UNIVERSIDADE DO VALE DO RIO DOS SINOS – UNISINOS
UNIDADE ACADÊMICA DE PESQUISA E PÓS-GRADUAÇÃO
PROGRAMA DE PÓS-GRADUAÇÃO EM GEOLOGIA
NÍVEL DOUTORADO

DISSERTAÇÃO DE DOUTORADO

GERMAN DAVID PATARROYO CAMARGO

PALEOENVIRONMENTAL AND BIOSTRATIGRAPHIC CONSTRAINTS FOR UPPERMOST CRETACEOUS (MAASTRICHTIAN) SEDIMENTARY SUCCESSIONS OF NORTHERN SOUTH AMERICA

Orientador: Karlos Guilherme Diemer Kochhann

Co-orientadora: Laia Alegret (Zaragoza University)

Línea de pesquisa: Paleontologia Aplicada

Banca examinadora:

Dra. Ana Luiza S. Albuquerque

Dra. Renata Guimarães Netto

Dr. Eduardo A. M. Koutsoukos

São Leopoldo, Brasil

2024

C173p Camargo, German David Patarroyo.
Paleoenvironmental and biostratigraphic constraints for uppermost cretaceous (Maastrichtian) sedimentary successions of northern South America / German David Patarroyo Camargo. – 2024.
182 f. : il. ; 30 cm.

Dissertação (doutorado) – Universidade do Vale do Rio dos Sinos, Programa de Pós-Graduação em Ciências Geologia, 2024.
“Orientador: Karlos Guilherme Diemer Kochhann
Co-orientadora: Laia Alegret (Zaragoza University)”.

1. Sedimentos (Geologia). 2. Geologia estratigráfica - Cretáceo. 3. Paleontologia - Cretáceo. I. Título.

CDU 551.7

Dados Internacionais de Catalogação na Publicação (CIP)
(Bibliotecária: Amanda Schuster – CRB 10/2517)

ABSTRACT

One of the major environmental and biotic turnovers of the Phanerozoic occurred at the Cretaceous-Paleogene (K-Pg) transition, being the focus of countless scientific studies that addressed the timing, mechanisms and consequences of this global event. Though less explored, Late Cretaceous oceanic settings also underwent significant paleoenvironmental changes, due to a combination of global or regional paleoceanographic and tectonic events. This study aims to reconstruct paleoenvironmental conditions on a series of Maastrichtian localities along the equatorial South American margin. To have a better understanding of low-latitude water masses during that time, we applied high-resolution micropaleontological (foraminifers) and geochemical (sediment elemental ratios, carbon isotopes, among others) methods in shallow marine units from northern Colombia, and in deep-sea sites from the tropical Atlantic Ocean.

Two Maastrichtian localities were considered in Colombia: (1) Core Diablito-1E (Colón Formation, Cesar-Ranchería Basin), and (2) the Aguablanca Creek section (Umir Formation, Middle Magdalena Valley). In general, foraminiferal assemblages were dominated by benthic taxa (Maastrichtian regional biozones *Siphogenerinoides bramletti* to *Ammobaculites colombiana*), and planktonic foraminiferal assemblages were mostly composed of *Guembelitria cretacea* and heterohelicids. Ostracods and calcareous nannofossil were also studied to provide integrated paleoenvironmental interpretations. Despite their potential, both microfossil groups had been poorly studied in this region. Integrated microfossil assemblages and sediment elemental ratios (Zr/Rb, Fe/Ca, V/Cr and Sr/Ba) in both localities clearly indicated a transition from inner platform settings, with moderately oxygenated bottom waters, to sublittoral conditions. Throughout the studied sections, weathering intensity increased, accompanied by increased input of terrigenous sediments. These environmental disturbances were related to the geological evolution of extensive epicontinental seas that occupied northern South America, and gradually disappeared due to sea level fluctuations, and the onset of the Andean orogeny since the Maastrichtian.

To track paleoenvironmental disturbances in the deep-sea, two Maastrichtian localities were surveyed in the tropical Atlantic Ocean: (1) Ocean Drilling Program (ODP) Hole 1258A (Demerara Rise), and (2) ODP Hole 1001B (Nicaraguan Rise). At Hole 1258A, high-resolution geochemical and benthic foraminiferal analyses suggest the occurrence of paleoenvironmental shifts during the entire Maastrichtian, related to changes in the intermediate to deep-water oxygenation and surface productivity, as well as a sudden dissolution episode in the earliest Maastrichtian. For instance, selected taxa (*Aragonia*, *Nuttallides truempyi*, *Coryphostoma*, *Strictoscomella*, among others), and the distribution of redox-sensitive trace metals (Ni, Cu) along the core, indicated suboxic bottom water

conditions, with oxygenation pulses during the mid-Maastrichtian event (MME), which was identified by a high-resolution stable carbon isotope ($\delta^{13}C$) record at the site. Moreover, sediment elemental ratios (log(Fe/Ca), Si/Ti, Fe/K) indicated fluctuations of biogenic silica and carbonate export via surface productivity, and probable disturbances of the regional hydroclimate since the early Maastrichtian. These disturbances of local surface productivity and bottom water oxygenation on Demerara Rise were likely related to the MME and the onset of the late Maastrichtian warming event, both linked to a higher interference of high-latitude deep-waters on the tropics and likely latitudinal migrations of the Paleo-Intertropical Convergence Zone (PITCZ). On the other hand, tracking paleoenvironmental disturbances at Hole 1001B was more challenging since diagenetic issues hampered good microfossils preservation, whose assemblages suggested a typical bathyal setting. However, the sedimentary archive of Hole 1001B was sensitive enough to allow identifying of the K-Pg boundary with a preliminary $\delta^{13}C$ survey, also indicating subtle changes of surface paleoproductivity and bottom water conditions during the late Maastrichtian, as suggested by sediment elemental ratios (log(Fe/Ca), Si/Al, Ba/Al, Fe/K) and concentrations of redox-sensitive trace metals (Ni, Zn, V) along the core.

Finally, the analysis of mercury (Hg) concentrations as a proxy for widespread volcanic activity was conducted in three of the studied localities: Sites Diablito-1E, ODP Holes 1258A and 100B. Considering the shallowing processes underwent by core Diablito-1E, and the poorly explored influence of the northern South American volcanism during Maastrichtian, Hg concentrations could not be exclusively linked to a single volcanic source (Deccan or regional volcanism). Bulk sediments $\delta^{13}C$ analyses at Core Diablito-1E, the first ones conducted in Maastrichtian rocks from this area, indicate that the low-latitude sedimentary record has the potential to track perturbations of the global carbon cycle. Moreover, the sedimentary records from Demerara Rise and Nicaraguan Rise illustrated significant Hg peaks along the Maastrichtian, which based on their proposed age models and comparisons with other Maastrichtian localities, would evidence the influence not only of Deccan volcanic episodes but also of the less studied volcanic pulses in the Caribbean during the late Maastrichtian. The role of those widespread processes on the low latitude climate is a promising field of study.

These results clearly pointed out that the northern South America region was particularly sensitive to paleoenvironmental disturbances during the Maastrichtian, reflecting their highly complex geological evolution during the latest Cretaceous.

ARCABOUÇO PALEOAMBIENTAL E BIOESTRATIGRÁFICO PARA SUCESSÕES SEDIMENTARES DO CRETÁCEO SUPERIOR NO NORTE DA AMÉRICA DO SUL

Uma das maiores perturbações ambientais e bióticas durante o Fanerozóico ocorreu na transição Cretáceo-Paleogeno (K-Pg), pelo que incontáveis trabalhos acadêmicos têm procurado compreender a cronologia, os mecanismos e consequências deste evento global. Entretanto, apenas alguns trabalhos têm documentado mudanças significativas nos ambientes marinos antes do limite K-Pg, explicadas por uma combinação de eventos paleoceanográficos e tectônicos de escala regional a global. Esta pesquisa procurou reconstruir as condições paleoambientais de diversas localidades com sedimentos do Maastrichtiano, ao longo da margem equatorial da América do Sul. Procurando obter um melhor conhecimento das massas de água de latitudes baixas durante aquele intervalo do tempo, foram aplicados diferentes métodos micropaleontológicas (foraminíferos) e geoquímicas (razoes elementais em sedimentos, isótopos de carbono) de alta resolução em unidades marinhas rasas do norte da América do Sul, e também em testemunhos de águas profundas do Oceano Atlântico tropical.

Duas localidades do Maastrichtiano da Colômbia foram estudadas: (1) Testemunho Diablito-1E (Formação Colón, Bacia de Cesar-Rancheria), e (2) a seção do Riacho Aguablanca (Formação Umir, Vale Médio de Magdalena). As associações de foraminíferos foram dominadas por espécies bentônicas (Biozonas regionais do Maastrichtiano *Siphogenerinoides bramletti* e *Ammobaculites colombiana*), enquanto as associações planctónicas foram representadas principalmente por *Guembelitria cretacea* e heterohelicidos. Com o propósito de obter uma ampla compreensão das condições paleoambientais nas duas localidades, os conteúdos de nanofósseis calcários e ostracodes também foram considerados nas interpretações. Apesar do potencial destes grupos de organismos fósseis, eles têm sido pouco explorados nesta região. A integração da informação micropaleontológica e diferentes razoes elementares (Zr/Rb, Fe/Ca, V/Cr, Sr/Ba) nos sedimentos das duas localidades, permitiu a identificação de uma transição de ambientes de plataforma interna, com águas de fundo moderadamente oxigenadas, e gradando para condições marinhas rasas, associadas a um maior aporte de material terrígeno. Essas mudanças ambientais estiveram relacionadas à evolução geológica dos mares epicontinentais que dominaram o norte da América do Sul, e que, gradualmente desapareceram devido a oscilações eustáticas, e a ativação da orogenia Andina, desde o começo do Maastrichtiano.

Dois testemunhos de águas profundas foram analisados para identificar mudanças paleoambientais no Oceano Atlântico tropical: (1) *Ocean Drilling Program* (ODP) Hole 1258A (Alto de Demerara), e (2) ODP Hole 1001B (Alto de Nicarágua). A análise micropaleontológico e geoquímico de alta resolução no Hole 1258A sugeriu a ocorrência de mudanças paleoambientais ao longo do Maastrichtiano, relacionada a perturbações na oxigenação das massas de água intermedias-profundas e à produtividade superficial, assim como um episódio súbito de dissolução de carbonatos no Maastrichtiano inicial. Taxa específicos (*Aragonia*, *Nuttallides truempyi*, *Coryphostoma*, *Strictoscomella*) e a distribuição de metais sensíveis (Ni, Cu) à oxigenação da água ao longo do testemunho, sugerem a ocorrência de condições subóxicas nos sedimentos de fundo, e pulsos de oxigenação durante o *mid-Maastrichtian Event* (MME), identificado por um registro de alta resolução de isótopos estáveis de carbono ($\delta^{13}C$). Razões elementais (log(Fe/Ca), Si/Ti, Fe/K) indicaram variações no aporte de sílica e carbonatos biogênicos via produtividade superficial, e prováveis perturbações hidroclimáticas desde o Maastrichtiano inicial. As perturbações de produtividade superficial e na oxigenação de águas de fundo no Alto de Demerara estariam relacionadas com o MME e com o começo do evento de aquecimento do Maastrichtiano tardio, ambos conectados com uma maior influência de massas de águas profundas, oriundas de latitudes altas, nos trópicos, além de possíveis migrações da paleo-Zona de Confluência Intertropical (PZCIT). Em contraste, reconhecer mudanças paleoambientais no Hole 1001B foi mais complexo por causa da intensa diagênese, dificultando um melhor diagnostico dos foraminíferos batiais que foram reconhecidos. Entretanto, esse registro sedimentar foi suficientemente sensível para capturar o limite K-Pg no registro de $\delta^{13}C$, enquanto variações sutis na produtividade superficial e da oxigenação de águas de fundo durante o Maastrichtiano tardio foram registradas por diferentes razoes elementares dos sedimentos (log(Fe/Ca), Si/Al, Ba/Al, Fe/K) e o conteúdo de metais sensíveis às condições redox (Ni, Zn, V).

Finalmente, as concentrações do mercúrio (Hg) como um indicador de vulcanismo de grande magnitude foram estudadas em três localidades: Diablito-1E, ODP *Hole* 1258A e ODP *Hole* 1001B. Por causa do ambiente marinho raso e o pouco conhecimento do vulcanismo regional da América do Sul durante o Maastrichtiano, as concentrações de Hg em Diablito-1E não puderam ser associadas com eventos vulcânicos exclusivos (Deccan ou vulcanismo regional). De qualquer forma, análises de $\delta^{13}C$, primeiras em rochas maastrichtianas desta região, sugerem seu potencial para registrar perturbações no ciclo global do carbono. Os registros sedimentares dos testemunhos ODP *Hole* 1258A e ODP *Hole* 1001B também apresentaram variações significativas no conteúdo de Hg ao longo do Maastrichtiano, as quais não somente evidenciariam a influência dos episódios vulcânicos da Província de Deccan, más também de episódios pouco estudados na região caribe durante o Maastrichtiano tardio. O impacto que aqueles episódios vulcânicos puderam ter no clima em baixas latitudes é uma oportunidade de pesquisa promissora.

Em conclusão, todos os resultados obtidos nesta investigação ilustraram a sensibilidade climática que América do Sul teve durante o Maastrichtiano, uma consequência da incrivelmente complexa história geológica desta área ao longo do Cretáceo tardio.

ACKNOWLEDGMENTS

It was a long journey…But, I will try to be brief this time…

Fueron cuatro años bastante extraños, y supongo que es normal. Después de todo, de eso se trata el aprendizaje en un doctorado: los ensayos optimistas y los errores torpes, las experiencias culturales, las amistades, los recuerdos buenos y amargos. Y bueno, la pandemia ciertamente influyó en ese coctel extraño durante los primeros años de estudio. Pero, agradecer es reconocer los aportes cuando se llega a este punto, el de celebrar los triunfos, la meta alcanzada. Por tal motivo hablaré en mi idioma natal, en reconocimiento a mi hogar y a la sinceridad que quiero plasmar, y como es habitual hablaré de esa gratitud en los términos que suele implicar el estudio: lo académico y lo personal.

A todos en itt-Oceaneon muchas gracias por haber creído en lo que se podía aportar desde los Andes de Colombia, en un ya lejano 2019. A Gerson, Simone, Mauro, Fernanda, Lilian, Bernardo, Andressa, muchas gracias por tenderme la mano durante este periodo que viví en el barrio Cristo Rei, fuera en trámites administrativos, dudas académicas, o simplemente en los rollos del día a día. Infinitas gracias a todos en el laboratorio: Luciana, Jordana, Lucas y Andressa E. Un buen equipo de laboratorio es fundamental en la investigación, y fue inspirador ver allí el ambiente cordial y la infraestructura que algún día quisiera emular en mi país. A mis compañeros de proyecto: Guilherme, Tamires, Sandro, Fernando y Eduarda, gracias por las conversas y la buena onda mientras lidiábamos con material no tan generoso en recobro (y preservación jaja). Ciertamente, muchas gracias a PETROBRAS porque fue debido a los recursos del proyecto "Bioestratigrafia de foraminíferos do Aptiano-Albiano da Margem Continental Brasileira" que mi estadía durante estos cuatro años fue posible. ¡La investigación en el Sur Global claro que es posible!

A mis compañeros de almuerzo que extraño un montón: Daiane, Marlone e Goti. Muchas gracias por su amistad sincera, sus consejos y cordialidad. Realmente espero que a futuro no solo sigamos creciendo juntos como colegas, sino como amigos en la distancia. Y también gracias a las compañías ocasionales como Leslie y Andreita, por su amistad y sororidad de pueblos andinos. A todos ellos, no sobra decir que se les espera por Colombia, así sea en plan turista.

A Karlos, mi supervisor bonachón, y a Deborah, su compañera de vida y de aventuras, gracias por los consejos académicos y los personales, su compañía y paciencia. Espero haber sido justo merecedor de su comprensión y apoyo. A Laia, mi supervisora tesa (término muy colombiano), muchas gracias por haber aceptado mi propuesta, y porque a pesar de la distancia hemos podido sacar a la luz los misterios de los bichines tropicales.

Hablemos ahora de lo que tuve que dejar atrás un tiempo y lo que conocí por el camino. Primero, y así parezca extraño, quisiera agradecer al azar de haber conocido en la pandemia a una especie de familia, o casa de estudio durante los primeros (los más duros) meses de la pandemia en Casa Cardoner: Rossane, Polyana y Ademir. Gracias por la compañía y los recuerdos.

A continuación, quisiera disculparme con mis amistades en Colombia, porque reconozco que durante buenos tramos de mi tiempo en Brasil, estuve en un modo más introspectivo del que hubiera deseado. Con o sin la locura de la pandemia, creo que hubiera sucedido igual. A pesar de eso, los pensé y les agradecí enormemente los momentos en que hablamos así fuera de forma remota. A Silvia, Claudia, Gyna, Andrés, Gustavo, Diego, Carolina y Nicté, muchas gracias, y prometo (solo prometo) ser mejor amigo al cerrar este ciclo de mi vida.

Y es curioso, o no, porque cuando llego al motor de mi vida, a la razón por la que nunca he desfallecido en la adversidad, y tercamente miro al futuro con optimismo, sí, mi familia, es el punto donde me suelo quedar corto en palabras, habladas y escritas. Tal vez por eso los quiero tanto: Ma, Pa, Mary, Diego, Antonio, porque con ustedes nunca tendré que fingir o anhelar cosas que no me corresponden, y en cambio, el amor opera en sus formas más puras y descomplicada. Y es curioso, nuevamente, porque fue al final de este camino, cuando tal vez ya no esperaba nuevas sorpresas, que apareciste, Juliana, y por ende, a ti, toda mi gratitud y cariño, así como los deseos infinitos de vivir contigo ese futuro optimista que por ahí está.

Finalmente, porque me lo prometí hace cuatro años, mientras daba vueltas sobre un diminuto sendero de hojas, recolectando bayas y viendo el paso de aves migratorias, en un encierro que no era encierro del todo (ahora finalmente entendí), dedico esta obra abstracta, (tú y yo lo sabemos, amigo lector) a mi salud mental, y a una resiliencia que nunca creí posible en mi inseguro ser.

I guess we made it, kid…

Ojalá el viento arrastrara mis pesares, y que allá, en la inmensidad del mar, estos se dispersaran por aguas heladas que nunca conocerán mi memoria. Un lugar donde en su continua degradación, en su merecido destierro, fueran engullidos por seres imaginarios, por alimañas de incontables ojos, por maquinaciones de mi infancia. Y más allá de una venerable desaparición, del olvido final, sus restos masticados a medias, descendieran a profundidades que codician la luz.

Y si allí, en la más completa oscuridad, en la inquietante paz del abismo, aquellos pesares creyeran que descansarían de mis deseos vengativos, pues se equivocarían, porque aquella fosa seguiría recibiendo restos hasta el final de mis tiempos, en una sucesión de carcasas que depositaría con macabro orgullo, y que solo podrían ser liberadas por cataclismos que sacudieran la tierra, o por almas que tuvieran el desafortunado rol de prospectar mi consciencia.

Ojalá los sonidos dejarán de acosarme, y que así, en el silencio más desolador, cautivos en una prisión que imite la arrogancia del granito, los recuerdos sonoros fueran susurros, y los susurros, fantasmas. Un lugar donde todos estos, ya cansados de ventilar sus frustraciones, fueran consumidos por el fuego de Vulcano, mientras aquel prepararía sus armas divinas, y el mundo arriba de este, el nuestro, se caería a pedazos.

Y si así, en la agonía del fuego primario, en el cautiverio más despiadado, aquellos sonidos malditos pensaran que descansarían de mis deseos vengativos, pues se equivocarían, porque el interior de la tierra es tan vasto y voraz como mis deseos de olvidar, desde el primer arrullo, hasta el suspiro que preceda el final de mis tiempos, en una sucesión ruidosa, aglutinada en el mayor desorden, y que solo podría ser rescatada por cataclismos que sacudieran la tierra, o por las almas que tuvieran el desafortunado rol de oír mis pensamientos.

Ojalá recordar no fuera el dolor punzante, y en cambio, fuera la caricia furtiva del viento, así sea uno rabioso, caótico, como el aire de los acantilados en Dover, donde ya en las alturas, en aquel peregrinaje anhelado, lo contemplara todo en absoluta paz: Desde la inmensidad del mar con sus secretos ocultos y sus criaturas sobrenaturales, hasta la rigidez del continente con el retumbar de sus martillos mecánicos y sus sonidos cautivos en siniestras catacumbas.

Y si en cambio, en vez de ascender hasta esas alturas inimaginables, de ser la aurora que maravilla al viajero en las noches polares, o ser la furia de los rayos que navegan entre tormentas colosales, tan solo consiguiera resistir el dolor que carcome mis entrañas, ese dolor de mirar hacia el pasado, de inventariar los sonidos y pesares que rigen y regirán mis acciones hasta el final de mis tiempos, no precisaría de monstruos aterradores, prisiones rocosas, abismos insondables o fuegos del Averno. Mucho menos de cataclismos que sacudieran a la tierra, o almas que tuvieran el desafortunado rol de visitar la mía.

Acantilados en Dover

German Patarroyo

TABLE OF CONTENTS

SUMMARY

The Cretaceous-Paleogene transition has been intensively studied in the literature due to the occurrence of the fifth largest mass extinction at the K-Pg boundary (e.g., Álvarez et al., 1980). There is a broad consensus that the impact of an asteroid 66 Ma caused global paleoclimatic and paleoenvironmental changes as well as the mass extinction, although the specific mechanisms are debated (e.g., D'Hondt, 2005; Schulte et al., 2010; Alegret et al., 2012, 2022; Henehan et al., 2019; Hull et al., 2020; Chiarenza et al., 2020; Carvalho et al., 2021; Goderis et al., 2021). Life and ecosystems also underwent significant paleobiological disturbances during the Late Cretaceous (Campanian-Maastrichtian), evidenced by faunal turnovers, diversity declines, and even extinction of representative marine groups, such as the inoceramids and the rudist bivalves (e.g., Johnson, 2002; Frank et al., 2005; Mateo et al., 2007; Stinnesbeck et al., 2012; Condamine et al., 2021; Coiffard et al., 2023). In general, Late Cretaceous climate was characterized by a shift from "hot greenhouse" conditions which dominated during most of Cretaceous, to a "cool greenhouse" scenario during the Maastrichtian, with a moderate latitudinal gradient and the development of stable deep-water masses at high latitudes.

This climatic shift has been tracked mostly on the deep-sea records using micropaleontological (foraminifers, calcareous nannofossils) and geochemical proxies (e.g., Friedrich et al., 2004; Voigt et al., 2013; Linnert et al., 2016; Huber et al., 2018; Ladant e al., 2020). The Late Cretaceous world also experienced an increase in global volcanic activity, commonly related to episodic volcanic pulses in India, as evidenced by the widespread Deccan Traps (e.g., Schoene et al., 2019; Sprain et al., 2019). How that recurrent activity was linked with the Campanian-Maastrichtian and the K-Pg climatic shifts, is also an issue widely explored in recent years (e.g., Percival et al., 2018; Keller et al., 2020; Hull et al., 2020; Font et al., 2021; Gu et al., 2022).

Considering that low-latitude ecosystems have operated as major triggers of biological diversity through geological time (Mittelbach et al., 2007), a better understanding of the Maastrichtian tropics, particularly their shallow marine and deep-sea environments, would help properly estimate how the marine biota responded to climate changes before the K-Pg extinction. In addition, this approach would provide more tools for Late Cretaceous climatic modelling (Ladant et al., 2020) and paleobiogeographical inferences.

Like in modern times, Late Cretaceous shallow marine ecosystems of northern South America were highly complex, being characterized by extensive epicontinental seas that gradually disappeared by a combination of sea level fluctuations and the onset of the Andean orogeny (Erlich et al., 2000; Bayona et al., 2020). On the other hand, low latitude open marine settings were likely influenced by changes

in water mass circulation in the Atlantic and Pacific realms (e.g., D´Hondt and Arthur, 2002; Friedrich et al., 2012; Batenburg et al., 2018). This study provides new data to improve our understanding of Maastrichtian marine settings, using an integrated analysis of micropaleontological (foraminifera) and geochemical (elemental ratios, isotopes, among others) proxies. One of the reasons why this study focused on the Maastrichtian interval is that foraminiferal assemblages were highly diverse in northern South America, with a moderate input of previous research (e.g., Tchegliakova and Mojica, 2001; Martinez, 2003; Koutsoukos, 2006).

Here, high-resolution studies were conducted at the stratigraphic core Diablito-1E and at the Aguablanca Creek section (northern Colombia). Micropaleontological and geochemical analyses in both localities aimed to establish a robust paleoenvironmental reconstruction for the latest Cretaceous of northern South America. To have a robust understanding of paleoceanographic conditions in the tropics, systematic studies (micropaleontological and geochemical) were also conducted at two deep-sea sections in the tropical Atlantic Ocean (ODP sites 1258 and 1001). High-resolution paleoenvironmental reconstructions for Maastrichtian deep-water masses and surface productivity were the major goals of this part of the study, tracking the likely influence of major perturbations in the global carbon cycle such as the Mid-Maastrichtian Event (MME) or the latest Maastrichtian warming event (LMWE), on northern South America.

An additionally explored issue was the tentative use of sedimentary mercury (Hg) concentrations as a chemostratigraphic tool for the Maastrichtian in tropics, and its link with not only the Deccan vulcanism, but also regional volcanic sources such as the Caribbean Large Igneous Province, and their possible consequences for low latitude climate. Results of Hg analyses in the surveyed shallow marine and deep-sea localities were compared with those reported in previous studies (e.g. Percival et al., 2018; Schoene et al., 2019; Sprain et al., 2019; Keller et al., 2020; Font et al., 2021).

THESIS STRUCTURE

An introductory chapter explains the main motivations for conducting this study, the geological context of the Late Cretaceous sedimentary successions in northern South America, the main research goals of this study, and additional topics that were explored during the doctorate. Main results are sorted in three major components: (1) paleoenvironmental inferences from shallow-marine units in northern South America (**CHAPTERS 1-2**), (2) paleoceanographic inferences from deep-sea settings in the tropical Atlantic Ocean (**CHAPTERS 3-4**), and (3) mercury chemostratigraphy in Maastrichtian low latitude locations (**CHAPTER 5**). Figure 1 summarizes the location of the studied sites.

CHAPTER 1 describes the results of an integrated micropaleontological and geochemical study of core Diablito-1E (Cesar-Rancheria Basin, Colombia). A paleoenvironmental reconstruction was made for the Colón Formation (Maastrichtian). This chapter was published at the *Journal of South American Earth Sciences* (Vol 119, 104015 Special Volume: "Stratigraphy and Micropaleontology of Caribbean Basins"), and it is entitled "**Paleoenvironmental changes recorded at a late Maastrichtian marine succession of northern South America".**

An additional shallow marine succession is explored in **CHAPTER 2**: Aguablanca Creek section (Middle Magdalena Valley, Colombia). An integrated micropaleontological and geochemical study surveyed the stratigraphic contact between La Luna-Umir formations, and the lower segment of the Umir Formation (Maastrichtian). This chapter was published at *Ameghiniana* (Vol 60 (4), p. 297-311), and it is entitled **"Maastrichtian microfossils of the shallow marine Umir Formation, North-eastern Colombia"**.

CHAPTER 3 comprises high-resolution benthic foraminiferal and geochemical analyses at Ocean Drilling Program (ODP) Hole 1258A (Demerara Rise, offshore Suriname). A series of paleoceanographic and paleoclimatic inferences were made for this locality (e.g., surface productivity, bottom water oxygenation, regional hydroclimate), comparing them with previous studies of high latitude locations in the Atlantic Ocean, and one site from the tropical Pacific Ocean. These results will be submitted to *Paleoceanography and Paleoclimatology* with the title "**Benthic foraminifera and paleoenvironmental turnover across the mid-Maastrichtian event in the tropical Atlantic Ocean (ODP Site 1258)**".

A similar approach is illustrated in **CHAPTER 4**, for ODP Hole 1001B (Nicaraguan Rise, Western Caribbean), where the paleoceanographic discussion was mostly focused on geochemical proxies, including stable carbon isotope and mercury (Hg) records along the Maastrichtian and the K-Pg boundary. Results of this chapter will be submitted to *Cretaceous Research* with the title "**Low latitude deep-sea paleoenvironmental evolution during the Maastrichtian**".

CHAPTER 5 deals with Hg concentrations and associated geochemical proxies (Hg/TOC, Hg/S ratios) from the studied localities described in CHAPTERS 1, 3 and 4. A tentative Hg chemostratigraphy is tested for the tropics, including a discussion about the likely volcanic sources of higher Hg concentrations (Deccan Traps and Caribbean Large Igneous Province). These results will be submitted to *Geology* as "**Mercury concentrations as a proxy for volcanic activity in the Maastrichtian low-latitude oceans**".

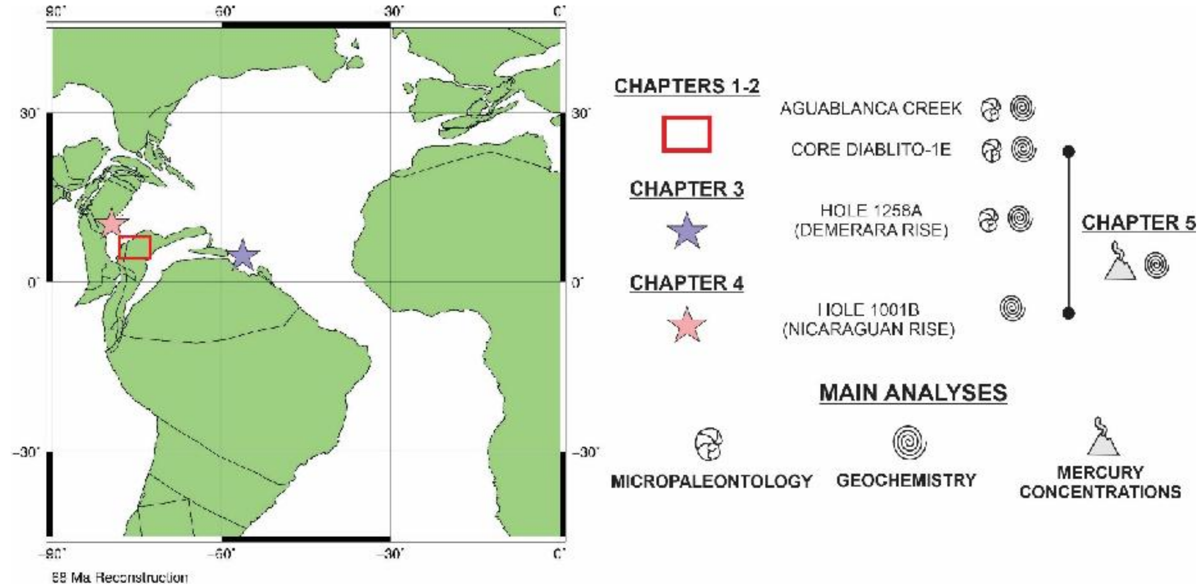

Figure 1. Geographic location of each chapter. 68 Ma paleogeographic reconstruction from the ODSN online tool (http://www.odsn.de/odsn/services/paleomap/paleomap.html). The location of the studied material described in the ADDENDA is in the same region as that of CHAPTER 1.

The concluding remarks of this dissertation are presented in **CHAPTER 6**, as well as an additional study (**ADDENDA**), submitted as second author to *Cretaceous Research*: "**Ostracod assemblages from the Upper Cretaceous Colón Formation, Colombia: Taxonomy and paleoecological inferences**"

INTRODUCTION

MOTIVATION

The “mysterious” Late Cretaceous seas of northern South America

When I wanted to discuss (or to argue, depending on context) with colleagues about the Late Cretaceous sedimentary successions in Colombia, I usually quoted Hermann Duque-Caro (1935-2015), a prominent Colombian micropaleontologist who used to say “ah, the mysterious Cretaceous seas”. Those seas were unusual indeed, not only in Colombia but in most of northern South America. In general, Cretaceous seas of this region were characterized by poorly ventilated intermediate water masses and anoxic-dysoxic to euxinic bottom water conditions, both associated with strong to moderate upwelling activity (Martinez and Hernández, 1992; Vergara, 1997; Villamil and Pindell, 1998; Bralower and Lorente, 2003; Martinez, 2003; Sarmiento-Rojas, 2019; Páez-Reyes et al., 2021). Consequently, the Late Cretaceous sedimentary units in northern South America, consist of thick sequences of organic-rich limestones and shales, cherts and silicified limestones, with scattered glauconitic and phosphatic levels (Figure 1; Macellari, 1988; Föllmi et al., 1992; Villamil and Arango, 1998, Erlich et al., 1999; Guerrero et al., 2000; Bayona, 2018; Sarmiento-Rojas, 2019). Due to those paleoenvironmental conditions, Late Cretaceous sedimentary successions are responsible for >70% of the extracted hydrocarbons in Venezuela, Colombia and northern Peru (Talukdar and Marcano, 1994; Pindell and Tabbutt, 1995; Villamil et al., 1999; Mann et al., 2006), and uncountable earth science professionals in Colombia and Venezuela have dealt with the geological concept of the La Luna Sea (LLS).

Proposed by Erlich et al., (2000), the LLS was originally dated as late Santonian, but the aforementioned paleoenvironmental conditions partially or completely extended from Early to Late Cretaceous, and were developed under a passive-margin regime (Figure 1). Considering that many studies have focused only on Oceanic Anoxic Event 2 (OAE2; e.g. Villamil and Pindell, 1998; Sarmiento-Rojas et al., 2019; Páez-Reyes et al., 2021), there are still major doubts about the timing and paleoceanographic settings of the LLS. Tracking the end of the LLS is equally challenging, since major facies changes and hiatuses are present at the end of the Campanian, with truncation of Cretaceous marine sequences in all the inter-mountainous basins from Colombia (Figure 2). For instance, in the Catatumbo, Cesar-Rancheria and Maracaibo basins, major unconformities have been identified between strata recording highly productive deeper water settings of the LLS, and the overlying successions that represent shallower and oligotrophic conditions (Guerrero et al., 2000; Patarroyo et al., 2017; Terraza, 2019).

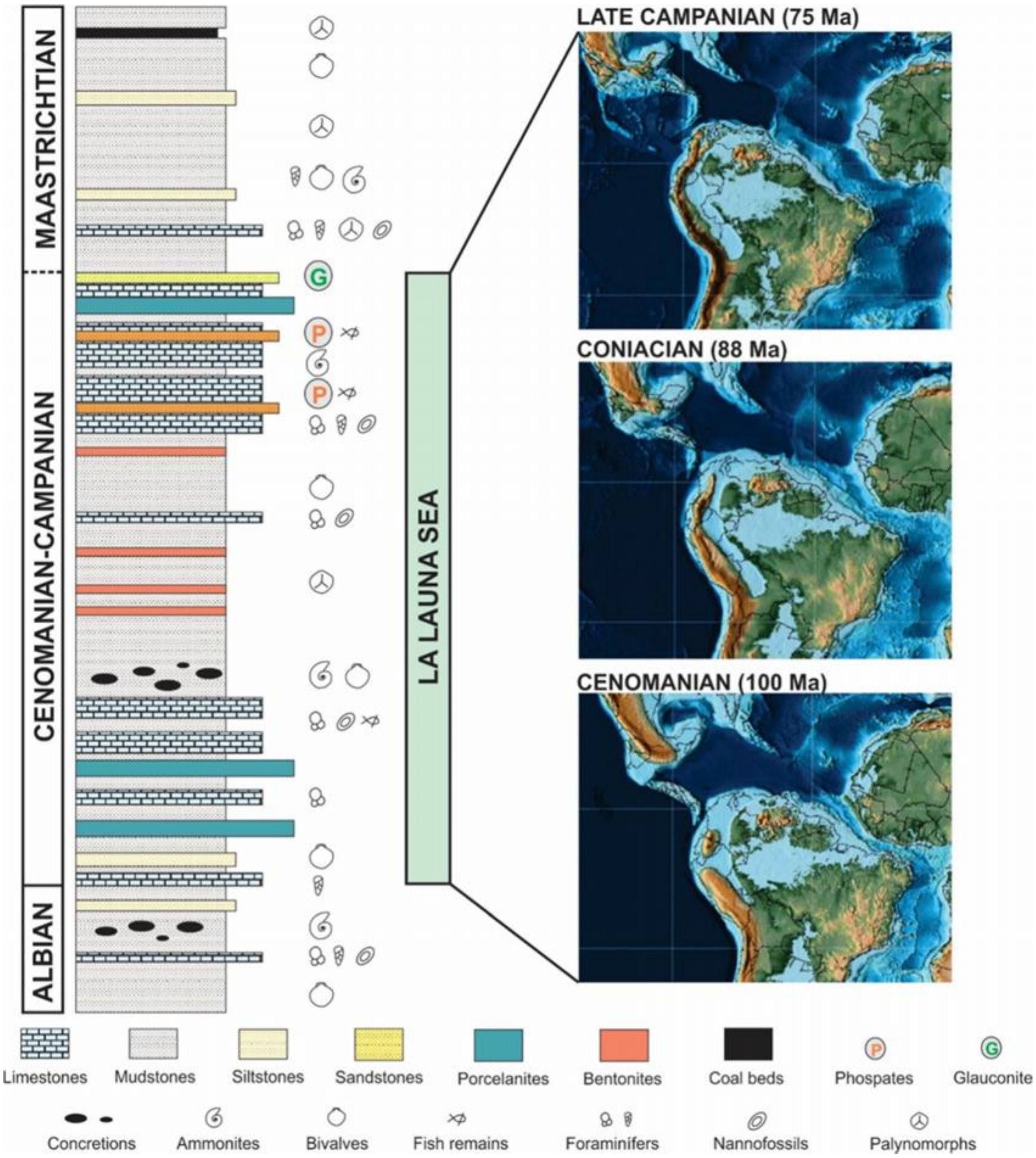

Figure 1. Main features of the La Luna Sea (LLS) in northern South America. Schematic stratigraphic synthesis of the Late Cretaceous sedimentary successions in Colombia (compiled from Vergara, 1997; Villamil and Arango, 1998; Guerrero et al., 2000; Erlich et al., 2000, Sarmiento-Rojas, 2019). Paleogeography of the Cenomanian-late Campanian interval from Scotese (2016).

An integration of sedimentological, biostratigraphic and seismic studies suggest that those facies changes and time gaps of late Campanian-early Maastrichtian were a consequence of gradational processes, linked to global sea level fluctuations, and the early stages of the Andean orogeny (Mora et al., 2006; 2010; Cooney and Lorente, 2009; Horton, 2018; Bayona, 2018; Bayona et al., 2020). Finally, though the highly productive water masses that defined the LLS disappeared for most of northern South America, restricted marine conditions continued until the Paleogene in the Perijá Range and the Maracaibo region (e.g. Hato Nuevo and Guasare Formations; Martínez and Hernández, 1992; Bayona et al., 2011). So far, the K-Pg boundary in this region of South America has been only described in a stratigraphic core from Cesar-Rancheria basin (Diablito-1E; De La Parra et al., 2022) and in a sedimentary outcrop from Gorgonilla Island, located in an open marine setting that was later accreted to South America (Bermúdez et al., 2019).

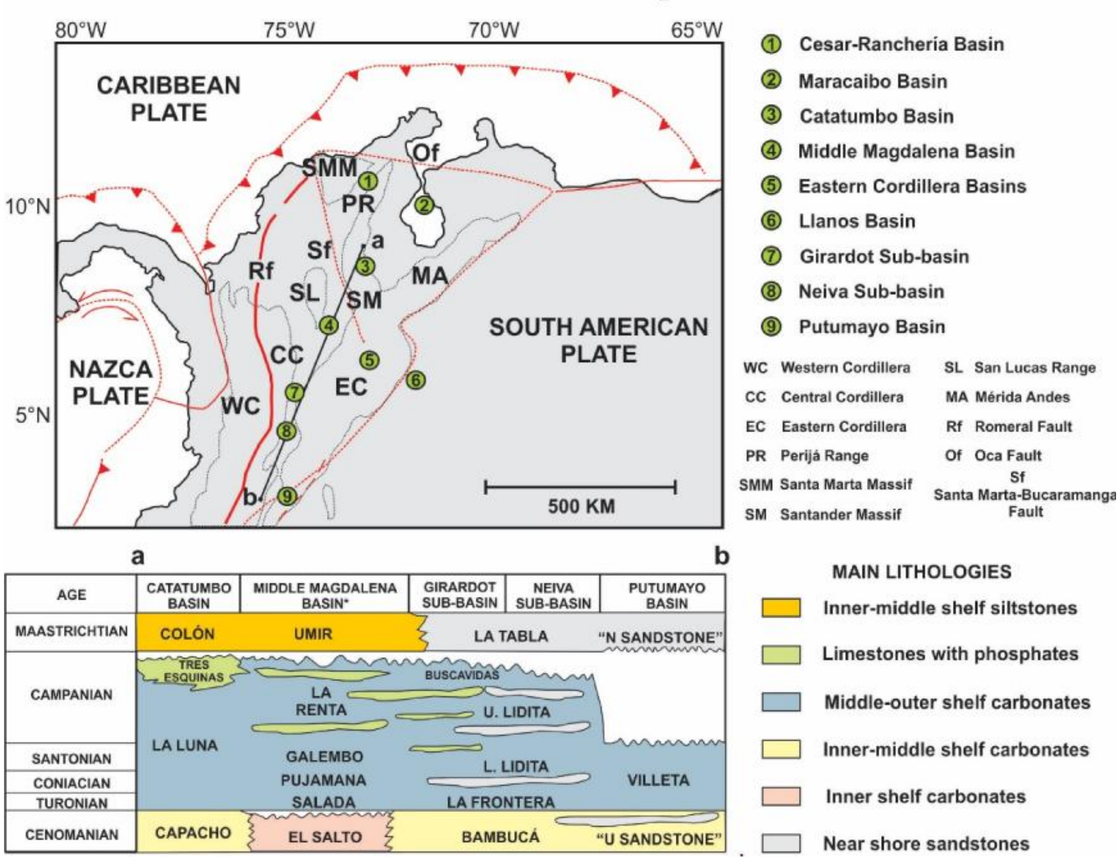

Figure 2. Regional tectonic setting of the northern Andes and general stratigraphic chart of the Late Cretaceous succession for the inter-mountainous basins of Colombia. Tectonic features based on Tschanz et al (1974), Bayona et al (2011) among others. Stratigraphy based on Montenegro and Barragán (2011), Pedraza and Ramírez (2011), Roncancio and Martínez (2011), Sarmiento-Rojas (2011). Stratigraphy for the Middle Magdalena basin followed the recent model of Terraza (2019).

It is already known that low latitude marine environments underwent significant shifts during the Campanian-Maastrichtian interval but, **what was the evolution of their associated ecosystems?** Previous paleontological studies have shown that marine microfossils (e.g., foraminifers, calcareous nannofossils, ostracods, dinoflagellates), which are key elements of the trophic chains, responded to these major changes. Marine microfossils were relatively abundant and diverse during the Maastrichtian, and they have been regularly used as paleoenvironmental proxies and chronostratigraphic markers (Bürgl and Dummit, 1954; Petters, 1955; Martinez, 1989; Tchegliakova, 1996; Vergara, 1997; Guerrero et al., 2000; Yepes, 2001; Tchegliakova and Mojica, 2001; Garzón et al., 2012; Juliao-Lemos et al., 2016; Patarroyo et al., 2017; Navarrete et al., 2018; Carvalho et al., 2021; De La Parra et al., 2022). However, most of these efforts, though effective, have relied on the distribution and abundance of the individual microfossil groups, an issue that could be troubling considering the dynamic paleoenvironmental context of this region. For instance, sedimentological (e.g., carbonate dissolution) and ecological (e.g., changes in bottom water oxygenation) processes could bias the potential of individual micropaleontological proxies. **In order to draw reliable paleoenvironmental and chronostratigraphic interpretations for the Late Cretaceous of northern South America, a multiproxy approach is ideal, not only for assessing the strengths and weaknesses of the selected microfossil groups, but also exploring the sedimentary record from a geochemical perspective**. For instance, sediment elemental ratios and organic geochemistry provide valuable data for reconstructing paleoclimatic (weathering intensity, paleohumidity, e.g., Stuut et al., 2005, Mulitza et al., 2008) and paleoceanographic parameters (surface productivity, sea level changes, e.g., Calvert and Pedersen, 2007, Agnihotri et al., 2008). Additionally, bulk sediment stable carbon isotope records have been used in chronostratigraphic correlations of uppermost Cretaceous sedimentary successions (Voigt et al., 2010, 2012; Vellekoop et al., 2022).

The multiproxy (micropaleontology and geochemistry) approach of this PhD thesis improves the understanding of northern South America marine ecosystems during the Maastrichtian in two ways: (1) providing robust paleoenvironmental and paleoceanographic schemes for the latest Cretaceous of northern South America and (2) assessing paleoclimate sensitivity of the low latitude regions to global and regional events such as the Andean orogeny or large-scale volcanism (Caribbean Large Igneous Province, Deccan Traps).

The Maastrichtian deep ocean in low latitude regions: “swimming on stranger tides”

There is a major consensus about the warmer nature of the Cretaceous climate (Figure 3; e.g., Barron, 1983; Jenkyns et al., 2004; O’Brien et al., 2017; Huber et al., 2018; Huber, 2020). Global paleotemperature compilations, based on paleontological (microfossils, plant remains) and geochemical data (oxygen isotopes, TEX_{86}) confirm this global warmth and reduced latitudinal temperature gradients during a long-time span of the Cretaceous, with an interval of maximum temperatures during the Cenomanian–Turonian (Wilson and Norris, 2001; Pucéat et al., 2003; Cramer et al., 2009; Friedrich et al., 2012; MacLeod et al., 2013; O’Brien et al., 2017; Huber et al., 2018). In contrast, a steady cooling trend has been recorded throughout the late Campanian-Maastrichtian, with arguably short-lived polar ice sheets in the late Maastrichtian (Davies et al., 2009; Bowman et al., 2013; Ladant and Donnadieu, 2016; Huber, 2020). As a response to warm intervals and changes of water masses circulation patterns, the Cretaceous world is also distinguished by major perturbations of the carbon cycle, known as ocean anoxic events (OAEs, e.g. Schlanger and Jenkyns, 1976; Jenkyns, 2010).

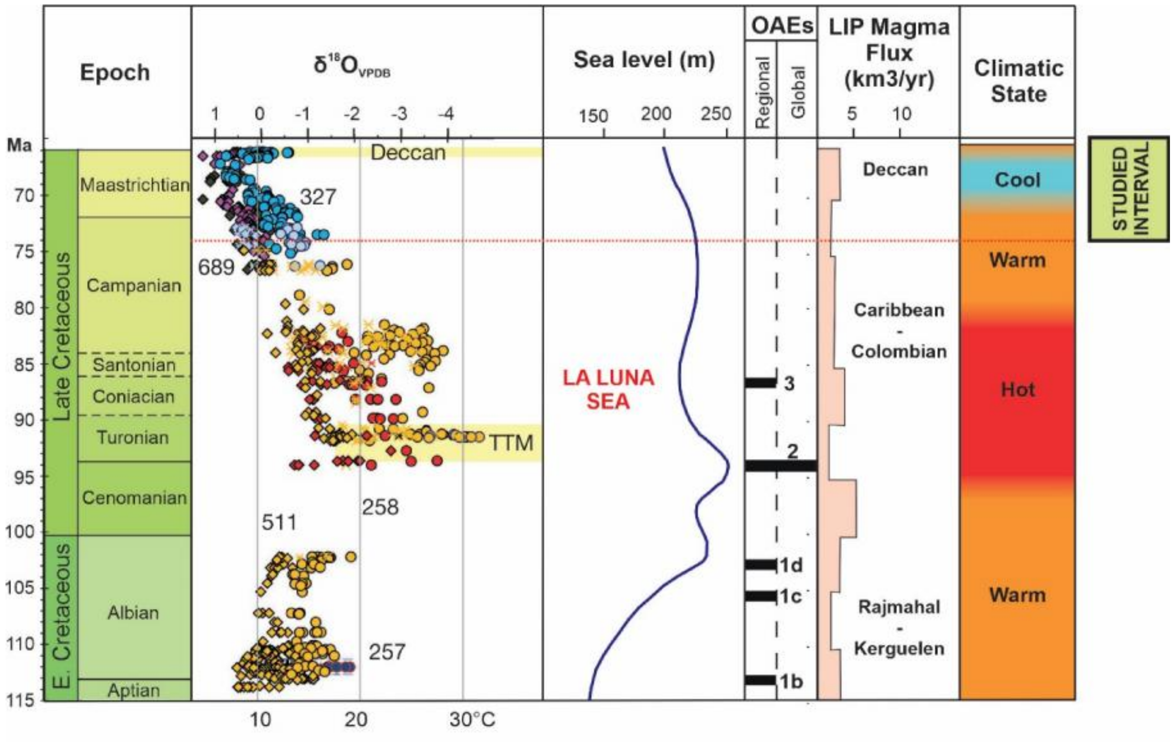

Figure 3. Compiled late Aptian-Maastrichtian planktonic and benthic foraminiferal stable oxygen isotope ($\delta^{18}O$) data and from Deep Sea Drilling Project (DSDP) sites 257, 258, 327, 511, and 689 by Huber et al. (2018). Note the occurrence of different Cretaceous greenhouse climatic states. Green square indicates the geochronological range of our studied material. Cretaceous sea level curve after Haq (2014). Regional and global Oceanic Anoxic Events after Takashima et al. (2015) and global large igneous provinces (LIP) magma flux estimations by Coffin et al. (2006). Figure modified from Li et al. (2019) and Huber (2020).

Oceanic Anoxic Events were characterized by widespread deposition of black shales and organic-rich limestones in marine environments (Schlanger and Jenkyns, 1976; Jenkyns, 2010; Jones et al., 2019). Many studies have focused on the onsets of OAEs, concluding that volcanism of large igneous provinces, likely caused these perturbations of the carbon cycle (e.g., Du Vivier et al., 2014; Huber, 2020). In contrast, OAE3 (Coniacian-Santonian) has only been discussed by Machado et al. (2016) in Venezuela, and its presence has been inferred from organic rich layers from central Colombia (e.g., Galembo Formation, Terraza, 2019). Late Cretaceous OAEs have been linked to rapid CO_2 degassing of the Caribbean Large Igneous Province and the High Arctic Large Igneous Province (Figure 3; Du Vivier et al., 2014; Schröder-Adams et al., 2019). The expression of OAEs in northern South America was likely favored by the openings of the Equatorial Atlantic Gateway and Southern Oceans between the Cenomanian and Maastrichtian (e.g., Martin et al., 2012). Similar conditions have been proposed for the deposition of organic-rich layers and the presence of the OAE2 in the U.S. Western Interior Seaway, where subtropical and Tethyan water masses interacted during the Albian-Maastrichtian time interval (e.g. He et al., 2005; Lowery et al., 2018). In the case of the LLS, the presence of OAE2 is beyond discussion, with most of the records located in Colombia and Venezuela (e.g., Villamil and Pindell, 1998; Davis et al., 1999; Erlich et al., 1999; Páez-Reyes et al., 2021). Additional features such as the phosphogenesis events recorded at the final stages of the LLS (Santonian-Campanian; Erlich et al., 2000; Martinez, 2003) also point to the combined effect of the post-Santonian cooling at high latitudes, sea level highstands, and the changing tectonic configuration of northern South America.

Open, relatively shallow, low latitude marine environments underwent significant environmental shifts before the Santonian but, **the evolution of the Maastrichtian deep-sea settings is debated**. Several studies, based on micropaleontological (foraminifers, calcareous nannofossils), geochemical (elemental ratios, organic matter and carbonate contents) and isotopic signatures ($\delta^{13}C$, $\delta^{18}O$, εNd) have proposed that, since the early and middle Maastrichtian, Atlantic water masses recorded a change in their source areas. For instance, warm-saline water masses in the equatorial Atlantic underwent a major influence of boreal deep-water masses since 69 Ma, rather than of the austral sources as recorded since the Albian-Cenomanian (e.g., Friedrich et al., 2004; Thibault and Gardin, 2006; Friedrich and Hemleben, 2007; MacLeod et al., 2011; Koch and Friedrich, 2012; Martin et al., 2012; Linnert et al., 2019). In the tropical Pacific Ocean (e.g., Shatsky Rise), changes in deep water masses have been recorded along the Maastrichtian, though with an ineffective oceanic circulation with the Atlantic and Tethyan realms. The recurrent presence of submarine barriers in the southern Atlantic (e.g., Rio Grande Rise) probably conditioned deep water formation in this region (e.g., Frank et al., 2005; Jung et al., 2013; Dameron et al., 2017; in press). The controlling mechanisms of deep-water formation in the Atlantic and Pacific realms have been proposed as possible triggers of at least two significant perturbations of the global carbon cycle: (1) the Campanian-Maastrichtian Boundary Event (CME; Friedrich et al., 2009), and (2) the mid-Maastrichtian Event (MME; Voigt et al., 2012). The MME (69 Ma) has been associated with ecological perturbations of the marine biota, reflected on the decline of several invertebrate groups (inoceramid and rudist bivalves, ammonoids; Johnson, 2002; Frank et al., 2005; Stinnesbeck et al., 2012), and changes in the benthic and planktonic microbiotas (e.g., Thibault and Husson, 2016; Dameron et al., 2017; in press; Vancoppenolle et al., 2022)

The question remains, **were major perturbations of the global carbon cycle such as the MME recorded in low-latitude settings?** The privileged geographic location of the low latitude Maastrichtian records favors a likely influence of this event, since the previously referred processes must have stimulated westward flowing of the Tethyan circumglobal current through the Caribbean Gateway (e.g., Soudry et al., 2006; Beil et al., 2020). Moreover, evidence for deep ocean circulation, linked to the aperture of the Equatorial Atlantic Gateway, has been documented in Cenomanian and even older sedimentary records of the northern South American margin (e.g., Koutsoukos and Merrick, 1986; Koutsoukos, 1992, 2006; Friedrich and Erbacher, 2006; Erbacher et al., 2009; Martin et al., 2012). Late Cretaceous climatic teleconnections between low and the high latitude processes (marine and continental) have been poorly explored, possibly undermining climatic modelling of this time interval, and discussions about the climatic transition at the K-Pg boundary (e.g., Hull et al., 2020; Ladant et al., 2020). For instance, studies based on geochemical proxies, such as Corentin et al (2022, 2023), have explored the possible role that tectonic pulses in South America could have played in the Late Cretaceous global cooling, due to chemical weathering feedback. Mercury (Hg) chronostratigraphy has tentatively linked Hg anomalies 400 k.y. before the K-Pg boundary with widespread volcanism of the Deccan Traps (Sial et al., 2014, 2016), but the role that Caribbean Plate volcanic activity might have played on global climate is still unclear.

Considering all these aspects, **ODP Holes 1258A (Demerara Rise) and 1001B (Nicaraguan Rise) are suitable candidates for testing climate sensitivity of the tropical oceans during the Maastrichtian**. Studies on the Maastrichtian record from Demerara Rise, would fill an important knowledge gap in the Cretaceous paleoceanographic history of the tropical Atlantic Ocean, comprising around 5 million years (Ma) before the K-Pg boundary extinction event (Friedrich and Erbacher, 2006; Friedrich et al., 2008; Schulte et al., 2009; Berndt et al., 2011; Martin et al., 2012; Thibault and Husson, 2016; MacLeod et al., 2017; Corentin et al., 2023). On the other hand, the Maastrichtian record of Nicaraguan Rise would not only provide insights about the nature of the deep-water circulation through this ancient gateway, but it also would complement studies about the geological evolution of the Caribbean Plate (Sigurdsson et al., 2000; Pindell et al., 2005; García-Reyes and Dyment, 2021).

The multiproxy (micropaleontological and geochemical) approach of this PhD thesis contributes to the understanding of low latitude marine ecosystems during the Maastrichtian, focusing on the following features: (1) Low latitude surface productivity and bottom water oxygenation, (2) paleoceanographic links with other oceanic settings (e.g., deep water formation) in the equatorial Pacific Ocean and high latitude settings in the Atlantic Ocean, as well as atmospheric circulation patterns, and (3) Hg chemostratigraphy of the Maastrichtian in low-latitude settings.

Based on the aforementioned questions, the main motivation of this study was imitating those ancient sea wolves while searching for new lands, though sailing will be this time in the mysterious Cretaceous seas.

RESEARCH HYPOTHESES

- Marine microorganisms (such as foraminifera), and water masses (surface and deep settings) from low-latitude seas responded to global climatic and paleoceanographic changes occurred during the Maastrichtian. Those changes should be reflected in the composition and abundance of the benthic foraminiferal assemblages or selected species, as well as fluctuations of selected geochemical proxies.
- Perturbations on the global carbon cycle, such as the MME, were reflected by changes of the surface productivity, deep-water circulation and bottom water oxygenation. Those fluctuations should be expressed in the distribution of selected foraminiferal taxa, estimations of benthic foraminiferal accumulation rates. Selected geochemical proxies and carbon stable isotope surveys must also reflected this perturbation.
- Regional tectonic features, such as the first pulses of the Andean orogeny, or volcanic episodes from the Deccan and Caribbean provinces, affected shallow marine settings and regional paleoclimatic parameters, such as weathering intensity. Mercury concentrations in the studied material, normalized with carbon and sulfur concentrations, can be used as a tracker of this volcanic activity.

MAIN RESEARCH GOAL

To explore Maastrichtian foraminiferal assemblages and selected geochemical proxies as tools for understanding paleoenvironmental and temporal constraints on latest Cretaceous water masses and epicontinental seas of northern South America, and coeval tropical Atlantic Ocean sedimentary successions.

ADDITIONAL RESEARCH GOALS

- To improve paleoenvironmental inferences for deep and surface water masses of the latest Cretaceous seas surrounding northern South America.
- To define paleoceanographic and paleoclimatic teleconnections of northern South America water masses and regional hydroclimate with surrounding areas of the Tethyan realm and high latitude locations of the Atlantic Ocean.
- To explore possible evidence of Deccan and Caribbean Plate volcanic activity in the low latitude paleoenvironments.

STUDIED LOCALITIES

A total of four localities were considered for this research (Figure 4).

- Stratigraphic core Diablito-1E (northern Colombia; 9°34'N, 73°16'W). The analyzed material spans the Colón Formation (Maastrichtian). Previous biostratigraphic data and sedimentary iridium concentration records, defined the K-Pg boundary at this core (De la Parra, 2022).
- Aguablanca Creek section (central Colombia; 7°7'N, 73°18'W). The surveyed material spans the Umir Formation (Maastrichtian). Detailed stratigraphy of the section was defined by Terraza (2019).
- ODP Hole 1258A (Demerara Rise; 9°26'N, 54°43'W). The analyzed material comprises the early to late Maastrichtian. Chronostratigraphy is based on Erbacher et al. (2004) and Suganuma and Ogg (2006).
- ODP Hole 1001B (Nicaraguan Rise; 15°45'N, 74°54'W). The studied material comprises the middle to late Maastrichtian. Chronostratigraphy is based on Sigurdsson et al. (1997) and Louvel and Galbrun (2000).

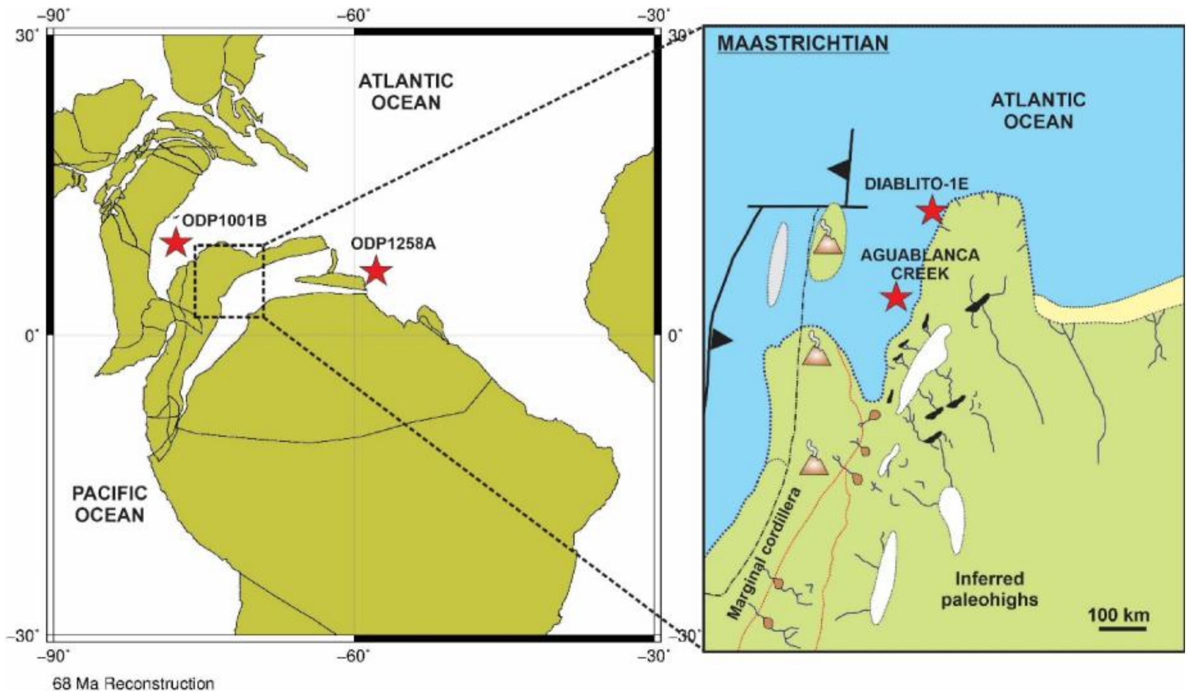

Figure 4. Geographic location of the studied sites. Left: 68 Ma paleogeographic reconstruction from the ODSN online tool (http://www.odsn.de/odsn/services/paleomap/paleomap.html). Right: Paleogeographic reconstruction of northern South America during the Maastrichtian interval (modified from Bayona, 2018).

CONTRIBUTION ROLES TAXONOMY

Considering the transdisciplinary approach that implies a multiproxy study, this research was possible due the contribution of several colleagues in Brazil and Colombia, where I was in charge of: (1) foraminiferal (sample preparation, foraminiferal counts and interpretation) analyses, (2) x-ray fluorescence analyses and sample preparation, and (3) the complete integration and discussion of the additional data. Here I provided the contribution of each colleague.

Karlos Kochhann (itt Oceaneon, Unisinos University). Foraminiferal, geochemical and paleoceanographical discussions.

Laia Alegret (Zaragoza University). Benthic foraminiferal ecology and taxonomic comments. Paleoceanographic discussions.

Daiane Ceolin (itt Oceaneon, Unisinos University). Ostracod taxonomy and ecology.

Rodrigo M. Guerra (itt Oceaneon, Unisinos University). Calcareous nannofossils taxonomy and ecology.

Marlone H.H. Bom (itt Oceaneon, Unisinos University). X-ray fluorescence methodological support and comments about geochemical proxies.

Andressa Esswein (itt Oceaneon, Unisinos University). Carbon and oxygen stable isotope analyses. Total organic carbon estimations.

Valeska Meirelles (Nova Analítica Imp. e Exp. Ltda). Mercury concentration analyses.

José Manuel Torres (Florida International University). Field support at the Aguablanca Creek section.

Gustavo Torres (Stratos Consultoría Geológica). Editing of selected SEM images.

Daniel Rincón (ECOPETROL-ICP). Data permits from stratigraphic core La Luna-3E.

REFERENCES

Agnihotri, R., Altabet, M.A., Herbert, T.D., Tierney, J.E., 2008. Subdecadally resolved paleoceanography of the Peru margin during the last two millennia. Geochemistry Geophysics Geosystems 9, Q05013, doi:10.1029/2007GC001744.

Alegret, L., Arreguín-Rodríguez, G. J., Thomas, E., 2022. Oceanic productivity after the Cretaceous/Paleogene impact: where do we stand? The view from the deep. In: Koeberl, C., Claeys, P., Montanari, A., eds., From the Guajira desert to the Apennines, and from Mediterranean microplates to the Mexican killer asteroid: Honoring the career of Walter Alvarez. Geological Society of America Special Paper 557, chapter 21.

Alegret, L., Thomas, E., Lohmann, K.C., 2012. End-Cretaceous marine mass extinction not caused by productivity collapse. PNAS (Proceedings of the National Academy of Sciences) 109 (3), 728-732.

Alvarez, L.W., Alvarez, W., Asaro, F., Michel, H.V., 1980. Extraterrestrial cause for the Cretaceous-Tertiary extinction. Science 208, 1195-1108.

Barron, E.J., 1983. A warm, equable Cretaceous: the nature of the problem. Earth Sci. Rev. 19, 305-338.

Batenburg, S.J., Voigt, S., Friedrich, O., Osborne, A.H., Bornemann, A., Klein, T., Pérez-Díaz, L., Frank, M., 2018. Major intensification of Atlantic overturning circulation at the onset of Paleogene greenhouse warmth. Nature Communications 9, 1-8.

Bayona, G., 2018. El inicio de la emergencia en los Andes del norte: una perspectiva a partir del registro tectónico-sedimentológico del Coniaciano al Paleoceno. Rev. Acad. Col. Cien. Ex. Fís. Nat. 42 (165), 364-378.

Bayona, G., Baquero, M., Ramírez, C., Tabares, M., Salazar, A.M., Nova, G., Duarte, E., Pardo, A., Plata, A., Jaramillo, C., Rodríguez, G., Caballero, V., Cardona, A., Montes, C. Gómez-Marulanda, S., Cárdenas-Rozo, A.L., 2020. Unravelling the widening of the earliest Andean northern orogen: Maastrichtian to early Eocene intra-basinal deformation in the northern Eastern Cordillera of Colombia. Basin Research 00, 1–37.

Bayona, G., Montes, C., Cardona, A., Jaramillo, C., Ojeda, G., Valencia, V., Ayala-Calvo, C., 2011. Intraplate subsidence and basin filling adjacent to an oceanic arc–continent collision: A case from the southern Caribbean-South America plate margin: Basin Research 23, 403–422.

Beil, S., Kuhnt, W., Holbourn, A., Scholz, F., Oxmann, J., Wallmann, K., Lorenzen, J., Aquit, M., Chellai, E-H., 2020. Cretaceous oceanic anoxic events prolonged by phosphorus cycle feedbacks. Climate of the Past 16(2), 757-782.

Bermúdez, H.D., Arenillas, I., Arz, J.A., Vajda, V., Renne, P.R., Gilabert, V., Rodríguez, J.V., 2019. The Cretaceous/Paleogene boundary deposits on Gorgonilla Island. In: Gómez, J., Mateus–Zabala, D. (Eds.), The Geology of Colombia, Volume 3 Paleogene – Neogene. Servicio Geológico Colombiano, Publicaciones Geológicas Especiales 37, 19 p.

Berndt, J., Deutsch, A., Schulte, P., Mezge, K., 2011. The Chicxulub ejecta deposit at Demerara Rise (western Atlantic): Dissecting the geochemical anomaly using laser ablation–mass spectrometry. Geology 39 (3), 279-282.

Bowman, V.C., Francis, J.E., Riding, J.B., 2013. Late Cretaceous winter sea ice in Antarctica? Geology 41(12), 1227-1230.

Bralower, T.J., Lorente, M.A., 2003. Paleogeography and stratigraphy of the La Luna Formation and related Cretaceous anoxic depositional systems. Palaios 18(4-5), 301-304.

Bürgl, H., Dummit, Y., 1954, El Cretáceo Superior en la región de Girardot: Boletín Geológico. Instituto Geológico Nacional 2, 23-48.

Calvert, S.E., Pedersen, T.F., 2007. Elemental proxies for palaeoclimatic and palaeoceanographic variability in marine sediments: Interpretation and application. In: Hillaire-Marcel, C., De Vernal, A. (Eds.), Proxies in Late Cenozoic Paleoceanography, Developments in Marine Geology 1, pp. 567-644.

Carvalho, M.R., Jaramillo, C., De La Parra, F., Caballero-Rodríguez, D., Herrera, F., Wing, S., Turner, B.L., D'Apolito, C., Romero-Báez, M., Narváez, P., Martínez, C., Gutierrez, M., Labandeira, C., Bayona, G., Rueda, M., Paez-Reyes, M., Cárdenas, D., Duque, A., Crowley, J.L., Santos, C., Silvestro, D., 2021. Extinction at the end-Cretaceous and the origin of modern Neotropical rainforests. Science 372, 63–68.

Chiarenza, A.A., Farnsworth, A., Mannion, P.D., Lunt, D.J., Valdes, P.J., Morgan, J.V., Allison, P.A., 2020. Asteroid impact, not volcanism, caused the end-Cretaceous dinosaur extinction. PNAS 117 (29), 17084-17093.

Coffin, M.F., Duncan, R.A., Eldholm, O., Fitton, J.G., F.A., Frey, Larsen, H.C., Mahoney, J.J., Saunders, A.D., Schlich, R., Wallace, P.J., 2006. Large igneous provinces and scientific ocean drilling. Status quo and look ahead. Oceanography 19 (4), 150-160.

Coiffard, C., El Atfy, H., Renaudie, J., Bussert, R., Dieter Uhl, D., 2023. The emergence of the tropical rainforest biome in the Cretaceous. Biogeosciences 20, 1145-1154.

Condamine, F.L., Guinot, G., Benton, M.J., Currie, P.J., 2021. Dinosaur biodiversity declined well before the asteroid impact, influenced by ecological and environmental pressures. Nature Communications 12, 3833.

Cooney, P.M., Lorente, M.A., 2009. A structuring event of Campanian age in western Venezuela, interpreted from seismic and paleontological data. Geological Society Special Publications 328, 687-703.

Corentin, P., Pucéat, E., Pellenard, P., Guiraud, M., Blondet, J., Bayon, G., Adatte, T., 2023. Late Cretaceous evolution of chemical weathering at the northeastern South American margin inferred from mineralogy and Hf-Nd isotopes. Marine Geology 455, 106968.

Corentin, P., Pucéat, E., Pellenard, P., Freslan, N., Guiraud, M., Blondet, J., Adatte, T., Bayon, G., 2022. Hafnium-neodymium isotope evidence for enhanced weathering and uplift-climate interactions during the Late Cretaceous. Chemical Geology 591, 120724.

Cramer, B.S., Toggweiler J., Wright, J.D., Katz, M.E., Miller, K.G., 2009. Ocean overturning since the Late Cretaceous: Inferences from a new benthic foraminiferal isotope compilation, Paleoceanography 24 (4), PA4216, doi:10.1029/2008PA001683.

D´Hondt, S., 2005. Consequences of the Cretaceous/Paleogene mass extinction for marine ecosystems. Annu. Rev. Ecol. Evol. Syst. 36, 295-317.

D'Hondt, S., Arthur, M.A., 2002. Deep water in the late Maastrichtian Ocean. Paleoceanography 17, 8-11.

Dameron, S., Leckie, M., Clark, K., Lees, J.A., 2017. Extinction, dissolution, and possible ocean acidification prior to the Cretaceous/Paleogene (K/Pg) boundary in the tropical Pacific. Palaeogeography Palaeoclimatology Palaeoecology, doi: 10.1016/j.palaeo.2017.06.032.

Dameron, S., Leckie, M., MacLeod, K.G., In press. Benthic Foraminiferal Assemblages and Deep-Sea Water Masses: A View from the Maastrichtian of Shatsky Rise, Northwest Pacific. Paleoceanography.

Davis, C., L. Pratt, W. Sliter, L. Mompart, Murat, B., 1999. Factors influencing organic carbon and trace metal accumulation in the Upper Cretaceous La Luna Formation of the western Maracaibo Basin, Venezuela. In Barrera, E., Johnson, C.C. (Eds.), Special Papers Geological Society of America, 332, pp. 203-230.

Davies, A., Kemp, A.E.S., Pike, J., 2009. Late Cretaceous seasonal ocean variability from the Arctic. Nature 460(7252), 254– 258.

De La Parra, F., Jaramillo, C., Kaskes, P., Goderis, S., Claeys, P., Villasante-Marcos, V., Bayona, G., Hatsukawa, Y., Caballero, D., 2022. Unraveling the record of a tropical continental Cretaceous-Paleogene boundary in northern Colombia, South America. Journal of South American Earth Sciences 114, 103717.

Du Vivier, A.D., Selby, D., Sageman, B.B., Jarvis, I., Gröcke, D.R., Voigt, S., 2014. Marine $^{187}Os/^{188}Os$ isotope stratigraphy reveals the interaction of volcanism and ocean circulation during Oceanic Anoxic Event 2, Earth Planet. Sci. Lett. 389, 23-33.

Erbacher, J., Mosher, D.C., Malone, M.J., 2004. Shipboard scientific party. In: Proc. ODP. In. Reports, 207.

Erlich, R.N., Macsotay, O., Nederbragt, A.J., Lorente, M.A., 1999. Palaeoecology, paleogeography and depositional environments of Upper Cretaceous rocks of western Venezuela. Palaeogeography, Palaeoclimatology, Palaeoecology 153 (1-4), 203-238.

Erlich, R.N., Nederbragt, A.J., Lorente, M.A., 2000. Birth and death of the Late Cretaceous "a Luna Sea", and origin of the Tres Esquinas phosphorites. Journal of South American Earth Sciences 13, 21–45.

Föllmi, K.B., Garrison, R.E., RamÍrez, P.C., Zambrano, F., Kennedy W.J., Lehner, B.L., 1992. Cyclic phosphate-rich successions in the upper Cretaceous of Colombia: Palaeogeography, Palaeoecology, Palaeoclimtology 93,151-182.

Font, E., Chen, J., Regelous, M., Adatte, T., 2021, Volcanic origin of the mercury anomalies at the Cretaceous-Paleogene transition of Bidart, France. Geology, https://doi.org/10.1130/G49458.1.

Frank, T.D., Thomas, D.J., Leckie, R.M., Arthur, M.A., Bown, P.R., Jones, K., Lees, J.A., 2005. The Maastrichtian record from Shatsky Rise (northwest Pacific): A tropical perspective on global ecological and oceanographic changes. Paleoceanography 20(1), PA1008. https://doi.org/10.1029/2004pa001052.

Friedrich, O., Erbacher, J., 2006. Benthic foraminiferal assemblages from Demerara Rise (ODP Leg 207, western tropical Atlantic): Possible evidence for a progressive opening of the Equatorial Atlantic Gateway. Cretaceous Research, 27, 377–397.

Friedrich, O., Hemleben, C., 2007. Early Maastrichtian benthic foraminiferal assemblages from the western North Atlantic (Blake Nose) and their relation to paleoenvironmental changes. Marine Micropaleontology, 62(1), 31–44.

Friedrich, O., Herrle, J.O., Kößler, P., Hemleben, C., 2004. Early Maastrichtian stable isotopes: Changing deep water sources in the North Atlantic? Palaeogeogr. Palaeoclimatol. Palaeoecol. 211, 171-184.

Friedrich, O., Herrle, J.O., Wilson, P.A., Cooper, M.J., Erbacher, J., Hemleben, C., 2009. The early Maastrichtian carbon cycle perturbation and cooling event: Implications from the South Atlantic Ocean. Paleoceanography 24, PA2211. doi:10.1029/2008PA001654.

Friedrich, O., Norris, R.D., Erbacher, J., 2012. Evolution of middle to Late Cretaceous oceans – A 55 m.y. record of Earth's temperature and carbon cycle, Geology, 40, 107-110.

García-Reyes, A., Dyment, J., 2021. Structure, age, and origin of the Caribbean Plate unraveled. Earth and Planetary Science Letters, 2021, 571, pp.117100. ff10.1016/j.epsl.2021.117100ff. ffhal-03452889f.

Garzón, S., Warny, S., Bart, P.J., 2012. A palynological and sequence-stratigraphic study of Santonian–Maastrichtian strata from the Upper Magdalena Valley basin in central Colombia. Palynology 36, 112-133.

Goderis, S., Sat, H., Ferriere, I., Schmitz, B., Burney, D., Kaskes, P., Vellekoop, J., Wittmann, A., Schultz, T., Chernonozhkin, S., Claeys, P., de Graff, S., Déhais, T., de Winter, N., Elfman, M., Feignon, J., Ishikawa, A., Koeberl, C., Kristiansson, P., Neal, C., Owens, J., Schmieder, M., Sinnesael, M., Vanhaecke, F., Van Malderen, S., Bralower, T., Gulick, S., Kring, D., Lowery, C., Morgan, J., Smit, J., Whalen, M., IODP-ICDP Expedition 364 Scientists, 2021. Globally distributed iridium layer preserved within the Chicxulub impact structure. Science Advances 7, eabe3647.

Gu, X., Zhang, L., Runsheng Yin, R., Grasby, S.E., Yao, H., Tan, J., Wang, C., 2022. Deccan volcanic activity and its links to the end-Cretaceous extinction in northern China. Global and Planetary Change 210, 103772.

Guerrero, J., Sarmiento, G., Navarrete, R.E., 2000. The Stratigraphy of the W side of the Cretaceous Colombian basin in the Upper Magdalena Valley. Reevaluation of selected areas and type localities including Aipe, Guaduas, Ortega, and Piedras. Geología Colombiana 25, 45-110.

Haq B.U., 2014. Cretaceous eustasy revisited. Global and Planetary Change 113, 44–58.

He S., Kyser T.K., Caldwell W.G.E. 2005. Paleoenvironment of the Western Interior Seaway inferred from $\delta^{18}O$ and $\delta^{13}C$ values of mollusks from the Cretaceous Bearpaw marine cyclothem. Palaeogeography, Palaeoclimatology, Palaeoecology 217(1–2), 67–85.

Henehan, M.J., Ridgwell, A., Thomas, E., Zhang, S., Alegret, L., Schmidt, D.N., Rae, J.W.B., Witts, J.D., Landman, N.H., Greene, S.E., Huber, B.T., Super, J.R., Planavsky, N.J., Hull, P.M., 2019. Rapid ocean acidification and protracted Earth system recovery followed the end-Cretaceous Chicxulub impact. PNAS 116 (4), 22500–22504.

Horton, B.K., 2018. Tectonic regimes of the central and southern Andes: Responses to variations in plate coupling during subduction. Tectonics 37, 402–429.

Huber, B., 2020. Cretaceous climate. Encyclopedia of Geology, 2nd edition https://doi.org/10.1016/B978-0-12-409548-9.12068-8.

Huber, B.T., MacLeod, K.G., Watkins, D.K., Coffind, M.L., 2018. The rise and fall of the Cretaceous Hot Greenhouse climate. Global and Planetary Change 167, 1-23.

Hull, P.M., Bornemann, A., Penman, D.E., Henehan, M.J., Norris, R.D., Wilson, P.A., Blum, P., Alegret, L., Batenburg, S.J., Bown, P.R., Bralower, T.J., Cournede, C., Deutsch, A., Donner, B., Friedrich, O., Jehle, S., Kim, H., Kroon, D., Lippert, P.C., Dominik Loroch, D., Moebius, I., Moriya, K., Peppe, D.J., Ravizza, G.E., Röhl, U., Schueth, J., Sepúlveda, J., Sexton, P.F., Sibert, E.C., Śliwińska, K.K., Summons, R.E., Thomas, E., Westerhold, T., Whiteside, J.H., Tatsuhiko Yamaguchi, T., Zachos, J.C., 2020. On impact and volcanism across the Cretaceous-Paleogene boundary. Science 367, 266–272.

Jenkyns, H.C., 2010, Geochemistry of oceanic anoxic events, Geochem. Geophys. Geosyst. 11 (3), 1-30.

Johnson, C.C., 2002. The Rise and Fall of Rudist Reefs. American Scientist 90(2), 148-153.

Jones, M.M., Sageman, B.B., Oakes, R.L., Parker, A.L., Leckie, R.M., Bralower, T.J., Sepúlveda, J., Fortiz V., 2019. Astronomical pacing of relative sea level during Oceanic Anoxic Event 2: Preliminary studies of the expanded SH# 1 Core, Utah, USA, GSA Bulletin 131(9-10), 1702-1722.

Juliao-Lemos, T., Carvalho, M., Torres, D., Plata, A., Parra, C., 2016. Paleoenvironmental reconstruction based on palynofacies analyses of the Cansona Formation (Late Cretaceous), Sinú-San Jacinto Basin, northwest Colombia. Journal of South American Earth Sciences 69, 103-118.

Jung, C., Koch, M.C., Voigt, S., Friedrich, O., 2013. Campanian-Maastrichtian ocean circulation in the tropical Pacific. Paleoceanography 28, doi:10.1002/palo.20051.

Keller, G., Mateo, P., Monkenbusch, J., Thibault, N., Punekar, J., Spangenberg, J.E., Abramovich, S., Ashckenazi-Polivoda, S., Schoene, B., Eddy, M.P., Samperton, K.M., Khadri, S.F.R., Adatte, T., 2020, Mercury linked to Deccan Traps volcanism, climate change and the end Cretaceous mass extinction. Global and Planetary Change 194, 103312.

Koch, M.C., Friedrich, O., 2012. Campanian-Maastrichtian intermediate- to deep-water changes in the high latitudes: Benthic foraminiferal evidence. Paleoceanography, 27(2), PA2209.

Koutsoukos, E.A.M., 1992. Late Aptian to Maastrichtian foraminiferal biogeography and palaeoceanography of the Sergipe Basin, Brazil. Palaeogeography, Palaeoclimatology, Palaeoecology 92 (3-4), 295-324.

Koutsoukos, E.A.M., 2006. The Cretaceous-Paleogene Boundary at the Poty Section, NE Brazil: Foraminiferal Record and Sequence of Events - A Review. Anuário do Instituto de Geociências - UFRJ 29 (1), 95-107.

Koutsoukos, E.A.M., Merrick, K.A., 1986. Foraminiferal paleoenvironments from the Barremian to Maastrichtian of Trinidad, West Indies. I Geological Conference of the Geological Society of Trinidad & Tobago, pp. 85-101.

Ladant J-B., Donnadieu, Y., 2016. Palaeogeographic regulation of glacial events during the Cretaceous supergreenhouse. Nature Communications 7, 12771.

Ladant, J-B., Poulsen, C.J., Fluteau, F., Tabor, C.R., MacLeod, K.J., Martin, E.L., Haynes, S.J., Rostami, M.A., 2020. Paleogeographic controls on the evolution of Late Cretaceous ocean circulation. Climate of the Past, doi.org/10.5194/cp-2019-157.

Li, X., Li, Y., Wang, J., Zhang, C., Wang, Y., Liu, L., 2019. Temporospatial variation in the late Mesozoic volcanism in southeast China, Solid Earth 10, 2089-2101.

Linnert, C., Engelke, J., Wilmsen, M., Mutterlose, J., 2016. The impact of the Maastrichtian cooling on the marine nutrient regime—Evidence from mid latitudinal calcareous nannofossils. Paleoceanography, 31, 694–714, doi:10.1002/2015PA002916.

Linnert, C., Engelke, J., Wilmsen, M., Mutterlose, J., 2019. Environmental footprints of the early Maastrichtian cooling – the record of benthic foraminifera from northern Germany. Cretaceous Research 97, 143-159.

Louvel, V., Galbrun, B., 2000. Magnetic polarity sequences from downhole measurements in ODP holes 998B and 1001A, leg 165, Caribbean Sea. Marine Geophysical Researches 21, 561-577.

Lowery, C.M., Leckie, M., Bryant, R., Elderbak, K., Parker, A., Polyak, D.E., Schmidt, M., Snoeyenbos-West, O., Sterzinar, E., 2018. The Late Cretaceous Western Interior Seaway as a model for oxygenation change in epicontinental restricted basins, Earth-Sci. Rev. 177, 545-564.

Macellari, C., 1988. Cretaceous paleogeography and depositional cycles of western South America. Journal of South American Earth Sciences 1(4), 373-418.

Machado, M.C., Chemale Jr. F., Kawashita, K., Rey, O., Moura, C.A.V., 2016. Isotope studies of carbonate rocks of La Luna Formation (Venezuela) to constrain the oceanic anoxic event 3 (OAE3). Journal of South American Earth Sciences 72, 38-48.

MacLeod, K.G., Huber, B.T., Berrocoso, Á.J., Wendler, I., 2013. A stable and hot Turonian without glacial δ18O excursions is indicated by exquisitely preserved Tanzanian foraminifera. Geology 41(10), 1083-1086.

MacLeod, K. G., Londoño, C. I., Martin, E. E., Jiménez Berrocoso, Á., Basak, C., 2011. Changes in North Atlantic circulation at the end of the Cretaceous greenhouse interval. Nature Geoscience 4, 779–782.

MacLeod, K.G., Whitney, D.L., Huber, B.T., Koeberl, K., 2017. Impact and extinction in remarkably complete Cretaceous-Tertiary boundary sections from Demerara Rise, tropical western North Atlantic. GSA Bulletin 119 (1-2), 101-115.

Mann, P., Escalona, A., Castillo, M.V., 2006. Regional geologic and tectonic setting of the Maracaibo supergiant basin, western Venezuela. AAPG Bulletin 90(4), 445-477.

Martin, E. E., MacLeod, K. G., Jiménez Berrocoso, Á., Bourbon, E., 2012. Water mass circulation on Demerara Rise during the Late Cretaceous based on Nd isotopes. Earth and Planetary Science Letters 327, 111–120.

Martínez, R. J.I., 1989. Foraminiferal biostratigraphy and paleoenvironments of the Maastrichtian Colón mudstones of Northern South America. Micropaleontology 35 (2), 97-113.

Martínez, J.I., 2003. The Paleoecology of late Cretaceous upwelling events from the Upper Magdalena Basin, Colombia. Palaios 18 (4-5), 305-320.

Martinez, J.I., Hernandez, R., 1992. Evolution and drowning of the Late Cretaceous Venezuelan carbonate platform. Journal of South American Earth Sciences 5(2), 197-210.

Mateo, P., Keller, G., Punekar, J., Spangenberg et al., 2007. Early to Late Maastrichtian environmental changes in the Indian Ocean compared with Tethys and South Atlantic. Palaeogeography, Palaeoclimatology, Palaeoecology 478, 121-138.

Mittelbach, G.G., Schemske, D.W., Cornell, H.V., Allen, A.P., Brown, J.M., Bush, M.B., Harrison, S.P., Hurlbert, A.H., Knowlton, N., Lessios, H.A., McCain, C.M., McCune, A.R., McDade, L.A., McPeek, M.A., Near, T.J., Price, T.D., Ricklefs, R.E., Roy, K., Sax, D.F., Schluter, D., Sobel, J.M., Turelli, M., 2007.

Evolution and the latitudinal diversity gradient: Speciation, extinction and biogeography. Ecology Letters 10, 315-331.

Montenegro, G., Barragán, M., 2011. Caguán and Putumayo basins. In: Cediel, F., Colmenares, F. (Eds.). Petroleum Geology of Colombia. Volume 4. ANH-Fondo Editorial Universidad EAFIT.

Mora, A., Garcia, A., 2006. Cenozoic tectono-stratigraphic relationships between the Cesar sub-basin and the southeastern Lower Magdalena Valley basin of northern Colombia: AAPG, search and discovery article, 30046. Search and Discovery 30046, 1–11.

Mulitza, S., Prange, M., Stuut, J.B., Zabel, M., von Dobeneck, T., Itambi, A.C., Nizou, J., Schulz, M., Wefer, G., 2008. Sahel megadroughts triggered by glacial slowdowns of Atlantic meridional overturning. Paleoceanography 23, PA4206.

Navarrete, R.E., Parra, F.J., Pérez-Panera, J.P., Daza, D., Sánchez, C., Prince, M., Rodríguez, M., 2018. Turonian-Campanian foraminifera zonation for the La Luna and lower Umir formations, Middle Magdalena Valley Basin, northern Colombia. In: Cusminski et al. (Eds.) Advances in South American Micropaleontology - Selected papers of the 11th Argentine Paleontological Congress. Springer Earth System Science Series, pp. 67-114.

O'Brien, C.L., Robinson, S.A., Pancost, R.D., Sinningeh Damsté, J.S., Schoulten, S., Lunt, D.J., Alsenz, H., Bornemann, A., Bottini, C., Brassell, S.C., Farnsworth, A., Forster, A., Huber, B.T., Inglis, G.N., Jenkyns, H.C., Linnert, C., Littler, K., Markwick, P., McAnena, A., Mutterlose, J., Naafs, B.D.A., Püttmann, W., Sluis, A., van Helmond, N.A.G.M., Vellekoop, J., Wagner, T., Wrobel, N.E., 2017. Cretaceous sea-surface temperature evolution: Constraints from TEX86 and planktonic foraminiferal oxygen isotopes. Earth-Science Reviews 172, 224–247.

Páez-Reyes, M., Carvajal-Ortiz, H., Sahoo, S.K., Varol, O., Miller, V.B., Hughes, G.W., Gaona-Narváez, T., Patarroyo, G.D., Curtis, J.H., Lerma, I., Copeland, P. 2021. Assessing the contribution of the La Luna Sea to the global sink of organic carbon during the Cenomanian-Turonian Oceanic Anoxic Event 2 (OAE2). Global and Planetary Change 199, 103424.

Patarroyo, G.D., Torres, G.A., Rincón, D.A., Cárdenas, C.P., Márquez, R.E., 2017. Bioestratigrafía e inferencias paleoambientales de las asociaciones de foraminíferos en las formaciones cretácicas La Luna-Colón (Cuenca del Catatumbo, Colombia). Boletín de Geología 39 (3), 25-40.

Pedraza, P., Ramírez, Y., 2011. Catatumbo Basin. In: Cediel, F., Colmenares, F. (Eds.), Petroleum Geology of Colombia. Volume 5. ANH-Fondo Editorial Universidad EAFIT.

Percival, L.M.E., Jenkyns, H.C., Mather, T.A., Dickson, A.J., Batenburg, S.J., Ruhl, M., Hesselbo, S.P., Barclay, R., Jarvis, I., Robinson, S.A., Woelders, L., 2018. Does large igneous province volcanism always perturb the mercury cycle? Comparing the records of Oceanic Anoxic Event 2 and the End-Cretaceous to other Mesozoic events. American Journal of Science 318, 799-860.

Petters, V., 1955. Development of Upper Cretaceous foraminiferal faunas in Colombia. Journal of Paleontology 29 (2), 212-225.

Pindell, J., Kennan, L., Maresch, W.V., Stanek, K., Draper, G., Higgs, R., 2005. Plate kinematics and crustal dynamics of circum Caribbean arc continent interactions: Tectonic controls on basin development in proto-Caribbean margins. Special Papper Geological Society of America 394, 7-52.

Pindell, J.L., Tabbutt, K.D., 1995. Mesozoic-Cenozoic Andean paleogeography and regional controls on hydrocarbon systems. In In: Tankard, A.J., Suárez-Soruco, R., Welsink, H.J. (Eds.), Petroleum basins of South America: AAPG Memoir 62, pp. 101-128.

Pucéat, E., Lécuyer, C., Reisberg, L., 2005. Neodymium isotope evolution of NW Tethyan upper ocean waters throughout the Cretaceous. Earth and Planetary Science Letters 236, 705-720.

Sarmiento-Rojas, L.F., 2019. Cretaceous stratigraphy and paleo-facies maps of northwestern South America. In: Cediel, F., Shaw, R.P., (Eds.), Geology and Tectonics of Northwestern South America. The Pacific Caribbean Andean Junction, pp. 673-747.

Schlanger, S.O., Jenkyns, H., 1976. Cretaceous oceanic anoxic events: causes and consequences, Netherlands Journal of Geosciences/Geologie en Mijnbouw 55(3-4), 179-184.

Schröder-Adams, C.J., Herrle, J.O., Selby, D., Quesnel, A., Froude, G., 2019. Influence of the High Arctic Igneous Province on the Cenomanian/Turonian boundary interval, Sverdrup Basin, High Canadian Arctic, Earth Planet. Sci. Lett. 511, 76-88.

Schoene, B., Eddy, M.P., Samperton, K.M., Keller, C.B., Keller, G., Adatte, T., Khadri, S.F., 2019. U-Pb constraints on pulsed eruption of the Deccan Traps across the end-Cretaceous mass extinction. Science 363, 862-866.

Schulte, P., Alegret, L., Arenillas, I., Arz, J.A., Barton, P.J., Bown, P.R., Bralower, T.J., Christeson, G.L., Claeys, P., Cockell, C.S., Collins, G.S., Deutsch, A., Goldin, T.J., Goto, K., Grajales-Nishimura, J.M., Grieve, R.A.F., Gulick, S.P.S., Johnson, K.R., Kiessling. W., Koeberl, C., Kring, D.A., Macleod, K.G., Matsui, T., Melosh, J., Montanari, A., Morgan, J.V., Neal, C.R., Nichols, D.J., Norris, R.D., Pierazzo, E., Ravizza, G., Rebolledo-Vieyra, M., Reimold, W.U., Robin, E., Salge, T., Speijer, R.P., Sweet, A.R., Urrutia-

Fucugauchi, J., Vajda, V., Whalen, M.T., Willumsen, P.S., 2010. The Chicxulub asteroid impact and mass extinction at the Cretaceous-Paleogene boundary. Science 327, 5970.

Schulte, P., Deutsch, A., Salge, T., Berndt, J., A. Kontny, A., MacLeod, K.G., Neuser, R.D., S. Krum, S., 2009. A dual-layer Chicxulub ejecta sequence with shocked carbonates from the Cretaceous–Paleogene (K–Pg) boundary, Demerara Rise, western Atlantic. Geochimica et Cosmochimica Acta 73 (4), 1180-1204.

Scotese, C., 2016. PALEOMAP PaleoAtlas for GPlates and the PaleoData Plotter Program, PALEOMAP Project (http://www.earthbyte.org/paleomap-paleoatlas-for-gplates/).

Sial, A.N., Chen, J.B., Lacerda, L.D., Peralta, S., Gaucher, C., Frei, R., Cirilli, S., Ferreira, V.P., Marquillas, R.A., Barbosa, J.A., Pereira, N.S., Belmino, I.K.C., 2014. High-resolution Hg chemostratigraphy: A contribution to the distinction of chemical fingerprints of the Deccan volcanism and Cretaceous-Paleogene boundary impact event. Palaeogeography, Palaeoclimatology, Palaeoecology 414, 98-115.

Sial, A.N., Chen, J.B., Lacerda, L.D., Frei, R., Tewari, V.C., Pandit, M.K., Gaucher, C., Ferreira, V.P., Cirilli, S., Peralta, S., Korte, C., Barbosa, J.A., Pereira, N.S., 2016. Mercury enrichment and Hg isotopes in Cretaceous-Paleogene boundary successions: Links to volcanism and palaeoenvironmental impacts. Cretaceous Research 66, 60-81.

Sigurdsson, H., Kelley, S., Leckie, R.M., Carey, S., Bralower, T., King, J., 2000. History of Circum-Caribbean explosive volcanism: 40Ar/ 39Ar dating of tephra layers. In: Leckie, R.M., Sigurdsson, H., Acton, G.D., and Draper, G. (Eds.), 2000. Proc. ODP, Sci. Results, 165: College Station, TX (Ocean Drilling Program).

Sigurdsson, H., Leckie, R.M., Acton, G.D., et al., 1997. Proc. ODP, Init. Repts., 165: College Station, TX (Ocean Drilling Program).

Soudry, D., Glenn, C.R., Nathan, Y., Segal, I., VonderHaar, D.L., 2006. Evolution of Tethyan phosphogenesis along the northern edges of the Arabian-African shield during the Cretaceous-Eocene as deduced from temporal variations of Ca and Nd isotopes and rates of P accumulation. Earth-Science Reviews 78, 27-57.

Sprain, G.A., Renne, P.R., Vanderkluysen, L., Pande, K., Self, S., Mittal, T., 2019. The eruptive tempo of Deccan volcanism in relation to the Cretaceous-Paleogene boundary. Science 363, 866-870.

Stinnesbeck, W. Ifrim, C. Salazar, C. 2012. The last Cretaceous ammonites in Latin America. Acta Palaeontologica Polonica 57, 717-728.

Stuut, J.B., Zabel, M., Ratmeyer, V., Helmke, P., Schefuß, E., Lavik, G., Schneider, R., 2005. Provenance of present-day eolian dust collected off NW Africa. Journal of Geophysical Research 110, D04202, doi:10.1029/2004JD005161.

Suganuma, Y., Ogg, J.G., 2006. Campanian through Eocene magnetostratigraphy of Sites 1257–1261, ODP Leg 207, Demerara Rise (western equatorial Atlantic). In Mosher, D.C., Erbacher, J., and Malone, M.J. (Eds.), Proc. ODP, Sci. Results, 207.

Takashima, R., Nishi, H., Ruciy L.E., Dercourt, J., Guiraud, R., 2015. Greenhouse world and the Mesozoic ocean. Oceanography 19 (4), 82-92.

Talukdar, S., Marcano, F., 1994. Petroleum System of the Maracaibo Basin, Venezuela. In: Magoon, L.B., Dow W.G. (Eds.), The petroleum system-from source to trap, pp. 463-481. AAPG Memoir, 60.

Tchegliakova, N., 1996. Registro de las biozonas de foraminíferos planctónicos Gansserina gansseri y Abathomphalus mayaroensis (Maastrichtiano medio y superior) en el extremo meridional del Valle Medio del Magdalena (Colombia, Suramérica). Geología Colombiana 20, 67-90.

Tchegliakova, N., Mojica, J., 2001. El Senoniano de la barrera de Girardot-Guataquí, Valle Alto del Magdalena, Colombia: Precisiones sobre la estratigrafía y establecimiento de una zonación micropaleontológica. Rev. Acad. Col. Cienc. Ex., Fís. Nat. 25 (94), 37-75.

Terraza, R., 2019. 'Formación La Luna': expresión espuria en la geología colombiana. En: Etayo-Serna, F. (Ed.). Estudios geológicos y paleontológicos sobre el Cretácico en la región del embalse del río Sogamoso, Valle Medio del Magdalena, pp. 305-362. Servicio Geológico Colombiano.

Thibault, N., Gardin, S., 2007. The late Maastrichtian nannofossil record of climate change in the South Atlantic DSDP Hole 525A. Marine Micropaleontology, 65, 163–184.

Tschanz, C.M., Marvin R.F., Cruz, J., Menhert, H.H., Cebula, G.T., 1974, Geologic evolution of the Sierra Nevada de Santa Marta, northeastern Colombia: GSA Bulletin 85, 273–284.

Vancoppenolle I., Vellekoop J., Doubrawa M., Kaskes P., Sinnesael M., Jagt J.W.M., Claeys P, Speijer R.P., 2022. The benthic foraminiferal response to the mid Maastrichtian event in the NW-European chalk sea of the Maastrichtian type area. Netherlands Journal of Geosciences 101, e12. https://doi.org/10.1017/njg.2022.10.

Vellekoop, J., Kaskes, P., Sinnesael, M., Huygh, J., Déhais, T., Jagt, J.W.M., Speijer, R.P., Claeys, P., 2022. A new age model and chemostratigraphic framework for the Maastrichtian type area (southeastern Netherlands, northeastern Belgium). Newsletters on Stratigraphy 4, 479-501.

Vergara, L.S., 1997. Stratigraphy, foraminiferal assemblages and paleoenvironments in the Late Cretaceous of the Upper Magdalena Valley, Colombia (Part I), Journal of South American Earth Sciences 10 (2), 111-132.

Villamil, T., Arango, C., Hay W.W., 1999. Plate tectonic paleoceanographic hypothesis for Cretaceous source rocks and cherts of northern South America. In: Barrera, E., Johnson, C.C. (Eds.), pp. 191-202. Special papers-Geological Society of America, 332.

Villamil, T., Pindell, J., 1998. Mesozoic paleogeographic evolution of northern South America. In: J. Pindell, J., Drake, C. (Eds.) Paleogeographic evolution and non-glacial eustacy, northern South America. SEPM Society for Sedimentary Geology 58, pp. 238-318.

Voigt, S., Friedrich, O., Norris, R. D., Schönfeld, J., 2010. Campanian–Maastrichtian carbon isotope stratigraphy: shelf-ocean correlation between the European shelf sea and the tropical Pacific Ocean. Newsletters on Stratigraphy 44(1), 57-72.

Voigt, S., Gale, A.S., Jung, C., Jenkyns, H.C., 2012. Global correlation of Upper Campanian-Maastrichtian successions using carbon-isotope stratigraphy: development of a new Maastrichtian timescale. Newsletters on Stratigraphy 45(1), 25-53.

Voigt, S., Jung, C., Friedrich, O., Frank, M., Teschner, C., Hoffmann, J., 2013. Tectonically restricted deep ocean circulation at the end of the Cretaceous greenhouse. Earth and Planetary Science Letters 369-370, 169-177.

Wilson, P.A., Norris, R.D., 2001. Warm tropical ocean surface and global anoxia during the mid-Cretaceous period. Nature 412(6845), 425– 429.

Earth, stream and tree encircled by sea

Waves sweep the sand from my island

My sunsets fade

Field and glade wait only for rain

Grain after grain love erodes my

High weathered walls which fend off the tide

Cradle the wind

To my island

Islands

King Crimson

CHAPTER 1

PALEOENVIRONMENTAL CHANGES RECORDED AT A LATE MAASTRICHTIAN MARINE SUCCESSION OF NORTHERN SOUTH AMERICA

Contribution roles taxonomy

German David Patarroyo (itt Oceaneon, Unisinos University). Micropaleontological and geochemical preparation. Foraminiferal taxonomy and geochemical analyses. Integration and discussion of results.

Karlos Kochhann (itt Oceaneon, Unisinos University). Foraminiferal, geochemical and paleoecological discussions.

Daiane Ceolin (itt Oceaneon, Unisinos University). Ostracod taxonomy and ecology.

Rodrigo M. Guerra (itt Oceaneon, Unisinos University). Calcareous nannofossils taxonomy and ecology.

Laia Alegret (Zaragoza University). Benthic foraminiferal ecology and taxonomic comments. Paleoecological discussions.

Marlone H.H. Bom (itt Oceaneon, Unisinos University). X-ray fluorescence methodological support and comments about geochemical proxies.

Article published at: Journal of South American Earth Sciences Volume 119, November 2022, 104015. Special Issue "Stratigraphy and Micropaleontology of Caribbean Basins"

https://doi.org/10.1016/j.jsames.2022.104015

Received 19 May 2022, Revised 16 August 2022, Accepted 25 August 2022, Available online 30 August 2022, Version of Record 15 September 2022.

Journal of South American Earth Sciences 119 (2022) 104015

Contents lists available at ScienceDirect

Journal of South American Earth Sciences

journal homepage: www.elsevier.com/locate/jsames

Paleoenvironmental changes recorded at a late Maastrichtian marine succession of northern South America

German D. Patarroyo[a,b,*], Karlos G.D. Kochhann[a,b], Daiane Ceolin[a], Rodrigo M. Guerra[a,c], Laia Alegret[d], Marlone H.H. Bom[a,b]

[a] Technological Institute for Paleoceanography and Climate Change (itt Oceaneon), UNISINOS University, São Leopoldo, 93.022–750, Brazil
[b] Geology Graduate Program. UNISINOS University, São Leopoldo, 93.022-750, Brazil
[c] Museu Itinerante de Ciências Naturais, Carlos Barbosa, 95.185-000, Brazil
[d] Dept. Ciencias de La Tierra, Universidad de Zaragoza, Zaragoza, Spain

A B S T R A C T

One of the major environmental and biotic turnovers of the Phanerozoic occurred at the Cretaceous-Paleogene (K-Pg) boundary, being the focus of countless scientific studies that addressed the timing, causes and consequences of this global event. Paleoenvironmental conditions that preceded the K-Pg boundary, however, have been less studied, especially at low latitudes. In order to help reconstructing late Maastrichtian marine environments along the equatorial South American margin, we apply micropaleontological and geochemical techniques to a stratigraphic core that recovered the Colón Formation in northern Colombia. Low abundance foraminiferal assemblages were overall dominated by benthic taxa (Maastrichtian local biozones *Siphogenerinoides bramletti* and *Ammobaculites colombiana*), and the planktonic species *Guembelitria cretacea*. Ostracod assemblages were mainly composed of the genera *Veenia*, *Cytherella*, *Paracypris*, and *Cythereis*. Calcareous nannofossils were typical of Upper Cretaceous low-latitude successions, with low abundance and diversity assemblages dominated by *Micula staurophora*, *Kamptnerius magnificus* and *Cervisiella operculata*. Sediment elemental ratios (Zr/Rb, Fe/Ca and Sr/Ba), as well foraminiferal, ostracod and nannofossils assemblages, indicate a shallowing upward trend, characterized by a transition from inner platform settings to sublittoral conditions. Input of terrigenous sediments and weathering intensity also increased upward in the section, probably related to the uplift pulses of the Andean orogeny. Proportions of benthic infauna, as well the V/Cr ratio and the distribution of redox-sensitive trace metals (Ni, Cu) along the core, mostly indicate suboxic bottom water conditions in the Colón Formation.

1. Introduction

Upper Cretaceous strata worldwide have been analyzed by countless studies addressing the mass extinction at the Cretaceous-Paleogene (K-Pg) boundary. The K-Pg mass extinction is attributed to a and asteroid impact at the Chicxulub impact site (Yucatán Peninsula, Mexico), evidenced by several features such as iridium anomalies, microspherules, among others (Alvarez et al., 1980; Simonson and Glass, 2004; Schulte et al., 2010; Goderis et al., 2021). This event triggered major environmental perturbations, causing significant ecosystem turnovers and widespread extinctions in terrestrial and marine ecosystems (e.g. D'Hondt, 2005; Schulte et al., 2010; Dameron et al., 2017; Chiarenza et al., 2020; Carvalho et al., 2021).

Though the mechanisms and possible causes of the K-Pg mass extinction are still a matter of discussion (Alvarez et al., 1980; Alegret et al., 2001; Punekar et al., 2014; Richards et al., 2015; Petersen et al., 2016; Schoene et al., 2019; Sprain et al., 2019; Chiarenza et al., 2020; Hull et al., 2020; Keller et al., 2020), there is a broad consensus that drastic biological, oceanic and climatic changes occurred at the K-Pg boundary (e.g. Culver, 2003; D'Hondt, 2005; Koutsoukos, 2006; Keller and Abramovich, 2009; Dameron et al., 2017; Guerra et al., 2021; Carvalho et al., 2021; Krahl et al., 2021). Even since the Campanian-Maastrichtian interval, major paleoenvironmental disturbances occurred (e.g. Abramovich et al., 2010; Thibault and Husson, 2016; O'Brien et al., 2017; Huber et al., 2018; Ladant et al., 2020). For instance, high resolution studies of deep-sea sites from the Atlantic and Southern oceans, and of the Maastrichtian type area (Netherlands), reconstructed perturbations of the global carbon cycle during the late Campanian and the mid-Maastrichtian (Voigt et al., 2012; Linnert et al., 2019; Vancoppenolle et al., 2022; Vellekoop et al., 2022). Moreover, foraminiferal assemblages and stable isotope analyses indicate steady global temperature decline during the Campanian-Maastrichtian interval, which likely promoted a gradual intensification of deep-water circulation in the Atlantic Ocean (MacLeod and Huber, 1996; Barrera et al., 1997; D' Hondt and Arthur, 2002; Friedrich et al., 2004; Cramer et al., 2009; Abramovich et al., 2010; Jung et al., 2013; Linnert et al., 2014;

* Corresponding author. Technological Institute for Paleoceanography and Climate Change (itt Oceaneon), UNISINOS University, São Leopoldo, 93.022–750, Brazil.

E-mail address: germanp@edu.unisinos.br (G.D. Patarroyo).

https://doi.org/10.1016/j.jsames.2022.104015
Received 19 May 2022; Received in revised form 16 August 2022; Accepted 25 August 2022
Available online 30 August 2022

Batenburg et al., 2018; Huber et al., 2018; Ladant et al., 2020).

However, these paleoenvironmental reorganizations that preceded the K-Pg boundary have not been yet explored in detail for tropical marine settings. So far, studies on latest Cretaceous records in areas such as northern South America have focused on the identification of the K-Pg boundary, and on how some selected biological groups (planktonic foraminifers, palynomorphs) responded across this transition (Sarmiento, 1994; Yepes, 2001; Koutsoukos, 2006; MacLeod et al., 2017; Gertsch et al., 2013; Bermúdez et al., 2019; Carvalho et al., 2021; De La Parra et al., 2022). Most of the Upper Cretaceous sedimentary successions of northern South America were deposited in extensive epicontinental seas, which gradually disappeared due to sea level fluctuations, and the onset of the Andean orogeny since the Campanian-Maastrichtian (Martinez and Hernandez, 1992; Villamil and Pindell, 1998; Erlich et al., 1999; Cooney and Lorente, 2009; Bayona, 2018; Sarmiento-Rojas, 2019; Montes et al., 2019; Bayona et al., 2020). Therefore, marine environments underwent significant shifts during the Campanian-Maastrichtian interval, not only of their depositional settings (retrogradational stacking and erosional episodes), but also of their associated ecosystems. Considering that Campanian-Maastrichtian sedimentary successions have a wide geographic distribution in Ecuador, Colombia and Venezuela, some studies have explored their geological evolution, mostly based on sedimentological and tectonic approaches (Veloza et al., 2008; Ayala-Calvo et al., 2009; Bayona et al., 2011, 2020; Montaño et al., 2016; Valencia-Gómez et al., 2020; Gramal-Aguilar et al., 2021). Previous paleontological studies, however, have shown that Maastrichtian marine microfossils were still relatively abundant and diverse, providing an opportunity to be used as paleoenvironmental proxies and chronostratigraphic markers (Bürgl and Dumit, 1954; Petters, 1955; Martínez, 1989; Tchegliakova, 1996; Vergara, 1997; Guerrero et al., 2000; Yepes, 2001; Tchegliakova and Mojica, 2001; Garzón et al., 2012; Juliao-Lemos et al., 2016; Patarroyo et al., 2017; Navarrete et al., 2018; Carvalho et al., 2021; De La Parra et al., 2022). In addition, Upper Cretaceous successions of northern South America were not yet studied with geochemical approaches, which are crucial to understand how tropical climates evolved during this time interval.

Here we provide an integrated micropaleontological (foraminifers, ostracods, and calcareous nannofossils) and geochemical (sediments elemental ratios derived by X-ray fluorescence) study for a stratigraphic core that recovered the Colón Formation (Maastrichtian) in northern Colombia. Our main goals are: (1) to build on the previously proposed tectono-sedimentary models for the uppermost Cretaceous successions of the region, and (2) to provide paleoenvironmental interpretations for those dynamic shallow marine settings. This integrated approach has been explored in regions with a similar geological evolution in South America such as in the Neuquén basin (Argentina; Guerra et al., 2021).

1.1. Study area and geological setting

The Cesar-Rancheria Basin (northeast Colombia) represents part of the tectonic domain of the Maracaibo Sub-Plate, conforming an asymmetric elongated depression with a N30°E orientation, and an area of 11.630 km^2 (Fig. 1). The geological evolution of the basin can be traced in four tectonic phases: 1) an extensional regime from the late Paleozoic (Carboniferous?) until the early Cretaceous (probably before the Aptian), which allowed deposition of volcanoclastic rocks (La Quinta and Rio Negro formations); 2) deposition of clastic and carbonate successions on a passive margin during most of the Cretaceous (Cogollo Group, La Luna Formation); 3) development of a foreland basin during the late Maastrichtian-Paleocene (Colón, Catatumbo/Barco and Cuervos formations); 4) infilling of the basin by alluvial and fluvial (molassic) deposits since the Eocene, which were related to several uplifting events of the Andean orogeny (Mora and Garcia, 2006; Ayala-Calvo et al., 2009; Bayona et al., 2011; Mesa and Rengifo, 2011; Montes et al., 2019).

The Colón Formation (also referred to as Molino Formation), described in the Cesar-Rancheria basin and in the proximal Catatumbo basin, can be divided into two major stratigraphic intervals: The basal Socuy Member (*sensu* Sellier de Civrieux, 1952), composed of

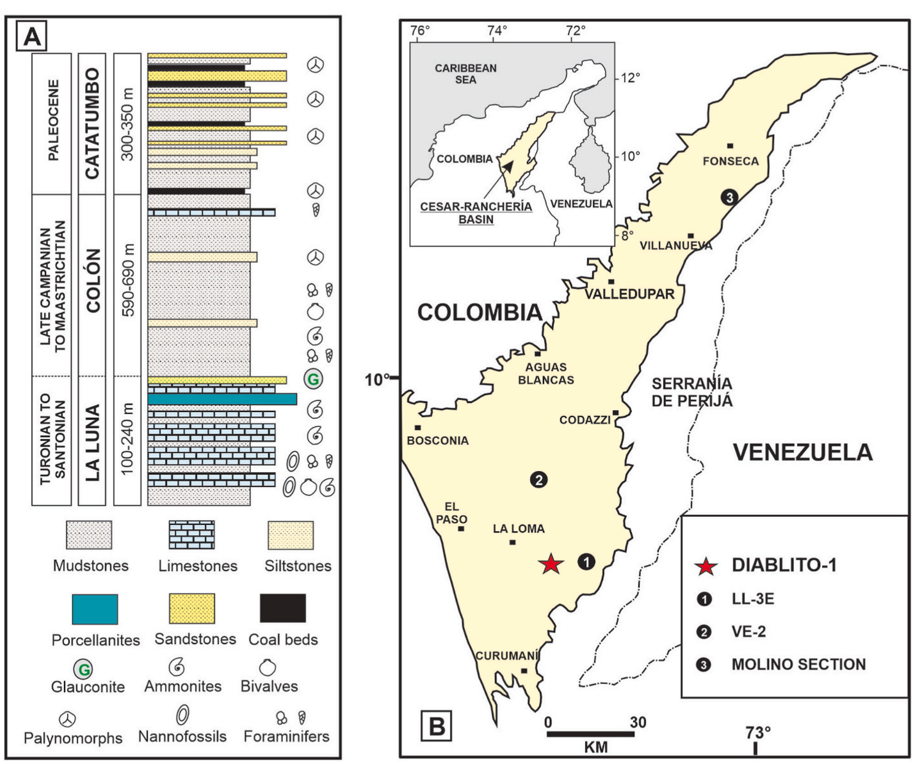

Fig. 1. Study area. A: Generalized stratigraphic column of the Cesar-Rancheria basin, northeast Colombia (adapted from Mesa and Rengifo, 2011). B: Location of Core Diablito-1. Sites 1 to 3 correspond to localities with previous biostratigraphic data for the Colón Formation. Sites 1 and 2 are stratigraphic cores (Ayala-Calvo et al., 2009; Malumián, 2010), and site 3 corresponds to the Molino River section (Gandolfi, 1955; Martínez, 1989).

moderately micritic levels and calcareous mudstones; and an uppermost segment, not yet formally named, which is composed of a monotonous succession of dark grey fine-grained rocks and sandy intervals (Ayala-Calvo et al., 2009; Avendaño-Suárez et al., 2021). An average thickness of 600 m is proposed for the formation, though most of the reports are related to exploratory wells and scattered outcrops in the Rancheria sub-basin (e.g. Molino River section; Martínez, 1989; Ayala-Calvo et al., 2009). The Colón Formation is underlaid by the La Luna Formation (Fig. 1). Although the lithological contrast between the La Luna and Colón formations is easy to identify on field and in subsurface, there are discussions about the stratigraphic and paleoenvironmental transitions between these two units. For instance, in the Catatumbo Basin some studies have suggested a concordant contact in the western part of the basin (e.g. Santa Elena Creek; Notestein et al., 1944; Pedraza and Ramírez, 2011), while other studies, mostly based on geophysical data and paleontological surveys, suggested a regional discordance at the boundary between these units (Sutton, 1946; Castillo and Mann, 2006; Cooney and Lorente, 2009; Patarroyo et al., 2017). Micropaleontological and geochemical data also suggest a condensed interval in the uppermost part of the La Luna Formation (formally assigned to the Tres Esquinas Member; De Romero and Galea-Alvarez, 1995; Parra et al., 2003). The upper part of the Colón Formation has been characterized by sedimentological and palynological data, mainly in the Cesar-Ranchería basin and the Mérida Range (e.g. Yepes, 2001; Ayala-Calvo et al., 2009; De La Parra et al., 2022). The Colón Formation is overlaid by the Catatumbo/Barco or Mito Juan (Catatumbo basin) formations, where both upper contacts seem to be conformable (Fig. 1).

A latest Campanian to Maastrichtian age has been proposed for the entire Colón Formation in both the Cesar-Rancheria and Catatumbo basins, mostly based on foraminiferal (planktonic and benthic) and palynological data (Cushman and Hedberg, 1930, 1941; Notestein et al., 1944; Sellier de Civrieux, 1952; Gandolfi, 1955; Martínez, 1989; Yepes, 2001; Mora and Garcia, 2006; Patarroyo et al., 2017; De La Parra et al., 2022). Additional biostratigraphic information has been registered in technical reports from petroleum companies (e.g. Jaramillo and De La Parra, 2005; Malumián, 2010). However, the major input of biostratigraphic data comes from foraminiferal assemblages. The first formal biostratigraphic scheme for the Colón Formation was proposed by Cushman and Hedberg (1941) who divided the unit into three benthic foraminiferal assemblage zones (from base to top of the formation): *Pullenia cretacea, Siphogenerinoides bramletti*, and *Ammobaculites colombiana* assemblage zones. Even though these zones still have a practical use, depending on depositional settings, Sellier de Civreaux (1952) later focused on the Socuy Member, and integrated both benthic and planktonic foraminiferal assemblages, assigning a Campanian-Maastrichtian age for this interval. Gandolfi (1955) focused only on planktonic assemblages from the Molino River section, making some stratigraphic indications, though most of his taxonomical proposals was later discarded. Martínez (1989) revisited that section, and using planktonic foraminiferal assemblages identified the *Globotruncana aegyptiaca* to *Abatomphalus mayaroensis* standard biozones (latest Campanian-mid Maastrichtian) within the Colón Formation. More recent studies on foraminiferal assemblages have discussed the chronology and the paleoenvironments of the La Luna-Colón formations (Martinez and Hernandez, 1992; Erlich et al., 1999; Villamil et al., 1999; De Romero et al., 2003; Parra et al., 2003; Cooney and Lorente, 2009; Patarroyo et al., 2017). Furthermore, palynological biostratigraphic schemes agree with the foraminiferal biostratigraphic framework, and have even recognized the K-Pg boundary at the uppermost part of the Colón Formation (Yepes, 2001; Mora and Garcia, 2006; Carvalho et al., 2021; De La Parra et al., 2022).

2. Methods

2.1. Core location and sample strategy

We studied a rock-core (Diablito-1), drilled by Drummond Coal Company, in the Jagua de Ibirico locality (Cesar Department, Colombia; 9°34′ N, 73°16’ W). The cored interval spanned a thickness of 701 m, recovering the Colón, Catatumbo/Barco formations (Figs. 1 and 2). At this site, the K-Pg boundary was identified between 501.80 and 501.72 m, based on palynological, sedimentological and geochemical analyses (De La Parra et al., 2022). We focused our study on the interval from 701.5 to 563.5 m, which comprises the middle to upper part of the Colón Formation. Lithological descriptions did not indicate the occurrence of the Socuy Member limestones at Core Diablito-1. Average sampling resolution in the studied interval of Core Diablito-1 was 1 m.

2.2. Micropaleontology

Calcareous microfossil samples (n = 40; interval 701.5–563.5 m) were prepared according to standard methods at the Technological Institute for Paleoceanography and Climate Change (itt Oceaneon – Unisinos University, Brazil). Approximately 20–30 g of dried rock were soaked into a 5% hydrogen peroxide (H_2O_2) solution for about 24 h, washed over 63 μm and 150 μm sieves, and dried at 40 °C (Sohn, 1961). Due to low abundances, all foraminifers and ostracods were handpicked. Planktonic foraminiferal taxonomy followed Caron (1985), Nederbragt (1991), Georgescu (2005), Premoli Silva and Verga (2011), among others. Benthic foraminiferal taxonomy followed previous studies of the Colón Formation (Cushman and Hedberg, 1930, 1941; Sellier de Civrieux, 1952; Petters, 1955; Martínez, 1989; Malumián, 2010; Patarroyo et al., 2017) and regional literature for the tropics and the U.S. Western Interior (Frizzell, 1954; Koutsoukos and Merrick, 1986; 1990; Bolli et al., 1994). The definition of benthic foraminiferal morphogroups and their ecological preferences followed to Frenzel (2000) and Cetean et al. (2011). Ostracod suprageneric classification follows Scott (1961) and taxa were classified only at genus level due to poor preservation. Selected foraminiferal and ostracod specimens were imaged using a Zeiss EVO MA15 scanning electron microscope (SEM) at itt Oceaneon. Diversity (Shannon-H) and richness (S) estimations were calculated for foraminiferal assemblages using the software Past (version 2.15; Hammer et al., 2001). All studied specimens were archived in the micropaleontological collection at itt Oceaneon. Total microfossil counts and their diversity estimates are available in Supplementary Tables S1 and S2.

Calcareous nannofossil samples (n = 33; interval 697.4–574.5 m) were also prepared at itt Oceaneon following the smear-slide technique detailed by Bown and Young (1988), and studied using a petrographic microscope Zeiss Axio Imager A2, at 1000 × magnification. In order to achieve a quantitative analysis of assemblages, 700 fields of view (FOV) were counted per slide. Preservation of calcareous nannofossils was evaluated under light microscope using qualitative criteria: “Good” indicating specimens with little or no etching and/or overgrowth; “moderate” for specimens exhibiting some degree of etching and/or overgrowth, but still easily recognizable; and “poor” for specimens exhibiting extreme etching and/or overgrowth (Roth and Thierstein, 1972; Roth, 1983). Considering the low abundances of the studied assemblages, we based our paleoenvironmental interpretations on the stratigraphic distributions of selected taxa, such as *Kamptnerius magnificus*. Total calcareous nannofossil counts are given in Supplementary Table S3.

2.3. Geochemistry

X-ray fluorescence (XRF) analyses were performed on 5–10 g of ground rock (n = 93; interval 700.3–574.7 m), with elemental concentrations reported as raw counts per second (cps). Samples were

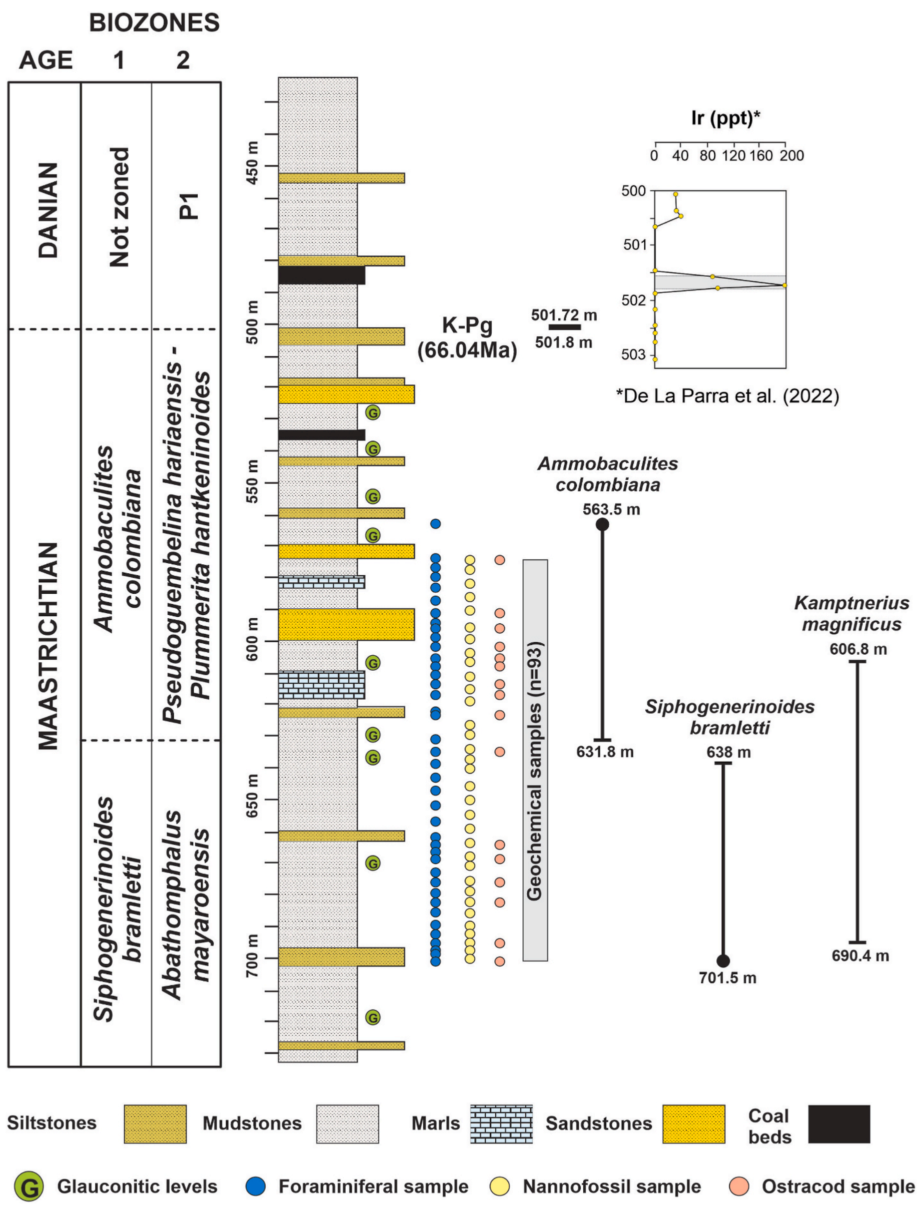

Fig. 2. General stratigraphic column of Core Diablito-1. Biozones 1 and 2 correspond to local assemblage zones of Cushman and Hedberg (1941) and the standard planktonic zonation for the Cretaceous (Caron, 1985; deduced from the occurrence of the local assemblage zones), respectively. The K-Pg boundary (66.04 Ma; Gradstein et al., 2012) was previously defined by palynology and geochemical analyses (De La Parra et al., 2022). According to Martínez (1989), the top of the regional foraminiferal zone *Siphogenerinoides bramletti*, correspond to the first occurrence of the planktonic foraminiferal marker *Pseudoguembelina hariaensis* (67.30 Ma; Gradstein et al., 2012). Biostratigraphic ranges of the most representative benthic foraminiferal taxa (*Ammobaculites colombiana*, *Siphogenerinoides bramletti*) and calcareous nannofossils (*Kamptnerius magnificus*) identified in our study are also shown.

measured at 10 kV (150 μA, no filter) for Al, Mg, and Si intensities; 12 kV (400 μA, Al-50 filter) for Ca, K, Ti and V intensities; 20 kV (250 μA, Al – 200 filter) for Co, Cr, Fe and Mn intensities; and 50 kV (100 μA, Ti filter) for Ba and Rb intensities. XRF analyses were performed with a PanAlytical Epsilon 1 XRF spectrometer, at itt Oceaneon. In order to prevent bias between contrasting values, data was mostly interpreted as logarithmic elemental ratios and normalized to a median-scaled (NMS) following Lyle et al. (2012).

The log (Zr/Rb) ratio was used as a proxy for sediment grain size changes. Zirconium resides mainly in relatively resistant and coarse grains, almost exclusively in zircons, while rubidium is mainly present in clays (aluminosilicates and related products; Calvert and Pedersen, 2007; Beil et al., 2018). The log (K/Fe) ratio was used to evaluate weathering intensity (regional hydroclimate), since potassium is mainly delivered to ocean basins as illite, which is preferentially generated in relatively dry climate conditions, whereas Fe oxides-hydroxides are mainly generated as products of intense chemical weathering under relatively wet climates (Piva et al., 2008; Govin et al., 2012). In addition, fluctuations in the log (Fe/Ca) ratio can be used as a tracer for terrigenous input and carbonate accumulation (Kujau et al., 2010; Govin et al., 2012). We used the Sr/Ba ratio as a paleosalinity proxy; strontium tends to be adsorbed onto fine-grained sediments deposited under high-salinity waters, whereas barium content is higher in freshwater delivered by continental runoff (e.g. Wei and Algeo, 2020; Yelwa et al., 2022). To reconstruct bottom water paleoredox conditions, we followed the classification scheme proposed by Tyson and Pearson (1991), defining improved or decreased oxygenation conditions based on the observations of Rivera et al. (2018) in Cretaceous rocks of Colombia. As a redox-sensitive element, vanadium (V) concentrations tend to be greater than other elements, such as the chromium (Cr), under suboxic to anoxic conditions. We thus considered the V/Cr ratio as a proxy for bottom water oxygenation where, according to Rivera et al. (2018), V/Cr values < 2.00 indicate oxic conditions, values between 2.00 and 4.25 suggest dysoxic conditions, and V/Cr > 4.25 indicate suboxic to anoxic conditions. In addition, bottom water oxygenation was also evaluated with the NMS intensities of the redox-sensitive trace metals (TM) Ni and Cu, normalized by NMS Al intensities (e.g. Dummann et al., 2021). All geochemical data are provided in Supplementary Table S4.

3. Results

3.1. Biostratigraphy of Core Diablito-1

A previous palynological study identified the K-Pg boundary within the interval 501.80–501.72 m at Core Diablito-1 (De La Parra et al., 2022). In general, most of the recovered planktonic foraminiferal taxa have wide chronostratigraphic ranges (*Guembelitria cretacea, Planoheterohelix globulosa*), but there are some species, such as *Spiroplecta americana*, *Pseudoguembelina excolata* and *Rugoglobigerina macrocephala* with late Campanian to late Maastrichtian chronostratigraphic ranges. Based on the distribution of benthic foraminiferal taxa in our study, we recognized the *Siphogenerinoides bramletti* (701.5–638 m) and *Ammobaculites colombiana* (631.8–563.5 m deep) assemblage zones. These zones have a mid to late Maastrichtian age, following the definitions of Cushman and Hedberg (1941) in the Colón Formation, and its calibration with the standard planktonic foraminiferal zonation (Martínez, 1989; Molino River section).

Considering our new biostratigraphic data, and the definition of the K-Pg boundary by De La Parra et al. (2022), the analyzed interval at the Core Diablito-1 comprises the late Maastrichtian (*Abathomphalus mayaroensis* to probably *Plummerita hantkeninoides* foraminiferal zones; Fig. 2). A first order estimate of sedimentation rate for the studied interval at Core Diablito-1 yields an approximated value of 100 mm/kyr, using the location level of the K-Pg boundary (66.04 Ma; Gradstein et al., 2012) proposed by De La Parra et al. (2022) and the first occurrence of *Pseudoguembelina hariaensis* (67.30 Ma; Gradstein et al., 2012). Despite *P. hariaensis* is not present at Core Diablito-1, according to Martínez (1989), its first occurrence would be probably correlated with the top of the regional biozone *Siphogenerinoides bramletti* (638 m at Core Diablito-1; Fig. 2). Therefore, the interval between 638.0 and 501.7 m at Core Diablito would span approximately span the time interval between 67.9 and 67.3 Ma. The estimated sedimentation rate for the Core Diablito-1 is in concordance with observations of modern shallow

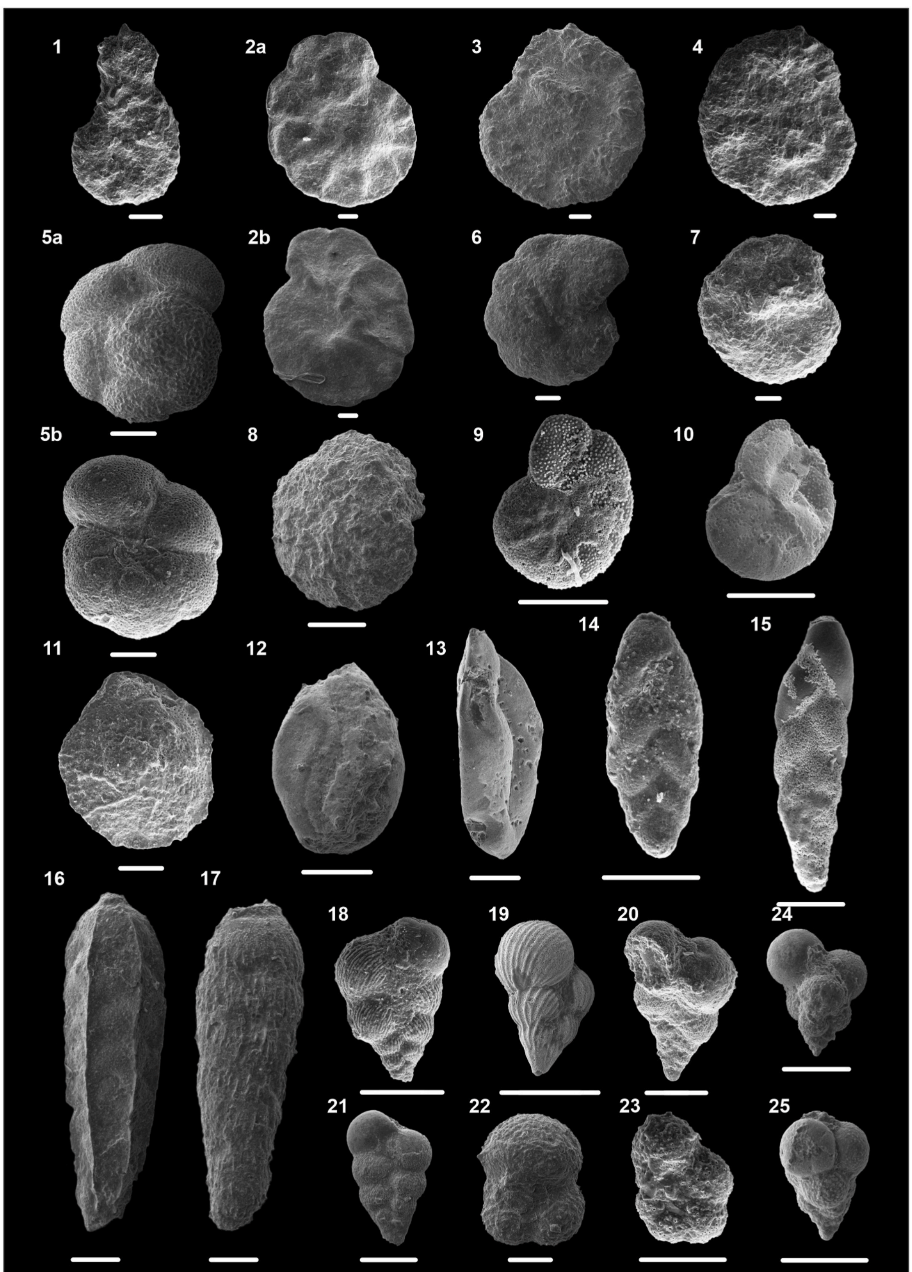

Fig. 3. Selected foraminifers from Core Diablito-1. Scale bars represent 100 μm. Benthic foraminifers are: 1. *Ammobaculites* sp. (574 m). 2a-b. *Haplophragmoides excavatum* (608.8 m). 3–4. *Ammobaculites colombiana* (574 m). 5a-b. *Cibicides coonensis* (661.6 m). 6. *Haplophragmoides glaber* (656.8 m). 7. *Evolutinella flageri* (574 m). 8. Undetermined rotaliid (595.2 m). 9. *Gavelinella spissocostata* (608.8 m). 10. *Gavelinella* sp. (594.5 m). 11. *Epistominella alata* (595.2 m). 12. *Triloculina neotica* (595.2 m). 13. *Triloculina* sp. (665.5 m). 14. *Coryphostoma incrassata* (661.6 m). 15. *Loxostomum minutissimum* (594.5 m). 16. *Siphogenerinoides bramletti* (661.6 m). 17. *Orthokarstenia parva* (661.6 m). Planktonic foraminifers are: 18. *Pseudoguembelina costulata* (661.6 m). 19. *Pseudoguembelina* sp. (594.5 m). 20. *Spiroplecta* cf. *americana* (668.8 m). 21. *Planoheterohelix globulosa* (668.8 m). 22. *Rugoglobigerina macrocephala* (689 m). 23. *Muricohedbergella* sp. (627.7 m). 24–25. *Guembelitria cretacea* (668.8 and 631.8 m).

marine settings, with values such as 0.3–1.0 mm/yr (Strasser and Samankassou, 2003; Restreppo et al., 2020), considering post-depositional compaction in the Colón Formation.

Calcareous nannofossil assemblages were also mostly composed of taxa with wide chronostratigraphic ranges (e.g. Aptian-Maastrichtian), though species such as *Arkhangelskiella maastrichtiensis* and *Prediscosphaera stoveri*, which ranged from Campanian to Maastrichtian, were present in low abundances. Among ostracod assemblages, *Sapucariella* spp. corresponds to the first record of this genus for the Maastrichtian of Colombia. In general, early brachycytherides were already widespread in the Maastrichtian, also occurring in Venezuela and together with the genera *Veenia*, and *Cythereis*, they represent a typical Cretaceous marine fauna (Puckett et al., 2016).

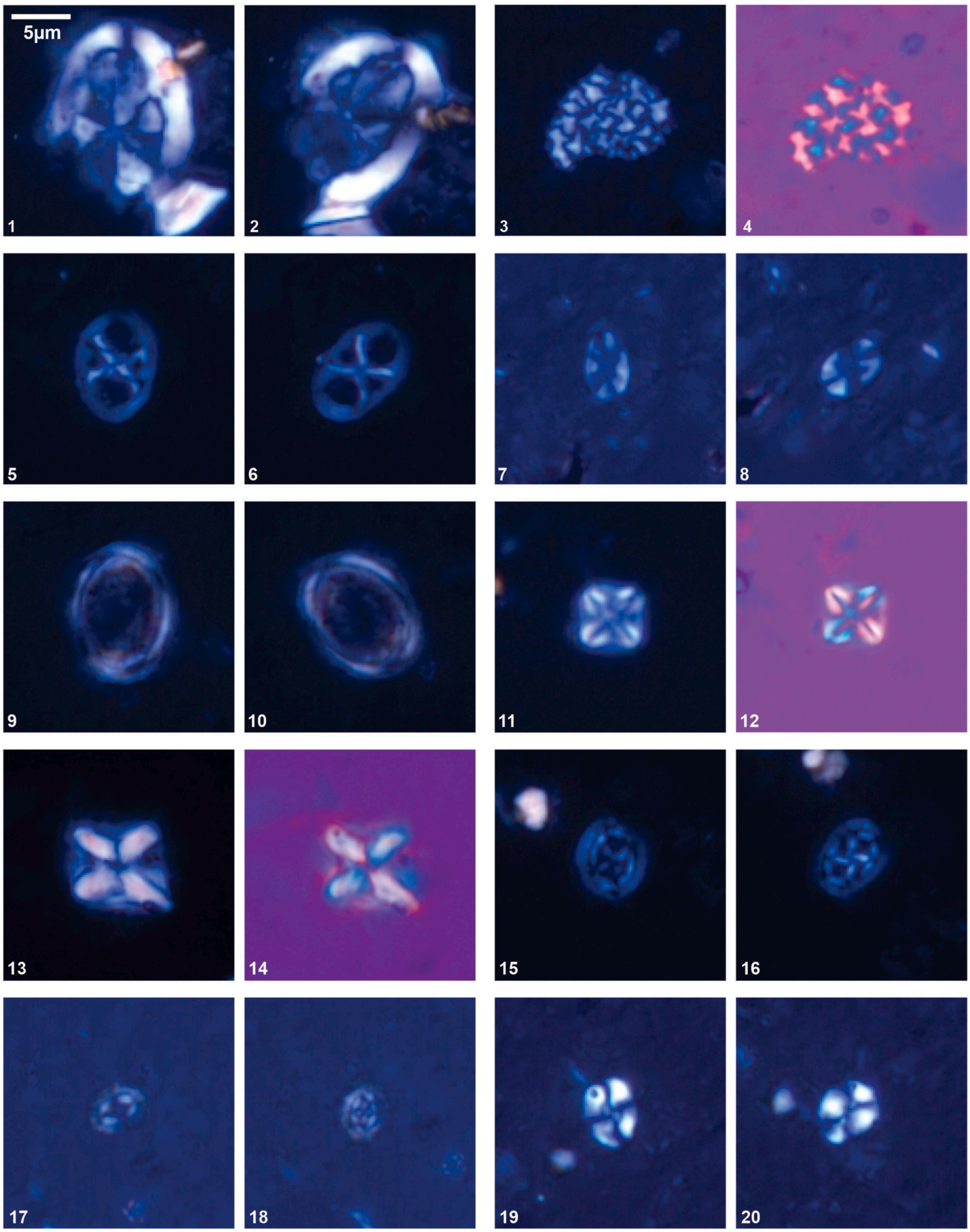

Fig. 4. Selected calcareous nannofossils from Core Diablito-1.1–2. *Arkhangelskiella maastrichtiana* (2167.5 m). 3–4. *Cervisiella operculata* (2204.2 m). 5–6. *Chiastozygus litterarius* (2265.2 m). 7–8. *Eiffelithus gorkae* (2265.2 m). 9–10. *Kamptnerius magnificus* (2120.5 m). 11–12. *Micula cubiformis* (2167.5 m). 13–14. *Micula staurophora* (2133.2 m). 15–16. *Prediscosphaera cretacea* (2133.2 m). 17–18. *Prediscosphaera stoveri* (2252 m). 19–20. *Watznaueria barnesiae* (2057.4 m).

3.2. Foraminiferal assemblages

Foraminiferal assemblages (planktonic and benthic) are moderately to poorly preserved and abundances along the core are moderate to scarce (usually 10–100 individuals/sample). Agglutinated taxa are common in the upper part of the core (563.5–617.8 m), mainly represented by the genera *Ammobaculites*, *Evolutinella* and *Haplophragmoides* (Fig. 3). Among those, *Ammobaculites colombiana* is the most abundant and recurrent species. Calcareous taxa include rotalids (*Cibicides*, *Epistominella*, *Gavelinella*, *Lenticulina*), buliminids (*Praebulimina*), and elongated uniserial/biserial forms such as the genera *Coryphostoma*, *Loxostomum*, and *Dentalina*, as well the species *Siphogenerinoides bramletti* and *Orthokarstenia cretacea* (Plate 1). Planktonic assemblages are mainly dominated by *Guembelitria cretacea* (highest abundances occur from 689 to 661.6 m), whereas both the biserial genera *Planoheterohelix, Pseudoguembelina* and *Spiroplecta*, and the trochospiral forms *Muricohedbergella* and *Rugoglobigerina* are present but scarce (Figs. 3 and 6). Despite the low abundance of foraminiferal assemblages, general estimates of diversity (Shannon-H) and richness (S) were tentatively calculated. Richness is relatively high ($S > 10$) in the intervals 668.8–656.8 m and 608.8–595.2 m, and at 698.1 m. Shannon-H diversity is > 2 within the interval 663.4–647.1 m, as well as at 601.6 m, 608.8 m, and 698.1 m.

3.3. Calcareous nannofossil assemblages

Assemblages of calcareous nannofossils are characterized by moderate to poor preservations and low abundances (<100 specimens/sample), except for those at 650.2 m and 660.6 m, which represented increased abundances (>150 specimens/sample). In general, occurrences are mostly restricted to the lower part of the Core Diablito-1 succession (Interval 690.4–611.4 m deep), with *Micula staurophora*, *Kamptnerius magnificus*, *Prediscosphaera cretacea* and *Watznaueria barnesiae* as the most representative taxa. *Micula cubiformis*, *Cervisiella operculata*, *Chiastozygus litterarius* and *Eiffelithus gorkae* occurrences were more scattered or less abundant throughout the studied interval (Figs. 4 and 6). Considering the low abundance of the calcareous nannofossil assemblages, we only estimated species richness (S). The highest richness values ($S > 10$) occur within the interval 660.6–627.1 m.

3.4. Ostracod assemblages

Among the set of samples analyzed for calcareous microfossils at Core Diablito-1, 11 samples yielded ostracods. Overall, ostracod assemblages are scarce (<5 specimens/sample), though samples at 595.2 m, 605.7 m and 613.8 m have higher abundances (>10 specimens/sample; Fig. 6). We identified ten species, belonging to four families,

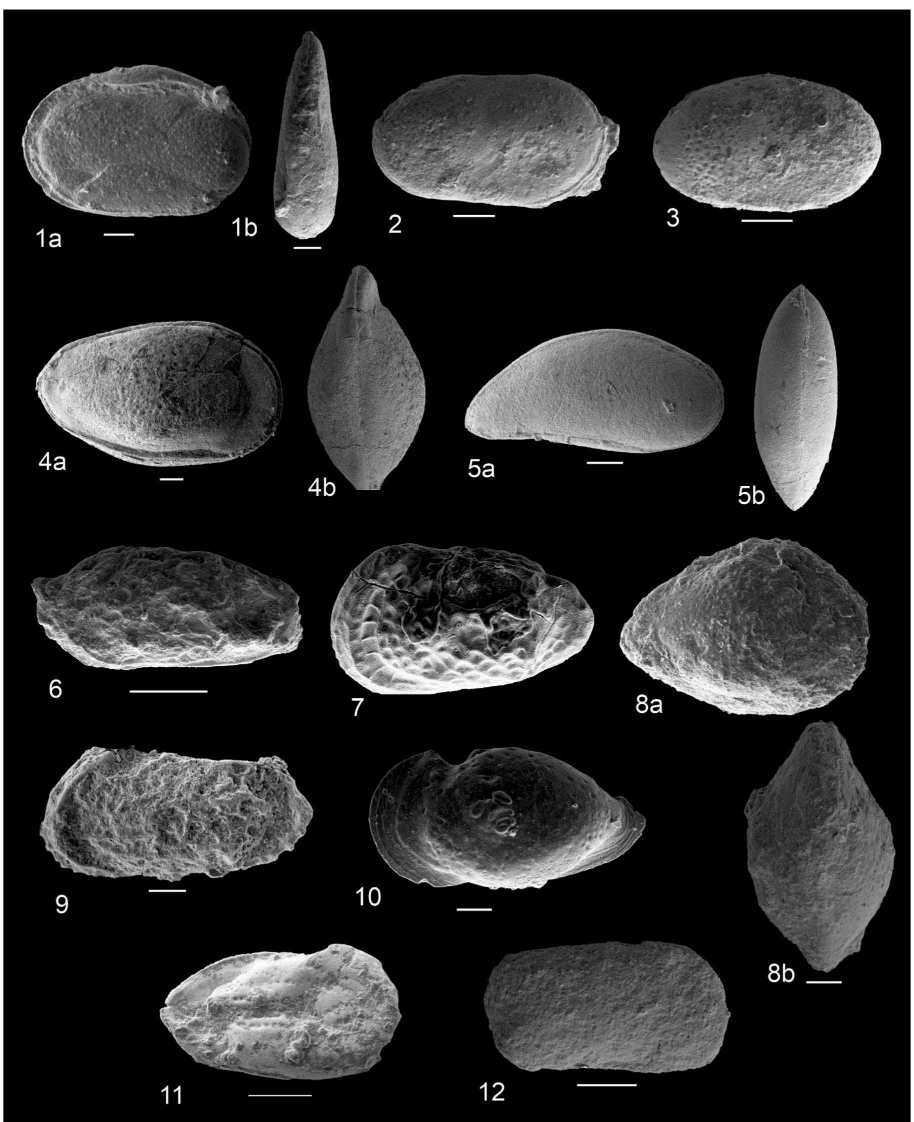

Fig. 5. Selected ostracods from Core Diablito-1. Scale bars represent 100 μm. 1a-b. *Cytherella* cf. *C. piacabucuensis* (574 m), 1a carapace, left view; 1 b, dorsal view. 2. *Cytherella* sp. 1, (676.5 m), right valve. 3. *Cytherella* sp. 2 (602.3 m), right valve. 4a-b. *Buntonia* sp. (574 m), 4a carapace, right view; 4 b dorsal view. 5a-b. *Paracypris* sp. (574 m), 5a carapace, right view, 5 b dorsal view. 6. *Munseyella*? sp. (595.2 m), left valve. 7. *Cythereis*? sp. (574 m), left valve. 8a-b. *Sapucariella* sp. (595.2 m); 8a carapace, right view; 8 b dorsal view. 9. *Paracosta* sp. (608.8 m), left valve. 10. *Veenia* sp., internal mold (613.8 m). 11. Gen et sp. indet. 1. (608.8 m), carapace, right view. 12. Gen et sp. indet. 2 (627.7 m), carapace, right view.

eight genera and two undetermined genera. Trachyleberididae and Cytherellidae are the richest families (5 and 3 species respectively), followed by Paracyprididae and Pectocytheridae with a single species each. The identified taxa were *Cytherella* cf. *C. piacabucuensis*, *Cytherella* sp.1, *Cytherella* sp.2, *Paracypris* sp., *Buntonia* sp., *Cythereis* sp., *Paracosta* sp., *Sapucariella* sp., *Veenia* sp., *Munseyella*? sp., Gen. et sp. indet. 1 and Gen. et sp. indet. 2. In general, the most abundant species were *Cytherella* sp.2 and *Veenia* sp. (particularly at 613.8 m), though they were mostly represented by molds (Fig. 5). Besides ostracods, micropaleontological samples contained mollusk remains (gastropods and bivalves), fish teeth, echinoderm spines, possible plant remains and charophytes.

3.5. Geochemistry

Log (Zr/Rb) values range between 0 and 1.20, steadily increasing from 700.3 to 623.8 m. High-amplitude fluctuations are recorded upward in the section, with the highest values at 599.1 m, 592.2 m and 578.5 m. In general, a decreasing upward trend is observed in the log (K/Fe) ratio, with values ranging from 1.4 to 1.7, and higher-amplitude fluctuations in the upper part of the core. The Sr/Ba ratio also depicts an overall decreasing upward trend, with values ranging between 16.7 and 30.7. Minimum Sr/Ba values (<8.5) are present at 599.1 and 582.8 m. In contrast, log (Fe/Ca) values tend to increase upward. Log (Fe/Ca) values range between −1.80 and −1.05, with the most negative spike at 662.8 m, and the highest values occurring within the interval 629.7–574.7 m (Fig. 6). A *t*-test showed that the differences in the log (Zr/Rb), and the Sr/Ba ratios between the lower (629.7–700.3 m) and upper (574.7–628.8 m) section of the Core Diablito-1, are statistically significant (*t*-test: 7.70, p: 3.43×10^{-9} for log (Zr/Rb); *t*-test: −6.86, p: 4.39×10^{-8} for Sr/Ba).

The V/Cr ratio presents little variations, with most values ranging from 3.4 to 4.2, and a slight increase is recorded in the upper part of Core Diablito-1. Spikes with lower values (<1.1) are present at 674.2 and 692.3 m. (Fig. 7). The Cu/Al and Ni/Al values mainly range between 3.0 $\times 10^{-2}$ to 6.0×10^{-2}, with increasing-upward trends between 700.3 and 687.4 m, and between 630 m and the top of the studied interval (Cu/Al). Spikes with anomalously high Cu/Al and Ni/Al ratios were observed at 687.4 m, 664 m, 644.7 m, and 585 m (Fig. 7).

4. Discussion

4.1. Relative sea level changes recorded at the upper maastrichtian Colón Formation

Our integration of micropaleontological and geochemical analyses indicates a transition from an inner platform setting, recorded in the lower part of the studied interval (700.3–629.7 m), to sublittoral conditions in the upper part of Core Diablito-1 (628.8–574.7 m; Figs. 6–8). Foraminiferal assemblages show two intervals that illustrate this transition: a lower assemblage (638–701.5 m) dominated by calcareous benthic foraminifers (mostly elongated and planispiral forms) and some planktonic taxa; and an upper assemblage (563.5–631.8 m) mostly dominated by agglutinated benthic taxa, commonly associated with relatively shallow conditions (Fig. 6; Cetean et al., 2011; Murray et al., 2011). The regressive trend in the uppermost part of the Colón Formation has been previously documented with foraminiferal assemblages, but without a clear stratigraphic control (Cushman and Hedberg, 1941). The detailed study of Martínez (1989) suggested a regressive pattern for this unit, based on the disappearance of keeled planktonic taxa, a drop in the planktonic/benthic ratio, and an increase in the proportion of textulariids upward in the succession. However, as previously mentioned, the study of Martínez (1989) focused on the lower (Socuy Member) and the middle part of the Colón Formation, only partially present at Core Diablito-1. This aspect explains why planktonic assemblages at Core Diablito-1 were mainly composed of *Guembelitria cretacea* and scarce non-keeled taxa, both characteristic of inner platforms and restricted marine settings (Leckie and Olson, 2003; Keller and Abramovich, 2009).

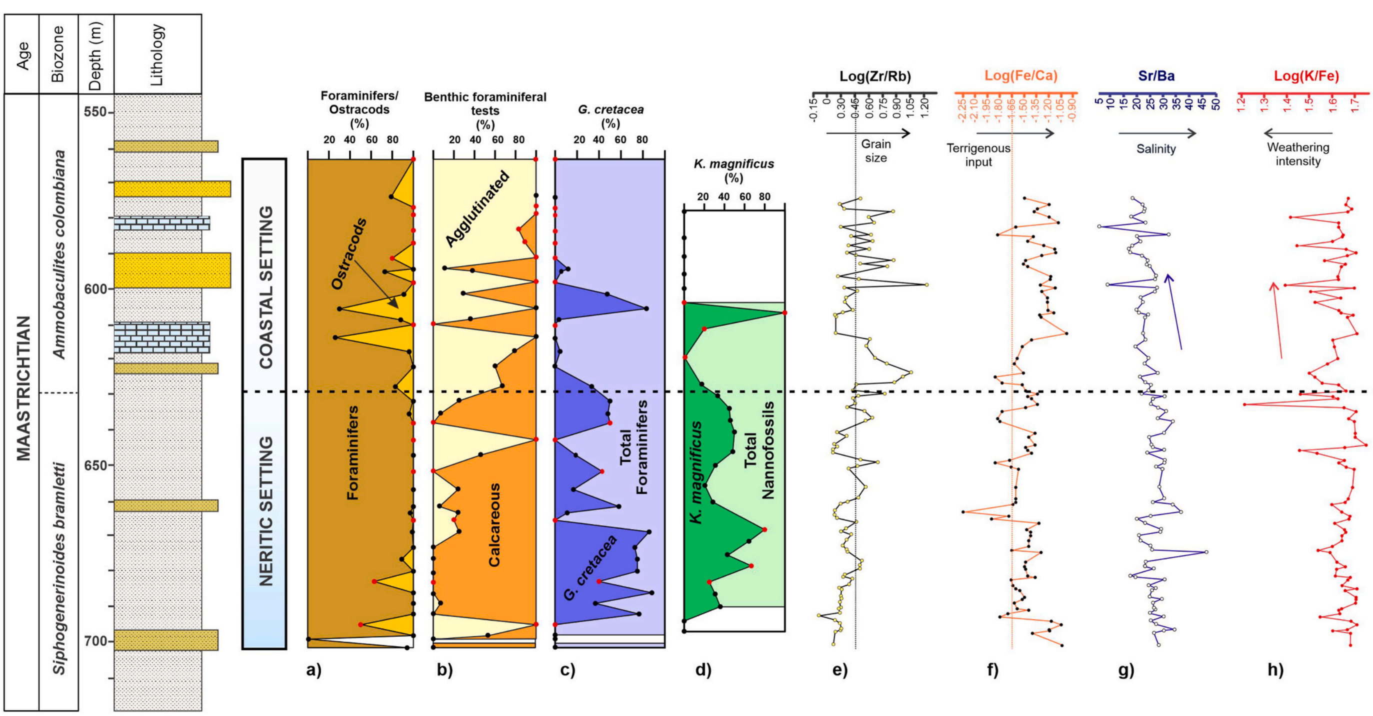

Fig. 6. General distribution of microfossils and geochemical proxies at Core Diablito-1. A) Foraminiferal and ostracod relative abundances. B) Relative abundances of the calcareous and agglutinated benthic foraminifers. C-D) Relative abundances of selected planktonic foraminifers and calcareous nannofossils (*Guembelitria cretacea*, *Kamptnerius magnificus*). Red points indicate samples barren of microfossils or presenting low abundances (<10 specimens/sample). E) Log (Zr/Rb) as a proxy for sediments grain sizes. F) Log (Fe/Ca) as a proxy for input of terrigenous sediments. G) Sr/Ba ratio as a proxy for paleosalinity. H) Log (K/Fe) as a proxy for weathering intensity.

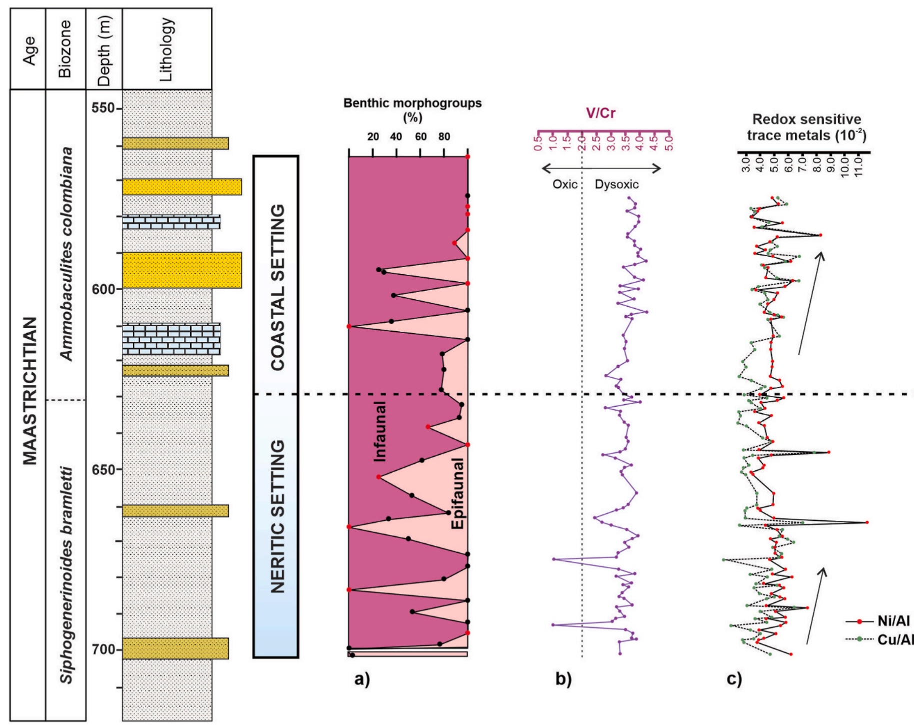

Fig. 7. Geochemical proxies and general distribution of benthic foraminifers at Core Diablito-1. A) Relative abundances of infaunal benthic foraminifers. B) V/Cr ratio as a proxy for bottom water oxygenation. C) Distribution of the redox-sensitive trace metals Ni and Cu, normalized to Al content.

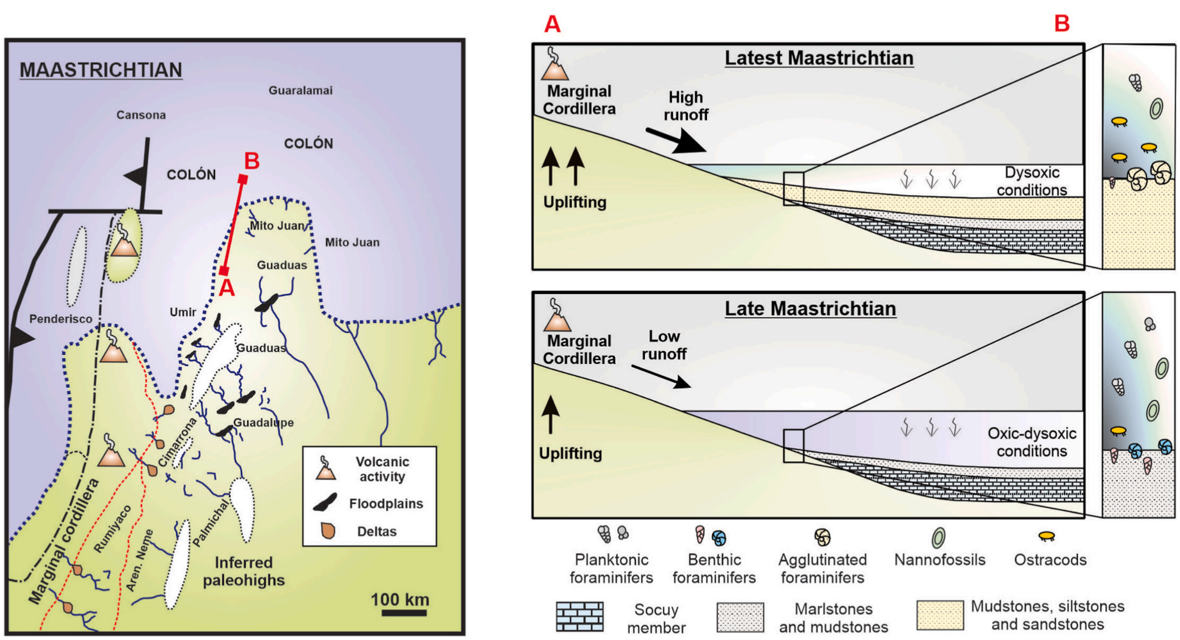

Fig. 8. Interpreted paleoenvironmental evolution for the succession at Core Diablito-1. Note the transition from inner platform to sublittoral conditions during the late Maastrichtian. Paleogeographic map adapted from Bayona (2018).

A similar deposition setting was observed at the nearby stratigraphic core LL-3E (Fig. 1), where foraminiferal assemblages (planktonic and benthic) also suggest middle to outer shelf settings and an early to middle Maastrichtian age (Malumián, 2010). In contrast, most of the foraminiferal assemblages recovered at Core Diablito-1 differ from those reported for localities in the Western Colombian Cordillera (e.g. Penderisco Formation), Gorgonilla Island, and the Colombian Caribbean (Cansona and Guaralamai formations), where open marine and deep-sea depositional settings have been proposed for uppermost Cretaceous strata (Fig. 5; Petters, 1955; Martínez, 1989; Bermúdez et al., 2019). We suggest that foraminiferal assemblages with *Ammobaculites*, *Evolutinella* and *Haplophragmoides* indicate proximal depositional conditions (Murray et al., 2011; Cetean et al., 2011) for the upper segment of the studied interval at Core Diablito-1. Previous micropaleontological and sedimentological analyses even inferred a highly dynamic coastal lagoon setting for other Maastrichtian units in Colombia (Umir, Guaduas and Buscavidas formations; Bürgl and Dumit, 1954; Tchegliakova, 1993–1996; Sarmiento, 1994; Vergara, 1997; Guerrero et al., 2000;

Tchegliakova and Mojica, 2001; Montaño et al., 2016).

Like planktonic foraminifers, calcareous nannofossil assemblages are mostly present in the lower part of the core (Fig. 6). Considering the scarcity of studies of Upper Cretaceous calcareous nannofossils in northern South America, we present here some general paleoenvironmental inferences for the Colón Formation. Despite low abundances of the recovered assemblages, well-known species such as *Micula staurophora* and *Watzneuria barnesiae* are present at Core Diablito-1. The paleobiogeographic distribution of both taxa and their relative abundance are commonly used to infer fluctuations in sea surface water temperatures (Wind, 1979). We suggest that higher proportions of *M. staurophora*, a taxon dominant at high latitudes (in comparison with the low-latitude adapted *W. barnesiae)*, might indicate relatively cold surface waters at the location of Core Diablito-1 during the Maastrichtian. However, according to Watkins and Self-Trail (2005) and Lees (2002), *M. staurophora* was relatively common in proximal environments, probably having an r-selected ecological strategy. Some studies have also emphasized the high resistance of *M. staurophora* to dissolution as an explanation for its higher abundance in some sections (e.g. Eshet and Almogi-Labin, 1996). In any case, high relative abundance of *M. staurophora* is a common feature of several Maastrichtian onshore (relatively proximal) localities in the Gulf of Mexico, Israel, and even at high latitude basins in Argentina (Eshet et al., 1992; Pospichal, 1996; Keller et al., 2007; Tantawi, 2011; Guerra et al., 2021). The species *Kamptnerius magnificus*, which is also abundant at the studied core (Fig. 3), had abundance episodes in deep-sea high-latitude localities in the South Atlantic Ocean, associated with sea-surface cooling during the late Campanian-Maastrichtian (Guerra et al., 2016). Considering the tropical location of Core Diablito-1, and the potential depositional/environmental biases of the succession, we suggest that the paleoenvironmental significance of *K. magnificus* in northern South America can only be elucidated with future sea surface temperature studies, such as those exploring the TEX_{86} proxy (O'Brien et al., 2017).

In contrast to planktonic foraminifers and calcareous nannofossils, ostracod assemblages were mostly present in the upper part of the studied interval at Core Diablito-1 (Fig. 6). The exception being *Cytherella* sp.1, which was identified between 701.5 and 676.5 m. The highest abundances of ostracods are recorded between 663.3 and 613.8 m, though assemblages of this interval are mostly composed of poorly preserved *Veenia* sp. and *Cytherella* sp. 2 molds. The best ostracod recovery (considering both preservation and species richness) was recorded in the uppermost part of the core (interval 601.6–574 m), where six species occurred (*Cythereis* sp. *Buntonia* sp., *Cytherella* cf. *C. piacabucuensis*, *Sapucariella* sp., *Paracypris* sp., and *Munseyella*? sp.) Among these, *Cythereis* was the most abundant genus followed by *Cytherella*. In general, *Cythereis* is an opportunistic genus, with exclusively marine habitat and can be found in infra-littoral to deep-water environments (Van Morkhoven, 1963). Most of the taxa belonging to the family Trachyleberididae were stenohaline and suggest shallow shelf settings (Bertels, 1975; Neale, 1975; Guerra et al., 2021). The genus *Paracypris* is exclusively marine, inhabiting infra-neritic to bathyal settings (Van Morkhoven, 1963), and, more specifically, it was reported for outer carbonate platforms, restricted coastal environments and open ocean contexts (Babinot and Colin, 1988; Andreu, 1991; Santos-Filho et al., 2017). In conclusion, ostracod assemblages from Core Diablito-1 indicate a shallow marine setting, characterized by the families Cytherellidae and Trachyleberididae. A more diversified ostracod fauna was reported by Malumián (2010) at the stratigraphic core LL-3E, but it has not been yet formally classified.

Our interpretation of a shallowing-upward trend for studied interval of the Colón Formation is also supported by geochemical records at Core Diablito-1. Higher values of the log (Zr/Rb) ratio in the upper part of the core (628.8–574.7 m) suggest an increase in sediments granulometry, since zirconium and rubidium concentrations are usually related to fluctuations in the accumulation of moderately resistant zircon grains versus aluminosilicates, respectively (Fig. 6; Calvert and Pedersen, 2007; Beil et al., 2018). This gradual increase in grain size is also associated with higher input of terrigenous sediments (Kujau et al., 2010; Govin et al., 2012), as evidenced by increased values of the log (Fe/Ca) ratios (Fig. 6). Previous sedimentological studies at Core Diablito-1, as well as at proximal sites in the basin (Cores LL-3E, VE-2, ANH-La Loma-1), described the upper part of the Colón Formation as a succession of siliceous mudstones, with scattered calcareous intervals (Ayala-Calvo et al., 2009; Avendaño-Sánchez et al., 2021). In addition, provenance and petrographic analyses of selected lithic sandstones of the upper segment of Core Diablito-1 indicated that the sedimentary lithics are more abundant than monocrystalline quartz grains and feldspars, being the main lithic fragments mica schists, sandstones, mudstones and cherts, likely characterizing a recycled orogenic material (Drummond, 2007). Macroscopic sedimentological descriptions of the Core Diablito-1 and coetaneous material (Core LL-3E, ANH La Loma-1) also suggested this transition from marine inner shelf to coastal plain depositional settings, with scattered mollusks remains and glauconitic/phosphatic levels, being superposed by a fluvio-estuarine depositional system, with common occurrences of plant remains, paleosols, coal beds, and sideritic levels (Drummond, 2007; Ayala-Calvo et al., 2009; Avendaño-Sánchez et al., 2021). These studies agree with our overall interpretation of a transition from an inner shelf setting to more proximal conditions (coastal plains), and a higher input of terrigenous sediments and freshwater (see below) for the upper part of the Colón Formation (Figs. 6 and 8).

The Sr/Ba ratio depicted lower values in the upper part of Core Diablito-1 (628.8–574.7 m), suggesting decreases in water salinity (Wei and Algeo, 2020; Yelwa et al., 2022). Even though we were not able to measure $CaCO_3$ content at Core Diablito-1, we do not consider that the Sr/Ba proxy is biased by sedimentological changes, since lithological descriptions do not suggest significant increases in $CaCO_3$ content. A possible bounding of Sr to carbonates can be discarded by the lack of correlation between the Sr/Ba ratio and Ca NMS values ($r^2 < 0.2$; Supplementary Fig. S1), assuming that most Ca in the studied sedimentary rocks occurs as carbonates.

In general, the Maastrichtian time interval was characterized by global sea-level fluctuations, which have been associated with the possible occurrence of intermittent icesheets at high latitudes (Kominz et al., 2008; Ray et al., 2019). Sea-level estimations, such as Haq (2014) propose five major eustatic events for the Maastrichtian. From these, the sedimentary succession at Core Diablito-1 could span eustatic events KMa4 and KMa5 (68.8 Ma and 66.8 Ma respectively). However, before assuming correlations with global sea level events, new localities must be surveyed in Cesar-Rancheria and proximal basins, using high resolution sequence stratigraphy approaches. In fact, the geological evolution of Maastrichtian coastal environments in northern South America was deeply influenced by the onset of tectonic activity in the Central and Eastern Cordilleras during the Campanian-Maastrichtian (Villamil and Pindell, 1998; Bayona, 2018; Sarmiento-Rojas, 2019; Montes et al., 2019). This tectonic activity makes it difficult to reconstruct the depositional evolution of the Cesar-Rancheria Basin, and other inter-mountainous basins in Colombia, due to the occurrence of several stages of basin deformation, local upliftings, xenoconformities, diachronism of units, and abrupt lateral facies shifts (Villamil, 1998; Veloza et al., 2008; Ayala-Calvo et al., 2009; Bayona et al., 2011, 2020; Montaño et al., 2016; Valencia-Gómez et al., 2020). So far, Maastrichtian sea-level fluctuations have been studied at the Umir Formation (Middle Magdalena basin), which records at least five maximum flooding surfaces over a major retro-gradational sequence (Montaño et al., 2016). Moreover, Bayona et al. (2020) proposed that the onset of tectonic deformation in the Cocuy region (southeastern of the Cesar-Rancheria basin) occurred in the earliest Maastrichtian, tracking the shift of depositional conditions from anoxic marine (typical of Cretaceous epicontinental seas of northern South America), to oxygenated shallow marine, coastal plains, continental swamps, fluvial and finally lacustrine environments, mostly deposited in closed basins. We suggest that the shallowing upward trend described at Core Diablito-1 shares a similar geological history with that described for the Cocuy region, and it was likely influenced by tectonic activity in the Central and Eastern cordilleras.

4.2. Late maastrichtian weathering intensity changes over northern South America

The log (K/Fe) record at Core Diablito-1 allows inferring Maastrichtian hydroclimate conditions. Log (K/Fe) values show transient decreases in the upper part of the studied interval (612.7–574.7 m), suggesting the occurrence of pulses of relatively humid climate conditions (Fig. 6). Increased continental runoff in the upper Colón Formation would have delivered higher amounts of Fe-bearing oxi-hydroxides, which are secondary minerals usually generated under enhanced chemical weathering (Piva et al., 2008; Govin et al., 2012). So far, Maastrichtian terrestrial ecosystems of northern South America have been interpreted as tropical rainforests (annual precipitation of 234–293 cm/year), with relatively open canopies (a mixture of angiosperms, ferns, and conifers), and evidence of intense host-specific insect herbivory, contrasting with the modern-like tropical rainforest of the Paleocene, with closed and sectorized angiosperms-dominated canopies (Carvalho et al., 2021). However, it is likely that the steady temperature decrease of the Campanian-Maastrichtian and the warming events at the end of the Cretaceous (Linnert et al., 2014; Huber et al., 2018) could be related to fluctuations in the regional precipitation patterns. Recent studies suggest that the paleo-intertropical convergence zone has been probably active since Aptian times (Santos et al., 2022). The nature of intertropical convergence during the late Maastrichtian may be tested in future studies at Core Diablito-1, and additional Campanian-Maastrichtian localities in Colombia.

Detailed paleopedological studies that explore precipitation shifts, combining proxies such as carbon isotopes, magnetic susceptibility or major oxides analyses, have not been yet conducted for the Late Cretaceous of northern South America. Considering the geographic extension of Campanian-Maastrichtian successions in Colombia, paleopedological analyses could be a promising field for paleoclimate research. For instance, studies with this approach have documented precipitation changes across the Paleocene-Eocene boundary in the Bogotá Basin (southwest of Core Diablito-1; Morón et al., 2013).

4.3. Bottom water oxygenation of the northern south American epicontinental sea during the late maastrichtian

V/Cr values are mostly constant (3.4–4.2) along Core Diablito-1, which, according to the thresholds of Rivera et al. (2018), indicate dysoxic conditions (V/Cr values 2.00–4.25). Exceptions occur at 692.3 m and 674.2 m, where V/Cr values are <1.1 (Fig. 7). However, these samples present anomalous spikes in several of the studied geochemical proxies (Fe/Ca, Sr/Ba), suggesting possible diagenetic or compositional biases. Increased Cu/Al ratios in the upper part of studied interval at Core Diablito-1 (700.3–687.4 m) correlate with the dominance of the infaunal foraminiferal taxa, suggesting decreased bottom water oxygenation (Fig. 7). Nevertheless, we cannot rule out that the anomalously high Cu/Al and Ni/Al values at 664 m, 644.7 m, and 585 m, were related with the higher input of terrigenous sediments and more proximal depositional settings in the upper part of the core (Fig. 7).

A dysoxic scenario can be also interpreted, based on the occurrence of benthic agglutinated morphogroups (rounded planispiral and elongated forms) at Core Diablito-1, such as *Ammobaculites colombiana* and *Haplophragmoides* spp., which are more common in the upper segment (617.8–563.5 m). In the Umir Formation, a similar benthic foraminiferal assemblage was reported by Tchegliakova (1993, 1995), which indicated poorly to moderately ventilated bottom waters in a marginal marine setting.

Despite major proportions of benthic infaunal taxa at Core Diablito-1, there is no record of high abundances of elongated (e.g. *Siphogenerinoides*, *Orthokarstenia*), ovoidal (buliminids) or elongated biserial (e.g. *Coryphostoma*, *Loxostomum*) forms. These morphotypes are usually thought to indicate poorly oxygenated bottom water conditions, related to water mass eutrophication (Frenzel, 2000; Van der Akker et al., 2000; Jorissen et al., 2007). Benthic foraminiferal assemblages at Core Diablito-1 contrast with those of Cenomanian-late Campanian successions of northern Colombia, where primary productivity was higher, anoxic episodes were recurrent, and benthic foraminiferal assemblages were mostly composed of deep infaunal forms (buliminids; De Romero and Galea-Alvarez, 1995; Vergara, 1997; Martínez, 2003; Parra et al., 2003; Rivera et al., 2018; Patarroyo et al., 2017).

Moreover, the moderately diverse ostracod assemblages and the presence of ichnofossils at Core Diablito-1 also favors a dysoxic environment instead of an anoxic one. Preliminary core descriptions reported the presence of intensely bioturbated facies with *Chondrites* burrows between 505 and 395 m (Drummond, 2007). In addition, geochemical and petrographical studies in other cores of the Colón Formation in Cesar-Rancheria (Cores LL-3E, ANH-La Loma-1) and Catatumbo basins (Core ECOPETROL-1) indicate low organic carbon concentrations ($\sim$0.8% for the calcareous Socuy Member, and $<$0.6% for fine-grained lithologies; Ayala-Calvo et al., 2009; Patarroyo et al., 2017; Avendaño-Sánchez et al., 2021).

5. Conclusions

The integrated micropaleontological (foraminifers, calcareous nannofossils, and ostracods) and geochemical (log (Zr/Rb), log (Fe/Ca), Sr/Ba ratios, and distribution of redox-sensitive trace metals Ni, Cu and V/Cr) analyses of the late Maastrichtian stratigraphic succession at Core Diablito-1 allowed us to recognize two paleoenvironmental scenarios for the Colón Formation: 1) A late Maastrichtian (regional foraminiferal zone *Siphogenerinoides bramletti*) inner platform setting, with mostly oxic-dysoxic bottom water conditions, and moderate continental runoff and input of terrigenous sediments; this interpretation is supported by the dominance of planktonic microfossils (*Guembelitria cretacea*, *Kamptnerius magnificus*) and calcareous benthic foraminifers (*Siphogenerinoides, Gavelinella*, among others), and low ostracod diversity; 2) shallower marine conditions for the latest Maastrichtian (regional foraminiferal zone *Ammobaculites colombiana*), with higher siliciclastic supply due to regional upliff events and enhanced continental runoff, and dysoxic bottom water conditions; this interval is characterized by the absence of planktonic microfossils, the dominance of agglutinated benthic foraminifers (*Ammobaculites*, *Haplophragmoides*, among others), and the occurrence of the ostracod families Cytherellidae and Trachyleberididae. Overall, micropaleontological and geochemical data (log (K/Fe), log (Fe/Ca) and Sr/Ba records) depict a shallowing upward trend for the studied interval of the Colón Formation. Given that northern South America was tectonically active during the Maastrichtian, it seems likely that the observed shallowing trend is mainly reflecting the earliest stages of uplift associated with the Andean orogeny.

Declaration of competing interest

The authors declare that they have no known competing financial interests or personal relationships that could have appeared to influence the work reported in this paper.

Data availability

Data will be made available on request.

Acknowledgments

We sincerely thank Drummond and Carlos Jaramillo (Smithsonian Tropical Research Institute) for providing the studied samples from Core

Diablito-1. G.D.P. thanks the PETROBRAS for a scholarship in the project "Bioestratigrafia de foraminíferos do Aptiano-Albiano da Margem Continental Brasileira". L.A. acknowledges funding from project PID 2019-105537RB-I00 (Spanish Ministry of Science and Innovation and FEDER funds). The authors thank the laboratory staff of itt-Oceaneon, Universidade do Vale do Rio dos Sinos (UNISINOS University). Gustavo Torres (Stratos Consultoría Geológica, Colombia) kindly assisted with the edition of the foraminiferal SEM images. Two anonymous reviewers provided key suggestions in order to improve the first version of this contribution, and to them we express our gratitude.

Appendix A. Supplementary data

Supplementary data to this article can be found online at https://doi.org/10.1016/j.jsames.2022.104015.

References

Abramovich, S., Yovel-Corem, S., Almogi-Labin, A., Benjamini, C., 2010. Global climate change and planktic foraminiferal response in the Maastrichtian. Paleoceanography 25, PA2201. https://doi.org/10.1029/2009PA001843.

Alegret, L., Molina, E., Thomas, E., 2001. Benthic foraminifera at the cretaceous- tertiary boundary around the Gulf of Mexico. Geology 29 (10), 891–894.

Alvarez, L.W., Alvarez, W., Asaro, F., Michel, H.V., 1980. Extraterrestrial cause for the Cretaceous-Tertiary extinction. Science 208, 1195-1108.

Andreu, B., 1991. Les Ostracodes du Crétacé moyen (Barrémien à Turonien), le long d'une transversale Agadir-Nador (Maroc). Strata Série 214 (2 volumes), 1–765.

Avendaño-Sánchez, G.M., García-González, M., Cruz-Guevara, L.E., Cruz-Ceballos, L.F., 2021. Geochemistry and petrographic analysis of los Cuervos and Molino formations, cesar sub-basin (Colombia): implications in the petroleum system evolution. Bol. Geol. 43 (2), 95–116.

Ayala-Calvo, R.C., Bayona-Chaparro, G.A., Ojeda-Marulanda, C., Cardona, A., Valencia, V., Padrón, C.E., Yoris, F., Mesa-Salamanca, J., García, A., 2009. Estratigrafía y procedencia de las unidades comprendidas entre el Campaniano y el Paleógeno en la subcuenca de Cesar: aportes a la evolución tectónica del área. Geol. Colomb. 34, 3–33.

Babinot, J.F., Colin, J.P., 1988. Paleobiogeography of Tethyan cretaceous marine ostracods. In: Hanai, T., Ikeya, N. (Eds.), Evolutionary Biology of Ostracoda, its Fundamentals and Applications, pp. 823–839.

Barrera, E., Savin, S.M., Thomas, E., Jones, C.E., 1997. Evidence for thermohaline circulation reversals controlled by sea-level change in the latest Cretaceous. Geology 25, 715–718.

Batenburg, S.J., Voigt, S., Friedrich, O., Osborne, A.H., Bornemann, A., Klein, T., Pérez-Díaz, L., Frank, M., 2018. Major intensification of Atlantic overturning circulation at the onset of Paleogene greenhouse warmth. Nat. Commun. 9, 1–8.

Bayona, G., 2018. El inicio de la emergencia en los Andes del norte: una perspectiva a partir del registro tectónico-sedimentológico del Coniaciano al Paleoceno. Rev. Acad. Col. Cien. Ex. Fís. Nat. 42 (165), 364–378.

Bayona, G., Baquero, M., Ramírez, C., Tabares, M., Salazar, A.M., Nova, G., Duarte, E., Pardo, A., Plata, A., Jaramillo, C., Rodríguez, G., Caballero, V., Cardona, A., Montes, C., Gómez-Marulanda, S., Cárdenas-Rozo, A.L., 2020. Unravelling the widening of the earliest Andean northern orogen: Maastrichtian to early Eocene intra-basinal deformation in the northern Eastern Cordillera of Colombia. Basin Res. 1–37.

Bayona, G., Montes, C., Cardona, A., Jaramillo, C., Ojeda, G., Valencia, V., 2011. Intraplate subsidence and basin filling adjacent to an oceanic arc-continental collision; a case from the southern Caribbean–South America plate margin. Basin Res. 23 https://doi.org/10.1111/j.1365-2117.2010.00495.x.

Beil, S., Kuhnt, W., Holbourn, A.E., Aquit, M., Flögel, S., Chellai, E.H., Jabour, H., 2018. New insights into Cenomanian paleoceanography and climate evolution from the Tarfaya Basin, southern Morocco. Cretac. Res. 84, 451–473.

Bermúdez, H.D., Arenillas, I., Arz, J.A., Vajda, V., Renne, P.R., Gilabert, V., Rodríguez, J. V., 2019. The cretaceous/paleogene boundary deposits on Gorgonilla Island. In: Gómez, J., Mateus–Zabala, D. (Eds.), The Geology of Colombia, Volume 3 Paleogene – Neogene. Servicio Geológico Colombiano, vol. 37. Publicaciones Geológicas Especiales, p. 19.

Bertels, A., 1975. Ostracod ecology during the upper cretaceous and cenozoic in Argentina. Bull. Am. Paleontol. 65 (282), 317–351.

Bolli, H.M., Beckmann, J.P., Saunders, J.B., 1994. Benthic Foraminiferal Biostratigraphy of the South Caribbean Region. Cambridge University Press, Cambridge, p. 411.

Bown, P.R., Young, J.R., 1988. Techniques. In: Bown, P.R. (Ed.), Calcareous Nannofossil Biostratigraphy. British Micropaleontological Society Series, pp. 16–28.

Bürgl, H., Dumit, Y., 1954. El Cretáceo Superior en la región de Girardot. Bol. Geol. 2, 23–48.

Calvert, S.E., Pedersen, T.F., 2007. Elemental proxies for palaeoclimatic and palaeoceanographic variability in marine sediments: interpretation and application. In: Hillaire-Marcel, C., De Vernal, A. (Eds.), Proxies in Late Cenozoic Paleoceanography, Developments in Marine Geology 1, 567–644.

Caron, M., 1985. Cretaceous planktic foraminifera. In: Bolli, H.M., Saunders, J., Perch-Nielsen, K. (Eds.), Plankton Stratigraphy, pp. 17–86.

Carvalho, M.R., Jaramillo, C., De La Parra, F., Caballero-Rodríguez, D., Herrera, F., Wing, S., Turner, B.L., D'Apolito, C., Romero-Báez, M., Narváez, P., Martínez, C., Gutierrez, M., Labandeira, C., Bayona, G., Rueda, M., Paez-Reyes, M., Cárdenas, D., Duque, A., Crowley, J.L., Santos, C., Silvestro, D., 2021. Extinction at the end-Cretaceous and the origin of modern Neotropical rainforests. Science 372, 63–68.

Castillo, M.V., Mann, P., 2006. Cretaceous to Holocene structural and stratigraphic development in south Lake Maracaibo, Venezuela, inferred from well and three-dimensional seismic data. AAPG (Am. Assoc. Pet. Geol.) Bull. 90 (4), 529–565.

Cetean, C.G., Bălc, R., Kaminski, M.A., Filipescu, S., 2011. Integrated biostratigraphy and palaeoenvironments of an upper Santonian – upper Campanian succession from the southern part of the Eastern Carpathians, Romania. Cretac. Res. 32 (5), 575–590.

Chiarenza, A.A., Farnsworth, A., Mannion, P.D., Lunt, D.J., Valdes, P.J., Morgan, J.V., Allison, P.A., 2020. Asteroid impact, not volcanism, caused the end-Cretaceous dinosaur extinction. Proc. Natl. Acad. Sci. USA 117 (29), 17084–17093.

Cooney, P.M., Lorente, M.A., 2009. A structuring event of Campanian age in western Venezuela, interpreted from seismic and paleontological data. Geol. Soc. Spec. Publ. 328, 687–703.

Cramer, B.S., Toggweiler, J., Wright, J.D., Katz, M.E., Miller, K.G., 2009. Ocean overturning since the Late Cretaceous: inferences from a new benthic foraminiferal isotope compilation. Paleoceanography 24 (4), PA4216. https://doi.org/10.1029/2008PA001683.

Culver, S.J., 2003. Benthic foraminifera across the Cretaceous–Tertiary (K–T) boundary: a review. Mar. Micropaleontol. 47, 177–226.

Cushman, J.A., Hedberg, H.D., 1930. Notes on some foraminifera from Venezuela and Colombia. Contribut. Cushman Lab. Foraminiferal Res. 6, 64–69.

Cushman, J.A., Hedberg, H.D., 1941. Upper Cretaceous foraminifera from Santander del Norte, Colombia. Contribut. Cushman Lab. Foraminiferal Res. 17, 79–100.

D'Hondt, S., 2005. Consequences of the Cretaceous/Paleogene mass extinction for marine ecosystems. Annu. Rev. Ecol. Evol. Syst. 36, 295–317.

D'Hondt, S., Arthur, M.A., 2002. Deep water in the late Maastrichtian ocean. Paleoceanography 17, 8–11.

Dameron, S., Leckie, M., Clark, K., Lees, J.A., 2017. Extinction, dissolution, and possible ocean acidification prior to the Cretaceous/Paleogene (K/Pg) boundary in the tropical Pacific. Palaeogeogr. Palaeoclimatol. Palaeoecol. https://doi.org/10.1016/j.palaeo.2017.06.032.

De La Parra, F., Jaramillo, C., Kaskes, P., Goderis, S., Claeys, P., Villasante-Marcos, V., Bayona, G., Hatsukawa, Y., Caballero, D., 2022. Unraveling the record of a tropical continental Cretaceous-Paleogene boundary in northern Colombia, South America. J. S. Am. Earth Sci. 114, 103717.

De Romero, L.M., Galea-Alvarez, F.A., 1995. Campanian *bolivinoides* and microfacies from Luna Formation, western Venezuela. Mar. Micropaleontol. 26 (1–4), 385–404.

De Romero, L., Truskowski, I., Bralower, T., Bergen, J.A., Odreman, O., Zachos, J.C., Galea-Alvarez, F.A., 2003. An integrated calcareous microfossil biostratigraphic and carbon-isotope stratigraphic framework for the La Luna Formation, western Venezuela. Palaios 18 (4/5), 349–366.

Drummond, L.T.D., 2007. Resumen de algunos aspectos estructurales y estratigráficos del Bloque La Loma. Informe técnico.

Dummann, W., Hofmann, P., Herrle, J.O., Wennrich, V., Wagner, T., 2021. A refined model of early cretaceous South Atlantic–Southern ocean gateway evolution based on high-resolution data from DSDP site 511 (falkland plateau). Palaeogeogr. Palaeoclimatol. Palaeoecol. 562, 110113.

Erlich, R.N., Macsotay, O., Nederbragt, A.J., Lorente, M.A., 1999. Palaeoecology, paleogeography and depositional environments of Upper Cretaceous rocks of western Venezuela. Palaeogeogr. Palaeoclimatol. Palaeoecol. 153 (1–4), 203–238.

Eshet, Y., Almogi-Labin, A., 1996. Calcareous nannofossil as paleoproductivity indicators in Upper Cretaceous organich rich sequences in Israel. Mar. Micropaleontol. 29, 37–61.

Eshet, Y., Moshkovitz, S., Habid, D., Benjamii, C., Magatitz, M., 1992. Calcareous nannofossil and dinoflagellate across the cretaceous/tertiary boundary at hor hahar, Israel. Mar. Micropaleontol. 18, 199–228.

Frenzel, P., 2000. Die benthischen Foraminiferen der Rügener Schreibkreide (unter Maastricht, NE Deutschland). In: Neue Paläontologischen Abhandlungen, vol. 3. C Press, Dresden, p. 361.

Friedrich, O., Herrle, J.O., Kößler, P., Hemleben, C., 2004. Early Maastrichtian stable isotopes: changing deep water sources in the North Atlantic? Palaeogeogr. Palaeoclimatol. Palaeoecol. 211, 171–184.

Frizzell, D.L., 1954. Handbook of Cretaceous Foraminifera of Texas. University of Texas Press, Austin, p. 232.

Gandolfi, R., 1955. The genus *Globotruncana* in northeastern Colombia. Bull. Am. Paleontol. 30 (155), 1–20.

Garzón, S., Warny, S., Bart, P.J., 2012. A palynological and sequence-stratigraphic study of Santonian–Maastrichtian strata from the Upper Magdalena Valley basin in central Colombia. Palynology 36, 112–133.

Georgescu, M.D., 2005. On the systematics of rugoglobigerinids (planktonic foraminifera, late Cretaceous). Stud. Geol. Pol. 124, 87–97.

Gertsch, B., Keller, G., Adatte, T., Berner, Z., 2013. The Cretaceous–Tertiary boundary (KTB) transition in NE Brazil. J. Geol. Soc. 170, 249–262.

Goderis, S., Sat, H., Ferriere, I., Schmitz, B., Burney, D., Kaskes, P., Vellekoop, J., Wittmann, A., Schultz, T., Chernonozhkin, S., Claeys, P., de Graff, S., Déhais, T., de Winter, N., Elfman, M., Feignon, J., Ishikawa, A., Koeberl, C., Kristiansson, P., Neal, C., Owens, J., Schmieder, M., Sinnesael, M., Vanhaecke, F., Van Malderen, S., Bralower, T., Gulick, S., Kring, D., Lowery, C., Morgan, J., Smit, J., Whalen, M., IODP-ICDP Expedition 364 Scientists, 2021. Globally distributed iridium layer preserved within the Chicxulub impact structure. Sci. Adv. 7, eabe3647.

Govin, A., Holzwarth, U., Heslop, D., Ford Keeling, L., Zabel, M., Mulitza, S., Collins, J. A., Chiessi, C.M., 2012. Distribution of major elements in Atlantic surface sediments

(36°N–49°S): imprint of terrigenous input and continental weathering. G-cubed 13, Q01013.
Gradstein, F.M., Ogg, J.G., Schmitz, M.D., Ogg, G.M., 2012. The Geological Time Scale 2012, vol. 2. Elsevier, Amsterdam, p. 1144.
Gramal-Aguilar, A., Carranco-Andino, F., Romero-Cóndor, C., Pulupa-Vela, R., Calderón-Romero, D., Toainga-Oñate, S., 2021. Evidencias de canibalización de secuencias Cretácicas y Paleógenas de la Cuenca Oriente en la cuña orogénica de los Andes ecuatorianos. Bol. Geol. 43 (3), 15–34.
Guerra, R.M., Concheyro, A., Kochhann, K.G.D., Bom, M.H.H., Ceolin, D., Musso, T., Savian, J.F., Fauth, G., 2021. Calcareous microfossils and paleoenvironmental changes across the cretaceous-paleogene (K-pg) boundary at the cerro azul section, Neuquén basin, Argentina. Palaeogeogr. Palaeoclimatol. Palaeoecol. 567, 110217.
Guerra, R.M., Concheyro, A., Wise, S.W., Fauth, G., 2016. Late campanian-maastrichtian *Kamptnerius magnificus* acme in the South atlantic section of the Southern ocean, ODP holes 690C and 700B. Micropaleontology 62 (3), 213–219.
Guerrero, J., Sarmiento, G., Navarrete, R.E., 2000. The stratigraphy of the W side of the cretaceous Colombian basin in the upper Magdalena valley. Reevaluation of selected areas and type localities including aipe, Guaduas, ortega, and piedras. Geol. Colomb. 25, 45–110.
Hammer, O., Harper, D.A.T., Ryan, P.D., 2001. PAST: paleontological statistics software package for education and data analysis. Palaeontol. Electron. 4 (1), 1–9.
Haq, B.U., 2014. Cretaceous eustasy revisited. Global Planet. Change 113, 44–45.
Huber, B.T., MacLeod, K.G., Watkins, D.K., Coffind, M.L., 2018. The rise and fall of the Cretaceous Hot Greenhouse climate. Global Planet. Change 167, 1–23.
Hull, P.M., Bornemann, A., Penman, D.E., Henehan, M.J., Norris, R.D., Wilson, P.A., Blum, P., Alegret, L., Batenburg, S.J., Bown, P.R., Bralower, T.J., Cournede, C., Deutsch, A., Donner, B., Friedrich, O., Jehle, S., Kim, H., Kroon, D., Lippert, P.C., Dominik Loroch, D., Moebius, I., Moriya, K., 20 Peppe, D.J., 21 Ravizza, G.E., Röhl, U., Schueth, J., Sepúlveda, J., Sexton, P.F., Sibert, E.C., Śliwińska, K.K., 28 Summons, R.E., Thomas, E., Westerhold, T., Whiteside, J.H., Tatsuhiko Yamaguchi, T., Zachos, J.C., 2020. On impact and volcanism across the Cretaceous-Paleogene boundary. Science 367, 266–272.
Jaramillo, C., De La Parra, F., 2005. Diablito 1E. Palynological Zonation, vol. 3. Informe Interno Drummond Ltd., Piedecuesta, Colombia.
Jorissen, F.J., Fontanier, C., Thomas, E., 2007. Paleoceanographical indicators based on deep-sea benthic foraminiferal assemblage characteristics. Dev. Marine Geol. 1, 263–325.
Juliao-Lemos, T., Carvalho, M., Torres, D., Plata, A., Parra, C., 2016. Paleoenvironmental reconstruction based on palynofacies analyses of the cansona formation (late cretaceous), sinú-san jacinto basin, northwest Colombia. J. S. Am. Earth Sci. 69, 103–118.
Jung, C., Koch, M.C., Voigt, S., Friedrich, O., 2013. Campanian-Maastrichtian ocean circulation in the tropical Pacific. Paleoceanography 28. https://doi.org/10.1002/palo.20051.
Keller, G., Abramovich, S., 2009. Lilliput effect in late Maastrichtian for foraminifera: response to environmental stress. Palaeogeogr. Palaeoclimatol. Palaeoecol. 284, 47–62.
Keller, G., Adatte, T., Tantawy, A.A., Berner, Z., Stinnesbeck, W., Stueben, D., Leanza, H. A., 2007. High stress late maastrichtian-early danian palaeoenvironment in the Neuquén basin, Argentina. Cretac. Res. 28, 939–960.
Keller, G., Mateo, P., Monkenbusch, J., Thibault, N., Punekar, J., Spangenberg, J.E., Abramovich, S., Ashckenazi-Polivoda, S., Schoene, B., Eddy, M.P., Samperton, K.M., Khadri, S.F.R., Adatte, T., 2020. Mercury linked to Deccan Traps volcanism, climate change and the end Cretaceous mass extinction. Global Planet. Change 194, 103312.
Kominz, M.A., Browning, J.V., Miller, K.G., Sugarman, P.J., Mizintsevaw, S., Scotese, C. R., 2008. Late Cretaceous to Miocene sea-level estimates from the New Jersey and Delaware coastal plain coreholes: an error analysis. Basin Res. 20, 211–226.
Koutsoukos, E.A.M., 2006. The cretaceous-paleogene boundary at the poty section, ne Brazil: foraminiferal record and sequence of events - a review. Anuário do Instituto de Geociências - UFRJ 29 (1), 95–107.
Koutsoukos, E.A.M., Merrick, K.A., 1986. Foraminiferal Paleoenvironments from the Barremian to Maastrichtian of Trinidad, West Indies. I Geological Conference of the Geological Society of Trinidad & Tobago, pp. 85–101.
Koutsoukos, E.A.M., Hart, M.B., 1990. Cretaceous foraminiferal morphogroup distribution patterns, paleocommunities and trophic structures: a case study from the Sergipe Basin, Brazil. Trans. R. Soc. Edinb. Earth Sci. 81, 221–246.
Krahl, G., Kochhann, K.G.D., Fauth, G., Sial, A.N., Lacerda, L.D., 2021. Evaluation of deep-water environmental conditions during the latest maastrichtian-early danian: insights from the western South Atlantic ocean. J. S. Am. Earth Sci. 112, 103630.
Kujau, A., Nürnberg, D., Zielhofer, C., Bahr, A., Röhl, U., 2010. Mississippi River discharge over the last ~560,000 years — indications from X-ray fluorescence core scanning. Palaeogeogr. Palaeoclimatol. Palaeoecol. 298, 311–318.
Ladant, J.-B., Poulsen, C.J., Fluteau, F., Tabor, C.R., MacLeod, K.J., Martin, E.L., Haynes, S.J., Rostami, M.A., 2020. Paleogeographic controls on the evolution of Late Cretaceous ocean circulation. Clim. Past. https://doi.org/10.5194/cp-2019-157.
Leckie, R.M., Olson, H.C., 2003. Foraminifera as proxies for sea-level change on siliciclastic margins. In: Olson, H.C., Leckie, R.M. (Eds.), Micropaleontologic Proxies for Sea-Level Change and Stratigraphic Discontinuities, vol. 75. SEPM Special Publication, pp. 5–19.
Lees, J.A., 2002. Calcareous nannofossil biogeography illustrates palaeoclimate change in the Late Cretaceous Indian Ocean. Cretac. Res. 23, 537–634.
Linnert, C., Engelke, J., Wilmsen, M., Mutterlose, J., 2019. Environmental footprints of the early Maastrichtian cooling – the record of benthic foraminifera from northern Germany. Cretac. Res. 97, 143–159.
Linnert, C., Robinson, S.A., Lees, J.A., Bown, P.R., Pérez-Rodríguez, I., Petrizzo, M.J., Falzoni, F., Littler, K., Arz, J.A., Russell, E.E., 2014. Evidence for global cooling in the late cretaceous. Nat. Commun. 5, 4194.
Lyle, M., Olivarez-Lyle, A., Gorgas, T., Holbourn, A., Westerhold, T., Hathorne, E.C., Kimoto, K., Yamamoto, S., 2012. Data report: raw and normalized elemental data along the U1338 splice from X-ray Fluorescence scanning. In: Proceedings of the Integrated Ocean Drilling Program, pp. 320–321. https://doi.org/10.2204/iodp.proc.320321.2010.
Malumián, N., 2010. Foraminíferos del Cretácico superior del Pozo Perijá-2. Informe Interno, vol. 21p. Instituto Colombiano del Petróleo. Grupo de Bioestratigrafía, Piedecuesta, Colombia.
Martínez, R.J.I., 1989. Foraminiferal biostratigraphy and paleoenvironments of the maastrichtian Colón mudstones of northern South America. Micropaleontology 35 (2), 97–113.
Martínez, J.I., 2003. The paleoecology of late cretaceous upwelling events from the upper Magdalena basin, Colombia. Palaios 18 (4–5), 305–320.
Martinez, J.I., Hernandez, R., 1992. Evolution and drowning of the Late Cretaceous Venezuelan carbonate platform. J. S. Am. Earth Sci. 5 (2), 197–210.
MacLeod, K.G., Huber, B.T., 1996. Reorganization of deep ocean circulation accompanying a Late Cretaceous extinction event. Nature 380, 422–425.
MacLeod, K.G., Whitney, D.L., Huber, B.T., Koeberl, K., 2017. Impact and extinction in remarkably complete Cretaceous-Tertiary boundary sections from Demerara Rise, tropical western North Atlantic. GSA Bulletin 119 (1–2), 101–115.
Mesa, A.M., Rengifo, S., 2011. Cesar-Rancheria basin. In: Cediel, F., Colmenares, F. (Eds.), Petroleum Geology of Colombia Volume 6. ANH-Fondo Editorial Universidad EAFIT.
Montaño, P.C., Nova, G., Bayona, G., Mahecha, H., Ayala, C., Jaramillo, C., De La Parra, F., 2016. Análisis de secuencias y procedencia en sucesiones sedimentarias de grano fino: un ejemplo de la Formación Umir y base de la Formación Lisama, en el sector de Simacota (Santander, Colombia). Bol. Geol. 38 (1), 51–72.
Montes, C., Rodríguez-Corcho, A.F., Bayona, G., Hoyos, N., Zapata, S., Cardona, A., 2019. Continental margin response to the multiple arc-continent collisions: the northern Andes-Caribbean margin. Earth Sci. Rev. 198, 102903.
Mora, A., Garcia, A., 2006. Cenozoic tectono-stratigraphic relationships between the cesar subbasin and the southeastern lower Magdalena valley basin of northern Colombia. AAPG, Search and Discovery 30046, 1–11.
Morón, S., Fox, D.L., Feinberg, J.M., Jaramillo, C., Bayona, G., Montes, C., Bloch, J.I., 2013. Climate change during the Early Paleogene in the Bogotá Basin (Colombia) inferred from paleosol carbon isotope stratigraphy, major oxides, and environmental magnetism. Palaeogeogr. Palaeoclimatol. Palaeoecol. 388, 115–127.
Murray, J.W., Alve, E., Jones, B.W., 2011. A new look at modern agglutinated benthic foraminiferal morphogroups: their value in palaeoecological interpretations. Palaeogeogr. Palaeoclimatol. Palaeoecol. 309 (3–4), 229–241.
Navarrete, R.E., Parra, F.J., Pérez-Panera, J.P., Daza, D., Sánchez, C., Prince, M., Rodríguez, M., 2018. Turonian-campanian foraminifera zonation for the La Luna and lower Umir formations, middle Magdalena valley basin, northern Colombia. In: Cusminski, et al. (Eds.), Advances in South American Micropaleontology - Selected Papers of the 11th Argentine Paleontological Congress. Springer Earth System Science Series, pp. 67–114.
Neale, J.W., 1975. The ostracod fauna of the santonian chalk (upper cretaceous) of gingin, western Australia. Spe. Papers in Paleontol. 16, 1–111.
Nederbragt, A., 1991. Late Cretaceous biostratigraphy and development of Heterohelicidae (planktic foraminifera). Micropaleontology 37 (4), 329–372.
Notestein, F., Hubman, C., Bowler, J., 1944. Geology of the barco concession, republic of Colombia, south America. Bull. Geol. Soc. Am. 55 (10), 1165–1216.
O'Brien, C.L., Robinson, S.A., Pancost, R.D., Sinninghe Damstéd, J.S., Schouten, S., Lunt, D.J., Alsenz, H., Bornemann, A., Bottini, C., Brassell, S.C., Farnsworth, A., Forster, A., Huber, B.T., Inglis, G.N., Jenkyns, H.C., Linnert, C., Littler, K., Markwick, P., McAnenao, A., Mutterlose, J., Naafs, B.D.A., Püttmann, W., Sluijse, A., van Helmond, N.A.G.M., Vellekoop, J., Wagner, T.7, Wrobel, N.E., 2017. Cretaceous sea-surface temperature evolution: constraints from TEX_{86} and planktonic foraminiferal oxygen isotopes. Earth Sci. Rev. 172, 224–247.
Parra, M., Moscardelli, L., Lorente, M.A., 2003. Late cretaceous anoxia and lateral microfacies changes in the Tres Esquinas member, La Luna Formation, western Venezuela. Palaios 18, 321–333.
Patarroyo, G.D., Torres, G.A., Rincón, D.A., Cárdenas, C.P., Márquez, R.E., 2017. Bioestratigrafía e inferencias paleoambientales de las asociaciones de foraminíferos en las formaciones cretácicas La Luna-Colón (Cuenca del Catatumbo, Colombia). Bol. Geol. 39 (3), 25–40.
Pedraza, P., Ramírez, Y., 2011. Catatumbo basin. In: Cediel, F., Colmenares, F. (Eds.), Petroleum Geology of Colombia, ume 5. ANH-Fondo Editorial Universidad EAFIT.
Petersen, S.V., Dutton, A., Lohmann, K.C., 2016. End-Cretaceous extinction in Antarctica linked to both Deccan volcanism and meteorite impact via climate change. Nat. Commun. https://doi.org/10.1038/ncomms12079.
Petters, V., 1955. Development of upper cretaceous foraminiferal faunas in Colombia. J. Paleontol. 29 (2), 212–225.
Piva, A., Asioli, A., Schneider, R.R., Trincardi, F., Andersen, N., Colmenero-Hidalgo, E., Dennillou, B., Flores, J.A., Vigliotti, L., 2008. Climatic cycles as expressed in sediments of the PROMESS1 borehole PRAD1-2, central Adriatic, for the last 370 ka. G-cubed 9 (1), 1–21.
Pospichal, J.J., 1996. Calcareous nannofossils and clastic sediments at the Cretaceous-Tertiary boundary, northeastern Mexico. Geology 24 (3), 255–258.
Puckett, T.M., Andreu, B., Colin, J.P., 2016. The evolution of the Brachycytheride ostracoda in the context of the breakup of Pangea. Rev. Micropaleontol. 59 (2), 97–167.

Punekar, J., Mateo, P., Keller, G., 2014. Effects of Deccan volcanism on paleoenvironment and planktic foraminifera: a global survey. In: Keller, G., Kerr, A. C. (Eds.), Volcanism, Impacts, and Mass Extinctions: Causes and Effects, vol. 505. Geological Society of America Special Paper, pp. 91–116.
Premoli Silva, I., Verga, D., 2011. Practical manual of Cretaceous planktonic foraminifera. In: New Editing by Marie Rose Petrizzo and Isabella Premoli Silva. International School on Planktonic Foraminifera 3rd Course: Cretaceous Planktonic Foraminifera, pp. 1–265.
Ray, D.C., van Buchem, F.S.P., Baines, G., Davies, A., Gréselle, B., Simmons, M.D., Robson, C., 2019. The magnitude and cause of short-term eustatic Cretaceous sea-level change: a synthesis. Earth Sci. Rev. 197, 102901.
Restreppo, G.A., Wood, W.T., 2 Phrampus, B.J., 2020. Oceanic sediment accumulation rates predicted via machine learning algorithm: towards sediment characterization on a global scale. Geo Mar. Lett. 40, 755–763.
Richards, M.A., Alvarez, W., Self, S., Karlstrom, L., Renne, P.R., Manga, M., Sprain, C.J., Smit, J., Vanderkluysen, L., Gibson, S.A., 2015. Triggering of the largest Deccan eruptions by the Chicxulub impact. Geol. Soc. Am. Bull. https://doi.org/10.1130/B31167.1.
Rivera, H.A., Le Roux, J.P., Sánchez, L.K., Mariño-Martínez, J.E., Salazar, C., Barragán, J. C., 2018. Palaeoredox conditions and sequence stratigraphy of the Cretaceous storm-dominated, mixed siliciclastic-carbonate ramp in the Eastern Cordillera Basin (Colombia): evidence from sedimentary geochemical proxies and facies analysis. Sediment. Geol. 372, 1–24.
Roth, P.H., 1983. Jurassic and Lower Cretaceous calcareous nannofossils in the Western North Atlantic (Site 534): biostratigraphy, preservation and some observations on biogeography and paleoceanography. Init. Rep. DSDP 76, 587–621.
Roth, P.H., Thierstein, H., 1972. Calcareous nannoplankton: leg 14 of the deep sea drilling project. Init. Rep. DSDP 14, 421–485.
Santos, A., De Lira Mota, M.A., Kern, H.P., Fautha, G., Paim, P.S.G., Netto, R.G., Sedorko, D., Lavina, E.L.C., Krahl, G., Fallgatter, C., Silveira, D.M., Aquino, C.D., Santos, M.O., Baecker-Fauth, S., Vieira, C.E.L., 2022. Earlier onset of the early cretaceous equatorial humidity belt. Global Planet. Change 208, 103724.
Santos-Filho, M.A.B., Fauth, G., Piovesan, E.K., 2017. Cretaceous ostracods of the Barreirinhas Basin: biostratigraphic considerations and paleoenvironmental inferences. J. S. Am. Earth Sci. 73, 130–152.
Sarmiento, G., 1994. Estratigrafía, palinología y paleoecología de la Formación Guaduas (Maastrichtiano–Paleoceno). Boletín Geológico. Publicación Especial 20.
Sarmiento-Rojas, L.F., 2019. Cretaceous stratigraphy and paleo-facies maps of northwestern South America. In: Cediel, F., Shaw, R.P. (Eds.), Geology and Tectonics of Northwestern South America. The Pacific Caribbean Andean Junction, pp. 673–747.
Schoene, B., Eddy, M.P., Samperton, K.M., Keller, C.B., Keller, G., Adatte, T., Khadri, S.F., 2019. U-Pb constraints on pulsed eruption of the Deccan Traps across the end-Cretaceous mass extinction. Science 363, 862–866.
Schulte, P., Alegret, L., Arenillas, I., Arz, J.A., Barton, P.J., Bown, P.R., Bralower, T.J., Christeson, G.L., Claeys, P., Cockell, C.S., Collins, G.S., Deutsch, A., Goldin, T.J., Goto, K., Grajales-Nishimura, J.M., Grieve, R.A.F., Gulick, S.P.S., Johnson, K.R., Kiessling, W., Koeberl, C., Kring, D.A., Macleod, K.G., Matsui, T., Melosh, J., Montanari, A., Morgan, J.V., Neal, C.R., Nichols, D.J., Norris, R.D., Pierazzo, E., Ravizza, G., Rebolledo-Vieyra, M., Reimold, W.U., Robin, E., Salge, T., Speijer, R.P., Sweet, A.R., Urrutia-Fucugauchi, J., Vajda, V., Whalen, M.T., Willumsen, P.S., 2010. The Chicxulub asteroid impact and mass extinction at the Cretaceous-Paleogene boundary. Science 327, 5970.
Scott, H.W., 1961. Classification of ostracoda. Q74-Q91. In: Moore, R.C., Pitrat, C.W. (Eds.), Treatise on Invertebrate Paleontology, Part Q, Arthropoda 3: Crustacea, Ostracoda. Geological Society of America and University of Kansas Press, p. 465.
Sellier de Civrieux, J.M., 1952. Estudio de la microfauna de la sección-tipo del Miembro Socuy de la Formación Colón, Distrito Mara, Estado Zulia. Boletín de Geología y Minas (Venezuela) 2 (5), 231–310.
Simonson, B.M., Glass, B.P., 2004. Spherule layers: records of ancient impacts. Annu. Rev. Earth Planet Sci. 32, 329–361.
Sohn, I.G., 1961. Techniques for preparation and study of fossil ostracodes. In: Moore, R. (Ed.), Treatise on Invertebrate Paleontology, Part Q, Arthropod 3. Crustacea Ostracoda. Geological Society of America and University of Kansas Press, pp. Q63–Q70.
Sprain, G.A., Renne, P.R., Vanderkluysen, L., Pande, K., Self, S., Mittal, T., 2019. The eruptive tempo of Deccan volcanism in relation to the Cretaceous-Paleogene boundary. Science 363, 866–870.
Strasser, A., Samankassou, E., 2003. Carbonate sedimentation rates today and in the past: holocene of Florida bay, Bahamas, and Bermuda vs. Upper jurassic and lower cretaceous of the jura mountains (Switzerland and France). Geologica Croatica 56 (1), 1–18.
Sutton, F.A., 1946. Geology of Maracaibo basin, Venezuela. Bull. Am. Assoc. Petrol. Geol. 30 (10), 1621–1739.
Tantawi, A.A., 2011. Calcareous nannofossils across the Cretaceous-Tertiary boundary at Brazos, Texas, USA: extinction and survivorship, biostratigraphy and paleoecology. In: Keller, G., Adatte, T. (Eds.), The End Cretaceous Mass Extinctions and the Chixculub Impact in Texas, vol. 10. SEPM Special Publications, pp. 157–178.
Tchegliakova, N., 1993. Los foraminíferos y los minerales antigénicos de la Formación Umir (sección Quebrada La Julia, Valle Medio del Magdalena): registro de laguna costera a finales del Cretácico Superior cuspidal (Maastrichtiano). Geol. Colomb. 18, 107–117.
Tchegliakova, N., 1995. Los Foraminíferos de la Formación Umir (Sección Quebrada La Julia): registro del Cretáceo Superior Cuspidal (Maestrichtiano) en el Valle Medio del Magdalena, Colombia. Geol. Colomb. 19, 109–130.
Tchegliakova, N., 1996. Registro de las biozonas de foraminíferos planctónicos *Gansserina gansseri* y *Abathomphalus mayaroensis* (Maastrichtiano medio y superior) en el extremo meridional del Valle Medio del Magdalena (Colombia, Suramérica). Geol. Colomb. 20, 67–90.
Tchegliakova, N., Mojica, J., 2001. El Senoniano de la barrera de Girardot-Guataquí, Valle Alto del Magdalena, Colombia: precisiones sobre la estratigrafía y establecimiento de una zonación micropaleontológica. Rev. Acad. Col. Cienc. Ex., Fís. Nat. 25 (94), 37–75.
Thibault, N., Husson, D., 2016. Climate fluctuations and sea-surface water circulation patterns at the end of the Cretaceous era: calcareous nannofossil evidence. Palaeogeogr. Palaeoclimatol. Palaeoecol. 441 (1), 152–164.
Tyson, R.V., Pearson, T.H., 1991. Modern and ancient continental shelf anoxia: an overview. In: Tyson, R.V., Pearson, T.H. (Eds.), Modern and Ancient Continental Shelf Anoxia, vol. 58. Geological Society of London, Special Publication, pp. 1–24.
Vancoppenolle, I., Vellekoop, J., Doubrawa, M., Kaskes, P., Sinnesael, M., Jagt, J.W.M., Claeys, P., Speijer, R.P., 2022. The benthic foraminiferal response to the mid Maastrichtian event in the NW-European chalk sea of the Maastrichtian type area. Neth. J. Geosci. 101, e12. https://doi.org/10.1017/njg.2022.10.
Van Morkhoven, F.P.C.M., 1963. Post-palaeozoic Ostracoda: Their Morphology, Taxonomy and Economic Use, vol. 2. Elsevier Publishing Company, p. 478.
Valencia-Gómez, J.C., Cardona, A., Bayona, G., Valencia, V., Zapata, S., 2020. Análisis de procedencia del registro sin-orogénico Maastrichtiano de la Formación Cimarrona, flanco Occidental de la Cordillera Oriental colombiana. Bol. Geol. 42 (3), 171–204.
Van der Akker, T.J.H.A., Kaminski, M.A., Gradstein, F.M., Wood, J., 2000. Campanian to palaeocene biostratigraphy and palaeoenvironments in the foula sub-basin, west of the shetland islands, UK. J. Micropalaeontol. 19, 23–43.
Vellekoop, J., Kaskes, P., Sinnesael, M., Huygh, J., Déhais, T., Jagt, J.W.M., Speijer, R.P., Claeys, P., 2022. A new age model and chemostratigraphic framework for the Maastrichtian type area (southeastern Netherlands, northeastern Belgium). Newsl. Stratigr. 4, 479–501.
Veloza, G.E., Mora, A., De Freitas, M., Mantilla, M., 2008. Dislocación de facies en el tope de la secuencia cretácica de la Subcuenca de Neiva, Valle Superior del Magdalena y sus implicaciones en el Modelo estratigráfico secuencial colombiano. Bol. Geol. 30 (1), 29–44.
Vergara, L.S., 1997. Stratigraphy, foraminiferal assemblages and paleoenvironments in the late cretaceous of the upper Magdalena valley, Colombia (Part I). J. S. Am. Earth Sci. 10 (2), 111–132.
Villamil, T., 1998. Chronology, relative sea level history and a new sequence stratigraphic model for basinal Cretaceous Facies of Colombia. In: Pindell, J.L., Drake, C. (Eds.), Paleogeographic Evolution and Non-glacial Eustacy, Northern South America, vol. 58. SEPM Society for Sedimentary Geology, pp. 161–216.
Villamil, T., Arango, C., Hay, W.W., 1999. In: Barrera, E., Johnson, C.C. (Eds.), Plate Tectonic Paleoceanographic Hypothesis for Cretaceous Source Rocks and Cherts of Northern South America, vol. 332. Geological Society of America, Special papers, pp. 191–202.
Villamil, T., Pindell, J., 1998. Mesozoic paleogeographic evolution of northern South America. In: Pindell, J., Drake, C. (Eds.), Paleogeographic Evolution and Non-glacial Eustacy, Northern South America, vol. 58. SEPM Society for Sedimentary Geology, pp. 238–318.
Voigt, S., Gale, A.S., Jung, C., Jenkyns, H.C., 2012. Global correlation of Upper Campanian-Maastrichtian successions using carbon-isotope stratigraphy: development of a new Maastrichtian timescale. Newsl. Stratigr. 45 (1), 25–53.
Watkins, D.K., Self-Trail, J.M., 2005. Calcareous nannofossil evidence for the existence of the Gulf stream during the maastrichtian. Paleoceanography 20, PA3006.
Wei, W., Algeo, T., 2020. Elemental proxies for paleosalinity analysis of ancient shales and mudrocks. Geochem. Cosmochim. Acta 287, 341–366.
Wind, F.H., 1979. Maastrichtian-Campanian nannofloral provinces of the Southern Atlantic and Indian oceans. In: Talwani, M., Hay, W., Ryan, W.B.F. (Eds.), Deep Sea Drilling Results in the Atlantic Ocean: Continental Margins and Paleoenvironment, pp. 123–137.
Yelwa, N.A., Mustapha, K.A., Opuwari, M., Aziz, A.A., 2022. Biomarkers, stable carbon isotope, and trace element distribution of source rocks in the Orange Basin, South Africa: implications for paleoenvironmental reconstruction, provenance, and tectonic setting. J. Pet. Explor. Prod. Technol. 12, 307–339.
Yepes, O., 2001. Maastrichtian/Danian dinoflagellate cyst biostratigraphy and biogeography from two equatorial sections in Colombia and Venezuela. Palynology 25, 217–249.

… Nada do que foi será

De novo do jeito que já foi um dia

Tudo passa, tudo sempre passará

… A vida vem em ondas

Como um mar

Num indo e vindo infinito

Como uma onda no mar

Lulu Santos / Nelson Motta

CHAPTER 2

MICROFOSSILS OF THE SHALLOW MARINE UMIR FORMATION, NORTHEASTERN COLOMBIA

Contribution roles taxonomy

German David Patarroyo (itt Oceaneon, Unisinos University). Micropaleontological and geochemical preparation. Foraminiferal taxonomy and geochemical analyses. Integration and discussion of results.

Karlos Kochhann (itt Oceaneon, Unisinos University). Foraminiferal, geochemical and paleoecological discussions.

Rodrigo M. Guerra (itt Oceaneon, Unisinos University). Calcareous nannofossils taxonomy and ecology.

Laia Alegret (Zaragoza University). Benthic foraminiferal ecology and taxonomic comments. Paleoecological discussions.

Daiane Ceolin (itt Oceaneon, Unisinos University). Ostracod taxonomy and ecology.

José Manuel Torres (Florida International University). Field support at the Aguablanca Creek section.

Article published at: Ameghiniana, 60 (4), 297-311. Special Issue "Gondwanan Perspectives: Mesozoic and Cenozoic Micropaleontology of South America, progresses and applications"

https://doi.org/10.5710/AMGH.02.03.2023.3525

Submitted: 21 June 2022 - Accepted: 2 March 2023 - Published: 23 June 2023.

AMEGHINIANA
A GONDWANAN PALEONTOLOGICAL JOURNAL

MAASTRICHTIAN MICROFOSSILS OF THE SHALLOW MARINE UMIR FORMATION, NORTHEASTERN COLOMBIA

GERMAN D. PATARROYO[1,2]
KARLOS G. D. KOCHHANN[1,2]
RODRIGO M. GUERRA[2,3]
LAIA ALEGRET[4]
DAIANE CEOLIN[2]
JOSÉ M. TORRES[5]

[1]Programa de Geologia, Universidade do Vale do Rio dos Sinos, Avenida Unisinos, 950, CP 93.022-970 São Leopoldo, RS, Brazil. germanp@edu.unisinos.br
[2]Instituto Tecnológico de Paleoceanografia e Mudanças Climáticas (itt Oceaneon), Universidade do Vale do Rio dos Sinos (UNISINOS) 950, CP 93.022-970 São Leopoldo, RS, Brazil.
[3]Museu Itinerante de Ciências Naturais. CP 95.185-000, Carlos Barbosa, RS, Brazil.
[4]Departamento de Ciencias de la Tierra & IUCA, Universidad de Zaragoza, Pedro Cerbuna 12, 50009 Zaragoza, Spain.
[5]Department of Earth and Environment, Florida International University, 11200 SW 8th St, Miami, FL, USA.

Submitted: 21 June 2022 - **Accepted:** 2 March 2023 - **Published:** 23 June 2023

To cite this article: German D. Patarroyo, Karlos G. D. Kochhann, Rodrigo M. Guerra, Laia Alegret, Daiane Ceolin, and José M. Torres (2023). Maastrichtian microfossils of the shallow marine Umir Formation, Northeastern Colombia. *Ameghiniana 60*(4), 297–311.

To link to this article: http://dx.doi.org/10.5710/AMGH.02.03.2023.3525

ISSN 0002-7014
AMEGHINIANA - 2023 - Volume 60(4): 297–311

MAASTRICHTIAN MICROFOSSILS OF THE SHALLOW MARINE UMIR FORMATION, NORTHEASTERN COLOMBIA

GERMAN D. PATARROYO[1,2], KARLOS G. D. KOCHHANN[1,2], RODRIGO M. GUERRA[2,3], LAIA ALEGRET[4], DAIANE CEOLIN[2], AND JOSÉ M. TORRES[5]

[1]Programa de Geologia, Universidade do Vale do Rio dos Sinos, Avenida Unisinos, 950, CP 93.022-970 São Leopoldo, RS, Brazil. *germanp@edu.unisinos.br*

[2]Instituto Tecnológico de Paleoceanografia e Mudanças Climáticas (itt Oceaneon), Universidade do Vale do Rio dos Sinos (UNISINOS) 950, CP 93.022-970 São Leopoldo, RS, Brazil. *kkochhann@unisinos.br*; *rmguerra@unisinos.br*; *daiaceolin@unisinos.br*

[3]Museu Itinerante de Ciências Naturais. CP 95.185-000, Carlos Barbosa, RS, Brazil.

[4]Departamento de Ciencias de la Tierra & IUCA, Universidad de Zaragoza, Pedro Cerbuna 12, 50009 Zaragoza, Spain. *laia@unizar.es*

[5]Department of Earth and Environment, Florida International University, 11200 SW 8th St, Miami, FL, USA. *manutorresgeo@gmail.com*

Abstract. During the Late Cretaceous, northern South America was characterized by broad epicontinental seas, with variable surface productivity and changing bottom-water oxygenation. Global sea-level fluctuations and local tectonic shifts caused their disappearance in the latest Cretaceous. We present an integrated micropaleontological and geochemical study of a section comprising the Umir Formation and its lower stratigraphic contact with the La Luna Formation, in the Middle Magdalena Valley, northeastern Colombia. Foraminiferal assemblages were moderately diverse and mainly dominated by benthic taxa, characterizing the biozones *Siphogenerinoides bramlettei* and *Ammobaculites colombiana* (Maastrichtian). Planktonic foraminiferal assemblages were less diversified, being species assigned to Heterohelicidae and scarce keeled forms (*Globotruncana* spp.) the most recurrent taxa. Ostracod recovery was very scarce, and we could only identify the genus *Actinocythereis*. In contrast, calcareous nannofossil assemblages were moderately diversified along the section, and composed of typical Late Cretaceous low-latitude taxa such as *Micula staurophora, Cribrosphaerella ehrenbergii, Gartnerago segmentatum*. The identified microfossils indicate a transition from middle-inner shelf conditions, with moderately oxygenated bottom waters within the La Luna Formation, to a shallower marine setting within the Umir Formation. This interpretation is supported by Sr/Ba and log(Fe/Ca) ratios measured in bulk sediment, which indicate increased continental runoff and terrigenous input in the upper part of the section. Moreover, a significant biotic turnover was identified at the base of the section, suggesting the presence of a xenoconformity at the La Luna-Umir contact, which has been previously described and proposed as a regional stratigraphic feature.

Key words. Paleoenvironments. Late Cretaceous. Colombia. Micropaleontology.

Resumen. MICROFÓSILES DEL MAASTRICHTIANO EN AMBIENTES MARINOS SOMEROS DE LA FORMACIÓN UMIR (NORESTE DE COLOMBIA). El Cretácico Tardío del norte de Sudamérica estuvo dominado por mares epicontinentales extensos, con fluctuaciones de la productividad superficial y oxigenación del agua de fondo. Cambios en los regímenes tectónicos locales y descensos globales en el nivel del mar, llevaron a la desaparición de dichos ambientes hacia fines del Cretácico. Presentamos un estudio micropaleontológico y geoquímico integrado de una sección de la Formación Umir y su contacto basal con la Formación La Luna en el Valle Medio del Magdalena, noreste de Colombia. Las asociaciones de foraminíferos fueron moderadamente diversas y estuvieron dominadas por formas bentónicas que definen las biozonas de asociación locales *Siphogenerinoides bramlettei* y *Ammobaculites colombiana* (Maastrichtiano). Las formas planctónicas, menos diversas, incluyeron ejemplares de Heterohelicidae y escasas formas quilladas (*Globotruncana* spp.). El registro de ostrácodos fue muy escaso, sólo pudimos reconocer al género *Actinocythereis*. En contraste, las asociaciones de nanofósiles calcáreos fueron moderadamente diversas y comprendieron formas típicas de bajas latitudes del Cretácico Tardío como *Micula staurophora*, *Cribrosphaerella ehrenbergii*, *Gartnerago segmentatum*. Las asociaciones de microfósiles indican una transición de condiciones de plataforma media-interna, moderadamente oxigenada en la Formación La Luna, a un ambiente más somero en la Formación Umir. Esta interpretación es corroborada por las relaciones de Sr/Ba y log(Fe/Ca) del sedimento que indican un aumento en la escorrentía continental y el aporte de terrígenos hacia la parte superior de la sección. De igual forma, la variación significativa en las asociaciones de microfósiles hacia la base sugiere la presencia de una xenoconformidad en el contacto La Luna-Umir, que fue previamente reportada como de carácter regional.

Palabras clave. Paleoambientes. Cretácico Tardío. Colombia. Micropaleontología.

NORTHERN SOUTH AMERICA underwent a series of geological reorganizations at the end of the Mesozoic era. For instance, the onset of the Andean orogeny likely occurred during the Campanian–Maastrichtian, causing significant shifts of regional sedimentary regimes, in progressively shallowing widespread epicontinental seas, with high surface productivity and the occurrence of recurrent anoxic episodes (Martínez & Hernandez, 1992; Villamil & Pindell, 1998; Erlich *et al*., 1999;

AMGHB2-0002-7014/12$00.00+.50

Sarmiento-Rojas, 2019; Montes *et al.*, 2019; Bayona *et al.*, 2020). In addition, the latest Cretaceous was characterized by a global sea-level fall, which has been associated with the possible occurrence of intermittent ice sheets at high latitudes (Hardenbol *et al.*, 1998; Kominz *et al.*, 2008; Huber *et al.*, 2018). Consequently, Campanian–Maastrichtian sedimentary successions of northern South America record a myriad of tectonic (basin deformation, local uplifts), stratigraphic (xenoconformities, diachronism of units), and sedimentary (abrupt lateral facies shifts, retrogradational stacking) features that make their depositional evolution highly complex (Ayala-Calvo *et al.*, 2009; Bayona *et al.*, 2011, 2020; Sarmiento *et al.*, 2015; Montaño *et al.*, 2016; Sarmiento-Rojas, 2019; Terraza, 2019; Valencia-Gómez *et al.*, 2020; Gramal-Aguilar *et al.*, 2021).

Marine microfossils have enabled paleoenvironmental reconstructions and chronostratigraphic constraints of the Upper Cretaceous sedimentary successions of northern South America (Bürgl & Dummit, 1954; Petters, 1955; Sole de Porta, 1972; Martínez, 1989, 2003; Sarmiento, 1992; Vergara, 1997; Guerrero *et al.*, 2000; Yepes, 2001; Tchegliakova & Mojica, 2001; Garzón *et al.*, 2012; Patarroyo *et al.*, 2017, 2022; Carvalho *et al.*, 2021; De La Parra *et al.*, 2022). This is the case for the Maastrichtian Umir Formation, cropping out in the Middle Magdalena Valley (MMV), northeastern Colombia (Fig. 1), where depositional and chronostratigraphic interpretations have been traditionally based on microfossils, and eventually, integrated with sedimentological studies (Tchegliakova, 1993, 1995, 1996; Santos, 2012; Montaño *et al.*, 2016; Navarrete *et al.*, 2018; Terraza, 2019). However, since most of these studies have focused on economically relevant coal-bearing strata of the middle and upper part of this unit, there is still debate on whether the lower part of the Umir Formation was deposited in a marine setting, and on the nature of its boundary with the underlying La Luna Formation. Previous works suggested the presence of an unconformity or a condensed section between the La Luna and Umir formations, as well as in coeval units in more proximal areas, such as in the Catatumbo and Cesar-Rancheria basins (Ward *et al.*, 1973; Sarmiento *et al.*, 2015; Terraza, 2019).

Here we present a micropaleontological (foraminifers,

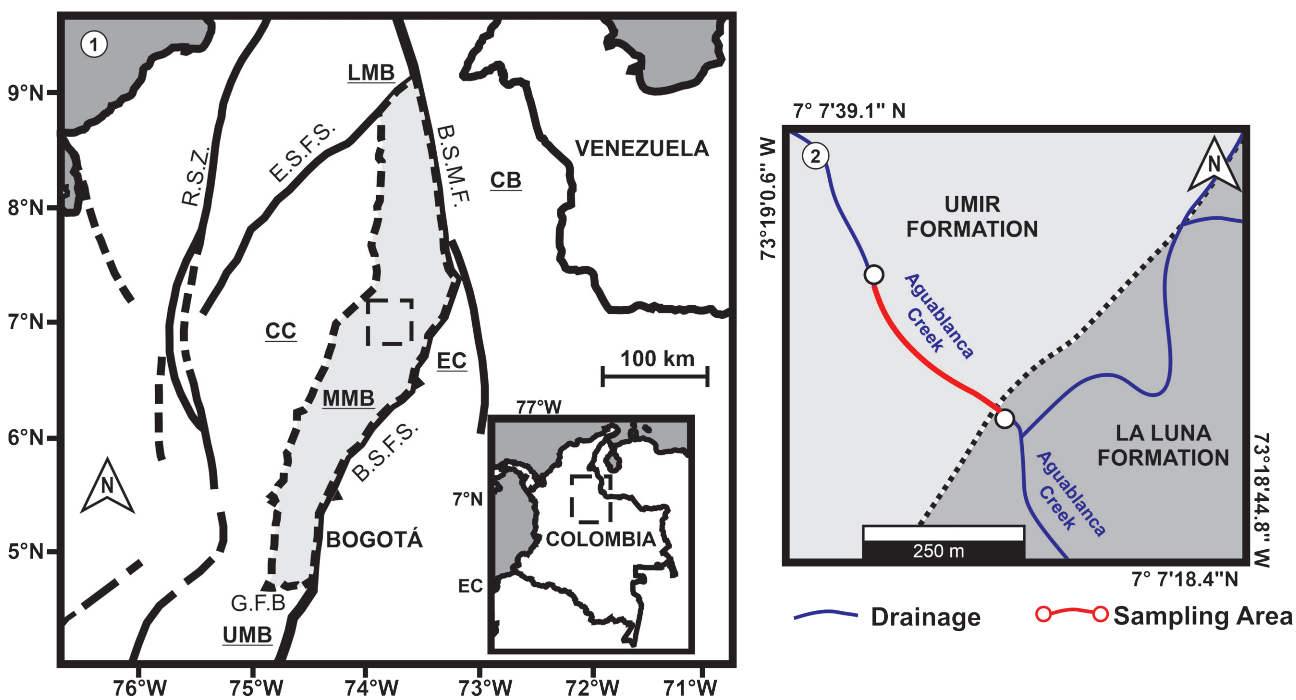

Figure 1. 1. Location of the Middle Magdalena Valley Basin. **2.** Map showing the location of the Aguablanca Creek section, northeastern Colombia. **Abbreviations**: **CC,** Central Cordillera; **EC,** Eastern Cordillera; **UMB,** Upper Magdalena basin; **MMB,** Middle Magdalena basin; **LMB,** Lower Magdalena basin; **CB,** Catatumbo basin; **RSZ,** Romeral suture zone; **ESFS,** Espiritu Santo fault system; **BSFS,** Bituima and La Salina fault system; **BSMF,** Bucaramanga-Santa Marta fault system.

ostracods, and calcareous nannofossils) and geochemical (sediments elemental ratios) survey for a stratigraphic section that spans the lowermost segment of the Umir Formation (Maastrichtian) and its contact with the underlying La Luna Formation. Our goals are to reconstruct the lower Umir Formation paleoenvironmental setting and assess the possible occurrence of a basal unconformity with the La Luna Formation.

Institutional abbreviations. UNISINOS, Universidade do Vale do Rio dos Sinos, São Leopoldo, Brasil; **itt OCEANEON,** Instituto Tecnológico de Paleoceanografia e Mudanças Climáticas, São Leopoldo, Brasil; **UIS,** Universidad Industrial de Santander, Bucaramanga, Colombia.

MATERIAL AND METHODS

Studied section

We sampled sediments from the Aguablanca Creek section in the Middle Magdalena Basin (7° 7′ N, 73° 18′ W; Eastern Colombian Cordillera). This locality was previously studied by Terraza (2019), and we focused on the uppermost interval investigated by this author (320.8–344.2 m stratigraphic height), which comprises the uppermost part of the La Luna Formation (La Renta Formation *sensu* Terraza, 2019) and the lower segment of Umir Formation (Figs. 1–3). The La Luna Formation is composed mainly of homogeneous limestones (mainly packstones) and a ~25 cm thick greenish glauconitic sandstone at its top. The Umir Formation is composed of a monotonous succession of dark grey marlstones, mudstones, and siltstones. The La Luna-Umir contact was proposed at 322.8 m by Terraza (2019).

Methods

Micropaleontological samples (n=28; interval 320.8–344.2 m stratigraphic height) were prepared according to standard methods at itt OCEANEON (UNISINOS). Approximately 30 g of dried rock were soaked into a 5% hydrogen peroxide (H_2O_2) solution for about 36 hours, washed over 63 and 150 μm sieves, and dried at 40°C (Sohn, 1961). Due to moderate and poor abundance, respectively, all foraminifers and ostracods were handpicked. Planktonic foraminiferal taxonomy followed Caron (1985), Nederbragt (1991), Georgescu (2005), Premoli Silva and Verga (2011), among others. Benthic foraminiferal taxonomy followed previous studies of Maastrichtian units in Colombia (Cushman & Hedberg, 1930, 1941; Martínez, 1989; Tchegliakova 1993, 1995; Tchegliakova & Mojica, 2001; Patarroyo *et al.*, 2017, 2022), and regional literature for the tropics and the US Western Interior (Sellier de Civrieux, 1952; Frizzell, 1954; Bolli *et al.*, 1994). Ostracod suprageneric classification follows Scott (1961). Selected foraminiferal specimens were imaged using an EVO MA15 Zeiss scanning electron microscope (SEM), and all studied specimens are archived in the micropaleontological collections at itt OCEANEON. Total microfossil counts and their diversity estimations are given in Supplementary Table S1.

Nannofossil samples (n=27; interval 321.2–344.2 m) were also prepared at itt OCEANEON following the smear-slide technique detailed by Bown and Young (1998), and studied using a Zeiss Axio Imager A2 petrographic microscope, at 1000x magnification. In order to achieve a quantitative analysis of the assemblages, 700 fields of view (FOV) were counted per slide. Preservation of calcareous nannofossils was evaluated under a light microscope using qualitative criteria: "Good" indicating specimens with little or no etching and/or overgrowth; "moderate" for specimens exhibiting some degree of etching and/or overgrowth, but still easily recognizable; and "poor" for specimens exhibiting extreme etching and/or overgrowth (Roth, 1983). Total calcareous nannofossil counts are given in Supplementary Table S2.

Diversity (Shannon-Weaver-H), richness (S) and evenness (E) estimations were calculated using the software Past version 2.15 (Hammer *et al.,* 2001), in addition to an SHEBI ("SHE Analysis for Biozone Identification") analysis, which is defined by the natural logarithm (ln) of the evenness estimations. SHEBI analysis searched general trends in ln(E) values in order to identify different assemblage intervals in the section (Buzas & Hayek, 1998, 2005).

A geochemical survey was conducted with bulk sediment samples from the section. Sample aliquots of 5 to 10 g ground rock (n = 29; interval 320.8–344.2 m height) were measured with a PanAlytical Epsilon 1 X-ray fluorescence (XRF) spectrometer at itt OCEANEON, with elemental concentrations reported as raw counts per second (cps). Results were normalized to a median-scaled (NMS) following Lyle *et al.* (2012) and interpreted as simple and logarithmic elemental ratios. We used the log(Fe/Ca) ratio as a proxy for terrigenous sediments input versus carbonate production (*e.g.*, Govin *et al.*, 2012), and the Sr/Ba ratio as a salinity proxy (*e.g.*, Wei & Algeo, 2019). Bottom water oxygenation was evaluated with the NMS intensities of redox-sensitive trace metals (TM) Ni, Cu, V, and Zn normalized by NMS Al intensities (*e.g.*, Dummann *et al.*, 2021). XRF measurements are provided in Supplementary Table S3.

RESULTS

Microfossil occurrences

The micropaleontological record of the Aguablanca Creek section yielded heterogeneous assemblages. Foraminiferal assemblages of the La Luna Formation and of the glauconitic level at the contact with the Umir Formation yielded few specimens of *Lenticulina* spp., undetermined rotaliids and planktonic foraminifera. Abundance and diversity increased along the succession of the Umir Formation (Figs. 2–3), where at least two intervals can be recognized based on the composition of foraminiferal assemblages: (1) a lower interval (329-338.2 m stratigraphic height) mainly composed of benthic taxa such as *Haplophragmoides excavatum*, *Gavelinella* spp., *Gyroidinoides depressus*, *Lenticulina muensteri*, *Orthokarstenia cretacea*, *Praebulimina* spp., *Pyramidina triangularis*, and *Siphogenerinoides bramletti*, while the planktonic assemblages were mainly composed of biserial taxa (*Planoheterohelix* spp., *Pseudoguembelina* spp., *Spiroplecta americana*) and scarce trochospiral forms

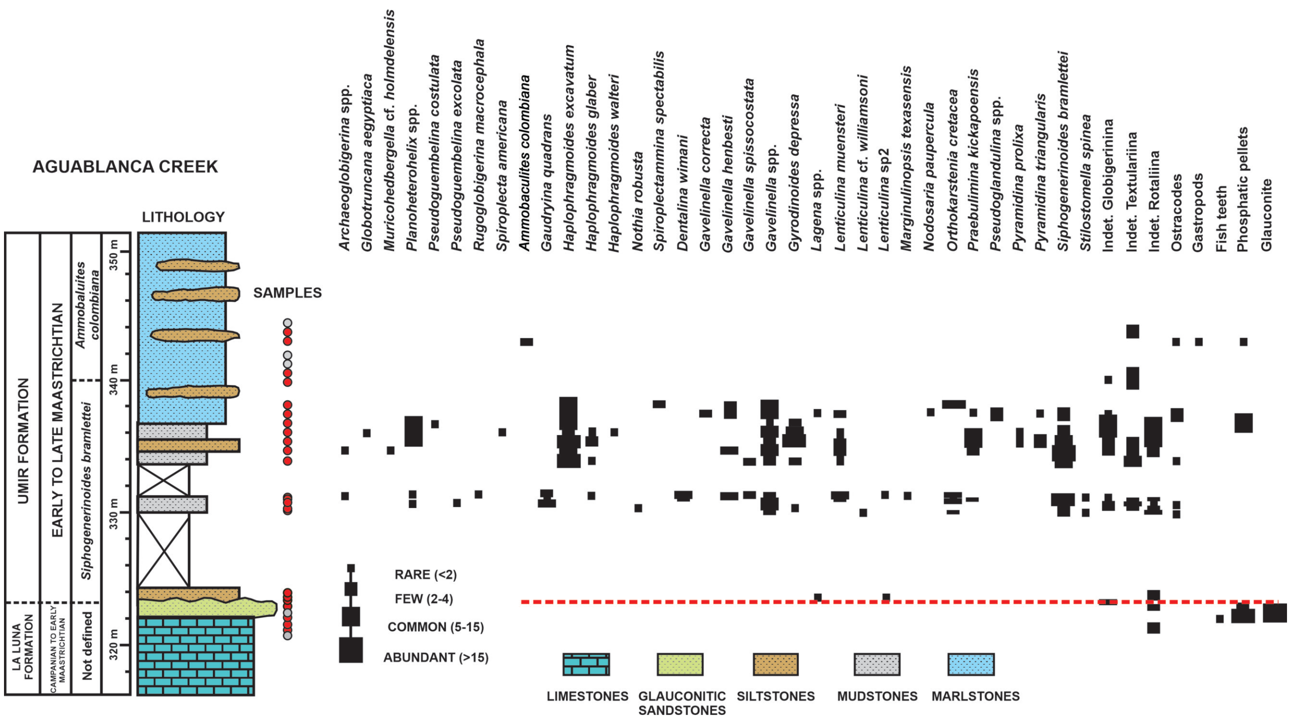

Figure 2. Stratigraphic distribution of foraminiferal taxa at Aguablanca Creek section. Biozones identification follows the local foraminiferal assemblage zones of Cushman and Hedberg (1941). Stratigraphic column based on descriptions of Terraza (2019). Gray dots indicate samples barren in foraminifers; red dashed line indicates the xenoconformity between the La Luna and Umir formations.

Figure 3. Selected foraminifers from Aguablanca Creek section. SEM Images. Scale bars represent 100 μm. **1.** ***Spiroplectammina spectabilis*** (337.6 m); **2.** ***Haplophragmoides walteri*** (334.9 m); **3.** ***Ammobaculites colombiana*** (343 m); **4.** ***Haplophragmoides excavatum*** (338.2 m); **5.** ***Haplophragmoides glaber*** (333.9 m); **6.** ***Gaudryina quadrans*** (329.9 m); **7.** ***Lenticulina muensteri*** (337.6 m); **8.** ***Lenticulina*** cf. ***williamsoni*** (329.9 m); **9.** ***Gavelinella henbesti*** (334.9 m); **10–11.** ***Gyroidinoides depressus*** (336 m); **12.** ***Marginulinopsis texasensis*** (331.3 m); **13.** ***Dentalina wimani*** (331 m); **14.** ***Stilostomella stimea*** (329.9 m); **15.** ***Nodosaria paupercula*** (337.6 m); **16.** ***Praebulimina*** spp. (334.9 m); **17.** ***Pyramidina prolixa*** (335.5 m); **18.** ***Spiroplecta americana*** (336 m); **19.** ***Pseudoguembelina costulata*** (336.9 m); **20.** ***Pseudoguembelina excolata*** (330.3 m); **21.** ***Siphogenerinoides bramletti*** (334.9 m); **22.** ***Orthokarstenia cretacea*** (331.3 m); **23.** ***Globotruncana aegyptiaca*** (336 m); **24.** ***Rugoglobigerina macrocephala*** (331.3 m); **25**. ***Muricohedbergella*** cf. ***holmdelensis*** (334.9 m).

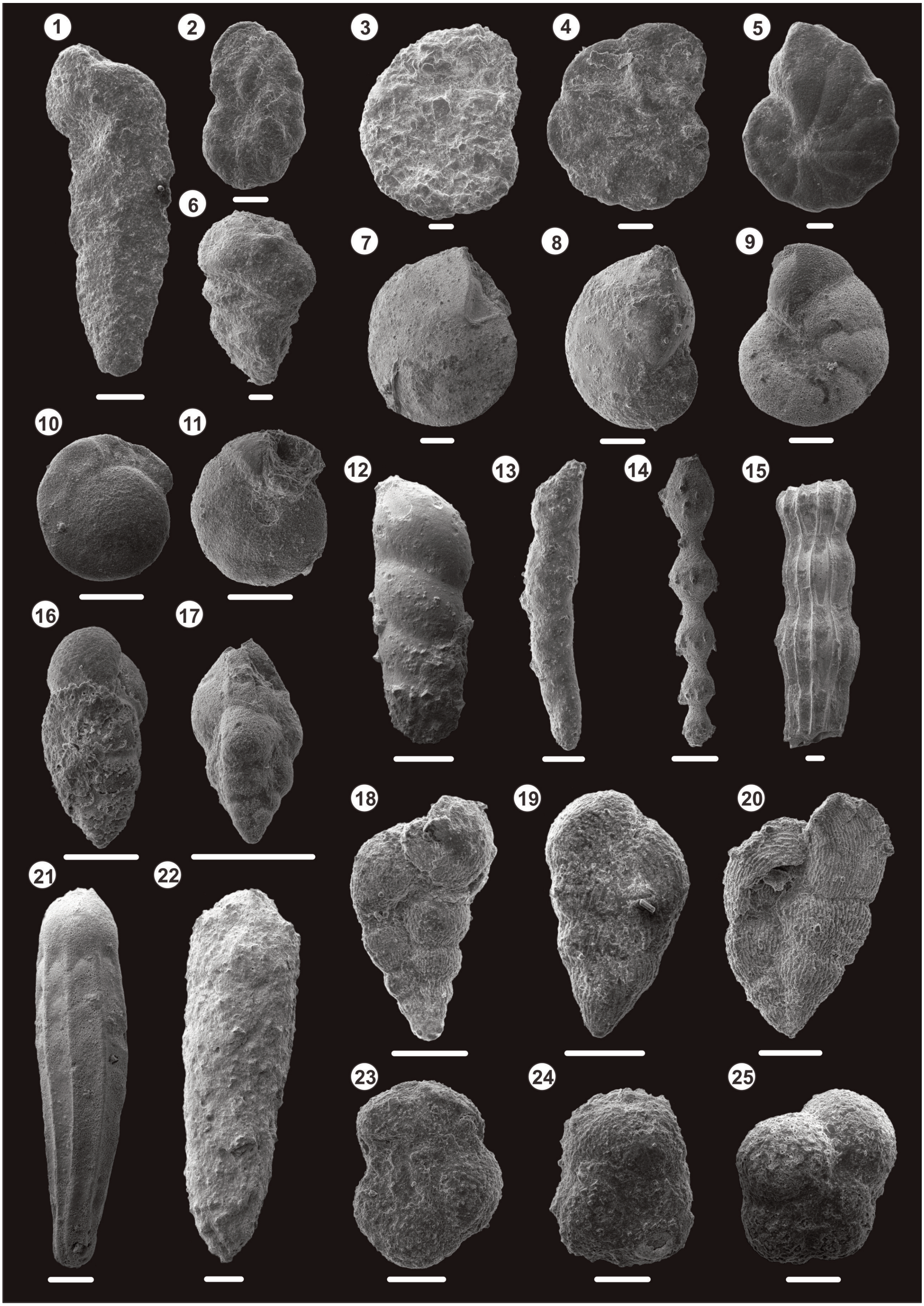
1
2
3
4
5
6
7
8
9
10
11
12
13
14
15
16
17
18
19
20
21
22
23
24
25

such as *Archaeoglobigerina* spp., *Rugoglobigerina* spp., *Muricohedbergella* spp., and *Globotruncana aegyptiaca* (Fig. 3); and (2) an upper interval (340–344.2 m) mainly dominated by undetermined textulariids and few specimens of *Ammobaculites colombiana* (sample 343 m; Figs. 2–3).

Nannofossil assemblages, in contrast, were equally abundant in the La Luna and Umir formations, though species such as *Cervisella operculata*, *Cribrosphaerella ehrenbergii*, *Micula staurophora,* or *Reinhardtites levis* were more common in the La Luna Formation (Figs. 4–5). *Chiastozygus synquadriperforatus*, *Cylindralithus biarcus*, *Cylindralithus serratus*, and *Predicosphaera stoveri* were only present in the Umir Formation, but with low abundances. The interval 340-344.2 m was barren of calcareous nannofossils, though samples at 340 m and 340.5 m yielded abundant (>300 fragments/sample) ascidian spicules (Fig. 4).

Other microfossils recovered from the Aguablanca Creek section include fish teeth, gastropod fragments, and ostracods (Fig. 2). Poor preservation and the scarcity of ostracods hampered taxonomic descriptions, and only a single specimen of *Actinocythereis*? sp. at 337.6 m was identified.

Diversity (Shannon-Weaver-H), evenness (E), and richness (S) estimations for foraminiferal and the calcareous nannofossil assemblages varied throughout the section. In the interval with better foraminiferal recovery (329.9–338.2 m), richness was relatively high (S>10), while the Shannon-Weaver-H index was >2 for most samples (Fig. 6). Calcareous nannofossil richness was also higher in this interval (S>10), and some other specific levels in the Umir Formation such as 331 and 331.3 m (reaching S>35). Regarding calcareous nannofossil diversity, the Shannon-Weaver-H index ranged from 1.2 to 2.0, with the highest values (H>2) at 322.5 m and 335.5. m, while the smallest value (H<1.1) was recorded in the lower part of the section (321.2–321.6 m). Evenness estimations in the calcareous nannofossil assemblages also presented a wide range of values along the section (0.1 to 0.7), though samples of the Umir Formation presented mostly values around 0.6 in the upper part of the section. Finally, SHEBI analysis, based on ln(E) values of calcareous nannofossil assemblages, suggests the occurrence of at least two assemblage intervals: (1) a lower assemblage (321.2–331.3 m) with most of the samples having values of ln(E)>-1.2, and (2) an upper assemblage, comprising samples of the Umir Formation (333.9-339 m) with values of ln(E)<-1.0 (Fig. 6).

Geochemical proxies

Log(Fe/Ca) presents an upward-increasing trend at the Aguablanca Creek section, with values ranging between –0.1 and 1.8. Conversely, the Sr/Ba ratio presents a decreasing-

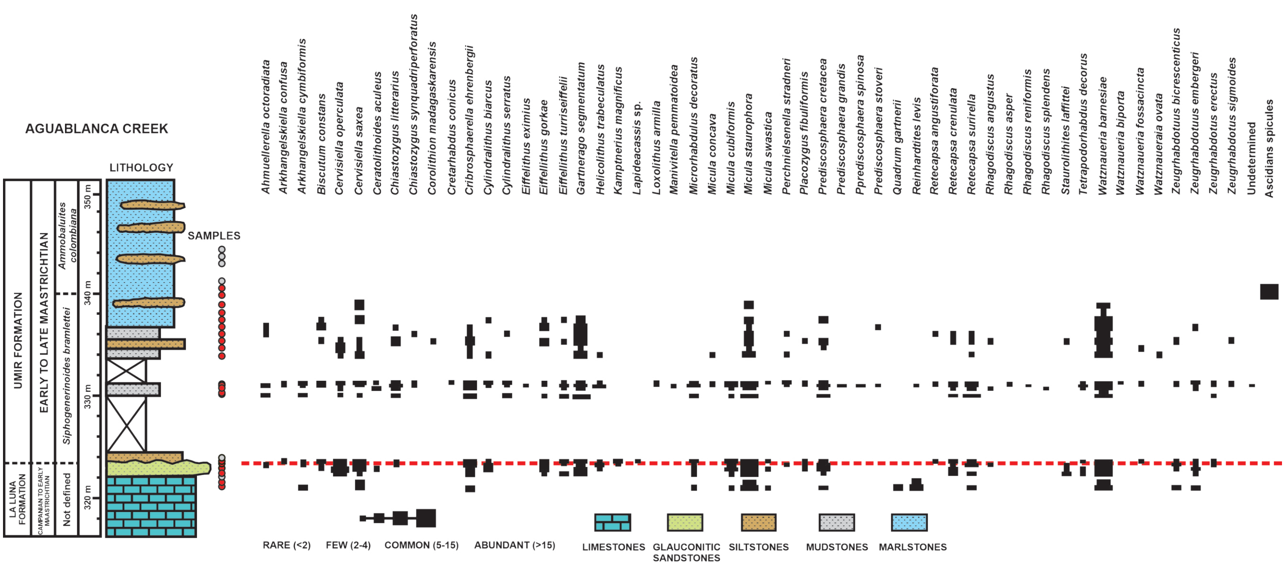

Figure 4. Stratigraphic distribution of calcareous nannofossil taxa at Aguablanca Creek section. Biozones identification follows the local foraminiferal assemblage zones of Cushman and Hedberg (1941). Stratigraphic column based on descriptions of Terraza (2019). Gray dots indicate samples barren in calcareous nannofossils; red dashed line indicates the xenoconformity between the La Luna and Umir formations.

upward trend, with values ranging from 130 to 90 in the lower part of the section and values <30 for most of the samples of the Umir Formation (Fig. 6). Most of the trace metals (TM)/Al ratios exhibit similar trends throughout the section, presenting a steady decrease above the contact between the La Luna and Umir formations. For instance, the Ni/Al, Cu/Al, and Zn/Al ratios present higher values in the La Luna Formation ($5\text{-}10*10^{-7}$ in the Ni/Al and Cu/Al, $>38*10^{-7}$ in the Zn/Al) and drop to average values of $4*10^{-7}$ and $25*10^{-7}$, respectively, within the Umir Formation. The V/Al ratio presents relatively high values in the La Luna Formation ($19\text{-}26*10^{-7}$), drops abruptly at the contact between the two formations, and shows an upward increasing trend across the Umir Formation (Fig. 6).

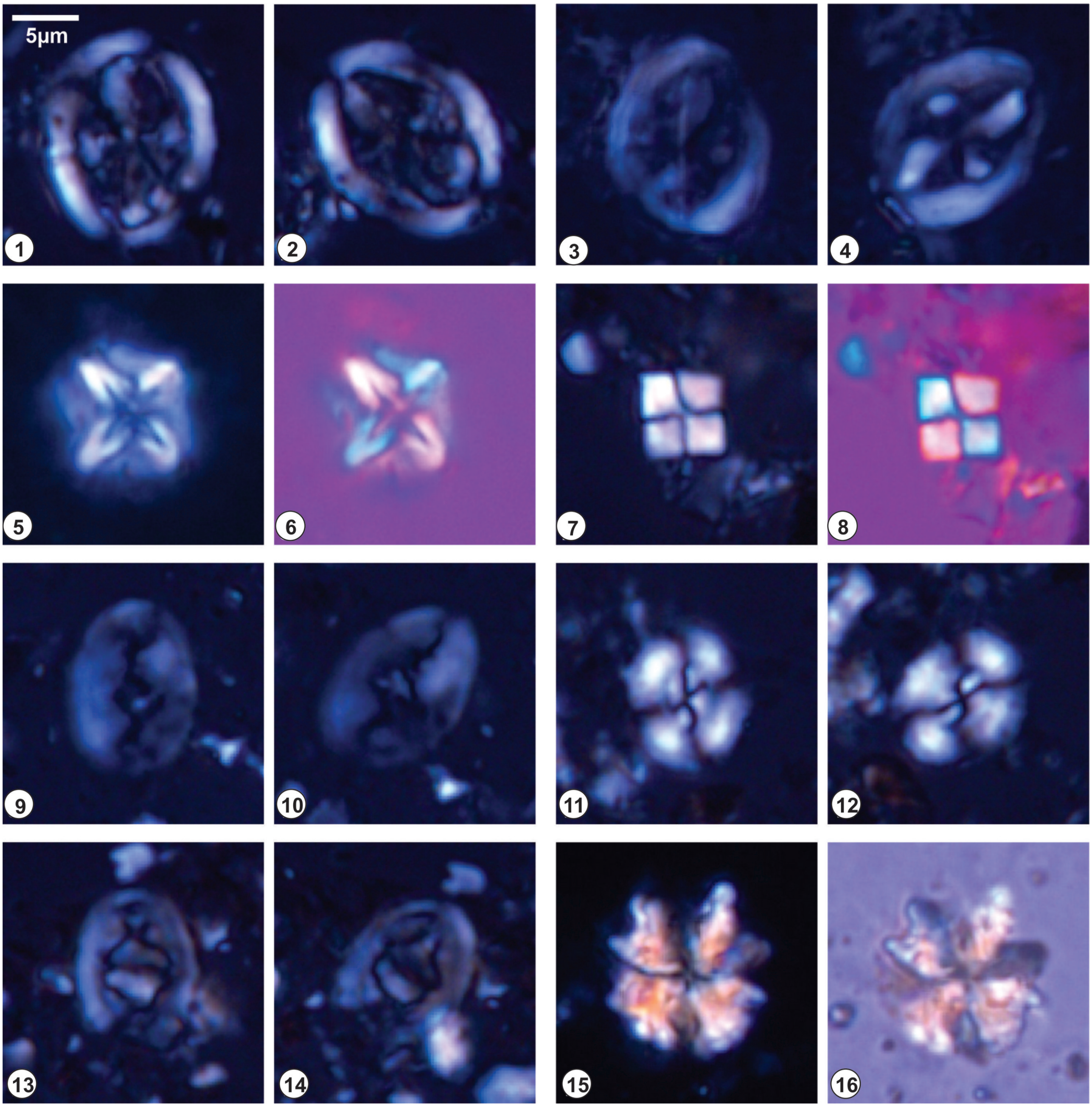

Figure 5. Selected calcareous nannofossils from Aguablanca Creek section. Scale bar represents 5 µm for all images. Petrographic microscopy images. **1–2.** ***Arkhangelskiella cymbiformis*** (321.2 m); **3–4.** ***Gartnerago segmentatum*** (329.9 m); **5–6.** ***Micula staurophora*** (323.4 m); **7–8.** ***Quadrum gartneri*** (321.2 m); **9–10.** ***Reinhardtites levis*** (331 m); **11–12.** ***Watznaueria barnesiae*** (321.2 m); **13–14.** ***Zeugrhabdotus bicrescenticus*** (321.2 m); **15–16.** Ascidian spicule (340 m).

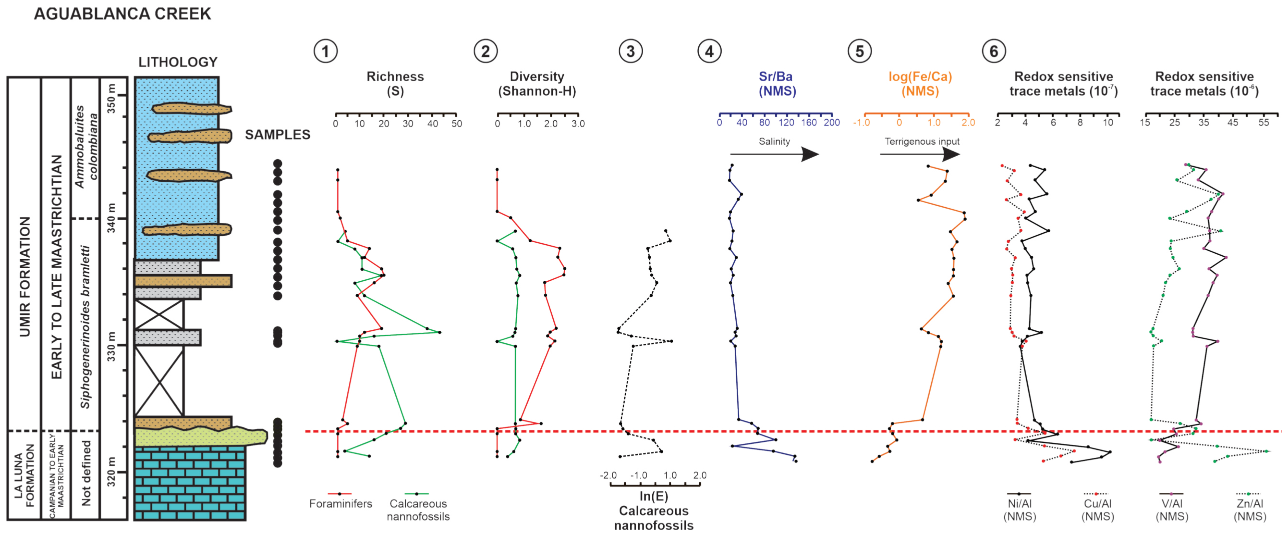

Figure 6. Records of foraminiferal and calcareous nannofossil distribution of diversity and richness estimates, and geochemical proxies at Aguablanca Creek section. **1.** Species richness of foraminiferal and calcareous nannofossil assemblages. **2.** Shannon-weaver-H diversity of foraminiferal and calcareous nannofossil assemblages. **3.** Ln (E) estimates for calcareous nannofossil assemblages. **4.** Log (Fe/Ca) as a proxy for terrigenous input. **5.** Sr/Ba ratio as a proxy for paleosalinity. **6.** Stratigraphic distribution of the redox-sensitive trace metals Ni, Cu, V, and Zn normalized to Al content. Red dashed line indicates the xenoconformity between the La Luna and Umir formations.

DISCUSSION

Biostratigraphic constraints for Maastrichtian strata at the Aguablanca Creek section

Micropaleontological evidence supports a latest Cretaceous (Campanian–Maastrichtian) age for the studied interval in the Aguablanca Creek section (Figs. 2, 4, 7). Most of the recovered planktonic foraminiferal taxa have wide chronostratigraphic ranges (*Planoheterohelix globulosa*, *Muricohedbergella* spp.), but there are some species such as *Spiroplecta americana*, *Pseudoguembelina excolata*, *Rugoglobigerina macrocephala*, and *Globotruncana aegyptiaca* with late Campanian–late Maastrichtian ranges. Benthic foraminiferal assemblages of the Umir Formation can be assigned to the *Siphogenerinoides bramletti* (329.9–337.6 m) and *Ammobaculites colombiana* (338.2–344.2 m) assemblage zones, according to the definitions of Cushman and Hedberg (1941) in the more proximal Catatumbo basin. Following these authors, as well as the chronostratigraphic update of Martínez (1989) based on planktonic foraminifera and new micropaleontological data for the Cesar-Ranchería and Catatumbo basins (Patarroyo *et al.*, 2017; 2022), the *S. bramletti* and *A. colombiana* assemblage zones comprise the late Maastrichtian (*Abathomphalus mayaroensis* Zone to probably *Plummerita hantkeninoides* Zone). In general, foraminiferal assemblages from the Aguablanca Creek section present the same sequence of biostratigraphic markers reported by Martínez (1989) and Patarroyo *et al.* (2017, 2022) for the coetaneous Colón Formation, located in the Catatumbo and Cesar-Ranchería basins (Fig. 7). The absence of diagnostic foraminifers in the upper part of the La Luna Formation hampered an age assignment for this unit.

The Umir Formation was originally dated as a Campanian–Maastrichtian by Petters (1955), using benthic foraminiferal assemblages that were also recognized in Western Venezuela. That scheme used the same biozones as Cushman and Hedberg (1941), with a difference in the definition of the oldest biozone (*Orthokarstenia cretacea* instead of *Pullenia cretacea*). A key aspect in the biostratigrahic zonation of Petters (1955) was the calibration with ammonite markers. For instance, in the southern MMV, the Campanian ammonite *Stantonoceras* occurred within the *O. cretacea* Zone. Ammonite genera such as *Coahuilites* and *Sphenodiscus* within the *S. bramlettei* and *A. colombiana* foraminiferal zones confirmed a Maastrichtian age for the upper part of the Umir Formation. However, the precise location and detailed description of that material remained unclear, hampering more detailed comparisons (*e.g.*, Ward *et al.*, 1973). Later, a series of studies by Tchegliakova (1993, 1995, 1996) in the

La Julia Creek section (northeastern MMV) and the Honda-Guaduas area (southern MMV) discussed the Campanian age assignment for the lower segment of the Umir Formation. At the La Julia Creek section, where the La Luna-Umir formations contact occurs, Tchegliakova (1995) reported the occurrences of *A. colombiana* and the planktonic species *Rugoglobigerina macrocephala*, constraining the age of the Umir Formation to middle-late Maastrichtian, and probably an early Maastrichtian age for the upper part of the La Luna Formation. Moreover, in localities from the Honda-Guaduas area, Tchegliakova (1996) identified the planktonic foraminiferal biozones *Gansserina gansseri* and *Abathomphalus mayaroensis*, extending the chronostratigraphic range of the lower Umir Formation from the middle Maastrichtian to the uppermost Campanian (Fig. 7). Considering our interpretation of a Maastrichtian age for the Umir Formation, based exclusively on the record of the foraminiferal assemblages, the absence of diagnostic elements of the *O. cretacea* Assemblage Zone (*e.g.*, *Pullenia cretacea*) in the studied material, and the location of the Aguablanca Creek section (middle part of the MMV), it is plausible that the lower boundary of the formation is diachronous along the MMV. However, it must be also considered that the lowermost segment of the Umir Formation is covered in the Aguablanca Creek section (324.1–329.9 m).

Considering these uncertainties, one of our goals was to explore an integrated approach (calcareous nannofossils, ostracods) in order to get higher accuracy for the age span of the studied section. Studies on calcareous nannofossils from the Late Cretaceous successions of Colombia are scarce, being Pérez-Panera *et al.* (2018) the only published work. That study focused mainly on the La Luna Formation and the lowermost part of the Umir Formation from an exploratory well in the northernmost MMV, and reported most of the species we recovered at the Aguablanca Creek section. Calcareous nannofossil assemblages in our locality were mainly composed of taxa with long chronostratigraphic ranges (*e.g.*, Aptian–Maastrichtian). However, species such as *Arkhangelskiella cymbiformis*, *Ceratolithoides aculeus*, *Perchnielsenella stradneri*, and *Prediscosphaera stoveri*, which ranged from Campanian to Maastrichtian, were present in low abundances along the section. The last occurrence of *Reinhardtites levis* at 331 m could be used as a boundary between the early and late Maastrichtian (top of UC18 zone), though its rare occurrence, and the presence of benthic foraminifer *S. bramletti* in this interval, could be

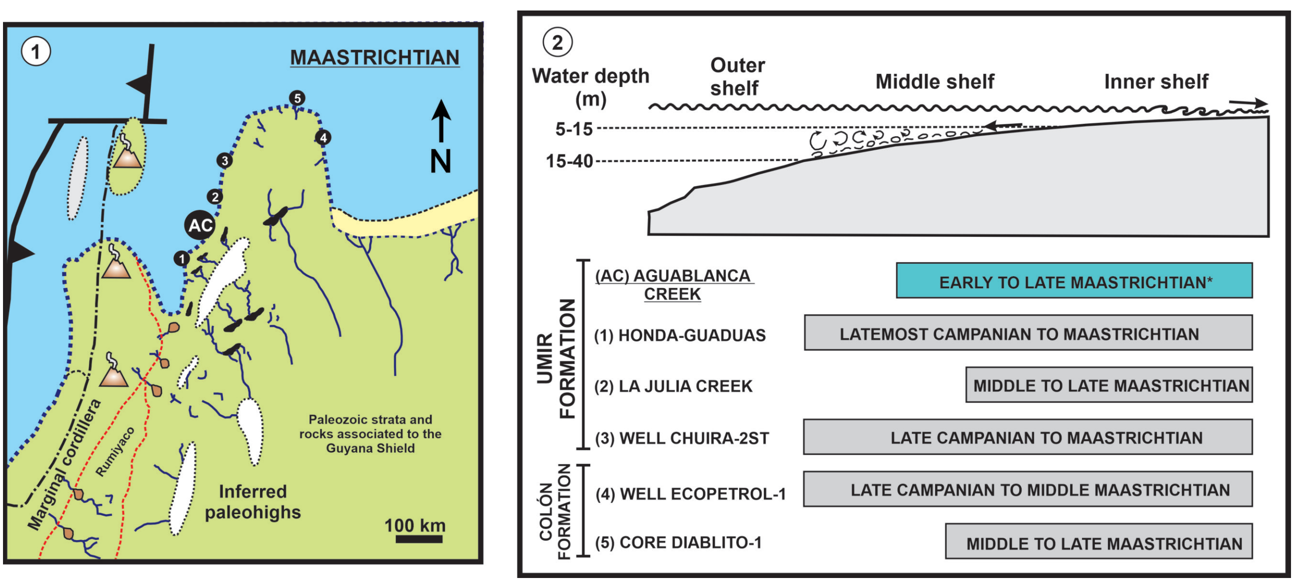

Figure 7. Interpreted paleoenvironmental settings of Maastrichtian successions in northern South America. **1.** Paleogeographic map adapted from Bayona (2018), indicating the location of the Aguablanca Creek section (AC) and additional localities with foraminiferal data numbers 1–5). **2.** Depositional setting and age assignments for latest Cretaceous sedimentary successions of northeastern Colombia. Age and paleoenvironmental assignments follow: **1–2.** Tchegliakova (1993, 1995, 1996); **3.** Navarrete *et al.* (2018) and Pérez-Panera *et al.* (2018); **4–5.** Patarroyo *et al.* (2017, 2022). The horizontal length of each bar indicates the proposed depositional setting range for each locality.

interpreted as a product of reworking. Using the calcareous nannofossil record, an age not older than early Maastrichtian could be assigned to the lowermost part of the Umir Formation (324.1–331 m).

Though calcareous nannofossil assemblages in the La Luna Formation were more abundant and diversified than foraminiferal assemblages, and the SHEBI analysis suggests a floristic turnover, taxa of the La Luna Formation consist of species with long chronostratigraphic ranges and Campanian-Maastrichtian markers. Therefore, based on the calcareous nannofossils assemblages we suggest a Campanian to early Maastrichtian age for the top of the La Luna Formation (Fig. 7). Our interpretation slightly modifies the original conclusions of Terraza (2019), who assigned a Campanian age to the upper part of the La Luna Formation (=La Renta Formation) in the Aguablanca Creek section. That age assignment was based on the presence of Santonian ammonites such as *Plesiotexanites*, *Texanites*, and *Cocuyites* in underlaying strata of the section (middle part of the La Luna Formation; Galembo Formation *sensu* Terraza, 2019), and the common presence of the benthic foraminifer *O. cretacea* in thin sections from the upper part of the La Luna Formation (=Galembo Formation). Additionally, the lithological contrast between the La Luna and Umir formations suggests the presence of an unconformity according to that author. The paleoenvironmental nature of the La Luna-Umir contact will be discussed in the following section.

Our biostratigraphic interpretation for the uppermost part of the Aguablanca Creek section (340-344.2 m) is tentative, considering the absence of calcareous nannofossils above 339 m, and the presence of scarce ostracods and benthic foraminifers, the latter represented mostly by agglutinated taxa. So far, we can only assign an age not older than late Maastrichtian, based on the first occurrence of the benthic foraminiferal species *A. colombiana* at 343 m, which defines the base of its homonym assemblage zone (Cushman & Hedberg, 1941). New micropaleontological data in the Cesar-Rancheria Basin and the identification of the Cretaceous-Paleogene (K-Pg) boundary in that area have provided a better age control for the *A. colombiana* assemblage zone (De La Parra *et al.*, 2022; Patarroyo *et al.*, 2022).

Considering the expected abundance decrease of marine microfossils in the uppermost strata at our section, palynological analyses could improve the chronostratigraphy of the middle and upper parts of the Umir Formation. Maastrichtian strata from the Umir Formation were originally studied by Van der Hammen (1954, 1957), who proposed three palynological zones (Maastrichtian A-C). However, since most of the morphotypes described by Van der Hammen (1954, 1957) have been revised and assigned to other genera, new biostratigraphic schemes have been proposed since then for Maastrichtian strata in Colombia (Sarmiento, 1992; Yepes, 2001; Santos, 2012; De La Parra *et al.*, 2022).

Paleoenvironmental settings recorded at the Aguablanca Creek section

The stratigraphic description of Terraza (2019), as well as the micropaleontological and geochemical data from our study at Aguablanca Creek section, highlight the differences between the La Luna Formation and the Umir Formation. Contrasting sedimentological and stratigraphical characteristics have been traditionally interpreted as evidence of a regional unconformity, related to the first pulses of the Andean orogeny (*e.g.*, Ward *et al.*, 1973; Sarmiento *et al.*, 2015). However, the nature of this boundary and its presence in other basins have been intensively debated in recent years. Based on sedimentological studies in the Cocuy region, Bayona *et al.* (2020) defined it as a xenoconformity, considering that it reflects a shift in the depositional regime (from dominant carbonate deposition to the onset of synorogenic terrigenous-dominated deposition), instead of a major hiatus within the Maastrichtian sedimentary successions. Petrographic, paleontological (microfossils), geochemical (total organic carbon, TOC), and seismic data also evidence marked differences between the La Luna Formation and the Colón Formation (coeval to the Umir Formation) in the Catatumbo and Cesar-Ranchería basins (Ayala-Calvo *et al.*, 2009; Cooney & Lorente, 2009; Bayona *et al.*, 2011; Patarroyo *et al.*, 2017).

The dominance of carbonate rocks and the presence of calcareous nannofossils in the Aguablanca Creek section suggest open marine conditions, probably in a middle shelf setting, for the upper part of the La Luna Formation (Fig. 7). This is also supported by our geochemical results, since sediment Sr/Ba values of the uppermost La Luna Formation indicate higher paleosalinity in comparison with the overlying strata. Strontium tends to be absorbed on fine-grained sediments deposited under high-salinity waters, whereas barium content is higher in freshwater delivered by continental runoff (Wei & Algeo, 2019). Additionally, increased concentrations of redox-sensitive TM, such as V, Ni, Cu and Zn, suggest that sediments were deposited under the influence of oxygen-depleted bottom waters (Fig. 6; *e.g.*, Dummann *et al.*, 2021). Previous studies in the upper part of the La Luna Formation in the MMV and other basins have reported an overall high total organic carbon (TOC) content, with values ranging from 3 to 7% (Patarroyo *et al.*, 2021). The low abundance of benthic foraminifers in this part of the section could be, in fact, a consequence of poorly oxygenated bottom waters. However, taphonomic controls are not discarded as a possible cause of low foraminiferal abundances, since some of the analyzed samples were collected from the greenish glauconitic sandstone below the La Luna-Umir contact. Special caution must additionally be taken for interpreting this interval, since reworked intraclasts were reported by Terraza (2019) and by studies in other localities recording the same glauconitic level in the MMV (*e.g.*, Ward *et al.*, 1973; Sarmiento *et al.*, 2015). In fact, glauconite precipitation supports our paleoenvironmental interpretation for the La Luna Formation, since glauconite has been reported from shallow marine poorly oxygenated settings in the Maracaibo area (*e.g.*, Erlich *et al.*, 1999; Parra *et al.*, 2003).

In contrast to the La Luna Formation, the microfossil content and geochemical proxies (Sr/Ba and log(Fe/Ca) ratios) of the uppermost part of our section indicate a progressive transition from an inner platform to sublittoral settings within the Umir Formation (Fig. 6).

Foraminiferal distributions depict two intervals that illustrate this transition: a lower assemblage (329–338.2 m) dominated by calcareous benthic foraminifers (mostly elongated and planispiral forms) and some planktonic taxa (mostly biserial forms); and an upper assemblage (340–344.2 m), characterized by lower recovery, but dominated by agglutinated benthic taxa, which tend to increase in abundance at relatively shallow conditions (Figs. 2, 7; *e.g.*, Cetean *et al.*, 2011). Like in other studies on latest Cretaceous foraminifera from Colombia, the disappearance of keeled planktonic taxa (only present in the interval 334.9–336 m), the predominance of the benthic foraminifera, and the increase in the proportion of textulariids upward in the succession, suggest a regressive pattern for this unit (Bürgl & Dummit, 1954; Martínez, 1989; 2003; Vergara, 1997; Guerrero *et al.*, 2000; Tchegliakova & Mojica, 2001; Patarroyo *et al.*, 2022). This regressive stacking trend was previously documented with foraminiferal assemblages within the Umir Formation, but without a broad stratigraphic control (Petters, 1955; Tchegliakova 1993, 1995). In the La Julia Creek section, Tchegliakova (1993, 1995) reported assemblages mostly composed of agglutinated forms (*Haplophragmoides*, *Bathysiphon*, *A. colombiana*), unidentified ostracods, calcareous algae, and high proportions of amorphous organic matter, suggesting paralic environments with intermittent influence of freshwater input.

Other micropaleontological evidence of this shallowing-upward trend include the disappearance of the calcareous nannofossil above 339 m, as well as the abundance of ascidian spicules (>300 specimens/sample) at 340 m and 340.5 m at the Aguablanca Creek section (Fig. 4). Considering that some species are temperature and salinity-sensitive (Shenkar & Swalla, 2011), future studies on these microfossils of the Umir Formation could provide new insights into its paleoenvironmental evolution.

Proxy records at the Aguablanca Creek section also provided clues about the shallowing trend recorded by the Umir Formation (Fig. 6). For instance, fluctuations in the log(Fe/Ca) ratio can be used as a tracer of terrigenous input relative to carbonate sedimentation (Govin *et al.*, 2012). The log(Fe/Ca) at the Aguablanca Creek section indicates a steady increase upward in the section, in comparison with the lower values within the La Luna Formation, implying increased supply of terrigenous sediments likely associated with progressively more proximal settings. Relatively lower sediment Sr/Ba values at the uppermost Aguablanca Creek section also suggest increased freshwater input (Wei & Algeo, 2019), which is consistent with more proximal depositional settings.

At a regional scale, Maastrichtian sea-level fluctuations within the Umir Formation include at least five maximum flooding surfaces over a major retro-gradational sequence (Montaño *et al.*, 2016). However, that study was mostly focused on the middle to upper interval of the unit, which yields economically relevant coal-bearing strata. The geological evolution of Maastrichtian coastal environments in northern South America was highly dynamic and was not solely affected by sea level fluctuations, but also deeply influenced by the onset of tectonic activity in the Central and Eastern Cordilleras during the Campanian–Maastrichtian (Fig. 7; Villamil & Pindell, 1998; Sarmiento-Rojas, 2019; Montes *et al*., 2019; Bayona *et al*., 2020).

Finally, our micropaleontological and geochemical results suggest moderate oxygenation of bottom waters for the lower part of the Umir Formation. In general, there is a high proportion of benthic infaunal taxa along the Aguablanca Creek section, comprising elongated (*e.g.*, *Siphogenerinoides*, *Orthokarstenia*, *Stilostomella*), ovoidal (buliminids) and elongated biserial (*e.g.*, *Coryphostoma*, *Loxostomum*) forms. These morphotypes are usually interpreted as indicative of poorly oxygenated bottom water conditions, related to water mass eutrophication (Van der Akker *et al*., 2000; Jorissen *et al*., 2007). However, there were still moderate abundance and richness of epifaunal or shallow infaunal taxa (*e.g.*, *Gavelinella*, *Gyroidinoides*, *Lenticulina*) within this interval at the Aguablanca Creek section. Overall, benthic foraminiferal assemblages at the Aguablanca Creek section contrast with those described for the La Luna Formation and coeval units in Colombia, which recorded relatively high primary productivity, recurrent anoxic episodes, and yielded benthic foraminiferal assemblages dominated by deep infaunal forms (*e.g.*, buliminids; Vergara, 1997; Guerrero *et al*., 2000; Tchegliakova & Mojica, 2001; Martínez, 2003; Parra *et al*., 2003; Patarroyo *et al*., 2017).

Values of TM/Al ratios within the Umir Formation are low in comparison to those of the La Luna Formation (Fig. 6), suggesting improved bottom water oxygenation (*e.g.*, Dummann *et al*., 2021). Nevertheless, fine-grained sediments of the lower part of the Umir Formation show TOC contents below 1.7%, while the organic carbon-rich levels from the middle and upper part of this unit have TOC values ranging from 12 to 40% (Rangel *et al*., 2000). An exception among the overall trends of TM/Al proxies at the Aguablanca Creek section is the V/Al ratio, which depicts a trend similar to that of the log(Fe/Ca) ratio, and in contrast to the remaining TM (Fig. 6). One likely explanation for the V/Al trend would be the input of V-rich terrigenous sediments.

CONCLUSIONS

The integrated micropaleontological (foraminifers, calcareous nannofossils, and ostracods) and geochemical [log(Fe/Ca), Sr/Ba, and redox-sensitive TM/Al ratios] study of the Maastrichtian stratigraphic succession at Aguablanca Creek section revealed a major paleoenvironmental shift between the La Luna and Umir formations. Based on the common presence of calcareous nannofossils and higher concentrations of redox-sensitive trace metals such as Ni, Cu, and Zn, we interpret the upper part of the La Luna Formation as a middle shelf setting, with poorly oxygenated bottom water conditions. In contrast, benthic foraminiferal, log(Fe/Ca), and Sr/Ba records depict a shallowing-upward trend for the studied interval of the Umir Formation in a retro-gradational inner platform setting. This interval is characterized by a gradual decrease of the planktonic biota (heterohelicids, keeled foraminifers, calcareous nannofossils), and the transition from moderately diverse calcareous benthic foraminifers (buliminids, elongated uniserial, trochospiral forms) to poorly diversified assemblages, composed of agglutinated benthic forms (*Ammobaculites*, unidentified textulariids). This interpretation is also supported by bulk sediment Sr/Ba and log(Fe/Ca) ratios, which indicate increased continental runoff and terrigenous input in the upper part of the section, likely associated with more proximal depositional settings. The recorded paleoenvironmental turnover suggests the presence of a xenoconformity at the La Luna-Umir stratigraphic contact. Our biostratigraphic results suggest an early Maastrichtian age (base of the regional foraminiferal Zone *Siphogenerinoides bramletti*) for this unconformity.

ACKNOWLEDGMENTS
The authors thank the staff of itt-OCEANEON for their support with sample preparation and analyses. G.D.P. thanks PETROBRAS for a scholarship in the project "Bioestratigrafia de foraminíferos do Aptiano–Albiano da Margem Continental Brasileira". L.A. acknowledges funding from project PID2019-105537RB-I00 funded by MCIN/AEI/10.13039/501100011033 and by "ERDF A way of making Europe". Gustavo Torres (Stratos Consultoría Geológica, Colombia) kindly assisted with edition of foraminiferal SEM images. Andrea Caramés (UBA) and an anonymous reviewer provided key suggestions in order to improve the first version of this contribution, and to them we express our gratitude.

REFERENCES
Ayala-Calvo, R. C., Bayona-Chaparro, G. A., Ojeda-Marulanda, C., Cardona, A., Valencia, V., Padrón, C. E., Yoris, F., Mesa-

Salamanca, J., & García, A. (2009). Estratigrafía y procedencia de las unidades comprendidas entre el Campaniano y el Paleógeno en la subcuenca de Cesar: aportes a la evolución tectónica del área. *Geología Colombiana*, *34*, 3–33.

Bayona, G., Baquero, M., Ramírez, C., Tabares, M., Salazar, A. M., Nova, G., Duarte, E., Pardo, A., Plata, A., Jaramillo, C., Rodríguez, G., Caballero, V., Cardona, A., Montes, C., Gómez-Marulanda, S., & Cárdenas-Rozo, A. L. (2020). Unravelling the widening of the earliest Andean northern orogen: Maastrichtian to early Eocene intra-basinal deformation in the northern Eastern Cordillera of Colombia. *Basin Research*, *33*(1), 809–845.

Bayona, G., Montes, C., Cardona, A., Jaramillo, C., Ojeda, G., & Valencia, V. (2011). Intraplate subsidence and basin filling adjacent to an oceanic arc-continental collision: a case from the southern Caribbean–South America plate margin. *Basin Research*, *23*(4), 403–422.

Bolli, H. M., Beckmann, J. P., & Saunders, J. B. (1994). *Benthic foraminiferal biostratigraphy of the South Caribbean region*. Cambridge University Press.

Bown, P. R., & Young, J. R. (1988). Techniques. In P. R. Bown (Ed.), *Calcareous Nannofossil Biostratigraphy* (pp. 16–28). British Micropaleontological Society Series.

Bürgl, H., & Dumit, Y. (1954). El Cretáceo Superior en la región de Girardot. *Boletín Geológico*, *2*, 23–48.

Buzas, M. A., & Hayek, L. A. C. (1998). SHE analysis for biofacies identification *Journal of Foraminiferal Research*, *28*(3), 233–239.

Buzas, M. A., & Hayek. L. A. C. (2005). On richness and evenness within and between communities. *Paleobiology*, *31*(2), 199–220.

Caron, M. (1985). Cretaceous planktic foraminifera. In H. M. Bolli, J. Saunders, & K. Perch-Nielsen (Eds.), *Plankton Stratigraphy* (pp. 17–86). Cambridge University Press.

Carvalho, M. R., Jaramillo, C., De La Parra, F., Caballero-Rodríguez, D., Herrera, F., Wing, S., Turner, B. L., D'Apolito, C., Romero-Báez, M., Narváez, P., Martínez, C., Gutierrez, M., Labandeira, C., Bayona, G., Rueda, M., Paez-Reyes, M., Cárdenas, D., Duque, A., Crowley, J. L., Santos, C., & Silvestro, D. (2021). Extinction at the end–Cretaceous and the origin of modern Neotropical rainforests. *Science*, *372*(6537), 63–68.

Cetean, C. G., Bălc, R., Kaminski, M. A., & Filipescu, S. (2011). Integrated biostratigraphy and palaeoenvironments of an upper Santonian–upper Campanian succession from the southern part of the Eastern Carpathians, Romania. *Cretaceous Research*, *32*(5), 575–590.

Cooney, P. M., & Lorente, M. A. (2009). A structuring event of Campanian age in western Venezuela, interpreted from seismic and paleontological data. *Geological Society Special Publications*, *328*, 687–703.

Cushman, J. A., & Hedberg, H. D. (1930). Notes on some foraminifera from Venezuela and Colombia. *Contributions from the Cushman Laboratory for Foraminiferal Research*, *6*, 64–69.

Cushman, J. A., & Hedberg, H. D. (1941). Upper Cretaceous foraminifera from Santander del Norte, Colombia. *Contributions from the Cushman Laboratory for Journa of the Foraminiferal Research*, *17*, 79–100.

De La Parra, F., Jaramillo, C., Kaskes, P., Goderis, S., Claeys, P., Villasante-Marcos, V., Bayona, G., Hatsukawa, Y., & Caballero, D. (2022). Unraveling the record of a tropical continental Cretaceous–Paleogene boundary in northern Colombia, South America. *Journal of South American Earth Sciences*, *114*, 103717. https://doi.org/10.1016/j.jsames.2022.103717

Dummann, W., Hofmann, P., Herrle, J. O., Wennrich, V., & Wagner, T. (2021). A refined model of Early Cretaceous South Atlantic–Southern Ocean gateway evolution based on high-resolution data from DSDP Site 511 (Falkland Plateau). *Palaeogeography, Palaeoclimatology, Palaeoecology*, *562*, 110113. https://doi.org/10.1016/j.palaeo.2020.110113

Erlich, R. N., Macsotay, O., Nederbragt, A. J., & Lorente, M. A. (1999). Palaeoecology, palaeogeography and depositional environments of Upper Cretaceous rocks of western Venezuela. *Palaeogeography, Palaeoclimatology, Palaeoecology*, *153*(1–4), 203–238.

Frizzell, D. L. (1954). *Handbook of Cretaceous Foraminifera of Texas*. University of Texas at Austin, Bureau of Economic Geology Report of Investigations, *22*, 1–237.

Garzón, S., Warny, S., & Bart, P. J. (2012). A palynological and sequence-stratigraphic study of Santonian–Maastrichtian strata from the Upper Magdalena Valley basin in central Colombia. *Palynology*, *36*(Suppl. 1), 112–133.

Georgescu, M. D. (2005). On the systematics of rugoglobigerinids (planktonic foraminifera, Late Cretaceous). *Studia Geologica Polonica*, *124*, 87–97.

Govin, A., Holzwarth, U., Heslop, D., Ford Keeling, L., Zabel, M., Mulitza, S., Collins, J. A., & Chiessi, C. M. (2012). Distribution of major elements in Atlantic surface sediments (36°N–49°S): Imprint of terrigenous input and continental weathering. *Geochemistry, Geophysics, Geosystems 13*, Q01013, https://doi/10.1029/ 2011gc 003785.

Gramal-Aguilar, A., Carranco-Andino, F., Romero-Cóndor, C., Pulupa-Vela, R., Calderón-Romero, D., & Toainga-Oñate, S. (2021). Evidencias de canibalización de secuencias Cretácicas y Paleógenas de la Cuenca Oriente en la cuña orogénica de los Andes ecuatorianos. *Boletín de Geología*, *43*(3), 15–34.

Guerrero, J., Sarmiento, G., & Navarrete, R. E. (2000). The Stratigraphy of the W side of the Cretaceous Colombian basin in the Upper Magdalena Valley. Reevaluation of selected areas and type localities including Aipe, Guaduas, Ortega, and Piedras. *Geología Colombiana*, *25*, 45–110.

Hammer, O., Harper, D. A. T., & Ryan, P. D. (2001). PAST: paleontological statistics software package for education and data analysis. *Palaeontologia Electronica*, *4*(1), 1–9.

Hardenbol, J., Thierry, J., Farley, M., Jacquin, T., De Graciansky, P., & Vail, P. (1998). Mesozoic and Cenozoic sequence chronostratigraphic framework of European basins. In P. Graciansky, J. Hardenbol, T. Jacquin, P. Vail, & M. Farley (Eds.), *Mesozoic and Cenozoic Sequences Stratigraphy of European Basins* (pp. 3–13). SEPM Special Publication 60.

Huber, B. T., MacLeod, K. G., Watkins, D. K., & Coffind, M. L. (2018). The rise and fall of the Cretaceous Hot Greenhouse climate. *Global and Planetary Change*, *167*, 1–23.

Jorissen, F. J., Fontanier, C., & Thomas, E. (2007). Paleoceanographical indicators based on deep-sea benthic foraminiferal assemblage characteristics. *Developments in Marine Geology*, *1*, 263–325.

Kominz, M. A., Browning, J. V., Miller, K. G., Sugarman, P. J., Mizintsevaw, S., & Scotese, C. R. (2008). Late Cretaceous to Miocene sea-level estimates from the New Jersey and Delaware coastal plain coreholes: an error analysis. *Basin Research*, *20*(2), 211–226.

Lyle, M., Olivarez-Lyle, A., Gorgas, T., Holbourn, A., Westerhold, T., Hathorne, E. C., Kimoto, K., & Yamamoto, S. (2012). Data report: raw and normalized elemental data along the U1338 splice from X-ray Fluorescence scanning. *Proceedings of the Integrated Ocean Drilling Program*, 320/321, DOI:10.2204/iodp.proc.320321.2010

Martínez, J. I. (1989). Foraminiferal biostratigraphy and paleoenvironments of the Maastrichtian Colón mudstones of Northern South America. *Micropaleontology*, *35*(2), 97–113.

Martínez, J. I. (2003). The Paleoecology of late Cretaceous upwelling events from the Upper Magdalena Basin, Colombia. *Palaios*, *18*(4–5), 305–320.

Martínez, J. I., & Hernandez, R. (1992). Evolution and drowning of the Late Cretaceous Venezuelan carbonate platform. *Journal of South American Earth Sciences, 5*(2), 197–210.

Montaño, P. C., Nova, G., Bayona, G., Mahecha, H., Ayala, C., Jaramillo, C., & De La Parra, F. (2016). Análisis de secuencias y procedencia en sucesiones sedimentarias de grano fino: un ejemplo de la Formación Umir y base de la Formación Lisama, en el sector de Simacota (Santander, Colombia). *Boletín de Geología*, *38*(1), 51–72.

Montes, C., Rodríguez-Corcho, A. F., Bayona, G., Hoyos, N., Zapata, S., & Cardona, A. (2019). Continental margin response to the multiple arc-continent collisions: The northern Andes-Caribbean margin. *Earth Science Reviews*, *198*, 102903. https://doi.org/10.1016/j.earscirev.2019.102903

Navarrete, R. E., Parra, F. J., Pérez-Panera, J. P., Daza, D., Sánchez, C., Prince, M., & Rodríguez, M. (2018). Turonian–Campanian foraminifera zonation for the La Luna and lower Umir formations, Middle Magdalena Valley Basin, northern Colombia. In Cusminsky *et al.* (Eds.), *Advances in South American Micropaleontology - Selected papers of the 11th Argentine Paleontological Congress* (pp. 67–114). Springer Earth System Science Series.

Nederbragt, A. (1991). Late Cretaceous biostratigraphy and development of Heterohelicidae (planktic foraminifera). *Micropaleontology, 37*(4), 329–372.

Parra, M., Moscardelli, L., & Lorente, M. A. (2003). Late Cretaceous anoxia and lateral microfacies changes in the Tres Esquinas Member, La Luna Formation, Western Venezuela. *Palaios*, *18*, 321–333.

Patarroyo, G. D, Alarcón, C. M., Torres, J. M., Díaz, J. S., Gómez, J. S., Márquez, J. J., Pontón, L. A., & Barragán, D. M. (2021). Reconocimiento geológico de la Formación La Luna en el sector de Matanza (Oeste del Macizo de Santander, Colombia). *Boletín de Geología*, *43*(1), 35–51.

Patarroyo, G. D., Kochhann, K. G. D., Ceolin, D., Guerra, R., Alegret, L., & Bom, M. H. H. (2022). Paleoenvironmental changes recorded at a late Maastrichtian marine succession of Northern South America. *Journal of South American Earth Sciences*, *119*, 104015. https://doi.org/10.1016/j.jsames.2022.104015

Patarroyo, G. D., Torres, G. A., Rincón, D. A., Cárdenas, C. P., & Márquez, R. E. (2017). Bioestratigrafía e inferencias paleoambientales de las asociaciones de foraminíferos en las formaciones cretácicas La Luna-Colón (Cuenca del Catatumbo, Colombia). *Boletín de Geología*, *39*(3), 25–40.

Pérez-Panera, J. P., Parra, F. J., Navarrete, R. E., Sánchez, C., Daza, D., Rodriguez, M., & Prince, M. (2018). Turonian–Santonian Calcareous Nannofossil Biozonation for La Luna Formation, Middle Magdalena Valley Basin, Northern Colombia. In Cusminski *et al.* (Eds.), *Advances in South American Micropaleontology-Selected papers of the 11th Argentine Paleontological Congress*. (pp. 46–66). Springer Earth System Science Series.

Petters, V. (1955). Development of Upper Cretaceous foraminiferal faunas in Colombia. *Journal of Paleontology*, *29*(2), 212–225.

Premoli Silva, I., & Verga, D. (2011). P*ractical manual of Cretaceous planktonic foraminifera. New Editing by Marie Rose Petrizzo and Isabella Premoli Silva. International School on Planktonic Foraminifera 3rd Course: Cretaceous Planktonic Foraminifera*. Milano University.

Rangel, A., Parra, P., & Niño, C. (2000). The La Luna formation: chemostratigraphy and organic facies in the Middle Magdalena Basin. *Organic Geochemistry*, *31*(12), 1267–1284.

Roth, P. H. (1983). Jurassic and Lower Cretaceous calcareous nannofossils in the Western North Atlantic (Site 534): biostratigraphy, preservation and some observations on biogeography and paleoceanography. *Initial Reports of the Deep Sea Drilling Project*, *76*, 587–621.

Santos, C. E. (2012). *Palynostratigraphy of the Umir Formation, Middle Magdalena Valley Basin (MMVB) Colombia*" (MSc Theses Louisiana State University, United States). Available from / Retrieved from [https://digitalcommons.lsu.edu/gradschool_theses/2122].

Sarmiento, G. (1992). Palinología de la Formación Guaduas. Estratigráfica y Sistemática. *Boletín Geológico*, *32*(1–3), 45–126.

Sarmiento, G., Puentes, J., & Sierra, C. (2015). Evolución geológica y estratigráfica del sector norte del Valle Medio del Magdalena. *Geología Norandina*, *12*, 51–82.

Sarmiento-Rojas, L.F. (2019). Cretaceous stratigraphy and paleofacies maps of northwestern South America. In F. Cediel, & R. P. Shaw (Eds.), *Geology and Tectonics of Northwestern South America. The Pacific Caribbean Andean Junction* (pp. 673–747). Springer.

Scott, H.W. (1961). Classification of Ostracoda. Q74-Q91. In R. C. Moore, & C. W. Pitrat (Eds.), *Treatise on invertebrate paleontology, Part Q, Arthropoda 3: Crustacea, Ostracoda*. Geological Society of America and University of Kansas Press.

Sellier de Civrieux, J. M. (1952). Estudio de la microfauna de la sección-tipo del Miembro Socuy de la Formación Colón, Distrito Mara, Estado Zulia. *Boletín de Geología y Minas (Venezuela)*, *2*(5), 231–310.

Shenkar, N., & Swalla, B. J. (2011). Global Diversity of Ascidiacea. *PLoS ONE*, 6, e20657, https://doi/10.1371/journal.pone.0020657.

Sole de Porta, N. (1972). Palinologia de la Formacion Cimarrona (Maastrichtiense) en el valle medio del Magdalena, Colombia. *Studia Geologica*, *4*, 103–142.

Sohn, I. G. (1961). Techniques for preparation and study of fossil ostracodes. In R. C. Moore, & C. W. Pitrat (Eds.), *Treatise on invertebrate paleontology, Part Q, Arthropoda 3: Crustacea, Ostracoda* (pp. Q63–Q70). Geological Society of America and University of Kansas Press.

Tchegliakova, N. (1993). Los foraminíferos y los minerales antigénicos de la Formación Umir (sección Quebrada La Julia, Valle Medio del Magdalena): registro de laguna costera a finales del Cretácico Superior cuspidal (Maastrichtiano). *Geología Colombiana*, *18*, 107–117.

Tchegliakova, N. (1995). Los Foraminíferos de la Formación Umir (Sección Quebrada La Julia): Registro del Cretáceo Superior Cuspidal (Maestrichtiano) en el Valle Medio del Magdalena, Colombia. *Geología Colombiana*, *19*, 109–130.

Tchegliakova, N. (1996). Registro de las biozonas de foraminíferos planctónicos *Gansserina gansseri* y *Abathomphalus mayaroensis* (Maastrichtiano medio y superior) en el extremo meridional del Valle Medio del Magdalena (Colombia, Suramérica). *Geología Colombiana*, *20*, 67–90.

Tchegliakova, N., & Mojica, J. (2001). El Senoniano de la barrera de Girardot-Guataquí, Valle Alto del Magdalena, Colombia: Precisiones sobre la estratigrafía y establecimiento de una zonación micropaleontológica. *Revista de la Academia Colombiana de Ciencias Exactas, Físicas y Naturales*, *25*(94), 37–75.

Terraza, R. (2019). "Formación La Luna": expresión espuria en la geología colombiana. In F. Etayo-Serna (Ed.), *Estudios geológicos y paleontológicos sobre el Cretácico en la región del embalse del río Sogamoso, Valle Medio del Magdalena* (pp. 305–362). Servicio Geológico Colombiano 23.

Valencia-Gómez, J. C., Cardona, A., Bayona, G., Valencia, V., & Zapata, S. (2020). Análisis de procedencia del registro sin-orogénico Maastrichtiano de la Formación Cimarrona, flanco occidental de la Cordillera Oriental colombiana. *Boletín de Geología*, *42*(3), 171–204.

Van der Akker, T. J. H. A., Kaminski, M. A., Gradstein, F. M., & Wood, J. (2000). Campanian to Palaeocene biostratigraphy and palaeoenvironments in the Foula Sub-basin, west of the Shetland Islands, UK. *Journal of Micropalaeontology*, *19*, 23–43.

Van der Hammen, T. (1954). El desarrollo de la flora colombiana en los periodos Geológicos. Maastrichtiano hasta Terciario más inferior. (Una investigación palinológica de la Formación Guaduas y equivalentes). *Boletín Geológico*, *2*(1), 49–106.

Van der Hammen, T. (1957). Climatic periodicity and evolution of South American Maastrichtian and Tertiary flora (a study based on pollen analysis in Colombia). *Boletín Geológico*, *5*(2), 57–91.

Vergara, L. S. (1997). Stratigraphy, foraminiferal assemblages and paleoenvironments in the Late Cretaceous of the Upper Magdalena Valley, Colombia (Part I), *Journal of South American Earth Sciences*, *10*(2), 111–132.

Villamil, T., & Pindell, J. (1998). Mesozoic paleogeographic evolution of northern South America. In J. Pindell, & C. Drake (Eds.), *Paleogeographic evolution and non-glacial eustacy, northern South America* (pp.238–318). SEPM Society for Sedimentary Geology 58.

Ward, D. E., Goldsmith, R., Cruz, J., & Restrepo, H. (1973). Geología de los cuadrángulos H-12 Bucaramanga y H-13 Pamplona, Departamento de Santander. *Boletín Geológico*, *21*(1–3), 1–134.

Wei, W., & Algeo, T. (2020). Elemental proxies for paleosalinity analysis of ancient shales and mudrocks. *Geochimica et Cosmochimica* Acta, *287*, 341–366.

Yepes, O. (2001). Maastrichtian/Danian dinoflagellate cyst biostratigraphy and biogeography from two equatorial sections in Colombia and Venezuela. *Palynology*, *25*(1), 217–249.

doi: 10.5710/AMGH.02.03.2023.3525

Submitted: 21 June 2022
Accepted: 2 March 2023
Published: 23 June 2023

Porque –eles sabiam– não era a verdadeira noite, a noite da lua e das estrelas, da música e do amor, que chegara. Esta só chegava na sua hora, quando os sinos tocavam e um negro cantava ao violão, no cais, uma cantiga de saudade. A que chegara carregada de nuvens, trazida pelo vento, fora a tempestade que derrubava aos navios e matava os homens. A tempestade é a falsa noite.

Mar Morto

Jorge Amado

CHAPTER 3

BENTHIC FORAMINIFERA AND PALEOENVIRONMENTAL TURNOVER ACROSS THE MID-MAASTRICHTIAN EVENT IN THE TROPICAL ATLANTIC OCEAN (ODP SITE 1258)

Contribution roles taxonomy

German David Patarroyo (itt Oceaneon, Unisinos University). Micropaleontological and geochemical preparation. Foraminiferal taxonomy and geochemical analyses. Integration and discussion of results.

Karlos Kochhann (itt Oceaneon, Unisinos University). Foraminiferal, geochemical and paleoceanographic discussions.

Laia Alegret (Zaragoza University). Benthic foraminiferal ecology and taxonomic comments. Paleoceanographic discussions.

Manuscript in preparation for: Paleoceanography and Paleoclimatology

BENTHIC FORAMINIFERA AND PALEOENVIRONMENTAL TURNOVER ACROSS THE MID-MAASTRICHTIAN EVENT IN THE TROPICAL ATLANTIC OCEAN (ODP SITE 1258)

ABSTRACT

In recent years, there has been an increasing number of studies describing significant disturbances of the global carbon cycle during the latest Cretaceous. One example of these disturbances is the Mid-Maastrichtian Event (MME), which was likely related to changes in deep ocean circulation, particularly in the Atlantic realm.

To track and characterize the influence of the MME in deep-water environments in the equatorial South American margin, we conducted micropaleontological (benthic foraminifers) and geochemical analyses of sediments from Ocean Drilling Program (ODP) Site 1258 (Demerara Rise, offshore Suriname). Both geochemical tracers and benthic foraminiferal assemblages suggest the occurrence of paleoenvironmental reorganizations during the entire Maastrichtian, related to changes of intermediate to deep-water oxygenation and surface productivity. Benthic foraminiferal assemblages, characterized by typical deep-sea taxa (*Aragonia*, *Nuttallides truempyi*, *Coryphostoma*, *Strictocostella*, among others), indicate suboxic bottom water conditions with some oxygenation pulses, which correlate with changes in elemental ratios of redox-sensitive trace metals (Ni/Al, Cu/Al). Sediment elemental ratios (log(Fe/Ca), Si/Ti, Fe/K) indicate fluctuations in the silica and carbonate export via surface productivity, and a probable hydroclimate disturbance since the early Maastrichtian. During the MME, three phases of environmental evolution occurred: (1) high surface productivity and reduced bottom water oxygenation during subinterval MME1, (2) moderate surface productivity and increased bottom water oxygenation in subinterval MME2, and (3) recovery in surface productivity, suboxic conditions in the deep-sea, and more humid conditions during subinterval MME3. These paleoenvironmental disturbances were probably caused by increased influence of high-latitude deep-waters (North Atlantic source instead of the Southern Ocean) on low latitudes, which likely influenced latitudinal migrations of the Paleo-Intertropical Convergence Zone.

INTRODUCTION

The latest Cretaceous (Campanian-Maastrichtian) was a time of significant changes in global climate. Sea-surface temperatures (SSTs) steadily drifted from a “hot greenhouse” state with reduced SST latitudinal gradient, to a “cool greenhouse” state, that characterized the Maastrichtian and early Paleocene, which likely had moderate latitudinal SSTs gradients (e.g., Friedrich et al., 2012; Linnert et al., 2014; Barnet et al., 2017; O´Brien et al., 2017; Huber et al., 2018; Hull et al., 2020). This drift of the mean ocean-climate state has been explained by a combination of changes, such as in: (1) global oceanic deep-water circulation, (2) atmospheric pCO_2 related to mid-ocean ridge and large igneous provinces activity, (3) eustatic sea-level (regional and global) and, (4) intensity of tectonic processes (e.g., Barrera et al., 1997; Coffin et al., 2006; Jarvis et al., 2006; McLeod et al., 2011; Martin et al., 2012; Voigt et al., 2013; Dameron et al., 2017; Linnert et al., 2018; Ladant et al., 2020). Those processes, and specially the controlling mechanisms of deep-water formation in the Atlantic and Pacific oceans have been described as possible triggers of at least two significant perturbations in the global carbon cycle during the latest Cretaceous: (1) the Campanian-Maastrichtian Boundary Event (CME; Friedrich et al., 2009), and (2) the mid-Maastrichtian Event (MME; Voigt et al., 2012).

In particular, the MME (69 Ma) has been studied in more detail due to its possible temporal correlation with major reorganizations of the marine biota. For instance, the MME was likely coeval with the decline of inoceramids and rudist reefs (Johnson, 2002; Frank et al., 2005; Huber et al., 2018), as well as with turnovers among benthic and planktonic foraminiferal assemblages, which were possibly related with changes of carbon influxes to the atmosphere and the ocean (Frank et al., 2015; Dameron et al., 2017; Vancoppenolle et al., 2022). Pelagic ecosystems after the MME (68-66.5 Ma) and before the Cretaceous-Paleogene (K-Pg) extinction event, could have been also affected by widespread Deccan Traps volcanism (e.g., Abramovich and Keller, 2003; Thibault and Gardin, 2007; Keller and Abramovich, 2009; Abramovich et al., 2010; Thibault and Husson, 2016; Linnert et al., 2016; Mateo et al., 2017; Keller et al., 2020; Hull et al., 2020; Guerra et al., 2021; Krahl et al., 2021). So far and based on carbon isotope records ($\delta^{13}C$), the MME is identified as an interval characterized by a plateau depicted by stable carbon isotope ($\delta^{13}C$) carbonate records, with onset above the base of geomagnetic polarity chron C31n, consisting of two positive inflections and a drop in between (MME1-MME3; ~69.2 to ~68.0 Ma; Voigt et al., 2012).

The MME has been correlated with deep-water circulation reconfigurations, when deep-water masses sources shifted from saline and warm low-latitude water masses, to cool and less saline high-latitude water masses (e.g., Frank et al., 2005; D´Hondt and Arthur, 2002; Friedrich et al., 2008; Cramer et al., 2009; Jung et al., 2013; Linnert et al., 2014; Moiroud et al., 2016; Dameron et al., 2017; Batenburg et al., 2018; Haynes et al., 2020; Ladant et al., 2020). In the Atlantic realm, micropaleontological (foraminifers, calcareous nannofossils), geochemical (elemental ratios, total organic carbon — TOC, and carbonate contents) and carbon, oxygen and neodymium isotope records ($\delta^{13}C$, $\delta^{18}O$, εNd) suggest that, since the early Maastrichtian, warm-saline water masses were developed in the equatorial Atlantic (e.g., Demerara Bottom Water, DBW), with an increasing influence of a northern-sourced water since 69 Ma. Before that time, the North Atlantic was still a semi-restricted basin, with estuarine circulation and deep-water masses coming from the eastern Tethys Ocean (Widmark and

Speijer, 1997a-b; Friedrich et al., 2004; Thibault and Gardin, 2006; Friedrich and Erbacher, 2006; Friedrich and Hemleben, 2007; MacLeod et al., 2011; Koch and Friedrich, 2012; Martin et al., 2012; Linnert et al., 2019; Vancoppenolle et al., 2022; Corentin et al., 2023). In addition to the intermediate/deep-water reorganization in the Atlantic Ocean, there were regional influences of epicontinental seas (northern South America/Africa, U.S. Western Interior, European Tethys), tectonic processes (e.g., first pulses of Andean orogeny) and global eustatic sea-level changes that might have influenced surface productivity and regional carbon fluxes (e.g., Martínez and Hernández, 1992; Friedrich et al., 2004; 2009; Linnert et al., 2018; Bayona et al., 2020; Vellekoop et al., 2022; Patarroyo et al., 2022; Farouk et al., 2023). On a global scale, intermediate and deep-water circulation between the Pacific Ocean and the Atlantic through the Caribbean gateway was ineffective, and the presence of submarine barriers in the South Atlantic, such as the Rio Grande Rise and the Walvis Ridge, likely restricted deep-water formation in the Pacific to the northern hemisphere (e.g., Frank et al., 2005; Jung et al., 2013; Dameron et al., 2017).

Considering the privileged geographic location of the Maastrichtian sedimentary record on the Demerara Rise (offshore Surinam, Equatorial Atlantic), we present a paleoenvironmental assessment of the equatorial Atlantic Ocean during the Maastrichtian in terms of: (1) surface productivity and bottom water oxygenation, (2) continental influence due weathering and tectonic activity, and (3) teleconnections with other equatorial (Pacific realm, eastern Tethys) and high latitude ocean basins. To achieve these goals, we integrated micropaleontological (benthic foraminifers) and geochemical (bulk sediments elemental ratios, and stable carbon isotope records) studies at Ocean Drilling Program (ODP) Hole 1258A, providing new insights on the influences of the MME on low latitude areas, and its link with paleoenvironmental perturbations in the high-latitude North Atlantic Ocean.

STUDY SITE

ODP Hole 1258A (15°06.99' N, 69°22.67' W; 3192 m depth) is located on the northwest-facing slope of the Demerara Rise (Suriname, South America; Figure 1). The studied interval comprises the earliest to late Maastrichtian (sections 28-2 to 34-4; 257.50-320.11 meters below seafloor; mbsf), and except for the coring gap between 279.11 and 284.13 mbsf, the studied section was sampled every ~40 cm (152 samples in total). Campanian to Maastrichtian sediments at Hole 1258A mostly consist of nannofossil chalks with foraminifers (subunits IIB-C and unit III; Erbacher et al., 2004). The main sedimentological transition within the studied interval is a drop of carbonate content from ~65 wt% in Subunit IIC to ~35 wt% in Unit III (Erbacher et al., 2004).

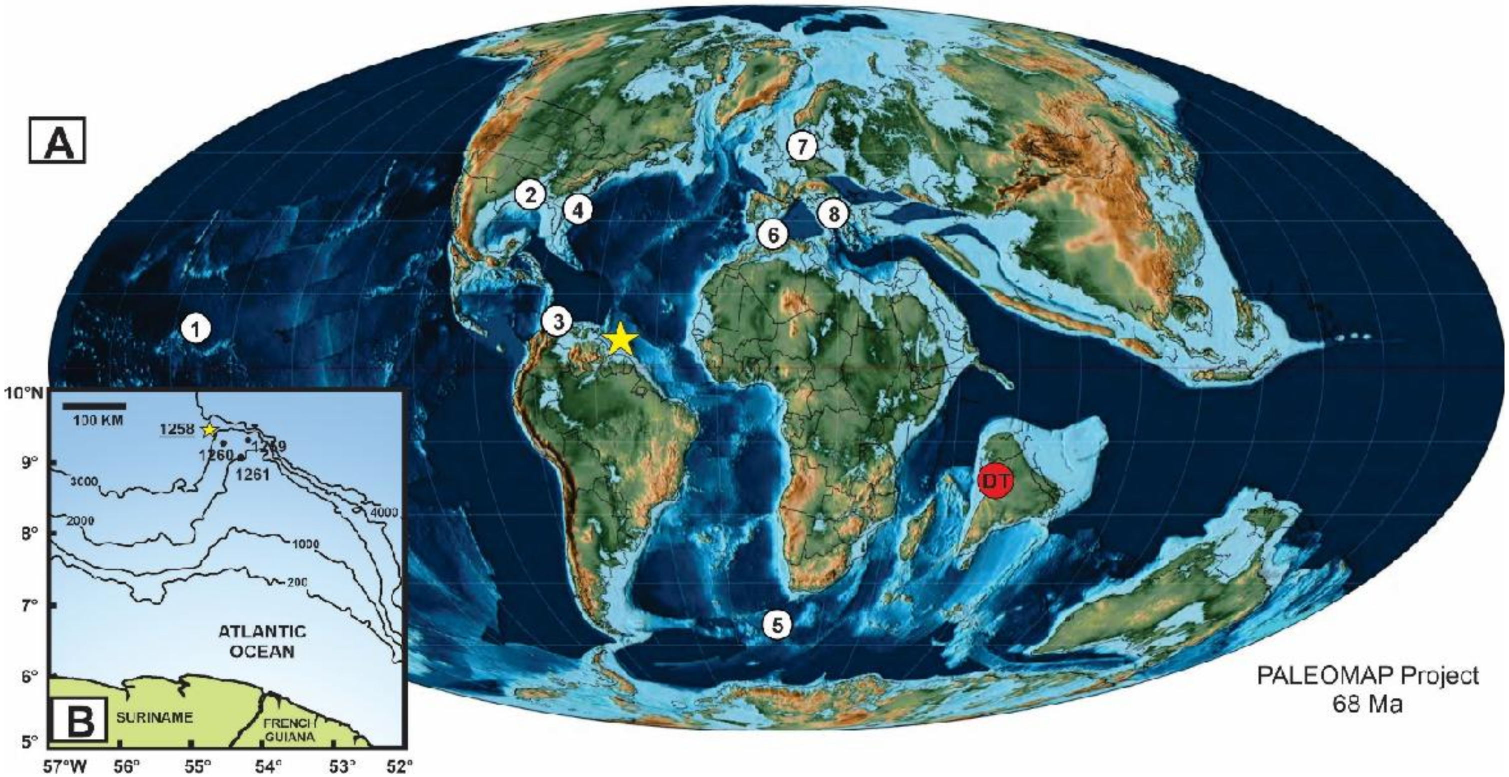

Figure 1. Location of the study sites and additional localities. (A) Paleogeographic map of the Maastrichtian (68 Ma, from Scotesse, 2014) showing the location of ODP Hole 1258A at Demerara Rise (yellow star) and other Campanian-Maastrichtian localities with available foraminiferal and isotopic data. (1) Shatsky Rise (Frank et al., 2005; Voigt et al., 2010; Dameron et al., 2017), (2) Shuqualak, Mississippi (Linert et al., 2014; 2018), (3) Core Diablito-1E (Patarroyo et al., 2022), (4) Blake Nose (Friedrich and Hemleben, 2006), (5) ODP site 690 (Koch and Friedrich, 2012), (6) Tunisia (Li et al., 1999; Bejaoui et al., 2019; Farouk et al., 2023), (7) Maastricht (Vancoppenolle et al., 2022; Vellekoop et al., 2022), (8) Gubbio (Voigt et al., 2012). (B) Topographic map of the Demerara Rise based on Erbacher et al. (2004).

The Campanian-Maastrichtian boundary at Hole 1258A was identified at 315.00 mbsf, and the K-Pg boundary is located at 252.58 mbsf, at the base of a well-preserved impact ejecta layer (base of subunit IIB; Erbacher et al., 2004). According to magnetostratigraphy, the studied interval comprises magnetochrons C31r to C29r, where the base of mid-Maastrichtian C31n magnetochron (broadly defined as C31n-C30r-C30n) was defined at 293.52 mbsf (Suganuma and Ogg, 2006). Planktonic foraminiferal KS30b to KS31 zones were identified for our studied interval, with typical Maastrichtian species such as *Globotruncanita stuarti*, *Rugoglobigerina rugosa*, *Abathomphalus mayarorensis* (FO at 279.31 mbsf), *Pseudoguembelina costillifera*, *Pseudoguembelina palpebra*, *Contusotruncana contusa* (Erbacher et al., 2004). Calcareous nannofossil zones CC22 to CC26 were reported by the same authors, while Thibault and Gardin (2006) proposed additional events (e.g., *Kamptnerius magnificus* acme event) and a more precise biostratigraphic scheme for the Maastrichtian (CC24 to CC26b).

METHODS

Benthic foraminifera

All foraminiferal samples (n = 80) were prepared according to standard methods at the Technological Institute for Paleoceanography and Climate Change (itt Oceaneon – Unisinos University, Brazil). Approximately 15–20 g of dry sediment aliquots were soaked in distilled water for about 24 hours, washed over 63 µm and 150 µm sieves, and dried in an oven at 40°C. To achieve statistically significant counts (Fatela and Taborda, 2002, Forcina, 2012), around 100-300 benthic foraminifers were handpicked from each sample. To avoid overestimations in the foraminiferal analyses, we omitted the uniserial/tubular agglutinated forms (e.g., *Nothia*, *Rhabdammina*) in the final counts, and we only considered the calcareous uniserial taxa (e.g., *Nodosaria*, *Strictocostella*) that were >60% complete.

Benthic foraminiferal taxonomy and palaeoenvironmental preferences followed regional literature for the tropics and the Atlantic realm (Frizzell, 1954; Koutsoukos and Merrick, 1986; Koutsoukos and Hart, 1990; Bolli et al., 1994; Widmark, 1997; Koutsoukos and Klasz, 2000; Koutsoukos, 1992; 2006; Alegret and Thomas, 2001; Friedrich and Hemleben, 2012; Koch and Friedrich et al., 2012; Dubicka and Peryt, 2016; Dameron et al., 2017; Bejaoui et al., 2019; Jaff and Lawa, 2019; Vancoppenolle et al., 2022). The definition of benthic foraminiferal morphogroups and their ecological preferences (epifaunal, infaunal) followed Frenzel (2000) and Cetean et al. (2011). Selected foraminiferal specimens were imaged using a Zeiss EVO MA15 scanning electron microscope (SEM) at itt Oceaneon.

To assess export productivity during the Maastrichtian, benthic foraminiferal numbers (BFN = number of benthic foraminifera per gram of dry sediment) were estimated for each sample, and benthic foraminiferal accumulation rates (BFAR, expressed in $cm^{-2}\ ky^{-1}$) were calculated by multiplying BFN by sediments dry bulk density and linear sedimentation rates (LSR; see section 4.1). Bulk sediment dry densities from Hole 1258A ranged between 1.41 and 1.76 g/cm^3 within the studied interval (Erbacher et al., 2004). BFN and BFAR estimations have been used to track changes in surface export productivity (Jorissen et al., 2007). Diversity (Shannon-H), richness (S) and evenness (E) estimations were calculated for foraminiferal assemblages using the software Past (version 2.15; Hammer et al., 2001). All studied specimens were archived in the micropaleontological collection at itt Oceaneon. Total foraminiferal counts and their diversity estimates are available in Supplementary Table S1.

Inorganic geochemistry

X-ray fluorescence (XRF) analyses were performed on 5 g of dry, ground, and homogenized sediment samples (*n* = 152), with elemental concentrations reported as raw counts per second (cps). Samples were measured at 10 kV (150 µA, no filter) for Al, Mg, and Si intensities; 12 kV (400 µA, Al-50 filter) for Ca, K, Ti and V intensities; 20 kV (250 µA, Al – 200 filter) for Co, Cr, Fe and Mn intensities; and 50 kV (100 µA, Ti filter) for Ba and Rb intensities. XRF analyses were performed with a PanAlytical Epsilon 1 XRF spectrometer, at itt Oceaneon. To reduce noise, data were normalized to a median-scaled (NMS) following Lyle et al. (2012).

We used several elemental ratios for paleoenvironmental inferences (Calvert et al., 2007). The log(Fe/Ca) ratio was used as a tracer for carbonate accumulation and terrigenous input (Kujau et al., 2010; Govin et al., 2012), while the Fe/K ratio is interpreted as a proxy for weathering intensity at sediments source area (e.g., Stuut et al., 2005; Mulitza et al., 2008; Govin et al., 2012). Silica export and surface productivity was explored using the Si/Ti ratio (e.g., Agnihotri et al., 2008). Finally, bottom water oxygenation was evaluated with the NMS intensities of the redox-sensitive trace metals Ni and Cu, normalized by NMS Al intensities (e.g. Dummann et al., 2021).

Bulk carbonate (*n* = 98) $\delta^{13}C$ and $\delta^{18}O$ values were measured with a MAT 253 (Thermo Scientific) isotope ratio mass spectrometer (IRMS), at itt Oceaneon. Samples were allowed to react with 105% phosphoric acid (H3PO4) at 73°C. All isotope values are reported in ‰, relative to the Vienna PeeDee Belemnite scale. Measurements accuracy and calibrations were performed with the standards IAEA - 203 and IAEA -CO-8 from the International Atomic Energy Agency (IAEA), and SHP2L from the University of São Paulo (USP; Crivellari et al., 2021).

All geochemical data are provided in Supplementary Table S2.

RESULTS

Stratigraphy of the Campanian-Maastrichtian at ODP Site 1258A

Erbacher et al (2004) suggested that LSRs for the Campanian-Maastrichtian interval of Hole 1258A were around 1 cm ky^{-1}. However, using the position of the K-Pg boundary given by those authors at 252.58 mbsf, and the estimated bases of geomagnetic polarity chrons C31r, C31n and C29r (330.34 mbsf, 293.52 mbsf, 262.77 mbsf respectively; Suganuma and Ogg, 2006; MacLeod et al., 2017), the resulting age model for Hole 1258A (Supplementary material Figure S1) indicates that the LSR ranged between 1.1 and 2.9 cm ky^{-1} (1.2 cm ky^{-1} for the mid-Maastrichtian). Considering these LSRs, the studied time interval spanned from 66.2 Ma to 70.8 Ma, and the beginning of the mid-Maastrichtian (69.3 Ma) is likely located at 293.48 mbsf. Our age model overall agrees with the original proposal of Erbacher et al. (2004), and with the more detailed study of Thibault and Gardin (2006) for the Maastrichtian. Additionally, our age model also agrees with Thibault and Gardin (2006) that the Campanian-Maastrichtian boundary is not recorded within the analyzed interval, since the earliest Maastrichtian calcareous nannofossils biozone CC24 occurs above 322.8 mbsf.

Benthic foraminiferal assemblages

Benthic foraminiferal assemblages are well to moderately preserved, and total abundances fluctuate along the studied interval of Hole 1258A (130-300 individuals/sample). At the species level, we identified 157 benthic foraminiferal taxa (81 genera, 110 species; supplementary table 1), with assemblages usually dominated by hyaline forms, typical of bathyal settings. Similar assemblages have been found in Campanian-Maastrichtian successions from tropical to mid-latitude settings in Trinidad (Koutsoukos and Merrick, 1986), northern Brazil (e.g., Koutsoukos and Hart, 1990; Koutsoukos and Klasz, 2000; Koutsoukos, 1992; 2006), northern Africa (Li et al., 1999; Bejaoui et al., 2019) and the middle East (Jaffa and Lawa, 2019; Jain et al., 2020). Benthic foraminifera are dominated by calcareous hyaline taxa (80-90% of the assemblages), which include trochospiral (*Cibicidoides*, *Gavelinella*, *Gyroidinoides*, *Nuttallides, Nuttallinella*), rounded planispiral (*Pullenia*), biconvex trochospiral (*Lenticulina*, *Osangularia*, *Saracenaria*), uniserial (*Laevidentalina*, *Nodosaria*, *Pleurostomella*, *Strictocostella*), biserial (*Aragonia*, *Bolivinoides*, *Coryphostoma*), elongated (*Praebulimina*, *Fursenkoina*), pyramidal (*Reussella*) and unilocular (*Oolina*) taxa. Agglutinated genera such as *Clavulinoides*, *Glomospira*, *Marssonella*, *Rhabdammina*, *Rzehakina*, *Spiroplectammina*, *Spiroplectinella*, among other taxa, make up 2-15% of the assemblages in most of the studied samples (Figure 2; Plates 1,2)

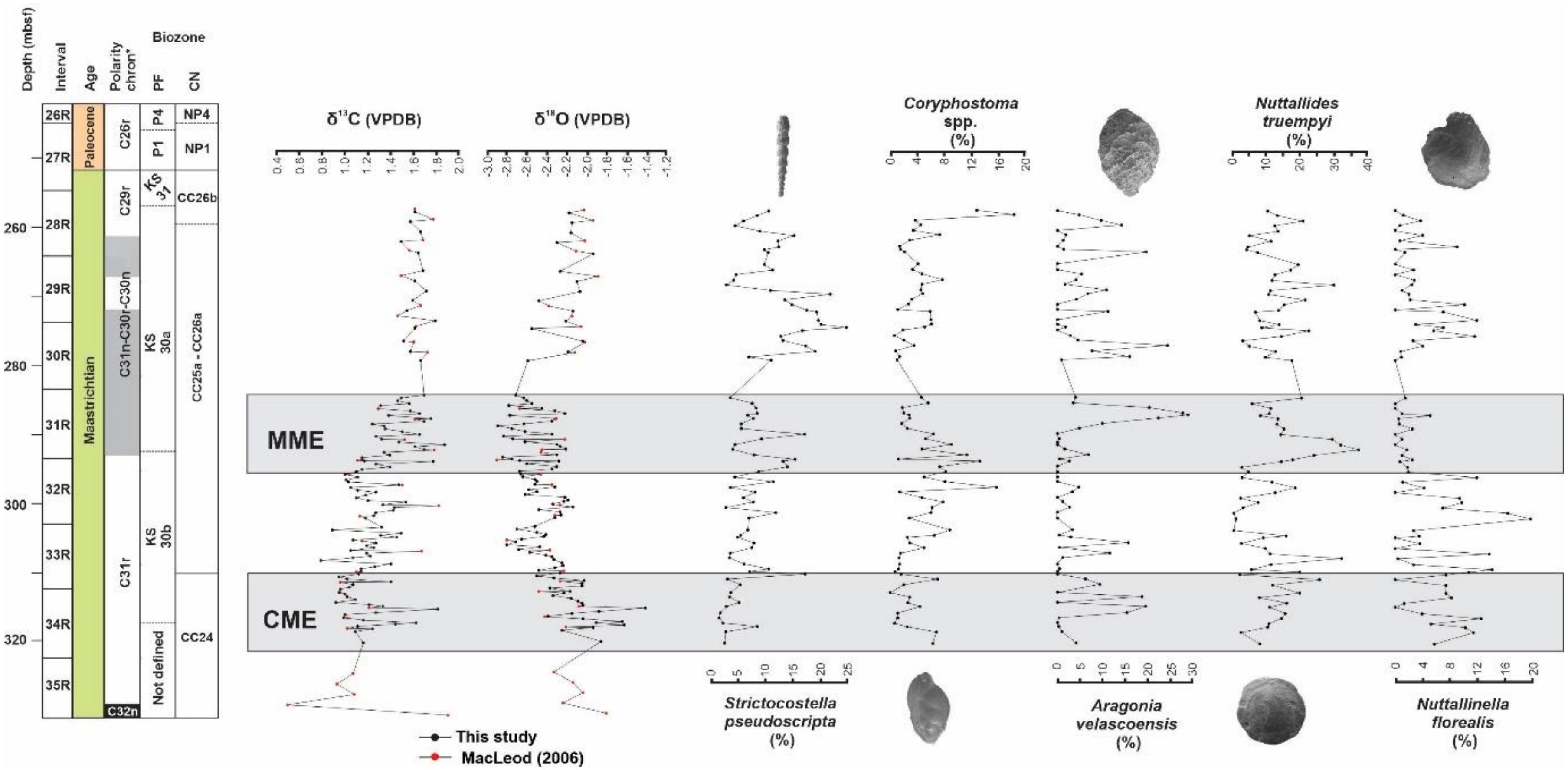

Figure 2. Bulk sediment $\delta^{13}C$ and $\delta^{18}O$, and relative abundance of selected benthic foraminifers across the Maastrichtian in Hole 1258A. *Chronostratigraphy based on Suganuma and Ogg (2006). Planktonic foraminifera (PF) and calcareous nannofossil (CN) biozones based on Erbacher et al. (2004) and Thibault and Gardin (2006). CME = Campanian-Maastrichtian Event, MME = Mid-Maastrichtian Event.

Plate 1. Selected benthic foraminifers from Hole 1258A (Demerara Rise). Scale bars represent 100 µm. 1. *Rhabdammina* sp. (34R3 64-66; 316,43 mbsf). 2. *Glomospira charoides* (34R3 142-144; 317,21 mbsf). 3. *Rzehakina epigona* (34R3 142-144; 317,21 mbsf). 4. *Marssonella oxycona* (33R3 20-22; 306,3 mbsf). 5. *Arenobulimina* sp. (33R5 25-27; 309,35 mbsf). 6. *Gaudryina* sp. (33R6 23-25; 310,83 mbsf). 7. *Spiroplectinella dentata* (31R2 143-145; 286,83 mbsf). 8-9. *Clavulinoides trilatera* (32R6 101-103, 33R1 60-62; 302,01 mbsf, 303,7 mbsf). 10. *Spiroplectammina spectabilis* (33R3 98-100; 307,1 mbsf). 11. *Pyrulina* sp. (34R3 142-144; 317,21 mbsf). 12. *Globulina* sp. (28R6 28-30; 262,7 mbsf). 13. *Lagena paucicosta* (33R3 20-22; 306,3 mbsf). 14. *Reussoolina apiculata* (29R6 20-22; 272,12 mbsf). 15. *Guttulina communis* (28R4 103-105; 260,41 mbsf). 16. *Fissurina laticarinata* (31R2 143-145; 286,83 mbsf). 17. *Fissurina* sp2 (33R4 103-105; 308,65 mbsf). 18. *Allomorphina trochoides* (33R7 68-70; 312,78 mbsf). 19. *Quadrimorphina allomorphinoides* (31R2 63-65; 286,03 mbsf). 20. *Marginulina* sp. (34R2 143-145; 315,73 mbsf). 21. *Laevidentalina communis* (34R4 118-119; 318,47 mbsf). 22. *Laevidentalina* sp. (33R4 15-17; 307,75 mbsf). 23. *Strictocostella pseudoscripta* (33R4 15-17; 307,75 mbsf). 24. *Pyramidulina majuscula* (34R3 142-144; 317,21 mbsf).

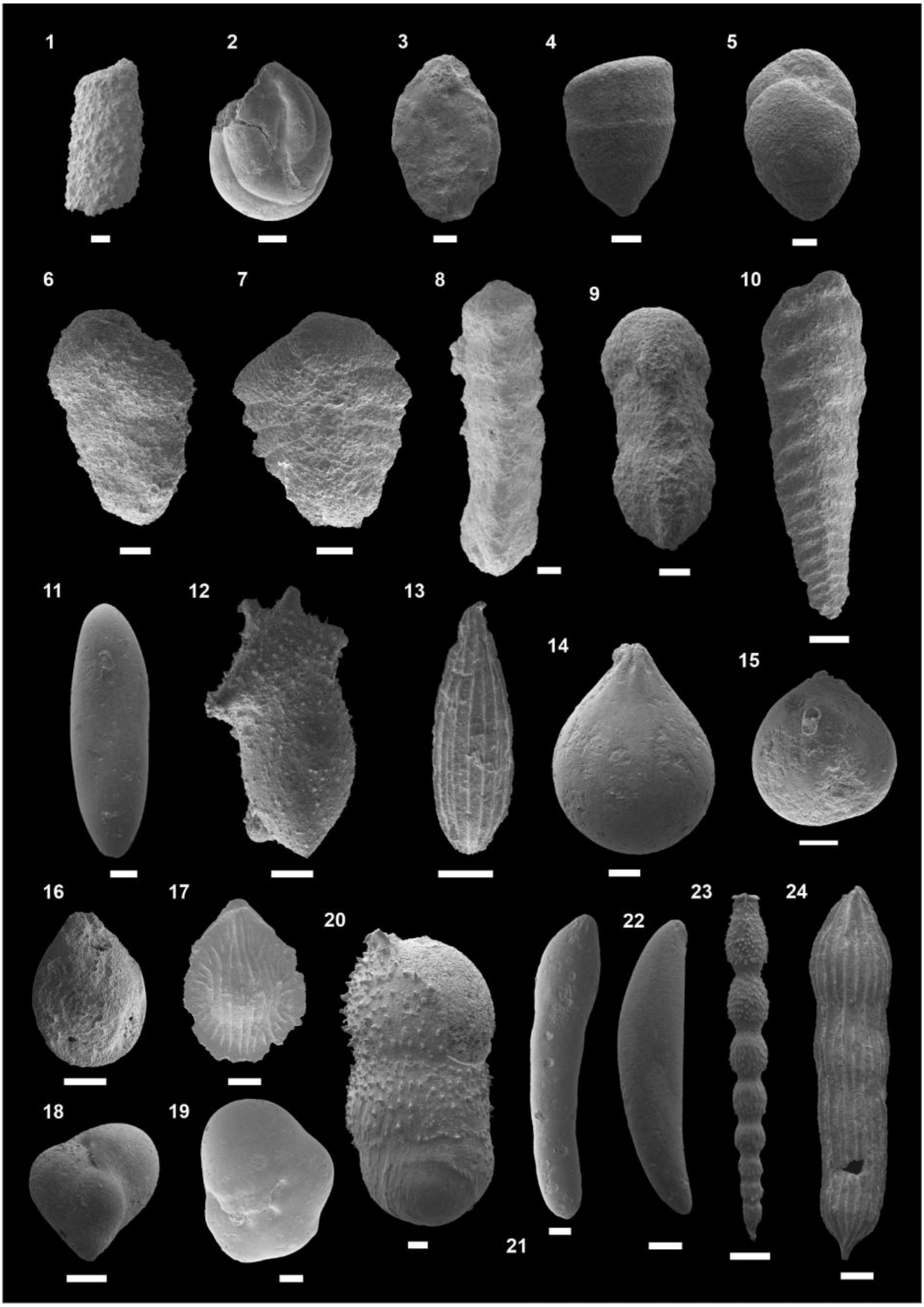
1
2
3
4
5
6
7
8
9
10
11
12
13
14
15
16
17
18
19
20
21
22
23
24

Plate 2. Selected benthic foraminifers from Hole 1258A (Demerara Rise). Scale bars represent 100 µm. 1. *Pleurostomella tenuis* (34R1 144-146; 314,24 mbsf). 2. *Nodosaria aspera* (34R1 144-146; 314,24 mbsf). 3. *Marginulina loisana* (31R1 65-67; 284,55 mbsf). 4. *Vaginulina trilobata* (30R4 41-43; 279,11 mbsf). 5. *Astacolus cretaceus* (33R5 25-27; 309,35 mbsf). 6. *Lenticulina rotulata* (34R4 118-119; 318,47 mbsf). 7. *Praebulimina spinata* (29R7 50-52; 273.92 mbsf). 8. *Coryphostoma incrassata* (34R2 143-145; 315.73 mbsf). 9. *Coryphostoma crassa* (29R7 50-52; 273,92 mbsf). 10. *Aragonia velascoensis* (34R2 143-145; 315,73 mbsf). 11. *Bolivinopsis draco* (28R3 103-105; 258,93 mbsf). 12. *Reussella szajnochae* (34R3 142-144; 317,21 mbsf). 13. *Neoflabellina* sp. (34R4 118-119; 318,47 mbsf). 14. *Pullenia jarvisi* (32R1 106-108; 294,56 mbsf). 15. *Pullenia cretacea* (28R4 103-105; 260,41 mbsf). 16. *Cibcidoides velascoensis*, dorsal view (28R2 110-112; 257,5 mbsf). 17. *Cibicidoides howelli*, dorsal view (31R2 63-65; 286,03 mbsf). 18. *Osangularia cordieriana,* dorsal view (28R2 110-112; 257,5 mbsf). 19. *Alabamina dorsoplana*, dorsal view (29RCC 3-5; 274,37 mbsf). 20. *Anomalimoides* cf. *acutus*, dorsal view (34R3 64-66; 316,43 mbsf). 21. *Gavelinella* cf. *correcta*, dorsal view (28R3 103-105; 258,93 mbsf). 22. *Nuttallides truempyi*, dorsal and ventral view (34R1 144-146; 314,24 mbsf). 23-24. *Nuttallinella florealis*, dorsal and ventral view (32R3 22-24, 33R6 103-105; 296,72 mbsf, 311,63 mbsf). 25. *Gyroidinoides girardanus*, dorsal and ventral view (33R7 68-70; 312,78 mbsf). 26. *Gyroidinoides globosus*, dorsal view (33R5 25-27; 309,35 mbsf). 27. *Gavelinella beccariformis*, ventral view (33R6 103-105; 311,63 mbsf). 28. *Gavelinella* sp., dorsal view (33R2 18-20; 304,78 mbsf). 29. *Gavelinella* cf. *nacatochensis*, dorsal view (28R3 103-105; 258,93 mbsf).

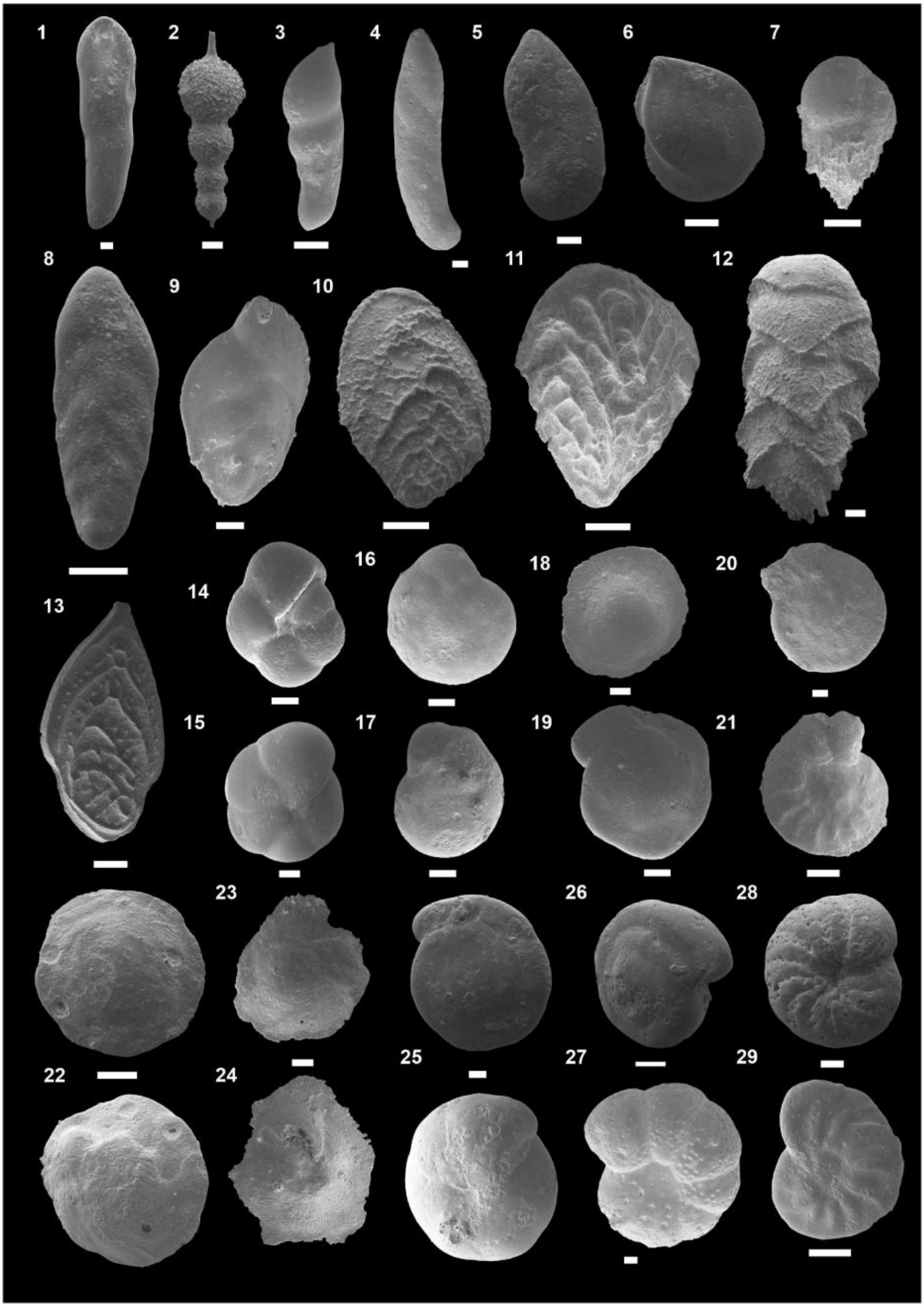
1
2
3
4
5
6
7
8
9
10
11
12
13
14
15
16
17
18
19
20
21
22
23
24
25
26
27
28
29

BFN and BFAR at Hole 1258A range from 4 to 17 specimens g^{-1} and from 10-38 specimens cm^{-2} ky^{-1}, respectively (Figure 3). For the early Maastrichtian, both the BFN and the BFAR depict general decreasing trends, while the mid-Maastrichtian interval contains two peak abundance intervals. BFN values for the late Maastrichtian are lower than in the preceding intervals, while BFARs depict a significant peak from 269.53 mbsf to 266.04 mbsf, and suggest a steady increase from 261.83 mbsf upward, although these uppermost values are biased by the high sedimentation rate in this part of the section (28.9 cm ky^{-1}).

The percentage of agglutinated taxa and the main infaunal morphogroups (uniserial, biserial) shift along the studied interval (Figures 2, 3). For example, agglutinated forms had significant peaks (>10% of total assemblages) in the lower (304.78-299.05 mbsf) and upper Maastrichtian (272.12-269.53, 2631.1-262.7 mbsf), being *Clavulinoides trilatera* the most common species in the lowermost interval. Calcareous uniserial forms depict an upward increasing trend, with values ranging from ~10% to >20% of the total assemblages above 279.11 mbsf. *Strictocostella* and *Laevidentalina* are the most common uniserial forms, with significant peaks between 279.11-269 mbsf (Figure 2). Abundances of biserial forms increased between 315.73-310.83 mbsf and 288.33-277.05 mbsf. For instance, *Coryphostoma* presented abundances >20% below 297.55 mbsf and at the interval 258.13-257.5 mbsf, while *Aragonia velascoensis* was abundant in several intervals along the studied interval. A significant abundance peak of this species was recorded in the mid-Maastrichtian (288.33-286.03 mbsf; figure 2). Other infaunal forms such as *Praebulimina* or the species *Reusella szajnochae* were common (>5% of total assemblages) in the lower Maastrichtian.

Richness estimates ranged between 25-55, with a decreasing trend in the lowermost Maastrichtian, and fluctuations during the middle and the uppermost Maastrichtian (Figure 4). In contrast, diversity and evenness depict significant shifts in the lower Maastrichtian, and especially before the mid-Maastrichtian, where there was a significant decreasing trend (H = 3.4 to 2.6; E = 0.72 to 0.37). After the mid-Maastrichtian, diversity and evenness estimates show increasing trends, with values like those of the lowermost Maastrichtian and the lower-mid Maastrichtian (Figure 3).

Geochemistry

Bulk sediment $\delta^{13}C$ values range between 0.5 and 1.9‰, while $\delta^{18}O$ values vary between −2.9 and −1.42‰ (Figure 2). $\delta^{13}C$ values depict an increasing-upward trend, with two positive excursions in the interval 284.13-293.6 mbsf, above the base of the C31n magnetochron. In general, isotopic values from our study are comparable to those of MacLeod (2005).

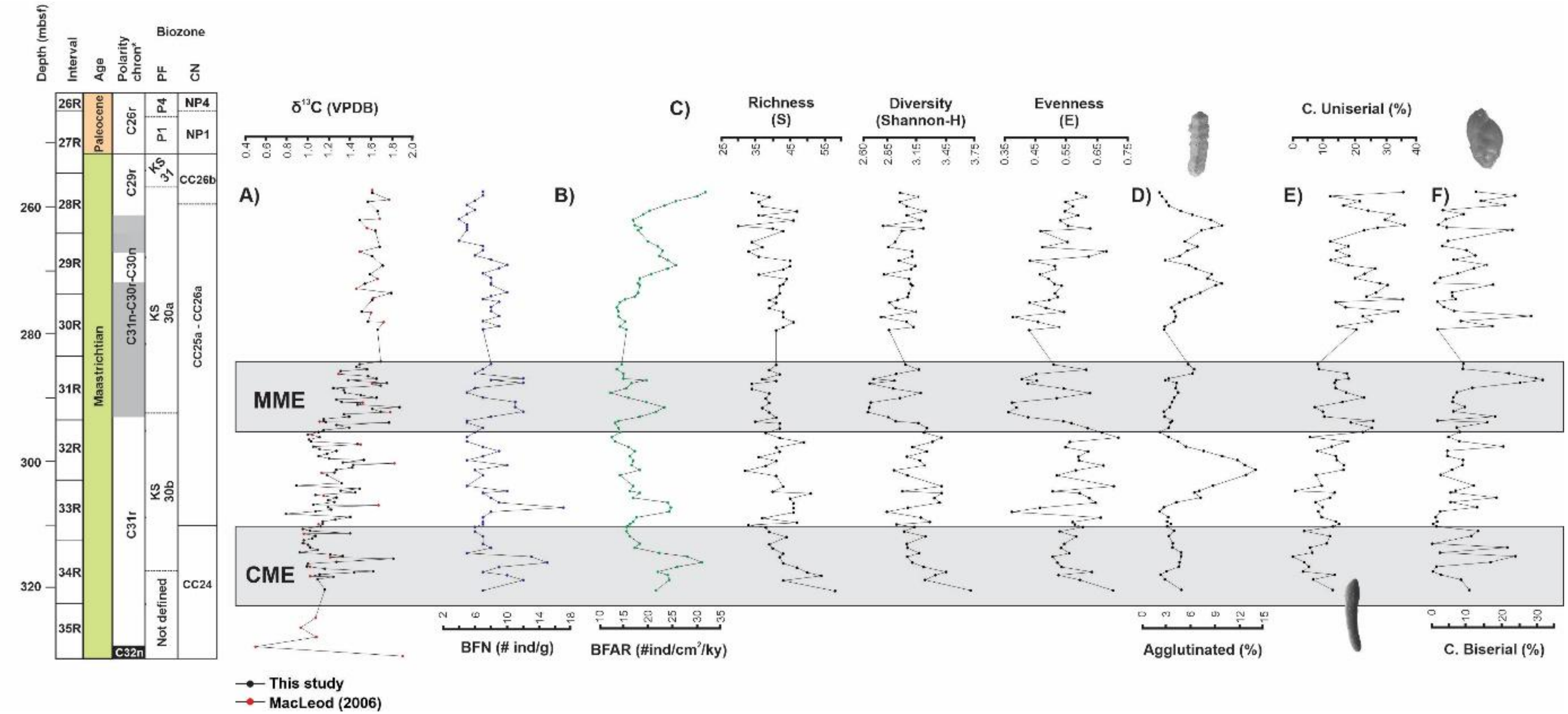

Figure 3. Bulk sediment $\delta^{13}C$ (A) and benthic foraminiferal indices (B-C) and relative abundance of selected groups (D-F) across the Maastrichtian in Hole 1258A. BFN = number of benthic foraminifera per gram of dry sediment; BFAR = benthic foraminiferal accumulation rate. D) Relative abundance of agglutinated foraminifera (the uniserial/tubular forms were omitted to avoid overestimations). E-F) Relative abundance of calcareous uniserial and biserial benthic forms. *Chronostratigraphy based on Suganuma and Ogg (2006). Planktonic foraminifera (PF) and calcareous nannofossil (CN) biozones based on Erbacher et al. (2004) and Thibault and Gardin (2006). CME = Campanian-Maastrichtian Event, MME = Mid-Maastrichtian Event.

Despite concerns about diagenetic biases at Site 1258, a cross plot shows no statistically significant correlation between bulk sediment $\delta^{18}O$ and $\delta^{13}C$ ($r^2 = 0.05$, $p = 0.006$), suggesting a limited diagenetic overprint (Jenkyns, 1995; Mitchell et al., 1997).

A decreasing-upward trend is depicted in the log(Fe/Ca) ratio, with values ranging from 2.7 to 1.9, and higher-amplitude fluctuations after the lowermost and the middle Maastrichtian. The positive spikes of the log(Fe/Ca) ratio in the interval 303.7-308-15 mbsf coincide with low carbonate content (<60 wt%) described at Hole 1258A (Figure 4). In general, carbonate content depicts an increasing-upward trend from the lower Maastrichtian (~55 to 70 wt%; Erbacher et al., 2004). Sediments Si/Ti values range from 2.5 to 5.9, with overall increasing-upward trends from the lowermost Maastrichtian and from the beginning of the mid-Maastrichtian. The Fe/K ratio depicts similar trends to those observed in the log(Fe/Ca) curve, with more pronounced positive spikes (>10) in the lower Maastrichtian (303.3-309.05 mbsf), and below the intervals 258.13-259.61 mbsf and 294.15-297.55 mbsf (Figure 4).

Sediments Cu/Al and Ni/Al values range between 2.0 $x10^{-2}$ and $8.0x10^{-2}$, with a slightly increasing-upward trend across the studied interval (Figure 4). Spikes with anomalously high Cu/Al ratios were observed in the interval 313.83-320.11 mbsf and especially, above 293.68 mbsf (>8.0 x 10^{-2}; Figure 4). Results from samples at 306.00 mbsf and 308.15 mbsf were discarded due to anomalously high (outliers) Cu/Al values.

INTERPRETATION

Maastrichtian carbon cycle perturbations recorded at Hole 1258A

The latest CME is depicted by a steady increasing upward $\delta^{13}C$ trend from 0.95 to 1.67‰ between 312.78-306.8 mbsf (70.41-70.06 Ma). This interpretation is supported by the occurrence of magnetochron C32n starting at 330.34 mbsf, and the updated calcareous nannofossil biostratigraphy of Thibault and Gardin (2006) for the same interval.

Based on the chronostratigraphy of Hole 1258A, at least two $\delta^{13}C$ isotope positive excursions (pCIE) can be assigned to the MME (Figure 2). The basal pCIE (subinterval MME1), which according to Voigt et al (2012) starts at ~69.2 Ma, can be traced as a positive $\delta^{13}C$ shift from 1.15 to 1.87‰ between 293.48-290.53 mbsf (69.27 to 68.99 Ma), starting slightly above the base of magnetochron C31n (293.52 mbsf; Suganuma and Ogg, 2006). Subinterval MME2, an abrupt but irregular negative inflection separating the two MME pCIEs (Voigt et al., 2012; Vellekoop et al., 2022), was identified between 290.53-288.33 mbsf (68.95 to 68.78 Ma), with values of ~1.2‰ and a positive spike at 289.83-289.43 mbsf. The upper pCIE (subinterval MME3), which ended at around 68 Ma (Voigt et al., 2012), was identified between 288.33-284.13 mbsf (68.78 to 68.39 Ma; 1.29 to 1.75‰).

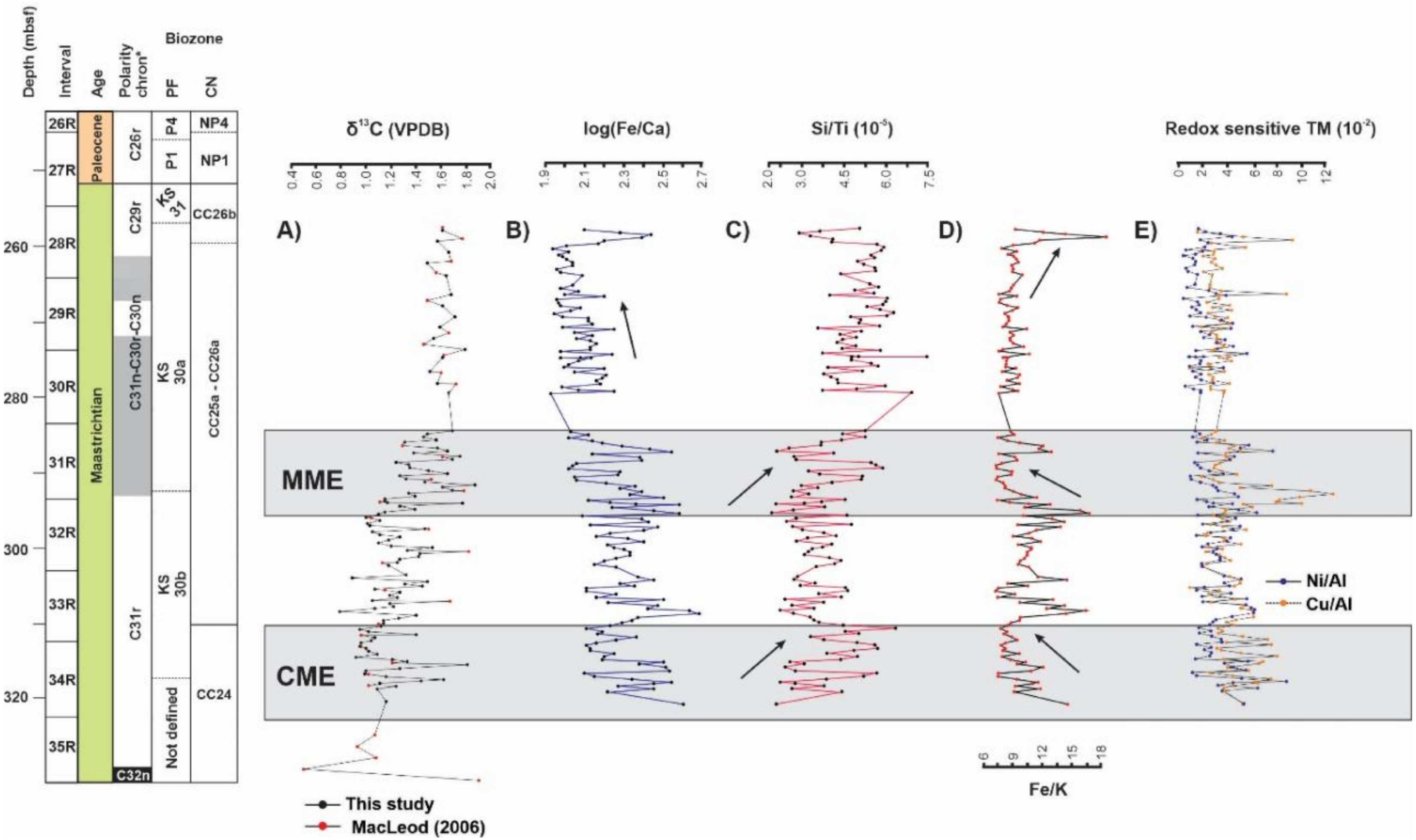

Figure 4. Bulk sediment $\delta^{13}C$ (A) and geochemical proxies across the Maastrichtian in Hole 1258A. B-C) Proxies of paleoproductivity. D) Fe/k ratio as a proxy of paleohumidity. E) Distribution of the redox-sensitive trace metals Ni and Cu, normalized to Al content. *Magnetostratigraphy based on Suganuma and Ogg (2006). Planktonic foraminifera (PF) and calcareous nannofossil (CN) biozones based on Erbacher et al. (2004) and Thibault and Gardin (2006). CME = Campanian-Maastrichtian Event, MME = Mid-Maastrichtian Event.

However, the gap between 284.13-279.11 mbsf, prevented the definition of the end of the MME at the studied interval (Figures 5-6). A tentative correlation of the $\delta^{13}C$ curve at Hole 1258A, with locations in Netherlands (ENCI Quarry; Vellekoop et al., 2022) and Italy (Gubbio; Voigt et al., 2012; Batenburg et al., 2018) is indicated in the supplementary material.

Paleoenvironmental turnover across the Maastrichtian at ODP Site 1258

Benthic foraminiferal assemblages and geochemical proxies point to significant paleoenvironmental changes across the Maastrichtian at Hole 1258A, likely associated with the physicochemical properties of the tropical water masses (Figures 5-6).

Fluctuations of BFAR and diversity curves, as well as the restricted distribution and abundances of some selected morphogroups/taxa (e.g., *Aragonia velascoensis*, *Nuttallides truempyi*, uniserials), suggest increasing availability of the organic matter (OM) across the MME. For instance, BFARs only depict positive excursions (>20 specimens cm^{-2} ky^{-1}) within the lowermost Maastrichtian (320.11-306.3 mbsf), the MME1 and MME3 subintervals, and above 274.4 mbsf. Shannon-H diversity and evenness dropped within the MME, suggesting stressful environmental conditions (Figure 5).

Some species and infaunal morphogroups depict abundance changes before and after the MME. For example, a typical Maastrichtian infaunal taxon, *Aragonia velascoensis* had significant abundance peaks (>10% of total assemblages) between 70.8-70.4 Ma and within the subinterval MME3 (Figure 5). This species has been used as a high-paleoproductivity indicator across the K-Pg transition in the tropical Pacific Ocean (Shatsky Rise; Alegret and Thomas, 2009). *Nuttallides truempyi* was also common to abundant (>20% of total assemblages) in the early Maastrichtian interval at Hole 1258A, though its highest abundances were restricted to subinterval MME1, decreasing steadily across the rest of the MME. For the upper Maastrichtian, the relative abundance of *N. truempyi* ranges between 10-25% of total assemblages (Figure 6). Assumed to be a predecessor of the epifaunal species *N. umbonifera*, the Late Cretaceous-Eocene *N. truempyi* has been associated with oligotrohic conditions and moderate-high bottom water oxygenation (Widmark and Speijer, 1997). Among buliminids, generally scarce in most of the analyzed assemblages, *Reussella szajnochae* was the most common species (4-12% of total assemblages), with common occurrences restricted to the lower Maastrichtian (320.11-304.5 mbsf). In general, occurrences of this species have been related to high surface productivity, low bottom water oxygenation, and warm saline water masses (Widmark, 1995). Distribution of infaunal morphogroups such as uniserials (e.g., *Strictoscotella pseudoscripta*, *Laevidentalina* spp.), flattened biserials (*Coryphostoma*), and the epifaunal planoconvex *Nuttallinella florealis*, might suggest changes in the bottom water oxygenation (Figures 2, 6; Jorissen et al., 2007).

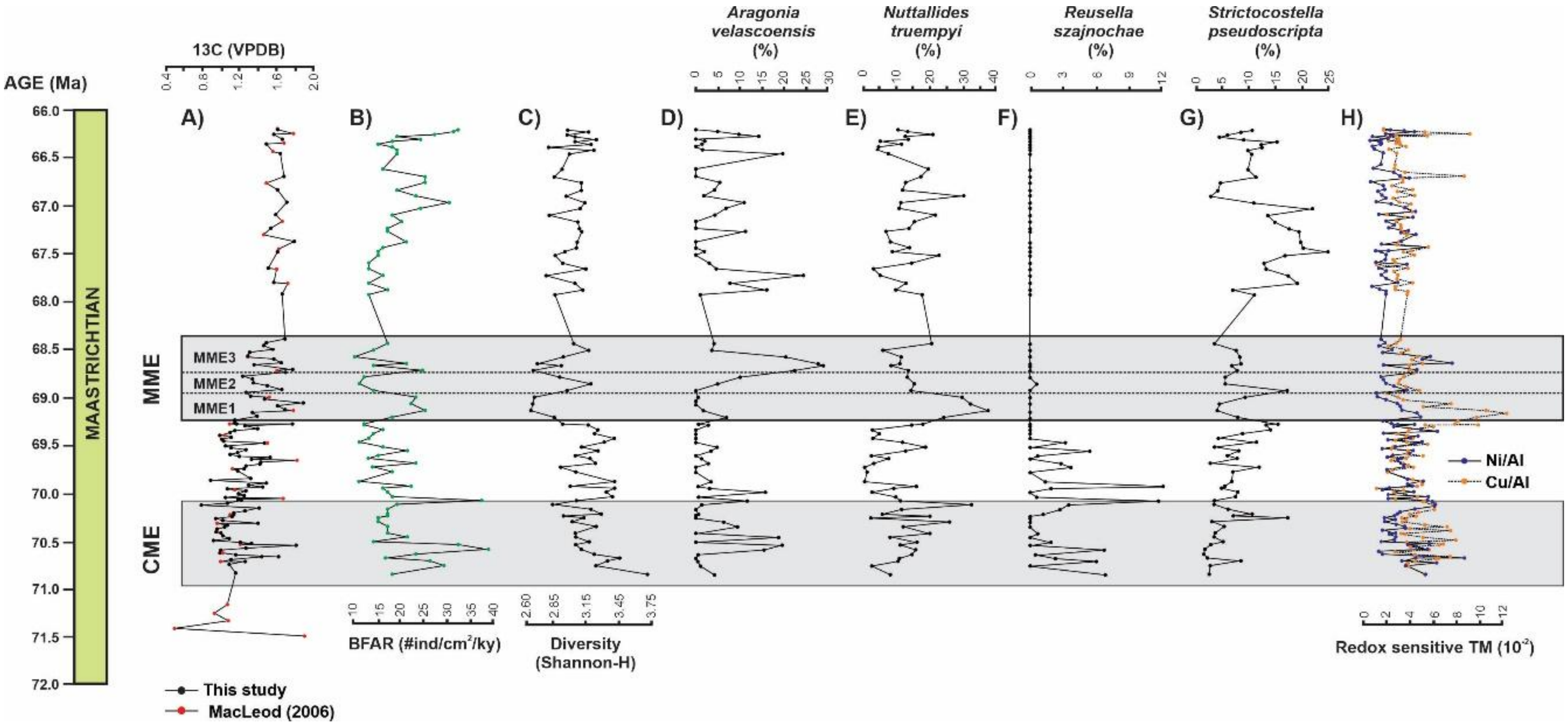

Figure 5. Distribution of geochemical and foraminiferal data along the Maastrichtian in Demerara Rise. A) Bulk sediment $\delta^{13}C$ curve. B-C) BFAR and Shannon-H diversity estimations. D-G) Relative abundances of *Aragonia velascoensis*, *Nuttallides truempyi*, *Reusella szajnochae*, *Strictocostella pseudoscripta*. H) Distribution of the redox-sensitive trace metals Ni and Cu, normalized to Al content. CME = Campanian-Maastrichtian Event, MME = Mid-Maastrichtian Event (Includes isotopic excursions MME1 to MME3).

However, those changes, reflected in a higher proportion of the uniserial forms (>10% of total assemblages), were not restricted to the MME. For example, relative abundances of *S. pseudoscripta* increased above 279.11 mbsf, while *Coryphostoma* spp. depicted increasing and decreasing trends before and after the MME (Figures 2, 6). The differences in the stratigraphic distribution of *N. florealis* and associated biserial-uniserial forms might suggest dissimilar food strategies, or changes in the type/abundance of the OM arriving to the seafloor after the MME. Other morphogroups in the foraminiferal assemblages of Hole 1258A such as the calcareous discoidal (Lenticulinidae), rounded-planispiral (*Pullenia*) and biconvex-trochospiral (Gavelinellidae) forms, did not illustrate major turnovers or sustained abundance peaks along the Maastrichtian.

We also explored bottom water oxygenation changes using the Ni/Al and Cu/Al elemental ratios. In general, both ratios do not suggest major changes during the early Maastrichtian. A slight decreasing-upward trend from 320.11-306.3 mbsf could account for the gradual disappearance of the high productivity species *R. szajnochae*. In contrast, high values of these ratios within MME subintervals MME1 and MME3 suggest oxygen-depleted waters during the mid-Maastrichtian, probably related to a second episode of increased surface productivity. These high productivity pulses might explain the positive BFAR excursions, as well as diversity decreases and increased relative abundances of *A. velascoensis* within the subinterval MME3 (Figure 6). However, high abundances of *N. truempyi* during subinterval MME1 would contradict the decreased bottom water oxygenation suggested by the Cu/Al ratio. This might reflect an alternative environmental mechanism that favored *N. truempyi* (e.g., bottom currents, interaction with more oxygenated intermediate to bottom waters), or a different source for Cu concentrations (e.g., atmospheric/submarine volcanism). An additional aspect is that TOC values do not reflect major changes along the core, and instead were generally low (~0.07; Erbacher et al., 2004, and selected samples from our study). After the MME, *A. velascoensis* and *N. truempyi* continued to present contrasting distributions, though with less amplitude than those within the MME, supporting dissimilar ecological preferences of these species (Figure 5).

DISCUSSION

Environmental shifts for the Campanian-Maastrichtian transition (73.0-70.5 Ma) have been described in southern high latitudes (ODP Site 690, Maud Rise), where benthic foraminiferal assemblages and benthic foraminiferal numbers (BFN) depicted a gradual turnover from less oxygenated and a high OM influx to well-oxygenated bottom conditions (Koch and Friedrich, 2012). As expected, foraminiferal assemblages at Site 690 were dominated by high latitude taxa such as *Paralabamina hillebrandti* or *R. szajnochae*. Other high productive indicators such as *Dorothia* spp., *Trochammina* spp. and

Coryphostoma incrassatum were common during the Campanian-Maastrichtian transition of Site 690. These taxa are also present in our early Maastrichtian material of Site 1258, but in minor abundances (<3% of total abundances). However, special caution must be taken with more detailed comparisons with Site 690, since the 71.2-70.1-71.2 Ma time interval was not recovered (Koch and Friedrich, 2012).

Paleoenvironmental changes have been also proposed for the early Maastrichtian interval in the North Atlantic Ocean Deep Sea Drilling Project (DSDP) Site 390 (Blake Nose). In general, BFN and diversity curves, as well as the relative abundances of selected benthic foraminiferal taxa, such as *Praebulimina reussi*, *Gavelinella beccariiformis*, *R. szajnochae* and *N. truempyi*, suggest three paleoceanographic scenarios, where there was a gradual increase in bottom water oxygenation and a decrease in OM supply (Friedrich and Hemleben, 2007). However, at Hole 1258A *R. szajnochae* was the most common element among elongated infaunal morphogroups, with the low relative abundances of other taxa, such as *Praebulimina* or *Pleurostomella*. This difference might suggest higher surface productivity conditions for the North Atlantic Ocean, as suggested by high abundances of *P. reussi* at DSDP Site 390 in comparison with those on Demerara Rise, or perhaps changes in the source of the deep-water masses (see following section).

At Hole 1258A, low productivity conditions occurred in the early Maastrichtian and continued until the base of the MME, when at least two high productivity episodes, and likely a dynamic source of the OM, occurred during subintervals MME1 and MME3. However, direct comparisons with the sedimentary record from the Maud Rise (ODP Site 690) and the Blake Nose Plateau (DSDP Site 390) are problematic due to stratigraphic issues. For example, a significant hiatus predated much of the middle Maastrichtian succession at Hole 390A (MacLeod et al., 2000; 2001). Considering the absence of magnetostratigraphy and the proposed duration of the hiatus (lower *Abathomphalus mayaroensis* to upper *Gansserina gansseri* planktonic foraminiferal biozones; ~68.5 to 70.2 Ma according to Gradstein et al., 2012), the MME would not be present in this locality. Micropaleontological surveys above 125.9 mbsf (cores 11-12) in this locality could bring insights about the transition between the MME and the late Maastrichtian. According to Friedrich and Hemleben (2007), foraminiferal assemblages from the interval 128.4-125.9 mbsf already suggest oligotrophic and well-oxygenated bottom-water conditions, mainly based on the dominance of *G. beccariiformis* and *R. szajnochae*.

Hole 690C also had a segment with no recovery, but in the early Maastrichtian interval (~71.2-70.1 Ma) recorded the base of magnetochron C31n at 272.25 mbsf (Hamilton, 1990). According to the age model of Koch and Friedrich (2012), the MME was recorded in their studied material (cores 17X and 18X). Foraminiferal assemblages in this interval were dominated by *N. truempyi*, *Pullenia* spp. and *Quadrimorphina* spp. which suggest well-oxygenated bottom waters and oligotrophic conditions. As referred above, *N. truempyi* was a common element during the subinterval MME1 on Demerara Rise, but in our case BFAR and diversity curves, as well as the Ni/Al and Cu/Al ratios would suggest higher surface productivity or changes in intermediate-deep water ventilation. Considering the low TOC values along Hole 1258A, we consider that those changes in the circulation could be related to a major interference of high-latitude deep waters from North Atlantic, as proposed by several authors (Widmark and Speijer, 1997a-b; Friedrich et al., 2004; Friedrich and Hemleben, 2007; MacLeod et al., 2011; Koch and Friedrich, 2012; Martin et al., 2012; Linnert et al., 2019; Vancoppenolle et al., 2022). *Pullenia* spp. and *Quadrimorphina* spp. were also present in low abundance (<3% of total assemblages) at Demerara Rise, but their abundances did not significantly change before, during, or after the MME. Additional calcareous nannofossil data from the Campanian-Maastrichtian interval at Hole 1258A and in Southern Ocean localities (ODP Sites 690, 700) suggest changes in surface productivity (indicated by acme-event of taxa such as *Kamptnerius magnificus*, *Gartnerago segmentatum*, among others), and sea-surface temperatures cooling during the latest Campanian-Maastrichtian (Thibault and Gardin, 2006; Guerra et al., 2016).

Previous studies for the late Maastrichtian suggest oligotrophic and well-oxygenated settings in the Atlantic realm. Calcareous nannofossil analyses at Hole 1258A suggest lower productivity and stressing environmental conditions prior to the K-Pg boundary, based on the disappearance of *Biscutum constans* and a significant increase in abundance of *Micula decussata* (Thibault and Gardin, 2006). Foraminiferal surveys in the western (present day Central and North Atlantic) and central Tethys (e.g., Caravaca, Spain; El Kef, Tunisia), identified a late Maastrichtian deep bathyal assemblage (DBA), in which Velasco-type foraminifera such as *G. beccariiformis*, *B. trinitatensis*, *N. truempyi*, *Aragonia* spp., among others, are common elements. These assemblages reflect oligotrophic conditions and fluctuating OM influx which depended on environmental setting (e.g., bathymetry, latitude; Widmark and Speijer, 1997a-b). Except for *B. trinitatensis*, all these taxa were recurrent elements in our late Maastrichtian material. Among the late Maastrichtian foraminiferal assemblages from Demerara Rise, a particular aspect is the common occurrence of *S. pseudoscripta* after the subinterval MM3, with significant peaks of complete specimens (>10% of total assemblages) between 67.9 and 66.6 Ma (Figure 5). The common presence of this infaunal species might suggest changes in the availability of OM, while the disappearance before the MME of the low-latitude and opportunistic species *R. szajnochae* clearly supports a change of bottom waters circulation in the tropical Atlantic Ocean, during and after the mid-Maastrichtian. Detailed surveys in the 68.0-68.0 Ma interval on other deep-water sites along the Atlantic (also complementing previous studies in Blake Nose and Maud Rise) would provide a clear understanding of the paleobiogeographic distribution of these taxa.

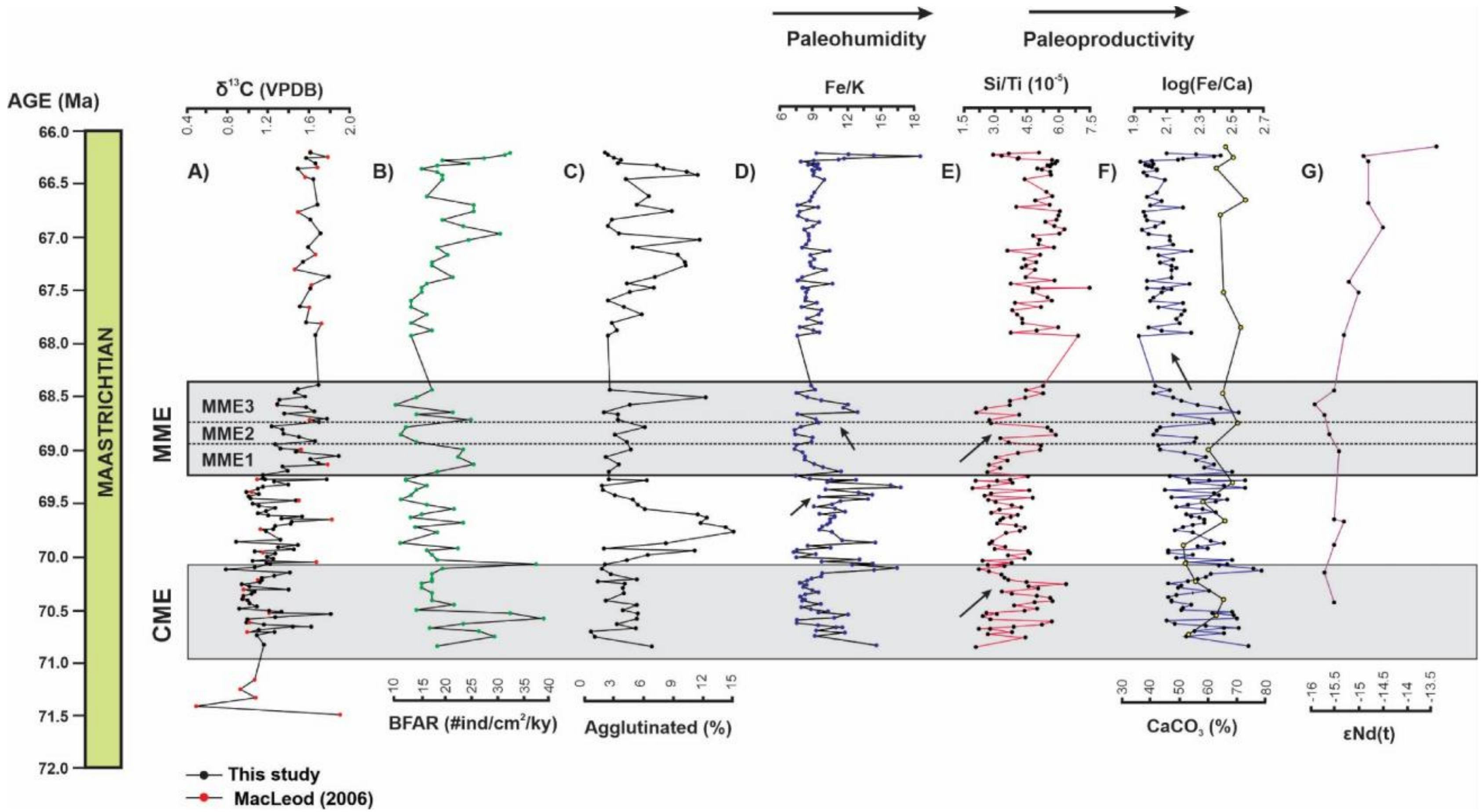

Figure 6. Distribution of paleoceanographic proxies along the Maastrichtian in Demerara Rise. A) Bulk sediment $\delta^{13}C$ curve. CME = Campanian-Maastrichtian Event, MME = Mid-Maastrichtian Event (Includes isotopic excursions MME1 to MME3). B-C) BFAR estimations and relative abundances of agglutinated foraminifera. D) Fe/k ratio as a proxy of paleohumidity. E-F) Log(Fe/Ca) and Si/Ti ratios as proxies of surface paleoproductivity. $CaCO_3$ data from Erbacher et al (2004). G) Distribution of Nd isotopes as an indicator of deep-water circulation in the Atlantic (Data of Martin et al., 2012).

Besides high-latitude localities in the Atlantic realm, the tropical Maastrichtian succession from Shatsky Rise provides information about paleoceanographic reorganizations during the MME (Frank et al., 2005; Jung et al., 2013; Dameron et al., 2017). In general, foraminiferal assemblages (planktonic and benthonic), $\delta^{13}C$ and $\delta^{18}O$ values measured on *N. truempyi* and *O. umbonatus*, as well as fish teeth Nd isotopes, suggest changing bottom water conditions during the Maastrichtian. Most of these changes have been related to episodes of deep-water cooling and warming due perturbations in thermohaline circulation, changes in source regions (Southern Ocean versus NW Pacific), modifications in the OM flux and dissolved oxygen content (i.e. high productive episodes at the MME), and even dissolution episodes in the latest Maastrichtian (~67.8-66.2 Ma; Henehan et al., 2016; Dameron et al., 2017). Coupled $\delta^{13}C$ and $\delta^{18}O$ isotope surveys on planktonic foraminiferal assemblages from Hole 1258A, would provide a clear idea of how interacted the high latitude deep-waters from the Atlantic and Pacific realms trough the Hispanic Corridor (e.g., D´Hondt and Arthur, 2002; Martin et al., 2012; Moiroud et al., 2016). This also would complement the models of surface and intermediate water circulation on the Maastrichtian tropics (e.g., Friedrich et al., 2008; Thibault and Husson, 2016; Ladant et al., 2020). However, Maastrichtian planktonic assemblages from Demerara Rise are a moderately preserved, mainly composed of globotruncanids, globular trochospiral, and biserial to multiserial-conical forms (Erbacher et al., 2004), so a detailed taphonomic revision of the assemblages will be needed first.

Finally, geochemical estimations of paleoproductity such as the Si/Ti and log(Fe/Ca) ratios suggest changes of surface productivity during the CME, and the early MME (Figure 6). Some of these changes coincide with the disturbances in bottom water oxygenation and OM influx that we suggested with BFAR and bulk $\delta^{13}C$ curves, concentrations of redox sensitive TM, as well as abundances of selected taxa such as *N. truempyi*, *R. szajnochae*, *A. velacoensis*, *S. psedoscripta*, among others.

Links between deep-ocean circulation and hydroclimatic changes in the low latitude areas

The Fe/K ratio (a paleohumidity proxy; Stuut et al., 2005; Mulitza et al., 2008) depicts coupled changes with paleoproductivity proxies (BFAR and selected species, and elemental ratios). Drier, or less humid conditions considering its tropical context, prevailed during the earliest Maastrichtian (71.0-70.0 Ma) and the MME. After 68.5 Ma, paleohumidity was lower, apart from a more humid episode between 66.2-66.3 Ma (Figure 6). This humid episode could be related with the onset of the late Maastrichtian warming event, an issue mainly explored on high-latitude settings (e.g., Barnet et al., 2017; Woelders et al., 2017). Considering that a paleo-intertropical convergence zone (PITCZ) was probably active since Aptian times (Santos et al., 2022), decreased Fe/K ratios within the CME and the MME could be related with a latitudinal migration of the PITCZ away from the source region of terrigenous sediments for Site 1258. This also could explain the steady increase of the estimated CIA (Chemical Index of Alteration) at nearby Hole 1259 since Campanian (2,354 m water depth; Corentin et al., 2023). An increased intensity of continental chemical weathering, as suggested by those authors, could be related to more humid conditions in this area, while a minor drop at ~70.0 Ma could be related with the interpreted less humid conditions during the MME. Unfortunately, sample resolution is still limited on the Campanian-Maastrichtian interval since studies such as Corentin et al (2023) have been more focused on a more extended time interval (Turonian to Maastrichtian), tracking the role that early tectonic pulses from South America could play in the global Late Cretaceous cooling via continental weathering.

Recent Nd isotopes data at Site 1258 and additional temperate localities (e.g., Cape Verde, Goban Spur, Bermuda Rise and Blake Nose), also support a major influence of the North Atlantic sourced deep waters in the tropics during the late Maastrichtian (Martin et al., 2012). In fact, changes in deep-ocean circulation, as depicted by Nd isotopes in Demerara Rise, may have changed inter-hemispherical heat exchange, leading to latitudinal migrations of the PITCZ. A similar scenario occurred during the last deglaciation due to weakening of the Atlantic Meridional Overturning Circulation (AMOC; Mulitza et al., 2017; Campos et al., 2022), resulting in latitudinal migrations of the Intertropical Convergence Zone. New high-resolution micropaleontological and geochemical surveys in other tropical Atlantic (e.g., Nicaraguan Rise) and supra-austral (e.g., Rio Grande Rise) deep-water localities, will provide a better understanding of Maastrichtian deep-water circulation and its role on the end Cretaceous tropical climate. In fact, climatic modelling for the Cenomanian-Maastrichtian time interval already suggested changes in paleohumidity patterns (expressed as precipitation minus evaporation; PME) of northern South America, exploring the likely role played by deep-water circulation (Ladant et al., 2020).

An additional element that should be considered for hydroclimate inferences during the latest Cretaceous is large scale atmospheric volcanism. During the latest Cretaceous global volcanic eruption rates increased, related to the Deccan Traps (e.g., Schoene et al., 2019; Sprain et al., 2019; Hull et al., 2020). The final emplacement of the Caribbean Plate and South American arc volcanism, though less studied in the sedimentary record, can be dated back to the Cenomanian, with a proposed magmatic hiatus during the middle-late Maastrichtian (e.g., Spikilings et al., 2015; Montes et al., 2020). Moreover, Deccan volcanic pulses, concentrated between ~65.3-66.2 Ma, could also influence the intensity of the PITCZ or the concentrations of trace elements on deep-sea sediments (e.g., Cu, Ni, Mo). Independent of probable volcanic-induced paleohumidity fluctuations, continental ecosystems in northern South America underwent significant changes after the K-Pg boundary extinction event, leading to the configuration of modern tropical rainforests (e.g., Carvalho et al., 2021).

Although taphonomic and diagenetic issues were not explored in detail here, we do not see evidence for significant deep ocean carbonate dissolution on Demerara Rise. Relative abundances of agglutinated forms reached >9% of total assemblages between 69-9 and 69.6 Ma, during the subinterval MME3 and after 67.5 Ma (Figure 6). Agglutinated assemblages were mainly composed of infaunal taxa *Clavulinoides trilatera*, *Marssonella* spp., and *Spiroplectinella dentata*. Given that we did not consider fragile forms such *Rhabdammina* in our estimations (Murray et al., 2011), we suggest that discrete carbonate dissolution may have occurred during these intervals. This could be supported by the $CaCO_3$ content curve (Erbacher et al., 2004), where a minor drop was observed between 70.5-69.7 Ma, before a gradual increase along the mid-late Maastrichtian (50 to 80% wt). Instead, increased carbon content could be related with increasing paleoproductivity, and agglutinated foraminifera abundance peaks within subinterval MME3 and the late Maastrichtian could be related to ecological preferences or changes in the OM availability/characteristics, since assemblages are mainly dominated by *S. dentata*. More detailed analyses in the late Maastrichtian assemblages from Demerara Rise, including a survey of the planktonic foraminifera preservation, would test the occurrence of deep ocean carbonate dissolution on low latitude areas, as the episodes reported in the Pacific Ocean (Shatsky Rise; Dameron et al., 2017).

CONCLUSIONS

We investigated the upper segment of the Campanian-Maastrichtian Event (CME) and the Mid-Maastrichtian Event (MME) in a deep-water environment along the equatorial South American margin (Demerara Rise; ODP Hole 1258A). Geochemical analyses (log(Fe/Ca), Si/Ti, Ni/Al, Cu/Al ratios) and benthic foraminiferal assemblages (BFN, BFAR curves, and selected taxa) suggest shifts of intermediate to deep-water oxygenation and surface productivity (OM flux, silica and carbonate export) during the entire Maastrichtian. Benthic foraminifers were typical of deep-sea settings (*Aragonia*, *Nuttallides truempyi*, among others), generally suggesting suboxic bottom water conditions, with some oxygenation pulses during the late Maastrichtian.

On Demerara Rise the MME was characterized by three major stages: (1) a lower subinterval (MME1) with high surface productivity and depleted bottom water conditions, (2) a middle subinterval (MME2) with moderate surface productivity and increased bottom water oxygenation, and (3) an upper subinterval (MME3) with increased surface productivity and suboxic bottom waters. Moreover, Fe/k ratios depict a hydroclimate drying at the source of terrigenous sediments during the CME and the MME (MME1 and MME2). This could be connected with latitudinal migrations of the PITCZ, and related changes in inter-hemispheric heat balance due to increased velocities of deep-waters coming generated in the North Atlantic Ocean.

ACKNOWLEDGMENTS

This research used samples provided by the International Ocean and Discovery Program (IODP). IODP is sponsored by the U.S. National Science Foundation (NSF) and participating countries. G.D.P. thanks to PETROBRAS for a scholarship in the project “Bioestratigrafia de foraminíferos do Aptiano-Albiano da Margem Continental Brasileira”. K.G.D.K thanks the Brazilian National Council for Scientific and Technological Development (CNPq) for grant number 307309/2023-1. L.A. acknowledges funding from project PID2019-105537RB-I00 (Spanish Ministry of Science and Innovation and FEDER funds). The authors thank the laboratory staff of itt-Oceaneon, Universidade do Vale do Rio dos Sinos (UNISINOS University). Gustavo Torres (Stratos Consultoría Geológica, Colombia) kindly assisted with the editing of foraminiferal SEM images.

Fue mi recuerdo y mi olvido,

fue mi noche y mi alborada,

fue mi calor y mi frío,

fue mi canto y mi tonada.

Por el norte, por el sur,

por el este, y por el oeste también.

Por el norte, por el sur

Magín Díaz

CHAPTER 4

LOW LATITUDE DEEP-SEA PALEOENVIRONMENTAL EVOLUTION DURING THE MAASTRICHTIAN

Contribution roles taxonomy

German David Patarroyo (itt Oceaneon, Unisinos University). Micropaleontological and geochemical preparation. Foraminiferal taxonomy and geochemical analyses. Integration and discussion of results.

Karlos Kochhann (itt Oceaneon, Unisinos University). Foraminiferal, geochemical and paleoceanographic discussions.

Laia Alegret (Zaragoza University). Benthic foraminiferal ecology and taxonomic comments. Paleoceanographic discussions.

Valeska Meirelles (Nova Analítica Imp. e Exp. Ltda). Mercury concentration analyses.

Andressa Esswein (itt Oceaneon, Unisinos University). Carbon and oxygen stable isotope analyses. Total organic carbon estimations.

Manuscript in preparation for: Cretaceous Research

LOW LATITUDE DEEP-SEA PALEOENVIRONMENTAL EVOLUTION DURING THE MAASTRICHTIAN

ABSTRACT

The Cretaceous-Paleogene (K-Pg) boundary extinction event is one of the most studied paleobiological turnover events. However, paleoenvironmental conditions that preceded the K-Pg boundary have been less studied, especially at tropical latitudes.

To assess the Maastrichtian deep-water environments along the equatorial South American margin, we conducted geochemical and micropaleontological analyses of sediments from Ocean Drilling Program (ODP) Site 1001 (Nicaraguan Rise, Caribbean region). Diagenetic processes hampered a proper recovery of the foraminiferal assemblages, though assemblages suggested a typical bathyal setting. Sediment elemental ratios (Si/Al, Ba/Al, Fe/K) indicated fluctuations of silica export via surface productivity, and a probable hydroclimate disturbance starting in the early Maastrichtian. Moreover, concentrations of redox-sensitive trace metals (Ni, Zn, V) along the core suggest increased changes in bottom water oxygenation (ventilation) during the late Maastrichtian. The K-Pg boundary and the mid-Maastrichtian Event (MME) were identified based on a new bulk sediment stable carbon isotope ($\delta^{13}C$) record. Paleoenvironmental disturbances on Nicaragua Rise during the Maastrichtian were probably caused by the reorganization of high-latitude sourced deep-waters in the Atlantic Ocean, and associated latitudinal migrations of the paleo-Intertropical Convergence Zone.

INTRODUCTION

The Cretaceous-Paleogene (K-Pg) extinction event is probably one of the most discussed biological events in the Phanerozoic. Numerous studies have focused on the paleoenvironmental mechanisms at work, geographical extent, environmental perturbations and their impact on the biota (e.g., Alvarez et al., 1980; Schulte et al., 2010; Punekar et al., 2014; MacLeod et al., 2017; Chiarenza et al., 2020; Hull et al., 2020; Keller et al., 2020; Goderis et al., 2021; Carvalho et al., 2021; Guerra et al., 2021; Alegret et al., 2022). To properly assess the nature of the Cretaceous climate, previous to the K-Pg extinction event, paleoceanographic studies have played a vital role, in which geochemical (isotopic and elemental composition) and micropaleontological (planktonic and benthonic organisms) analyses have provided a deeper understanding of issues such as surface ocean productivity and temperature, bottom water conditions, global water masses circulation, among others. For example, high-resolution paleoceanographic studies of deep-sea settings point out to a steady global temperature decline for the Campanian-Maastrichtian interval, a gradual re-organization of deep-water masses circulation, geographically variable fluctuations of surface productivity, deep ocean carbonate dissolution episodes, and faunal turnovers (e.g., D´Hondt and Arthur, 2002; Friedrich et al., 2004, 2008, 2009; Mateo et al., 2007; Abramovich et al., 2010; Hull and Norris, 2011; Jung et al., 2013; Linnert et al., 2014, 2016; Thibault and Husson, 2016; Dameron et al., 2017; Huber et al., 2018; Ladant et al., 2020).

Additional topics such as the role of continental chemical weathering and tectonics (e.g., orogenic pulses, geographic barriers) on the global Late Cretaceous cooling, or the response of tropics (e.g., hydroclimate) to these disturbances are still lacking deeper discussions. For instance, Chemical Index of Alteration (CIA) and Hf-Nd isotope records at Ocean Drilling Program (ODP) Site 1259 (Demerara Rise, offshore Suriname) have suggested changes in continental weathering intensity since Campanian times (Corentin et al., 2023). These authors, as well as several studies on low latitude neritic successions, agreed with the idea that significant environmental disturbances occurred during the Campanian-Maastrichtian time, which were likely linked to global sea-level fluctuations and the first stages of the Andean orogeny. These disturbances were particularly severe and dynamic in proximal settings of northern South America, and they have been tracked using a combination of sedimentological (e.g., facies analyses, ichnology), geochemical (elemental ratios), and micropaleontological (foraminifers, calcareous nannofossils, palynomorphs) proxies (Martinez, 1989, 2003; Erlich et al., 1999, 2000; Bayona et al., 2011, 2020; Sarmiento-Rojas, 2019; Patarroyo et al., 2022, 2023; Giraldo-Villegas et al., 2023). Rather than exclusive changes in the physicochemical properties of water masses, related to shifts in global oceanic circulation, low latitude marine successions recorded a complex mixture of climatic and tectonic-induced paleoenvironmental disturbances during the latest Cretaceous. Considering the scarcity of well-exposed and non-tectonically disturbed outcrops recording deep-sea deposits in northern South America, ODP Sites 999 and 1001 (Nicaraguan Rise) are crucial locations to generate high-resolution paleoceanographic records in open marine settings.

Here we present high-resolution geochemical (sedimentary elemental ratios, Hg content) records across the Maastrichtian at ODP Hole 1001B, lower resolution stable carbon isotope ($\delta^{13}C$) and Hg content records across the K-Pg transition, as well as a low-resolution benthic and planktonic foraminiferal survey. The location of ODP Site 1001B makes it an ideal location to trace direct comparisons with, not only the sedimentary record of northern South America, but also with tropical and mid-latitude locations in the Pacific and Tethyan oceans.

METHODS

Study material

ODP Hole 1001B (15°45.41' N, 74°54.63' W; 3271 m depth) is located on the edge of the southern Nicaraguan Rise, next to the Hess Escarpment (Modern central Caribbean; Figure 1). The Caribbean Plate as well as the Nicaraguan Rise and the Hess Escarpment were formed in the Pacific Ocean during the Late Jurassic and later moved through the gap created between North and South America during the opening of the proto-Caribbean Sea (e.g., Pindell and Kennan, 2009; Carvajal-Arenas and Mann, 2018). The recovered sediments at Hole 1001B consists of a middle Miocene to Pleistocene pelagic succession overlying a Cretaceous to upper Eocene section (Sigurdsson et al., 1997). The K-Pg boundary interval was identified based on the presence of rare grains of shocked quartz and dark green spherules at 352.9 mbsf (Sigurdsson et al., 1997).

Sampling for our study comprised different intervals, depending on the type of analysis: x-ray fluorescence (XRF) elemental ratios, δ^{13}C, or Hg content. For the XRF analyses, the middle to upper Maastrichtian (sections 20-1 to 24-4; 362.2-403.9 meters below seafloor; mbsf) was sampled, in 20-40 cm resolution. For δ^{13}C and Hg content analyses, we also studied scattered samples of across the K-Pg transition and the lower Danian: interval 341.83-403.53 mbsf (sections 17-1 to 24-4) for carbon isotopes, and interval 332.15-403.9 mbsf (sections 16-1 to 24-4) for Hg content. Sampling resolution for Hg analyses was 20-40 cm, and 40-80 cm for carbon isotopes.

The earliest Danian to Maastrichtian sediments at Hole 1001B are mainly characterized by calcareous chalks with interbedded foraminiferal-rich sand layers and some volcanic ash layers (Danian), and calcareous limestones (subunits IIB and IIIA; Sigurdsson et al., 1997). The K-Pg boundary interval was recorded at 352.9 mbsf (Section 18R-5; Sigurdsson et al., 1997). According to magnetostratigraphy, the studied interval comprises magnetochrons C31r to C29n (Louvel and Galbrun, 200). The base of magnetochron C31n (identified as C30n-C31n), which defined the mid-Maastrichtian onset, is located at 392.8 mbsf. Planktonic foraminiferal biozones P1-Pα have been recognized for the early Danian segment, while the *Abathompalus mayaroensis* and *Gansserina gansseri* biozones were identified for our studied Maastrichtian interval, with the base of the *A. mayaroensis* biozone at 393.7 mbsf (Sigurdsson et al., 1997). Sedimentation rates at Hole 1001B range between 0.8 cm/ky and 1.9 cm/ky according our age model proposal (Supplementary material S2). Calcareous nannofossils have been roughly assigned to the CP1/CP3 to CP23-CP25 biozones, and radiolarian and ostracod surveys in the same hole recognized typical Maastrichtian taxa at cores 21 and 20 (Aumond et al., 2009).

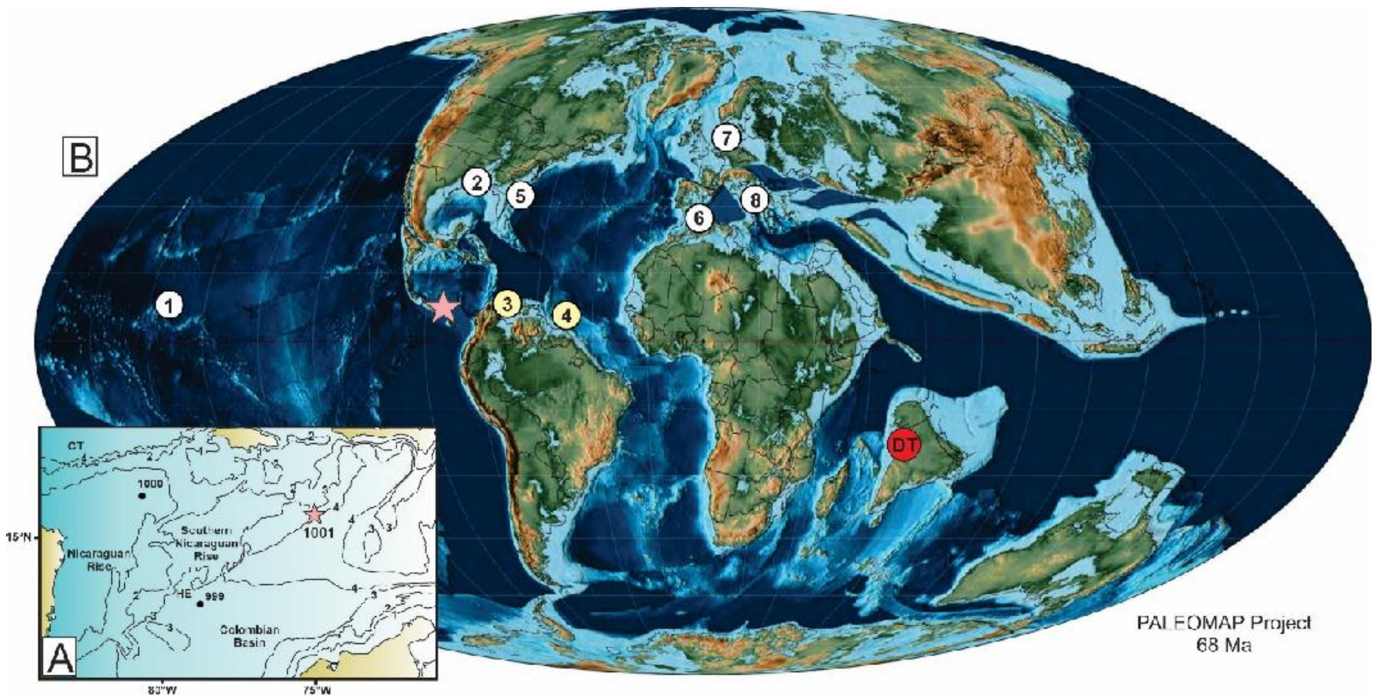

Figure 1. Location of the study sites and additional localities. (A) Location of the ODP Hole 1001B (Nicaraguan Rise). HE: Hess Escarpment, CT: Cayman Through. Topographic map of the Nicaraguan Rise based on Sigurdsson et al. (1997). (B) Paleogeographic map of the Maastrichtian (68 Ma, from Scotesse, 2014) showing the location of ODP Hole 1001B at Nicaraguan Rise (pink star) and other Campanian-Maastrichtian localities with available foraminiferal and isotopic data. (1) Shatsky Rise (Frank et al., 2005; Voigt et al., 2010; Dameron et al., 2017), (2) Shuqualak, Mississippi (Linert et al., 2014; 2018), (3) Core Diablito-1E and Aguablanca Creek (CHAPTERS 1 and 2; Patarroyo et al., 2022, 2023), (4) Demerara Rise (CHAPTER 3; Patarroyo et al., Submitted), (5) Blake Nose (Friedrich and Hemleben, 2006), (6) Tunisia (Li et al., 1999; Bejaoui et al., 2019; Farouk et al., 2023), (7) Maastricht (Vancoppenolle et al., 2022; Vellekoop et al., 2022), (8) Gubbio (Voigt et al., 2012). DC: Deccan Traps.

Geochemistry

X-ray fluorescence (XRF) analyses were performed on 5 g of ground and homogenized sediment aliquots (*n* = 120), with elemental concentrations reported as raw counts per second (cps). Samples were measured at 10 kV (150 µA, no filter) for Al, Mg, and Si intensities; 12 kV (400 µA, Al-50 filter) for Ca, K, Ti and V intensities; 20 kV (250 µA, Al – 200 filter) for Co, Cr, Fe and Mn intensities; and 50 kV (100 µA, Ti filter) for Ba and Rb intensities. XRF measurements were performed with a PanAlytical Epsilon 1 XRF spectrometer, at the Technological Institute for Paleoceanography and Climate Change (itt Oceaneon – Unisinos University, Brazil). To prevent bias between contrasting values, measurements were normalized to a median-scaled (NMS) following Lyle et al. (2012).

Several elemental ratios were used for paleoenvironmental inferences (Calvert et al., 2007). The Fe/K ratio has been used as a proxy for weathering intensity at the source of terrigenous components (e.g., Stuut et al., 2005; Mulitza et al., 2008; Govin et al., 2012). Silica export and surface productivity was explored using the Si/Ti and Ba/Al ratios (e.g., Agnihotri et al., 2008; Jaccard et al., 2005). Finally, bottom water oxygenation was evaluated with the NMS intensities of the redox-sensitive trace metals (TM) Ni, Zn and V, normalized with NMS Al intensities (e.g. Dummann et al., 2021).

Bulk sediment (*n* = 43) $\delta^{13}C$ values were measured with an isotope ratio mass spectrometer (IRMS) model 253 Plus – Thermo Scientific, at itt Oceaneon. Samples were allowed to react with 105% phosphoric acid (H_3PO_4) at 73°C. All isotope values are reported as ‰ deviations relative to the Vienna PeeDee Belemnite scale. Measurements accuracy and calibrations were performed with the standards IAEA -203 and IAEA -CO-8 from the International Atomic Energy Agency (IAEA), and SHP2L from the University of São Paulo (USP; Crivellari et al., 2021).

Finally, mercury concentrations (*n* = 148) were measured with a direct mercury analyzer DMA-80 evo Milestone at itt Oceaneon, via thermal decomposition of homogenized powdered samples (300 mg) on a nickeled boat. The analyzer converts Hg^{+} and Hg^{2+} of each sample into gaseous Hg^{0} and traps it on a gold amalgamator. The amalgamator is then heated at 850°C and the concentrations are estimated by atomic absorption (Hg lamp at 254 nm) in parts per billion (ppb). To make a proper diagnosis of a likely volcanic source for sedimentary Hg contents, we normalized the results with sulfur (S) contents from our XRF measurements and extrapolated total organic carbon (TOC) values from Sigurdsson et al (1997) at the same hole (mean TOC = 0.09 wt%).

All geochemical data are provided in Supplementary Table S1.

Micropaleontological analyses

Due to enhanced lithological hardness, our foraminiferal survey of scattered Maastrichtian samples resulted in negligible extraction of well-preserved microfossils with several tested solutions (e.g., distilled water, H_2O_2, sodium hexametaphosphate). Therefore, we surveyed the micropaleontological content of 20 petrographic thin sections within the studied interval (sections 24-4 to 20-1; 403.53-362.87 mbsf). This material was characterized at the Petrography Laboratory of Universidad Industrial de Santander (Colombia). Moreover, we handpicked and counted benthic foraminifers from the Maastrichtian set of samples (*n* = 10, 403.96-372.75 mbsf) of Aumond et al. (2009). That study only focused on the radiolarian and ostracod contents and considering their extraction methodology (40% H_2O_2 solution for 72 hours), our foraminiferal results will be assumed as merely exploratory. Benthic foraminiferal taxonomy followed regional literature for the tropics and the Atlantic realm (Frizzell, 1954; Koutsoukos and Merrick, 1986; Koutsoukos and Hart, 1990; Bolli et al., 1994; Widmark, 1997; Koutsoukos and Klasz, 2000; Alegret and Thomas, 2001; Vancoppenolle et al., 2022). Planktonic foraminiferal taxonomy was based on the Mikrotax portal (mikrotax.org/pforams/mesozoic) and Premoli Silva and Verga (2011). Selected foraminiferal specimens were imaged using a Zeiss EVO MA15 scanning electron microscope (SEM) at itt Oceaneon.

RESULTS

Geochemistry

A steady increasing-upward trend within the lower to middle Maastrichtian (403.9-374.08 mbsf) was depicted by the Si/Al ratio, with values ranging from 15 to 25, followed by a drop between 381.1-373.67 mbsf (middle to upper Maastrichtian), and again an increasing-upward trend in the uppermost Maastrichtian (Si/Al ratios of 20-25; 373.75-362.2 mbsf; Figure 2). Samples 394.58 mbsf and 394.17 mbsf were not considered, since they are outliers with anomaly high ratios. The Ba/Al ratio also depicted an increasing-upward trend above 370 mbsf, with values ranging from ~1.6 to 4.1 (Figure 2). Like in the Si/Al curve, samples 394.17 mbsf and 394.58 mbsf were not considered due to anomaly high ratios. The Fe/K ratio illustrated an opposite trend from previous geochemical proxies, with a steady decreasing upward trend along the Maastrichtian (Figure 2). In general, Fe/K ratios ranged from 6.1 to 9.5, with maximum values (>11) at 400.25 mbsf and 369.02 mbsf. Sample 381.1 mbsf was not considered for presenting an anomaly low ratio (K/Fe <1).

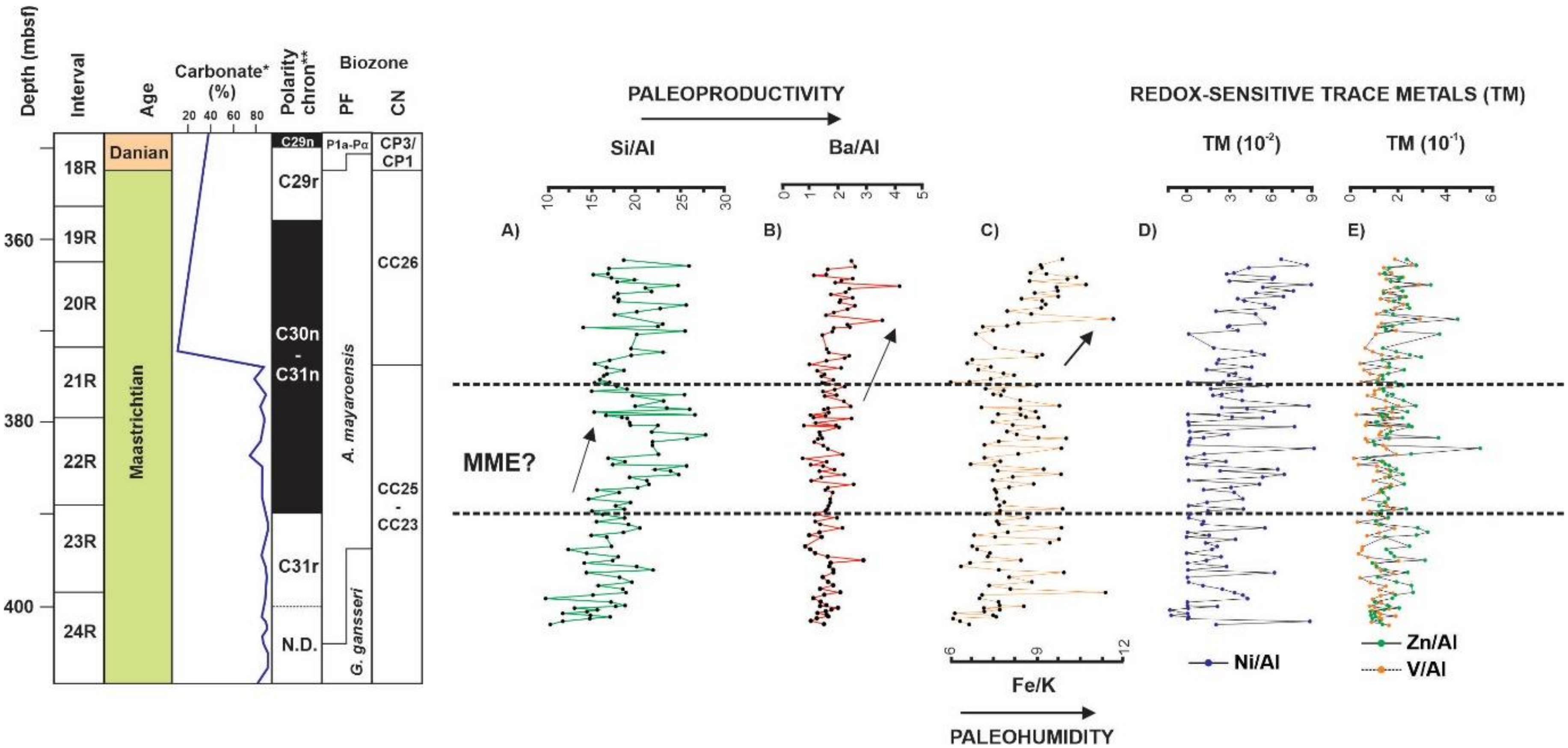

Figure 2. Distribution of paleoceanographic proxies along the Maastrichtian interval at Hole 1001B (Nicaraguan Rise). A-B) Si/Al and Ba/Al ratios as proxies of surface paleoproductivity. C) Fe/K ratio as a proxy for weathering intensity. D-E) Distribution of the redox-sensitive trace metals Ni, Zn and V, normalized to Al content. *Carbonate content and planktonic foraminifera (PF) and calcareous nannofossil (CN) biozones based on Sigurdsson et al. (1997). **Magnetostratigraphy based on Louvel and Galbrun (2000).

Redox-sensitive trace metals Ni, Zn and V had dissimilar trends at Hole 1001B. For instance, the NI/Al ratio depicted a general increasing-upward trend, ranging from ~1.0 x10^{-2} in the lower Maastrichtian to 7.0x10^{-2} in the upper Maastrichtian, while spikes with anomalously high Zn/Al values (>4.0 x10^{-1}) were observed along the middle-upper Maastrichtian (e.g., samples at 387.44 mbsf, 383.79 mbsf, and 369.02 mbsf). In general, the V/Al ratio was low (<2.0 10^{-1}) but its values mimicked most of the trends of the Zn/Al curve (Figure 2).

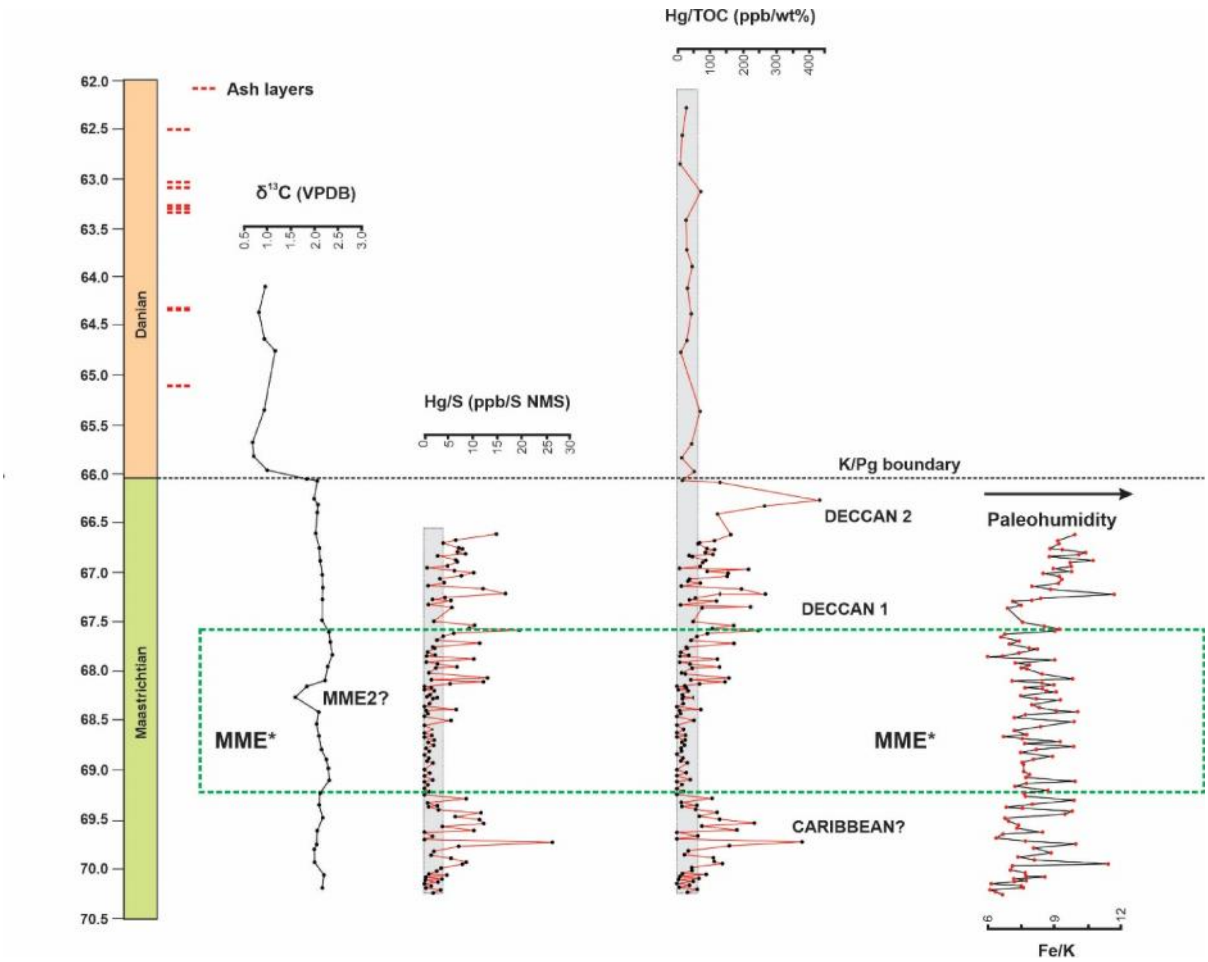

Figure 3. Carbon stable isotopes on bulk sediments, Hg/S and Hg/TOC at Hole 1001B (Nicaraguan Rise). Position of the K-Pg boundary, location of ash layers, and chronostratigraphy are based on Sigurdsson et al. (1997) and Louvel and Galbrun (2000). *MME: Mid-Maastrichtian Event. Gray areas indicate average Hg/S and Hg/TOC values. TOC estimations based on Sigurdsson et al. (1997). Tentative chronology of the Deccan eruption based on previous studies (Renne et al., 2015; Sprain et al., 2019; Schoene et al., 2015; 2019; 2021). Tentative chronology of the Campanian-Maastrichtian Caribbean volcanic episodes based on Sigurdsson et al (2000).

Bulk sediment $\delta^{13}C$ values ranged between 0.9 and 2.3‰, with a marked negative excursion at the K-Pg boundary (values <1.1‰; samples 352.27 mbsf and 351.13 mbsf). Despite the lower sampling resolution, there is a negative inflection (values <2.04‰) at the interval 384.43-379.27 mbsf (68.54 to 68.1 Ma; Figure 2). Moreover, Hg concentrations normalized to S and TOC values depicted peaks before and after the negative $\delta^{13}C$ excursion at 384.43-379.27 mbsf. Values of the Hg/S ratio were >10 in the interval 379.27-368.45 mbsf (68.1-67.16 Ma) and in the interval 400.25-392.86 mbsf (69.92-69.28 Ma), while the Hg/TOC ratio depicted two major spikes (Hg/TOC >80) in the lower Maastrichtian (400.53-394.58 mbsf; 69.94-69.42 Ma) and above 378.5 mbsf, with its highest peak ~4 m above the K-Pg boundary (Figure 3), considering the chronostratigraphy of Sigurdsson et al. (1997) and Louvel and Galbrun (2000).

Foraminiferal assemblages

In general, foraminiferal assemblages had a moderate to poor preservation. Planktonic forms were dominated by globotruncanids and biserial/multiserial taxa. In the analyzed thin sections, several specimens of Maastrichtian markers such as *Globotruncana aegyptiaca*, among others, were identified (Supplementary material Figure S1). Among benthic foraminifera, assemblages were scarce (<20 specimens/sample), with typical Maastrichtian calcareous taxa such as *Nuttallides truempyi*, *Coryphostoma incrassata* and *Gyroidinoides girardanus*, or *Clavulinoides trilatera* and *Marssonella oxycona* among agglutinated forms (Plate 1, Figure 4).

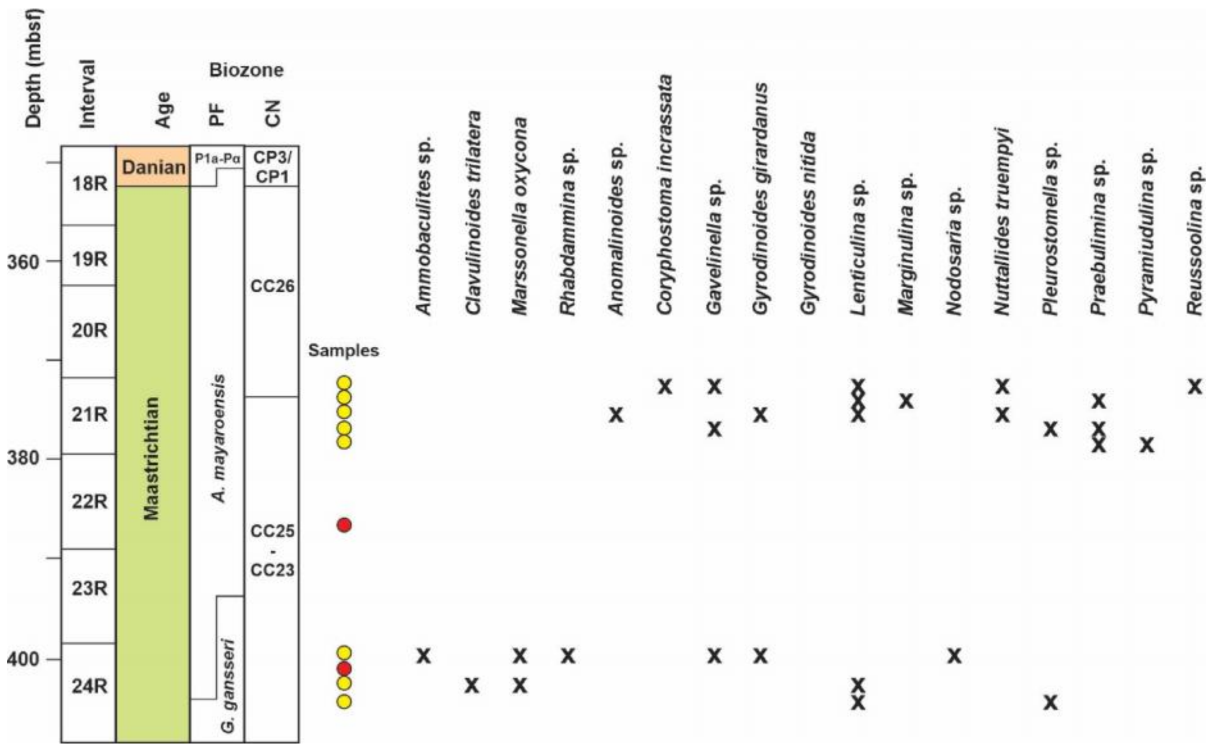

Figure 4. Stratigraphic distribution of benthic foraminiferal taxa at Hole 1001B (Nicaraguan Rise). Specimens were handpicked from samples studied by Aumond et al. (2009). For samples in red, benthic foraminiferal recovery was very low (and <20 total specimens/sample in samples marked with yellow dots), being dominated by undetermined textulariids and rotaliids. Planktonic foraminifera (PF) and calcareous nannofossil (CN) biozones based on Sigurdsson et al (1997).

Considering preservational biases, and the low abundance of benthic foraminifera, we can only propose a deep-sea setting for this locality, in agreement with the previous study of Aumond et al. (2009). Those authors suggested bathyal to outer shelf conditions for Hole 1001B, based on the occurrence of ostracod taxa such as *Paleoabyssocythere* or *Krithe*.

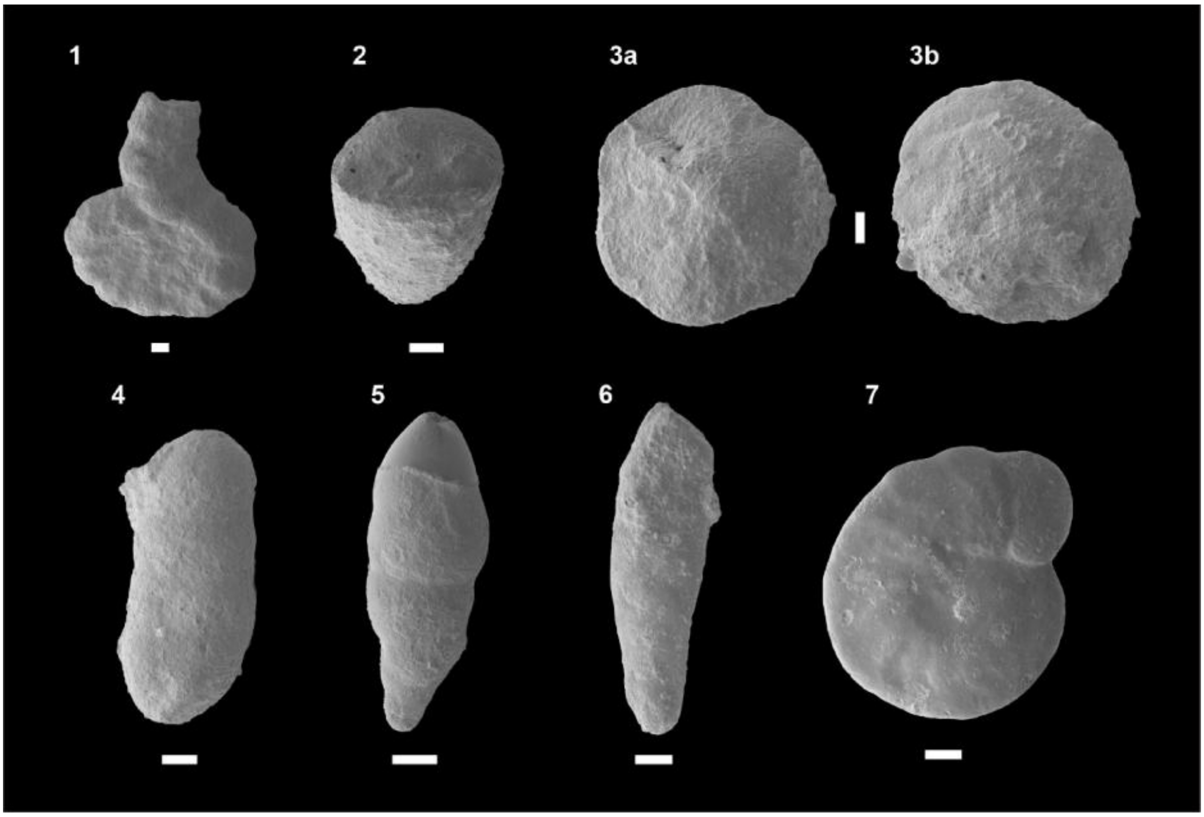

Plate 1. Selected benthic foraminifers from Hole 1001B. Scale bars represent 100 µm. 1. *Ammobaculites* sp. (21R4 71-76, 376,96 mbsf). 2. *Marssonella oxycona* (24R1 68-73, 399,53 mbsf). 3a-b. *Nuttallides truempyi*: 3a ventral view (21R1 70-75, 372,75 mbsf); 3b dorsal view (21R3 71-76, 375,46 mbsf). 4. *Clavulinoides trilatera* (24R3 70-75, 402,43 mbsf). 5. Buliminidae (21R4 71-76, 376,96 mbsf). 6. *Coryphostoma incrassata* (21R1 70-75, 372,75 mbsf). 7. *Gavelinella* sp. (dorsal view; 21R1 70-75, 372,75 mbsf).

DISCUSSION

The dominance of highly lithified limestones in the studied interval of Hole 1001B hampered a detailed micropaleontological survey, and most paleoceanographic and chronostratigraphic inferences were based on geochemical proxies. Despite low sampling resolution, the negative $\delta^{13}C$ excursion across interval 384.43-379.27 mbsf (68.54 to 68.1 Ma) is here tentatively associated with the intermediate part of the mid-Maastrichtian event (MME, subinterval MME2; Figure 3). Based on the position of the K-Pg boundary and the updated magnetostratigraphy proposal for Hole 1001B by Louvel and Galbrun (2000), we considered that MME would fall within 392.45 and 373.67 mbsf (69.24 to 67.61 Ma;

Supplementary figure S2). Considering linear sedimentation rates, the negative excursion within 384.43-379.27 mbsf would fall between 68.54 to 68.1Ma, in accordance with age estimates for the $\delta^{13}C$ excursion defining sub-interval MME2 (Figure 3), as defined elsewhere (e.g., Voigt et al., 2012; Batenburg et al., 2018; Vellekoop et al., 2022). However, special caution must be taken with the magnetostratigraphy proposal of Louvel and Galbrun (2000), considering the near-Equator location of Nicaraguan Rise, and its possible impact on magnetic declination data. Therefore, a detailed $\delta^{13}C$ survey between 69.36-67.49 Ma (393.9-372.33 mbsf) would be desirable to properly define the MME and improve our age model.

Surface productivity and bottom water oxygenation

The explored paleoproductivity proxies (Si/Al, Ba/Al) suggest a gradual increase of surface productivity through the middle Maastrichtian at Site 1001, with a short disturbance episode in the upper Maastrichtian (381.1-373.67 mbsf, 68.25-67.61 Ma; Figure 2). Considering the carbonate content drop that was described at Hole 1001B above 375 mbsf (Sigurdsson et al., 1997), this paleoproductivity disturbance episode could have caused decreased carbonate accumulation rates or, alternatively, the carbonate content drop could have been related to short-live dissolution events. The latter would be like the deep ocean carbonate dissolution events described for the latest Cretaceous in the tropical Pacific Ocean (Shatsky Rise; Dameron et al., 2017). A detailed carbonate content survey would allow disentangling these hypotheses for Site 1001, since previous analyses focused mostly on the Cenozoic interval (Sigurdsson et al., 1997).

Increased surface paleoproductivity in the middle Maastrichtian interval at Hole 1001B might also explain reduced bottom water oxygenation, suggested by increased values of the Ni/Al ratio (Figure 2). However, in the absence of detailed studies of the benthic foraminiferal assemblages, we cannot relate these changes of bottom water oxygenation solely to increasing surface productivity in the low latitude oceans. In fact, there were major changes of deep-water circulation in the Atlantic realm during the Campanian-Maastrichtian. Several studies, based on foraminiferal assemblages and geochemical proxies, have proposed that deep-water masses shifted from a major influence of saline and warm masses originating in the South Atlantic Ocean, to a cool and less saline North Atlantic source (e.g., D´Hondt and Arthur, 2002; Friedrich et al., 2008; Cramer et al. 2009; Linnert et al., 2014; Moiroud et al., 2016; Batenburg et al., 2018; Ladant et al., 2020). This environmental shift has been linked to the MME global carbon cycle disruption, which likely triggered the decline of marine organisms such as the inoceramid and rudist bivalves (Johnson, 2002; Frank et al., 2005; Voigt et al., 2012; Huber et al., 2018).

Late Cretaceous volcanism (subaereal and submarine) could have played a role in controlling paleoceanographic settings of this area, or influenced TM concentrations in bottom sediments, especially those observed in the Ni/Al during the late Maastrichtian (Figure 2). In general, the late Maastrichtian was characterized by enhanced volcanic activity globally, commonly linked to the Deccan Traps, and the resulting climatic shifts (e.g., transient global warming events, alterations on surface productivity) have been proposed before and after the K-Pg boundary extinction event (e.g., Punekar et al., 2014; Petersen et al., 2016; Percival et al., 2018; Schoene et al., 2019; Sprain et al., 2019; Hull et al., 2020; Keller et al., 2020; Font et al., 2021; Krahl et al., 2021; Gu et al., 2022). However, the key element for the Atlantic Ocean was the geological evolution of the Caribbean Large Igneous Province (CLIP), which favored the presence of a widespread and thick (~600,000 km^2; ~20 km) oceanic plateau. The onset of the CLIP has been dated as Turonian for the Colombia Basin, southeastward of Nicaraguan Rise, and at least as Albian for the Venezuela Basin (e.g. Sigurdsson et al., 2000; Pindell et al., 2005; García-Reyes and Dyment, 2021). The description of ash-layers and their $^{40}Ar/^{39}Ar$ dating at ODP Site 1001, indicates that ash accumulation rates were high (10-75 cm/m.y.) between 75-77 Ma and around 72 Ma (late Campanian to early Maastrichtian according to Gradstein et al., 2012). Along the Maastrichtian, ash accumulation rates were negligible, and 1 m.y. after the K-Pg boundary they increased again, with a major peak in the early Eocene (>75 cm/m.y.; Sigurdsson et al., 2000). According to Whattam and Stern (2015), the CLIP formed in three magmatic pulses: 124-112 Ma, 92-88 Ma and 76-72 Ma. Magnetic anomalies in the Lower Nicaragua Rise, and in the western part of the Colombia Basin have been related to the youngest pulse (García-Reyes and Dyment, 2021). At Hole 1001B, ash layers were only reported between 65.1 and 62.5 Ma (Sigurdsson et al., 2000; Figure 3).

Sedimentary Hg concentrations have become a common proxy to evaluate the influence of widespread volcanic activity, considering its minor variations due to non-volcanic processes, such as changes in bottom water conditions or increased continental weathering (e.g., Percival et al., 2018). In recent years, Hg concentrations have been studied in Late Cretaceous localities, to test extensive (e.g., Deccan episodes) and regional volcanic activity (e.g. Font et al, 2016, 2021; Sial et al., 2014, 2016; Keller et al., 2020; Krahl et al., 2021; Yao et al., 2021). Mercury concentrations are typically normalized by total organic carbon (TOC) or sulfur content of the sediments, to account for Hg bounding to organic matter, and elevated Hg/TOC and Hg/S values support an external volcanic source (Percival et al., 2018). Considering the age model for Hole 1001B (Supplementary figure S2), Hg/TOC and Hg/S positive spikes between ~70.3-69.4 Ma at Hole 1001B could be related to the ~72.0 Ma CLIP volcanic episode (Figure 4). Tentatively, the late Maastrichtian Hg/S and Hg/TOC major peaks at Hole 1001B were associated with Deccan vulcanism. Moreover, Hg/TOC and Hg/S positive spikes before 67.8 Ma, could be linked to a non-CLIP source, likely the Deccan volcanism, which according to recent estimations had two major episodes (Deccan 1 and 2) during the latest Maastrichtian (Schoene et al., 2019; Sprain et al., 2019). Additional regional evidence of a reduced CLIP influence during the Maastrichtian on northern South America is a magmatic hiatus between 70.0 Ma and 60.0 Ma (e.g., Spikings et al., 2015; Duque-Trujillo et al., 2019).

Low latitude regions hydroclimate

Low latitude hydroclimate is a key component of the climate system, and Maastrichtian and Paleogene sedimentary successions of this area can provide insights into its evolution through time. For instance, studies with this approach have suggested precipitation changes across the Paleocene-Eocene boundary in the Bogotá Basin (Colombia; Moron et al., 2013), or increased continental chemical weathering since the Campanian, recorded at deep-sea sediments from Demerara Rise (Corentin et al., 2023). Maastrichtian terrestrial ecosystems in northern South America have been generally associated with developed rainforests (open canopies with mixed gymnosperm-angiosperm assemblages; Carvalho et al., 2021), where a paleo-intertropical convergence zone (PITCZ) was probably active since the Aptian (Santos et al., 2022). Here we used the sedimentary Fe/K ratio as a weathering intensity proxy, and therefore as a hydroclimate indicator, at the source area of terrigenous components. This is because Fe is mostly delivered to ocean basins as oxy-hydroxide under wetter climate conditions, and K only survives weathering in the structure of clays such as illite, generated under drier climate settings (Stuut et al., 2005; Mulitza et al., 2008).

The Fe/K ratio at Hole 1001B indicates more humid episodes during the early Maastrichtian (~70.0 Ma) and after the MME (Figure 3). This low latitude hydroclimate reorganization was likely related to changes in deep ocean circulation in the Atlantic Ocean (Patarroyo et al., submitted; CHAPTER 3). This would have affected inter-hemispheric heat transfer and allowed for latitudinal migrations of the PITCZ. Latitudinal migrations of the modern Inter-Tropical Convergence Zone (ITCZ) were recorded during the last deglaciation, and related to weakening of the Atlantic Meridional Overturning Circulation (AMOC; Mulitza et al., 2017; Campos et al., 2022). High-resolution geochemical surveys in successions from northern South America, especially those related from epicontinental seas (e.g., Villamil and Pindell, 1998; Erlich et al., 1999; Martínez, 2003; Sarmiento-Rojas et al., 2019), and less explored deep-sea localities from the Caribbean realm (e.g., ODP site 999, DSDP 146/149) and the Equatorial Pacific Ocean (Gorgonilla Island; Bermúdez et al., 2011), will provide a better understanding of how the low latitude climate operated during the Late Cretaceous.

CONCLUSIONS

We explored the Maastrichtian deep-water environmental changes recorded at Nicaraguan Rise ODP Hole 1001B across the Maastrichtian, including the MME carbon cycle perturbation. Geochemical analyses (Si/Al, Ba/Al, Fe/K ratios) suggest shifts of intermediate to deep-water oxygenation and surface productivity (OM flux, silica and export) during the Maastrichtian. Benthic foraminifers were typical of deep-sea settings (*Nuttallides truempyi*, *Coryphostoma*, among others), and despite diagenetic issues, foraminiferal assemblages and the concentrations of redox sensitive metals (Ni, Zn, V) suggest suboxic bottom water conditions, with episodic oxygenation pulses during the late Maastrichtian. Paleoenvironmental disturbances at Nicaragua Rise during the Maastrichtian were likely influenced by the reorganization of high-latitude deep-water sources in the Atlantic Ocean, and associated latitudinal migrations of the PTICZ.

ACKNOWLEDGMENTS

This research used samples provided by the International Ocean and Discovery Program (IODP). IODP is sponsored by the U.S. National Science Foundation (NSF) and participating countries. G.D.P. thanks to PETROBRAS for a scholarship in the project “Bioestratigrafia de foraminíferos do Aptiano-Albiano da Margem Continental Brasileira”. K.G.D.K thanks the Brazilian National Council for Scientific and Technological Development (CNPq) for grant number 307309/2023-1. L.A. acknowledges funding from project PID2019-105537RB-I00 (Spanish Ministry of Science and Innovation and FEDER funds).

A light kindled in the sky, a blaze of yellow fire behind dark barriers. Pippin cowered back, afraid for a moment, wondering into what dreadful country Gandalf was bearing him. He rubbed his eyes, and then he saw that it was the moon rising above the eastern shadows, now almost at the full. So the night was not yet old and for hours the dark journey would go on. He stirred and spoke.

'Where are we, Gandalf?' he asked.

'In the realm of Gondor,' the wizard answered. 'The land of Anórien is still passing by.'

The return of the king

J.R.R. Tolkien.

CHAPTER 5

MERCURY CONCENTRATIONS AS A PROXY FOR VOLCANIC ACTIVITY IN THE MAASTRICHTIAN LOW-LATITUDE OCEANS

Contribution roles taxonomy

German David Patarroyo (itt Oceaneon, Unisinos University). Micropaleontological and geochemical preparation. Foraminiferal taxonomy and geochemical analyses. Integration and discussion of results.

Karlos Kochhann (itt Oceaneon, Unisinos University). Foraminiferal, geochemical and paleoceanographic discussions.

Laia Alegret (Zaragoza University). Benthic foraminiferal ecology and taxonomic comments. Paleoceanographic discussions.

Andressa Esswein (itt Oceaneon, Unisinos University). Carbon and oxygen stable isotope analyses. Total organic carbon estimations.

Valeska Meirelles (Nova Analítica Imp. e Exp. Ltda). Mercury concentration analyses.

Manuscript in preparation for: Geology

MERCURY CONCENTRATIONS AS A PROXY FOR VOLCANIC ACTIVITY IN THE MAASTRICHTIAN LOW-LATITUDE OCEANS

ABSTRACT

In recent years, the possible links between widespread volcanic activity and the Latest Cretaceous climatic shifts have become a common research scope. However, the evidence of volcanic activity on the tropics is still poorly traced for that time interval. To explore regional and distal (e.g., Deccan Traps) impacts on tropical environmental conditions, we track Hg enrichments in Maastrichtian low-latitude localities from: (1) Shallow marine strata of the Colón Formation (Core Diablito-1E, northern Colombia) and, (2) deep sea records from the Ocean Drilling Program (ODP) Sites 1258 (Demerara Rise, Tropical Atlantic Ocean) and 1001 (Nicaraguan Rise, Caribbean Sea).

Mercury concentrations, Hg/TOC and H/S values could not be exclusively linked to a single volcanic source (Deccan or regional volcanism) at core Diablito-1E, due to the shallowing processes of the sedimentary succession, and the poorly explored influence of the northern South American volcanism during the Maastrichtian. To improve age control for core Diablito-1E, we measured stable carbon isotopes ($\delta^{13}C$) of bulk carbonates, the first one conducted in Maastrichtian rocks from this area, which indicate that low latitude strata potentially recorded the mid-Maastrichtian event (MME). Mercury, Hg/TOC and H/S records at Sites 1258 and 1001 suggest the record of at least, three volcanic episodes during the Maastrichtian, which could be related with proximal and/or distal volcanic sources, such as the Caribbean Plate volcanic arc, or the Deccan volcanic pulses. Significant Hg spikes were observed before the K-Pg transition but not in the early Danian from Site 1001.

INTRODUCTION

Among the proxies used to evaluate the influence of widespread volcanic activity, mercury concentrations and osmium isotopes have become promising tracers, being less affected by changes in continental weathering rates or marine redox conditions (Percival et al., 2018; Grasby et al., 2019; Shen et al., 2020). In recent years, Hg concentrations have been studied in Cretaceous localities recording extensive volcanism (e.g. Deccan episodes), regional volcanic activity, and even possible links with Cretaceous oceanic anoxic events (e.g. Font et al, 2016, 2021; Sial et al., 2014, 2016; Percival et al., 2018; Fendley et al., 2019; Keller et al., 2020; Matsumoto et al., 2020; Krahl et al., 2021, 2023; Yao et al., 2021; Gu et al., 2022).

Unequivocal assignment of increased Hg concentrations to widespread Maastrichtian volcanism in the tropics requires some previous considerations. Volcanism is indeed the main source of Hg to the atmosphere, and due to its atmospheric residence time (5-24 months) this metal has a high potential of worldwide deposition in terrestrial and marine environments (e.g. Percival et al., 2018; Grasby et al., 2019). Oxidation processes allow Hg precipitation in aqueous compounds (as Hg^{2+}), and long-term Hg sequestration in marine sediments is possible due to adsorption in organic matter (OM; Selin, 2009). In terrestrial environments and reducing freshwater settings (lakes, wetlands), features such as type of soil and vegetation, biotic and abiotic processes cause high Hg mobilization in its oxidized forms (Monomethyl-mercury, dimethyl-mercury; Benoit et al., 2001; Ravichandran, 2004; Emili et al., 2011). Terrestrial Hg may also be deposited into soils or peats, and it can be transported to aquatic settings via runoff (e.g. Grasby et al., 2017). Therefore, changes of Hg concentrations in marine records, and mostly in shallow marine settings, could not only be associated with variations in Hg emissions to the atmosphere (mostly via volcanism), but also with shifts in marine environmental conditions (e.g. subaqueous volcanism, upwelling processes, bottom water oxygenation, runoff intensity). Considering that most of Hg geochemical species have a considerable affinity with OM, sedimentary Hg concentrations are typically normalized against the total organic carbon (TOC) content of the sediments. Therefore, elevated Hg/TOC values point to an external source such as volcanism for Hg enrichments, rather than just increased flux of OM, and consequently Hg bounding to the sediments (review in Percival et al., 2018; Grasby et al., 2019; Shen et al., 2020; Keller et al., 2020).

The use of Hg chemostratigraphy as a proxy for volcanic activity through geological time also requires detailed chronostratigraphic frameworks, based on isotopic geology, magnetostratigraphy, biostratigraphic datums, among others. This aspect has been crucial when discussing environmental and biotic impacts of the Maastrichtian-Danian Deccan volcanic episodes (e.g., Keller and Abramovich, 2009; Schulte et al., 2010; Font et al, 2016, 2021; Sial et al., 2014, 2016; Barnet et al., 2018; Fendley et al., 2019; Schoene et al., 2019; Sprain et al., 2019; Hull et al., 2020; Keller et al., 2020; Gilabert et al., 2021; Krahl et al., 2021, 2023; Alegret et al., 2022; Nauter-Alves, 2022).

So far, few studies have compiled published Hg analyses to infer chemostratigraphic correlations between localities, and to constrain the proposed volcanic episodes in the Maastrichtian (Percival et al., 2018; Keller et al., 2020; Gu et al., 2022), and available studies mostly deal with high-latitude localities and open marine settings. Preliminary surveys at selected low-latitude (northern Brazil) and shallow-marine austral localities (Neuquén basin, Argentina) also recorded Hg enrichments before the K-Pg boundary for South America (Sial et al., 2014, 2016). Considering that despite low sampling resolution, Maastrichtian tropics were likely sensitive to global or regional volcanic events, we evaluate Hg concentrations at two deep-sea sites (ODP Holes 1001B, Nicaragua Rise; 1258A, Demerara Rise) and a shallow marine locality (Core Diablito-1E, Colombia) in northern South America. High-resolution Hg chemostratigraphy, $\delta^{13}C$ records, and additional geochemical proxies (TOC content, S and trace metal concentrations) were used to explore possible sources (volcanic or sedimentary) for Hg enrichments, and their possible links with Maastrichtian climate shifts.

METHODS

Studied localities and sampling strategy

Three localities were considered in this study: A shallow-marine succession in northern Colombia (Core Diablito-1E), and two deep-sea cores in the Tropical Atlantic (ODP Holes 1001B and 1258A; Figure 1). Core Diablito-1E was drilled in the Upper Cretaceous succession of the Cesar-Rancheria Basin (northern Colombia; 9°34’ N, 73°16’ W), and it spans 701 m of the Colón, and Catatumbo/Barco formations. At this site, the K-Pg boundary iridium anomaly was previously identified between 501.72 and 501.80 m by De La Parra et al. (2022). Our studied interval spans from 574.3 m to 700.9 m, which comprises the middle to upper part of the Colón Formation (Late Maastrichtian; Patarroyo et al., 2022). A total of 102 samples (574.7-700.9 m) were analyzed for carbon isotope analysis, and 93 samples were analyzed for Hg (574.7-700.3 m), and total organic content (TOC).

Ocean Drilling Program (ODP) Hole 1258A (15°06.99' N, 69°22.67' W; 3192 m depth) is located on the northwest-facing slope of Demerara Rise (Suriname, northeastern South America), on a ridge of Paleogene sediments that outcrop on the seafloor bed (Erbacher et al, 2004). The studied interval comprises the earliest to late Maastrichtian (257.5-320.11 mbsf; planktonic foraminiferal biozones KS30a to KS31). The K-Pg boundary was defined at 252.58 mbsf, based on the presence of a well-preserved 1.5-cm thick impact ejecta layer of green microspherules. According to magnetostratigraphy, the studied interval comprises magnetochrons C31n to C29r, where the base of the magnetochron C31n was defined at 293.52 mbsf (Suganuma and Ogg, 2006; MacLeod et al., 2017). A total of 152 samples were considered for Hg content, and scattered samples (*n* = 24) were also analyzed for TOC content, to corroborate low TOC contents (<0.1 wt%) across the Maastrichtian interval as reported by Erbacher et al. (2004). As an additional reference on the chronology of this locality, we also considered the bulk sediment $\delta^{13}C$ curve of **CHAPTER 3**.

ODP Hole 1001B (15°45.41' N, 74°54.63' W; 3271 m depth) is located on the northern sector of the Hess Escarpment, a 1000-km-long tectonic feature that separates the lower Nicaraguan Rise from the Colombian Basin (Modern central Caribbean). The recovered sedimentary succession consists of a middle Miocene to Pleistocene section overlying a Cretaceous to upper Eocene section (Sigurdsson et al., 1997). The K-Pg boundary interval was recovered at 352.9 mbsf based on biostratigraphy and the presence of rare grains of shocked quartz and dark green spherules. (Sigurdsson et al., 1997).

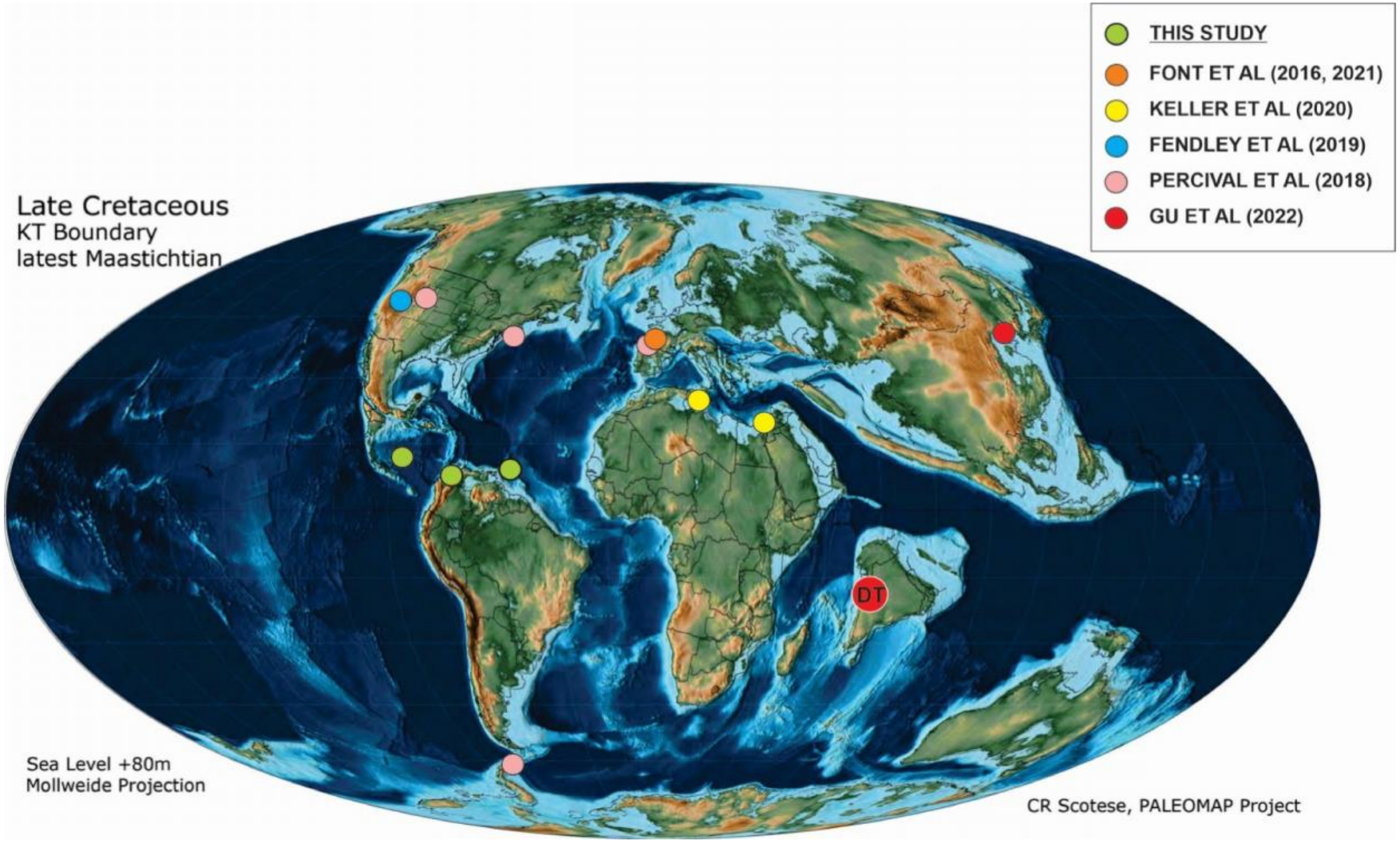

Figure 1. Location of selected localities with Hg chemostratigraphy in the Maastrichtian-Danian transition. This study: ODP Hole 1001B (Nicaragua Rise), ODP Hole 1258A (Demerara Rise), Core Diablito-1E (Colombia). Paleogeographic map from Scotesse (2014). Previous studies: Bidart (France; Font et al., 2016, 2021), Elles and Hor Hahar (Tunisia and Israel; Keller et al., 2020), Nirvana (United States, Fendley et al., 2019), ODP Site 174AX, Montana and Seymour Island (Bass River, United States and Antarctica; Percival et al., 2018), SK-In borehole (China; Gu et al., 2022).

The studied interval comprises magnetochrons C31r to C29n (Louvel and Galbrun, 2000). The base of magnetochron C31n (broadly identified as C30n-C31n), defining the mid-Maastrichtian, is located at 392.8 mbsf. Besides the Maastrichtian interval, we also sampled in lower resolution the K-Pg transition for Hg analyses (n = 148; 332.15-403.9 mbsf). Based on previous surveys, TOC content was particularly low along the early Danian and Maastrichtian at Hole 1001B (TOC ~0.1 wt%; Sigurdsson et al., 1997). Considering its low sampling resolution, we did not include the $\delta^{13}C$ record of **CHAPTER 4** in our chronology discussion.

Geochemistry

Mercury concentrations were measured with a direct mercury analyzer DMA-80 evo Milestone at the Technological Institute for Paleoceanography and Climate Change (itt OCEANEON, UNISINOS University), via thermal decomposition of homogenized powdered samples (300 mg) on a nickeled boat. The analyzer converts Hg^{+} and Hg^{2+} of each sample into gaseous Hg^{0}, and traps it on a gold amalgamator. The amalgamator is then heated at 850°C, and concentrations are estimated by atomic absorption (Hg lamp at 254 nm) in parts per billion (ppb).

To make a proper diagnosis of a likely volcanic source for Hg concentrations at Core Diablito-1E, we normalized the results with new TOC content analyses, and sulfur (S) elemental intensities reported in Patarroyo et al (2022). For most samples from Holes 1001B and 1258A, we interpolated TOC from lower resolution site report records (Sigurdsson et al., 1997; Erbacher et al., 2004), measured TOC values of selected samples at Hole 1258A, and considered S elemental intensities reported in **CHAPTERS 3-4**. For selected TOC measurements at Core Diablito-1E and at Hole 1258, we analyzed 10 mg sample aliquots, after acidification with hydrochloric acid (HCl) with a FlashSmart Elemental Analyser (Thermo Scientific) at itt OCEANEON.

At Core Diablito-1E, bulk sediments $\delta^{13}C$ was measured with an isotope ratio mass spectrometer (IRMS) MAT 253 Plus – Thermo Scientific, at itt Oceaneon. Samples were allowed to react with 105% phosphoric acid (H_3PO_4) at 74°C. All isotope values are reported as ‰, deviations in relation to the Vienna PeeDee Belemnite standard value. Measurements were calibrated and monitored (reproducibility and accuracy) using standards IAEA -203 and IAEA -CO-8 from the International Atomic Energy Agency (IAEA), and SHP2L from the University of São Paulo (USP; Crivellari et al., 2021).

All geochemical data are provided in Supplementary Table S1.

RESULTS

Core Diablito-1E

Based on the location of the K-Pg boundary (De La Parra et al., 2022) and the presence of the regional benthic foraminiferal zones *Siphogenerinoides bramletti* and *Ammobaculites colombiana* (Patarroyo et al. (2022), the studied interval at Core Diablito-1E encompasses the latest Maastrichtian (66.71 to 67.99 Ma). $\delta^{13}C$ values within the interval 700.9-619 m (67.99 to 67.13 Ma) ranged between -6.5 and -2.5‰. Considering our age model, the positive excursion between 67.27 and 67.63 Ma (630.4-673.6 m) could be tentatively associated with the upper part of the mid-Maastrichtian event (MME3; Figure 2).

TOC contents were <0.7 wt% for most of the studied interval, in contrast with a marked positive excursion (TOC 1.0-1.8 wt%) starting at 66.96 Ma (609.4-578.5 m).

At Core Diablito-1E, Hg concentrations were moderately high throughout the studied interval (~50 ppb), with significant spikes (>100 ppb) in the oldest interval (Figure 3). Mercury concentrations normalized against normalized median-scaled (NMS; Lyle et al., 2012) S intensities (derived from XRF analyses) depicted the highest ratios (Hg/S >40) between 66.71 and 67.06 Ma (574.7-612.7 m). Mercury concentrations against TOC depicted higher values between 67.27 and 67.08 Ma, and through the oldest interval (Hg/TOC >150; 67.8 to 67.54 Ma, 692.3-664 m) at Core Diablito-1E. In addition, we compared Hg concentrations with NMS Al, S, K, and Fe intensities, as well as with the V/Cr ratio, as a rough estimate of the influence of clay minerals (aluminosilicates, phyllosilicates), runoff intensity (Fe) and bottom water oxygenation (V/Cr, S) on Hg concentrations. In general, correlations were negligible (r^2<0.01-0.2; Supplementary Figure S1) in all cases, suggesting that these processes were not the main drivers of Hg variability at Core Diablito-1E.

ODP Holes 1001B and 1258A

Based on the age model of Hole 1258A (**CHAPTER 3**), the studied interval comprises most of the Maastrichtian, with the two positive excursions that define the mid-Maastrichtian event (MME; Figure 3). In general, Hg concentrations where particularly high (>30 ppb) in the earliest Maastrichtian (70.75 to 70.29 Ma; 318.47-310.83 mbsf), in the younger interval of the MME (MME1; 69.28 to 69.02 Ma, 293.68-290.93 mbsf), and an outlier sample at 66.26 Ma. To distinguish non-volcanic sources of the Hg, we normalized Hg concentrations by TOC and NMS sulfur measurements in the same interval. We assumed average TOC values of 0.1 wt% across the studied interval, since previous surveys indicated TOC values between 0.06-0.17 wt% (Erbacher et al., 2004).

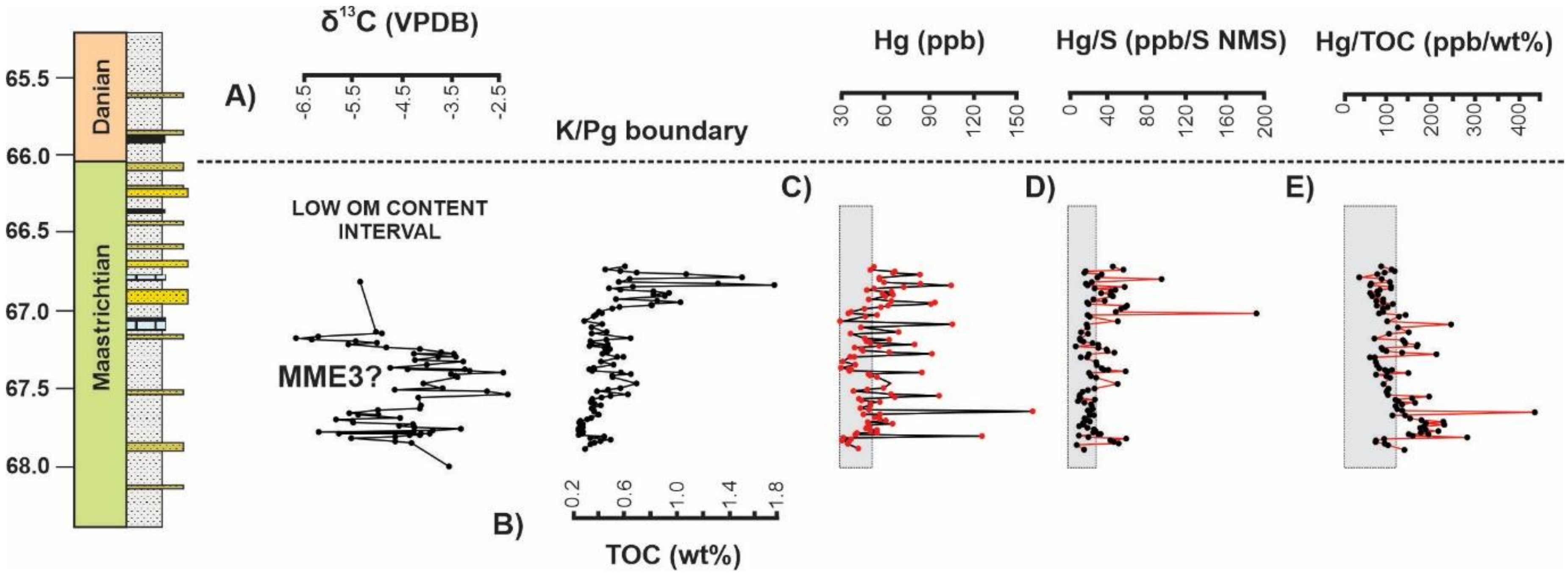

Figure 2. Geochemical survey and Hg chemostratigraphy of core Diablito-1E. A) $\delta^{13}C$ curve (MME3: Mid-Maastrichtian excursion 3). B) Total organic carbon (TOC) measurements. C-E) Hg concentrations, Hg/S and Hg/TOC ratios. Age model based on De La Parra et al (2022) and Patarroyo et al (2022).

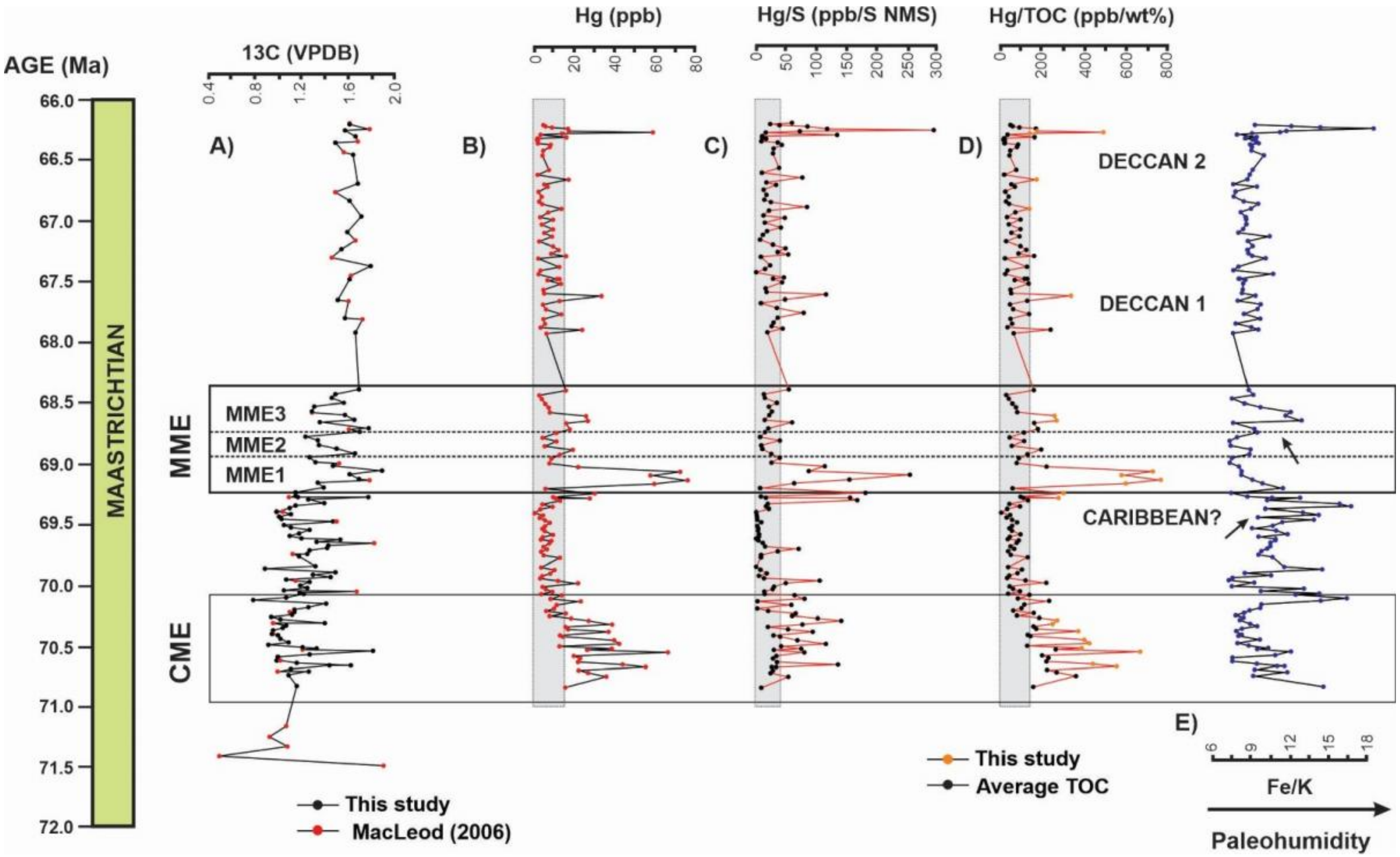

Figure 3. Geochemical survey and Hg chemostratigraphy of Hole 1258A (Demerara Rise). B-D) Hg concentrations, Hg/S and Hg/TOC ratios. TOC measurements from our study and previous surveys (Erbacher et al., 2004). E) Fe/K ratio as a proxy for geochemical weathering intensity (hydroclimate). Age model based on Erbacher et al. (2004) and Suganuma and Ogg (2006). Tentative chronology of the Deccan eruption based on previous studies (Sprain et al., 2019; Schoene et al., 2019). Tentative chronology of the Campanian-Maastrichtian Caribbean volcanic episodes based on Sigurdsson et al. (2000).

Our TOC measurements for samples with anomalously high Hg concentrations also resulted in negligible TOC values (TOC 0.00-0.12 wt%; Figure 3). Covariation between Hg and TOC values (previous results and our estimations) or sulfur concentrations show a weak correlation (r^2<0.2; see supplementary material). Both Hg/TOC and Hg/S trends are similar to those of the Hg curve, with significant spikes in the earliest Maastrichtian (70.75-70.29 Ma), during the MME (69.28-68.6 Ma), and at least in two segments of the late Maastrichtian (67.89-67.61 Ma and 66.3-66.25 Ma). Figure 3 also includes the Fe/K curve from the same set of data (**CHAPTER 3**). The Fe/K ratio depicts an increasing-upward trend, with positive spikes (>10) in the lower Maastrichtian (303.3-309.05 mbsf), before the mid-Maastrichtian and the upper Maastrichtian (258.13-259.61 mbsf; 294.15-297.55 mbsf) intervals.

At least two intervals with elevated Hg concentrations (>10 ppb) are present in Hole 1001B: early Maastrichtian (69.42 to 69.94 Ma; 394.58-400.53 mbsf), and late Maastrichtian (66.96 to 68.06 Ma; 366.13-378.92 mbsf), with a major peak in the latest Maastrichtian (66.08 to 66.61 Ma; 353.79-362.2 mbsf). Across the Danian interval (65.97 to 62.28 Ma; 352.27-332.15 mbsf), Hg measurements depicted concentrations <5 ppb (**CHAPTER 4**). To distinguish volcanic sources of Hg during the Maastrichtian, we normalized Hg concentrations by the mean TOC content of 0.09 wt% reported by Sigurdsson et al (2004). Therefore, the Hg/TOC curve depicted the same trends as those of Hg content. New TOC measurements of samples with anomalous Hg concentrations like those on the latest Maastrichtian (e.g., 353.79-362.87 mbsf) would be desirable. To make tentative comparisons with Hg concentrations of Hole 1258A, the K-Pg boundary at both sites was used as a datum (Figure 4).

In general, the Hg curves at both ODP sites were similar, with 40-80 ppb as their highest values, and suggesting the record of at least three major volcanic episodes during the Maastrichtian. However, due to uncertainties in the age model for 1001B (based on magnetostratigraphy, see discussion in **CHAPTER 4**), we cannot assert whether the Hg spike between 69.42 and 69.94 Ma corresponds to the one observed between 70.75-70.29 Ma and 69.28-69.02 Ma at Hole 1258A. Though of smaller magnitude at Hole 1258A, Hg positive excursions between 68.2 and 66.7 Ma can be correlated within the late Maastrichtian, particularly for its last 600 k.y. (Figure 4).

PRELIMINARY DISCUSSIONS

Tracking volcanic activity recorded in Maastrichtian tropical shallow-marine settings

Considering the record in northern Brazil (Paraiba Basin; Sial et al., 2013), our study at Core Diablito-1E is the second Maastrichtian high-resolution Hg record in South America. Based on the age model of this locality, which includes the location of the K-Pg (De La Parra et al., 2022), biostratigraphy (Patarroyo et al., 2022), and the $\delta^{13}C$ record, our studied interval likely spans from 67.0 to 68.0 Ma

(Figure 2). In general, Hg concentrations *per se* are promising as a chemostratigraphic tool, with significant contrasts along the studied interval (Figure 2). Normalization of these concentrations with the estimations of TOC and sulfur content, suggests several Hg sources (sin-sedimentary, organic, volcanic), as expected for a shallow marine setting. Low TOC content at the lower part of Core Diablito-1E (~0.7 wt%) advocates for a likely volcanic origin for Hg enrichments. These results agreed with previous studies that reported overall low TOC content for the Colón Formation, with values of ~0.8 wt% for the calcareous Socuy Member (lower Colón Formation), and <0.6 wt% for the fine-grained successions of the same unit in the Cesar-Rancheria and Catatumbo basins (Patarroyo et al., 2017; Avendaño et al., 2021). Considering the age model of Core Diablito-1E, we suggest that the Hg/TOC spikes between 68 and 67.5 Ma could be correlated with Hg/TOC enrichment episodes recorded in the late Maastrichtian from Nicaragua and Demerara Rise (Figure 4). In contrast, higher TOC contents in the upper part of Core Diablito-1E (>1.0 wt%; 609.4-578.5 m), and the distribution of the Hg/S ratio, suggest a non-volcanic source for these Hg concentrations. More proximal settings, and therefore oxygen-depleted bottom and pore waters, as suggested by micropaleontological and geochemical proxies by Patarroyo et al (2022), might explain Hg enrichments in the upper segment of Core Diablito-1E. In terrestrial and shallow marine environments, Hg concentrations vary constantly and are mostly controlled by biological (e.g., soil moisture, bioturbation) and sedimentological (e.g., aquatic transport via runoff, sediment winnowing) processes (Grasby et al., 2017; Percival et al., 2018).

The geological and geographical context of northern South America presents additional issues that should be addressed before continuing to test Hg chemostratigraphy in the Late Cretaceous. One of them is segregating the likely record of the Deccan (distal) volcanism from the potential influence of the arc-continent collisional event in northern South America, which occurred between the Late Cretaceous and Paleogene, and the final emplacement of the Caribbean Plate (e.g. Pindell et al., 2005; Montes et al., 2019; Zapata-Villada et al., 2021). For the Cretaceous-Paleogene transition, several authors have proposed magmatic episodes associated to this arc-continent collisional event, and even the occurrence of a magmatic hiatus between 70 Ma and 60 Ma (Villagómez et al., 2011; Spikings et al., 2015; Duque-Trujillo et al., 2019). This hiatus encompasses the depositional time span of the studied interval at core Diablito-1E, where a key aspect is the absence of volcanic ash layers (bentonites) in the Campanian-Maastrichtian interval. The accumulation of bentonite deposits, related to the Caribbean Large Igneous Province (CLIP), is a common feature of the Cenomanian-Santonian successions of Colombia (e.g. Villamil, 1998; Terraza, 2019; Paez-Reyes et al., 2021).

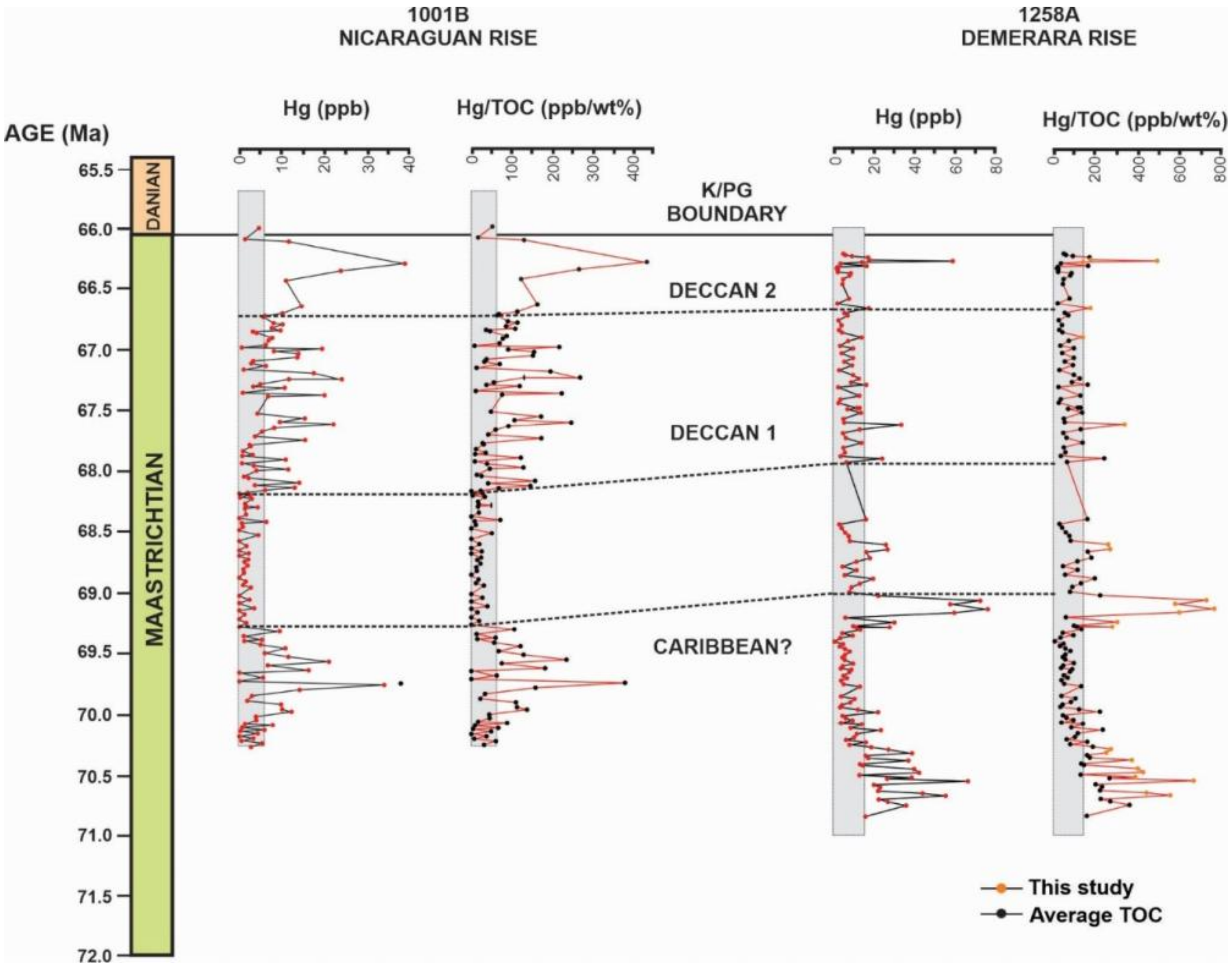

Figure 4. Mercury chemostratigraphy of Holes 1001B (Nicaraguan Rise) and 1258A (Demerara Rise). TOC measurements at Hole 1258A from our study and previous surveys (Erbacher et al., 2004). Tentative chronology of the Deccan eruption based on previous studies (Sprain et al., 2019; Schoene et al., 2019). Tentative chronology of Campanian-Maastrichtian Caribbean volcanic episodes based on Sigurdsson et al (2000).

Despite environmental complexities of the Maastrichtian shallow marine environments of northern South America, and the singular geographic and geological context of this area, one could speculate that the major Hg enrichments at the lower segment of core Diablito-1E might be related to Deccan volcanism, providing additional chronostratigraphic constrains for the Colón Formation. This hypothesis, however, is still tentative and purely speculative, and future studies (e.g. magnetostratigraphy) are needed to test it at our core and in coetaneous localities. Additional Hg spikes may be also explored in the Paleocene record of core Diablito-1E (Catatumbo/Barco formations) since Hg enrichments have been reported in lower Paleocene marine records and associated with late pulses of Deccan volcanism (e.g., Sial et al., 2013, 2016; Font et al., 2021; Krahl et al., 2021, 2023). A similar approach would be also desirable in the Santonian-Campanian successions of this area to track the influence of CLIP volcanism.

A final consideration is the role that the Maastrichtian tropical rainforest could have played in the regional Hg biogeochemical cycle. Coniferous trees, a major component of the Cretaceous tropical forests of northern South America (Carvalho et al., 2021), tend to intake more Hg into both foliage and woody tissues than deciduous species, eventually promoting soil Hg enrichment (Obrist et al., 2012; Percival et al., 2018). This mechanism could be tested with further integrated paleobotanical and geochemical studies of tropical Maastrichtian successions.

Record of Deccan volcanic activity at tropical deep-sea settings

Several studies have explored sedimentary Hg concentrations in the upper Maastrichtian and their possible links with the Deccan volcanic episodes. Surveyed localities comprise from open marine to continental settings, proximal and distal to the Deccan Traps large igneous province (e.g., Font et al, 2016, 2021; Sial et al., 2014, 2016; Percival et al., 2018; Fendley et al., 2019; Keller et al., 2020; Krahl et al., 2021; Gu et al., 2022). Supplementary figure 2 (SF2) summarizes Hg concentrations at our tropical sites, as well as at selected sections where Hg studies have been published across the Maastrichtian-Danian transition. All the selected localities presented low TOC contents, and Hg/TOC normalizations support mostly volcanic Hg sources. Following Percival et al (2018) and Gu et al (2022), we used the position of the K-Pg boundary as a correlation datum, since magnetostratigraphy and biostratigraphy were not conclusive enough in some intervals. Apart from ODP Site 174 (New Jersey Coastal Plain), all localities depict a general Hg enrichment in the latest Maastrichtian. Additional studies that were not included in the SF2 due to low sampling resolution or short time span (e.g., 66.05-65.9 Ma), also reported higher Hg concentrations before the K-Pg boundary (e.g., northern Brazil, Montana, Zumaia, Israel, Southern Atlantic, among others; Sial et al., 2014, 2016; Percival et al., 2018; Keller et al., 2020; Krahl et al., 2021, 2023). Based on the Deccan Traps chronology of Chenet et al (2009), Percival et al (2018) tentatively related these Hg spikes to the Igatpuri-Poladpur interval, which comprises magnetochron C29r. Maastrichtian localities in Tunisia and Israel, which display Hg enrichments 550 k.y. before the K-Pg boundary, were also related to Deccan Traps volcanic episodes, based on orbitally tuned age models (Keller et al., 2020).

Correlation of middle to late Maastrichtian (magnetochrons C30 to C31) Hg enrichments is less clear due to uncertainties in magnetostratigraphy and varying sampling resolutions, since most previous studies focused on the K-Pg transition. For instance, we did not consider the Hg surveys of Percival et al (2018) in Zumaia (Spain) because there were not TOC measurements, and we could not derive an age model for it. This reinforces the need for more high-resolution records, in both marine (deep-sea and shallow) and continental settings, with robust chronostratigraphic frameworks for the Maastrichtian. Recent chronostratigraphic re-evaluations in the Global Stratotype Section and Point (GSSP) of the K-Pg boundary (Jones et al., 2022), or reference Maastrichtian localities such as ENCY quarry (Netherlands; Vellekoop et al., 2022), made them suitable candidates for high-resolution Hg chemostratigraphy of the Maastrichtian.

Notwithstanding, our tentative Hg chemostratigraphic correlation for the early Maastrichtian allowed comparison between Holes 1001B and 1258A with Seymour Island (Antarctic Peninsula). Considering the likely influence of CLIP volcanic pulses, as well as of regional volcanic activity in Antarctica (Da Silva et al., 2021), additional studies are necessary to disentangling regional (CLIP, Antarctica) from widespread (Deccan) volcanic activity. For instance, osmium isotopes ($^{187}Os/^{188}Os$) are being applied as a proxy for large igneous provinces activity and related processes (Percival et al., 2018; Matsumoto et al., 2020). In addition, surveys using any of the seven natural stable isotopes of mercury, or the mass-independent fractionation of this element (Hg-MIF) could provide hints about the influence of photochemical processes on Hg concentrations (e.g., Bergquist and Blum, 2009; Percival et al., 2018, Grasby et al., 2019; Gu et al., 2022).

In conclusion, Hg chemostratigraphy in Maastrichtian localities is promising, not only for tracking the influence of Deccan volcanism before the K-Pg boundary, but also for detecting regional volcanic episodes in poorly explored locations as the tropics, and testing likely links of these episodes with climate variability. For example, Figure 3 suggests a likely relation between Maastrichtian volcanic pulses and the hydroclimate changes in northern South America, suggested by the distribution of the sedimentary Fe/K ratio (Stuut et al., 2005; Mulitza et al., 2008) at Hole 1258A. Less humid conditions are tentatively associated with volcanic pulses of the early and middle Maastrichtian (Caribbean?, Deccan 1), while the latest Maastrichtian volcanic pulse (Deccan 2) probably strengthened the precipitation on low latitude regions. A revised chronology for the late Maastrichtian warming event at Site 1262 (Walvis Ridge), proposed synchronism between the onset of the main phase of Deccan volcanism, with the late Maastrichtian warming event, about 300 k.y. before the K-Pg boundary (Barnet et al., 2018).

To test the climatic and chronostratigraphic significance of the Hg concentration records in the latest Cretaceous low latitude settings, we need to increase the number of high-resolution surveys in this area, including open and shallow marine localities, as well as detailed geochemical tests (e.g., TOC and trace metal concentrations, Hg isotopes) of the analyzed material. Suitable candidates could be the deep-sea sediments of Gorgonilla Island (Colombian Pacific, Bermúdez et al., 2019) or ODP sites such as those on Shatsky Rise (Dameron et al., 2017) and Blake Nose (Martínez-Ruiz et al., 2001).

CONCLUSIONS

To track evidence of widespread volcanism during the latest Cretaceous we surveyed Hg concentrations in three Maastrichtian low-latitude localities: (1) Core Diablito-1E (Colón Formation, northern Colombia), (2) Ocean Drilling Program (ODP) Hole 1258A (Demerara Rise, offshore Suriname) and, (3) ODP Hole 1001B (Nicaraguan Rise, Caribbean Sea).

Mercury, Hg/TOC and H/S chemostratigraphy at Core Diablito-1E was problematic due to the shallowing processes underwent by this sedimentary succession, and the poorly explored influence of northern South American volcanism during the Maastrichtian. Stable carbon isotopes ($\delta^{13}C$) surveys at the same core, the first of its type in Maastrichtian strata from this area, suggested that low latitude sedimentary successions potentially recorded the MME global carbon cycle perturbation. Furthermore, Hg, Hg/TOC and H/S chemostratigraphy at Holes 1258A and 1001B suggest the record of at least three volcanic episodes during the Maastrichtian, likely related with proximal and/or distal volcanic sources, such as from the Caribbean Plate volcanic arc, and Deccan volcanic pulses. Significant Hg/TOC spikes were observed before the K-Pg transition, but not in the early Danian from Site 1001.

ACKNOWLEDGMENTS

This research used samples provided by the International Ocean and Discovery Program (IODP). IODP is sponsored by the U.S. National Science Foundation (NSF) and participating countries. G.D.P. thanks to PETROBRAS for a scholarship in the project “Bioestratigrafia de foraminíferos do Aptiano-Albiano da Margem Continental Brasileira”. K.G.D.K thanks the Brazilian National Council for Scientific and Technological Development (CNPq) for grant number 307309/2023-1. L.A. acknowledges funding from project PID2019-105537RB-I00 (Spanish Ministry of Science and Innovation and FEDER fund

REFERENCES (CHAPTER 3-6)

Abramovich, S., Keller, G., 2003. Planktonic foraminiferal response to the latest Maastrichtian abrupt warm event: A case study from South Atlantic DSDP Site 525A. Marine Micropaleontology, 48(3–4), 225–249.

Abramovich, S., Yovel-Corem, S., Almogi-Labin, A., Benjamini, C., 2010. Global climate change and planktic foraminiferal response in the Maastrichtian, Paleoceanography 25, PA2201, doi:10.1029/2009PA001843.

Agnihotri, R., Altabet, M.A., Herbert, T.D., Tierney, J.E., 2008. Subdecadally resolved paleoceanography of the Peru margin during the last two millennia. Geochemistry Geophysics Geosystems 9, Q05013, doi:10.1029/2007GC001744.

Alegret, L., Arreguín-Rodríguez, G. J., Thomas, E., 2022. Oceanic productivity after the Cretaceous/Paleogene impact: where do we stand? The view from the deep. In: Koeberl, C., Claeys, P., Montanari, A., eds., From the Guajira desert to the Apennines, and from Mediterranean microplates to the Mexican killer asteroid: Honoring the career of Walter Alvarez. Geological Society of America Special Paper 557, chapter 21.

Alegret L., Thomas, E., 2001. Upper Cretaceous and lower Paleogene benthic foraminifera from northeastern Mexico. Micropaleontology 47 (4), 269-316.

Alegret, L., Thomas, E., 2009. Food supply to the seafloor in the Pacific Ocean after the Cretaceous/Paleogene boundary event. Marine Micropaleontology 73(1–2), 105-116.

Alvarez, L.W., Alvarez, W., Asaro, F., Michel, H.V., 1980. Extraterrestrial cause for the Cretaceous-Tertiary extinction. Science 208, 1195-1108.

Avendaño-Sánchez, G.M., García-González, M., Cruz-Guevara, L.E., Cruz-Ceballos, L.F., 2021. Geochemistry and petrographic analysis of Los Cuervos and Molino formations, Cesar Sub-Basin (Colombia): Implications in the petroleum system evolution. Boletín de Geología 43 (2), 95-116.

Barrera, E., Savin, S.M., Thomas, E., Jones, C.E., 1997. Evidence for thermohaline circulation reversals controlled by sea-level change in the latest Cretaceous. Geology 25, 715-718.

Barnet, J.S.K., Littler, K., Kroon, D., Leng, M.J., Westerhold, T., Röhl, U., Zachos, J.C., 2017. A new high-resolution chronology for the late Maastrichtian warming event: Establishing robust temporal links with the onset of Deccan volcanism. Geology 46, 147–150.

Batenburg, S.J., Voigt, S., Friedrich, O., Osborne, A.H., Bornemann, A., Klein, T., Pérez-Díaz, L., Frank, M., 2018. Major intensification of Atlantic overturning circulation at the onset of Paleogene greenhouse warmth. Nature Communications 9, 1-8.

Bayona, G., Baquero, M., Ramírez, C., Tabares, M., Salazar, A.M., Nova, G., Duarte, E., Pardo, A., Plata, A., Jaramillo, C., Rodríguez, G., Caballero, V., Cardona, A., Montes, C. Gómez-Marulanda, S., Cárdenas-Rozo, A.L., 2020. Unravelling the widening of the earliest Andean northern orogen: Maastrichtian to early Eocene intra-basinal deformation in the northern Eastern Cordillera of Colombia. Basin Research 00, 1–37.

Bayona, G., Montes, C., Cardona, A., Jaramillo, C., Ojeda, G., Valencia, V., 2011. Intraplate subsidence and basin filling adjacent to an oceanic arc-continental collision; a case from the southern Caribbean–South America plate margin. Basin Research 23. http://dx.doi.org/10.1111/j.1365-2117.2010.00495.x.

Bejaoui, A., Saïdi, E., Zaghbib-Turki, D., 2019. Small benthic foraminiferal biostratigraphy and palaeoecology during the CampanianMaastrichtian transition in north-western Tunisia. Turkish Journal of Earth Sciences 28, 500-530.

Benoit, J.M., Mason, R.P., Gilmour, C.C., Aiken, G.R., 2001. Constants for mercury binding by dissolved organic matter isolates from the Florida Everglades. Geochimica et Cosmochimica Acta 65 (24), 4445-4451.

Bermúdez, H.D., Arenillas, I., Arz, J.A., Vajda, V., Renne, P.R., Gilabert, V., Rodríguez, J.V., 2019. The Cretaceous/Paleogene boundary deposits on Gorgonilla Island. In: Gómez, J., Mateus–Zabala, D. (Eds.), The Geology of Colombia, Volume 3 Paleogene – Neogene. Servicio Geológico Colombiano, Publicaciones Geológicas Especiales 37, 19 p.

Bergquist, B.A., Blum, J.D., 2009. The Odds and Evens of Mercury Isotopes: Applications of Mass-Dependent and Mass-Independent Isotope Fractionation. Elements 5 (6), 353-357.

Bolli, H.M., Beckmann, J.P., and Saunders, J.B. 1994. Benthic foraminiferal biostratigraphy of the South Caribbean region. Cambridge University Press. Cambridge, 411 p.

Calvert, S.E., Pedersen, T.F., 2007. Elemental proxies for palaeoclimatic and palaeoceanographic variability in marine sediments: Interpretation and application. In: Hillaire-Marcel, C., De Vernal, A. (Eds.), Proxies in Late Cenozoic Paleoceanography, Developments in Marine Geology 1, pp. 567-644.

Campos, M.C., Chiessi, C.M., Novello, V.F., Crivellari, S., Campos, J.L.P.S., Albuquerque, A.L.S., Venancio, I.M., Santos, T.P., Melo, D.B., Cruz, F.W., Sawakuchi, A.O., Mendes, V.R., 2022. South

American precipitation dipole forced by interhemispheric temperature gradient. Scientific Reports 12, 10527.

Carvajal-Arenas, L.C., Mann, P., 2018. Western Caribbean intraplate deformation: Defining a continuous and active microplate boundary along the San Andres rift and Hess Escarpment fault zone, Colombian Caribbean Sea. AAPG Bulletin 102 (8), 1523-1563.

Carvalho, M.R., Jaramillo, C., De La Parra, F., Caballero-Rodríguez, D., Herrera, F., Wing, S., Turner, B.L., D'Apolito, C., Romero-Báez, M., Narváez, P., Martínez, C., Gutierrez, M., Labandeira, C., Bayona, G., Rueda, M., Paez-Reyes, M., Cárdenas, D., Duque, A., Crowley, J.L., Santos, C., Silvestro, D., 2021. Extinction at the end-Cretaceous and the origin of modern Neotropical rainforests. Science 372, 63–68.

Cetean, C.G., Bălc, R., Kaminski, M.A., Filipescu, S., 2011. Integrated biostratigraphy and palaeoenvironments of an upper Santonian – upper Campanian succession from the southern part of the Eastern Carpathians, Romania. Cretaceous Research 32 (5), 575-590.

Chiarenza, A.A., Farnsworth, A., Mannion, P.D., Lunt, D.J., Valdes, P.J., Morgan, J.V., Allison, P.A., 2020. Asteroid impact, not volcanism, caused the end-Cretaceous dinosaur extinction. PNAS 117 (29), 17084-17093.

Chenet, A.L., Courtillot, V., Fluteau, F., Gérard, M., Quidelleur, X., Khadri, S.F.R., Subbarao, K.V., Thordarson, T., 2009. Determination of rapid Deccan eruptions across the Cretaceous-Tertiary boundary using paleomagnetic secular variation: 2. Constraints from analysis of eight new sections and synthesis for a 3500-m-thick composite section: Journal of Geophysical Research: Solid Earth 114 (B6), B06103.

Coffin, M.F., Duncan, R.A., Eldholm, O., Fitton, J.G., Frey, F.A., Larsen, H. C., Mahoney, J.J., Saunders, A.D., Schlich, R., Wallace, P.J., 2006. Large igneous provinces and scientific ocean drilling, status quo and a look ahead. Oceanography 19, 150–160.

Corentin, P., Pucéat, E., Pellenard, P., Guiraud, M., Blondet, J., Bayon, G., Adatte, T., 2023. Late Cretaceous evolution of chemical weathering at the northeastern South American margin inferred from mineralogy and Hf-Nd isotopes. Marine Geology 455, 106968.

Cramer, B.S., Toggweiler J., Wright, J.D., Katz, M.E., Miller, K.G., 2009. Ocean overturning since the Late Cretaceous: Inferences from a new benthic foraminiferal isotope compilation, Paleoceanography 24 (4), PA4216, doi:10.1029/2008PA001683.

Crivellari, S., Junia-Viana, P., de Carvalho-Campos, M., Kuhnert, H., Machado-Lopes, A.B., da Cruz, Jr., F.W., Mazur-Chiessi, C., 2021. Development and characterization of a new in-house reference material for stable carbon and oxygen isotopes analyses. Journal of Analytical Atomic Spectrometry 36 (6), 1125-1134.

D'Hondt, S., Arthur, M.A., 2002. Deep water in the late Maastrichtian Ocean. Paleoceanography 17, 8-11.

Dameron, S., Leckie, M., Clark, K., Lees, J.A., 2017. Extinction, dissolution, and possible ocean acidification prior to the Cretaceous/Paleogene (K/Pg) boundary in the tropical Pacific. Palaeogeography Palaeoclimatology Palaeoecology, doi: 10.1016/j.palaeo.2017.06.032.

Da Silva, R.R., Kochhann, K.G.D., Guerra, R.M., Fauth, G., Carvalho, M.A., Ramos, R.R.C., 2022. Why do calcareous microfossils preferentially occur in tuffaceous sandstones of the Santa Marta formation (James Ross Island, Antarctica)? Journal of South American Earth Sciences 113, 103682.

De La Parra, F., Jaramillo, C., Kaskes, P., Goderis, S., Claeys, P., Villasante-Marcos, V., Bayona, G., Hatsukawa, Y., Caballero, D., 2022. Unraveling the record of a tropical continental Cretaceous-Paleogene boundary in northern Colombia, South America. Journal of South American Earth Sciences 114, 103717.

Dubicka, Z., Peryt, D., 2016. *Bolivinoides* (Benthic foraminifera) from the Upper Cretaceous of Poland and western Ukraine: Taxonomy, evolutionary changes and stratigraphic significance. Journal of Foraminiferal Research 46 (1), 75–94

Dummann, W., Hofmann, P., Herrle, J.O., Wennrich, V., Wagner, T., 2021. A refined model of Early Cretaceous South Atlantic–Southern Ocean gateway evolution based on high-resolution data from DSDP Site 511 (Falkland Plateau). Palaeogeography, Palaeoclimatology, Palaeoecology 562, 110113.

Duque-Trujillo, J., Bustamante, C., Solari, L., Gómez-Mafla, A., Toro-Villegas, G., Hoyos, S., 2019, Reviewing the Antioquia batholith and satellite bodies: a record of Late Cretaceous to Eocene syn- to post-collisional arc magmatism in the central Cordillera of Colombia. Andean Geology 46 (1), 82-101.

Emili, A., Koron, N., Covelli, S., Faganeli, J., Acquavita, A., Predonzani, S., De Vittor, C., 2011. Does anoxia affect mercury cycling at the sediment-water interface in the Gulf of Trieste (Northern Adriatic Sea)? Incubation experiments using benthic flux chambers. Applied Geochemistry 26 (2), 194-204.

Erbacher, J., Mosher, D.C., Malone, M.J., 2004. Shipboard scientific party. In: Proc. ODP. In. Reports, 207.

Erlich, R.N., Macsotay, O., Nederbragt, A.J., Lorente, M.A., 1999. Palaeoecology, paleogeography and depositional environments of Upper Cretaceous rocks of western Venezuela. Palaeogeography, Palaeoclimatology, Palaeoecology 153 (1-4), 203-238.

Erlich, R.N., Nederbragt, A.J., Lorente, M.A., 2000. Birth and death of the Late Cretaceous "a Luna Sea", and origin of the Tres Esquinas phosphorites. Journal of South American Earth Sciences 13, 21–45.

Farouk, S., Jain, S., Bazeen, Y.S., Ahmad, F., Elamri, Z., Al-Kahtany, K., Abdeldaim, A., 2023. Palaeoenvironmental changes across the Mid and latest Maastrichtian events: Planktic foraminiferal inference from the Elles section (central Tunisia). Geological Journal 1–18.

Fatela, F., Taborda, R., 2002. Confidence limits of species proportions in microfossil assemblages. Marine Micropaleontology 45, 169-174.

Fendley, I.M., Mittal, T., Sprain, C.J., Marvin-DiPasquale, M., Tobin, T.S., Renne, P.R., 2019. Constraints on the volume and rate of Deccan Traps flood basalt eruptions using a combination of high-resolution terrestrial mercury records and geochemical box models. Earth and Planetary Science Letters 524, 115721.

Font, E., Adatte, T., Sial, A.N., Drude de Lacerda, L., Keller, G., Punekar, J., 2016. Mercury anomaly, Deccan volcanism, and the end-cretaceous mass extinction. Geology 44, 171-174.

Font, E., Adatte, T., Sial, A.N., Drude de Lacerda, L., Keller, G., Punekar, J., 2016. Mercury anomaly, Deccan volcanism, and the end-cretaceous mass extinction. Geology 44, 171-174.

Forcino, F.L., 2012. Multivariate assessment of the required sample size for community paleoecological research. Palaeogeography, Palaeoclimatology, Palaeoecology 315-316, 134-141.

Frank, T.D., Thomas, D.J., Leckie, R.M., Arthur, M.A., Bown, P.R., Jones, K., Lees, J.A., 2005. The Maastrichtian record from Shatsky Rise (northwest Pacific): A tropical perspective on global ecological and oceanographic changes. Paleoceanography 20(1), PA1008. https://doi.org/10.1029/2004pa001052.

Frenzel, P., 2000. Die benthischen Foraminiferen der Rügener Schreibkreide (unter Maastricht, NE Deutschland). In: Neue Paläontologischen Abhandlungen. C Press, Dresden, 3, 361 p.

Friedrich, O., Erbacher, J., 2006. Benthic foraminiferal assemblages from Demerara Rise (ODP Leg 207, western tropical Atlantic): Possible evidence for a progressive opening of the Equatorial Atlantic Gateway. Cretaceous Research, 27, 377–397.

Friedrich, O., Erbacher, J., Moriya, K., Wilson, P. A., Kuhnert, H., 2008. Warm saline intermediate waters in the Cretaceous tropical Atlantic Ocean. Nature Geoscience, 1(7), 453–457.

Friedrich, O., Hemleben, C., 2007. Early Maastrichtian benthic foraminiferal assemblages from the western North Atlantic (Blake Nose) and their relation to paleoenvironmental changes. Marine Micropaleontology, 62(1), 31–44.

Friedrich, O., Herrle, J.O., Kößler, P., Hemleben, C., 2004. Early Maastrichtian stable isotopes: Changing deep water sources in the North Atlantic? Palaeogeogr. Palaeoclimatol. Palaeoecol. 211, 171-184.

Friedrich, O., Herrle, J.O., Wilson, P.A., Cooper, M.J., Erbacher, J., Hemleben, C., 2009. The early Maastrichtian carbon cycle perturbation and cooling event: Implications from the South Atlantic Ocean. Paleoceanography 24, PA2211. doi:10.1029/2008PA001654.

Friedrich, O., Norris, R.D., Erbacher, J., 2012. Evolution of middle to Late Cretaceous oceans – A 55 m.y. record of Earth's temperature and carbon cycle, Geology, 40, 107–110.

Frizzell, D.L. 1954. Handbook of Cretaceous Foraminifera of Texas. Bureau of Economic Geology, Report of Investigations 22, University of Texas, 232 p.

García-Reyes, A., Dyment, J., 2021. Structure, age, and origin of the Caribbean Plate unraveled. Earth and Planetary Science Letters, 2021, 571, pp.117100. ff10.1016/j.epsl.2021.117100ff. ffhal-03452889f.

Gilabert, V., Batenburg, S.J., Arenillas, I., Arz, J.A., 2021. Contribution of orbital forcing and Deccan volcanism to global climatic and biotic changes across the Cretaceous-Paleogene boundary at Zumaia, Spain. Geology 50 (1), 22-25.

Giraldo-Villegas, C.A., Rodríguez-Tovar, F.J., Celis, S.A., Pardo-Trujillo, A., Duque-Castaño, M.L., 2023. Paleoenvironmental conditions over the Caribbean Large Igneous Province during the Late Cretaceous in NW of South American Margin: A sedimentological and ichnological approach. Cretaceous Research 142, 105407.

Goderis, S., Sat, H., Ferriere, I., Schmitz, B., Burney, D., Kaskes, P., Vellekoop, J., Wittmann, A., Schultz, T., Chernonozhkin, S., Claeys, P., de Graff, S., Déhais, T., de Winter, N., Elfman, M., Feignon, J., Ishikawa, A., Koeberl, C., Kristiansson, P., Neal, C., Owens, J., Schmieder, M., Sinnesael, M., Vanhaecke, F., Van Malderen, S., Bralower, T., Gulick, S., Kring, D., Lowery, C., Morgan, J., Smit, J., Whalen, M., IODP-ICDP Expedition 364 Scientists, 2021. Globally distributed iridium layer preserved within the Chicxulub impact structure. Science Advances 7, eabe3647.

Govin, A., Holzwarth, U., Heslop, D., Ford Keeling, L., Zabel, M., Mulitza, S., Collins, J.A., Chiessi, C. M. 2012. Distribution of major elements in Atlantic surface sediments (36°N–49°S): Imprint of terrigenous input and continental weathering. Geochem. Geophys. Geosyst. 13, Q01013.

Gradstein, F.M., Ogg, J.G., Schmitz, M.D., Ogg, G.M., 2012. The Geological Time Scale 2012, vol. 2. Elsevier, Amsterdam, p. 1144.

Grasby, S.E., Shen, W., Yin, R., Gleason, J.D., Blum, J.D., Lepak, R.F., Hurley, J.P., Beauchamp, B., 2017. Isotopic signatures of mercury contamination in latest Permian oceans. Geology 45, 55-68.

Grasby, S.E., Them, T.R., Chen, Z., Yin, R., Ardakani, O.H., 2019. Mercury as a proxy for volcanic emissions in the geologic record. Earth Science Reviews 196, 102880.

Gu, X., Zhang, L., Runsheng Yin, R., Grasby, S.E., Yao, H., Tan, J., Wang, C., 2022. Deccan volcanic activity and its links to the end-Cretaceous extinction in northern China. Global and Planetary Change 210 (2022) 103772.

Guerra, R.M., Concheyro, A., Kochhann, K.G.D., Bom, M.H.H., Ceolin, D., Musso, T., Savian, J.F., Fauth, G., 2021. Calcareous microfossils and paleoenvironmental changes across the Cretaceous-Paleogene (K-Pg) boundary at the Cerro Azul Section, Neuquén Basin, Argentina. Palaeogeography, Palaeoclimatology, Palaeoecology 567, 110217.

Guerra, R.M., Concheyro, A., Wise, S.W., Fauth, G., 2016. Late Campanian-Maastrichtian *Kamptnerius magnificus* acme in the South Atlantic section of the Southern Ocean, ODP Holes 690C and 700B. Micropaleontology 62 (3), 213-219.

Hammer, O., Harper, D.A.T., Ryan, P.D., 2001. PAST: paleontological statistics software package for education and data analysis. Palaeontologia Electrononica 4 (1), 1-9.

Haynes, S.J., MacLeod, K.G., Ladant, J.B., Guchte, A.V., Rostami, M.A., Poulsen, C.J., Martin, E.E., 2020. Constraining sources and relative flow rates of bottom waters in the Late Cretaceous Pacific Ocean. Geology, 48(5), 509–513.

Henehan, M.J., Hull, P.M., Penman, D.E., Rae, J.W.B., Schmidt, D.N., 2016. Biogeochemical significance of pelagic ecosystem function: An end-Cretaceous case study: Royal Society of London Philosophical Transactions, ser. B, 371, p. 1-10.

Huber, B.T., MacLeod, K.G., Watkins, D.K., Coffind, M.L., 2018. The rise and fall of the Cretaceous Hot Greenhouse climate. Global and Planetary Change 167, 1-23.

Hull, P.M., Bornemann, A., Penman, D.E., Henehan, M.J., Norris, R.D., Wilson, P.A., Blum, P., Alegret, L., Batenburg, S.J., Bown, P.R., Bralower, T.J., Cournede, C., Deutsch, A., Donner, B., Friedrich, O., Jehle, S., Kim, H., Kroon, D., Lippert, P.C., Dominik Loroch, D., Moebius, I., Moriya, K., Peppe, D.J., Ravizza, G.E., Röhl, U., Schueth, J., Sepúlveda, J., Sexton, P.F., Sibert, E.C., Śliwińska, K.K., Summons, R.E., Thomas, E., Westerhold, T., Whiteside, J.H., Tatsuhiko Yamaguchi, T., Zachos, J.C., 2020. On impact and volcanism across the Cretaceous-Paleogene boundary. Science 367, 266–272.

Jaccard, S.L., Haug, G.H., Sigman, D.M., Pedersen, T.F., Thierstein, H.R., Röhl, U., 2005. Glacial/interglacial changes in subarctic North Pacific stratification. Science 308(5724), 1003-1006.

Jaff, R.B.N., Lawa, F.A., 2019. Palaeonenvironmental signature of the Late Campanian-Early Maastrichtian benthonic foraminiferal assemblages of Kurdistan, Northeast Iraq. Journal of African Earth Sciences 151, 255-273.

Jarvis, I., Gale, A.S., Jenkyns, H.C., Pearce, M.A., 2006. Secular variation in Late Cretaceous carbon isotopes: a new $\delta^{13}C$ carbonate reference curve for the Cenomanian–Campanian (99.6–70.6 Ma). Geological Magazine 143, 561–608.

Jenkyns, H.C., 1995. Carbon-isotope stratigraphy and paleoceanographic significance of the Lower Cretaceous shallow-water carbonates of Resolution Guyot, Mid-Pacific Mountains. In: Winterer E.L., Sager W.W., Firth J.V, Sinton J.M. (eds): Proceedings of the ocean drilling program, scientific results. Ocean Drilling Program (College Station, TX): 99–104.

Johnson, C.C., 2002. The Rise and Fall of Rudist Reefs. American Scientist 90(2), 148-153.

Jones, H., Westerhold, T., Birch, H., Hull, P., Negra, M.H., Röhl, U., Sepúlveda, J., Vellekoop, J., Whiteside, J., Alegret, L., Henehan, M., Robinson L., van Dijk, J., Bralower, T., 2023. Stratigraphy of the Cretaceous/Paleogene (K/Pg) boundary at the Global Stratotype Section and Point (GSSP) in El Kef, Tunisia: New insights from the El Kef Coring Program. GSA Bulletin 135 (9-10), 2451-2477.

Jorissen, F.J., Fontanier, C., Thomas, E., 2007. Paleoceanographical indicators based on deep-sea benthic foraminiferal assemblage characteristics. Developments in Marine Geology 1, 263-325.

Jung, C., Koch, M.C., Voigt, S., Friedrich, O., 2013. Campanian-Maastrichtian ocean circulation in the tropical Pacific. Paleoceanography 28, doi:10.1002/palo.20051.

Keller, G., Abramovich, S., 2009. Lilliput effect in late Maastrichtian for foraminifera: Response to environmental stress. Palaeogeography, Palaeoclimatology, Palaeoecology 284, 47-62.

Keller, G., Mateo, P., Monkenbusch, J., Thibault, N., Punekar, J., Spangenberg, J.E., Abramovich, S., Ashckenazi-Polivoda, S., Schoene, B., Eddy, M.P., Samperton, K.M., Khadri, S.F.R., Adatte, T., 2020, Mercury linked to Deccan Traps volcanism, climate change and the end Cretaceous mass extinction. Global and Planetary Change 194, 103312.

Koch, M.C., Friedrich, O., 2012. Campanian-Maastrichtian intermediate- to deep-water changes in the high latitudes: Benthic foraminiferal evidence. Paleoceanography, 27(2), PA2209.

Koutsoukos, E.A.M., 1992. Late Aptian to Maastrichtian foraminiferal biogeography and palaeoceanography of the Sergipe Basin, Brazil. Palaeogeography, Palaeoclimatology, Palaeoecology 92 (3-4), 295-324.

Koutsoukos, E.A.M., 2006. The Cretaceous-Paleogene Boundary at the Poty Section, NE Brazil: Foraminiferal Record and Sequence of Events - A Review. Anuário do Instituto de Geociências - UFRJ 29 (1), 95-107.

Koutsoukos, E.A.M., Klasz, I., 2000. Late Cretaceous foraminiferal biogeography (Families Bolivinidae, Buliminellidae, Gavelinellidae, Siphogenerinoididae, Turrilinidae) in northeastern Brazilian shelf and central West African basins. Cretaceous Research 21, 381–405.

Koutsoukos, E.A.M., Merrick, K.A., 1986. Foraminiferal paleoenvironments from the Barremian to Maastrichtian of Trinidad, West Indies. I Geological Conference of the Geological Society of Trinidad & Tobago, pp. 85-101.

Koutsoukos, E.A.M., Hart, M.B., 1990. Cretaceous foraminiferal morphogroup distribution patterns, paleocommunities and trophic structures: A case study from the Sergipe Basin, Brazil. Transactions of the Royal Society of Edinburgh, Earth Sciences 81, 221-246.

Krahl, G., Kochhann, K.G.D., Fauth, G., Sial, A.N., Lacerda, L.D., 2021. Evaluation of deep-water environmental conditions during the latest Maastrichtian-early Danian: Insights from the western South Atlantic Ocean. Journal of South American Earth Sciences 112, 103630.

Krahl, G., Kochhann, K.G.D., Hunning Bom, M., Fauth, G., 2023. Mercury stratigraphy of early Danian sediments from the Rio Grande Rise and the timing of Deccan volcanism. Journal of South American Earth Sciences 128, 104488.

Kujau, A., Nürnberg, D., Zielhofer, C., Bahr, A., Röhl, U., 2010. Mississippi River discharge over the last ~560,000 years — Indications from X-ray fluorescence core scanning. Palaeogeogr. Palaeoclimatol. Palaeoecol. 298, 311-318.

Ladant, J-B., Poulsen, C.J., Fluteau, F., Tabor, C.R., MacLeod, K.J., Martin, E.L., Haynes, S.J., Rostami, M.A., 2020. Paleogeographic controls on the evolution of Late Cretaceous ocean circulation. Climate of the Past, doi.org/10.5194/cp-2019-157.

Li, L., Keller, G., Stinnesbeck, W., 1999. The Late Campanian and Maastrichtian in northwestern Tunisia: palaeoenvironmental inferences from lithology, macrofauna and benthic foraminifera. Cretaceous Research 20(2), 231-252.

Linnert, C., Engelke, J., Wilmsen, M., Mutterlose, J., 2016. The impact of the Maastrichtian cooling on the marine nutrient regime—Evidence from mid latitudinal calcareous nannofossils. Paleoceanography, 31, 694–714, doi:10.1002/2015PA002916.

Linnert, C., Engelke, J., Wilmsen, M., Mutterlose, J., 2019. Environmental footprints of the early Maastrichtian cooling – the record of benthic foraminifera from northern Germany. Cretaceous Research 97, 143-159.

Linnert, C., Robinson, S.A., Lees, J.A., Bown, P.R., Pérez-Rodríguez, I., Petrizzo, M.J., Falzoni, F., Littler, K., Arz, J.A., Russell, E.E., 2014. Evidence for global cooling in the Late Cretaceous. Nature Communications 5, 4194.

Linnert, C., Robinson, S., Lees, J., Pérez-Rodríguez, I., Jenkyns, H., Petrizzo, M., Arz, J., Bown, P., Falzoni, F., 2018. Did Late Cretaceous cooling trigger the Campanian–Maastrichtian Boundary Event? Newsletters on Stratigraphy, 51(2), 145–166.

Louvel, V., Galbrun, B., 2000. Magnetic polarity sequences from downhole measurements in ODP holes 998B and 1001A, leg 165, Caribbean Sea. Marine Geophysical Researches 21, 561-577.

Lyle, M., Olivarez-Lyle, A., Gorgas, T., Holbourn, A., Westerhold, T., Hathorne, E. C., Kimoto, K., Yamamoto, S., 2012. Data report: raw and normalized elemental data along the U1338 splice from X-ray Fluorescence scanning. Proceedings of the Integrated Ocean Drilling Program, 320/321,doi: 10.2204/iodp.proc.320321.2010.

MacLeod, K.G., 2006. Data report: stable isotopic ratios in bulk carbonate from upper Campanian and Maastrichtian samples (Demerara Rise, western tropical North Atlantic). In Mosher, D.C., Erbacher, J., and Malone, M.J. (Eds.), Proc. ODP, Sci. Results, 207: College Station, TX (Ocean Drilling Program), 1–9. doi:10.2973/odp.proc.sr.207.110.2006

MacLeod, K. G., Londoño, C. I., Martin, E. E., Jiménez Berrocoso, Á., Basak, C., 2011. Changes in North Atlantic circulation at the end of the Cretaceous greenhouse interval. Nature Geoscience 4, 779–782.

MacLeod, K.G., Huber, B.T., Le Ducharme, M., 2000. Paleontological and geochemical constraints on the deep ocean during the Cretaceous greenhouse interval. In: Huber, B.T., MacLeod, K.G., Wing, S.L. (Eds.), Warm Climates in Earth History. Cambridge University Press, Cambridge, pp. 241–274.

MacLeod, K.G., Huber, B.T., Pletsch, T., Röhl, U., 2001. Maastrichtian foraminiferal and paleoceanographic changes on Milankovitch timescales. Paleoceanography 16, 133-154.

MacLeod, K.G., Whitney, D.L., Huber, B.T., Koeberl, K., 2017. Impact and extinction in remarkably complete Cretaceous-Tertiary boundary sections from Demerara Rise, tropical western North Atlantic. GSA Bulletin 119 (1-2), 101-115.

Martin, E. E., MacLeod, K. G., Jiménez Berrocoso, Á., Bourbon, E., 2012. Water mass circulation on Demerara Rise during the Late Cretaceous based on Nd isotopes. Earth and Planetary Science Letters 327, 111–120.

Martínez, R. J.I., 1989. Foraminiferal biostratigraphy and paleoenvironments of the Maastrichtian Colón mudstones of Northern South America. Micropaleontology 35 (2), 97-113.

Martínez, J.I., 2003. The Paleoecology of late Cretaceous upwelling events from the Upper Magdalena Basin, Colombia. Palaios 18 (4-5), 305-320.

Martinez, J.I., Hernandez, R., 1992. Evolution and drowning of the Late Cretaceous Venezuelan carbonate platform. Journal of South American Earth Sciences 5(2), 197-210.

Martínez-Ruiz, F., Ortega-Huertas, M., Palomo-Delgado, I., Smit, J., 2001. K-T boundary spherules from Blake Nose (ODP Leg 171B) as a record of the Chicxulub ejecta deposits. Geological Society, London, Special Publications 183, 149-161.

Mateo, P., Keller, G., Punekar, J., Spangenberg et al., 2007. Early to Late Maastrichtian environmental changes in the Indian Ocean compared with Tethys and South Atlantic. Palaeogeography, Palaeoclimatology, Palaeoecology 478, 121-138.

Matsumoto, H., Kuroda, J., Coccioni, R., Frontalini, F., Sakai, S., Ogawa, N.O., Ohkouchi, N., 2020. Marine Os isotopic evidence for multiple volcanic episodes during Cretaceous Oceanic Anoxic Event 1b. Scientific Reports 10, 12601.

Mitchell, S.F., Ball, J.D., Crowley, S.F., Marshall, J.D., Paul, C.R.C., Veltkamp, C.J., Samir, A., 1997. Isotope data from Cretaceous chalks and foraminifera: environmental or diagenetic signals? Geology 25, 691-694.

Moiroud, M., Pucéat, E., Donnadieu, Y., Bayon, G., Guiraud, M., Voigt, S., Deconinck, J.F., Mona, F., 2016. Evolution of neodymium isotopic signature of seawater during the Late Cretaceous: Implications for intermediate and deep circulation. Gondwana Research, 36, 503–522.

Montes, C., Rodríguez-Corcho, A.F., Bayona, G., Hoyos, N., Zapata, S., Cardona, A., 2019. Continental margin response to the multiple arc-continent collisions: The northern Andes-Caribbean margin. Earth Science Reviews 198, 102903.

Morón, S., Fox, D.L., Feinberg, J.M., Jaramillo C. Bayona, G., Montes, C., Bloch, J.I., 2013. Climate change during the Early Paleogene in the Bogotá Basin (Colombia) inferred from paleosol carbon isotope stratigraphy, major oxides, and environmental magnetism. Palaeogeography, Palaeoclimatology, Palaeoecology 388, 115-127.

Mulitza, S., Prange, M., Stuut, J.B., Zabel, M., von Dobeneck, T., Itambi, A.C., Nizou, J., Schulz, M., Wefer, G., 2008. Sahel megadroughts triggered by glacial slowdowns of Atlantic meridional overturning. Paleoceanography 23, PA4206.

Mulitza, S. Chiessi, C.M., Schefuß, E., Lippold, J., Wichmann, D., Antz, B., Mackensen, A., Paul, A., Prange, M., Rehfeld, K., Werner, M., Bickert, T., Frank, N., Kuhnert, H., Lynch-Stieglitz, J., Portilho-Ramos, R.C., Sawakuchi, A.O., Schulz, M., Schwenk, T., Tiedemann, R., Vahlenkamp, M., Zhang, Y., 2017. Synchronous and proportional deglacial changes in Atlantic meridional overturning and northeast Brazilian precipitation, Paleoceanography,32, 622-633.

Murray, J.W., Alve, E., Jones, B.W., 2011. A new look at modern agglutinated benthic foraminiferal morphogroups: their value in palaeoecological interpretations. Palaeogeography, Palaeoclimatology, Palaeoecology 309 (3–4), 229-241.

Nauter-Alves, A., Dunkley-Jones, T., Rodrigues Bruno, M.D., De Lira Mota, M.A., Cachão, M., Krahl, G., Fauth, G., 2023. Biotic turnover and carbon cycle dynamics in the early Danian event (Dan-C2): New insights from Blake Nose, North Atlantic. Global and Planetary Change 221, 104046.

Nunes-Aumond, G., Kochhann, K.G.D., Santos-Florisbal, L., Baecker-Fauth, S., Trescastro-Bergue, C., Fauth, G., 2009. Maastrichtian-early Danian radiolarians and ostracodes from ODP Site 1001b, Caribbean Sea. Rev. bras. paleontol. 12(3), 195-210.

O'Brien, C.L., Robinson, S.A., Pancost, R.D., Sinninghe Damstéd, J.S., Schouten, S., Lunt, D.J., Alsenz, H., Bornemann, A., Bottini, C., Brassell, S.C., Farnsworth, A., Forster, A., Huber, B.T., l, Inglis, G.N., Jenkyns, H.C., Linnert, C., Littler, K., Markwick, P., McAnenao, A., Mutterlose, J., Naafs, B.D.A., Püttmann, W., Sluijse, A., van Helmond, N.A.G.M., Vellekoop, J., Wagner, T., 7, Wrobel, N.E., 2017. Cretaceous sea-surface temperature evolution: Constraints from TEX_{86} and planktonic foraminiferal oxygen isotopes. Earth-Science Review 172, 224-247.

Obrist, D., Johnson, D.W., Edmonds, R.I., 2012. Effects of vegetation type on mercury concentrations and pools in two adjacent coniferous and deciduous forest. Journal of Plant Nutrition and Soil Science 175, 68-77.

Páez-Reyes, M., Carvajal-Ortiz, H., Sahoo, S.K., Varol, O., Miller, V.B., Hughes, G.W., Gaona-Narváez, T., Patarroyo, G.D., Curtis, J.H., Lerma, I., Copeland, P. 2021. Assessing the contribution of the La Luna Sea to the global sink of organic carbon during the Cenomanian-Turonian Oceanic Anoxic Event 2 (OAE2). Global and Planetary Change 199, 103424.

Patarroyo, G., Kochhann, K.G.D., Ceolin, D., Guerra, R.M., Alegret, L., Bom, M.H.H., 2022. Paleoenvironmental changes recorded at a late Maastrichtian marine succession of northern South America. Journal of South American Earth Sciences, 119: 104015.

Patarroyo, G., Kochhann, K.G.D., Guerra, R.M., Alegret, L., Ceolin, D., Torres, J.M. 2023. Maastrichtian microfossils of the shallow marine Umir Formation, North-eastern Colombia. Ameghiniana 60(4), 297-311.

Percival, L.M.E., Jenkyns, H.C., Mather, T.A., Dickson, A.J., Batenburg, S.J., Ruhl, M., Hesselbo, S.P., Barclay, R., Jarvis, I., Robinson, S.A., Woelders, L., 2018. Does large igneous province volcanism always perturb the mercury cycle? Comparing the records of Oceanic Anoxic Event 2 and the End-Cretaceous to other Mesozoic events. American Journal of Science 318, 799-860.

Petersen, S.V., Dutton, A., Lohmann, K.C., 2016. End-Cretaceous extinction in Antarctica linked to both Deccan volcanism and meteorite impact via climate change. Nature Communications, DOI: 10.1038/ncomms12079.

Pindell, J.L., Kennan, L., 2009. Tectonic evolution of the Gulf of Mexico, Caribbean and northern South America in the mantle reference frame: An update. In: James, K.H., Lorente, M.A., Pindell, J.L. (Eds.) The geology and evolution of the region between North and South America: Geological Society, London, Special Publications 328, p. 1–55

Pindell, J., Kennan, L., Maresch, W.V., Stanek, K., Draper, G., Higgs, R., 2005. Plate kinematics and crustal dynamics of circum Caribbean arc continent interactions: Tectonic controls on basin development in proto-Caribbean margins. Special Papper Geological Society of America 394, 7-52.

Premoli Silva I., Verga, D., 2011. Practical manual of Cretaceous planktonic foraminifera. New Editing by Marie Rose Petrizzo and Isabella Premoli Silva. International School on Planktonic foraminifera 3rd Course: Cretaceous Planktonic Foraminifera. Perugia, 16-20 February 2004, 265p.

Punekar, J., Mateo, P., Keller G., 2014. Effects of Deccan volcanism on paleoenvironment and planktic foraminifera: A global survey. In: Keller G., A.C., Kerr (Eds.) Volcanism, Impacts, and Mass Extinctions: Causes and Effects. Geological Society of America Special Paper 505, pp. 91-116.

Ravichandran, M., 2004. Interaction between mercury and dissolved organic matter – a review. Chemosphere 55 (3), 319-331.

Renne, P.R., Sprain, C.J., Richards, M.A., Self, S., Vanderkluysen, L., Pande, K., 2015. State shift in Deccan volcanism at the Cretaceous–Paleogene boundary, possibly induced by impact. Science 350, 76-78.

Santos, A., De Lira Mota, M.A., Kern, H.P., Fautha, G., Paim, P.S.G. Netto, R.G., Sedorko, D. Lavina, E.L.C., Krahl, G., Fallgatter, C., Silveira, D.M., Aquino, C.D., Santos, M.O., Baecker-Fauth, S., Vieira, C.E.L., 2022. Earlier onset of the Early Cretaceous Equatorial humidity belt. Global and Planetary Change 208, 103724.

Sarmiento-Rojas, L.F., 2019. Cretaceous stratigraphy and paleo-facies maps of northwestern South America. In: Cediel, F., Shaw, R.P., (Eds.), Geology and Tectonics of Northwestern South America. The Pacific Caribbean Andean Junction, pp. 673-747.

Schoene, B., Eddy, M.P., Samperton, K.M., Keller, C.B., Keller, G., Adatte, T., Khadri, S.F., 2019. U-Pb constraints on pulsed eruption of the Deccan Traps across the end-Cretaceous mass extinction. Science 363, 862-866.

Schoene, B., Eddy, M.P., Keller, C.B., Samperton, K.M., 2021. An evaluation of Deccan Traps eruption rates using geochronologic data. Geochronology, 3(1), 181-198.

Schoene, B., Samperton, K. M., Eddy, M. P., Keller, G., Adatte, T., Bowring, S. A., Khadri, S. F., and Gertsch, B., 2015. U−Pb geochronology of the Deccan Traps and relation to the end-Cretaceous mass extinction. Science 347, 182-184.

Schulte, P., Alegret, L., Arenillas, I., Arz, J.A., Barton, P.J., Bown, P.R., Bralower, T.J., Christeson, G.L., Claeys, P., Cockell, C.S., Collins, G.S., Deutsch, A., Goldin, T.J., Goto, K., Grajales-Nishimura, J.M., Grieve, R.A.F., Gulick, S.P.S., Johnson, K.R., Kiessling. W., Koeberl, C., Kring, D.A., Macleod, K.G., Matsui, T., Melosh, J., Montanari, A., Morgan, J.V., Neal, C.R., Nichols, D.J., Norris, R.D., Pierazzo, E., Ravizza, G., Rebolledo-Vieyra, M., Reimold, W.U., Robin, E., Salge, T., Speijer, R.P., Sweet, A.R., Urrutia-Fucugauchi, J., Vajda, V., Whalen, M.T., Willumsen, P.S., 2010. The Chicxulub asteroid impact and mass extinction at the Cretaceous-Paleogene boundary. Science 327, 5970.

Scotese, C., 2016. PALEOMAP PaleoAtlas for GPlates and the PaleoData Plotter Program, PALEOMAP Project (http://www.earthbyte.org/paleomap-paleoatlas-for-gplates/).

Selin, N.E., 2009. Global biogeochemical cycling of mercury: A review. Annual Review of Environment and Resources 34, 43-63. Earth and Planetary Science Letters 543, 1163333.

Shen, J., Feng, Q., Algeo, T.J., Liu, J., Zhou, C., Wei, W., Liu, J., Them II, T.R., Gill, B.C., Chen, J., 2020. Sedimentary host phases of mercury (Hg) and implications for use of Hg as a volcanic proxy.

Sial, A.N., Chen, J.B., Lacerda, L.D., Peralta, S., Gaucher, C., Frei, R., Cirilli, S., Ferreira, V.P., Marquillas, R.A., Barbosa, J.A., Pereira, N.S., Belmino, I.K.C., 2014. High-resolution Hg chemostratigraphy: A contribution to the distinction of chemical fingerprints of the Deccan volcanism and Cretaceous-Paleogene boundary impact event. Palaeogeography, Palaeoclimatology, Palaeoecology 414, 98-115.

Sial, A.N., Chen, J.B., Lacerda, L.D., Frei, R., Tewari, V.C., Pandit, M.K., Gaucher, C., Ferreira, V.P., Cirilli, S., Peralta, S., Korte, C., Barbosa, J.A., Pereira, N.S., 2016. Mercury enrichment and Hg isotopes in Cretaceous-Paleogene boundary successions: Links to volcanism and palaeoenvironmental impacts. Cretaceous Research 66, 60-81.

Sigurdsson, H., Kelley, S., Leckie, R.M., Carey, S., Bralower, T., King, J., 2000. History of Circum-Caribbean explosive volcanism: 40Ar/ 39Ar dating of tephra layers. In: Leckie, R.M., Sigurdsson, H., Acton, G.D., and Draper, G. (Eds.), 2000. Proc. ODP, Sci. Results, 165: College Station, TX (Ocean Drilling Program).

Sigurdsson, H., Leckie, R.M., Acton, G.D., et al., 1997. Proc. ODP, Init. Repts., 165: College Station, TX (Ocean Drilling Program).

Spikings, R., Cochrane, R., Villagómez, D., Van der Lelij, R., Vallejo, C., Winkler, W., Beate, B., 2015. The geological history of northwestern South America: from Pangea to the early collision of the Caribbean Large Igneous Province (290-75 Ma). Gondwana Research 27, 95-139.

Sprain, G.A., Renne, P.R., Vanderkluysen, L., Pande, K., Self, S., Mittal, T., 2019. The eruptive tempo of Deccan volcanism in relation to the Cretaceous-Paleogene boundary. Science 363, 866-870.

Stinnesbeck, W. Ifrim, C. Salazar, C. 2012. The last Cretaceous ammonites in Latin America. Acta Palaeontologica Polonica 57, 717-728.

Stuut, J.B., Zabel, M., Ratmeyer, V., Helmke, P., Schefuß, E., Lavik, G., Schneider, R., 2005. Provenance of present-day eolian dust collected off NW Africa. Journal of Geophysical Research 110, D04202, doi:10.1029/2004JD005161.

Suganuma, Y., Ogg, J.G., 2006. Campanian through Eocene magnetostratigraphy of Sites 1257–1261, ODP Leg 207, Demerara Rise (western equatorial Atlantic). In Mosher, D.C., Erbacher, J., and Malone, M.J. (Eds.), Proc. ODP, Sci. Results, 207.

Terraza, R., 2019. “Formación La Luna”: expresión espuria en la geología colombiana. in: Etayo-Serna, F. (Ed.). Estudios geológicos y paleontológicos sobre el Cretácico en la región del embalse del río Sogamoso, Valle Medio del Magdalena, p. 305-362. Servicio Geológico Colombiano.

Thibault, N., Gardin, S., 2007. The late Maastrichtian nannofossil record of climate change in the South Atlantic DSDP Hole 525A. Marine Micropaleontology, 65, 163–184.

Thibault, N., Husson, D., 2016. Climate fluctuations and sea-surface water circulation patterns at the end of the Cretaceous era: calcareous nannofossil evidence, Palaeogeography, Palaeoclimatology, Palaeoecology 441 (1), 152-164.

Vancoppenolle I., Vellekoop J., Doubrawa M., Kaskes P., Sinnesael M., Jagt J.W.M., Claeys P, Speijer R.P., 2022. The benthic foraminiferal response to the mid Maastrichtian event in the NW-European chalk sea of the Maastrichtian type area. Netherlands Journal of Geosciences 101, e12. https://doi.org/10.1017/njg.2022.10.

Vellekoop, J., Kaskes, P., Sinnesael, M., Huygh, J., Déhais, T., Jagt, J.W.M., Speijer, R.P., Claeys, P., 2022. A new age model and chemostratigraphic framework for the Maastrichtian type area (southeastern Netherlands, northeastern Belgium). Newsletters on Stratigraphy 4, 479-501.

Villagómez, D., Spikings, R., Magna, T., Kammer, A., Winkler, W., Beltrán, A., 2011. Geochronology, geochemistry and tectonic evolution of the Western and Central cordilleras of Colombia. Lithos 125, 875-896.

Villamil, T., Pindell, J., 1998. Mesozoic paleogeographic evolution of northern South America. In: J. Pindell, J., Drake, C. (Eds.) Paleogeographic evolution and non-glacial eustacy, northern South America. SEPM Society for Sedimentary Geology 58, pp. 238-318.

Voigt, S., Friedrich, O., Norris, R. D., Schönfeld, J., 2010. Campanian–Maastrichtian carbon isotope stratigraphy: shelf-ocean correlation between the European shelf sea and the tropical Pacific Ocean. Newsletters on Stratigraphy 44(1), 57-72.

Voigt, S., Gale, A.S., Jung, C., Jenkyns, H.C., 2012. Global correlation of Upper Campanian-Maastrichtian successions using carbon-isotope stratigraphy: development of a new Maastrichtian timescale. Newsletters on Stratigraphy 45(1), 25-53.

Voigt, S., Jung, C., Friedrich, O., Frank, M., Teschner, C., Hoffmann, J., 2013. Tectonically restricted deep ocean circulation at the end of the Cretaceous greenhouse. Earth and Planetary Science Letters 369-370, 169-177.

Whattam, S.A., Stern, R.J., 2015. Late Cretaceous plume-induced subduction initiation along the southern margin of the Caribbean and NW South America: The first documented example with implications for the onset of plate tectonics. Gondwana Research 27, 38-63.

Widmark, J.G.V., 1997. Deep-sea benthic foraminifera from Cretaceous-Paleogene boundary strata in the South Atlantic - taxonomy and paleoecology. Fossils & Strata 43, 1-94.

Widmark, J.G.V., Speijer, R.P., 1997a. Benthic foraminiferal faunas and trophic regimes at the terminal Cretaceous Tethyan seafloor. PALAIOS 12(4), 354–371.

Widmark, J.G.V., Speijer, R.P., 1997b. Benthic foraminiferal faunas and trophic regimes of the terminal Cretaceous Tethyan seafloor. Palaios 12, 354-371.

Woelders, L., Vellekoop, L.J., Kroon, D., Smit, J., Casadío, S., Prámparo, M.B., Dinarès-Turell, J., Peterse, F., Sluijs, A., Lenaerts, J.T.M., Speijer, R.P., 2017. Latest Cretaceous climatic and environmental change in the South Atlantic region. Paleoceanography 32, 466-483.

Yao, H., Chen, X., Yin, R., Grasby, S. E., Weissert, H., Gu, X., Wang, C., 2021. Mercury evidence of intense volcanism preceded Oceanic Anoxic Event 1d. Geophysical Research Letters, 48, e2020GL091508.

Zapata-Villada, J.P., Cardona, A., Serna, S., Rodríguez, G., 2021. Late Cretaceous to Paleocene magmatic record of the transition between collision and subduction in the Western and Central Cordillera of northern Colombia. Journal of South American Earth Sciences 112 (1), 103557.

Alguna vez se hacía un gran silencio sobre las aguas, presentíase el Acontecimiento y aparecía, enorme, tardo, desusado, un pez de otras épocas, de cara mal ubicada en un extremo de la masa, encerrado en un eterno miedo a su propia lentitud, con el pellejo cubierto de vegetaciones y parásitos, como casco sin carenar, que sacaba el vasto lomo en un hervor de rémoras, con solemnidad de galeón rescatado, de patriarca abisal, de Leviatán traído a la luz, largando espuma a mares en una salida a flote que acaso fuera la segunda desde que el astrolabio llegara a estos parajes. Abría el monstruo sus ojillos de paquidermo, y, al saber que cerca le bogaba un desclavado cayuco sardinero, se hundía nuevamente, angustiado y medroso, hacia la soledad de sus trasfondos, a esperar algún otro siglo para regresar a un mundo colmado de peligros.

El siglo de las luces

Alejo Carpentier

CHAPTER 6

FINAL CONSIDERATIONS

Low latitude marine environments underwent several environmental changes during the latest Cretaceous (Maastrichtian, Figure 1). Those disturbances were recorded in both shallow marine and deep-sea settings from northern South America (Tropical Atlantic), reflecting a complex combination of widespread and regional oceanographic, tectonic and paleoenvironmental processes. Bearing in mind the dynamic geological context of this area, two different paleoenvironmental settings were investigated: (1) shallow marine successions of epicontinental seas from northern South America and (2) deep ocean settings from the tropical Atlantic Ocean.

Integrated micropaleontological (foraminifers, calcareous nannofossils, ostracods) and geochemical (elemental ratios) surveys of the Colón and Umir formations (Maastrichtian, Colombia) were conducted to track environmental variations recorded in both units (**CHAPTERS 1-2**). In general, microfossil assemblages and sediment elemental ratios (Zr/Rb, Fe/Ca, V/Cr, Sr/Ba, among others) recorded a transition from inner platform settings, with moderately oxygenated bottom waters, to sublittoral conditions, characterized by increased input of terrigenous material and weathering intensity. This environmental shift developed on an extensive epicontinental sea setting, which gradually disappeared due to global sea level fluctuations and the onset of the Andean orogeny, the latter probably active since the Campanian. Despite possible sedimentological biases due to the retro-gradational context of this region, this Maastrichtian record was likely sensitive to the paleoclimatic disturbances (e.g., hydroclimate) that occurred before the K-Pg boundary extinction event. However, to properly assess the influence of the tectonic processes due to Andean orogeny, future studies need a robust chronostratigraphic framework. This was the case of the Aguablanca Creek section, where a previously proposed unconformity (xenoconformity) for the early Maastrichtian was clearly identified with microfossil and geochemical proxies.

Tropical deep-water masses also recorded changes in their physicochemical properties, but in this case related to reconfigurations of global circulation during the Maastrichtian (**CHAPTERS 3-4**). High-resolution analyses (benthic foraminifers, elemental ratios, carbon isotopes) at ODP Hole 1258A (Demerara Rise), pointed out changes of intermediate to deep-water oxygenation and surface productivity, as well as a sudden dissolution episode in the Maastrichtian. Typical deep-sea taxa such as *Aragonia*, *Nuttallides truempyi*, *Coryphostoma*, *Strictostomella*, among others, and the distribution of redox-sensitive trace metals (Ni, Cu), supported the presence of suboxic bottom water conditions, with some oxygenation pulses during the mid-Maastrichtian event (MME). The MME, a major global carbon cycle perturbation was identified with a high-resolution $\delta^{13}C$ record at the site. Fluctuations in silica and carbonate export via surface productivity, and a probable disturbance of regional hydroclimate during the MME, were depicted by several sediment elemental ratios (log(Fe/Ca), Si/Ti, Fe/K). These disturbances of local surface productivity and bottom water oxygenation recorded on Demerara Rise were likely related to the MME and the onset of the late Maastrichtian warming event, both linked to a stronger influence of high-latitude deep-waters on the tropics. In contrast, tracking paleoenvironmental disturbances at ODP Hole 1001B (Nicaraguan Rise) was more challenging likely due to diagenesis. Even though this issue hampered geochemical studies on microfossils, geochemical analyses (elemental ratios, $\delta^{13}C$) of bulk sediments allowed the identification of the K-Pg boundary. Subtle changes of surface productivity and bottom water conditions during the late Maastrichtian were also identified along the core. However, the record of the MME is still not certain at this site due to low sampling resolution of the $\delta^{13}C$ record and possible biases of the available magnetostratigraphy.

Considering the presence of widespread volcanic activity during the Maastrichtian, Hg chemostratigraphy was conducted in both the shallow marine and the deep ocean localities (**CHAPTER 5**). However, due to the lack of robust chronostratigraphic frameworks, retro-gradational processes that characterize the Maastrichtian sedimentary successions, and the poorly studied influence of Caribbean Plate volcanism, Hg concentrations could not be exclusively linked to Deccan volcanic activity at Core Diablito-1E. In contrast, tracking the influence of volcanic activity on low latitude deep-sea settings provided more robust correlations. The sedimentary records from Demerara Rise and Nicaraguan Rise depicted significant Hg enrichment peaks along the Maastrichtian, which, based on the proposed age models for these sites and comparisons with other Maastrichtian localities, support the influence not only of Deccan volcanic episodes, but also of less studied volcanic pulses in the Caribbean. In summary, Hg chemostratigraphy could allow future correlations between shallow and deep marine sedimentary successions, as suggested in this thesis, and the role of widespread volcanic processes on low latitude climate reveals itself as a key field for further studies.

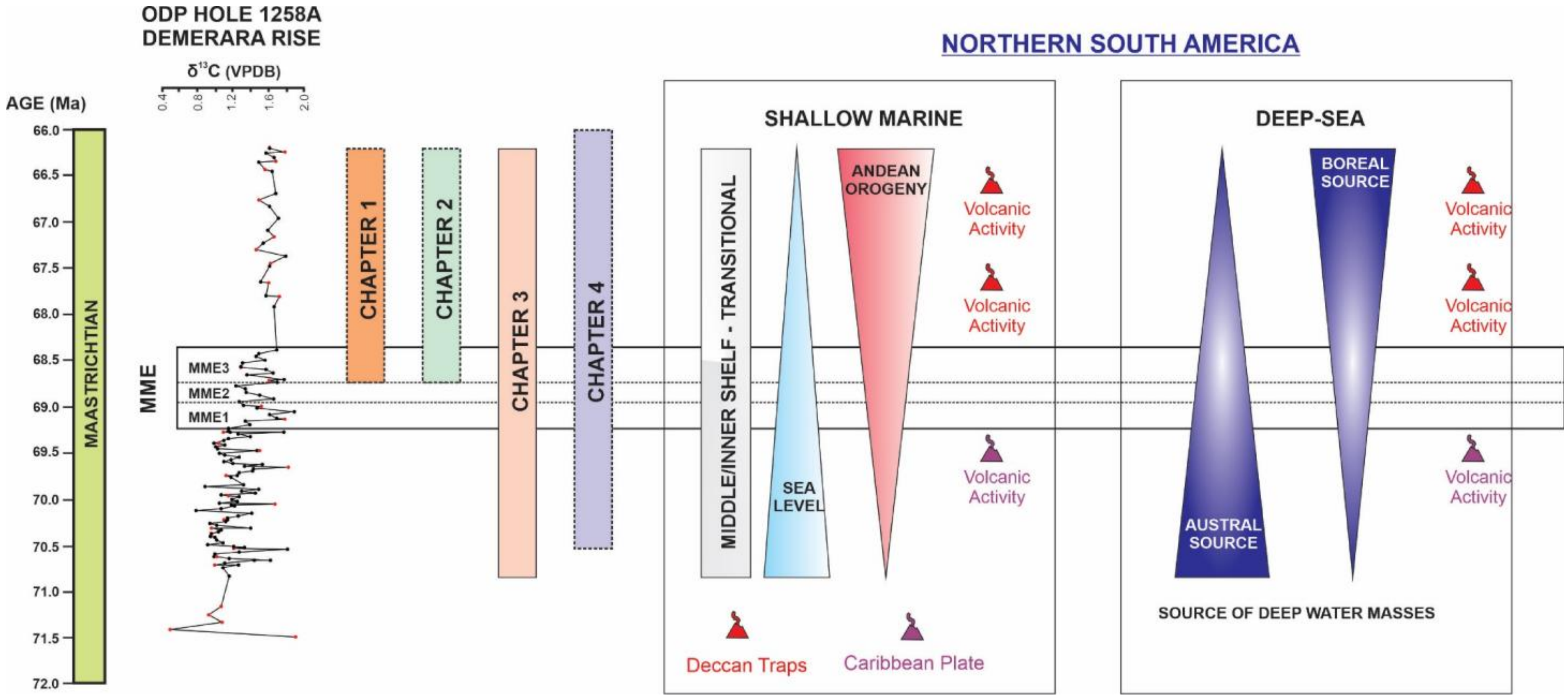

Figure 1. Summary of the chronostratigraphic intervals studied in each chapter, as well as the regional and global oceanographic and tectonic events recorded during the Maastrichtian in northern South America. MME Mid-Maastrichtian Event.

ADDENDA

OSTRACOD ASSEMBLAGES FROM THE UPPER CRETACEOUS COLÓN FORMATION, COLOMBIA: TAXONOMY AND PALEOECOLOGICAL INFERENCES

Contribution roles taxonomy

Daiane Ceolin (itt Oceaneon, Unisinos University). Ostracod taxonomy and ecology.

German David Patarroyo (itt Oceaneon, Unisinos University). Foraminiferal ecology and discussion of results.

Karlos Kochhann (itt Oceaneon, Unisinos University). Foraminiferal and paleoecological discussions.

Gustavo Torres (Stratos Consultoría Geológica). Editing of selected SEM images.

Daniel Rincón (ECOPETROL-ICP). Data permits from stratigraphic core La Luna-3E.

Article submitted at: Cretaceous Research

Received 13 November 2023.

OSTRACOD ASSEMBLAGES FROM THE UPPER CRETACEOUS COLÓN FORMATION, COLOMBIA: TAXONOMY AND PALEOECOLOGICAL INFERENCES

Daiane Ceolin[1], German D. Patarroyo[1,2], Karlos G.D. Kochhann[1,2], Gustavo A. Torres[3], Daniel A. Rincón[4]

[1]Technological Institute for Paleoceanography and Climate Change (itt Oceaneon), UNISINOS University. São Leopoldo, 93.022-750, Brazil.

[2]Geology Graduate Program. UNISINOS University. São Leopoldo, 93.022-750, Brazil.

[3]Stratos Consultoría Geológica. Bucaramanga, Colombia.

[4]Instituto Colombiano del Petróleo (ICP), ECOPETROLS.A. Piedecuesta, Colombia

RESEARCH HIGHLIGHTS

- First study with ostracods for the Colón Formation, Colombia
- 14 marine ostracods species are identified, with likely endemism in some of them
- Ostracod assemblage indicative of two paleoenvironments: open marine and neritic environment

ABSTRACT

In this paper, 14 ostracod species from Maastrichtian strata of Colombia (Colón Formation, core La Luna-3E) were described in detail. Assemblages were characterized by taxa assigned to the genera *Cytherella*, *Bairdoppilata*, *Argilloecia*, *Krithe*, *Loxoconcha*, *Sapucariella*, among others, including some endemic forms. Moreover, the ostracod association can be divided in two assemblages: the first in the lower segment of the core, characterized by the dominance of species indicative of open marine conditions with relatively cold waters; and the second assemblage, with a more diversified fauna characteristic of neritic environments. This environmental shift is in concordance with previous sedimentological and foraminiferal studies of the Colón Formation and coeval units from northern South America.

INTRODUCTION

The late Cretaceous was a time of significant environmental changes recorded in the sedimentary successions of northern South America. In general, units had been deposited in extensive epicontinental seas since the late Albian (e.g., La Luna Sea), which gradually disappeared due to sea level fluctuations and the onset of the Andean orogeny, especially since the Campanian-Maastrichtian (Martinez and Hernandez, 1992; Villamil and Pindell, 1998; Erlich et al., 1999; Sarmiento-Rojas, 2019; Montes et al., 2019; Bayona et al., 2020). Therefore, for the latest Cretaceous, marine settings underwent significant shifts, reflected by different depositional environments (e.g., coastal plains, inner platforms) and the preserved biota.

Several studies have explored the micropaleontological the response of different groups to these environmental changes, but mainly with a chronostratigraphic approach (e.g., Tchegliakova, 1996; Vergara, 1997; Guerrero et al., 2000; Tchegliakova and Mojica, 2001; Yepes, 2001; Garzón et al., 2012; Patarroyo et al., 2017; Navarrete et al., 2018). However, new studies have proposed a holistic approach to better understand environmental disturbances at that time, integrating high-resolution geochemical and sedimentological studies with the micropaleontological record (e.g., Bayona et al., 2020; Carvalho et al., 2021; De La Parra et al., 2022; Patarroyo et al., 2022; Patarroyo et al., 2023).

This study summarizes the results of an ostracod survey from subsurface sedimentary rocks assigned to the Colón Formation (Maastrichtian; northeastern Colombia). This unit has been explored in detail for several microfossil groups (Cushman and Hedberg, 1930, 1941; Sellier de Civrieux, 1952; Petters, 1955; Martínez, 1989; Malumián, 2010; Yepes, 2001; De La Parra et al., 2022; Patarroyo et al., 2017; 2022), but its ostracod content has been usually relegated to brief mentions. Therefore, detailed taxonomic descriptions, as well as paleoenvironmental inferences based on this group, are proposed for the first time for the latest Cretaceous of Colombia. We also integrate our new results with previously published foraminiferal data for the same sedimentary core.

GEOLOGICAL SETTING

The Cesar-Rancheria Basin (northeastern Colombia; Figure 1) shared a similar geological evolution with other inter-mountainous basins in northern South America. At least three tectonic phases occurred during the Mesozoic in the basin: 1) an extensional regime spanning the late Paleozoic to the early Cretaceous, with the emplacement of volcanoclastic rocks (La Quinta and Rio Negro formations); 2) development of clastic and carbonate successions on a passive margin during most of the Cretaceous (Cogollo Group, La Luna Formation) and; 3) formation of a foreland basin during the late Maastrichtian to Paleocene (Colón, Catatumbo/Barco and Cuervos formations). Cenozoic sedimentary successions were related to several uplifting event of the Andean orogeny (Ayala-Calvo et al., 2009; Bayona et al., 2011).

The Colón Formation is usually divided into two major stratigraphic intervals: The basal Socuy Member, composed of moderately micritic levels and calcareous mudstones; and an uppermost segment, which is composed of a monotonous succession of dark grey fine-grained rocks and sandy intervals (Ayala-Calvo et al., 2009). A latest Campanian to Maastrichtian age has been proposed for the entire Colón Formation in both the Cesar-Rancheria and the Venezuelan Andes, mostly based on foraminiferal (planktonic and benthic) and palynological data (Cushman and Hedberg, 1930, 1941; Sellier de Civrieux, 1952; Martínez, 1989; Yepes, 2001; Patarroyo et al., 2017; De La Parra et al., 2022). So far, ostracod assemblages have been described in unpublished technical reports (Malumián, 2010), and the core Diablito-1E (Figure 1; Patarroyo et al., 2022).

MATERIAL AND METHODS

Core La Luna-3E, drilled by Drummond Coal Company, is located in the Jagua de Ibirico locality (Cesar Department, Colombia; 9°33’ N, 73°23’ W). The cored interval spanned a thickness of 578.7 m, recovering the Colón, La Luna and Capacho formations (Figures 1, 2). At this site, the Colón Formation was originally described between 0 and 292.5 m, but based on foraminiferal analyses (Malumián, 2010; Torres et al., 2011), the La Luna-Colón contact is located at 256.9 m (Figure 2). Both studies identified the *Pullenia cretacea* (121-256.9 m) and *Siphogenerinoides bramletti* (0-121 m) regional assemblage zones, following the definitions of Cushman and Hedberg (1941). Considering the correlation of these assemblage zones with the standard planktonic foraminiferal zonation for the Colón Formation by Martínez (1989), the studied interval at the core La Luna-3E comprises the early to Middle Maastrichtian (*Gansserina gansseri* to *Abathomphalus mayaroensis* foraminiferal zones).

All the ostracod material (n=22 samples; interval 13.7-211.8 m) was extracted of the analyzed samples of Malumián (2010) and Torres et al. (2011). Samples of dry sedimentary rocks (20–30 g) were soaked into a 5% hydrogen peroxide (H_2O_2) solution for about 24 hours, washed over 63 µm and 150 µm sieves, and dried at 40°C (Sohn et al. 1965). Ostracod suprageneric classification of the extracted material followed Scott (1961). Selected ostracod specimens were imaged using an EVOMA15 Zeiss scanning electron microscope (SEM) at the Technological Institute for Paleoceanography and Climate Change (itt Oceaneon – Unisinos University, Brazil).

RESULTS

Faunal aspects and species distributions

The analyzed samples yielded a total of 14 ostracod taxa, distributed in 12 genera and eight families: Cytherellidae, Bairdiidae, Paracyprididae, Pontocyprididae, Cytherideidae, Loxoconchidae, Pectocytheridae, and Trachyleberididae (supplementary material S1). Most of the taxa were identified only at the genus level. Ostracod abundances were low (<6 individuals/sample), and, in some cases, specimens were not well preserved, making it difficult to identify taxa at the species level. Levels with poor ostracod preservation occurred at 47.7 m, 58.4 m, 102.4 m, 110.3 m, 202.7 m, 208.8 m and 211.8 m at core La Luna-3E.

Despite low abundances, ostracod assemblages were diverse. The identified taxa were *Cytherella* sp., *Bairdoppilata* sp., *Paracypris* sp. *sensu* Patarroyo et al., 2022, *Argilloecia* sp. 1, *Argilloecia* sp. 2, *Krithe* sp. 1, *Krithe* sp. 2, *Loxoconcha* sp., *Munseyella* sp., *Sapucariella* sp. *sensu* Patarroyo et al., 2022, *Paragrenocythere* sp., *Trachyleberis* sp., *Langiella reymenti* (Neufville, 1973), *Platycythereis*? sp., and one undetermined genus (Figures 2, 3, 4). The most abundant species was *Langiella reymenti* with four specimens and the most diverse family was Trachyleberididae with five species (see supplementary material S1).

In general, the ostracod assemblages in the core La Luna-3E are characteristic of marine environments. Despite low abundances, two main ostracod assemblages were identified in the studied core, based on the species distributions (Figure 2):

Assemblage 1 occurs between 169.2 m. and 63 m. This assemblage displays higher species richness than assemblage 2, and low abundances. Characteristic ostracod species are *Krithe* sp. 1, *Krithe* sp. 2, *Argilloecia* sp. 1, *Argilloeica* sp. 2, *Paragrenocythere* sp., *Paracypris* sp. *sensu* Patarroyo, et al., 2022, *Bairdoppilata* sp., *Langiella reymenti*, and *Loxoconcha* sp.

Assemblage 2 occurs between the depths of 58.4 m and 13.7 m. This assemblage displays lower species richness but higher abundance, when compared with assemblage 1. Ostracods that compose this association are *Krithe* sp. 2, *Paragrenocythere* sp., *Langiella reymenti*, *Platycythereis*? sp., *Sapucariella* sp. *sensu* Patarroyo et al., 2022, *Cytherella* sp., *Munseyella* sp., and Gen. *et*. sp. indet.

Systematic paleontology

The studied material is housed in the paleontological collection of the Museu de História Geológica do Rio Grande do Sul, Universidade do Vale do Rio dos Sinos, Brazil, under the prefix ULVG: 12925 to 12943. Abbreviations are: L, length; H, height; W, width.

Class OSTRACODA Latreille, 1806

Order PLATYCOPIDA Sars, 1866

Suborder PLATYCOPINA Sars, 1866

Family CYTHERELLIDAE Sars, 1866

Genus CYTHERELLA Jones, 1849

Cytherella sp.

Fig. 3A-B

Material. One specimen from sample 21.3 m.

Dimensions. Carapace from sample 21.3 m; ULVG: 12925; L.: 0.781 mm; H.: 0.478 mm.

Remarks. Although this specimen was laterally crushed, it is similar to *Cytherella* sp.1 *sensu* Piovesan et al. (2009), recovered from the lower Maastrichtian of Pará-Maranhão Basin, northeastern of Brazil. *Cytherella* sp. is characterized by having a posteroventral overlap, absent in the aforementioned species (Piovesan et al., 2009). *Cytherella* sp. is also similar to *Cytherella* cf. *C. piacabucuensis* identified in the middle-upper part of the Colón Formation (middle to late Maastrichtian) at core Diablito-1E (Patarroyo et al., 2022). Although both species are poorly preserved, the characteristic overhang present in the dorsal region of *C. piacabucuensis* Neufville, 1973, is absent in *Cytherella* sp.

Order PODOCOPIDA Sars, 1866

Suborder PODOCOPINA Sars, 1866

Superfamily BAIRDIOIDEA Sars, 1888

Family BAIRDIIDAE Sars, 1888

Genus BAIRDOPPILATA Coryell et al., 1935

Bairdoppilata sp.

Fig. 3C-D

Material. One specimen from sample 144.8 m.

Dimensions. ULVG: 12926; L.: 1.102 mm H.: 0. 751 mm; W.: 0.553 mm.

Remarks. It is difficult to compare this species with other taxa since it is broken. However, it resembles the species *Bairdia* sp. Majoran, 1999, (pl.1, fig. 4). identified in the Maastrichtian succession at Ocean Drilling Project (ODP) Site 1052, in the Western North Atlantic, but differing in a less truncated anterior region, and a more convex ventral margin.

Superfamily CYPRIDOIDEA Baird, 1845

Family PARACYPRIDIDAE Sars, 1923

Genus PARACYPRIS Sars, 1866

Paracypris sp. *sensu* Patarroyo et al., 2022

Fig. 3E-F

2022 *Paracypris* sp. Patarroyo et al., fig.5a-b.

Material. One juvenile specimen from sample 158.5 m.

Dimensions. Carapace from sample 158.5 m; ULVG: 12927; L.: 0.411 mm; H.: 0.202 mm; W.: 0.145 mm.

Remarks. It differs from *Paracypris* sp. *sensu* Donze et al., 1982 (pl. 2, fig.7) by having a less developed overlap, and a shorter posterior margin. *Paracypris* sp. was identified in the middle-upper part of the Colón Formation (middle to late Maastrichtian) at core Diablito-1E. The small differences in size and the overlap between *Paracypris* sp. (Patarroyo et al., 2022) and the specimen found herein is due to the fact that the latter is a juvenile.

Family PONTOCYPRIDIDAE Müller, 1894

Genus ARGILLOECIA Sars, 1866

Argilloecia sp. 1

Fig. 3G-I

Material. Two specimens from sample 169.2 m.

Dimensions. Valve, right lateral view (fig. 3G); ULVG: 12928; L.: 0.390 mm; H.: 0.145 mm; Carapace, left lateral view (fig. 3H); ULVG: 12929; L.: 0.412 mm; H.: 0.153 mm; W.: 0.121mm.

Remarks: It is similar to *Macrocypris* sp. (Donze et al. 1982, pl. 2, fig. 6) identified from Maastrichtian strata at La Coupe du Kef, Tunisia (Donze et al., 1982). It differs from the latter in the size, being much smaller in the overlap, having a less arched dorsal region, and a less acuminated posterior region.

Argilloecia sp. 2

Fig. 3J-K

Material. Three specimens from samples 63 m and 66 m.

Dimensions. Carapace from sample 63 m; ULVG: 12930; L.: 0.466 mm; H.: 0.198 mm W.: 0.153 mm (lost).

Remarks. It differs from *Macrocypris longana* Bold, 1960, which was also identified by Piovesan et al. (2009; pl.1, fig. 13) in Maastrichtian units of the Pará-Maranhão Basin, by being smaller, having a concave ventral margin, and a more arched dorsal margin.

Family CYTHERIDEIDAE Sars, 1925

Subfamily KRITHINAE Mandelstam in Bubikyan, 1958

Genus KRITHE Brady et al., 1874

Krithe sp. 1

Fig. 3L-M

Material. Two specimens from samples 63 m and 169.2 m

Dimensions. Carapace from sample 63 m (fig. 3L); ULVG: 12931; L.: 0.752 mm, H.: 0.372 mm, W.: 0.291.

Remarks: It differs from *Krithe crepidus* Ceolin and Whatley, 2015 (Fig. 5R and figs. 6A-C), identified in Danian strata of Neuquén Basin, Argentina (Ceolin et al., 2015), by the absence of overlap in the anterior margin, being more developed in the ventral and posterodorsal regions. Differs from *Krithe* sp. 2 of this study in being more rounded, with the overlap developed in the ventral margin, and a more subtle posterior region. Differs from *Krithe guatemalensis* van den Bold in Neufville, 1979 (Fig. 6, 4a-c) by the absence of overlap in anterior margin, having a less arched dorsal margin, and having a more inflated carapace in dorsal view.

Krithe sp. 2

Fig. 3N-O

Material. Two specimens from samples 29.7 m and 169.2 m

Dimensions. Carapace from sample 29.7 m (fig. 3O); ULVG: 12932; L.: 0.789 mm; H.: 0.418 mm; W.: 0.294 mm.

Remarks: It differs from *Krithe nibelaensis* Dingle, 1985 (fig. 31a-f), identified in Campanian strata of the Nibela Peninsula, South Africa, by having a more acuminated anterior margin in dorsal view, and a bigger size. It differs from *Krithe* sp. P1 (Viviers et al., 2000; fig. 16, 15-16), identified in Cretaceous rocks of the Potiguar Basin, Northeastern of Brazil, by having a more compressed carapace, overlap in the ventral margin, and a more acuminated anterior region in dorsal view.

Family LOXOCONCHIDAE Sars, 1925

Genus LOXOCONCHA Sars, 1866

Loxoconcha sp.

Fig. 3P-R

Material. One carapace from sample 63 m.

Dimensions. ULVG: 12933; L.: 0.310 mm; H.: 0.179 mm; W.: 0.162 mm.

Remarks: It differs from *Loxoconcha corrugata* Alexander in Neufville, 1979 (pl. 7, fig. 9a-b) in presenting a more elongated outline, a less compressed anterior end in dorsal view, more acuminated posterior end, and thicker ribs. It differs from *Loxoconcha mariafarinhensis* Fauth et al. (2005, fig. 7, 7-12), identified in Danian strata of the Paraíba Basin, Brazil, in the pattern and position of ribs, which are more developed, and also in dorsal view, with the posterior end more acuminated.

Family PECTOCYTHERIDAE Hanai, 1957

Genus MUNSEYELLA Van den Bold, 1957b

Munseyella sp.

Fig. 3S-T

Material. One carapace from sample 13.7 m.

Dimensions. ULVG: 12934; L.: 0.395 mm; H.: 0.230 mm; W.: 0.206 mm.

Remarks: It differs from *Munseyella costaevermiculatus* Ceolin and Whatley, 2015 (fig.10 C-F), described for the Maastrichtian interval of the Neuquén Basin, Argentina, in being more compressed, and in the distribution pattern of the ribs.

Family BRACHYCYTHERIDAE Puri (1954).

Subfamily BRACHYCYTHERINAE Puri (1954).

Genus SAPUCARIELLA Puckett et al. (2016).

Sapucariella sp. *sensu* Patarroyo et al., 2022

2022 *Sapucariella* sp. Patarroyo et al., fig. 5, 8a-b

Fig.4A-D

Material. Two specimens from samples 13.7 m and 24.4 m.

Dimensions. Carapace from sample 24.4 m; ULVG: 12935; L.: 0.893 mm; H.: 0.589 mm; W.: 0.522 mm; valve from sample 13.7 m; ULVG: 12936; L.: 0.936 mm; H.: 0.577 mm.

Remarks: It differs from *Sapucariella* sp. 2, identified by Piovesan et al. (2009; pl. II, fig. 15) (*Brachycythere* sp. 2 in their usage) to be shorter and less inflated ventrolaterally, with a shorter caudal process. It differs from *Brachycythere* sp. P1 aff. *B*. *oguni* Reyment, 1960 in Viviers et al. (2000; fig. 11, 19-20) by having punctuations on the surface, ventral margin less inflated, and being less inflated in dorsal view. Most likely this is a new species. However, due to the scarcity of material, it is not possible to describe it herein. This species has been also recorded within the Maastrichtian interval at Core Diablito-1, Cesar-Rancheria Basin, Colombia (Patarroyo et al., 2022, fig.5, 8a-b).

Family TRACHYLEBERIDIDAE Sylvester-Bradley, 1948

Genus *Paragrenocythere* Benson, 1974

Paragrenocythere sp.

Fig. 4E-I

Material. Five specimens from samples 38.4 m and 158.5 m.

Dimensions. Carapace, female from sample 38.4 m (figs. 4E-G) ULVG: 12937; L.: 0.954 mm; H.: 0.571 mm; W.: 0.478 mm; carapace, male from sample 158.5 m (figs. 4H, I); ULVG: 12938; L.: 1.129 mm; H.: 0.551 m; W.: 0.486 mm.

Remarks. Differs from *Paragrenocythere gravis* Al-Furaih, 1980, described to Aruma Formation, Maastrichtian of Saudi Arabia (Al-Furaih, 1984; pl. 2, fig. 5) in a less developed ornamentation and the ocular tubercle, and overlap more pronounced in the posterodorsal, dorsal and anterodorsal regions, and in having a more acute posterior margin.

Genus *Trachyleberis* Brady, 1898

Type species. *Cythere scabrocuneata* Brady, 1880

Trachyleberis sp.

Fig. 4J-L

Material. One carapace from sample 98 m.

Dimensions. ULVG:12939; Carapace, L.: 0.924 mm; H.: 0.480 mm; W.: 0.443 mm.

Remarks. It differs from *Acanthocythereis multispinosa* Al-Furaih, 1984, described for the Maastrichtian of Aruma Formation, Saudi Arabia (Al-Furaih, 1984, pl.1, fig.1-2), by presenting a less acute posterior margin, the absence of an ocular tubercle and having a less spinose carapace. It is, most likely, a new species.

Subfamily Thaerocytherinae Hazel, 1967

Genus *Langiella* Fauth et al., 2005

Type species. "*Henryhowella*" *reymenti* Neufville, 1973

Langiella reymenti (Neufville, 1973)

Fig. 4M-O

1973. "*Henryhowella*" *reymenti* Neufville, p. 89-91, pl. 5, fig. 1a-c.

1979. "*Henryhowella*" *reymenti* Neufville. - Neufville, p.151-152, pl. 5, fig. 2a-c.

2005. *Langiella reymenti* (Neufville) Fauth et al. - Fauth et al., p. 297, fig. 6 (9,12-16).

2009. *Langiella reymenti* (Neufville, 1973) Fauth et al. – Piovesan et al., p. 444, Pl. II, fig. 11.

Material. Six carapaces from samples 15.2 m, 21.3 m; 24.4 m, 29.6 m, 38.4 m, and 121 m.

Dimensions. Carapace, right view, (fig. 4M), ULVG: 12940; L.: 0.828 mm; H.: 0.481 mm; W.:0.333; carapace, left view (fig. 4O); ULVG: 12941; L.: 0.839 mm; H.: 0.466 mm; W.: 0.480 mm.

Remarks. This species was originally described for the Danian interval of the Sergipe-Alagoas and Pernambuco basins (northeastern Brazil; Neufville, 1973; Fauth et al., 2005), and later identified in Maastrichtian strata of the Pará-Maranhão Basin (northern Brazil; Piovesan et al., 2009).

Subfamily TRACHYLEBERIDINAE Sylvester-Bradley, 1948

Genus *Platycythereis* Triebel, 1940

Platycythereis? sp.

Fig. 4P-R

Material. Two specimens from sample 55.3 m.

Dimensions. Carapace from sample 55.3 m; ULVG: 12942; L.: 0.921 mm; H.: 0.444 mm; W.: 0.354 mm.

Remarks. It. Differs from *Patycythereis minuita* Damote, 1971 (pl.3, figs.17a-c), described for Cenomanian strata of Dordogne, France, by having more compressed dorsal and anterior regions, and being more elongated, as well as more compressed anteriorly, in dorsal view.

INDETERMINATE TAXA

Gen et sp. indet.

Fig. 4S

Material. Two carapaces from sample 29.6 m.

Dimensions. ULVG: 12943; L: 0.769 mm H: 0.411 mm.

Remarks. The scarcity of material and poor preservation of the specimens hampers a proper identification of this taxon. It might have affinity to the genus *Langiella*, though the diagnostic ventral and anterior regions are not preserved.

DISCUSSION

Paleoecological preferences of taxa assigned to assemblage 1, mostly the predominance of the genera *Argilloecia* and *Krithe*, allow us to draw paleoenvironmental inferences for the interval between 169.2 m. and 63 m at core La Luna-3E. The genus *Argilloecia* usually occurs in larger abundances in a marine context of relatively deep waters (infra-neritic and bathyal; Morkhoven, 1963). The genus *Krithe* is exclusively marine found in infra-littoral to deep-water environments, usually associated to carbonate substrate (Morkhoven, 1963; Andreu, 1992; Andreu et al., 2013). Therefore, this genus has been extensively studied due to its possible applications for reconstructing oxygen levels, paleobathymetry and paleotemperature. For instance, studies on the size of vestibules of *Krithe* species suggested that the size of the anterior vestibule has a direct relationship with the dissolve oxygen levels in the water (Peypouquet, 1975; Puckett, 1997). However, studies by Whatley and Zhao (1993), Zhao and Whately (1997) and Coles at al. (1994), found no evidence of this relationship. In Late Cenozoic records from the North Atlantic, Coles et al. (1994) recognized the genus as being mainly restricted to low energy substrates in shallow waters, but being highly diversified and abundant in bathyal to abyssal depths. In Holocene records, it was observed that *Krithe* had a preference for deep water settings, once its abundances increase alongside depth (Dingle et al., 1990). According to Dingle (1980), the presence of *Argilloecia* and *Krithe* may suggest the influence of deeper and cooler waters, which is our overall paleoenvironmental interpretation for the interval assigned to assemblage 1 at core La Luna-3E.

The presence of the genus *Paracypris*, also occurring in assemblage 1, has already been recognized in the studied area, at the more proximal core Diablito-1E (Patarroyo et al., 2022). At that core, it occurred associated with benthic foraminiferal assemblages indicative of shallow marine environments (dominated by benthic agglutinated foraminifera). The genus *Bairdoppilata*, with only one occurrence at the core (14.8 m), features a wide environmental distribution, extending from very shallow to very deep waters (Morkhoven, 1963; Maddocks, 1969), and having greater abundances in warm and shallow carbonate environments (Kornicker, 1961; Horne, 2005). *Loxoconcha,* another found taxa at core La Luna-3E, is a cosmopolitan genus, common in shallow marine environments (Morkhoven, 1963; Cronin et al., 2005). A similar association with the taxa *Argilloecia*, *Paracypris*, *Bairdoppilata* and *Loxoconcha* was described for the Maastrichtian interval of the Pará-Maranhão Basin (Brazil) in a neritic environment (Piovesan et al., 2009). Moreover, in the Barreirinhas Basin (Brazil; Santos-Filho et al., 2017) ostracod assemblages with the dominance of *Argilloecia*, *Krithe*, and *Paracypris* were identified for Turonian-Coniacian middle neritic (shelf) environments.

As referred above, ostracod assemblage 2 at core La Luna-3E is composed of genus *Krithe* sp. 2*,* *Paragrenocythere* sp., *Langiella reymenti*, *Platicythereis*? sp., *Sapucariella* sp. *sensu* Patarroyo et al., (2022), *Cytherella* sp., *Munseyella* sp., and Gen. *et.* sp. indet. Although it is a mixed fauna, with the presence of several species assigned to different families, there is a predominance of the family Trachyleberididae, specifically of the species *Langiella reymenti* and *Paragrenocythere* sp. This family is more abundant in open marine environments with normal salinity and many of its species display strong ornamentation and visible ocular tubercles, characteristics of species that inhabit the photic zone, and live on surface sediments of shelf environments (Morkhoven 1963, Fauth et al. 2002). At core La Luna-3E, we also observed an association of the genera *Sapucariella*, *Cytherella* and *Munseyella* that have been previously recorded at core Diablito-1E (Patarroyo et. al., 2022). Moreover, the presence of *Sapucariella* indicates well oxygenated environments (Piovesan et al., 2014).

To further explore the paleoenvironmental significance of ostracod assemblages at core La Luna-3E, we also considered the stratigraphic distribution of selected foraminiferal morphogroups from Malumián (2010) and Torres et al. (2011) for the same core (Figure 5). A general survey of the agglutinated taxa indeed suggests an environmental shift above 50 m at core La Luna-3E, where relative abundances of agglutinated taxa decrease from ~60% to <15%. Intervals in the middle part of the core (113.4-118 m, 125.9-151.2), with higher relative abundances of agglutinated taxa (>40% of total abundance) could have been related with dissolution episodes, or moderate eustatic changes since benthic foraminiferal diversity remained high (Malumián, 2010; Torres et al., 2011). A similar decreasing-upward trend is observed for relative abundances of keeled planktonic taxa (e.g., *Globotruncana*, *Contusotruncana*), which slightly decrease from 15% to <10% in the upper segment of the core (13.7 - 49.2 m). Notwithstanding, planktonic assemblages at core La Luna-3E indicate open marine conditions (middle to inner shelf settings) along the studied interval, where the assemblages are mainly dominated by heterohelicids (*Braunella*, *Planoheterohelix*, *Pseudoguembelina*) as indicated in Figure 5. The presence of radiolarians in the studied interval is also an indicative of relatively deep waters, according to Malumián (2010).

In summary, our new and compiled data indicate open marine paleoenvironmental conditions for the studied interval, likely grading upward from middle to inner shelf settings. Stable physicochemical water properties, such as salinity and oxygenation, could be inferred for most of the deposition of Maastrichtian sediments at core La Luna-3E, based on the described ostracod assemblages and the previously published foraminiferal data. The paleoenvirromental significance of the higher abundances of agglutinated foraminiferal taxa for the middle part of the core must be explored with more detailed foraminiferal analyses and geochemical proxies (*e.g.*, Sr/Ba as a paleosalinity proxy). Eventually, the Colón Formation continues this shallowing-upward trend in its upper portion, which is not recorded at core La Luna-3E. Micropaleontological (foraminifers, calcareous nannofossils, and palynomorphs), sedimentological and geochemical studies have recorded this environmental shift from inner shelf settings to more restricted marine, and even continental ecosystems in the uppermost Colón Formation (Cushman and Hedberg, 1941; Martinez, 1989; Yepes, 2001; Ayala-Calvo et al., 2009; De La Parra et al., 2022; Patarroyo et al., 2022). This shallowing process has been also identified in other inter-mountainous basins in northern South America, and related to global eustatic sea level changes at the end of the Maastrichtian, as well as the early stages of the Andean orogeny (e.g., Tchegliakova 1995, Sarmiento-Rojas, 2019; Bayona et al., 2020; Patarroyo et al., 2023).

CONCLUSIONS

A total of 14 ostracod species were identified and described in detail for the first time for the Maastrichtian marine successions of northern Colombia. The studied interval of core La Luna-3E records the Colón Formation, and allowed the definition of two ostracode assemblages: (1) an open marine, with likely colder waters, basal (169.2-63.0 m) assemblage dominated by taxa such as *Krithe* sp. 2, *Argilloecia* sp., *Bairdoppilata* sp.; (2) an uppermost, ostracod assemblage with a the predominance of species assigned to the Trachyleberididae family (*Langiella reymenti* and *Paragrenocythere* sp.), which suggest an upward shallowing trend. This environmental shift was also recorded by previously published foraminiferal data, and illustrates the first stages of a regional retrogradational process recorded by upper Cretaceous sedimentary successions of northern South America.

ACKNOWLEDGEMENTS

Authors thank to Marcos Antonio Batista dos Santos Filho for SEM images (itt OCEANEON – UNISINOS University). Special thanks to the Instituto Colombiano del Petróleo (ICP-ECOPETROL S.A.) by allowing the publication of this research.

REFERENCES

Al-Furaih, A.A.F. 1984. Maastrichtian Ostracoda from the Aruma Formation of Saudi Arábia. Revue de Micropaléontologie, 27 (3): 159-170.

Andreu, B., 1992. Associations d'ostracodes et paléoécologie du Crétacé (Barrémien à Turonien) le long d'une transversale Agadir-Nador (Maroc). Paleogeogrsphy, Palaeoclimatology, Palaeoecology, 99, 291-319.

Andreu, B., Levedel, V., Wallez, M.-J., Lézin, C., Ettachfini, El M., 2013. The upper Cenomanian-lower Turonian carbonate platform of the Preafrican Trough, Morocco: biostratigraphic, paleoecological and paleobiogeographical distribution of ostracods. Cretaceous Research, 45, 216-246.

Ayala-Calvo, R.C., Bayona-Chaparro, G.A., Ojeda-Marulanda, C., Cardona, A., Valencia, V., Padrón, C.E., Yoris, F., Mesa-Salamanca, J., García, A., 2009. Estratigrafía y procedencia de las unidades comprendidas entre el Campaniano y el Paleógeno en la subcuenca de Cesar: aportes a la evolución tectónica del área. Geología Colombiana 34, 3-33.

Bayona, G., Baquero, M., Ramírez, C., Tabares, M., Salazar, A.M., Nova, G., Duarte, E., Pardo, A., Plata, A., Jaramillo, C., Rodríguez, G., Caballero, V., Cardona, A., Montes, C. Gómez-Marulanda, S., Cárdenas-Rozo, A.L., 2020. Unravelling the widening of the earliest Andean northern orogen: Maastrichtian to early Eocene intra-basinal deformation in the northern Eastern Cordillera of Colombia. Basin Research 00, 1–37.

Bayona, G., Montes, C., Cardona, A., Jaramillo, C., Ojeda, G., Valencia, V., 2011. Intraplate subsidence and basin filling adjacent to an oceanic arc-continental collision; a case from the southern Caribbean–South America plate margin. Basin Research 23. http://dx.doi.org/10.1111/j.1365-2117.2010.00495.x.

Bold, W. A. van den (1960) - Eocene and Oligocene Ostracoda of Trinidad. Micropaleontology, 6(2): 145-196.

Carvalho, M.R., Jaramillo, C., De La Parra, F., Caballero-Rodríguez, D., Herrera, F., Wing, S., Turner, B.L., D'Apolito, C., Romero-Báez, M., Narváez, P., Martínez, C., Gutierrez, M., Labandeira, C., Bayona, G., Rueda, M., Paez-Reyes, M., Cárdenas, D., Duque, A., Crowley, J.L., Santos, C., Silvestro, D., 2021. Extinction at the end-Cretaceous and the origin of modern Neotropical rainforests. Science 372, 63–68.

Ceolin, D., Whatley, R.C., Fauth, G. and Concheyro, A. 2015. New genera and species of Ostracoda from the Maastrichtian and Danian of the Neuquén Basin, Argentina. Papers in Palaeontology, 1 (4), 425–495.

Coles, G., Whately, R.C., Moguilevsky, A., 1994. The Ostracod Genus Krithe from the Cainozoic of the North Atlantic, vol. 37. Palaeontology, Oxford, pp. 71-120.

Cronin T.M., Kamiya T., Dwyer, G.S., Belkin, H., Vann C.D., Schwede S., Wagne, R., 2005. Ecology and shell chemistry of *Loxoconcha matagordensis,* Palaeogeography, Palaeoclimatology, Palaeoecology, 225, 14– 67.

Cushman, J.A., Hedberg, H.D., 1930. Notes on some foraminifera from Venezuela and Colombia. Contributions from the Cushman Laboratory for Foraminiferal Research 6, 64-69.

Cushman, J.A., Hedberg, H.D., 1941. Upper Cretaceous foraminifera from Santander del Norte, Colombia. Contributions from the Cushman Laboratory for Foraminiferal Research 17, 79-100.

Damote, R. 1971. Quelques Ostracodes du Cénomanien de Dordogne et de Touraine. *Revue de Micropaléontologie*, 14 (1): 3-20.

De La Parra, F., Jaramillo, C., Kaskes, P., Goderis, S., Claeys, P., Villasante-Marcos, V., Bayona, G., Hatsukawa, Y., Caballero, D., 2022. Unraveling the record of a tropical continental Cretaceous-Paleogene boundary in northern Colombia, South America. Journal of South American Earth Sciences 114, 103717.

Dingle, R.V., 1980. Marine Santonian and Campanian ostracods from a borehole at Richards Bay, Zululand. Annals of the South African Museum 82:1-70.

Dingle, R.V., Lord, A.R., Boomer, I., 1990. Deep-sea Quaternary Ostracoda from the continental margin off south-western Africa (SE Atlantic Ocean). Annals South African Museum, 99 (9), 245-366.

Dingle, R.V. 1985. Turonian, Coniacian, and Santonian Ostracoda from south-east Africa. Annals of the South African Museum 96:123-239.

Donze P., Colin J.P., Damotte R., Oertli H.J., Peypouquet J.P., Said R. 1982. Les Ostracodes du Campanien terminal à l'Èocène inférieur de la coupe du Kef, Tunisie Nord-Occidentale. Bulletin des Centres de Researches Exploration-Production Elf-Aquitain, 6: 273-335.

Erlich, R.N., Macsotay, O., Nederbragt, A.J., Lorente, M.A., 1999. Palaeoecology, paleogeography and depositional environments of Upper Cretaceous rocks of western Venezuela. Palaeogeography, Palaeoclimatology, Palaeoecology 153 (1-4), 203-238.

Fauth, G., Colin, J.P., Koutsoukos E.A.M. & Bengtson, P. (2005) - Cretaceous/Tertiary boundary ostracodes from the Poty Quarry, Pernambuco, northeastern Brazil. Journal of South American Earth Sciences, 19(3): 285-305.

Fauth, G., Seeling, J., and Luther, A. 2002. Campanian (Upper Cretaceous) ostracods from southern James Ross Island, Antarctica, Micropaleontology, 49(1):95-107.

Garzón, S., Warny, S., Bart, P.J., 2012. A palynological and sequence-stratigraphic study of Santonian–Maastrichtian strata from the Upper Magdalena Valley basin in central Colombia. Palynology 36, 112-133.

Guerrero, J., Sarmiento, G., Navarrete, R.E., 2000. The Stratigraphy of the W side of the Cretaceous Colombian basin in the Upper Magdalena Valley. Reevaluation of selected areas and type localities including Aipe, Guaduas, Ortega, and Piedras. Geología Colombiana 25, 45-110.

Horne, D.J., 2005. Ostracoda. In: Selley, R.C., Cocks, R.M., Plimer, I.R. (Eds.), Encyclopedia of Geology. Elsevier, Oxford, pp. 453-463.

Kornicker, L.S., 1961. Ecology, taxonomy Recent Bairdiinae (Ostracoda) Micropaleontology, 7 (1), 55-70.

Maddocks, R.F., 1969. Revision of Recent Bairdiidae (Ostracoda), vol. 295. United States National Museum Bulletin, p. 126.

Majoran, S.1999. Palaeoenvironment of Maastrichtian ostracods from ODP Holes 1049B, 1050C and 1052E in the Western North Atlantic. Journal of Micropalaeontology, 18: 125-1 36.

Malumián, N., 2010. Foraminíferos del Cretácico superior del Pozo Perijá-2. Informe Interno. Instituto Colombiano del Petróleo. Grupo de Bioestratigrafía, 21p. Piedecuesta, Colombia.

Martínez, R. J.I., 1989. Foraminiferal biostratigraphy and paleoenvironments of the Maastrichtian Colón mudstones of Northern South America. Micropaleontology 35 (2), 97-113.

Martinez, J.I., Hernandez, R., 1992. Evolution and drowning of the Late Cretaceous Venezuelan carbonate platform. Journal of South American Earth Sciences 5(2), 197-210.

Montes, C., Rodríguez-Corcho, A.F., Bayona, G., Hoyos, N., Zapata, S., Cardona, A., 2019. Continental margin response to the multiple arc-continent collisions: The northern Andes-Caribbean margin. Earth Science Reviews 198, 102903.

Morkhoven, F.P.C.M., 1963. Post-palaeozoic Ostracoda: Their Morphology, Taxonomy and Economic Use e Volume II e Generic Descriptions. Elsevier Publishing Company, p. 478.

Navarrete, R.E., Parra, F.J., Pérez-Panera, J.P., Daza, D., Sánchez, C., Prince, M., Rodríguez, M., 2018. Turonian-Campanian foraminifera zonation for the La Luna and lower Umir formations, Middle Magdalena Valley Basin, northern Colombia. In: Cusminski et al. (Eds.) Advances in South American Micropaleontology - Selected papers of the 11th Argentine Paleontological Congress. Springer Earth System Science Series, pp. 67-114.

Neufville, M. H. 1973. Upper Cretaceous-Paleogene Ostracoda from the South Atlantic. Publications from the Paleontological Institution of the University of Uppsala, 1: 1-193.

Neufville, M. H. 1979. Upper Cretaceous-Paleogene marine ostracods from the Sergipe-Alagoas Basin, northeastern Brazil. Bulletin of the Geological Institutions of the University of Uppsala, 8: 132-172.

Patarroyo, G.D., Kochhann, K.G.D., Ceolin, D., Guerra, R.M., Alegret, L. and Bom, M.H.H. 2022. Paleoenvironmental changes recorded at a late Maastrichtian marine succession of northern South America. Journal of South American Earth Sciences, 119: 104015.

Patarroyo, G., Kochhann, K.G.D., Guerra, R.M., Alegret, L., Ceolin, D., Torres, J.M. 2023. Maastrichtian microfossils of the shallow marine Umir Formation, North-eastern Colombia. Ameghiniana, 60 (4): 297–311.

Patarroyo, G.D., Torres, G.A., Rincón, D.A., Cárdenas, C.P., Márquez, R.E., 2017. Bioestratigrafía e inferencias paleoambientales de las asociaciones de foraminíferos en las formaciones cretácicas La Luna-Colón (Cuenca del Catatumbo, Colombia). Boletín de Geología 39 (3), 25-40.

Petters, V., 1955. Development of Upper Cretaceous foraminiferal faunas in Colombia. Journal of Paleontology, 29(2), 212–225.

Peypouquet, J.P., 1975. Les Variations des Caracteres Morphologiques Internes chez les Ostracodes des Genres *Krithe* et *Parakrithe*: relation possible avec la teneur em 02 dissous am l'eau. Bull. l'Institut Geologie Bassin d'Aquitaine 17, 81-88.

Piovesan, E.K., Cabral, M.C., Colin, J-P.; Fauth, G., Bergue, C.T., 2014 Ostracodes from the Upper Cretaceous deposits of the Potiguar Basin, northeastern Brazil: taxonomy, paleoecology and paleobiogeography. Part 2: Santonian-Campanian. Carnets de Géologie [Notebooks on Geology], 14, (15): 315-351.

Piovesan, E.K., Bergue, C.T. and Fauth, G. 2009. Cretaceous ostracodes from Pará-Maranhão Basin, Brazil: taxonomy and preliminary paleoecological and paleobiogeographical inferences. Revue de Paléobiologie 28, 457-470.

Puckett, T.M., 1997. The genus *Krithe* (ostracoda) from the Campanian and Maastrichtian (upper Cretaceous) of the northern US gulf coastal plain. Journal of Micropalaeontology, 16, 145-157.

Santos-Filho, M.A.B., Fauth, G., Piovesan, E.K., 2017. Cretaceous ostracods of the Barreirinhas Basin: biostratigraphic considerations and paleoenvironmental inferences. Journal of South American Earth Science, 73, 130–152.

Sarmiento-Rojas, L.F., 2019. Cretaceous stratigraphy and paleo-facies maps of northwestern South America. In: Cediel, F., Shaw, R.P., (Eds.), Geology and Tectonics of Northwestern South America. The Pacific Caribbean Andean Junction, pp. 673-747.

Scott, H.W. 1961. Classification of Ostracoda. Q74–Q91 In MOORE, R. C. and PITRAT, C. W. (eds). Treatise on invertebrate paleontology, Part Q, Arthropoda 3: Crustacea, Ostracoda. Geological Society of America, Boulder, CO &University of Kansas Press, Lawrence, KS, 465 pp.

Sellier de Civrieux, J.M., 1952. Estudio de la microfauna de la sección-tipo del Miembro Socuy de la Formación Colón, Distrito Mara, Estado Zulia. Boletín de Geología y Minas (Venezuela) 2 (5), 231-310.

Sohn I.G., Berclan J.M., Peck R.E. 1965. Ostracods. In: Kummel B. & Raup D. (eds) Handbook of Paleontological Techniques, W.H. Freeman & Co. 77-89pp.

Tchegliakova, N., 1995. Los Foraminíferos de la Formación Umir (Sección Quebrada La Julia): Registro del Cretáceo Superior Cuspidal (Maestrichtiano) en el Valle Medio del Magdalena, Colombia. Geología Colombiana 19, 109-130.

Tchegliakova, N., 1996. Registro de las biozonas de foraminíferos planctónicos Gansserina gansseri y Abathomphalus mayaroensis (Maastrichtiano medio y superior) en el extremo meridional del Valle Medio del Magdalena (Colombia, Suramérica). Geología Colombiana 20, 67-90.

Tchegliakova, N., Mojica, J., 2001. El Senoniano de la barrera de Girardot-Guataquí, Valle Alto del Magdalena, Colombia: Precisiones sobre la estratigrafía y establecimiento de una zonación micropaleontológica. Rev. Acad. Col. Cienc. Ex., Fís. Nat. 25 (94), 37-75.

Torres, G.A., Parra, D.C., Caicedo, C., Rincón, D.A. 2011. Reconstrucción Paleoambiental de los shales de la Formación Molino (Formación Colón) de la Cuenca Cesar-Ranchería, Cretácico superior del norte de Colombia, basado en foraminíferos. XIV Congreso Latinoamericano de Geología-XIII Congreso Colombiano de Geología. Medellín, Colombia.

Vergara, L.S., 1997. Stratigraphy, foraminiferal assemblages and paleoenvironments in the Late Cretaceous of the Upper Magdalena Valley, Colombia (Part I), Journal of South American Earth Sciences 10 (2), 111-132.

Villamil, T., Pindell, J., 1998. Mesozoic paleogeographic evolution of northern South America. In: J. Pindell, J., Drake, C. (Eds.) Paleogeographic evolution and non-glacial eustacy, northern South America. SEPM Society for Sedimentary Geology 58, pp. 238-318.

Viviers, M. C., E. A. M. Koutsoukos, A.C. Silva-Telles & P. Bengtson (2000) - Stratigraphy and biogeographic affinities of the late Aptian-Campanian ostracods of the Potiguar and Sergipe Basins in northeastern Brazil. Cretaceous Research, 21: 407-455.

Whatley, R.C., Zhao, Q., 1993. The *Krithe* Problem: a Case History of the Distribution of *Krithe* and *Parakrithe* (Crustacea, Ostracoda) in the South China Sea, vol. 103.Palaeogeography, Palaeoecology, Palaeoclimatology, Amsterdam, pp. 281-297

Yepes, O., 2001. Maastrichtian/Danian dinoflagellate cyst biostratigraphy and biogeography from two equatorial sections in Colombia and Venezuela. Palynology 25, 217-249.

Zhao, Q., Whately, R.C., 1997. Distribution of the Genera *Krithe* and *Parakrithe* in bottom sediments of the East China and Yellow Seas, vol. 32. Marine Micropaleontology, Amsterdam, pp. 195-207.

LIST OF FIGURES

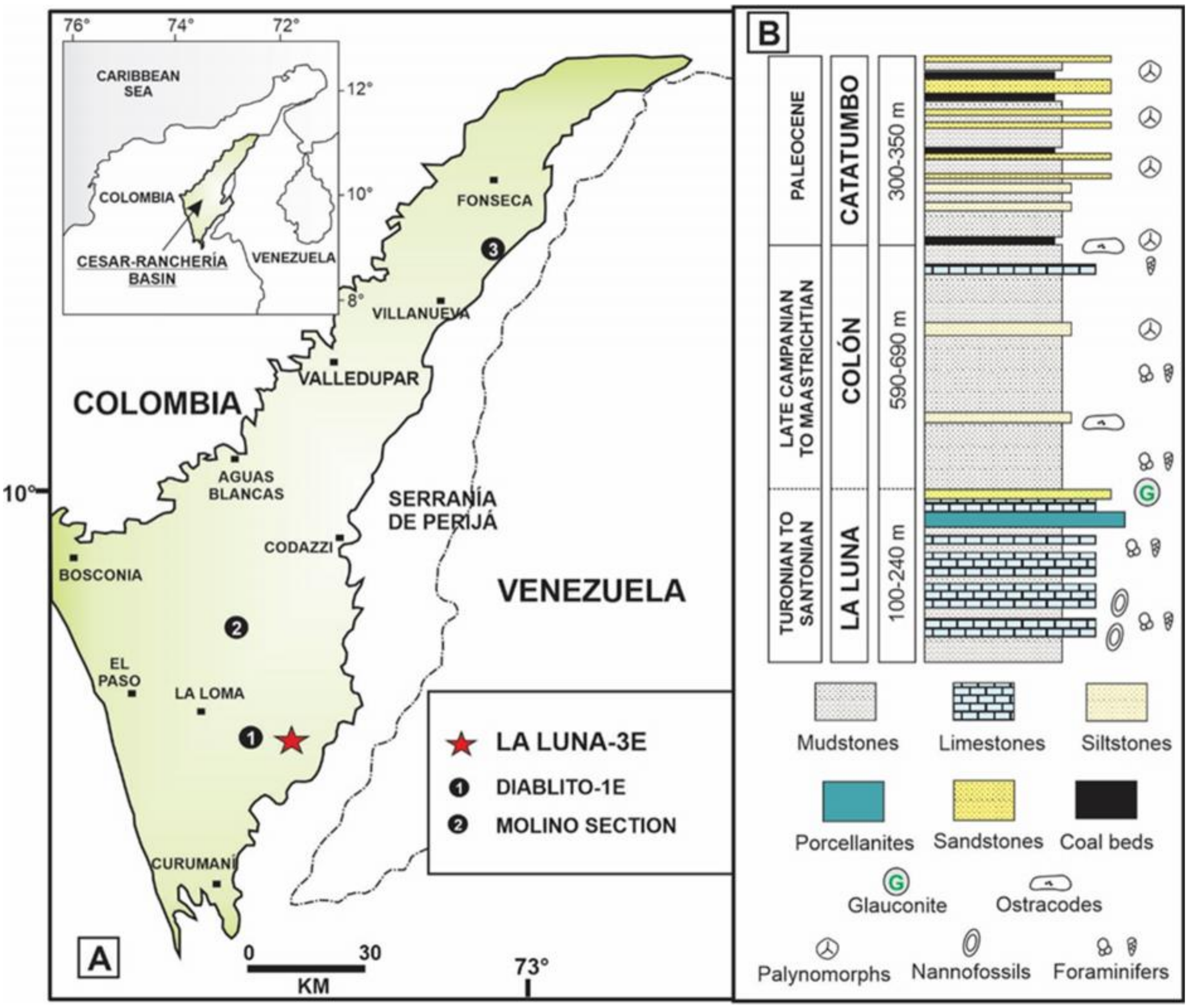

Figure 1. Study area. A: Generalized stratigraphic column of the Cesar-Rancheria Basin, northeast Colombia. B: Location of core La Luna-3E. Sites 1 to 3 correspond to localities with previous biostratigraphic data for the Colón Formation. Sites 1 and 2 are stratigraphic cores (Ayala-Calvo et al., 2009; Malumián, 2010; Torres et al., 2011; Patarroyo et al., 2022), and site 3 corresponds to the Molino River section (Martinez, 1989).

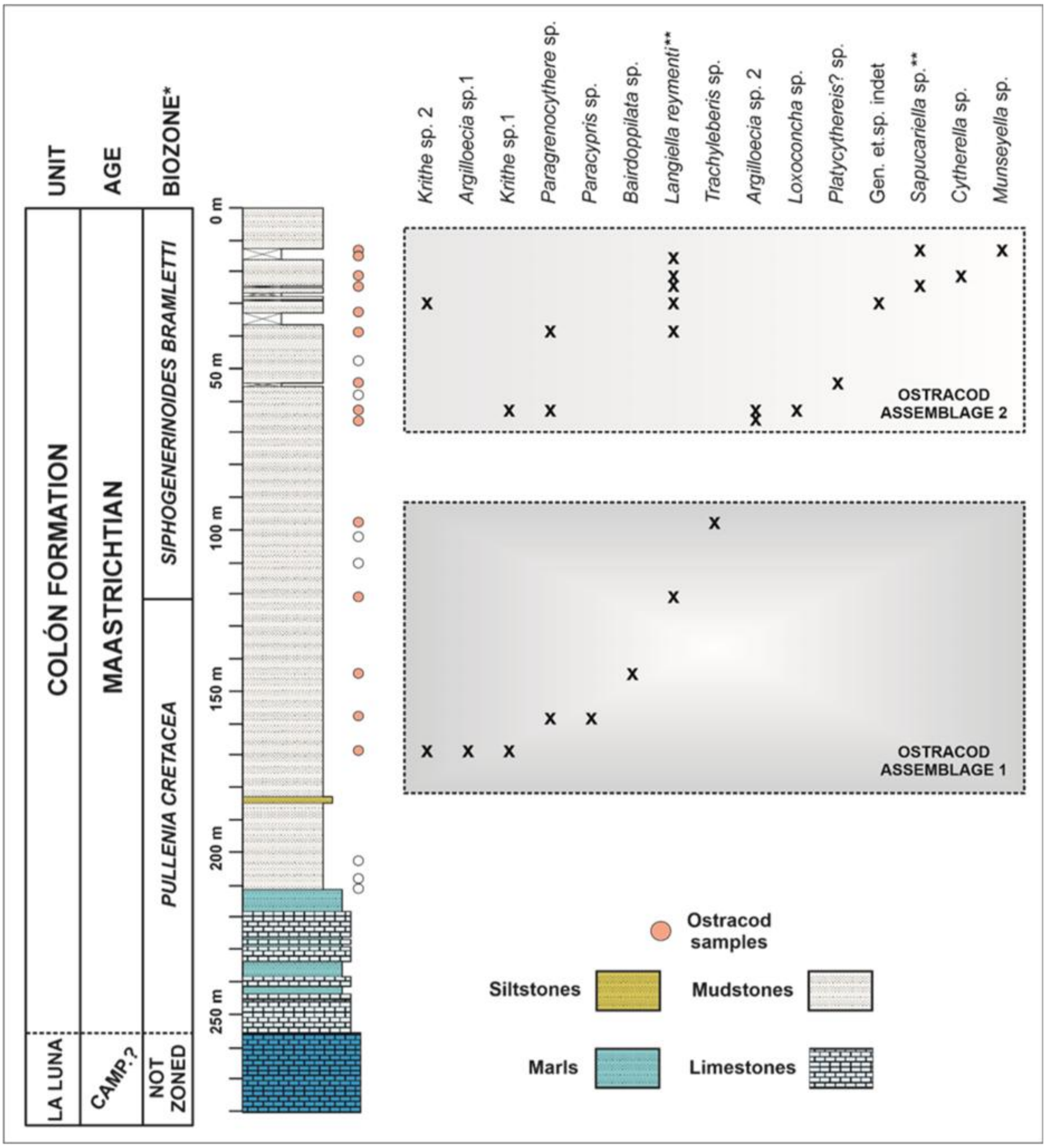

Figure 2. Ostracod distributions at core La Luna-3E, Cesar-Rancheria Basin, northeast Colombia. White dots indicate samples with low to null ostracod recovery. ***Langiella reymenti* and Sapucariella sp. *sensu* Patarroyo et al. (2022).

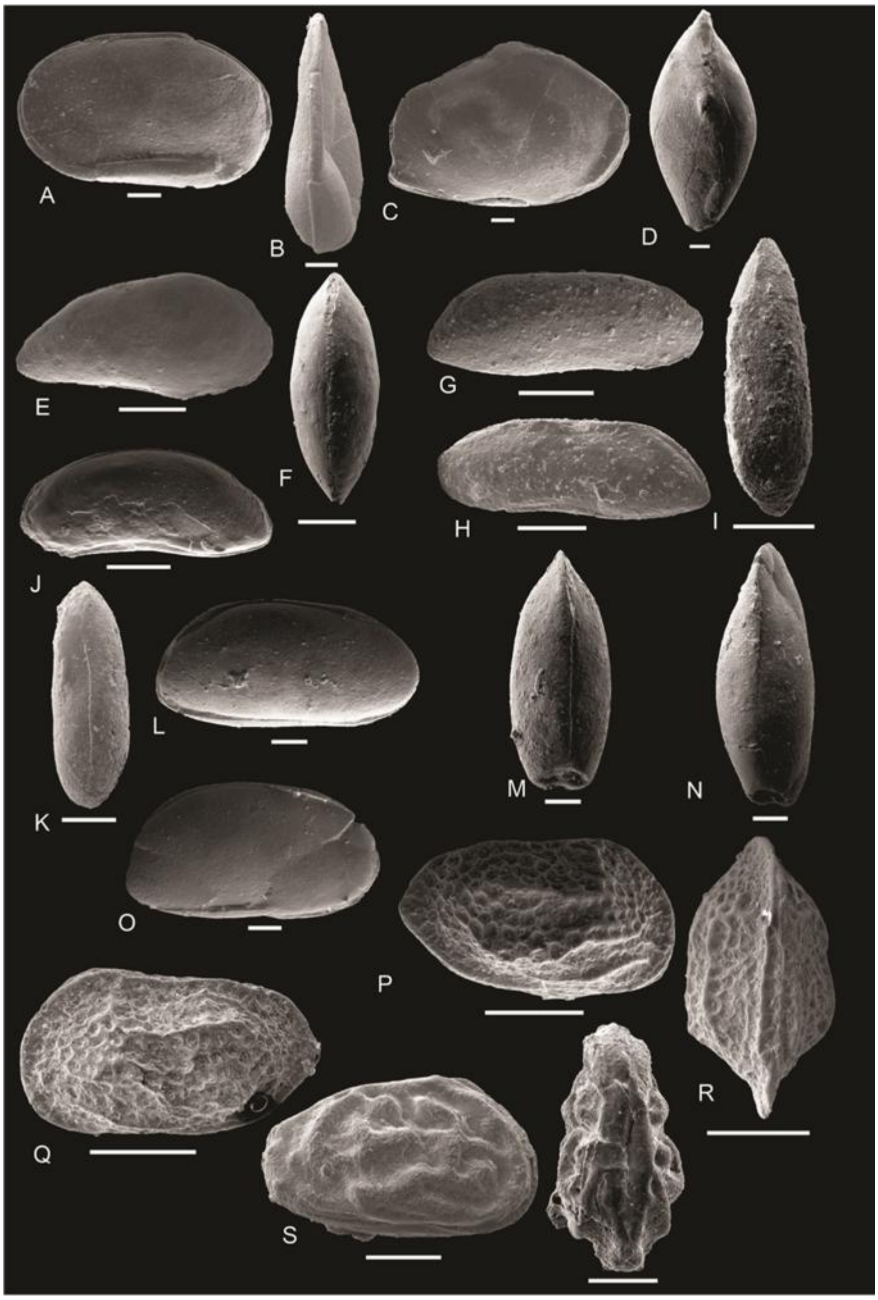

Figure 3. Ostracod species recovered from core La Luna-3E, Cesar-Rancheria Basin, northeast Colombia. A-B. *Cytherella* sp., ULVG 12925; A, adult, carapace, left lateral view; B, dorsal view. C-D. *Bairdoppilata* sp., ULVG 12926, C, adult, carapace, left lateral view; D, dorsal view. E-F, *Paracypris* sp. *sensu* Patarroyo et al., 2022; ULVG 12927; E, carapace, right lateral view, F, dorsal view. G-I, *Argilloecia* sp. 1, ULVG 12928; G, adult, carapace, right lateral view, H, ULVG 12929, adult, carapace, left lateral view, I, dorsal view. J-K, *Argilloecia* sp. 2, ULVG 12930; J, adult, carapace, left lateral view; K, dorsal view. L-M, *Krithe* sp.1, ULVG 12931; L, adult, carapace, right lateral view, M, dorsal view. N-O, *Krithe* sp. 2, ULVG 12932; N, carapace, adult, dorsal view, O, carapace, adult right lateral view. P-R, *Loxoconcha* sp., P, ULVG 12933, P, adult, carapace, right lateral view, Q, left lateral view, R, dorsal view. S-T, *Munseyella* sp., S, ULVG 12934 adult, carapace, right lateral view, T, dorsal view. All scale bars represent 100 µm.

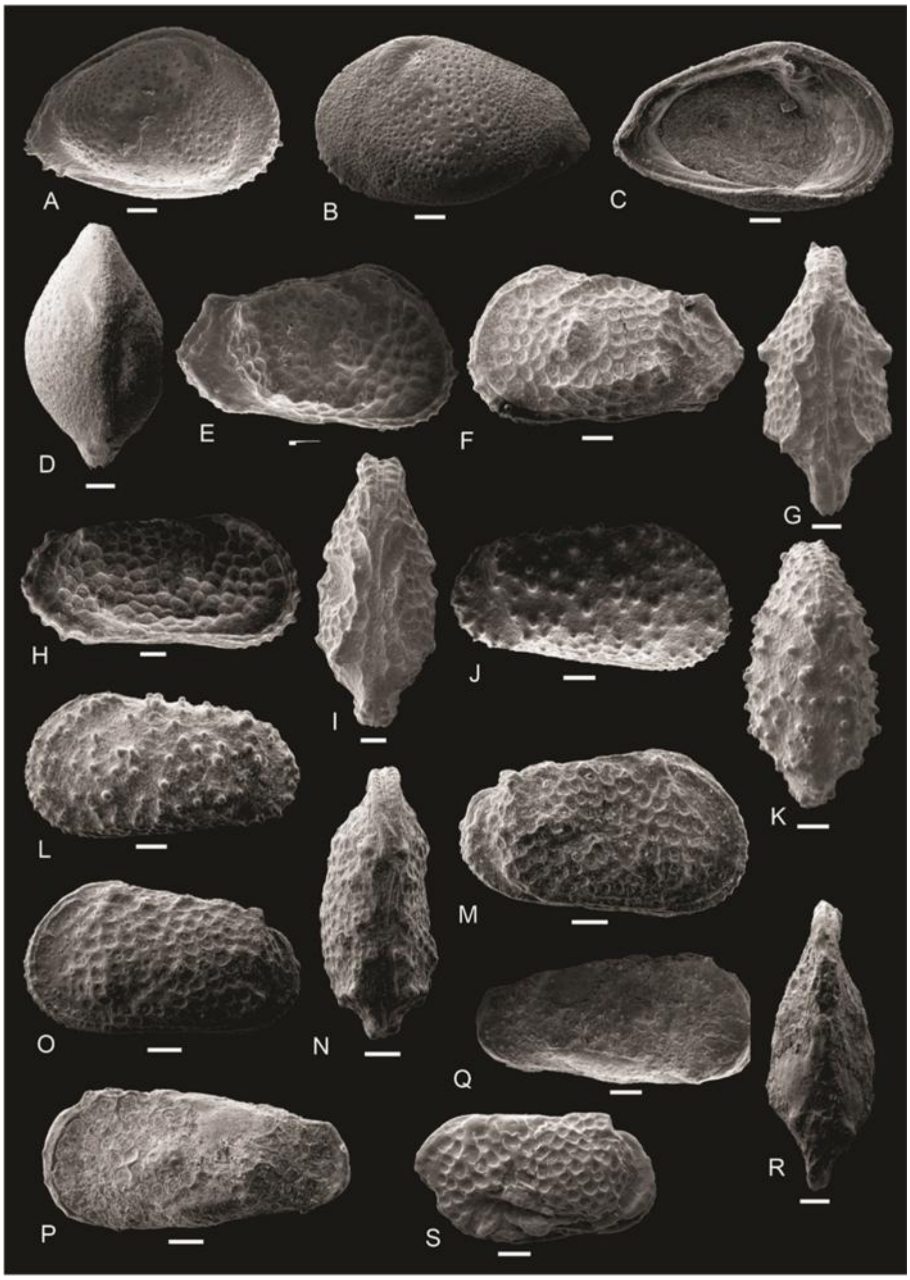

Figure 4. Ostracod species recovered from core La Luna-3E, Cesar-Rancheria Basin, northeast Colombia. A-D. *Sapucariella* sp. *sensu* Patarroyo et al. 2022, ULVG 12935 A, carapace, right lateral view, B, valve, left lateral view, ULVG 12936; C, valve, internal view; D, carapace, dorsal view. E-I. *Paragrenocythere* sp., ULVG 12937, E, adult, carapace, female, left lateral view; F, carapace, ULVG 12938, female, right lateral view; G, female, dorsal view; H, carapace, male, right view; I, dorsal view. J-L. *Trachyleberis* sp. ULVG 12939; J, carapace, right lateral view, K, dorsal view; L, carapace, left lateral view. M-O. *Langiella reymenti* (Neufville, 1973) ULVG 12940, M, adult, carapace, right lateral view; N, dorsal view, O, ULVG 12941; left lateral view. P-R, *Platycythereis* sp., ULVG 12942; P, adult carapace, left lateral view, Q, adult, carapace, right lateral view, R, dorsal view. S, Gen *et* sp. indet., ULVG 12943, adult, carapace, left lateral view. All scale bars represent 100 µm.

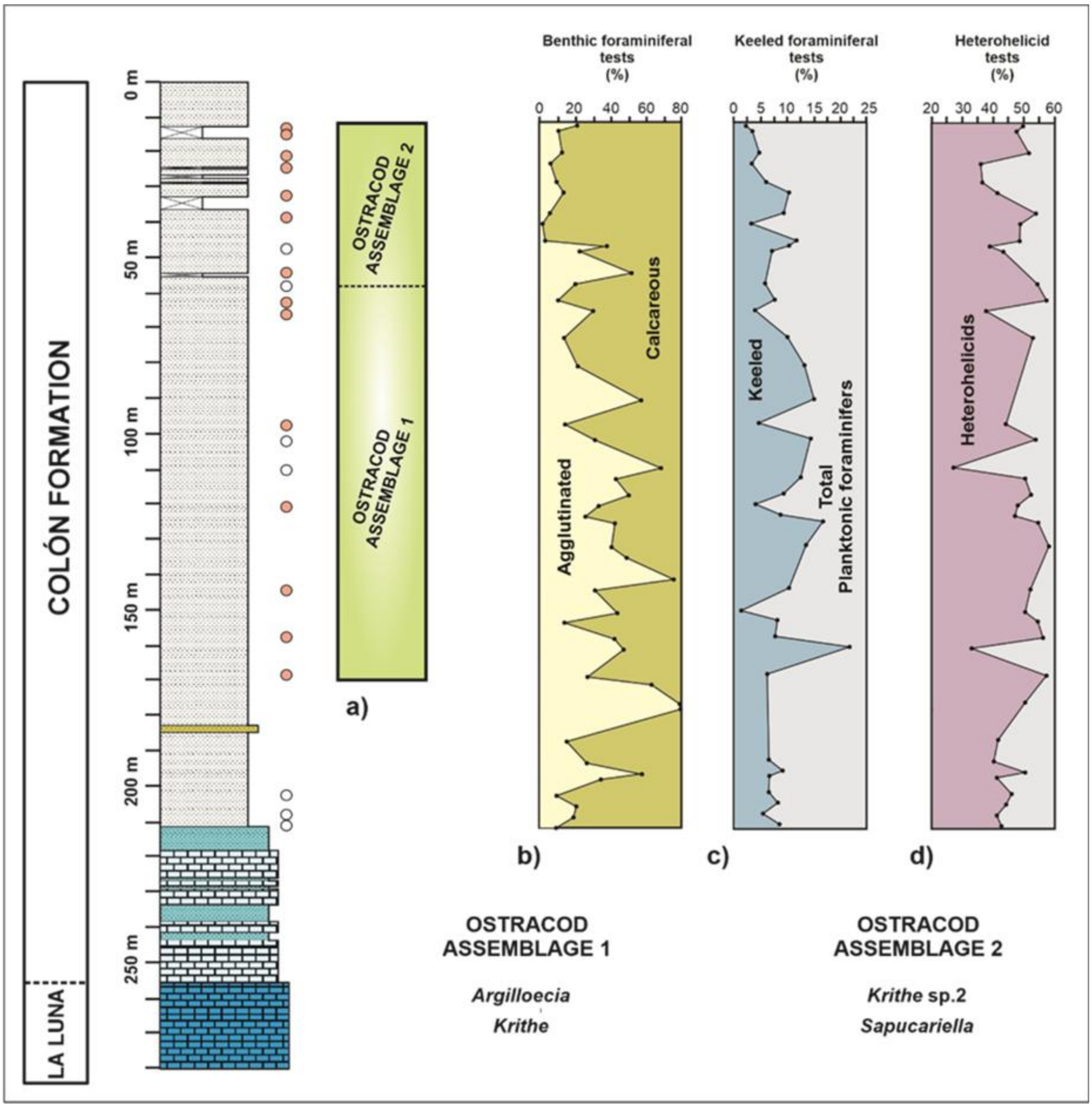

Figure 5 General distribution of microfossils at Core La Luna-3E. a) Distribution of the ostracod assemblages 1 and 2 (63-169.2 m; 13.7-58.4 m). b) Relative abundances of the calcareous and agglutinated benthic foraminifers. c) Relative abundances of the keeled planktonic foraminifers. d) Relative abundances of the biserial (Heterohelicids) foraminifers. Foraminiferal data from Malumián (2010) and Torres et al. (2011).

SUPPLEMENTARY MATERIAL

Supplementary material S1. Quantitative analyses of the total amount of genera belonging to the different families of ostracods recovered for the Maastrichtian interval, showing the dominance of the Trachyleberididae family.

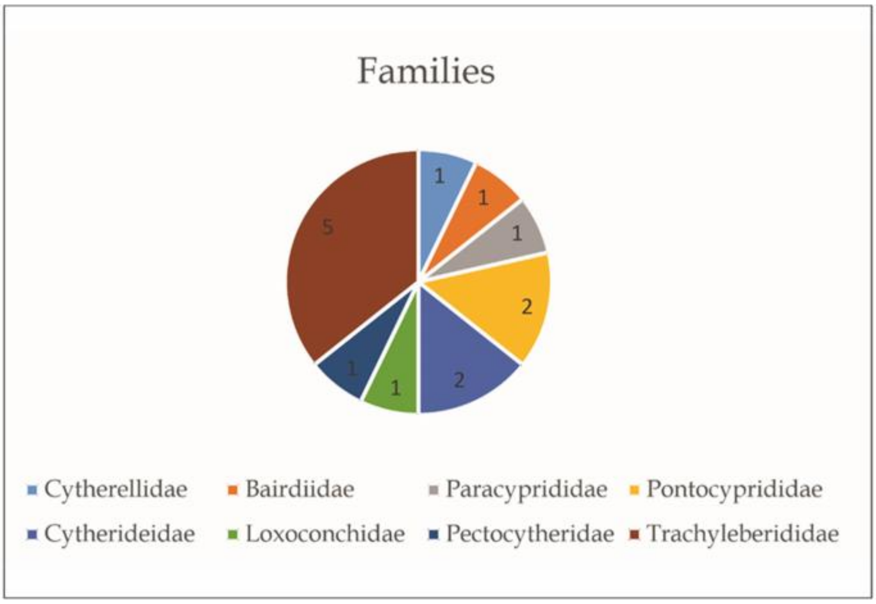

SUPPLEMENTARY MATERIAL

CHAPTER 1

Table S1 Total foraminifer counts of Core Diablito-1.

Table S2 Total calcareous nannofossil counts of Core Diablito-1.

Table S3 Total ostracod counts of Core Diablito-1.

Table S4 Geochemical data (XRF analyses) of Core Diablito-1.

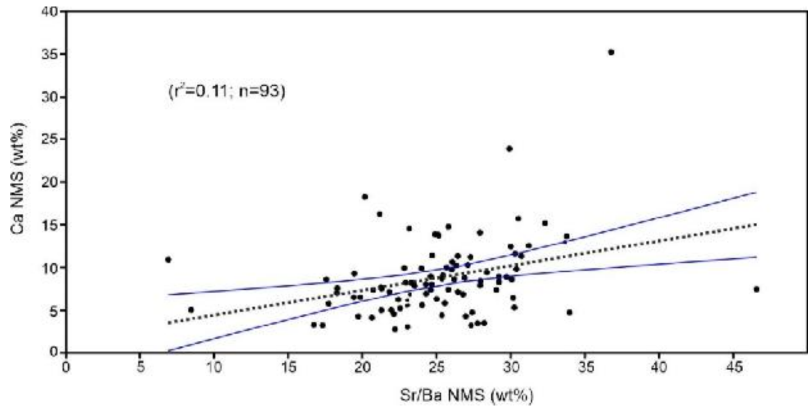

Figure S1 Cross-plot of Sr/Ba ratio and normalized (NMS) Ca intensity at core Diablito-1.

Foraminiferal reference list

Guembelitria cretacea Cushman, 1933

Laeviheterohelix dentata (Stenestad, 1968)

Planoheterohelix globulosa (Ehrenberg, 1840)

Rugoglobigerina macrocephala Brönnimann, 1952

Alabamina creta (Finlay, 1940)

Anomalina nelsoni Berry, 1929

Ammobaculites colombiana Cushman and Hedberg, 1930

Coryphostoma incrassata (Reuss, 1851)

Evolutinella flageri Cushman and Hedberg, 1941

Gavelinella correcta (Carsey, 1926)

Gavelinella henbesti (Plummer, 1936)

Gavelinella pinguis (Jennings, 1936)

Gavelinella spissocostata (Cushman, 1938)

Haplophramoides excavatum Cushman and Waters, 1927

Haplophragmoides glabra Cushman and Waters, 1927

Lenticulina muensteri (Roemer, 1839)

Loxostomum minutissimum (Spandel, 1929)

Nonionella austiniana Cushman, 1933

Praebulimina carseyae (Plummer, 1931)

Praebulimina kickapoensis (Cole, 1938)

Rzehakina epigona (Rzehak, 1895)

Siphogenerinoides bramletti Cushman, 1929

Siphogenerinoides parva Cushman, 1929

Nannofossil reference list

Ahmuellerella regularis (Górka, 1957) Reinhardt and Górka, 1967

Ahmuellerella octoradiata (Górka, 1957) Reinhardt, 1966

Arkhangelskiella cymbiformis Vekshina, 1959

Arkhangelskiella maastrichtiensis Burnett, 1997

Biscutum constans (Górka, 1957) Black in Black and Barnes, 1959

Calculites obscurus (Deflandre, 1959) Prins and Sissingh in Sissingh, 1977

Cervisiellla operculata (Bramlette and Martini 1964) Streng, Hildebrand-Habel and Williams 2004

Cervisiella saxea (Stradner 1961) Hildebrand-Habel, Willems, and Versteegh 1999

Chiastozygus amphipons (Bramlette and Martini, 1964) Gartner, 1968

Chiastozygus litterarius (Górka, 1957) Manivit, 1971

Cribrosphaerella ehrenbergii (Arkhangelsky, 1912) Deflandre in Piveteau, 1952

Cyclagelosphaera reinhardtii (Perch-Nielsen, 1968) Romein, 1977

Eiffelithus gorkae (Stover, 1966) Perch-Nielsen, 1968

Eiffelithus turrisseiffelii (Deflandre in Deflandre and Fert, 1954) Reinhardt, 1965

Helicolithus anceps (Górka, 1957) Noël, 1970

Helicolithus compactus (Bukry, 1969) Varol and Girgis, 1994

Helicolithus trabeculatus (Górka, 1957) Verbeek, 1977

Kamptnerius magnificus Deflandre, 1959

Loxolithus armilla (Black in Black and Barnes, 1959) Noël, 1965

Microrhabdulus decoratus Deflandre, 1959

Micula adumbrata Burnett, 1997

Micula concava (Stradner in Martini and Stradner, 1960) Verbeek, 1976

Micula cubiformis Forchheimer, 1972

Micula staurophora (Gardet, 1955) Stradner, 1963

Micula swastica Stradner and Steinmetz, 1984

Placozygus fibuliformis (Reinhardt, 1964) Hoffmann, 1970

Prediscosphaera cretacea (Arkhangelsky, 1912) Gartner, 1968

Prediscosphaera spinosa (Bramlette and Martini, 1964) Gartner, 1968

Prediscosphaera stoveri (Perch-Nielsen, 1968) Shafik & Stradner, 1971

Retecapsa crenulata (Bramlette and Martini, 1964) Grün in Grün and Allemann, 1975

Retecapsa surirella (Deflandre and Fert, 1954) Grün in Grün and Allemann, 1975

Rhagodiscus angustus (Stradner, 1963) Reinhardt, 1971

Rhagodiscus reniformis Perch-Nielsen, 1973

Rhagodiscus splendens (Deflandre, 1953) Verbeek, 1977

Staurolithites laffittei Caratini, 1963

Staurolithites mielnicensis (Górka, 1957) Perch-Nielsen, 1968 sensu Crux 1982

Tetrapodorhabdus decorus (Deflandre in Deflandre and Fert, 1954) Wind and Wise 1983

Watznaueria barnesiae (Black in Black and Barnes, 1959) Perch-Nielsen, 1968

Zeugrhabdotuus erectus (Deflandre in Deflandre and Fert, 1954) Reinhardt, 1965

Ostracod reference list

Cytherella cf. C. piacabucuensis Neufville 1973

Cytherella sp. 1

Cytherella sp. 2

Buntonia sp.

Paracypris sp.

Munseyella sp.

Cythereis sp.

Sapucariella sp.

Paracosta sp.

Veenia sp.

Gen. *et* sp. Indet. 1

Gen. *et* sp. Indet. 2

TABLE S1 TOTAL FORAMINIFER COUNTS OF CORE DIABLITO (COUNTS)

Depth (ft)	Depth (m)	*Globigerinelloides* spp.	*Guembelitria cretacea*	*Guembelitria* spp.	Heterohelicidae indet.	*Laeviheterohelix dentata*	*Laeviheterohelix* spp.	*Muricohedbergella* spp.	*Muricohedbergella?* spp.	*Planoheterohelix globulosa*
1848.7	563.5				1					
1883.1	574									
1893.11	577									
1900	579.1				1					
1914.3	583.5									
1926.1	587.1									
1940.3	591.4				1					
1950.5	594.5		4	2						1
1952.7	595.2		1	1						
1962.8	598.3									
1973.6	601.6		18	10			1	2		4
1987.1	605.7		1	4						
1997.5	608.8		1							
2002	610.2									
2013.9	613.8				2				1	
2027	617.8		1	1						
2041	622.1									
2059.4	627.7	1	5							
2072.8	631.8		21	1			1			1
2084.5	635.4		9	4						
2093.2	638		1	2						
2109	642.8									
2123	647.1		2	1						
2138	651.7		2	1						
2155	656.8		3	1	2					1
2170.6	661.6		49	1	1	1		1		2
2176.5	663.4		2	6	17					15
2183.5	665.5									
2194.3	668.8		58	14	1		2			4
2208.5	673.2		27	5			1			2
2219.5	676.5		6	6						1
2230.5	679.9		27	12	1		1			1
2240	682.8		2							1
2250.5	686		49	18						
2260.5	689		10	1	1					1
2270.5	692		7	6			1			
2280.3	695									
2290.5	698.1				1					
2293.5	699.1									
2301.4	701.5									

Depth (ft)	*Rugoglobigerina macrocephala*	*Alabamina creta*	*Anomalina nelsoni*	*Anomalina* spp.	*Ammobaculites colombiana*	*Ammobaculites sp2*	*Coryphostoma incrassata*	*Dentalina* spp.	*Evolutinella flageri*	*Evolutinella* spp.
1848.7					2					
1883.1					17	2			3	1
1893.11					1					
1900										
1914.3					1					
1926.1										
1940.3										
1950.5					5		2			
1952.7		7	1		2		1			
1962.8										
1973.6										1
1987.1										
1997.5					1					
2002		1								
2013.9					10				2	
2027					30					
2041			1		3					
2059.4					2					
2072.8					1					
2084.5		1								
2093.2										
2109										
2123			1							
2138										
2155										
2170.6		2	6				2	1		
2176.5				2						
2183.5										
2194.3	1									
2208.5										
2219.5										
2230.5										
2240										
2250.5										
2260.5	2	6								
2270.5										
2280.3										
2290.5									1	
2293.5										
2301.4		1								

Depth (ft)	*Gavelinella correcta*	*Gavelinella henbesti*	*Gavelinella pinguis*	*Gavelinella spissocostata*	*Gavelinella* spp.	*Haplophramoides excavatum*	*Haplophragmoides glabra*	*Haplophragmoides sp2*	*Haplophragmoides* spp.	*Lenticulina muensteri*	*Loxostomum minutissimum*	*Nonionella austiniana*	*Osangularia* spp.
1848.7													
1883.1									10				
1893.11									2				
1900													
1914.3								2	1				
1926.1								3					
1940.3													
1950.5		14	3		16						4		
1952.7	8				2	3							
1962.8									1				
1973.6			3	2	8			1	3				
1987.1						1							
1997.5		2	8	3	4	4	1						
2002		1			1								
2013.9													
2027	1	4		1	3				2				
2041	1				1				2				
2059.4					2			2	2			1	
2072.8				1					3				
2084.5													
2093.2				1									
2109													
2123			4		1		2		2				
2138					2								
2155	1			2	2		2		2				
2170.6					1		1			1			1
2176.5	3	1		1	8	1			2	2	1		
2183.5					4								
2194.3				1									
2208.5													
2219.5													
2230.5					1								
2240			1		1								
2250.5													
2260.5													
2270.5													
2280.3													
2290.5	1			1	2		1	4	2				
2293.5													
2301.4	1		1	18	7								

Depth (ft)	*Praebulimina carseyae*	*Praebulimina kickapoensis*	Rotaliina Indet.	*Rzehakina epigona*	*Rzehakina* spp.	*Siphogenerinoides bramletti*	*Siphogenerinoides cf. bramletti*	*Siphogenerinoides parva*	Textulariina Indet.	Total foraminifera
1848.7										3
1883.1									1	34
1893.11										3
1900									5	6
1914.3		1							1	6
1926.1		1		1					4	9
1940.3									3	4
1950.5										51
1952.7		2		7					1	36
1962.8									3	4
1973.6		4		2						59
1987.1										6
1997.5		1		1					3	29
2002										3
2013.9									3	18
2027									1	44
2041		1							1	10
2059.4										15
2072.8		14							1	44
2084.5		12							1	27
2093.2		1					1			6
2109									2	2
2123		1							2	16
2138		1	1							7
2155		5	3							24
2170.6		3			1	8		4		86
2176.5			6		1	1			4	73
2183.5				1						5
2194.3	1	1			1					84
2208.5		9								44
2219.5		3								16
2230.5		8	1							52
2240										5
2250.5	1	8								76
2260.5		7	1						1	30
2270.5		3								17
2280.3									1	1
2290.5						2		2	1	18
2293.5										0
2301.4						1				29

Depth (ft)	Bivalve remains	Bivalve remains?	Charophytes	Diatoms?	Echinoids (fragments)	Echinoids (espines)	Fish remains	Fish tooth	Gastropodes	Ostracodes (molds)	Ostracodes (molds?)	Ostracodes (valves)	Otholiths	Plant remains	Chert fragments	Glauconite	Phosphates	Pyrite	Siderite
1848.7		4				4									4	2			
1883.1	16				2	3			6	6		3				3			
1893.11																			
1900			1						2							1			
1914.3														1					
1926.1														1		2			
1940.3											1								
1950.5					1	14													
1952.7	13				1	2	7	1	1	9	1	3				13			
1962.8					1											2			
1973.6										1		5				3			
1987.1										9	2	3				3			
1997.5	1	1				1	7		1			4				3			
2002	2					1										64	6		
2013.9					9	5	2		9	44	2	6				1			
2027	4					3	1			1	1								
2041	2					5			5							6			
2059.4										1		2				2			
2072.8					1	1													
2084.5												1							
2093.2						2													
2109																	14		
2123																13	1		
2138						1													
2155				1		1													
2170.6																2			
2176.5						5	2	2	1	2						25			8
2183.5							5	5								15	16		
2194.3						1						1				2			
2208.5	1					1	4									1			
2219.5					1	12				1		1							
2230.5						1							1				3	5	
2240	3					6	1			2		1							
2250.5							3										4		
2260.5																	2		
2270.5					1											1	4		
2280.3	1								5		1						1		
2290.5	1				1	6	2	1								71	9		
2293.5	1						3	5								59	16		
2301.4						1	4				1	1				4	10		

TABLE S1 TOTAL FORAMINIFER COUNTS OF CORE DIABLITO (DIVERSITY)

Depth (ft)	Depth (m)	Taxa_S	Individuals	Dominance_D	Simpson_1-D	Shannon_H	Evenness_e^H/S	Brillouin	Menhinick	Margalef	Equitability_J	Fisher_alpha	Berger-Parker	Chao-1
1848.7	563.5	2.0	3.0	0.5556	0.4444	0.6365	0.9449	0.3662	1155.0	0.9102	0.9183	2622.0	0.6667	2.0
1883.1	574.0	6	34	0.3495	0.6505	1,295	0.6084	1,103	1,029	1,418	0.7226	2,114	0.5	6.5
1893.11	577.0	2	3	0.5556	0.4444	0.6365	0.9449	0.3662	1,155	0.9102	0.9183	2,622	0.6667	2
1900	579.1	2	6	0.7222	0.2778	0.4506	0.7846	0.2986	0.8165	0.5581	0.65	1,051	0.8333	2
1914.3	583.5	5	6	0.2222	0.7778	1,561	0.9524	0.981	2,041	2,232	0.9697	14.12	0.3333	8
1926.1	587.1	4	9	0.3333	0.6667	1,215	0.8425	0.8702	1,333	1,365	0.8764	2,759	0.4444	5
1940.3	591.4	2	4	0.625	0.375	0.5623	0.8774	0.3466	1	0.7213	0.8113	1,592	0.75	2
1950.5	594.5	9	51	0.2026	0.7974	1,843	0.7019	1,612	1.26	2,035	0.8389	3,171	0.3137	9
1952.7	595.2	12	36	0.1451	0.8549	2,158	0.7209	1,783	2	3.07	0.8683	6,303	0.2222	14.5
1962.8	598.3	2	4	0.625	0.375	0.5623	0.8774	0.3466	1	0.7213	0.8113	1,592	0.75	2
1973.6	601.6	13	59	0.1589	0.8411	2,153	0.6626	1,871	1,692	2,943	0.8395	5,157	0.3051	13.75
1987.1	605.7	3	6	0.5	0.5	0.8676	0.7937	0.5669	1,225	1,116	0.7897	2,388	0.6667	4
1997.5	608.8	11	29	0.1463	0.8537	2,136	0.7697	1,725	2,043	2.97	0.8908	6.46	0.2759	16
2002	610.2	3	3	0.3333	0.6667	1,099	1	0.5973	1,732	1.82	1	0	0.3333	6
2013.9	613.8	5	18	0.3642	0.6358	1,274	0.715	1,006	1,179	1,384	0.7916	2,293	0.5556	5
2027	617.8	9	44	0.4824	0.5176	1,233	0.3812	1,023	1,357	2,114	0.561	3,424	0.6818	14
2041	622.1	7	10	0.18	0.82	1,834	0.8945	1,262	2,214	2,606	0.9427	10.36	0.3	12
2059.4	627.7	7	15	0.1911	0.8089	1,802	0.8659	1,356	1,807	2,216	0.926	5,109	0.3333	7.2
2072.8	631.8	9	44	0.3368	0.6632	1,417	0.4581	1,204	1,357	2,114	0.6447	3,424	0.4773	24
2084.5	635.4	5	27	0.3333	0.6667	1,254	0.7006	1,059	0.9623	1,214	0.7789	1,805	0.4444	6
2093.2	638.0	5	6	0.2222	0.7778	1,561	0.9524	0.981	2,041	2,232	0.9697	14.12	0.3333	8
2109	642.8	1	2	1	0	0	1	0	0.7071	0		0.7959	1	1
2123	647.1	9	16	0.1406	0.8594	2,079	0.8889	1,545	2.25	2,885	0.9464	8,505	0.25	10.2
2138	651.7	5	7	0.2245	0.7755	1.55	0.9421	1.02	1.89	2,056	0.963	7,824	0.2857	6
2155	656.8	11	24	0.1146	0.8854	2,279	0.8882	1,789	2,245	3,147	0.9505	7,859	0.2083	11.5
2170.6	661.6	18	86	0.3445	0.6555	1,767	0.3253	1,528	1,941	3,816	0.6114	6,936	0.5698	29.25
2176.5	663.4	17	73	0.1308	0.8692	2,355	0.6197	2.06	1.99	3,729	0.8311	6,965	0.2329	20
2183.5	665.5	2	5	0.68	0.32	0.5004	0.8247	0.3219	0.8944	0.6213	0.7219	1,235	0.8	2
2194.3	668.8	10	84	0.5082	0.4918	1,105	0.3019	0.9739	1,091	2,031	0.4798	2,958	0.6905	17.5
2208.5	673.2	5	44	0.4339	0.5661	1,098	0.5996	0.9654	0.7538	1,057	0.6822	1,452	0.6136	5
2219.5	676.5	4	16	0.3203	0.6797	1,223	0.8492	0.9826	1	1,082	0.882	1,712	0.375	4
2230.5	679.9	8	52	0.3484	0.6516	1,347	0.4805	1,177	1,109	1,772	0.6476	2.64	0.5192	18
2240	682.8	4	5	0.28	0.72	1,332	0.9473	0.8189	1,789	1,864	0.961	9,284	0.4	5.5
2250.5	686.0	4	76	0.483	0.517	0.9181	0.6261	0.8507	0.4588	0.6927	0.6623	0.8991	0.6447	4
2260.5	689.0	9	30	0.2156	0.7844	1,775	0.6556	1,459	1,643	2,352	0.8079	4,359	0.3333	14
2270.5	692.0	4	17	0.3287	0.6713	1,206	0.8348	0.977	0.9701	1,059	0.8697	1,649	0.4118	4
2280.3	695.0	1	1	1	0	0	1	0	1	0		0	1	1
2290.5	698.1	11	18	0.1173	0.8827	2,274	0.8837	1,691	2,593	3.46	0.9484	12.01	0.2222	14
2293.5	699.1	0	0	0	0	0	0	0	0	0	0	0	0	0
2301.4	701.5	6	29	0.4483	0.5517	1,104	0.5025	0.9082	1,114	1,485	0.6159	2,297	0.6207	12

TABLE S1 TOTAL FORAMINIFER COUNTS OF CORE DIABLITO (MORPHOGROUPS P)					
Depth (ft)	Depth (m)	Total foraminifera	Guembelitria spp.	Heterohelicidae	Total planktonics
1848,7	563.5	3	0	1	1
1883,1	574.0	34	0	0	0
1893,11	577.0	3	0	0	0
1900	579.1	6	0	1	1
1914,3	583.5	6	0	0	0
1926,1	587.1	9	0	0	0
1940,3	591.4	4	0	1	1
1950,5	594.5	51	6	0	7
1952,7	595.2	36	2	0	2
1962,8	598.3	4	0	0	0
1973,6	601.6	59	28	1	35
1987,1	605.7	6	5	0	5
1997,5	608.8	29	1	0	1
2002	610.2	3	0	0	0
2013,9	613.8	18	0	2	3
2027	617.8	44	2	0	2
2041	622.1	10	0	0	0
2059,4	627.7	15	5	0	6
2072,8	631.8	44	22	1	24
2084,5	635.4	27	13	0	13
2093,2	638.0	6	3	0	3
2109	642.8	2	0	0	0
2123	647.1	16	3	0	3
2138	651.7	7	3	0	3
2155	656.8	24	4	2	7
2170,6	661.6	86	50	2	55
2176,5	663.4	73	8	17	40
2183,5	665.5	5	0	0	0
2194,3	668.8	84	72	3	80
2208,5	673.2	44	32	1	35
2219,5	676.5	16	12	0	13
2230,5	679.9	52	39	2	42
2240	682.8	5	2	0	3
2250,5	686.0	76	67	0	67
2260,5	689.0	30	11	1	15
2270,5	692.0	17	13	1	14
2280,3	695.0	1	0	0	0
2290,5	698.1	18	0	1	1
2293,5	699.1	0	0	0	0
2301,4	701.5	29	0	0	0

TABLE S1 TOTAL FORAMINIFER COUNTS OF CORE DIABLITO (MORPHOGROUPS B)										
Depth (ft)	Depth (m)	Total foraminifera	Total planktonics	Total benthonics	Total agglutinated	Total calcareous	Total infauna	Total epifauna	Elongated benthics	*Ammobaculites* spp.
1848,7	563.5	3	1	2	2	0	2	0	0	2
1883,1	574.0	34	0	34	34	0	34	0	0	19
1893,11	577.0	3	0	3	3	0	3	0	0	1
1900	579.1	6	1	5	5	0	5	0	0	0
1914,3	583.5	6	0	6	5	1	6	0	1	1
1926,1	587.1	9	0	9	8	1	8	1	1	0
1940,3	591.4	4	1	3	3	0	3	0	0	0
1950,5	594.5	51	7	44	5	39	11	33	6	5
1952,7	595.2	36	2	34	13	21	10	24	3	2
1962,8	598.3	4	0	4	4	0	4	0	0	0
1973,6	601.6	59	35	24	7	17	9	15	4	0
1987,1	605.7	6	5	1	1	0	1	0	0	0
1997,5	608.8	29	1	28	10	18	10	18	1	1
2002	610.2	3	0	3	0	3	0	3	0	0
2013,9	613.8	18	3	15	15	0	15	0	0	10
2027	617.8	44	2	42	33	9	33	9	0	30
2041	622.1	10	0	10	6	4	8	2	1	3
2059,4	627.7	15	6	9	6	3	7	2	0	2
2072,8	631.8	44	24	20	5	15	19	1	14	1
2084,5	635.4	27	13	14	1	13	13	1	12	0
2093,2	638.0	6	3	3	0	3	2	1	2	0
2109	642.8	2	0	2	2	0	2	0	0	0
2123	647.1	16	3	13	6	7	8	5	1	0
2138	651.7	7	3	4	0	4	1	3	1	0
2155	656.8	24	7	17	4	13	9	8	5	0
2170,6	661.6	86	55	31	2	29	26	5	18	0
2176,5	663.4	73	40	33	8	25	11	22	2	0
2183,5	665.5	5	0	5	1	4	0	5	0	0
2194,3	668.8	84	80	4	1	3	2	2	2	0
2208,5	673.2	44	35	9	0	9	9	0	9	0
2219,5	676.5	16	13	3	0	3	3	0	3	0
2230,5	679.9	52	42	10	0	10	8	2	8	0
2240	682.8	5	3	2	0	2	0	2	0	0
2250,5	686.0	76	67	9	0	9	9	0	9	0
2260,5	689.0	30	15	15	1	14	8	7	7	0
2270,5	692.0	17	14	3	0	3	3	0	3	0
2280,3	695.0	1	0	1	1	0	1	0	0	0
2290,5	698.1	18	1	17	9	8	13	4	4	0
2293,5	699.1	0	0	0	0	0	0	0	0	0
2301,4	701.5	29	0	29	0	29	1	28	1	0

TABLE S2 TOTAL CALCAREOUS NANNOFOSSIL COUNTS OF CORE DIABLITO

				Age		Tur-Maa	Tur-Maa	Cam-Maa	Cam-Maa		Jur-Maa	Tur-Maa	Maa-Eoc	Maa-Mio	San-Maa	Bar-Maa	Alb-Maa	Alb-Pal
Depth (ft)	Depth (m)	Nº Field of View (FOV)	Preservation	Species richness	TOTAL	*Ahmuellerella regularis*	*Ahmuellerella octoradiata*	*Arkhangelskiella cymbiformis*	*Arkhangelskiella maastrichtiensis*	*Arkhangelskiella sp.*	*Biscutum constans*	*Calculites obscurus*	*Cervisiellla operculata*	*Cervisiella saxea*	*Chiastozygus amphipons*	*Chiastozygus litterarius*	*Cribrosphaerella ehrenbergii*	*Cyclagelosphaera reinhardtii*
1895.3	577.7	700	-	0	0													
1921	585.5	700	-	0	0													
1921.2	585.6	700	-	0	0													
1938.5	590.8	700	-	0	0													
1954.7	595.8	700	-	0	0													
1968.2	599.9	700	-	0	0													
1981.3	603.9	700	P	1	2													
1991	606.8	700	P	1	1													
2006	611.4	700	P	3	5													
2033	616.9	700	P	3	5									1				
2057.4	627.1	700	M	15	40		1				1		3			1	2	
2068.3	630.4	700	M	13	24	1					1		1					
2080.1	634	700	P	13	69									5			1	
2091.3	637.4	700	P	12	37			1					3				1	1
2102	640.7	700	P	6	18								2					
2120.5	646.3	700	M	14	58								5	2		2		
2133.2	650.2	700	M	16	203			1					3	3		1	1	
2152	655.9	700	M	14	63			1						1				
2167.5	660.6	700	M	15	165								1	1				
2193.4	668.5	700	P	2	5													
2204.2	671.8	700	P	5	14											1	1	
2216.4	675.6	700	P	13	28			1	1			1	1	1		2	1	
2227.2	678.8	700	P	4	9			1									1	
2242.3	683.4	700	P	3	4									1				
2253.3	686.8	700	M	12	26					1			1	1		3	1	
2265.2	690.4	700	M	18	78				3		1		1		1	17	2	
2278.5	694.4	700	-	0	0													
2288.2	697.4	700	-	0	0	?	?	?	?	?	?	?	?	?	?	?	?	?

Age	Tur-Maa	Alb-Maa	Cen-Maa	Alb-Maa	Apt-Maa	Cen-Maa	Hau-Maa	Cen-Maa	Con-San	San-Maa	Con-Maa		Con-Maa	Con-Maa
Depth (ft)	*Eiffelithus gorkae*	*Eiffelithus turrisseiffelii*	*Helicolithus anceps*	*Helicolithus compactus*	*Helicolithus trabeculatus*	*Kamptnerius magnificus*	*Loxolithus armilla*	*Microrhabdulus decoratus*	*Micula adumbrata*	*Micula concava*	*Micula cubiformis*	*Micula prinsii?*	*Micula staurophora*	*Micula swastica*
1895.3						?								
1921						?								
1921.2						?								
1938.5						?								
1954.7						?								
1968.2						?								
1981.3						?								
1991						1								
2006						1							1	
2033						?					3		1	
2057.4	2			1		7				1			6	
2068.3	1				1	8					1		1	
2080.1				1	1	31				2	2	1	18	
2091.3	1				3	17	2				2		4	
2102	1					9		2					3	
2120.5	1			1		28					1		1	
2133.2	3	1				63		4			10		76	
2152	1	1				13					2		20	
2167.5						47				1	12		85	1
2193.4						4							1	
2204.2						9							1	
2216.4			1			12							3	
2227.2						6								
2242.3						1							2	
2253.3					1	8			1				1	
2265.2	10				1	28	1						2	
2278.5						?								
2288.2	?	?	?	?	?	?	?	?	?	?	?	?	?	?

Age	Cen-Maa	Alb-Maa	Apt-Maa	Cam-Maa	Ber-Maa	Ber-Maa	Apt-Maa	Tur-Maa	Ber-Maa		San-Maa	Cen-Maa	Jur-Maa	Jur-Maa
Depth (ft)	*Placozygus fibuliformis*	*Prediscosphaera cretacea*	*Prediscosphaera spinosa*	*Prediscosphaera stoveri*	*Retecapsa crenulata*	*Retecapsa surirella*	*Rhagodiscus angustus*	*Rhagodiscus reniformis*	*Rhagodiscus splendens*	*Staurolithites laffittei*	*Staurolithites mielnicensis*	*Tetrapodorhabdus decorus*	*Watznaueria barnesiae*	*Zeugrhabdotus erectus*
1895.3														?
1921														?
1921.2														?
1938.5														?
1954.7														?
1968.2														?
1981.3													2	?
1991														?
2006													3	?
2033														?
2057.4		1			1	1						1	11	?
2068.3								1	1	1	1		5	?
2080.1		2			1	2							2	?
2091.3										1			1	?
2102											1			?
2120.5		10	1	3		1					1		1	?
2133.2		23		2		1							2	9
2152		14		1		1			1		1		3	3
2167.5	1	3		2		1	1			1	1		5	2
2193.4														?
2204.2													2	?
2216.4				1		2							1	?
2227.2													1	?
2242.3														?
2253.3		2				1							5	?
2265.2	1	1		2			1		1	1			4	?
2278.5														?
2288.2	?	?	?	?	?	?	?	?	?	?	?	?	?	?

TABLE S3 TOTAL OSTRACOD COUNTS OF CORE DIABLITO

Depth (ft)	Depth (m)	*Buntonia sp.*	*Cythereis sp.*	*Cytherella* cf. *C. piacabucuensis*	*Cytherella sp. 1*	*Cytherella sp. 2*	*Munseyella?* sp.	*Paracosta* sp.	*Paracypris sp.*	*Sapucariella sp.*	*Veenia sp.*
1883.1	574	2	5	3	0	0	0	0	1	0	0
1952.7	595.2	0	0	1	0	0	1	0	0	1	0
1973.6	601.6	0	0	1	0	0	0	0	1	0	0
1987.1	605.7	0	0	0	0	0	0	0	7	0	1
1997.5	608.8	0	0	0	0	0	0	1	0	0	0
2013.9	613.8	0	3	0	0	10	0	0	0	0	20
2059.4	627.7	0	0	0	0	0	0	0	0	0	0
2176.5	663.4	0	0	0	0	0	0	0	0	0	0
2219.5	676.5	0	0	0	2	0	0	0	0	0	0
2240	682.8	0	0	0	1	0	0	0	0	0	0
2301.4	701.5	0	0	0	1	0	0	0	0	0	0

TABLE S4 GEOCHEMICAL DATA (XRF ANALYSES) OF CORE DIABLITO-1 (XRF DATA)

Label	Depth (ft)	Depth (m)	Mg	Al	Si	S	K	Ca	Ti	Cr	Mn	Fe	Ni	Cu	Zn	Rb	Sr	Zr	Ba	Co	V	Ga
DI1885.5	1885.5	574.7	3,792	488,400	6,799,652	189,245	1,840,492	1,243,174	2,349,815	52,348	178,566	39238.91	23,824	26,050	140,768	489,064	772,881	1,118,127	42,229	366,200	189,687	30,141
DI1891.5	1891.5	576.5	0.163	447,529	5,618,966	123,942	1,863,932	634,693	2,067,069	49,569	219,083	40737.35	23,659	26,262	133,559	533,533	739,791	740,069	33,448	366,812	190,291	31,947
DI1895.3	1895.3	577.7	-0.063	624,101	6,736,979	604,437	2,045,107	919,824	2,394,232	51,451	140,543	42059.84	24,375	23,341	105,228	556,701	865,356	849,679	37,636	384,745	195,986	31,558
DI1898	1898	578.5	0.830	559,021	6,579,187	680,543	1,825,657	929,152	2,470,200	54,365	177,164	39108.41	21,382	22,223	151,835	474,931	814,177	2,336,881	36,117	360,813	193,412	29,325
DI1902.8	1902.8	580.0	2,021	565,112	6,351,934	438,991	1,788,430	1,040,482	2,753,996	48,721	1,727,605	66548.64	19,235	21,253	103,212	410,717	748,364	1,175,109	42,214	505,795	192,541	23,945
DI1908.3	1908.3	581.6	1,598	395,891	6,550,258	282,578	1,626,046	461,852	2,280,058	44,319	374,974	38240.25	21,642	19,013	139,295	400,934	653,565	1,293,193	28,351	349,200	174,897	26,399
DI1912.2	1912.2	582.8	1,375	574,671	6,304,188	103,017	1,979,836	1,887,510	2,274,634	47,405	869,606	46563.85	21,384	25,305	130,327	540,634	947,049	771,464	136,779	402,335	181,410	28,927
DI1919.4	1919.4	585.0	-0.185	217,459	4,063,271	282,636	1,222,602	1,772,165	1,565,316	35,089	224,052	27448.14	18,028	17,152	95,081	288,975	597,934	825,892	18,501	256,712	125,673	17,226
DI1921	1921	585.5	0.911	467,016	6,094,880	716,450	1,882,979	1,036,355	2,196,263	51,043	389,355	42681.67	24,321	24,793	143,828	498,813	771,671	940,303	38,828	382,247	182,268	26,290
DI1925.2	1925.2	586.8	-0.062	475,489	6,366,144	863,977	1,768,537	1,264,989	2,257,009	45,422	400,562	44272.94	22,319	23,637	134,987	444,399	726,297	1,343,590	34,087	389,106	173,109	25,409
DI1929.1	1929.1	588.0	3,107	512,148	6,416,586	214,611	1,899,292	1,193,052	2,467,045	50,381	1,235,199	66167.37	19,225	27,212	121,241	449,799	721,189	790,051	39,456	496,667	192,169	26,686
DI1932.3	1932.3	589.0	0.901	514,184	6,978,525	312,295	1,826,215	533,064	2,445,432	46,966	176,442	39801.01	22,524	25,123	119,743	483,803	735,526	1,322,379	44,023	374,894	188,945	29,424
DI1935.6	1935.6	590.0	0.684	585,081	6,907,756	161,346	2,042,282	524,912	2,604,564	52,022	161,081	40228.99	21,387	27,928	119,942	564,266	812,593	939,689	46,927	370,852	204,472	31,643
DI1938.3	1938.3	590.8	-1,333	374,875	5,829,480	204,586	1,673,308	699,059	2,152,792	43,191	194,637	36028.11	18,361	24,692	122,901	427,909	692,218	881,979	31,541	332,453	169,620	27,684
DI1943	1943	592.2	0.349	303,155	6,307,056	245,612	1,209,706	989,046	1,951,884	32,217	190,600	32504.58	18,468	17,519	119,369	297,933	580,727	1,472,107	23,907	301,668	135,322	18,947
DI1946.2	1946.2	593.2	0.946	523,392	6,657,838	253,036	1,871,811	1,314,922	2,415,730	46,521	228,248	41093.5	21,682	23,438	122,526	492,608	887,786	1,216,078	37,722	370,178	177,817	28,970
DI1948.4	1948.4	593.9	0.395	460,882	7,038,848	224,519	1,654,623	1,073,750	2,408,648	46,734	196,539	37859.17	21,035	21,024	115,075	436,179	806,171	1,863,166	32,261	355,005	160,942	27,068
DI1957.8	1957.8	596.7	-2,664	363,064	5,470,054	259,918	1,846,736	658,109	1,992,182	42,336	741,399	43778.93	15,987	19,169	105,699	428,061	718,376	578,050	26,210	368,129	161,291	23,038
DI1960.2	1960.2	597.5	1,075	310,645	5,420,926	227,517	1,583,583	569,063	2,097,983	39,441	355,072	37307.88	19,602	20,089	112,884	391,461	649,980	863,104	24,108	335,195	161,638	21,513
DI1965.6	1965.6	599.1	1,368	358,685	7,038,972	729,891	953,828	778,932	1,572,907	33,113	160,755	38623.22	20,653	14,989	162,130	196,139	512,735	2,364,502	60,774	364,300	110,593	14,200
DI1968.2	1968.2	599.9	2,248	555,969	6,351,745	688,891	2,115,305	561,529	2,294,711	51,083	141,856	42410.2	21,357	21,186	120,802	566,050	1,052,560	903,331	37,897	388,042	197,708	29,851
DI1971.4	1971.4	600.9	2,034	453,823	6,442,867	169,009	1,888,266	1,117,366	2,161,604	51,839	716,875	57831.69	23,717	20,747	157,230	459,029	861,870	970,705	32,183	486,150	171,330	24,093
DI1977.2	1977.2	602.7	2,069	376,801	5,633,484	137,428	1,829,756	696,693	1,991,902	45,461	506,090	42549.48	18,749	17,899	128,737	446,097	730,027	718,553	34,285	369,276	171,377	23,813
DI1981.3	1981.3	603.9	-1,794	401,394	5,655,286	125,389	1,880,471	913,936	1,984,408	51,163	968,647	55935.79	18,242	17,186	99,062	423,166	706,659	654,876	31,518	438,258	166,200	23,404
DI1989	1989	606.2	-1,376	436,003	6,725,188	115,035	1,679,038	638,869	2,202,756	40,708	286,411	39391.85	18,713	21,234	202,239	447,799	652,708	840,627	33,088	363,911	171,108	26,282
DI1991	1991	606.9	-0.371	517,038	6,540,108	29,273	2,059,742	649,622	2,381,289	51,424	367,980	47246.14	25,818	27,626	176,198	538,965	806,157	796,682	39,079	411,214	190,222	33,624
DI1993	1993	607.5	-1,350	408,435	5,719,448	377,801	1,908,946	785,927	2,015,708	50,787	142,042	38756.35	22,418	23,201	119,593	508,345	723,414	626,067	30,105	341,391	178,270	29,035
DI1995	1995	608.1	1,006	545,309	6,581,958	336,503	2,123,590	900,979	2,291,144	52,878	180,834	45667.07	25,971	25,899	141,003	581,964	881,344	723,546	38,148	404,389	197,055	28,649
DI2010.2	2010.2	612.7	-1,670	419,947	5,753,985	79,127	1,986,524	367,790	1,987,566	49,252	125,658	38785.13	20,699	22,828	117,193	513,114	695,754	635,486	31,341	352,653	168,367	26,827
DI2016	2016	614.5	-0.386	467,071	6,662,553	908,958	1,768,191	1,145,282	2,204,430	50,664	237,308	44125.52	22,268	17,575	136,495	438,593	717,010	1,264,724	30,897	394,803	178,525	24,541
DI2022.2	2022.2	616.4	0.715	443,703	6,451,658	356,113	1,832,474	1,525,095	2,145,620	51,327	294,940	45004.63	21,063	17,615	141,800	459,182	785,667	1,224,056	40,377	387,460	177,105	24,861
DI2033	2033	619.7	1,926	434,500	6,632,869	876,345	1,723,157	1,549,494	2,266,376	45,540	275,985	40870.89	21,213	14,129	133,907	441,365	785,736	1,467,253	31,923	375,206	161,965	23,533
DI2037.9	2037.9	621.2	1,611	385,051	6,949,981	303,721	1,566,925	1,694,169	2,104,948	44,920	331,356	41271.81	18,667	13,288	123,711	398,746	729,644	1,754,454	31,993	370,924	145,514	21,798
DI2046.5	2046.5	623.8	5,821	363,762	6,416,917	557,295	1,190,079	1206769	1,733,150	36,883	429,873	37735.18	17,165	11,042	81,545	210,912	761,649	1,727,191	27,257	314,607	104,165	10,192
DI2050.3	2050.3	624.9	4,796	360,072	6,697,964	882,963	1,343,129	2,955,679	1,995,285	40,417	230,818	40218.52	19,354	13,565	109,006	294,776	672,972	1,953,568	31,803	360,897	134,481	19,320
DI2055.8	2055.8	626.6	0.585	323,313	6,224,625	482,191	1,417,610	2,365,121	1,938,110	43,346	189,837	39410.13	18,039	14,806	130,920	306,129	590,533	1,652,986	25,500	340,994	137,499	17,558
DI2057.4	2057.4	627.1	3,583	451,411	6,871,311	338,186	1,970,097	1,539,046	2,210,389	52,292	379,552	46340.45	21,465	19,610	119,820	485,796	820,786	1,010,985	32,260	402,450	170,599	25,231
DI2062.9	2062.9	628.8	1,644	517,898	6,487,654	431,930	2,030,517	1,341,205	2,284,640	50,054	334,947	44295.44	20,735	17,434	131,913	534,336	822,197	1,019,917	33,861	393,841	170,976	26,760
DI2065.8	2065.8	629.7	-1,705	270,489	5,691,627	943,266	1,329,755	1,007,839	1,711,527	32,555	355,118	46170.17	15,255	12,696	162,668	281,236	508,900	1,185,518	23,318	384,586	120,543	16,470
DI2068.3	2068.3	630.4	-1,364	356,352	5,478,753	180,202	1,704,959	1,215,515	1,934,379	41,348	476,323	42517.82	18,554	12,887	113,882	411,739	710,471	888,432	23,629	373,530	142,928	22,461
DI2070.1	2070.1	631.0	2,233	457,952	6,192,479	177,982	1,900,932	1,170,136	2,143,888	42,077	553,516	45237.75	18,614	17,226	127,184	494,401	872,276	945,629	33,807	390,156	166,032	28,278
DI2075.3	2075.3	632.6	4,967	419,660	5,666,258	190,265	1,724,182	2,315,811	1,923,158	53,817	1,775,721	105439	18,196	18,081	109,800	337,477	653,824	681,903	25,994	646,393	152,781	17,554
DI2078.4	2078.4	633.5	1,025	564,883	6,962,646	229,650	2,116,028	1,448,306	2,258,417	55,234	315,659	47120.64	20,615	17,050	135,644	543,657	913,520	907,706	32,664	407,980	183,940	30,281
DI2082.1	2082.1	634.6	-0.914	383,691	5,625,196	652,110	1,654,194	1,917,374	1,905,098	40,708	188,208	32577.78	18,433	11,968	99,863	414,210	802,517	1,050,405	25,704	298,570	133,558	21,369
DI2088.5	2088.5	636.6	0.774	502,200	6,970,014	368,943	1,904,309	2,615,735	2,189,678	44,255	291,284	40446.2	19,571	14,885	136,861	479,811	938,075	1,477,653	33,586	367,705	152,623	24,516
DI2091.3	2091.3	637.4	-0.549	393,878	6,146,256	448,653	1,756,500	2,249,596	2,034,718	41,924	221,881	35199.58	16,955	13,675	126,095	439,934	879,914	1,159,121	26,042	315,397	150,868	21,770
DI2102	2102	640.7	-0.042	365,525	5,314,469	143,073	1,834,350	839,951	1,786,126	43,876	224,535	36441.14	16,445	16,239	119,357	455,727	715,915	593,069	23,730	316,543	153,974	24,999
DI2105.5	2105.5	641.8	0.069	364,440	5,546,060	189,460	1,881,147	1,029,825	1,908,592	45,073	260,080	37389.81	17,852	18,082	142,836	478,399	708,292	773,256	28,785	334,926	162,474	24,451
DI2113	2113	644.0	-0.177	547,917	6,422,609	138,618	2,212,216	911,995	2,132,834	52,436	128,817	39343.29	21,632	18,554	144,082	629,248	911,524	756,716	35,653	356,603	182,738	31,381
DI2115	2115	644.7	0.754	123,655	2,869,726	70,337	1,115,313	757,632	1,097,556	27,882	163,257	24653.18	10,987	9,273	92,698	269,359	440,327	341,711	16,908	220,864	92,008	15,518
DI2117.8	2117.8	645.5	-2,659	402,356	5,594,073	148,304	1,958,121	1,902,160	1,868,437	51,373	747,809	66829.57	19,274	15,442	140,169	440,929	735,099	513,319	24,499	494,045	142,505	21,962
DI2120.5	2120.5	646.3	1,347	505,129	6,089,473	99,480	2,133,182	1,592,056	2,011,334	52,025	642,702	62479.19	19,543	16,842	142,738	527,026	842,905	609,791	35,154	486,809	163,419	26,298
DI2127	2127	648.3	-0.064	499,385	6,521,632	691,427	1,943,975	2,010,388	2,269,187	47,777	239,182	43124.97	21,402	18,073	124,171	504,077	1,021,399	1,158,190	33,249	381,558	176,223	27,176
DI2129.3	2129.3	649.0	-0.286	441,444	6,479,621	385,340	1,710,022	2,823,275	2,124,096	40,481	251,300	40152.92	18,486	14,546	134,970	447,401	941,657	1,546,987	30,850	359,757	139,952	21,364
DI2133.2	2133.2	650.2	0.395	549,400	6,816,008	375,799	1,997,990	1,996,401	2,262,092	51,005	281,054	43522.09	18,366	17,468	129,904	517,255	1,000,339	1,096,155	36,650	384,856	170,223	29,364
DI2135.2	2135.2	650.8	0.654	567,748	6,608,583	321,345	2,061,221	1,508,236	2,276,333	50,608	195,624	41410.52	19,822	19,471	111,009	557,948	1,033,896	954,604	34,780	378,821	170,726	30,224
DI2152	2152	655.9	-1,770	368,158	6,005,607	193,224	1,732,808	1,437,891	2,039,355	38,848	307,380	35388.4	18,244	15,108	128,702	432,795	844,341	1,123,605	29,735	325,886	150,802	23,974
DI2162.4	2162.4	659.1	2,579	363,006	5,532,771	308,601	1,628,733	1,399,833	1,936,301	40,258	293,206	34756.44	17,814	14,877	119,511	403,820	774,645	868,969	25,486	311,981	144,341	24,149
DI2165.6	2165.6	660.1	1,438	554,485	6,609,021	397,296	1,985,246	1,740,977	2,202,157	51,089	261,704	43691.2	21,220	19,417	138,785	534,427	918,156	891,842	34,886	395,414	174,907	27,331
DI2167.5	2167.5	660.7	2,418	523,244	6,326,666	429,793	1,978,082	2,200,130	2,038,151	52,311	341,407	49860	20,984	17,733	143,259	517,727	921,181	718,839	27,368	428,670	166,483	27,446
DI2174.7	2174.7	662.8	-3,231	424,353	4,942,655	973,521	1,737,960	6,803,201	1,487,801	50,498	223,266	39618.75	21,099	14,460	120,853	417,950	1,042,131	501,637	28,345	342,890	122,518	22,063
DI2178.6	2178.6	664.0	2,410	103,670	2,305,341	568,683	970,206	999,728	918,724	30,304	63,284	20331.85	11,575	7,071	67,222	243,848	327,991	292,300	13,062	191,752	81,171	12,303
DI2181	2181	664.8	-0.086	505,469	6,106,099	926,945	2,074,693	3,297,941	1,897,137	53,449	207,429	43939.46	22,362	15,489	145,519	545,143	914,925	696,904	45,384	384,234	159,948	25,409
DI2185.2	2185.2	666.0	0.064	416,541	6,270,295	233,877	1,838,274	930,365	2,183,183	50,208	322,902	45007.72	21,647	23,389	134,857	449,143	679,083	913,677	29,478	392,087	177,890	24,783
DI2190.8	2190.8	667.8	-0.766	403,194	5,378,551	594,743	1,806,764	1,188,634	1,993,521	44,595	252,028	40029.71	22,409	21,861	125,047	451,855	695,351	720,686	23,811	355,290	175,041	23,798
DI2193.4	2193.4	668.5	2,214	496,219	6,566,247	552,047	2,113,384	1,230,831	2,269,320	52,953	349,126	46214.77	23,483	29,372	129,516	564,301	770,943	809,368	26,553	402,161	197,522	28,623
DI2196.5	2196.5	669.5	-1,110	442,236	6,553,770	340,566	2,002,773	1,202,437	2,256,448	55,388	393,515	45566.12	22,771	27,755	149,706	490,940	740,802	899,499	35,731	391,764	191,351	28,163
DI2201	2201	670.9	1,124	512,451	6,725,041	351,021	2,097,240	1,314,999	2,341,347	57,003	445,571	47702.89	25,852	25,827	162,164	539,005	845,719	879,058	39,770	422,141	206,012	28,421
DI2206.4	2206.4	672.5	2,027	432,493	5,999,218	267,294	1,938,214	1,357,597	2,104,082	54,140	485,278	48616.73	21,878	24,103	141,679	524,824	769,580	774,750	30,329	428,138	174,995	28,316
DI2210	2210	673.6	-0.327	295,487	4,853,069	318,492	1,531,135	1,960,840	1,678,649	46,710	361,694	44145.77	16,386	15,902	91,303	351,095	597,995	568,685	23,165	366,477	148,571	17,200
DI2211.9	2211.9	674.2	0.812	386,836	5,752,362	1,062,275	2,218,738	1124355	1,245,192	110,664	256,540	56969.39	18,074	11,088	157,330	382,503	1,000,144	640,695	21,469	458,653	111,445	10,154
DI2220.7	2220.7	676.9	3,302	372,204	6,149,894	254,595	1,712,812	1,226,628	2,058,980	47,953	327,822	40981.69	21,594	18,531	124,536	406,200	673,034	960,870	28,900	360,551	156,424	21,789
DI2225	2225	678.2	-3,083	419,206	5,924,952	372,962	1,768,202	1,217,776	2,027,074	45,196	272,956	38844.89	20,729	15,767	121,349	419,787	653,378	942,174	28,518	343,236	170,477	22,771
DI2227.2	2227.2	678.9	1,249	375,431	5,850,775	466,853	1,775,768	1,308,223	2,040,119	52,187	328,123	42649.86	23,246	17,707	155,988	439,530	704,614	995,485	26,893	376,692	167,105	24,846
DI2233.7	2233.7	680.8	1,575	509,575	6,520,157	496,078	2,054,963	1,443,159	2,200,954	49,310	457,815	49979.36	22,153	20,739	137,918	513,113	799,205	806,849	45,470	436,884	182,223	27,906
DI2235	2235	681.2	-0.783	391,701	5,783,625	383,428	1,892,860	932,751	1,989,850	51,969	279,616	39543.75	20,362	21,290	114,890	465,918	668,818	698,231	34,419	352,453	177,012	26,150
DI2237.3	2237.3	681.9	2,706	398,754	5,937,286	475,755	1,818,432	1,792,752	1,984,215	45,053	244,471	38940.95	22,665	15,683	121,202	445,536	722,271	829,686	23,835	351,079	162,399	25,385
DI2242.3	2242.3	683.5	1,659	472,116	6,501,291	695,151	2,016,501	1,975,099	2,142,899	53,423	321,460	45810.85	22,607	20,071	156,620	522,003	821,390	897,886	33,251	409,041	180,076	26,787
DI2245.5	2245.5	684.4	-2,589	371,276	5,328,136	587,934	1,851,182	1,466,734	1,851,782	48,482	195,443	36505.18	20,049	18,929	115,841	460,277	718,900	624,091	26,527	323,748	158,621	23,374
DI2247.2	2247.2	684.9	-1,758	378,785	5,485,221	349,613	1,816,610	1,418,420	1,881,505	47,034	289,475	39982.98	21,768	17,747	124,982	445,764	652,266	637,721	25,389	357,475	162,285	22,892
DI2253.3	2253.3	686.8	-0.251	536,524	6,625,185	292,421	2,132,072	1,328,186	2,195,579	51,727	256,721	41974.73	24,118	19,159	133,527	587,271	893,724	828,959	36,222	381,812	192,862	27,709
DI2255.2	2255.2	687.4	0.498	232,181	4,142,027	211,130	1,494,181	970,397	1,543,651	42,979	176,099	29444.96	17,101	14,661	91,863	366,230	573,300	517,172	19,643	271,837	136,038	20,019
DI2258.4	2258.4	688.4	0.067	509,444	6,764,026	336,093	2,199,196	1,847,026	2,190,850	55,074	279,966	43550.53	25,944	21,880	148,879	575,283	907,114	786,823	34,794	384,533	181,703	28,698
DI2263.7	2263.7	690.0	-0.585	340,924	5,238,537	239,522	1,750,110	1,543,911	1,759,522	43,925	307,928	39917.38	19,733	16,961	120,702	416,533	656,156	581,929	24,827	341,336	152,093	22,216
DI2265.2	2265.2	690.4	2,431	491,877	6,756,701	205,788	2,171,408	1,461,667	2,109,101	58,124	362,366	50979.32	22,611	19,915	144,022	538,365	837,996	719,076	31,169	437,949	183,232	27,536
DI2268.5	2268.5	691.4	0.464	344,152	5,391,060	503,912	1,763,341	2,010,757	1,734,205	50,219	245,438	40990.62	20,066	16,093	117,708	428,256	682,315	585,286	27,410	351,577	152,145	23,493
DI2271.4	2271.4	692.3	3,551	439,175	6,445,742	1,209,871	2,693,324	4,858,664	1,499,205	147,135	200,565	75341.88	23,868	11,589	217,841	551,364	754,517	456,037	25,217	567,349	144,816	14,762
DI2275.4	2275.4	693.5	0.790	507,865	6,466,570	86,574	2,323,852	705,360	2,205,622	51,690	472,008	48190.85	20,276	18,825	112,234	592,448	950,954	731,555	37,500	413,856	180,959	30,660
DI2278.5	2278.5	694.5	-1,302	373,622	5,698,839	115,654	1,988,060	432,920	2,015,067	43,693	118,142	38834.86	19,111	16,068	117,376	491,627	690,594	680,939	25,273	341,783	163,709	25,371
DI2283.2	2283.2	695.9	2,335	523,026	6,253,502	104,870	2,209,273	738,083	2,266,788	52,903	261,705	47571.64	22,302	20,450	161,000	582,653	883,579	827,578	26,001	410,393	195,998	30,257
DI2284.2	2284.2	696.2	0.915	554,702	6,666,957	112,664	2,321,289	869,056	2,278,827	50,445	295,224	56550	21,529	17,958	149,380	550,690	883,983	769,718	29,222	471,955	193,619	28,237
DI2286.5	2286.5	696.9	0.037	557,186	6,603,213	634,630	2,347,524	1,212,485	2,147,494	56,233	119,879	48914.56	21,055	18,503	152,559	601,580	1,004,138	735,194	37,979	432,659	184,191	30,103
DI2297.5	2297.5	700.3	3,002	191,694	3,326,606	210,908	1,353,488	295,960	1,256,844	32,279	61,890	28245.93	11,914	9,444	85,163	318,900	476,921	373,763	16,900	249,946	106,819	18,905

TABLE S4 GEOCHEMICAL DATA (XRF ANALYSES) OF CORE DIABLITO-1 (XRF DATA NORMALIZED)

Depth (meters)	Mg NMS	Al NMS	Si NMS	S NMS	K NMS	Ca NMS	Ti NMS	Cr NMS	Mn NMS	Fe NMS	Ni NMS	Cu NMS	Zn NMS	Rb NMS	Sr NMS	Zr NMS	Ba NMS	Co NMS	V NMS	Ga NMS
574.7004	0.02	2.98	41.50	1.16	11.23	7.59	14.34	0.32	1.09	0.24	0.15	0.16	0.86	2.99	4.72	6.82	0.26	2.24	1.16	0.18
576.5292	0.00	3.22	40.47	0.89	13.42	4.57	14.89	0.36	1.58	0.29	0.17	0.19	0.96	3.84	5.33	5.33	0.24	2.64	1.37	0.23
577.68744	0.00	3.75	40.50	3.63	12.30	5.53	14.39	0.31	0.84	0.25	0.15	0.14	0.63	3.35	5.20	5.11	0.23	2.31	1.18	0.19
578.5104	0.00	3.15	37.05	3.83	10.28	5.23	13.91	0.31	1.00	0.22	0.12	0.13	0.86	2.67	4.59	13.16	0.20	2.03	1.09	0.17
579.97344	0.01	3.13	35.24	2.44	9.92	5.77	15.28	0.27	9.58	0.37	0.11	0.12	0.57	2.28	4.15	6.52	0.23	2.81	1.07	0.13
581.64984	0.01	2.61	43.20	1.86	10.72	3.05	15.04	0.29	2.47	0.25	0.14	0.13	0.92	2.64	4.31	8.53	0.19	2.30	1.15	0.17
582.83856	0.01	3.33	36.49	0.60	11.46	10.93	13.17	0.27	5.03	0.27	0.12	0.15	0.75	3.13	5.48	4.47	0.79	2.33	1.05	0.17
585.03312	0.00	1.86	34.81	2.42	10.48	15.18	13.41	0.30	1.92	0.24	0.15	0.15	0.81	2.48	5.12	7.08	0.16	2.20	1.08	0.15
585.5208	0.00	2.94	38.31	4.50	11.83	6.51	13.80	0.32	2.45	0.27	0.15	0.16	0.90	3.14	4.85	5.91	0.24	2.40	1.15	0.17
586.80096	0.00	2.83	37.89	5.14	10.52	7.53	13.43	0.27	2.38	0.26	0.13	0.14	0.80	2.64	4.32	8.00	0.20	2.32	1.03	0.15
587.98968	0.02	3.02	37.88	1.27	11.21	7.04	14.56	0.30	7.29	0.39	0.11	0.16	0.72	2.66	4.26	4.66	0.23	2.93	1.13	0.16
588.96504	0.00	3.17	43.03	1.93	11.26	3.29	15.08	0.29	1.09	0.25	0.14	0.15	0.74	2.98	4.53	8.15	0.27	2.31	1.16	0.18
589.97088	0.00	3.61	42.59	0.99	12.59	3.24	16.06	0.32	0.99	0.25	0.13	0.17	0.74	3.48	5.01	5.79	0.29	2.29	1.26	0.20
590.79384	-0.01	2.69	41.83	1.47	12.01	5.02	15.45	0.31	1.40	0.26	0.13	0.18	0.88	3.07	4.97	6.33	0.23	2.39	1.22	0.20
592.2264	0.00	2.13	44.27	1.72	8.49	6.94	13.70	0.23	1.34	0.23	0.13	0.12	0.84	2.09	4.08	10.33	0.17	2.12	0.95	0.13
593.20176	0.00	3.13	39.79	1.51	11.19	7.86	14.44	0.28	1.36	0.25	0.13	0.14	0.73	2.94	5.31	7.27	0.23	2.21	1.06	0.17
593.87232	0.00	2.71	41.45	1.32	9.74	6.32	14.18	0.28	1.16	0.22	0.12	0.12	0.68	2.57	4.75	10.97	0.19	2.09	0.95	0.16
596.73744	-0.02	2.62	39.47	1.88	13.33	4.75	14.37	0.31	5.35	0.32	0.12	0.14	0.76	3.09	5.18	4.17	0.19	2.66	1.16	0.17
597.46896	0.01	2.35	40.94	1.72	11.96	4.30	15.84	0.30	2.68	0.28	0.15	0.15	0.85	2.96	4.91	6.52	0.18	2.53	1.22	0.16
599.11488	0.01	2.32	45.45	4.71	6.16	5.03	10.16	0.21	1.04	0.25	0.13	0.10	1.05	1.27	3.31	15.27	0.39	2.35	0.71	0.09
599.90736	0.01	3.44	39.34	4.27	13.10	3.48	14.21	0.32	0.88	0.26	0.13	0.13	0.75	3.51	6.52	5.60	0.23	2.40	1.22	0.18
600.88272	0.01	2.79	39.60	1.04	11.61	6.87	13.29	0.32	4.41	0.36	0.15	0.13	0.97	2.82	5.30	5.97	0.20	2.99	1.05	0.15
602.65056	0.01	2.71	40.47	0.99	13.14	5.00	14.31	0.33	3.64	0.31	0.13	0.13	0.92	3.20	5.24	5.16	0.25	2.65	1.23	0.17
603.90024	-0.01	2.75	38.70	0.86	12.87	6.25	13.58	0.35	6.63	0.38	0.12	0.12	0.68	2.90	4.84	4.48	0.22	3.00	1.14	0.16
606.2472	-0.01	2.92	45.02	0.77	11.24	4.28	14.74	0.27	1.92	0.26	0.13	0.14	1.35	3.00	4.37	5.63	0.22	2.44	1.15	0.18
606.8568	0.00	3.30	41.69	0.19	13.13	4.14	15.18	0.33	2.35	0.30	0.16	0.18	1.12	3.44	5.14	5.08	0.25	2.62	1.21	0.21
607.4664	-0.01	2.91	40.71	2.69	13.59	5.59	14.35	0.36	1.01	0.28	0.16	0.17	0.85	3.62	5.15	4.46	0.21	2.43	1.27	0.21
608.076	0.01	3.39	40.86	2.09	13.18	5.59	14.22	0.33	1.12	0.28	0.16	0.16	0.88	3.61	5.47	4.49	0.24	2.51	1.22	0.18
612.70896	-0.01	3.14	42.97	0.59	14.83	2.75	14.84	0.37	0.94	0.29	0.15	0.17	0.88	3.83	5.20	4.75	0.23	2.63	1.26	0.20
614.4768	0.00	2.79	39.86	5.44	10.58	6.85	13.19	0.30	1.42	0.26	0.13	0.11	0.82	2.62	4.29	7.57	0.18	2.36	1.07	0.15
616.36656	0.00	2.70	39.28	2.17	11.16	9.29	13.06	0.31	1.80	0.27	0.13	0.11	0.86	2.80	4.78	7.45	0.25	2.36	1.08	0.15
619.6584	0.01	2.51	38.33	5.06	9.96	8.95	13.10	0.26	1.59	0.24	0.12	0.08	0.77	2.55	4.54	8.48	0.18	2.17	0.94	0.14
621.15192	0.01	2.26	40.80	1.78	9.20	9.95	12.36	0.26	1.95	0.24	0.11	0.08	0.73	2.34	4.28	10.30	0.19	2.18	0.85	0.13
623.7732	0.04	2.39	42.09	3.66	7.81	7.92	11.37	0.24	2.82	0.25	0.11	0.07	0.53	1.38	5.00	11.33	0.18	2.06	0.68	0.07
624.93144	0.03	1.98	36.88	4.86	7.40	16.27	10.99	0.22	1.27	0.22	0.11	0.07	0.60	1.62	3.71	10.76	0.18	1.99	0.74	0.11
626.60784	0.00	1.99	38.29	2.97	8.72	14.55	11.92	0.27	1.17	0.24	0.11	0.09	0.81	1.88	3.63	10.17	0.16	2.10	0.85	0.11
627.09552	0.02	2.66	40.49	1.99	11.61	9.07	13.02	0.31	2.24	0.27	0.13	0.12	0.71	2.86	4.84	5.96	0.19	2.37	1.01	0.15
628.77192	0.01	3.10	38.86	2.59	12.16	8.03	13.68	0.30	2.01	0.27	0.12	0.10	0.79	3.20	4.92	6.11	0.20	2.36	1.02	0.16
629.65584	-0.01	1.92	40.37	6.69	9.43	7.15	12.14	0.23	2.52	0.33	0.11	0.09	1.15	1.99	3.61	8.41	0.17	2.73	0.86	0.12
630.41784	-0.01	2.52	38.73	1.27	12.05	8.59	13.67	0.29	3.37	0.30	0.13	0.09	0.80	2.91	5.02	6.28	0.17	2.64	1.01	0.16
630.96648	0.01	2.90	39.24	1.13	12.05	7.42	13.59	0.27	3.51	0.29	0.12	0.11	0.81	3.13	5.53	5.99	0.21	2.47	1.05	0.18
632.55144	0.03	2.49	33.65	1.13	10.24	13.75	11.42	0.32	10.54	0.63	0.11	0.11	0.65	2.00	3.88	4.05	0.15	3.84	0.91	0.10
633.49632	0.01	3.29	40.50	1.34	12.31	8.42	13.14	0.32	1.84	0.27	0.12	0.10	0.79	3.16	5.31	5.28	0.19	2.37	1.07	0.18
634.62408	0.00	2.51	36.82	4.27	10.83	12.55	12.47	0.27	1.23	0.21	0.12	0.08	0.65	2.71	5.25	6.88	0.17	1.95	0.87	0.14
636.5748	0.00	2.70	37.53	1.99	10.25	14.08	11.79	0.24	1.57	0.22	0.11	0.08	0.74	2.58	5.05	7.96	0.18	1.98	0.82	0.13
637.42824	0.00	2.39	37.30	2.72	10.66	13.65	12.35	0.25	1.35	0.21	0.10	0.08	0.77	2.67	5.34	7.03	0.16	1.91	0.92	0.13
640.6896	0.00	2.81	40.80	1.10	14.08	6.45	13.71	0.34	1.72	0.28	0.13	0.12	0.92	3.50	5.50	4.55	0.18	2.43	1.18	0.19
641.7564	0.00	2.61	39.75	1.36	13.48	7.38	13.68	0.32	1.86	0.27	0.13	0.13	1.02	3.43	5.08	5.54	0.21	2.40	1.16	0.18
644.0424	0.00	3.50	40.97	0.88	14.11	5.82	13.61	0.33	0.82	0.25	0.14	0.12	0.92	4.01	5.82	4.83	0.23	2.27	1.17	0.20
644.652	0.00	1.59	36.98	0.91	14.37	9.76	14.14	0.36	2.10	0.32	0.14	0.12	1.19	3.47	5.67	4.40	0.22	2.85	1.19	0.20
645.50544	-0.02	2.63	36.60	0.97	12.81	12.45	12.22	0.34	4.89	0.44	0.13	0.10	0.92	2.88	4.81	3.36	0.16	3.23	0.93	0.14
646.3284	0.01	3.15	37.92	0.62	13.28	9.91	12.52	0.32	4.00	0.39	0.12	0.10	0.89	3.28	5.25	3.80	0.22	3.03	1.02	0.16
648.3096	0.00	2.82	36.78	3.90	10.96	11.34	12.80	0.27	1.35	0.24	0.12	0.10	0.70	2.84	5.76	6.53	0.19	2.15	0.99	0.15
649.01064	0.00	2.46	36.09	2.15	9.53	15.73	11.83	0.23	1.40	0.22	0.10	0.08	0.75	2.49	5.25	8.62	0.17	2.00	0.78	0.12
650.19936	0.00	3.09	38.35	2.11	11.24	11.23	12.73	0.29	1.58	0.24	0.10	0.10	0.73	2.91	5.63	6.17	0.21	2.17	0.96	0.17
650.80896	0.00	3.35	39.01	1.90	12.17	8.90	13.44	0.30	1.15	0.24	0.12	0.11	0.66	3.29	6.10	5.63	0.21	2.24	1.01	0.18
655.9296	-0.01	2.41	39.38	1.27	11.36	9.43	13.37	0.25	2.02	0.23	0.12	0.10	0.84	2.84	5.54	7.37	0.19	2.14	0.99	0.16
659.09952	0.02	2.55	38.84	2.17	11.43	9.83	13.59	0.28	2.06	0.24	0.13	0.10	0.84	2.83	5.44	6.10	0.18	2.19	1.01	0.17
660.07488	0.01	3.26	38.87	2.34	11.68	10.24	12.95	0.30	1.54	0.26	0.12	0.11	0.82	3.14	5.40	5.25	0.21	2.33	1.03	0.16
660.654	0.01	3.09	37.37	2.54	11.68	12.99	12.04	0.31	2.02	0.29	0.12	0.10	0.85	3.06	5.44	4.25	0.16	2.53	0.98	0.16
662.84856	-0.02	2.20	25.59	5.04	9.00	35.22	7.70	0.26	1.16	0.21	0.11	0.07	0.63	2.16	5.40	2.60	0.15	1.78	0.63	0.11
664.03728	0.03	1.43	31.88	7.86	13.42	13.83	12.71	0.42	0.88	0.28	0.16	0.10	0.93	3.37	4.54	4.04	0.18	2.65	1.12	0.17
664.7688	0.00	2.80	33.79	5.13	11.48	18.25	10.50	0.30	1.15	0.24	0.12	0.09	0.81	3.02	5.06	3.86	0.25	2.13	0.89	0.14
666.04896	0.00	2.75	41.42	1.55	12.14	6.15	14.42	0.33	2.13	0.30	0.14	0.15	0.89	2.97	4.49	6.04	0.19	2.59	1.18	0.16
667.75584	0.00	2.82	37.57	4.15	12.62	8.30	13.92	0.31	1.76	0.28	0.16	0.15	0.87	3.16	4.86	5.03	0.17	2.48	1.22	0.17
668.54832	0.01	2.98	39.41	3.31	12.69	7.39	13.62	0.32	2.10	0.28	0.14	0.18	0.78	3.39	4.63	4.86	0.16	2.41	1.19	0.17
669.4932	-0.01	2.72	40.28	2.09	12.31	7.39	13.87	0.34	2.42	0.28	0.14	0.17	0.92	3.02	4.55	5.53	0.22	2.41	1.18	0.17
670.8648	0.01	3.00	39.40	2.06	12.29	7.70	13.72	0.33	2.61	0.28	0.15	0.15	0.95	3.16	4.96	5.15	0.23	2.47	1.21	0.17
672.51072	0.01	2.77	38.44	1.71	12.42	8.70	13.48	0.35	3.11	0.31	0.14	0.15	0.91	3.36	4.93	4.96	0.19	2.74	1.12	0.18
673.608	0.00	2.22	36.52	2.40	11.52	14.76	12.63	0.35	2.72	0.33	0.12	0.12	0.69	2.64	4.50	4.28	0.17	2.76	1.12	0.13
674.18712	0.00	2.57	38.28	7.07	14.77	7.48	8.29	0.74	1.71	0.38	0.12	0.07	1.05	2.55	6.66	4.26	0.14	3.05	0.74	0.07
676.86936	0.02	2.49	41.09	1.70	11.44	8.20	13.76	0.32	2.19	0.27	0.14	0.12	0.83	2.71	4.50	6.42	0.19	2.41	1.05	0.15
678.18	-0.02	2.83	39.97	2.52	11.93	8.22	13.68	0.30	1.84	0.26	0.14	0.11	0.82	2.83	4.41	6.36	0.19	2.32	1.15	0.15
678.85056	0.01	2.47	38.56	3.08	11.70	8.62	13.45	0.34	2.16	0.28	0.15	0.12	1.03	2.90	4.64	6.56	0.18	2.48	1.10	0.16
680.83176	0.01	3.04	38.87	2.96	12.25	8.60	13.12	0.29	2.73	0.30	0.13	0.12	0.82	3.06	4.76	4.81	0.27	2.60	1.09	0.17
681.228	0.00	2.73	40.37	2.68	13.21	6.51	13.89	0.36	1.95	0.28	0.14	0.15	0.80	3.25	4.67	4.87	0.24	2.46	1.24	0.18
681.92904	0.02	2.58	38.41	3.08	11.76	11.60	12.84	0.29	1.58	0.25	0.15	0.10	0.78	2.88	4.67	5.37	0.15	2.27	1.05	0.16
683.45304	0.01	2.73	37.55	4.01	11.65	11.41	12.38	0.31	1.86	0.26	0.13	0.12	0.90	3.01	4.74	5.19	0.19	2.36	1.04	0.15
684.4284	-0.02	2.61	37.46	4.13	13.01	10.31	13.02	0.34	1.37	0.26	0.14	0.13	0.81	3.24	5.05	4.39	0.19	2.28	1.12	0.16
684.94656	-0.01	2.67	38.70	2.47	12.82	10.01	13.28	0.33	2.04	0.28	0.15	0.13	0.88	3.15	4.60	4.50	0.18	2.52	1.15	0.16
686.80584	0.00	3.23	39.95	1.76	12.85	8.01	13.24	0.31	1.55	0.25	0.15	0.12	0.81	3.54	5.39	5.00	0.22	2.30	1.16	0.17
687.38496	0.00	2.14	38.11	1.94	13.75	8.93	14.20	0.40	1.62	0.27	0.16	0.13	0.85	3.37	5.27	4.76	0.18	2.50	1.25	0.18
688.36032	0.00	2.94	39.05	1.94	12.70	10.66	12.65	0.32	1.62	0.25	0.15	0.13	0.86	3.32	5.24	4.54	0.20	2.22	1.05	0.17
689.97576	0.00	2.50	38.47	1.76	12.85	11.34	12.92	0.32	2.26	0.29	0.14	0.12	0.89	3.06	4.82	4.27	0.18	2.51	1.12	0.16
690.43296	0.01	2.96	40.62	1.24	13.06	8.79	12.68	0.35	2.18	0.31	0.14	0.12	0.87	3.24	5.04	4.32	0.19	2.63	1.10	0.17
691.4388	0.00	2.38	37.21	3.48	12.17	13.88	11.97	0.35	1.69	0.28	0.14	0.11	0.81	2.96	4.71	4.04	0.19	2.43	1.05	0.16
692.32272	0.02	2.16	31.69	5.95	13.24	23.89	7.37	0.72	0.99	0.37	0.12	0.06	1.07	2.71	3.71	2.24	0.12	2.79	0.71	0.07
693.54192	0.00	3.18	40.52	0.54	14.56	4.42	13.82	0.32	2.96	0.30	0.15	0.12	0.70	3.71	5.96	4.58	0.24	2.59	1.13	0.19
694.4868	-0.01	2.79	42.54	0.86	14.84	3.23	15.04	0.33	0.88	0.29	0.14	0.12	0.88	3.67	5.16	5.08	0.19	2.55	1.22	0.19
695.91936	0.01	3.35	40.03	0.67	14.14	4.73	14.51	0.34	1.68	0.30	0.14	0.13	1.03	3.73	5.66	5.30	0.17	2.63	1.25	0.19
696.22416	0.00	3.40	40.85	0.69	14.22	5.32	13.96	0.31	1.81	0.35	0.13	0.11	0.92	3.37	5.42	4.72	0.18	2.89	1.19	0.17
696.9252	0.00	3.29	38.97	3.75	13.85	7.16	12.67	0.33	0.71	0.29	0.12	0.11	0.90	3.55	5.93	4.34	0.22	2.55	1.09	0.18
700.278	0.04	2.27	39.46	2.50	16.06	3.51	14.91	0.38	0.73	0.34	0.14	0.11	1.01	3.78	5.66	4.43	0.20	2.97	1.27	0.22

TABLE S4 GEOCHEMICAL DATA (XRF ANALYSES) OF CORE DIABLITO-1 (GRAIN SIZE-WEATHERING INTENSITY)

Consecutive	Depth (m)		Zr	Rb	Log(Zr/Rb)		K	Fe	Log(K/Fe)
1	574.7		1,118,127	489,064	0.36		1,840,492	39238.91	1.67
2	576.5		740,069	533,533	0.14		1,863,932	40737.35	1.66
3	577.7		849,679	556,701	0.18		2,045,107	42059.84	1.69
4	578.5		2,336,881	474,931	0.69		1,825,657	39108.41	1.67
5	580.0		1,175,109	410,717	0.46		1,788,430	66548.64	1.43
6	581.6		1,293,193	400,934	0.51		1,626,046	38240.25	1.63
7	582.8		771,464	540,634	0.15		1,979,836	46563.85	1.63
8	585.0		825,892	288,975	0.46		1,222,602	27448.14	1.65
9	585.5		940,303	498,813	0.28		1,882,979	42681.67	1.64
10	586.8		1,343,590	444,399	0.48		1,768,537	44272.94	1.60
11	588.0		790,051	449,799	0.24		1,899,292	66167.37	1.46
12	589.0		1,322,379	483,803	0.44		1,826,215	39801.01	1.66
13	590.0		939,689	564,266	0.22		2,042,282	40228.99	1.71
14	590.8		881,979	427,909	0.31		1,673,308	36028.11	1.67
15	592.2		1,472,107	297,933	0.69		1,209,706	32504.58	1.57
16	593.2		1,216,078	492,608	0.39		1,871,811	41093.5	1.66
17	593.9		1,863,166	436,179	0.63		1,654,623	37859.17	1.64
18	596.7		578,050	428,061	0.13		1,846,736	43778.93	1.63
19	597.5		863,104	391,461	0.34		1,583,583	37307.88	1.63
20	599.1		2,364,502	196,139	1.08		953,828	38623.22	1.39
21	599.9		903,331	566,050	0.20		2,115,305	42410.2	1.70
22	600.9		970,705	459,029	0.33		1,888,266	57831.69	1.51
23	602.7		718,553	446,097	0.21		1,829,756	42549.48	1.63
24	603.9		654,876	423,166	0.19		1,880,471	55935.79	1.53
25	606.2		840,627	447,799	0.27		1,679,038	39391.85	1.63
26	606.9		796,682	538,965	0.17		2,059,742	47246.14	1.64
27	607.5		626,067	508,345	0.09		1,908,946	38756.35	1.69
28	608.1		723,546	581,964	0.09		2,123,590	45667.07	1.67
29	612.7		635,486	513,114	0.09		1,986,524	38785.13	1.71
30	614.5		1,264,724	438,593	0.46		1,768,191	44125.52	1.60
31	616.4		1,224,056	459,182	0.43		1,832,474	45004.63	1.61
32	619.7		1,467,253	441,365	0.52		1,723,157	40870.89	1.62
33	621.2		1,754,454	398,746	0.64		1,566,925	41271.81	1.58
34	623.8		1,727,191	210,912	0.91		1,190,079	37735.18	1.50
35	624.9		1,953,568	294,776	0.82		1,343,129	40218.52	1.52
36	626.6		1,652,986	306,129	0.73		1,417,610	39410.13	1.56
37	627.1		1,010,985	485,796	0.32		1,970,097	46340.45	1.63
38	628.8		1,019,917	534,336	0.28		2,030,517	44295.44	1.66
39	629.7		1,185,518	281,236	0.62		1,329,755	46170.17	1.46
40	630.4		888,432	411,739	0.33		1,704,959	42517.82	1.60
41	631.0		945,629	494,401	0.28		1,900,932	45237.75	1.62
42	632.6		681,903	337,477	0.31		1,724,182	105439	1.21
43	633.5		907,706	543,657	0.22		2,116,028	47120.64	1.65
44	634.6		1,050,405	414,210	0.40		1,654,194	32577.78	1.71
45	636.6		1,477,653	479,811	0.49		1,904,309	40446.2	1.67
46	637.4		1,159,121	439,934	0.42		1,756,500	35199.58	1.70
47	640.7		593,069	455,727	0.11		1,834,350	36441.14	1.70
48	641.8		773,256	478,399	0.21		1,881,147	37389.81	1.70
49	644.0		756,716	629,248	0.08		2,212,216	39343.29	1.75
50	644.7		341,711	269,359	0.10		1,115,313	24653.18	1.66
51	645.5		513,319	440,929	0.07		1,958,121	66829.57	1.47
52	646.3		609,791	527,026	0.06		2,133,182	62479.19	1.53
53	648.3		1,158,190	504,077	0.36		1,943,975	43124.97	1.65
54	649.0		1,546,987	447,401	0.54		1,710,022	40152.92	1.63
55	650.2		1,096,155	517,255	0.33		1,997,990	43522.09	1.66
56	650.8		954,604	557,948	0.23		2,061,221	41410.52	1.70
57	655.9		1,123,605	432,795	0.41		1,732,808	35388.4	1.69
58	659.1		868,969	403,820	0.33		1,628,733	34756.44	1.67
59	660.1		891,842	534,427	0.22		1,985,246	43691.2	1.66

TABLE S4 GEOCHEMICAL DATA (XRF ANALYSES) OF CORE DIABLITO-1 (TERRIGENOUS INPUT-PALEOSALINITY)

Consecutive	Depth (m)	Fe	Ca	Log(Fe/Ca)	Sr	Ba	Sr/Ba	Ca NMS	Sr/Ba
1	574.7	39238.91	1,243,174	-1.501	772,881	42,229	18.30	7.59	18.30
2	576.5	40737.35	634,693	-1.193	739,791	33,448	22.12	4.57	22.12
3	577.7	42059.84	919,824	-1.340	865,356	37,636	22.99	5.53	22.99
4	578.5	39108.41	929,152	-1.376	814,177	36,117	22.54	5.23	22.54
5	580.0	66548.64	1,040,482	-1.194	748,364	42,214	17.73	5.77	17.73
6	581.6	38240.25	461,852	-1.082	653,565	28,351	23.05	3.05	23.05
7	582.8	46563.85	1,887,510	-1.608	947,049	136,779	6.92	10.93	6.92
8	585.0	27448.14	1,772,165	-1.810	597,934	18,501	32.32	15.18	32.32
9	585.5	42681.67	1,036,355	-1.385	771,671	38,828	19.87	6.51	19.87
10	586.8	44272.94	1,264,989	-1.456	726,297	34,087	21.31	7.53	21.31
11	588.0	66167.37	1,193,052	-1.256	721,189	39,456	18.28	7.04	18.28
12	589.0	39801.01	533,064	-1.127	735,526	44,023	16.71	3.29	16.71
13	590.0	40228.99	524,912	-1.116	812,593	46,927	17.32	3.24	17.32
14	590.8	36028.11	699,059	-1.288	692,218	31,541	21.95	5.02	21.95
15	592.2	32504.58	989,046	-1.483	580,727	23,907	24.29	6.94	24.29
16	593.2	41093.5	1,314,922	-1.505	887,786	37,722	23.53	7.86	23.53
17	593.9	37859.17	1,073,750	-1.453	806,171	32,261	24.99	6.32	24.99
18	596.7	43778.93	658,109	-1.177	718,376	26,210	27.41	4.75	27.41
19	597.5	37307.88	569,063	-1.183	649,980	24,108	26.96	4.30	26.96
20	599.1	38623.22	778,932	-1.305	512,735	60,774	8.44	5.03	8.44
21	599.9	42410.2	561,529	-1.122	1,052,560	37,897	27.77	3.48	27.77
22	600.9	57831.69	1,117,366	-1.286	861,870	32,183	26.78	6.87	26.78
23	602.7	42549.48	696,693	-1.214	730,027	34,285	21.29	5.00	21.29
24	603.9	55935.79	913,936	-1.213	706,659	31,518	22.42	6.25	22.42
25	606.2	39391.85	638,869	-1.210	652,708	33,088	19.73	4.28	19.73
26	606.9	47246.14	649,622	-1.138	806,157	39,079	20.63	4.14	20.63
27	607.5	38756.35	785,927	-1.307	723,414	30,105	24.03	5.59	24.03
28	608.1	45667.07	900,979	-1.295	881,344	38,148	23.10	5.59	23.10
29	612.7	38785.13	367,790	-0.977	695,754	31,341	22.20	2.75	22.20
30	614.5	44125.52	1,145,282	-1.414	717,010	30,897	23.21	6.85	23.21
31	616.4	45004.63	1,525,095	-1.530	785,667	40,377	19.46	9.29	19.46
32	619.7	40870.89	1,549,494	-1.579	785,736	31,923	24.61	8.95	24.61
33	621.2	41271.81	1,694,169	-1.613	729,644	31,993	22.81	9.95	22.81
34	623.8	37735.18	1206769	-1.505	761,649	27,257	27.94	7.92	27.94
35	624.9	40218.52	2,955,679	-1.866	672,972	31,803	21.16	16.27	21.16
36	626.6	39410.13	2,365,121	-1.778	590,533	25,500	23.16	14.55	23.16
37	627.1	46340.45	1,539,046	-1.521	820,786	32,260	25.44	9.07	25.44
38	628.8	44295.44	1,341,205	-1.481	822,197	33,861	24.28	8.03	24.28
39	629.7	46170.17	1,007,839	-1.339	508,900	23,318	21.82	7.15	21.82
40	630.4	42517.82	1,215,515	-1.456	710,471	23,629	30.07	8.59	30.07
41	631.0	45237.75	1,170,136	-1.413	872,276	33,807	25.80	7.42	25.80
42	632.6	105439	2,315,811	-1.342	653,824	25,994	25.15	13.75	25.15
43	633.5	47120.64	1,448,306	-1.488	913,520	32,664	27.97	8.42	27.97
44	634.6	32577.78	1,917,374	-1.770	802,517	25,704	31.22	12.55	31.22
45	636.6	40446.2	2,615,735	-1.811	938,075	33,586	27.93	14.08	27.93
46	637.4	35199.58	2,249,596	-1.806	879,914	26,042	33.79	13.65	33.79
47	640.7	36441.14	839,951	-1.363	715,915	23,730	30.17	6.45	30.17
48	641.8	37389.81	1,029,825	-1.440	708,292	28,785	24.61	7.38	24.61
49	644.0	39343.29	911,995	-1.365	911,524	35,653	25.57	5.82	25.57
50	644.7	24653.18	757,632	-1.488	440,327	16,908	26.04	9.76	26.04
51	645.5	66829.57	1,902,160	-1.454	735,099	24,499	30.01	12.45	30.01
52	646.3	62479.19	1,592,056	-1.406	842,905	35,154	23.98	9.91	23.98
53	648.3	43124.97	2,010,388	-1.669	1,021,399	33,249	30.72	11.34	30.72
54	649.0	40152.92	2,823,275	-1.847	941,657	30,850	30.52	15.73	30.52
55	650.2	43522.09	1,996,401	-1.662	1,000,339	36,650	27.29	11.23	27.29
56	650.8	41410.52	1,508,236	-1.561	1,033,896	34,780	29.73	8.90	29.73
57	655.9	35388.4	1,437,891	-1.609	844,341	29,735	28.40	9.43	28.40
58	659.1	34756.44	1,399,833	-1.605	774,645	25,486	30.39	9.83	30.39
59	660.1	43691.2	1,740,977	-1.600	918,156	34,886	26.32	10.24	26.32

TABLE S4 GEOCHEMICAL DATA (XRF ANALYSES) OF CORE DIABLITO-1 (BOTTOM WATER OXYGENATION)

Consecutive	Depth (m)	V	Cr	V/Cr	Cu	Al	Cu/Al	Cu/Al (*10-2)	Ni	Al	Ni/Al	Ni/Al (*10-2)	Zn	Al	Zn/Al	Zn/Al (*10-1)	V	Al	V/Al	V/Al (*10-1)
1	574.7	189,687	52,348	3.62	26,050	488,400	0.053337	5.33	23,824	488,400	0.04878	4.88	140,768	488,400	0.288223	2.88	189,687	488,400	0.388385	3.88
2	576.5	190,291	49,569	3.84	26,262	447,529	0.058682	5.87	23,659	447,529	0.052866	5.29	133,559	447,529	0.298437	2.98	190,291	447,529	0.425204	4.25
3	577.7	195,986	51,451	3.81	23,341	624,101	0.037399	3.74	24,375	624,101	0.039056	3.9	105,228	624,101	0.168607	1.69	195,986	624,101	0.314029	3.14
4	578.5	193,412	54,365	3.56	22,223	559,021	0.039753	3.97	21,382	559,021	0.038249	3.82	151,835	559,021	0.271609	2.72	193,412	559,021	0.345983	3.46
5	580.0	192,541	48,721	3.95	21,253	565,112	0.037608	3.76	19,235	565,112	0.034038	3.4	103,212	565,112	0.18264	1.83	192,541	565,112	0.340713	3.41
6	581.6	174,897	44,319	3.95	19,013	395,891	0.048026	4.8	21,642	395,891	0.054667	5.47	139,295	395,891	0.351852	3.52	174,897	395,891	0.441781	4.42
7	582.8	181,410	47,405	3.83	25,305	574,671	0.044034	4.4	21,384	574,671	0.037211	3.72	130,327	574,671	0.226785	2.27	181,410	574,671	0.315676	3.16
8	585.0	125,673	35,089	3.58	17,152	217,459	0.078875	7.89	18,028	217,459	0.082903	8.29	95,081	217,459	0.437236	4.37	125,673	217,459	0.577916	5.78
9	585.5	182,268	51,043	3.57	24,793	467,016	0.053088	5.31	24,321	467,016	0.052077	5.21	143,828	467,016	0.307972	3.08	182,268	467,016	0.390282	3.9
10	586.8	173,109	45,422	3.81	23,637	475,489	0.049711	4.97	22,319	475,489	0.046939	4.69	134,987	475,489	0.283891	2.84	173,109	475,489	0.364065	3.64
11	588.0	192,169	50,381	3.81	27,212	512,148	0.053133	5.31	19,225	512,148	0.037538	3.75	121,241	512,148	0.23673	2.37	192,169	512,148	0.375222	3.75
12	589.0	188,945	46,966	4.02	25,123	514,184	0.04886	4.89	22,524	514,184	0.043805	4.38	119,743	514,184	0.23288	2.33	188,945	514,184	0.367466	3.67
13	590.0	204,472	52,022	3.93	27,928	585,081	0.047734	4.77	21,387	585,081	0.036554	3.66	119,942	585,081	0.205001	2.05	204,472	585,081	0.349476	3.49
14	590.8	169,620	43,191	3.93	24,692	374,875	0.065867	6.59	18,361	374,875	0.048979	4.9	122,901	374,875	0.327845	3.28	169,620	374,875	0.452471	4.52
15	592.2	135,322	32,217	4.20	17,519	303,155	0.057789	5.78	18,468	303,155	0.060919	6.1	119,369	303,155	0.393756	3.94	135,322	303,155	0.446379	4.46
16	593.2	177,817	46,521	3.82	23,438	523,392	0.044781	4.48	21,682	523,392	0.041426	4.14	122,526	523,392	0.2341	2.34	177,817	523,392	0.33974	3.4
17	593.9	160,942	46,734	3.44	21,024	460,882	0.045617	4.56	21,035	460,882	0.045641	4.56	115,075	460,882	0.249684	2.5	160,942	460,882	0.349204	3.49
18	596.7	161,291	42,336	3.81	19,169	363,064	0.052798	5.28	15,987	363,064	0.044034	4.4	105,699	363,064	0.29113	2.91	161,291	363,064	0.444249	4.44
19	597.5	161,638	39,441	4.10	20,089	310,645	0.064669	6.47	19,602	310,645	0.063101	6.31	112,884	310,645	0.363386	3.63	161,638	310,645	0.52033	5.2
20	599.1	110,593	33,113	3.34	14,989	358,685	0.041789	4.18	20,653	358,685	0.05758	5.76	162,130	358,685	0.452012	4.52	110,593	358,685	0.308329	3.08
21	599.9	197,708	51,083	3.87	21,186	555,969	0.038106	3.81	21,357	555,969	0.038414	3.84	120,802	555,969	0.217282	2.17	197,708	555,969	0.35561	3.56
22	600.9	171,330	51,839	3.31	20,747	453,823	0.045716	4.57	23,717	453,823	0.05226	5.23	157,230	453,823	0.346457	3.46	171,330	453,823	0.377526	3.78
23	602.7	171,377	45,461	3.77	17,899	376,801	0.047503	4.75	18,749	376,801	0.049758	4.98	128,737	376,801	0.341658	3.42	171,377	376,801	0.454821	4.55
24	603.9	166,200	51,163	3.25	17,186	401,394	0.042816	4.28	18,242	401,394	0.045447	4.54	99,062	401,394	0.246795	2.47	166,200	401,394	0.414057	4.14
25	606.2	171,108	40,708	4.20	21,234	436,003	0.048701	4.87	18,713	436,003	0.042919	4.29	202,239	436,003	0.463848	4.64	171,108	436,003	0.392447	3.92
26	606.9	190,222	51,424	3.70	27,626	517,038	0.053431	5.34	25,818	517,038	0.049934	4.99	176,198	517,038	0.340783	3.41	190,222	517,038	0.367907	3.68
27	607.5	178,270	50,787	3.51	23,201	408,435	0.056805	5.68	22,418	408,435	0.054888	5.49	119,593	408,435	0.292808	2.93	178,270	408,435	0.436471	4.36
28	608.1	197,055	52,878	3.73	25,899	545,309	0.047494	4.75	25,971	545,309	0.047626	4.76	141,003	545,309	0.258574	2.58	197,055	545,309	0.361364	3.61
29	612.7	168,367	49,252	3.42	22,828	419,947	0.054359	5.43	20,699	419,947	0.04929	4.93	117,193	419,947	0.279066	2.79	168,367	419,947	0.400924	4.01
30	614.5	178,525	50,664	3.52	17,575	467,071	0.037628	3.76	22,268	467,071	0.047676	4.77	136,495	467,071	0.292236	2.92	178,525	467,071	0.382222	3.82
31	616.4	177,105	51,327	3.45	17,615	443,703	0.0397	3.97	21,063	443,703	0.047471	4.75	141,800	443,703	0.319583	3.2	177,105	443,703	0.399152	3.99
32	619.7	161,965	45,540	3.56	14,129	434,500	0.032518	3.25	21,213	434,500	0.048822	4.88	133,907	434,500	0.308186	3.08	161,965	434,500	0.372762	3.73
33	621.2	145,514	44,920	3.24	13,288	385,051	0.03451	3.45	18,667	385,051	0.048479	4.85	123,711	385,051	0.321285	3.21	145,514	385,051	0.377908	3.78
34	623.8	104,165	36,883	2.82	11,042	363,762	0.030355	3.04	17,165	363,762	0.047187	4.72	81,545	363,762	0.224171	2.24	104,165	363,762	0.286355	2.86
35	624.9	134,481	40,417	3.33	13,565	360,072	0.037673	3.77	19,354	360,072	0.05375	5.38	109,006	360,072	0.302734	3.03	134,481	360,072	0.373484	3.73
36	626.6	137,499	43,346	3.17	14,806	323,313	0.045795	4.58	18,039	323,313	0.055794	5.58	130,920	323,313	0.404933	4.05	137,499	323,313	0.425281	4.25
37	627.1	170,599	52,292	3.26	19,610	451,411	0.043442	4.34	21,465	451,411	0.047551	4.76	119,820	451,411	0.265434	2.65	170,599	451,411	0.377924	3.78
38	628.8	170,976	50,054	3.42	17,434	517,898	0.033663	3.37	20,735	517,898	0.040037	4	131,913	517,898	0.254708	2.55	170,976	517,898	0.330135	3.3
39	629.7	120,543	32,555	3.70	12,696	270,489	0.046937	4.69	15,255	270,489	0.056398	5.64	162,668	270,489	0.601385	6.01	120,543	270,489	0.445648	4.46
40	630.4	142,928	41,348	3.46	12,887	356,352	0.036164	3.61	18,554	356,352	0.052066	5.21	113,882	356,352	0.319577	3.2	142,928	356,352	0.401087	4.01
41	631.0	166,032	42,077	3.95	17,226	457,952	0.037615	3.76	18,614	457,952	0.040646	4.06	127,184	457,952	0.277723	2.78	166,032	457,952	0.362553	3.62
42	632.6	152,781	53,817	2.84	18,081	419,660	0.043085	4.31	18,196	419,660	0.043359	4.34	109,800	419,660	0.26164	2.62	152,781	419,660	0.364059	3.64
43	633.5	183,940	55,234	3.33	17,050	564,883	0.030183	3.02	20,615	564,883	0.036494	3.65	135,644	564,883	0.240128	2.4	183,940	564,883	0.325625	3.26
44	634.6	133,558	40,708	3.28	11,968	383,691	0.031192	3.12	18,433	383,691	0.048041	4.8	99,863	383,691	0.260269	2.6	133,558	383,691	0.348087	3.48
45	636.6	152,623	44,255	3.45	14,885	502,200	0.02964	2.96	19,571	502,200	0.038971	3.9	136,861	502,200	0.272523	2.72	152,623	502,200	0.303909	3.04
46	637.4	150,868	41,924	3.60	13,675	393,878	0.034719	3.47	16,955	393,878	0.043046	4.3	126,095	393,878	0.320137	3.2	150,868	393,878	0.383032	3.83
47	640.7	153,974	43,876	3.51	16,239	365,525	0.044427	4.44	16,445	365,525	0.04499	4.5	119,357	365,525	0.326536	3.26	153,974	365,525	0.421241	4.21
48	641.8	162,474	45,073	3.60	18,082	364,440	0.049616	4.96	17,852	364,440	0.048985	4.9	142,836	364,440	0.391933	3.92	162,474	364,440	0.445818	4.46
49	644.0	182,738	52,436	3.48	18,554	547,917	0.033863	3.39	21,632	547,917	0.03948	3.95	144,082	547,917	0.262963	2.63	182,738	547,917	0.333514	3.33
50	644.7	92,008	27,882	3.30	9,273	123,655	0.074991	7.5	10,987	123,655	0.088852	8.88	92,698	123,655	0.74965	7.5	92,008	123,655	0.74407	7.44
51	645.5	142,505	51,373	2.77	15,442	402,356	0.038379	3.84	19,274	402,356	0.047903	4.79	140,169	402,356	0.348371	3.48	142,505	402,356	0.354176	3.54
52	646.3	163,419	52,025	3.14	16,842	505,129	0.033342	3.33	19,543	505,129	0.038689	3.87	142,738	505,129	0.282577	2.82	163,419	505,129	0.323519	3.24
53	648.3	176,223	47,777	3.69	18,073	499,385	0.036191	3.62	21,402	499,385	0.042857	4.28	124,171	499,385	0.248648	2.49	176,223	499,385	0.35288	3.53
54	649.0	139,952	40,481	3.46	14,546	441,444	0.032951	3.3	18,486	441,444	0.041876	4.19	134,970	441,444	0.305747	3.06	139,952	441,444	0.317032	3.17
55	650.2	170,223	51,005	3.34	17,468	549,400	0.031795	3.18	18,366	549,400	0.033429	3.34	129,904	549,400	0.236447	2.36	170,223	549,400	0.309834	3.1
56	650.8	170,726	50,608	3.37	19,471	567,748	0.034295	3.43	19,822	567,748	0.034913	3.49	111,009	567,748	0.195525	1.96	170,726	567,748	0.300707	3.01
57	655.9	150,802	38,848	3.88	15,108	368,158	0.041037	4.1	18,244	368,158	0.049555	4.96	128,702	368,158	0.349584	3.5	150,802	368,158	0.409612	4.1
58	659.1	144,341	40,258	3.59	14,877	363,006	0.040983	4.09	17,814	363,006	0.049074	4.91	119,511	363,006	0.329226	3.29	144,341	363,006	0.397627	3.98
59	660.1	174,907	51,109	3.42	19,417	554,485	0.035018	3.5	21,220	554,485	0.03827	3.83	138,785	554,485	0.250295	2.5	174,907	554,485	0.31544	3.15
60	660.7	166,483	52,311	3.18	17,733	523,244	0.03389	3.39	20,984	523,244	0.040104	4.01	143,259	523,244	0.27379	2.74	166,483	523,244	0.318175	3.18
61	662.8	122,518	50,498	2.43	14,460	424,353	0.034075	3.41	21,099	424,353	0.04972	4.97	120,853	424,353	0.284794	2.85	122,518	424,353	0.288717	2.89
62	664.0	81,171	30,304	2.68	7,071	103,670	0.068207	6.82	11,575	103,670	0.111652	11.6	67,222	103,670	0.648423	6.48	81,171	103,670	0.782975	7.83
63	664.8	159,948	53,449	2.99	15,489	505,469	0.030643	3.06	22,362	505,469	0.04424	4.44	145,519	505,469	0.287889	2.88	159,948	505,469	0.316435	3.16
64	666.0	177,890	50,208	3.54	23,389	416,541	0.056151	5.62	21,647	416,541	0.051968	5.2	134,857	416,541	0.323754	3.24	177,890	416,541	0.427065	4.27
65	667.8	175,041	44,595	3.93	21,861	403,194	0.05422	5.42	22,409	403,194	0.055579	5.58	125,047	403,194	0.310141	3.1	175,041	403,194	0.434136	4.34
66	668.5	197,522	52,953	3.73	29,372	496,219	0.059192	5.92	23,483	496,219	0.047324	4.73	129,516	496,219	0.261006	2.62	197,522	496,219	0.398054	3.98
67	669.5	191,351	55,388	3.45	27,755	442,236	0.062761	6.28	22,771	442,236	0.051491	5.15	149,706	442,236	0.338521	3.38	191,351	442,236	0.43269	4.33
68	670.9	206,012	57,003	3.61	25,827	512,451	0.050399	5.04	25,852	512,451	0.050448	5.04	162,164	512,451	0.316448	3.16	206,012	512,451	0.402013	4.02
69	672.5	174,995	54,140	3.23	24,103	432,493	0.05573	5.57	21,878	432,493	0.050586	5.06	141,679	432,493	0.327587	3.28	174,995	432,493	0.404619	4.05
70	673.6	148,571	46,710	3.18	15,902	295,487	0.053816	5.38	16,386	295,487	0.055454	5.54	91,303	295,487	0.308992	3.09	148,571	295,487	0.5028	5.03
71	674.2	111,445	110,664	1.01	11,088	386,836	0.028663	2.29	18,074	386,836	0.046723	4.67	157,330	386,836	0.40671	4.07	111,445	386,836	0.288094	2.89
72	676.9	156,424	47,953	3.26	18,531	372,204	0.049787	4.98	21,594	372,204	0.058017	5.8	124,536	372,204	0.334591	3.34	156,424	372,204	0.420264	4.2
73	678.2	170,477	45,196	3.77	15,767	419,206	0.037612	3.76	20,729	419,206	0.049448	4.94	121,349	419,206	0.289473	2.89	170,477	419,206	0.406666	4.07
74	678.9	167,105	52,187	3.20	17,707	375,431	0.047164	4.72	23,246	375,431	0.061918	6.19	155,988	375,431	0.41549	4.15	167,105	375,431	0.445102	4.45
75	680.8	182,223	49,310	3.70	20,739	509,575	0.040699	4.07	22,153	509,575	0.043473	4.35	137,918	509,575	0.270653	2.71	182,223	509,575	0.357598	3.58
76	681.2	177,012	51,969	3.41	21,290	391,701	0.054353	5.44	20,362	391,701	0.051984	5.2	114,890	391,701	0.29331	2.93	177,012	391,701	0.451906	4.52
77	681.9	162,399	45,053	3.60	15,683	398,754	0.03933	3.93	22,665	398,754	0.05684	5.68	121,202	398,754	0.303952	3.04	162,399	398,754	0.407266	4.07
78	683.5	180,076	53,423	3.37	20,071	472,116	0.042513	4.25	22,607	472,116	0.047884	4.79	156,620	472,116	0.331741	3.32	180,076	472,116	0.381423	3.81
79	684.4	158,621	48,482	3.27	18,929	371,276	0.050984	5.1	20,049	371,276	0.054	5.4	115,841	371,276	0.312008	3.12	158,621	371,276	0.427232	4.27
80	684.9	162,285	47,034	3.45	17,747	378,785	0.046852	4.68	21,768	378,785	0.057468	5.75	124,982	378,785	0.329955	3.3	162,285	378,785	0.428436	4.28
81	686.8	192,862	51,727	3.73	19,159	536,524	0.035709	3.57	24,118	536,524	0.044952	4.5	133,527	536,524	0.248874	2.49	192,862	536,524	0.359466	3.6
82	687.4	136,038	42,979	3.17	14,661	232,181	0.063145	6.31	17,101	232,181	0.073654	7.36	91,863	232,181	0.395653	3.96	136,038	232,181	0.585914	5.86
83	688.4	181,703	55,074	3.30	21,880	509,444	0.042949	4.29	25,944	509,444	0.050926	5.09	148,879	509,444	0.292238	2.92	181,703	509,444	0.356669	3.57
84	690.0	152,093	43,925	3.46	16,961	340,924	0.04975	4.98	19,733	340,924	0.057881	5.79	120,702	340,924	0.354044	3.54	152,093	340,924	0.44612	4.46
85	690.4	183,232	58,124	3.15	19,915	491,877	0.040488	4.05	22,611	491,877	0.045969	4.6	144,022	491,877	0.292801	2.93	183,232	491,877	0.372516	3.72
86	691.4	152,145	50,219	3.03	16,093	344,152	0.046761	4.68	20,066	344,152	0.058306	5.83	117,708	344,152	0.342023	3.42	152,145	344,152	0.442087	4.42
87	692.3	144,816	147,135	0.98	11,589	439,175	0.026388	2.64	23,868	439,175	0.054347	5.44	217,841	439,175	0.496023	4.96	144,816	439,175	0.329746	3.3
88	693.5	180,959	51,690	3.50	18,825	507,865	0.037067	3.71	20,276	507,865	0.039924	3.99	112,234	507,865	0.220992	2.21	180,959	507,865	0.356313	3.56
89	694.5	163,709	43,693	3.75	16,068	373,622	0.043006	4.3	19,111	373,622	0.051151	5.12	117,376	373,622	0.314157	3.14	163,709	373,622	0.438167	4.38
90	695.9	195,998	52,903	3.70	20,450	523,026	0.039099	3.91	22,302	523,026	0.04264	4.26	161,000	523,026	0.307824	3.08	195,998	523,026	0.374739	3.75
91	696.2	193,619	50,445	3.84	17,958	554,702	0.032374	3.24	21,529	554,702	0.038812	3.89	149,380	554,702	0.269298	2.69	193,619	554,702	0.34905	3.49
92	696.9	184,191	56,233	3.28	18,503	557,186	0.033208	3.32	21,055	557,186	0.037788	3.78	152,559	557,186	0.273803	2.74	184,191	557,186	0.330574	3.3
93	700.3	106,819	32,279	3.31	9,444	191,694	0.049266	4.93	11,914	191,694	0.062151	6.22	85,163	191,694	0.444265	4.44	106,819	191,694	0.557237	5.57

CHAPTER 2

Table S1 Total foraminifer counts at Aguablanca Creek section.

Table S2 Total calcareous nannofossil counts at Aguablanca Creek section.

Table S3 Sediments geochemical data (XRF analysis) at Aguablanca Creek section.

TABLE S1. TOTAL FORAMINIFER COUNTS AT AGUABLANCA CREEK SECTION (COUNTS)

Consecutive	Height (m)	Sample	PLANCKTONIC: Archaeoglobigerina spp.	Archaeoglobigerina ?sp.	Globotruncana aegyptiaca	Globotruncana spp.	Muricohedbergella cf. holmdelensis	Muricohedbergella spp.	Planoheterohelix spp.	Pseudoguembelina costulata	Pseudoguembelina excolata	Pseudoguembelina spp.	Rugoglobigerina macrocephala	Rugoglobigerina spp.	Spiroplecta americana	Globigerinina indet.
1	344.2	AG-01														
2	343.8	AG-02														
3	343	AG-03														
4	341.9	AG-05														
5	341.5	AG-06														
6	340.5	AG-07														
7	340	AG-08														1
8	338.2	AG-10														
9	337.6	AG-11														1
10	336.9	AG-12							5	1				1		7
11	336	AG-13			1	1			12			1			1	5
12	335.5	AG-14						1	14			1		1		2
13	334.9	AG-15		1		1	1									3
14	333.9	AG-16														
15	331.3	AG-17		3					1				1	5		1
16	331	AG-18														1
17	330.7	AG-19						1	1							2
18	330.3	AG-20									1	1				4
19	329.9	AG-21												1		
20	324.1	AG-22														
21	323.8	AG-23						3								
22	323.4	AG-24														7
23	323	AG-25														
24	322.5	AG-26														
25	322	AG-27														
26	321.6	AG-28														
27	321.2	AG-29														
28	320.8	AG-30														

Consecutive	Height (m)	Sample	BENTHIC: Ammobaculites colombiana	Gaudyina quadrans	Gaudryina spp.	Haplophragmoides excavatum	Haplophragmoides glaber	Haplophragmoides walteri	Haplophragmoides spp.	Nothia robusta	Nothia spp.	Spiroplectammina spectabilis	Textulariina indet.
1	344.2	AG-01											
2	343.8	AG-02											2
3	343	AG-03	4										
4	341.9	AG-05											
5	341.5	AG-06											
6	340.5	AG-07											3
7	340	AG-08											4
8	338.2	AG-10				8			6				
9	337.6	AG-11				11			4			2	
10	336.9	AG-12				5			1				
11	336	AG-13				2	1	1	4		1		
12	335.5	AG-14			1	17	2		18				3
13	334.9	AG-15				14			7				4
14	333.9	AG-16				19	1		13				10
15	331.3	AG-17		2			1		2				
16	331	AG-18		1									2
17	330.7	AG-19		11									6
18	330.3	AG-20								1			2
19	329.9	AG-21									1		
20	324.1	AG-22											
21	323.8	AG-23											
22	323.4	AG-24											
23	323	AG-25											
24	322.5	AG-26											
25	322	AG-27											
26	321.6	AG-28											
27	321.2	AG-29											
28	320.8	AG-30											

Consecutive	Height (m)	Sample	BENTHIC (cont.): Dentalina wimani	Dentalina spp.	Gavelinella correcta	Gavelinella henbesti	Gavelinella spissocostata	Gavelinella spp.	Gyroidinoides depressa	Lagena spp.	Lenticulina muensteri	Lenticulina cf. williamsoni	Lenticulina sp2	Lenticulina spp.	Marginulinopsis texasensis	Nodosaria paupercula	Orthokarstenia cretacea
1	344.2	AG-01															
2	343.8	AG-02															
3	343	AG-03															
4	341.9	AG-05															
5	341.5	AG-06															
6	340.5	AG-07															
7	340	AG-08															
8	338.2	AG-10				2		7									32
9	337.6	AG-11			2	4		8		1	3					1	
10	336.9	AG-12		2				1	3								
11	336	AG-13						10	11		1						
12	335.5	AG-14		1				3	23		3						
13	334.9	AG-15		1		10		5			2						
14	333.9	AG-16					2	3	2		1						
15	331.3	AG-17	5	12		10	2	11			6		1		1		10
16	331	AG-18	2	4				4			2						1
17	330.7	AG-19		1				7									11
18	330.3	AG-20						5	1								
19	329.9	AG-21		1				2				1					2
20	324.1	AG-22		8													
21	323.8	AG-23		2							1		1				
22	323.4	AG-24															
23	323	AG-25															
24	322.5	AG-26															
25	322	AG-27															
26	321.6	AG-28												2			
27	321.2	AG-29												2			
28	320.8	AG-30															

Consecutive	Height (m)	Sample	BENTHIC (cont.): Praebulimina kickapoensis	Praebulimina spp.	Pseudoglandulina spp.	Pyramidina prolixa	Pyramidina triangularis	Siphogenerinoides bramlettei	Siphogenerinoides spp.	Stilostomella spinea	Rotaliina indet.	OTHERS: Echinoid remains	Fish teeth	Gastropods	Invertebrate remains	Ostracodes	Phosphatic peloids	Glauconite
1	344.2	AG-01																
2	343.8	AG-02																
3	343	AG-03										3		1	2	1	1	
4	341.9	AG-05																
5	341.5	AG-06																
6	340.5	AG-07																
7	340	AG-08																
8	338.2	AG-10																
9	337.6	AG-11	1		2		1	4								2		
10	336.9	AG-12		1					4		6						5	
11	336	AG-13	13	2		1		4			6				1			
12	335.5	AG-14	7	2		1	2	6			9							
13	334.9	AG-15	2	1				65	1		3	1						
14	333.9	AG-16						7								1		
15	331.3	AG-17						49		1								
16	331	AG-18	3					18		1	2							
17	330.7	AG-19						18			1					1		
18	330.3	AG-20						2	2		2							
19	329.9	AG-21						2		1	6					1		
20	324.1	AG-22							1		4							
21	323.8	AG-23									3							
22	323.4	AG-24																
23	323	AG-25									2						3	100
24	322.5	AG-26															100	100
25	322	AG-27											1				100	100
26	321.6	AG-28																
27	321.2	AG-29																
28	320.8	AG-30																

Sterile

TABLE S1. TOTAL FORAMINIFER COUNTS AT AGUABLANCA CREEK SECTION (DIVERSITY)

Sample	Height (m)	Taxa_S	Individuals	Shannon_H	Evenness_e^H/S
AG-02	343.8	1	2	0	1
AG-03	343	1	4	0	1
AG-07	340.5	1	3	0	1
AG-08	340	2	5	0.5004	0.8247
AG-10	338.2	5	55	1.22	0.6775
AG-11	337.6	14	45	2,315	0.7236
AG-12	336.9	12	37	2,241	0.7834
AG-13	336	19	78	2,495	0.6379
AG-14	335.5	20	117	2,464	0.5878
AG-15	334.9	16	121	1,755	0.3616
AG-16	333.9	9	58	1,785	0.6618
AG-17	331.3	19	124	2,181	0.4662
AG-18	331	12	41	1,958	0.5907
AG-19	330.7	10	59	1,865	0.6456
AG-20	330.3	10	21	2,133	0.8442
AG-21	329.9	9	17	1,956	0.7858
AG-22	324.1	3	13	0.8587	0.7867
AG-23	323.8	5	10	1,505	0.9006
AG-24	323.4	1	7	0	1
AG-25	323	1	2	0	1
AG-28	321.6	1	2	0	1
AG-29	321.2	1	2	0	1

TABLE S2. TOTAL CALCAREOUS NANNOFOSSIL COUNTS AT AGUABLANCA CREEK SECTION (COUNTS)

Consecutive	Height (m)	Nº Field of View (FOV)	Preservation	Species richness	TOTAL	Ascidians spicles	Ahmuellerella octoradiata	Arkhangelskiella confusa	Arkhangelskiella cymbiformis	Biscutum constans	Cervisiella operculata	Cervisiella saxea	Ceratolithoides aculeus	Chiastozygus litterarius	Chiastozygus synquadriperforatus	Corolithion madagaskarensis	Cretarhabdus conicus
1	344.2	700	-	-	-												
2	343.8	700	-	-	-												
3	343	700	-	-	-												
4	341.5	700	-	-	-												
5	340.5	278	P	1	304	304											
6	340	284	P	1	306	306											
7	339	700	P	4	11							3					
8	338.2	700	P	1	1												
9	337.6	700	M	8	35					1		2					
10	336.9	700	M	11	33		1			2				1			
11	336	700	M	11	30		1								1		
12	335.5	700	M	19	53					1	1	1		2		1	
13	334.9	700	M	8	18						2	1					
14	333.9	700	M	12	44						1	3					
15	331.3	132	M	38	316												
16	331	167	M	43	306			1	2	4	2	7	1	2	1		1
17	330.7	700	M	16	136		2	1	1	3	1	4		5	1		
18	330.3	700	P	1	2						1		2	2			
19	329.9	700	M	18	296												
20	324.1	700	-	-	-		3		3		1	1		2			
21	323.8	81	M	29	305												
22	323.4	112	M	27	320												
23	323	271	M	21	302			1	1	2	7	5		1			
24	322.5	700	M	16	66		1		1	1	11	10		1			
25	322	700	-	-	-					1	19	12	1				
26	321.6	700	P	4	28						5	1					
27	321.2	480	M	14	300												
												2					
									3			4					

Consecutive	Cribrosphaerella ehrenbergii	Cylindralithus biarcus	Cylindralithus serratus	Eiffelithus eximius	Eiffellithus gorkae	Eiffellithus turriseiffelii	Gartnerago segmentatum	Helicolithus trabeculatus	Kamptnerius magnificus	Lapideacassis sp.	Loxolithus armilla	Manivitella pemmatoidea	Microrhabdulus decoratus	Microrhabdulus undosus	Micula concava	Micula cubiformis	Micula staurophora	Micula swastica	Perchnielsenella stradneri	Placozygus fibuliformis
1																				
2																				
3																				
4																				
5																				
6																				
7	1																2			
8																				
9		1			1		2										2			
10	1				2	1	5										1			
11	1		1				8										1		1	
12	3				2	1	12										3			1
13	1						1										2			
14	1	1					7	1							1		9		1	
15																				
16	13	2	2		1	1	3	1			1		4	2	1	5	58	1	2	1
17	9	1	1	1	1	2	6	6			1	1	5	1	1	7	28		1	1
18	11					1	4									1	15			
19																				
20	12		3		1	2	38						2			1	41			
21																				
22																				
23	9	1			4	2	5	1	2	1			2			6	149	1		1
24	12	2			2	1	4	2	1				1			4	148		1	1
25	4	2			2		6	1					1			6	144	1		1
26	4				1	3	6						1			1	18			
27																				
																	11			
	3												1			1	33	1		

Consecutive	Prediscosphaera cretacea	Prediscosphaera grandis	Prediscosphaera spinosa	Prediscosphaera stoveri	Quadrum gartnerii	Reinhardtites levis	Retecapsa angustiforata	Retecapsa crenulata	Retecapsa surirella	Rhagodiscus angustus	Rhagodiscus asper	Rhagodiscus reniformis	Rhagodiscus splendens	Staurolithites laffittei	Tetrapodorhabdus decorus	Watznaueria barnesiae	Watznaueria biporta	Watznaueria fossacincta	Watznaueraia ovata	Zeugrhabdotus bicrescenticus	Zeugrhabdotus embergeri	Zeugrhabdotus erectus	Zeugrhabdotus sigmoides
1																							
2																							
3																							
4																							
5																							
6																							
7																5							
8																1							
9	4															22							
10				1												17					1		
11							1	1	1							13							
12	3							1	1	1				1		16				1			1
13	1															9		1					
14									1							17			1				
15																							
16	4						1	3	15		1				1	165	1	1		1	2	1	1
17	10	2	2	1		1	1	4	10		1	1			2	174		1		1	1	1	1
18	4							1	5	1			1		1	85					1		
19																2							
20	9							4	16							156						1	
21																							
22																							
23	4						1	4	3						1	87		1		1	1	1	
24	10							1	5	1				1		94				2	1	1	
25	10							3						1	1	83				1	2		
26	1							3	2					2	1	16					1		
27																							
						2										13							
	3				4	8			2							231				4	2		

TABLE S2. TOTAL CALCAREOUS NANNOFOSSIL COUNTS AT AGUABLANCA CREEK SECTION (DIVERSITY)

Sample	Depth	Taxa_S	Individuals	Shannon_H	Evenness_e^H/S		SHEBI ln(E)
AG-9A	339	4	11	1.241	0.8645		-0.145603974
AG-10	338.2	1	1	0	1		0
AG-11	337.6	8	35	1.335	0.4751		-0.744229971
AG-12	336.9	11	33	1.709	0.5022		-0.688756832
AG-13	336	11	30	1.735	0.5155		-0.662617976
AG-14	335.5	19	53	2.332	0.5419		-0.612673796
AG-15	334.9	8	18	1.638	0.6429		-0.441766088
AG-16	333.9	12	44	1.856	0.533		-0.629233855
AG-17	331.3	38	316	1.933	0.1819		-1.704298193
AG-18	331	43	306	2.033	0.1776		-1.728221448
AG-19	330.7	16	136	1.482	0.2752		-1.290257173
AG-20	330.3	1	2	0	1		0
AG-21	329.9	18	296	1.664	0.2933		-1.226559303
AG-23	323.8	29	305	1.721	0.1927		-1.646620704
AG-24	323.4	27	320	1.726	0.2081		-1.569736546
AG-25	323	21	302	1.652	0.2484		-1.392714929
AG-26	322.5	16	66	2.219	0.5746		-0.554081132
AG-28	321.6	4	28	1.1	0.7513		-0.28595024
AG-29	321.2	14	300	0.9754	0.1894		-1.663894098

TABLE S3. GEOCHEMICAL DATA (XRF ANALYSIS) AT AGUABLANCA CREEK (XRF DATA NMS)

	Consecutive	Sample	Height (m)	Mg NMS	Al NMS	Si NMS	S NMS	K NMS	Ca NMS	Ti NMS	Cr NMS	Mn NMS	Fe NMS	Ni NMS	Cu NMS	Zn NMS	Rb NMS	Sr NMS	Zr NMS	Ba NMS	Co NMS	V NMS	Ga NMS
[illegible]	1	AG-01	344,2	8.7E-02	0,847218242	1.7E+09	1.6E+09	2.3E+09	8.2E+09	3.6E+09	0,056430647	0,422674336	5.5E+09	0,03682025	0,019581394	0,252211126	0,467793867	1.1E+09	9.0E+09	0,048660111	0,520235505	0,243862763	0,032686226
	2	AG-02	343,8	-0,002502898	0,759311509	1.5E+08	1.2E+09	3.3E+09	2.7E+09	4.2E+09	0,064540034	0,220758066	6.4E+09	0,040987739	0,024196705	0,238320777	0,784037479	1.1E+09	5.6E+09	0,059766548	0,599719918	0,271609932	0,042217978
	3	AG-03	343	7.0E-02	0,867819281	1.3E+09	1.2E+09	3.6E+09	3.2E+09	3.7E+09	0,070316769	0,231535642	6.7E+08	0,040704318	0,023227998	0,223825286	0,876831766	1.2E+09	4.0E+09	0,067924656	0,619533365	0,287561916	0,041841852
	4	AG-05	341,9	5.3E-03	0,656360015	2.1E+09	0,487149852	2.0E+09	6.3E+09	4.6E+09	0,050951579	0,368597886	5.2E+08	0,036517169	0,024108373	0,260804121	0,454002753	1.0E+09	9.7E+09	0,025901832	0,527182507	0,272927189	0,031300066
	5	AG-06	341,5	1.8E-01	0,630783066	1.9E+09	0,48095925	2.1E+09	1.4E+09	4.1E+08	0,056296712	0,616332953	4.9E+09	0,026865919	0,01650712	0,235324342	0,41938809	1.2E+09	7.5E+09	0,034696729	0,494260277	0,252784777	0,028077425
	6	AG-07	340,5	0,003713254	0,791391755	8.8E+09	0,151367451	3.4E+09	1.1E+08	3.4E+09	0,082599752	0,628953388	7.7E+09	0,03724972	0,030989189	0,230555698	0,910620154	1.0E+09	1.2E+08	0,05394984	0,648457125	0,2980168	0,048867004
	7	AG-08	340	1.3E-01	0,814845675	8.5E+09	0,063366736	3.4E+09	1.0E+09	3.3E+09	0,079239156	0,649481167	7.8E+07	0,032619731	0,028309603	0,190604843	0,910554807	1.1E+09	1.1E+09	0,061059424	0,639600039	0,297357336	0,04519987
	8	AG-09	339	-7.2E-02	0,737709633	1.5E+09	1.1E+09	2.8E+09	2.2E+09	4.3E+09	0,066110798	0,264059274	6.5E+09	0,041965603	0,027038845	0,299020007	0,651064669	0,971316477	6.0E+08	0,040318044	0,633555783	0,272931087	0,041129758
	9	AG-10	338,2	5.5E-02	1.1E+09	1.1E+09	0,272079742	4.8E+09	1.6E+09	4.0E+09	0,105094387	0,177419445	7.2E+09	0,039981542	0,029608996	0,256885192	1.2E+09	1.4E+09	1.3E+09	0,061455175	0,664090803	0,398245234	0,060144468
	10	AG-11	337,6	0,007798774	0,973038412	1.0E+09	0,48648771	4.2E+08	2.3E+09	3.6E+08	0,08757335	0,205115747	7.3E+09	0,03863128	0,025700924	0,229441592	1.0E+08	1.1E+09	1.2E+09	0,06105506	0,640183171	0,34072008	0,050599847
	11	AG-12	336,9	-2.4E-02	0,749218633	8.8E+08	0,124942696	3.8E+09	2.1E+09	3.4E+09	0,088060039	0,304311788	7.6E+09	0,033237991	0,024412592	0,183730589	0,912862441	1.0E+09	1.1E+09	0,033625886	0,660752079	0,319570046	0,04465298
	12	AG-13	336	0,005903126	0,945042211	1.0E+09	0,220422535	4.4E+09	2.0E+09	3.7E+09	0,094139819	0,201430073	7.3E+09	0,04334129	0,028295212	0,251630143	1.1E+09	1.2E+09	1.2E+09	0,059631285	0,666033344	0,347405542	0,051920249
	13	AG-14	335,5	0,005467067	0,836541484	8.9E+09	0,117220849	3.8E+09	2.1E+09	3.3E+09	0,082490497	0,262642818	7.6E+09	0,034328994	0,025751404	0,196491883	0,942763696	1.1E+09	1.0E+09	0,04448478	0,665263472	0,331511518	0,043135931
	14	AG-15	334,9	0,00467763	0,866442561	9.8E+09	0,513141104	4.1E+09	2.9E+09	3.6E+09	0,091378356	0,206428718	7.3E+09	0,035989664	0,026460768	0,190895001	1.0E+09	1.2E+09	1.2E+09	0,059344595	0,638393773	0,330923423	0,048138214
	15	AG-16	333,9	-2.0E-02	1.1E+08	1.1E+09	0,323751583	4.8E+09	2.0E+09	4.1E+09	0,10398159	0,171492948	7.1E+09	0,046642308	0,031248682	0,225329468	1.2E+09	1.4E+09	1.3E+09	0,05835649	0,650932166	0,388168433	0,062626017
	16	AG-17	331,3	0,001993964	0,986241163	8.8E+09	0,726883001	4.2E+08	1.5E+09	2.7E+09	0,09350434	0,153116006	6.3E+09	0,04222179	0,028648706	0,175952386	0,908627302	1.8E+09	0,935691827	0,055732072	0,5682781	0,308805324	0,041411644
	17	AG-18	331	-3.6E-03	0,673491091	6.6E+09	0,346675266	3.1E+09	1.1E+09	2.1E+09	0,082232944	0,217249285	7.3E+09	0,034726826	0,020429886	0,115126387	0,568894055	1.1E+09	0,58795222	0,040953962	0,579553414	0,210321697	0,024709549
	18	AG-19	330,7	0,004099676	0,998365067	9.3E+09	0,198222992	4.4E+09	5.4E+09	3.2E+09	0,091951758	0,17523395	7.1E+09	0,041221578	0,031646851	0,17826389	1.0E+09	1.5E+09	1.0E+09	0,051414929	0,624872859	0,313719231	0,041115779
	19	AG-20	330,3	-0,008184808	1.2E+09	1.4E+08	0,145531412	6.7E+09	3.8E+09	5.2E+08	0,12798931	0,17747225	6.2E+09	0,046886899	0,050590149	0,25883326	1.7E+09	2.1E+09	1.8E+09	0,105410788	0,609813399	0,497350118	0,077313798
	20	AG-21	329,9	2.1E-02	1.4E+09	1.3E+09	0,059910171	6.2E+09	4.0E+09	4.9E+09	0,111192474	0,119341847	6.2E+09	0,049028676	0,05136134	0,245104929	1.7E+09	2.5E+09	1.9E+09	0,091339193	0,600129194	0,490829339	0,081329243
	21	AG-22	324,1	0,002232744	0,701411632	6.3E+09	0,379632465	2.9E+09	1.5E+09	2.2E+09	0,071598901	0,31988823	6.9E+09	0,032602167	0,023766546	0,120987723	0,539165092	1.1E+09	0,616194754	0,030894603	0,581185272	0,227496352	0,026775322
	22	AG-23	323,8	-0,001970082	0,97220944	8.9E+09	1.6E+09	3.7E+09	4.7E+09	2.2E+09	0,075643587	0,149535189	3.0E+08	0,049331363	0,033138117	0,261065635	0,640777804	3.7E+09	1.1E+09	0,064935208	0,28367742	0,203192442	0,028161541
	23	AG-24	323,4	0,002380113	0,84836295	9.2E+09	1.5E+09	3.6E+09	5.0E+09	2.1E+09	0,084210106	0,098773708	2.6E+09	0,044507919	0,035648279	0,272939429	0,613976211	4.0E+08	1.2E+09	0,058333547	0,246265542	0,209230348	0,022675376
	24	AG-25	323	-0,003748828	0,739312716	8.2E+09	2.1E+09	3.2E+09	4.7E+09	1.8E+09	0,114022411	0,064501952	3.0E+09	0,046881079	0,040155298	0,230376242	0,542670004	4.1E+09	1.1E+09	0,060435293	0,269838629	0,188943697	0,019281097
[illegible]	25	AG-26	322,5	0,010287145	0,325105711	3.4E+09	4.3E+08	1.8E+09	4.7E+09	0,481395209	0,144027339	0,089655915	3.9E+09	0,013701969	0,010559014	0,057502188	0,255747339	2.3E+08	0,378548146	0,023669698	0,322066382	0,064639062	0,007184421
	26	AG-27	322	0,004179544	0,288012114	3.5E+08	2.6E+09	1.6E+09	6.0E+09	0,424014789	0,141879131	0,066872702	2.8E+09	0,024748357	0,015532895	0,113285009	0,232874051	3.2E+09	0,299332575	0,129674278	0,230364619	0,075689822	0,006232162
	27	AG-28	321,6	-0,002687972	0,858265087	7.8E+08	2.8E+09	2.6E+08	5.1E+09	1.7E+09	0,242204478	0,068383864	2.7E+09	0,087387796	0,064878021	0,478557913	0,470857494	3.7E+09	0,811356303	0,038605723	0,244535329	0,185989826	0,014077577
	28	AG-29	321,2	3.2E-02	0,620957077	6.3E+09	1.9E+09	2.1E+09	6.5E+09	1.1E+09	0,156011842	0,048320671	1.7E+09	0,059428588	0,040866503	0,265499391	0,345366313	4.2E+09	0,661554922	0,031540442	0,164502885	0,120826366	0,011562457
	29	AG-30	320,8	6,91E-08	0,467558713	7.1E+09	1.4E+09	1.5E+09	7.1E+09	0,724998948	0,101825505	0,059281942	1.2E+09	0,034466211	0,024848075	0,17987766	0,223413618	4.3E+09	0,535341429	0,03335767	0,101455011	0,093715808	0,011472075

TABLE S3. GEOCHEMICAL DATA (XRF ANALYSIS) AT AGUABLANCA CREEK (TERRIGENOUS INPUT)

Consecutive	Sample	Height (m)	Fe NMS	Ca NMS	log(Fe/Ca)
1	AG-01	344.2	54.6523254	8.15121443	0.82638633
2	AG-02	343.8	63.5740242	2.68540397	1.37427008
3	AG-03	343	66.8454443	3.19755032	1.32025443
4	AG-05	341.9	52.0431907	6.32884328	0.91503957
5	AG-06	341.5	49.0891326	13.998083	0.5449168
6	AG-07	340.5	77.1728649	1.06594841	1.85972844
7	AG-08	340	77.710497	1.0118135	1.88537922
8	AG-09	339	64.9543913	2.22439198	1.4653972
9	AG-10	338.2	71.6501437	1.58863465	1.65419304
10	AG-11	337.6	73.4681236	2.27879533	1.50839363
11	AG-12	336.9	76.4217311	2.08267152	1.56459609
12	AG-13	336	73.1621335	2.04416102	1.55377126
13	AG-14	335.5	76.1911006	2.13982483	1.55152602
14	AG-15	334.9	73.340099	2.92015902	1.39993499
15	AG-16	333.9	71.0602964	1.99821747	1.55098426
16	AG-17	331.3	62.7813932	14.6711347	0.63136725
17	AG-18	331	72.9013684	10.6889721	0.83379974
18	AG-19	330.7	71.3870646	5.41417422	1.1200873
19	AG-20	330.3	61.5109924	3.82364611	1.20647504
20	AG-21	329.9	61.9851103	4.03777165	1.18614562
21	AG-22	324.1	68.9901999	14.8666998	0.66657283
22	AG-23	323.8	29.5549103	46.5272317	-0.19707757
23	AG-24	323.4	25.9664016	49.8456438	-0.28321544
24	AG-25	323	30.168215	46.9925368	-0.19247928
25	AG-26	322.5	39.4773623	46.5324319	-0.07140762
26	AG-27	322	27.5641347	59.5109066	-0.3342522
27	AG-28	321.6	27.1678269	50.7026186	-0.27097549
28	AG-29	321.2	17.1591389	64.7604459	-0.57681434
29	AG-30	320.8	11.8584261	71.2085771	-0.77850526

TABLE S3. GEOCHEMICAL DATA (XRF ANALYSIS) AT AGUABLANCA CREEK (PALEOSALINITY)

Consecutive	Sample	Height (m)	Sr NMS	Ba NMS	Sr/Ba
1	AG-01	344.2	1.08725932	0.04866011	22.3439549
2	AG-02	343.8	1.10483674	0.05976655	18.4858717
3	AG-03	343	1.20485842	0.06792466	17.73816
4	AG-05	341.9	1.01137813	0.02590183	39.0465872
5	AG-06	341.5	1.15436632	0.03469673	33.2701775
6	AG-07	340.5	1.04837674	0.05394984	19.4324346
7	AG-08	340	1.07847251	0.06105942	17.6626709
8	AG-09	339	0.97131648	0.04031804	24.0913592
9	AG-10	338.2	1.3543974	0.06145518	22.0387853
10	AG-11	337.6	1.1166474	0.06105506	18.2891869
11	AG-12	336.9	1.00180843	0.03362589	29.7927741
12	AG-13	336	1.23271777	0.05963129	20.6723327
13	AG-14	335.5	1.07581954	0.04448478	24.1839918
14	AG-15	334.9	1.15658243	0.0593446	19.4892632
15	AG-16	333.9	1.37189041	0.05835649	23.508789
16	AG-17	331.3	1.75247119	0.05573207	31.4445728
17	AG-18	331	1.13099186	0.04095396	27.616177
18	AG-19	330.7	1.51183548	0.05141493	29.4046013
19	AG-20	330.3	2.10281028	0.10541079	19.9487198
20	AG-21	329.9	2.53198121	0.09133919	27.7206436
21	AG-22	324.1	1.05259935	0.0308946	34.0706553
22	AG-23	323.8	3.6971612	0.06493521	56.9361572
23	AG-24	323.4	3.99171689	0.05833355	68.4291819
24	AG-25	323	4.07805767	0.06043529	67.4780819
25	AG-26	322.5	2.34055825	0.0236697	98.8841617
26	AG-27	322	3.17517307	0.12967428	24.4857586
27	AG-28	321.6	3.69003911	0.03860572	95.5826967
28	AG-29	321.2	4.21899989	0.03154044	133.764768
29	AG-30	320.8	4.33857454	0.03335767	130.062277

TABLE S3. GEOCHEMICAL DATA (XRF ANALYSIS) AT AGUABLANCA CREEK (REDOX-SENSITIVE TM)

Consecutive	Sample	Height (m)	Ni NMS	Cu NMS	V NMS	Zn NMS	Al NMS	Ni/Al (*10-7)	Cu/Al (*10-7)	V/Al (*10-6)	Zn/Al (*10-6)
1	AG-01	344.2	0.03682025	0.019581394	0.243862763	0.252211126	0.847218242	4.35	2.31	2.88	2.98
2	AG-02	343.8	0.040987739	0.024196705	0.271609932	0.238320777	0.759311509	5.4	3.19	3.58	3.14
3	AG-03	343	0.040704318	0.023227998	0.287561916	0.223825286	0.867819281	4.69	2.68	3.31	2.58
4	AG-05	341.9	0.036517169	0.024108373	0.272927189	0.260804121	0.656360015	5.56	3.67	4.16	3.97
5	AG-06	341.5	0.026865919	0.01650712	0.252784777	0.235324342	0.630783066	4.26	2.62	4.01	3.73
6	AG-07	340.5	0.03724972	0.030989189	0.2980168	0.230555698	0.791391755	4.71	3.92	3.77	2.91
7	AG-08	340	0.032619731	0.028309603	0.297357336	0.190604843	0.814845675	4	3.47	3.65	2.34
8	AG-09	339	0.041965603	0.027038845	0.272931087	0.299020007	0.737709633	5.69	3.67	3.7	4.05
9	AG-10	338.2	0.039981542	0.029608996	0.398245234	0.256885192	1.072810047	3.73	2.76	3.71	2.39
10	AG-11	337.6	0.03863128	0.025700924	0.34072008	0.229441592	0.973038412	3.97	2.64	3.5	2.36
11	AG-12	336.9	0.033237991	0.024412592	0.319570046	0.183730589	0.749218633	4.44	3.26	4.27	2.45
12	AG-13	336	0.04334129	0.028295212	0.347405542	0.251630143	0.945042211	4.59	2.99	3.68	2.66
13	AG-14	335.5	0.034328994	0.025751404	0.331511518	0.196491883	0.836541484	4.1	3.08	3.96	2.35
14	AG-15	334.9	0.035989664	0.026460768	0.330923423	0.190895001	0.866442561	4.15	3.05	3.82	2.2
15	AG-16	333.9	0.046642308	0.031248682	0.388168433	0.225329468	1.06227166	4.39	2.94	3.65	2.12
16	AG-17	331.3	0.04222179	0.028648706	0.308805324	0.175952386	0.986241163	4.28	2.9	3.13	1.78
17	AG-18	331	0.034726826	0.020429886	0.210321697	0.115126387	0.673491091	5.16	3.03	3.12	1.71
18	AG-19	330.7	0.041221578	0.031646851	0.313719231	0.17826389	0.998365067	4.13	3.17	3.14	1.79
19	AG-20	330.3	0.046886899	0.050590149	0.497350118	0.25883326	1.249601775	3.75	4.05	3.98	2.07
20	AG-21	329.9	0.049028676	0.05136134	0.490829339	0.245104929	1.357978118	3.61	3.78	3.61	1.8
21	AG-22	324.1	0.032602167	0.023766546	0.227496352	0.120987723	0.701411632	4.65	3.39	3.24	1.72
22	AG-23	323.8	0.049331363	0.033138117	0.203192442	0.261065635	0.97220944	5.07	3.41	2.09	2.69
23	AG-24	323.4	0.044507919	0.035648279	0.209230348	0.272939429	0.84836295	5.25	4.2	2.47	3.22
24	AG-25	323	0.046881079	0.040155298	0.188943697	0.230376242	0.739312716	6.34	5.43	2.56	3.12
25	AG-26	322.5	0.013701969	0.010559014	0.064639062	0.057502188	0.325105711	4.21	3.25	1.99	1.77
26	AG-27	322	0.024748357	0.015532895	0.075689822	0.113285009	0.288012114	8.59	5.39	2.63	3.93
27	AG-28	321.6	0.087387796	0.064878021	0.185989826	0.478557913	0.858265087	10.2	7.56	2.17	5.58
28	AG-29	321.2	0.059428588	0.040866503	0.120826366	0.265499391	0.620957077	9.57	6.58	1.95	4.28
29	AG-30	320.8	0.034466211	0.024848075	0.093715808	0.17987766	0.467558713	7.37	5.31	2	3.85

CHAPTER 3

Table S1 Foraminiferal data (total counts and relative abundances) of Hole 1258A.

Table S2 $\delta^{13}C$ and $\delta^{18}O$ values, and elemental composition data (XRF analyses) of Hole 1258A.

Figure S1 Age model of Hole 1258A. Chronostratigraphic datums based on Suganuma and Ogg (2006). Planktonic foraminifera and calcareous nannofossil biozones based on Erbacher et al. (2004) and Thibault and Gardin (2006).

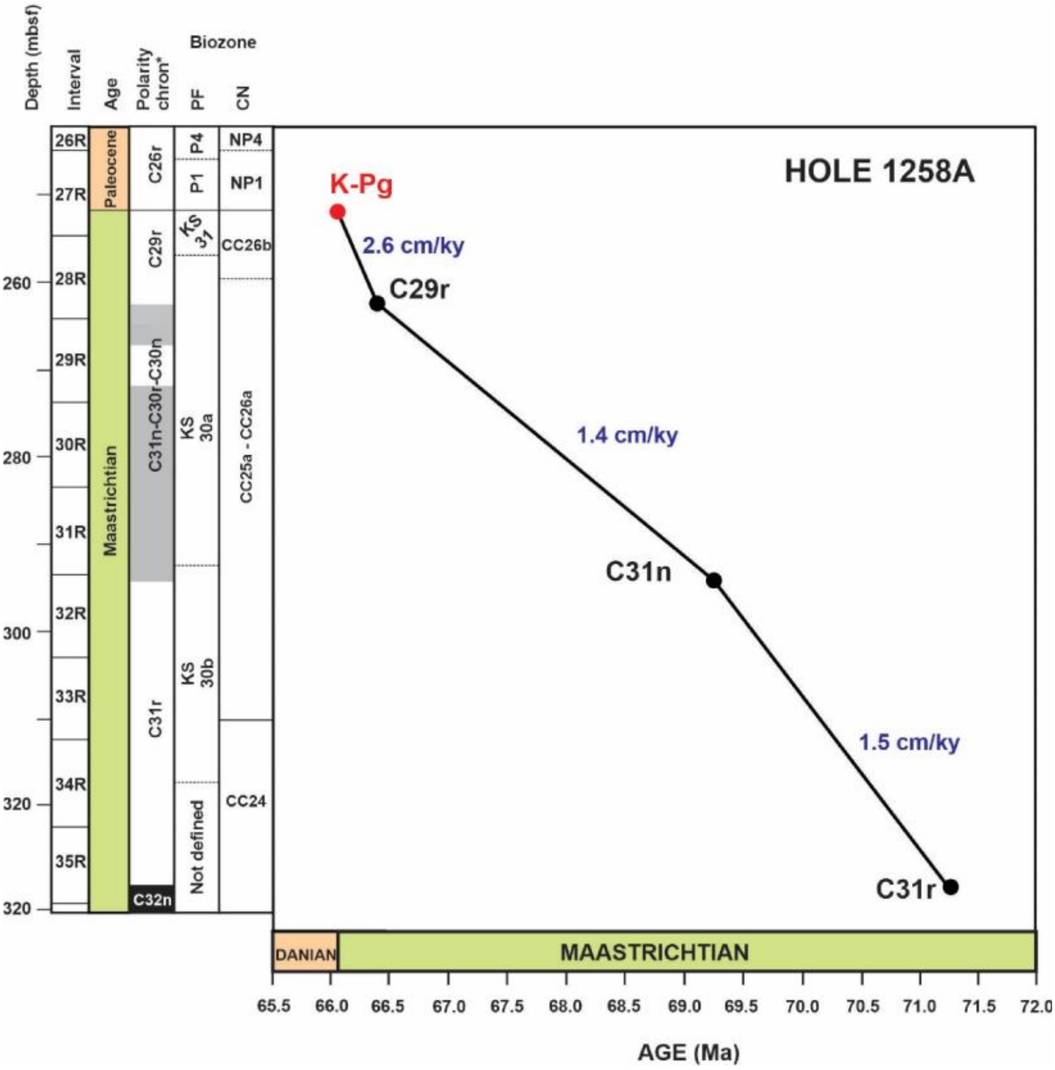

Figure S2 δ^{13}C correlation of Hole 1258A and Maastrichtian localities from Netherlands (ENCI Quarry; Vellekoop et al., 2022) and Italy (Gubbio; Voigt et al., 2012; Batenburg et al., 2018).

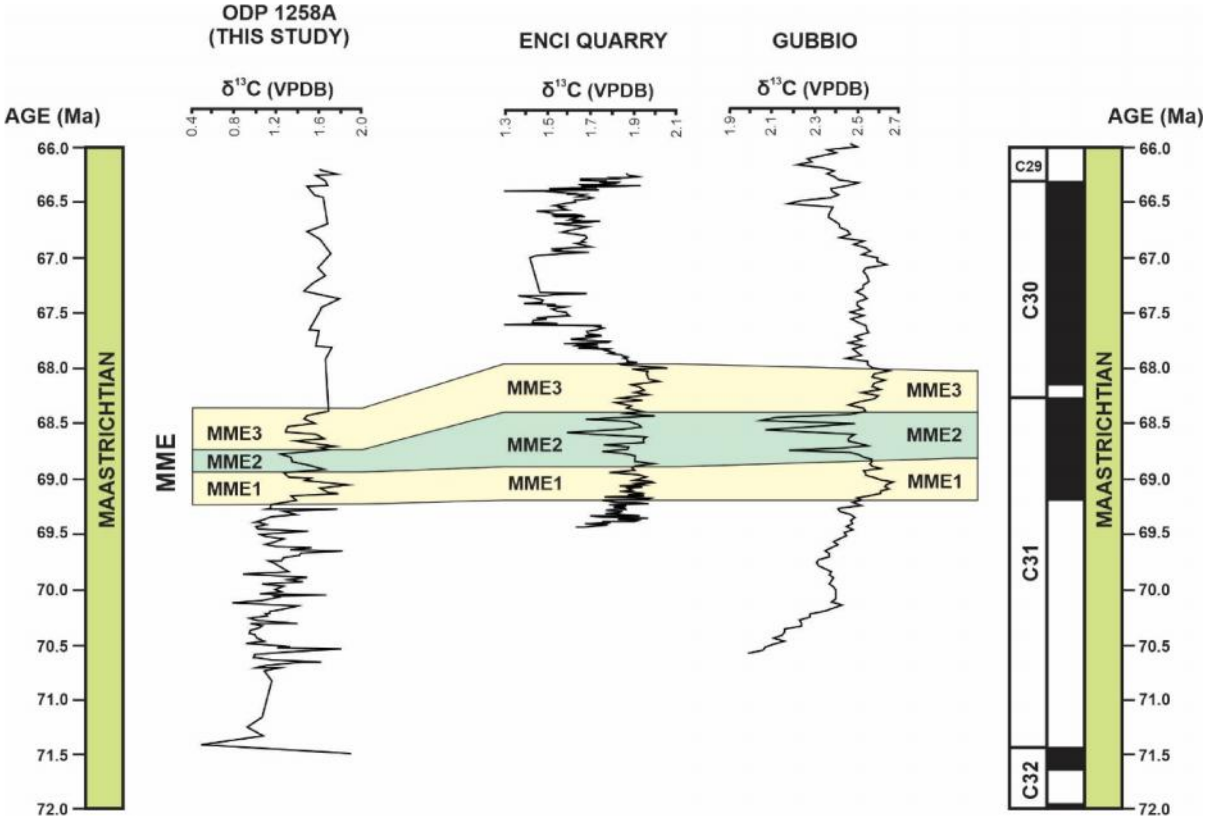

TABLE S1 FORAMINIFERAL DATA (TOTAL COUNT AND RELATIVE ABUNDANCES) OF HOLE 1258A (TOTAL COUNTS)

Consecutive	Ident	Sample	Depth (mbsf)	Total foraminifers*	Total agglutinated (tubular)	Total	*Arenobulimina puschi*	*Arenobulimina* sp.	*Clavulinoides trilatera*
1	DEM28R2-110-112	28R2 110-112	257.5	135	0	145			
2	DEM28R3-23-25NEW	28R3 23-25	258.13	153	0	166			
3	DEM28R3-103-105	28R3 103-105	258.93	129	0	140			
4	DEM28R4-21-23	28R4 21-23	259.61	126	0	138			
5	DEM28R4-103-105	28R4 103-105	260.41	175	0	183			
6	DEM28R5-13-15	28R5 13-15	261.03	147	0	159			
7	DEM28R5-93-95	28R5 93-95	261.83	135	0	144			
8	DEM28R6-30-32	28R6 28-30	262.7	133	0	148			
9	DEM28R6 70-72	28R6 70-72	263.1	121	0	132			
10	DEM28R6-110-112	28R6 110-112	263.5	136	1	149			
11	DEM29R1-63-65	29R1 63-65	265.23	111	0	131			
12	DEM29R1-144-146	29R1 144-146	266.04	135	0	152			
13	DEM29R2-59-61	29R2 59-61	266.69	135	0	148			
14	DEM29R2-143-145	29R2 143-145	267.53	131	0	147			
15	DEM29R3-58-60	29R3 58-60	268.18	166	0	172			
16	DEM29R3-140-142	29R3 140-142	269	199	0	208			
17	DEM29R4-43-45	29R4 43-45	269.53	145	0	154		1	
18	DEM29R4-125-127	29R4 125-127	270.35	180	0	194		1	
19	DEM29R5-63-65	29R5 63-65	271.05	145	0	154			
20	DEM29R5-143-145	29R5 143-145	271.85	183	0	197			
21	DEM29R6-20-22	29R6 20-22	272.12	186	0	192			
22	DEM29R6-140-142	29R6 140-142	273.32	161	1	172	2		
23	DEM29R7-50-52	29R7 50-52	273.92	159	0	171			
24	DEM29R-CC3-5	29R CC 3-5	274.37	151	1	162			
25	DEM30R1-60-62	30R1 60-62	274.8	198	0	227			
26	DEM30R1-143-145	30R1 143-145	275.63	146	0	171	1		
27	DEM30R2-55-57new	30R2 55-57	276.25	142	0	159			
28	DEM30R2-135-137	30R2 135-137	277.05	215	0	231			
29	DEM30R3-63-65	30R3 63-65	277.83	228	0	252			
30	DEM30R3-143-145	30R3 143-145	278.63	199	0	221			
31	DEM30R4-41-43	30R4 41-43	279.11	191	0	215			
32	DEM31R1-65-67	31R1 65-67	284.55	183	0	208			
33	DEM31R1-145-147	31R1 145-147	285.35	183	0	214			
34	DEM31R2-63-65	31R2 63-65	286.03	206	0	220	1		
35	DEM31R2-143-145	31R2 143-145	286.83	192	0	201			
36	DEM31R3 18-20	31R3 18-20	287.08	169	0	179			
37	DEM31R3-63-65	31R3 63-65	287.53	205	0	212			
38	DEM31R3-143-145	31R3 143-145	288.33	168	0	190		1	
39	DEM31R4-63-65	31R4 63-65	289.03	153	0	172			
40	DEM31R4-143-145	31R4 143-145	289.83	173	9	206			
41	DEM31R5-63-65	31R5 63-65	290.53	184	0	198			
42	DEM31R5-143-145	31R5 143-145	291.33	171	0	183			
43	DEM31R6-64-66	31R6 64-66	292.04	164	1	177			
44	DEM31R6-143-145	31R6 143-145	292.83	194	0	212			
45	DEM31R7-58-60	31R7 58-60	293.48	153	0	164			
46	DEM32R1-24-28	32R1 24-28	293.76	137	2	150			
47	DEM32R1-105-108	32R1 105-108	294.56	147	0	165			
48	DEM32R2-25-27	32R2 25-27	295.25	143	0	162			
49	DEM32R2-105-107	32R2 105-107	296.05	140	0	160		1	
50	DEM32R3-22-24	32R3 22-24	296.72	177	0	192			
51	DEM32R3-105-107	32R3 105-107	297.55	156	1	168			
52	DEM32R4-23-25	32R4 23-25	298.23	131	0	155			
53	DEM32R4-105-107	32R4 105-107	299.05	132	0	161			16
54	DEM32R5-16-18	32R5 16-18	299.66	143	0	160			15
55	DEM32R5-95-97	32R5 95-97	300.45	129	0	148			7
56	DEM32R6-20-22	32R6 20-22	301.2	122	0	142			6
57	DEM32R6-101-103	32R6 101-103	302.01	131	0	155	1		18
58	DEM33R1-60-62	33R1 60-62	303.7	127	0	154			3
59	DEM33R1-140-142	33R1 140-142	304.5	178	0	219			
60	DEM33R2-18-20	33R2 18-20	304.78	143	0	170			1
61	DEM33R2-97-100	33R2 97-100	305.58	128	0	143			
62	DEM33R320-22	33R3 20-22	306.3	145	0	166		2	
63	DEM33R3-98-100	33R3 98-100	307.1	324	1	337			
64	DEM33R4-15-17NEW2	33R4 15-17	307.75	219	0	237	1		
65	DEM33R4-103-105	33R4 103-105	308.65	137	5	159			
66	DEM33R5-25-27	33R5 25-27	309.35	153	2	174		1	
67	DEM33R5 63-65	33R5 63-65	309.73	130	2	146			
68	DEM33R5-102-104	33R5 102-104	310.12	109	10	142			
69	DEM33R6-23-25	33R6 23-25	310.83	116	13	146			
70	DEM33R6-103-105	33R6 103-105	311.63	133	11	164		1	
71	DEM33R7-68-70	33R7 68-70	312.78	123	6	143			
72	DEM34R1-62-64	34R1 62-64	313.42	166	15	191			
73	DEM34R1-144-146	34R1 144-146	314.24	137	29	192			
74	DEM34R2-60-62	34R2 60-62	314.8	190	5	214			
75	DEM34R2-143-145	34R2 143-145	315.73	277	10	307			
76	DEM34R3-64-66	34R3 64-66	316.43	175	10	195			
77	DEM34R3-142-144NEW2	34R3 142-144	317.21	153	8	186			
78	DEM34R4-41-43	34R4 41-43	317.71	263	4	302			
79	DEM34R4-118-119	34R4 118-119	318.47	160	0	178			
80	DEM34RCC-5-7	34RCC 5-7	320.11	193	4	213			1

TABLE S1 FORAMINIFERAL DATA (TOTAL COUNT AND RELATIVE ABUNDANCES) OF HOLE 1258A (RELATIVE ABUNDANCE)

Consecutive	Sample	Depth (mbsf)	Total foraminifers*	Arenobulimina puschi	Arenobulimina sp.	Clavulinoides trilatera	Clavulinoides spp.	Cribrostomoides sp.	Dorothia bulletta	Dorothia pupa	Dorothia retusa	Gaudryina pyramidata	Glomospira charoides	Glomospira gordialis	Haplophragmoides sp.	Hormosinella sp.
1	28R2 110-112	257.5	135	0.0	0.0	0.0	0.0	0.0	0.0	0.0	0.0	0.0	0.0	0.0	0.0	0.0
2	28R3 23-25	258.13	153	0.0	0.0	0.0	0.0	0.0	0.7	0.0	0.0	0.0	0.0	0.0	0.0	0.0
3	28R3 103-105	258.93	129	0.0	0.0	0.0	0.0	0.0	0.0	0.0	0.0	0.0	0.0	0.0	0.0	0.0
4	28R4 21-23	259.61	126	0.0	0.0	0.0	0.0	0.0	0.0	0.8	0.0	0.0	0.0	0.0	0.0	0.0
5	28R4 103-105	260.41	175	0.0	0.0	0.0	0.0	0.6	0.0	1.1	0.0	0.0	0.0	0.0	0.0	0.0
6	28R5 13-15	261.03	147	0.0	0.0	0.0	0.0	0.7	0.0	0.0	0.0	0.0	0.0	0.0	0.0	0.0
7	28R5 93-95	261.83	135	0.0	0.0	0.0	0.0	0.0	0.0	0.0	0.7	0.0	0.0	0.0	0.0	0.0
8	28R6 28-30	262.7	133	0.0	0.0	0.0	0.0	0.0	0.0	0.0	0.0	0.0	0.0	0.0	0.0	0.0
9	28R6 70-72	263.1	121	0.0	0.0	0.0	0.0	0.0	0.0	0.0	0.0	0.0	0.0	0.0	0.0	0.0
10	28R6 110-112	263.5	137	0.0	0.0	0.0	0.0	0.7	0.0	0.0	0.0	0.0	0.0	0.0	0.0	0.0
11	29R1 63-65	265.23	111	0.0	0.0	0.0	0.0	0.0	0.0	0.0	0.0	0.0	0.0	0.0	0.0	0.0
12	29R1 144-146	266.04	135	0.0	0.0	0.0	0.0	0.0	0.0	0.0	0.0	0.0	0.0	0.0	0.0	0.0
13	29R2 59-61	266.69	135	0.0	0.0	0.0	0.0	0.0	0.0	0.0	0.0	0.0	0.0	0.0	0.0	0.0
14	29R2 143-145	267.53	131	0.0	0.0	0.0	0.0	0.0	0.0	0.0	0.0	0.0	0.0	0.0	0.0	0.0
15	29R3 58-60	268.18	166	0.0	0.0	0.0	0.0	0.0	0.0	0.0	0.0	0.0	0.0	0.0	0.0	0.0
16	29R3 140-142	269	199	0.0	0.0	0.0	0.0	0.5	0.0	0.0	0.0	0.0	0.0	0.0	0.0	0.0
17	29R4 43-45	269.53	145	0.0	0.7	0.0	0.0	2.1	0.0	0.0	0.0	0.7	0.0	0.0	0.0	0.0
18	29R4 125-127	270.35	180	0.0	0.6	0.0	0.0	0.0	0.0	1.1	0.6	0.0	0.0	0.0	0.0	0.0
19	29R5 63-65	271.05	145	0.0	0.0	0.0	0.0	0.7	0.0	0.0	0.0	0.7	0.0	0.0	0.0	0.0
20	29R5 143-145	271.85	183	0.0	0.0	0.0	0.0	1.1	0.0	0.0	0.5	0.0	0.0	0.0	0.0	0.0
21	29R6 20-22	272.12	186	0.0	0.0	0.0	0.0	0.0	0.0	0.0	0.0	0.0	0.0	0.0	0.0	0.0
22	29R6 140-142	273.32	162	1.2	0.0	0.0	0.0	0.6	0.0	0.0	0.0	0.0	0.0	0.0	0.0	0.0
23	29R7 50-52	273.92	159	0.0	0.0	0.0	0.0	0.0	0.0	0.0	0.0	0.0	0.0	0.0	0.0	0.0
24	29R CC 3-5	274.37	152	0.0	0.0	0.0	0.0	0.0	0.0	0.0	0.0	0.0	0.0	0.0	0.0	0.0
25	30R1 60-62	274.8	198	0.0	0.0	0.0	0.5	0.0	0.0	0.5	0.0	0.0	0.0	0.0	0.0	0.0
26	30R1 143-145	275.63	146	0.7	0.0	0.0	0.0	0.0	0.0	0.0	0.0	0.0	0.0	0.0	0.7	0.0
27	30R2 55-57	276.25	142	0.0	0.0	0.0	0.0	0.0	0.0	0.0	0.0	0.0	0.0	0.0	0.0	0.0
28	30R2 135-137	277.05	215	0.0	0.0	0.0	0.0	0.0	0.0	2.3	0.0	0.0	0.0	0.0	0.0	0.0
29	30R3 63-65	277.83	228	0.0	0.0	0.0	0.0	0.0	0.0	0.4	0.4	0.0	0.0	0.0	0.0	0.0
30	30R3 143-145	278.63	199	0.0	0.0	0.0	0.0	1.0	0.0	0.0	0.0	0.0	0.0	0.0	0.0	0.0
31	30R4 41-43	279.11	191	0.0	0.0	0.0	0.0	0.0	0.0	0.0	0.0	0.5	0.0	0.0	0.5	0.0
32	31R1 65-67	284.55	183	0.0	0.0	0.0	0.0	0.0	0.0	0.5	0.0	0.0	0.0	0.0	0.0	0.0
33	31R1 145-147	285.35	183	0.0	0.0	0.0	0.0	0.0	0.0	1.6	0.0	1.6	0.0	0.0	0.0	0.0
34	31R2 63-65	286.03	206	0.5	0.0	0.0	0.0	0.0	0.0	0.5	0.0	0.0	0.0	0.0	0.0	0.0
35	31R2 143-145	286.83	192	0.0	0.0	0.0	0.0	1.0	0.0	0.0	0.0	0.0	0.0	0.0	0.0	0.0
36	31R3 18-20	287.08	169	0.0	0.0	0.0	0.0	0.0	0.0	0.0	0.0	0.6	0.0	0.0	0.0	0.0
37	31R3 63-65	287.53	205	0.0	0.0	0.0	0.0	0.5	0.0	0.0	0.0	0.0	0.0	0.0	0.0	0.0
38	31R3 143-145	288.33	168	0.0	0.6	0.0	0.0	0.0	0.0	0.0	0.0	0.0	0.0	0.0	0.0	0.0
39	31R4 63-65	289.03	153	0.0	0.0	0.0	0.0	0.0	0.0	0.7	0.0	0.7	0.0	0.0	0.0	0.7
40	31R4 143-145	289.83	182	0.0	0.0	0.0	0.0	1.1	0.0	0.5	0.5	0.0	0.0	0.0	0.0	0.0
41	31R5 63-65	290.53	184	0.0	0.0	0.0	0.0	0.0	0.0	0.5	0.0	1.6	0.0	0.0	0.0	0.0
42	31R5 143-145	291.33	171	0.0	0.0	0.0	0.0	0.0	0.0	0.0	0.0	0.0	0.0	0.0	0.0	0.0
43	31R6 64-66	292.04	165	0.0	0.0	0.0	0.0	0.0	0.0	0.0	0.0	0.6	0.0	0.0	0.0	0.0
44	31R6 143-145	292.83	194	0.0	0.0	0.0	0.0	0.5	0.0	0.0	0.0	0.0	0.0	0.0	0.0	0.0
45	31R7 58-60	293.48	153	0.0	0.0	0.0	0.0	0.0	0.0	0.0	0.0	1.3	0.0	0.0	0.0	0.0
46	32R1 24-28	293.76	139	0.0	0.0	0.0	0.0	0.0	0.0	0.0	0.0	0.7	0.0	0.0	0.0	0.0
47	32R1 105-108	294.56	147	0.0	0.0	0.0	0.0	0.0	0.0	0.0	0.0	0.0	0.0	0.0	0.0	0.0
48	32R2 25-27	295.25	143	0.0	0.0	0.0	0.0	0.0	0.7	0.0	0.0	0.7	0.0	0.0	0.0	0.0
49	32R2 105-107	296.05	140	0.0	0.7	0.0	0.0	0.0	0.0	0.0	0.0	1.4	0.0	0.0	0.0	0.0
50	32R3 22-24	296.72	177	0.0	0.0	0.0	0.6	0.0	0.0	0.6	0.0	0.0	0.0	0.0	0.0	0.0
51	32R3 105-107	297.55	157	0.0	0.0	0.0	0.0	0.0	0.0	0.0	0.0	0.0	0.0	0.0	0.0	0.0
52	32R4 23-25	298.23	131	0.0	0.0	0.0	0.0	0.0	0.0	0.0	0.8	0.8	0.0	0.0	0.0	0.0
53	32R4 105-107	299.05	132	0.0	0.0	12.1	0.0	0.0	0.0	0.8	0.0	0.0	0.0	0.0	0.0	0.0
54	32R5 16-18	299.66	143	0.0	0.0	10.5	0.0	0.0	0.0	0.0	0.0	0.0	0.0	0.0	0.0	0.0
55	32R5 95-97	300.45	129	0.0	0.0	5.4	0.8	0.0	0.0	1.6	0.0	0.0	0.0	0.0	0.0	0.0
56	32R6 20-22	301.2	122	0.0	0.0	4.9	0.0	0.0	0.0	1.6	0.0	0.8	0.0	0.0	0.0	0.0
57	32R6 101-103	302.01	131	0.8	0.0	13.7	0.0	0.0	0.0	0.0	0.0	0.0	0.0	0.0	0.0	0.0
58	33R1 60-62	303.7	127	0.0	0.0	2.4	0.0	0.0	0.0	0.0	0.0	2.4	0.0	0.0	0.0	0.0
59	33R1 140-142	304.5	178	0.0	0.0	0.0	0.0	0.0	0.0	0.6	0.0	0.6	0.0	0.0	0.0	0.0
60	33R2 18-20	304.78	143	0.0	0.0	0.7	0.0	0.0	1.4	0.0	0.0	1.4	0.0	0.0	0.0	0.0
61	33R2 97-100	305.58	128	0.0	0.0	0.0	0.0	0.0	0.0	0.8	0.0	2.3	0.0	0.0	0.0	0.0
62	33R3 20-22	306.3	145	0.0	1.4	0.0	0.0	0.0	0.0	0.0	0.0	0.7	0.0	0.0	0.0	0.0
63	33R3 98-100	307.1	325	0.0	0.0	0.0	0.0	0.0	0.0	0.0	0.0	0.3	0.0	0.0	0.0	0.0
64	33R4 15-17	307.75	219	0.5	0.0	0.0	0.0	0.0	0.0	0.0	0.0	0.5	0.0	0.0	0.0	0.0
65	33R4 103-105	308.65	142	0.0	0.0	0.0	0.0	0.7	0.0	0.7	0.0	0.0	0.0	0.0	0.7	0.0
66	33R5 25-27	309.35	155	0.0	0.6	0.0	0.0	1.3	0.0	0.0	0.0	0.0	0.0	0.0	0.0	0.0
67	33R5 63-65	309.73	132	0.0	0.0	0.0	0.0	0.0	0.0	0.0	0.0	0.0	0.0	0.0	0.0	0.0
68	33R5 102-104	310.12	119	0.0	0.0	0.0	0.0	0.0	0.0	0.0	0.0	1.7	0.0	0.0	0.0	0.0
69	33R6 23-25	310.83	129	0.0	0.0	0.0	0.0	0.0	0.0	0.0	0.0	0.8	0.0	0.0	0.0	0.0
70	33R6 103-105	311.63	144	0.0	0.7	0.0	0.0	0.0	0.0	0.0	0.7	0.0	0.0	0.0	0.0	0.0
71	33R7 68-70	312.78	129	0.0	0.0	0.0	0.0	0.0	0.0	0.8	0.0	0.8	0.0	0.0	0.0	0.0
72	34R1 62-64	313.42	181	0.0	0.0	0.0	0.0	0.0	0.0	1.1	0.0	1.1	0.0	0.0	0.0	0.0
73	34R1 144-146	314.24	166	0.0	0.0	0.0	0.0	0.0	0.0	0.0	0.0	3.0	0.0	0.0	0.0	0.0
74	34R2 60-62	314.8	195	0.0	0.0	0.0	0.0	0.0	0.0	0.0	0.0	4.1	0.0	0.0	0.0	0.0
75	34R2 143-145	315.73	287	0.0	0.0	0.0	0.0	0.0	0.0	0.0	0.0	4.2	0.0	0.3	0.0	0.0
76	34R3 64-66	316.43	185	0.0	0.0	0.0	0.0	0.0	0.0	0.5	0.0	1.6	0.0	0.0	0.0	0.0
77	34R3 142-144	317.21	161	0.0	0.0	0.0	0.0	0.6	0.0	0.0	0.0	0.6	1.2	0.0	0.6	0.0
78	34R4 41-43	317.71	267	0.0	0.0	0.0	0.0	0.0	0.0	0.0	0.0	0.0	0.0	0.4	0.0	0.0
79	34R4 118-119	318.47	160	0.0	0.0	0.0	0.0	0.0	0.0	0.0	0.0	0.0	0.0	0.0	0.0	0.6
80	34R CC 5-7	320.11	197	0.0	0.0	0.5	0.0	0.0	0.0	0.5	0.0	0.5	0.0	0.0	0.0	0.0

lcareous uniserial forms (fragmented)

TABLE S1 FORAMINIFERAL DATA (TOTAL COUNT AND RELATIVE ABUNDANCES) OF HOLE 1258A (DIVERSITY)															
Sample	Depth (mbsf)	Taxa_S	Individuals	Dominance_D	Simpson_1-D	Shannon_H	Evenness_e^H/S	Brillouin	Menhinick	Margalef	Equitability_J	Fisher_alpha	Berger-Parker	Chao-1
DEM28R2-110-112	257.5	34	135	0.07029	0.9297	2,985	0.582	2,661	2,926	6,727	0.8465	14.62	0.1111	51.14
DEM28R3-23-25NEW	258.13	39	153	0.06113	0.9389	3,173	0.6122	2,835	3,153	7,554	0.8661	16.9	0.1438	52.13
DEM28R3-103-105	258.93	36	129	0.08503	0.915	2.98	0.5468	2,631	3.17	7,202	0.8316	16.56	0.2171	93
DEM28R4-21-23	259.61	37	124	0.0731	0.9269	3,051	0.5713	2,682	3,323	7,468	0.845	17.85	0.1532	65.5
DEM28R4-103-105	260.41	47	175	0.06344	0.9366	3,243	0.5452	2,898	3,553	8,906	0.8424	21.07	0.1371	80
DEM28R5-13-15	261.03	36	146	0.06887	0.9311	3,051	0.5874	2,729	2,979	7,023	0.8515	15.27	0.1575	70
DEM28R5-93-95	261.83	46	135	0.06491	0.9351	3,196	0.531	2,796	3,959	9,174	0.8347	24.6	0.1259	139
DEM28R6-30-32	262.7	30	133	0.09085	0.9092	2,812	0.5547	2,516	2,601	5.93	0.8267	12.06	0.203	38.25
DEM28R6 70-72	263.1	40	118	0.05918	0.9408	3,221	0.6261	2,807	3,682	8,175	0.8731	21.3	0.1271	82
DEM28R6-110-112	263.5	43	136	0.08942	0.9106	3	0.4671	2.63	3,687	8,549	0.7976	21.66	0.2059	106
DEM29R1-63-65	265.23	34	111	0.09017	0.9098	2,934	0.5532	2.56	3,227	7,007	0.8321	16.72	0.2162	43.55
DEM29R1-144-146	266.04	37	135	0.0986	0.9014	2,863	0.4736	2,529	3,184	7,339	0.793	16.82	0.1926	56
DEM29R2-59-61	266.69	33	135	0.05909	0.9409	3,108	0.6782	2,776	2.84	6,524	0.889	13.93	0.1407	40.86
DEM29R2-143-145	267.53	36	131	0.0687	0.9313	3,108	0.6218	2.75	3,145	7,179	0.8674	16.39	0.1679	45.75
DEM29R3-58-60	268.18	45	166	0.1183	0.8817	2,971	0.4338	2,634	3,493	8,607	0.7806	20.3	0.3072	66
DEM29R3-140-142	269	45	197	0.06918	0.9308	3,139	0.513	2,837	3,206	8,328	0.8247	18.23	0.132	60.3
DEM29R4-43-45	269.53	43	143	0.08318	0.9168	3,097	0.5149	2,729	3,596	8,463	0.8235	20.86	0.2238	79.14
DEM29R4-125-127	270.35	36	180	0.1009	0.8991	2,819	0.4654	2,553	2,683	6.74	0.7866	13.53	0.2222	47.38
DEM29R5-63-65	271.05	44	145	0.0771	0.9229	3,076	0.4928	2,714	3,654	8.64	0.813	21.49	0.1586	119.6
DEM29R5-143-145	271.85	43	183	0.07635	0.9236	3,091	0.5116	2,783	3,179	8,062	0.8218	17.71	0.1803	58.3
DEM29R6-20-22	272.12	42	186	0.07486	0.9251	3,112	0.5347	2,807	3.08	7,846	0.8325	16.9	0.1935	48.5
DEM29R6-140-142	273.32	42	162	0.08078	0.9192	3,071	0.5134	2,739	3.3	8,059	0.8216	18.4	0.2037	54.75
DEM29R7-50-52	273.92	41	159	0.08287	0.9171	3,063	0.5219	2,732	3,252	7,891	0.8249	17.9	0.2075	75.2
DEM29R-CC3-5	274.37	39	152	0.09687	0.9031	2.96	0.4949	2,635	3,163	7,564	0.808	16.97	0.2566	67.5
DEM30R1-60-62	274.8	41	198	0.1103	0.8897	2,873	0.4316	2,598	2,914	7,564	0.7737	15.71	0.2475	48.58
DEM30R1-143-145	275.63	39	146	0.08594	0.9141	2.94	0.485	2,612	3,228	7,625	0.8025	17.42	0.1644	89.6
DEM30R2-55-57new	276.25	43	141	0.08043	0.9196	3,149	0.5423	2,769	3,621	8,487	0.8373	21.08	0.2128	70.14
DEM30R2-135-137	277.05	43	214	0.1189	0.8811	2.79	0.3787	2,532	2,939	7,827	0.7418	16.2	0.257	81.5
DEM30R3-63-65	277.83	46	228	0.08764	0.9124	3.05	0.4588	2,774	3,046	8,288	0.7965	17.37	0.2061	51.2
DEM30R3-143-145	278.63	43	197	0.0715	0.9285	3,121	0.5269	2,825	3,064	7.95	0.8297	16.96	0.1726	47.59
DEM30R4-41-43	279.11	41	190	0.09596	0.904	2,871	0.4307	2,595	2,974	7,623	0.7732	16.07	0.1947	58.1
DEM31R1-65-67	284.55	41	180	0.08278	0.9172	3,039	0.5093	2.74	3,056	7,703	0.8183	16.58	0.2222	88.5
DEM31R1-145-147	285.35	39	183	0.0622	0.9378	3,175	0.6137	2,876	2,883	7,294	0.8667	15.18	0.1475	46.86
DEM31R2-63-65	286.03	42	206	0.09072	0.9093	2,945	0.4525	2,675	2,926	7,695	0.7878	15.95	0.2136	59
DEM31R2-143-145	286.83	37	192	0.1237	0.8763	2,712	0.407	2.46	2.67	6,847	0.751	13.64	0.2865	50.33
DEM31R3 18-20	287.08	41	169	0.1139	0.8861	2,927	0.4552	2,614	3,154	7,797	0.7881	17.22	0.2959	53
DEM31R3-63-65	287.53	33	205	0.1129	0.8871	2,675	0.4266	2.45	2,375	6,199	0.7584	11.62	0.2244	47
DEM31R3-143-145	288.33	34	167	0.07799	0.922	2,913	0.5416	2,639	2,631	6,448	0.8261	12.9	0.1437	42.67
DEM31R4-63-65	289.03	39	153	0.06087	0.9391	3,194	0.6256	2,855	3,153	7,554	0.872	16.9	0.1634	63
DEM31R4-143-145	289.83	38	182	0.08109	0.9189	2,981	0.5186	2,699	2,817	7.11	0.8195	14.62	0.1758	48.11
DEM31R5-63-65	290.53	39	184	0.1358	0.8642	2,685	0.3758	2,419	2,875	7,287	0.7329	15.13	0.3098	62.75
DEM31R5-143-145	291.33	37	171	0.1418	0.8582	2.67	0.3902	2.4	2,829	7,002	0.7394	14.53	0.3333	94.75
DEM31R6-64-66	292.04	39	164	0.173	0.827	2,654	0.3642	2,358	3,045	7,451	0.7243	16.18	0.3902	60.38
DEM31R6-143-145	292.83	41	194	0.1038	0.8962	2,863	0.4272	2,591	2,944	7,593	0.771	15.88	0.2526	62.11
DEM31R7-58-60	293.48	35	153	0.08744	0.9126	2,939	0.54	2,634	2.83	6,759	0.8267	14.19	0.1895	43.25
DEM32R1-24-28	293.76	42	139	0.06951	0.9305	3.17	0.5666	2,791	3,562	8,309	0.848	20.45	0.1511	52.46
DEM32R1-105-108	294.56	42	146	0.06052	0.9395	3,257	0.6184	2,885	3,476	8,227	0.8714	19.74	0.1575	61.43
DEM32R2-25-27	295.25	38	143	0.0555	0.9445	3,227	0.6633	2,872	3,178	7,455	0.8872	16.92	0.1329	51
DEM32R2-105-107	296.05	42	140	0.04612	0.9539	3,404	0.7163	3,007	3.55	8,297	0.9107	20.34	0.1357	53.38
DEM32R3-22-24	296.72	49	177	0.05685	0.9432	3,314	0.5609	2,959	3,683	9,273	0.8514	22.42	0.1243	74.3
DEM32R3-105-107	297.55	41	156	0.07479	0.9252	3.11	0.5468	2,772	3,283	7,921	0.8374	18.12	0.1987	58
DEM32R4-23-25	298.23	42	131	0.05926	0.9407	3,258	0.6191	2,858	3.67	8.41	0.8717	21.39	0.145	61
DEM32R4-105-107	299.05	36	132	0.0722	0.9278	3,054	0.5888	2,704	3,133	7,168	0.8522	16.31	0.1667	47.67
DEM32R5-16-18	299.66	41	143	0.06088	0.9391	3,186	0.5902	2,822	3,429	8.06	0.858	19.22	0.1119	52.33
DEM32R5-95-97	300.45	38	129	0.05751	0.9425	3,235	0.6686	2,852	3,346	7,613	0.8893	18.16	0.1628	53
DEM32R6-20-22	301.2	32	122	0.0821	0.9179	2,921	0.5798	2,585	2,897	6,453	0.8427	14.12	0.1803	40.67
DEM32R6-101-103	302.01	41	131	0.08572	0.9143	3,058	0.5191	2,678	3,582	8,205	0.8234	20.5	0.2137	60
DEM33R1-60-62	303.7	43	127	0.04681	0.9532	3,407	0.7019	2,978	3,816	8.67	0.9059	22.88	0.126	58.11
DEM33R1-140-142	304.5	40	178	0.08124	0.9188	3,008	0.5064	2,712	2,998	7,526	0.8156	16.05	0.1798	57
DEM33R2-18-20	304.78	51	143	0.05707	0.9429	3,408	0.5925	2,976	4,265	10.07	0.8669	28.35	0.1678	86.1
DEM33R2-97-100	305.58	45	128	0.05957	0.9404	3,333	0.623	2,901	3,977	9,068	0.8757	24.7	0.1719	57.21
DEM33R320-22	306.3	46	145	0.04685	0.9532	3,388	0.6435	2,989	3.82	9,042	0.8849	23.24	0.1103	74.11
DEM33R3-98-100	307.1	46	325	0.07488	0.9251	3,063	0.4652	2,853	2,552	7.78	0.8001	14.63	0.1415	54.25
DEM33R4-15-17NEW2	307.75	46	219	0.1348	0.8652	2,849	0.3753	2,577	3,108	8.35	0.744	17.76	0.3333	74.88
DEM33R4-103-105	308.65	37	142	0.05713	0.9429	3,195	0.66	2,847	3,105	7,264	0.8849	16.26	0.1268	55.2
DEM33R5-25-27	309.35	47	155	0.06148	0.9385	3,287	0.5696	2,907	3,775	9,121	0.8538	22.95	0.1548	63.15
DEM33R5 63-65	309.73	33	131	0.08339	0.9166	2,947	0.577	2,619	2,883	6,564	0.8427	14.19	0.2061	51.2
DEM33R5-102-104	310.12	38	119	0.06829	0.9317	3,131	0.6027	2,737	3,483	7,742	0.8608	19.29	0.1765	55
DEM33R6-23-25	310.83	39	129	0.09344	0.9066	3,026	0.5285	2,652	3,434	7,819	0.8259	19	0.2558	50.33
DEM33R6-103-105	311.63	44	144	0.05883	0.9412	3,242	0.5816	2,862	3,667	8,652	0.8568	21.6	0.125	67.1
DEM33R7-68-70	312.78	39	129	0.07998	0.92	3,053	0.543	2,682	3,434	7,819	0.8333	19	0.2093	60.11
DEM34R1-62-64	313.42	40	181	0.07213	0.9279	3,059	0.5326	2,765	2,973	7,502	0.8292	15.89	0.1768	57
DEM34R1-144-146	314.24	43	166	0.07272	0.9273	3,179	0.5589	2,837	3,337	8,216	0.8453	18.82	0.1747	49
DEM34R2-60-62	314.8	42	195	0.08003	0.92	3,057	0.5064	2,769	3,008	7,775	0.8179	16.45	0.2051	67.5
DEM34R2-143-145	315.73	43	287	0.07152	0.9285	3,109	0.5209	2,885	2,538	7,421	0.8266	14.02	0.1568	49.88
DEM34R3-64-66	316.43	47	185	0.06489	0.9351	3,224	0.5348	2,894	3,456	8,812	0.8375	20.32	0.1459	73.25
DEM34R3-142-144NEW2	317.21	50	161	0.04664	0.9534	3,453	0.6319	3,057	3,941	9,643	0.8827	24.85	0.118	65
DEM34R4-41-43	317.71	54	267	0.05582	0.9442	3,344	0.5248	3,063	3,305	9,486	0.8384	20.42	0.1124	69.55
DEM34R4-118-119	318.47	43	160	0.05914	0.9409	3,239	0.5934	2.89	3,399	8,276	0.8613	19.29	0.125	58.3
DEM34RCC-5-7	320.11	58	197	0.03327	0.9667	3,703	0.6992	3,308	4,132	10.79	0.9119	27.71	0.07614	66.5

TABLE S1 FORAMINIFERAL DATA (TOTAL COUNT AND RELATIVE ABUNDANCES) OF HOLE 1258A (MORPHOGROUPS)

Consecutive	Ident	Sample	Depth (mbsf)	Age (My)	Total foraminifers	Total foraminifers*	Agglutinated	Total agglutinated (tubular)	Total agglutinated*	Total biserial**	Total uniserial***	Lenticulinids	Gavelinellids	Buliminids	Agglutinated (%)	Calcareous biserial (%)	Calcareous uniserial (%)	Lenticulinids (%)	Gavelinellids (%)	Buliminids (%)
1	**DEM28R2-110-112**	28R2 110-112	257.5	66.2	145	141	3	0	3	18	50	7	3	0	2.1	12.8	35.5	5.0	2.1	0.0
2	DEM28R3-23-25NEW	28R3 23-25	258.13	66.22	166	164	4	0	4	39	20	5	4	3	2.4	23.8	12.2	3.0	2.4	1.8
3	**DEM28R3-103-105**	28R3 103-105	258.93	66.25	140	134	4	0	4	19	29	3	12	0	3.0	14.2	21.6	2.2	9.0	0.0
4	DEM28R4-21-23	28R4 21-23	259.61	66.27	138	134	5	0	5	28	22	7	6	1	3.7	20.9	16.4	5.2	4.5	0.7
5	**DEM28R4-103-105**	28R4 103-105	260.41	66.3	183	177	6	0	6	6	43	6	30	2	3.4	3.4	24.3	3.4	16.9	1.1
6	DEM28R5-13-15	28R5 13-15	261.03	66.32	159	151	11	0	11	14	49	5	19	0	7.3	9.3	32.5	3.3	12.6	0.0
7	**DEM28R5-93-95**	28R5 93-95	261.83	66.35	144	138	11	0	11	6	41	6	12	1	8.0	4.3	29.7	4.3	8.7	0.7
8	DEM28R6-30-32	28R6 28-30	262.7	66.38	148	145	15	0	15	3	52	1	8	0	10.3	2.1	35.9	0.7	5.5	0.0
9	DEM28R6 70-72	28R6 70-72	263.1	66.41	132	132	15	0	15	6	36	5	5	5	11.4	4.5	27.3	3.8	3.8	3.8
10	**DEM28R6-110-112**	28R6 110-112	263.5	66.45	149	143	7	1	6	33	33	3	3	5	4.2	23.1	23.1	2.1	2.1	3.5
11	DEM29R1-63-65	29R1 63-65	265.23	66.61	131	123	8	0	8	6	15	1	9	1	6.5	4.9	12.2	0.8	7.3	0.8
12	**DEM29R1-144-146**	29R1 144-146	266.04	66.69	152	150	8	0	8	5	27	14	8	2	5.3	3.3	18.0	9.3	5.3	1.3
13	DEM29R2-59-61	29R2 59-61	266.69	66.75	148	148	13	0	13	15	21	5	11	0	8.8	10.1	14.2	3.4	7.4	0.0
14	**DEM29R2-143-145**	29R2 143-145	267.53	66.83	147	143	4	0	4	18	26	3	16	2	2.8	12.6	18.2	2.1	11.2	1.4
15	DEM29R3-58-60	29R3 58-60	268.18	66.89	172	170	4	0	4	11	21	5	26	2	2.4	6.5	12.4	2.9	15.3	1.2
16	**DEM29R3-140-142**	29R3 140-142	269	66.96	208	201	7	0	7	32	36	13	41	7	3.5	15.9	17.9	6.5	20.4	3.5
17	DEM29R4-43-45	29R4 43-45	269.53	67.02	154	147	17	0	17	18	39	5	14	2	11.6	12.2	26.5	3.4	9.5	1.4
18	**DEM29R4-125-127**	29R4 125-127	270.35	67.09	194	185	9	0	9	14	43	8	24	0	4.9	7.6	23.2	4.3	13.0	0.0
19	DEM29R5-63-65	29R5 63-65	271.05	67.16	154	149	14	0	14	4	30	2	12	4	9.4	2.7	20.1	1.3	8.1	2.7
20	**DEM29R5-143-145**	29R5 143-145	271.85	67.23	197	189	19	0	19	2	53	11	17	3	10.1	1.1	28.0	5.8	9.0	1.6
21	DEM29R6-20-22	29R6 20-22	272.12	67.26	192	187	19	0	19	33	57	8	6	2	10.2	17.6	30.5	4.3	3.2	1.1
22	**DEM29R6-140-142**	29R6 140-142	273.32	67.37	172	168	13	1	12	10	45	11	10	5	7.1	6.0	26.8	6.5	6.0	3.0
23	DEM29R7-50-52	29R7 50-52	273.92	67.43	171	164	7	0	7	10	39	3	30	5	4.3	6.1	23.8	1.8	18.3	3.0
24	DEM29R-CC3-5	29R CC 3-5	274.37	67.47	162	158	12	1	11	11	56	2	14	5	7.0	7.0	35.4	1.3	8.9	3.2
25	DEM30R1-60-62	30R1 60-62	274.8	67.51	227	216	10	0	10	4	30	6	15	4	4.6	1.9	13.9	2.8	6.9	1.9
26	DEM30R1-143-145	30R1 143-145	275.63	67.59	171	164	4	0	4	6	28	3	3	0	2.4	3.7	17.1	1.8	1.8	0.0
27	**DEM30R2-55-57new**	30R2 55-57	276.25	67.65	159	151	6	0	6	10	51	8	11	3	4.0	6.6	33.8	5.3	7.3	2.0
28	DEM30R2-135-137	30R2 135-137	277.05	67.72	231	226	13	0	13	64	51	9	13	1	5.8	28.3	22.6	4.0	5.8	0.4
29	**DEM30R3-63-65**	30R3 63-65	277.83	67.8	252	248	7	0	7	21	63	16	16	2	2.8	8.5	25.4	6.5	6.5	0.8
30	DEM30R3-143-145	30R3 143-145	278.63	67.87	221	213	7	0	7	37	31	11	18	0	3.3	17.4	14.6	5.2	8.5	0.0
31	**DEM30R4-41-43**	30R4 41-43	279.11	67.92	215	209	5	0	5	4	43	6	35	0	2.4	1.9	20.6	2.9	16.7	0.0
32	DEM31R1-65-67	31R1 65-67	284.55	68.43	208	195	5	0	5	18	16	7	18	0	2.6	9.2	8.2	3.6	9.2	0.0
33	**DEM31R1-145-147**	31R1 145-147	285.35	68.5	214	197	24	0	24	18	17	7	36	0	12.2	9.1	8.6	3.6	18.3	0.0
34	DEM31R2-63-65	31R2 63-65	286.03	68.57	220	217	10	0	10	48	38	16	10	1	4.6	22.1	17.5	7.4	4.6	0.5
35	**DEM31R2-143-145**	31R2 143-145	286.83	68.64	201	199	4	0	4	59	36	4	29	1	2.0	29.6	18.1	2.0	14.6	0.5
36	**DEM31R3 18-20**	31R3 18-20	287.08	68.66	178	177	6	0	6	56	25	4	8	1	3.4	31.6	14.1	2.3	4.5	0.6
37	DEM31R3-63-65	31R3 63-65	287.53	68.71	212	206	7	0	7	52	28	7	48	0	3.4	25.2	13.6	3.4	23.3	0.0
38	**DEM31R3-143-145**	31R3 143-145	288.33	68.78	190	180	11	0	11	21	25	5	25	0	6.1	11.7	13.9	2.8	13.9	0.0
39	DEM31R4-63-65	31R4 63-65	289.03	68.85	172	162	5	0	5	12	28	10	16	0	3.1	7.4	17.3	6.2	9.9	0.0
40	**DEM31R4-143-145**	31R4 143-145	289.83	68.92	206	187	17	9	8	12	43	4	21	0	4.3	6.4	23.0	2.1	11.2	0.0
41	DEM31R5-63-65	31R5 63-65	290.53	68.99	198	193	9	0	9	12	31	3	28	0	4.7	6.2	16.1	1.6	14.5	0.0
42	**DEM31R5-143-145**	31R5 143-145	291.33	69.06	183	178	4	0	4	17	13	9	30	5	2.2	9.6	7.3	5.1	16.9	2.8
43	DEM31R6-64-66	31R6 64-66	292.04	69.13	177	172	7	1	6	11	17	9	8	0	3.5	6.4	9.9	5.2	4.7	0.0
44	**DEM31R6-143-145**	31R6 143-145	292.83	69.2	212	203	5	0	5	37	21	8	18	4	2.5	18.2	10.3	3.9	8.9	2.0
45	DEM31R7-58-60	31R7 58-60	293.48	69.27	164	162	4	0	4	3	42	13	10	0	2.5	1.9	25.9	8.0	6.2	0.0
46	**DEM32R1-24-28**	32R1 24-28	293.76	69.28	150	144	11	2	9	23	27	8	11	2	6.3	16.0	18.8	5.6	7.6	1.4
47	DEM32R1-105-108	32R1 105-108	294.56	69.33	165	164	3	0	3	12	42	10	13	0	1.8	7.3	25.6	6.1	7.9	0.0
48	**DEM32R2-25-27**	32R2 25-27	295.25	69.37	162	159	3	0	3	13	36	11	20	1	1.9	8.2	22.6	6.9	12.6	0.6
49	DEM32R2-105-107	32R2 105-107	296.05	69.42	160	159	5	0	5	8	9	11	27	1	3.1	5.0	5.7	6.9	17.0	0.6
50	**DEM32R3-22-24**	32R3 22-24	296.72	69.46	192	185	9	0	9	15	33	20	20	3	4.9	8.1	17.8	10.8	10.8	1.6
51	DEM32R3-105-107	32R3 105-107	297.55	69.51	168	166	10	1	9	34	21	5	9	0	5.4	20.5	12.7	3.0	5.4	0.0
52	**DEM32R4-23-25**	32R4 23-25	298.23	69.55	155	148	9	0	9	7	12	5	19	4	6.1	4.7	8.1	3.4	12.8	2.7
53	DEM32R4-105-107	32R4 105-107	299.05	69.6	161	149	17	0	17	7	21	5	3	0	11.4	4.7	14.1	3.4	2.0	0.0
54	**DEM32R5-16-18**	32R5 16-18	299.66	69.63	160	154	19	0	19	14	22	6	13	2	12.3	9.1	14.3	3.9	8.4	1.3
55	DEM32R5-95-97	32R5 95-97	300.45	69.68	148	145	17	0	17	13	24	4	12	0	11.7	9.0	16.6	2.8	8.3	0.0
56	**DEM32R6-20-22**	32R6 20-22	301.2	69.72	142	134	19	0	19	8	22	3	13	0	14.2	6.0	16.4	2.2	9.7	0.0
57	DEM32R6-101-103	32R6 101-103	302.01	69.77	155	142	23	0	23	4	11	6	10	1	16.2	2.8	7.7	4.2	7.0	0.7
58	**DEM33R1-60-62**	33R1 60-62	303.7	69.87	154	147	12	0	12	18	14	10	5	13	8.2	12.2	9.5	6.8	3.4	8.8
59	DEM33R1-140-142	33R1 140-142	304.5	69.92	219	200	4	0	4	14	2	9	19	2	2.0	7.0	1.0	4.5	9.5	1.0
60	DEM33R2-18-20	33R2 18-20	304.78	69.94	170	162	18	0	18	9	22	7	10	2	11.1	5.6	13.6	4.3	6.2	1.2
61	**DEM33R2-97-100**	33R2 97-100	305.58	69.98	143	140	9	0	9	26	17	8	8	5	6.4	18.6	12.1	5.7	5.7	3.6
62	DEM33R320-22	33R3 20-22	306.3	70.03	166	161	7	0	7	9	12	13	16	4	4.3	5.6	7.5	8.1	9.9	2.5
63	**DEM33R3-98-100**	33R3 98-100	307.1	70.07	337	336	8	1	7	44	33	21	36	0	2.1	13.1	9.8	6.3	10.7	0.0
64	DEM33R4-15-17NEW2	33R4 15-17	307.75	70.11	237	226	4	0	4	6	19	10	40	8	1.8	2.7	8.4	4.4	17.7	3.5
65	**DEM33R4-103-105**	33R4 103-105	308.65	70.16	159	147	9	5	4	2	14	10	12	2	2.7	1.4	9.5	6.8	8.2	1.4
66	DEM33R5-25-27	33R5 25-27	309.35	70.21	174	170	11	2	9	3	24	13	8	3	5.3	1.8	14.1	7.6	4.7	1.8
67	DEM33R5 63-65	33R5 63-65	309.73	70.23	145	140	4	2	2	1	21	16	14	4	1.4	0.7	15.0	11.4	10.0	2.9
68	**DEM33R5-102-104**	33R5 102-104	310.12	70.25	142	122	15	10	5	2	16	10	13	2	4.1	1.6	13.1	8.2	10.7	1.6
69	DEM33R6-23-25	33R6 23-25	310.83	70.29	146	128	18	13	5	17	5	7	6	1	3.9	13.3	3.9	5.5	4.7	0.8
70	**DEM33R6-103-105**	33R6 103-105	311.63	70.34	164	149	17	11	6	17	18	5	10	1	4.0	11.4	12.1	3.4	6.7	0.7
71	DEM33R7-68-70	33R7 68-70	312.78	70.41	143	135	9	6	3		15	13	10	4	2.2	0.0	11.1	9.6	7.4	3.0
72	**DEM34R1-62-64**	34R1 62-64	313.42	70.45	191	171	24	15	9	37	10	2	15	8	5.3	21.6	5.8	1.2	8.8	4.7
73	DEM34R1-144-146	34R1 144-146	314.24	70.5	192	154	35	29	6	4	10	10	10	6	3.9	2.6	6.5	6.5	6.5	3.9
74	**DEM34R2-60-62**	34R2 60-62	314.8	70.53	214	205	16	5	11	49		15	13	19	5.4	23.9	0.0	7.3	6.3	9.3
75	DEM34R2-143-145	34R2 143-145	315.73	70.58	307	285	25	10	15	48	11	10	39	7	5.3	16.8	3.9	3.5	13.7	2.5
76	**DEM34R3-64-66**	34R3 64-66	316.43	70.63	195	184	16	10	6	3	10	16	19	2	3.3	1.6	5.4	8.7	10.3	1.1
77	DEM34R3-142-144NEW2	34R3 142-144	317.21	70.67	186	172	17	8	9	1	6	11	24	2	5.2	0.6	3.5	6.4	14.0	1.2
78	**DEM34R4-41-43**	34R4 41-43	317.71	70.7	302	284	6	4	2	8	39	15	18	2	0.7	2.8	13.7	5.3	6.3	0.7
79	DEM34R4-118-119	34R4 118-119	318.47	70.75	178	176	2	0	2	15	12	5	36	7	1.1	8.5	6.8	2.8	20.5	4.0
80	DEM34RCC-5-7	34RCC 5-7	320.11	70.84	204	192	17	4	13	21	25	11	26	5	6.8	10.9	13.0	5.7	13.5	2.6

TABLE S1 FORAMINIFERAL DATA (TOTAL COUNT AND RELATIVE ABUNDANCES) OF HOLE 1258A (SELECTED TAXA)

Sample	Total foraminifers*	Depth (mbsf)	Age (My)	*Aragonia velascoensis*	*Clavulinoides trilatera*	*Gyroidinoides* spp.	*Strictocostella pseudoscripta*	*Reusella szajnochae*	*Nuttallides truempyi*	*Nuttalinella florealis*	*Pullenia* spp.	*Coryphostoma* spp.	*Pleurosomella* spp.		*Aragonia velascoensis* (%)	*Clavulinoides trilatera* (%)	*Gyroidinoides* spp. (%)	*Strictocostella pseudoscripta* (%)	*Reusella szajnochae* (%)	*Nuttallides truempyi* (%)	*Nuttalinella florealis* (%)	*Pullenia* spp. (%)	*Coryphostoma* spp. (%)	*Pleurostomella* spp. (%)
28R2 110-112	141	257.5	66.2			6	15		15		3	18	10		0.0	0.0	4.3	10.6	0.0	10.6	0.0	2.1	12.8	7.1
28R3 23-25	164	258.13	66.22	8		3	14		22	2	5	30	1		4.9	0.0	1.8	8.5	0.0	13.4	1.2	3.0	18.3	0.6
28R3 103-105	134	258.93	66.25	13		4	8		28	5	4	5	6		9.7	0.0	3.0	6.0	0.0	20.9	3.7	3.0	3.7	4.5
28R4 21-23	134	259.61	66.27	19		5	6		17	1	4	6	3		14.2	0.0	3.7	4.5	0.0	12.7	0.7	3.0	4.5	2.2
28R4 103-105	177	260.41	66.3			12	16		24		3	6	2		0.0	0.0	6.8	9.0	0.0	13.6	0.0	1.7	3.4	1.1
28R5 13-15	151	261.03	66.32	3		4	23		8	6	1	11	5		2.0	0.0	2.6	15.2	0.0	5.3	4.0	0.7	7.3	3.3
28R5 93-95	138	261.83	66.35	2		2	17		16	1	3	4	2		1.4	0.0	1.4	12.3	0.0	11.6	0.7	2.2	2.9	1.4
28R6 28-30	145	262.7	66.38			3	18		7	13	3	2	7		0.0	0.0	2.1	12.4	0.0	4.8	9.0	2.1	1.4	4.8
28R6 70-72	132	263.1	66.41	2		4	13		6		3	2	14		1.5	0.0	3.0	9.8	0.0	4.5	0.0	2.3	1.5	10.6
28R6 110-112	143	263.5	66.45	28		6	15		11	2	1	3	7		19.6	0.0	4.2	10.5	0.0	7.7	1.4	0.7	2.1	4.9
29R1 63-65	123	265.23	66.61			6	12		24		1	5			0.0	0.0	4.9	9.8	0.0	19.5	0.0	0.8	4.1	0.0
29R1 144-146	150	266.04	66.69			1	17		26	4	1	5			0.0	0.0	0.7	11.3	0.0	17.3	2.7	0.7	3.3	0.0
29R2 59-61	148	266.69	66.75	8		4	7		19		5	7			5.4	0.0	2.7	4.7	0.0	12.8	0.0	3.4	4.7	0.0
29R2 143-145	143	267.53	66.83	6		5	6		17	4	3	11	2		4.2	0.0	3.5	4.2	0.0	11.9	2.8	2.1	7.7	1.4
29R3 58-60	170	268.18	66.89	3		10	5		51	4	5	8	2		1.8	0.0	5.9	2.9	0.0	30.0	2.4	2.9	4.7	1.2
29R3 140-142	201	269	66.96	22		5	22		23	2	1	9	2		10.9	0.0	2.5	10.9	0.0	11.4	1.0	0.5	4.5	1.0
29R4 43-45	147	269.53	67.02	10		3	32		16	3	4	7	1		6.8	0.0	2.0	21.8	0.0	10.9	2.0	2.7	4.8	0.7
29R4 125-127	185	270.35	67.09	8		6	25		40	4	5	6	7		4.3	0.0	3.2	13.5	0.0	21.6	2.2	2.7	3.2	3.8
29R5 63-65	149	271.05	67.16			1	22		23	15	2	4	1		0.0	0.0	0.7	14.8	0.0	15.4	10.1	1.3	2.7	0.7
29R5 143-145	189	271.85	67.23			3	33		26		9	2	7		0.0	0.0	1.6	17.5	0.0	13.8	0.0	4.8	1.1	3.7
29R6 20-22	187	272.12	67.26	21		3	36		13	13	3	11	6		11.2	0.0	1.6	19.3	0.0	7.0	7.0	1.6	5.9	3.2
29R6 140-142	168	273.32	67.37			8	33		14	20		10	5		0.0	0.0	4.8	19.6	0.0	8.3	11.9	0.0	6.0	3.0
29R7 50-52	164	273.92	67.43			4	33		23	5		10	2		0.0	0.0	2.4	20.1	0.0	14.0	3.0	0.0	6.1	1.2
29RCC 3-5	158	274.37	67.47	3		3	39		14	11		8	10		1.9	0.0	1.9	24.7	0.0	8.9	7.0	0.0	5.1	6.3
30R1 60-62	216	274.8	67.51			11	36		49	12	4	4			0.0	0.0	5.1	16.7	0.0	22.7	5.6	1.9	1.9	0.0
30R1 143-145	164	275.63	67.59	5		4	21		24	19	5	1	4		3.0	0.0	2.4	12.8	0.0	14.6	11.6	3.0	0.6	2.4
30R2 55-57	151	276.25	67.65	7		6	20		5	4	2	3	4		4.6	0.0	4.0	13.2	0.0	3.3	2.6	1.3	2.0	2.6
30R2 135-137	226	277.05	67.72	55		5	39		12	9		8	1		24.3	0.0	2.2	17.3	0.0	5.3	4.0	0.0	3.5	0.4
30R3 63-65	248	277.83	67.8	19		11	47		32	2	3	2	1		7.7	0.0	4.4	19.0	0.0	12.9	0.8	1.2	0.8	0.4
30R3 143-145	213	278.63	67.87	34		10	15		21	2	2	3	5		16.0	0.0	4.7	7.0	0.0	9.9	0.9	0.9	1.4	2.3
30R4 41-43	209	279.11	67.92	2		4	23		37			2	3		1.0	0.0	1.9	11.0	0.0	17.7	0.0	0.0	1.0	1.4
31R1 65-67	195	284.55	68.43	8		3	7		40	3	8	9	7		4.1	0.0	1.5	3.6	0.0	20.5	1.5	4.1	4.6	3.6
31R1 145-147	197	285.35	68.5	7		12	15		12		3	11	1		3.6	0.0	6.1	7.6	0.0	6.1	0.0	1.5	5.6	0.5
31R2 63-65	217	286.03	68.57	44		6	18		25		1	4	2		20.3	0.0	2.8	8.3	0.0	11.5	0.0	0.5	1.8	0.9
31R2 143-145	199	286.83	68.64	55		7	17		22	2	1	4	1		27.6	0.0	3.5	8.5	0.0	11.1	1.0	0.5	2.0	0.5
31R3 18-20	177	287.08	68.66	51		5	12		15	9	3	5	9		28.8	0.0	2.8	6.8	0.0	8.5	5.1	1.7	2.8	5.1
31R3 63-65	206	287.53	68.71	46		9	16		28	1	4	6			22.3	0.0	4.4	7.8	0.0	13.6	0.5	1.9	2.9	0.0
31R3 143-145	180	288.33	68.78	18		3	10		24	1	3	3	1		10.0	0.0	1.7	5.6	0.0	13.3	0.6	1.7	1.7	0.6
31R4 63-65	162	289.03	68.85	8		10	9	1	25	4	2	4			4.9	0.0	6.2	5.6	0.6	15.4	2.5	1.2	2.5	0.0
31R4 143-145	187	289.83	68.92			3	32		27		1	12			0.0	0.0	1.6	17.1	0.0	14.4	0.0	0.5	6.4	0.0
31R5 63-65	193	290.53	68.99	1		1	18		57	2	7	10	1		0.5	0.0	0.5	9.3	0.0	29.5	1.0	3.6	5.2	0.5
31R5 143-145	178	291.33	69.06			6	8		57		1	16			0.0	0.0	3.4	4.5	0.0	32.0	0.0	0.6	9.0	0.0
31R6 64-66	172	292.04	69.13	3		9	7		64	3	3	8			1.7	0.0	5.2	4.1	0.0	37.2	1.7	1.7	4.7	0.0
31R6 143-145	203	292.83	69.2	14		8	16		49	2	5	23			6.9	0.0	3.9	7.9	0.0	24.1	1.0	2.5	11.3	0.0
31R7 58-60	162	293.48	69.27	1		5	25		29	4	5	2	2		0.6	0.0	3.1	15.4	0.0	17.9	2.5	3.1	1.2	1.2
32R1 24-28	144	293.76	69.28	4		4	19		21	1	1	19	1		2.8	0.0	2.8	13.2	0.0	14.6	0.7	0.7	13.2	0.7
32R1 105-108	164	294.56	69.33			12	23		5	3	4	12	2		0.0	0.0	7.3	14.0	0.0	3.0	1.8	2.4	7.3	1.2
32R2 25-27	159	295.25	69.37			6	14		8	3	1	13			0.0	0.0	3.8	8.8	0.0	5.0	1.9	0.6	8.2	0.0
32R2 105-107	159	296.05	69.42			10	7		5	19	3	8	7		0.0	0.0	6.3	4.4	0.0	3.1	11.9	1.9	5.0	4.4
32R3 22-24	185	296.72	69.46			9	21	6	22	2	4	15	5		0.0	0.0	4.9	11.4	3.2	11.9	1.1	2.2	8.1	2.7
32R3 105-107	166	297.55	69.51	8		2	6		31	7	7	26			4.8	0.0	1.2	3.6	0.0	18.7	4.2	4.2	15.7	0.0
32R4 23-25	148	298.23	69.55	5		6	12	8	19		1	2			3.4	0.0	4.1	8.1	5.4	12.8	0.0	0.7	1.4	0.0
32R4 105-107	149	299.05	69.6		16	7	9	1	4	14	1	7	3		0.0	10.7	4.7	6.0	0.7	2.7	9.4	0.7	4.7	2.0
32R5 16-18	154	299.66	69.63	2	15	2	12		12	15	3	12	3		1.3	9.7	1.3	7.8	0.0	7.8	9.7	1.9	7.8	1.9
32R5 95-97	145	300.45	69.68	4	7	1	4	4	5	10	1	9	2		2.8	4.8	0.7	2.8	2.8	3.4	6.9	0.7	6.2	1.4
32R6 20-22	134	301.2	69.72		6	3	16	5	1	22		8	2		0.0	4.5	2.2	11.9	3.7	0.7	16.4	0.0	6.0	1.5
32R6 101-103	142	302.01	69.77		18	5	10		2	28	3	4	3		0.0	12.7	3.5	7.0	0.0	1.4	19.7	2.1	2.8	2.1
33R1 60-62	147	303.7	69.87	5	3	4	10	2	1	4	2	13			3.4	2.0	2.7	6.8	1.4	0.7	2.7	1.4	8.8	0.0
33R1 140-142	200	304.5	69.92	1		7	11	26	32	7	1	13	1		0.5	0.0	3.5	5.5	13.0	16.0	3.5	0.5	6.5	0.5
33R2 18-20	162	304.78	69.94	5	1	3	8	3	15		2	4			3.1	0.6	1.9	4.9	1.9	9.3	0.0	1.2	2.5	0.0
33R2 97-100	140	305.58	69.98	22		4	11		4	5	1	4	2		15.7	0.0	2.9	7.9	0.0	2.9	3.6	0.7	2.9	1.4
33R3 20-22	161	306.3	70.03	1		9	12	1	16			8			0.6	0.0	5.6	7.5	0.6	9.9	0.0	0.0	5.0	0.0
33R3 98-100	336	307.1	70.07	39		11	12	39	38	46	4	5			11.6	0.0	3.3	3.6	11.6	11.3	13.7	1.2	1.5	0.0
33R4 15-17	226	307.75	70.11	3		6	8	8	73	1		3	2		1.3	0.0	2.7	3.5	3.5	32.3	0.4	0.0	1.3	0.9
33R4 103-105	147	308.65	70.16			19	9	4	17	4	1	2			0.0	0.0	12.9	6.1	2.7	11.6	2.7	0.7	1.4	0.0
33R5 25-27	170	309.35	70.21	1		10	18	2	10	24	2	2	1		0.6	0.0	5.9	10.6	1.2	5.9	14.1	1.2	1.2	0.6
33R5 63-65	140	309.73	70.23			7	10		28	15		1	11		0.0	0.0	5.0	7.1	0.0	20.0	10.7	0.0	0.7	7.9
33R5 102-104	122	310.12	70.25			8	21		3	9	2	2	1		0.0	0.0	6.6	17.2	0.0	2.5	7.4	1.6	1.6	0.8
33R6 23-25	128	310.83	70.29	8		3	4		33		3	9	2		6.3	0.0	2.3	3.1	0.0	25.8	0.0	2.3	7.0	1.6
33R6 103-105	149	311.63	70.34	14		3	8		18	11		3	2		9.4	0.0	2.0	5.4	0.0	12.1	7.4	0.0	2.0	1.3
33R7 68-70	135	312.78	70.41			9	5	1	27	10			2		0.0	0.0	6.7	3.7	0.7	20.0	7.4	0.0	0.0	1.5
34R1 62-64	171	313.42	70.45	32		3	6		14	14	2	5	1		18.7	0.0	1.8	3.5	0.0	8.2	8.2	1.2	2.9	0.6
34R1 144-146	154	314.24	70.5			6	8	3	25	2	5	4	5		0.0	0.0	3.9	5.2	1.9	16.2	1.3	3.2	2.6	3.2
34R2 60-62	205	314.8	70.53	40		10	6		23		4	9			19.5	0.0	4.9	2.9	0.0	11.2	0.0	2.0	4.4	0.0
34R2 143-145	285	315.73	70.58	44		7	5	19	45	11	13	3	4		15.4	0.0	2.5	1.8	6.7	15.8	3.9	4.6	1.1	1.4
34R3 64-66	184	316.43	70.63	1		4	3	1	27	23	1	2	4		0.5	0.0	2.2	1.6	0.5	14.7	12.5	0.5	1.1	2.2
34R3 142-144	172	317.21	70.67			18	4	4	19	9	3	1	3		0.0	0.0	10.5	2.3	2.3	11.0	5.2	1.7	0.6	1.7
34R4 41-43	284	317.71	70.7	1		10	24	17	30	29	2	7	19		0.4	0.0	3.5	8.5	6.0	10.6	10.2	0.7	2.5	6.7
34R4 118-119	176	318.47	70.75	2		7	5		5	20	3	12			1.1	0.0	4.0	2.8	0.0	2.8	11.4	1.7	6.8	0.0
34RCC 5-7	192	320.11	70.84	8	1	6	5	13	16	11	4	12	11		4.2	0.5	3.1	2.6	6.8	8.3	5.7	2.1	6.3	5.7

*Total counts without agglutinated tubular and calcareous uniserial forms (fragmented)

TABLE S1 FORAMINIFERAL DATA (TOTAL COUNT AND RELATIVE ABUNDANCES) OF HOLE 1258A (BFAR)

Sample	Total ostracodes	Total foraminifers*	Final weight (g)	Dry weight (g)	>63 fraction (%)	Dry density estimation (g/cm3)	Depth (mbsf)	ON (ostracods/g)	ON (ostracods/10g)	BFN (foraminifers/g)	Age (My)	LSR (m/my)	LSR (cm/ky)	BFAR (foraminifers/cm2/ky)	LSR Sci Report (cm/ky)	BFAR (foraminifers/cm2/ky) Sci Report		Tie points				OAR (ostracods/cm2/ky)
28R2 110-112	4	135	10.35	20.42	50.7	1.63	257.5	0.2	2	7	66.2	28.9	2.9	32	1	11		K/Pg	252,58 m	66,04 Ma		1
28R3 23-25	6	153	6.24	24.08	25.9	1.63	258.13	0.2	2	7	66.22	28.3	2.8	31	1	11		C29r*	262,77 m	66,38 Ma		1
28R3 103-105	8	129	8.29	22.21	37.3	1.62	258.93	0.4	4	6	66.25	27.4	2.7	27	1	10		C31n*	293,52 m	69,27 Ma		2
28R4 21-23	17	126	10.33	29.54	35.0	1.59	259.61	0.6	6	5	66.27	26.8	2.7	19	1	7		C31r*	330,34 m	71,45 Ma		2
28R4 103-105	19	175	10.89	30.04	36.3	1.57	260.41	0.6	6	6	66.3	26	2.6	24	1	9						3
28R5 13-15	17	147	11.57	31.92	36.2	1.52	261.03	0.5	5	5	66.32	25.3	2.5	18	1	7						2
28R5 93-95	14	135	8.9	34.3	25.9	1.50	261.83	0.4	4	4	66.35	24.5	2.5	15	1	6	*Magneto (Suganuma & Ogg, 2006)					1
28R6 28-30	13	133	11.17	30.73	36.3	1.63	262.7	0.4	4	4	66.38	23.6	2.4	18	1	8						2
28R6 70-72	8	121	10.39	27.98	37.1	1.70	263.1	0.3	3	5	66.41	23.2	2.3	19	1	8						1
28R6 110-112	8	136	7.03	28.81	24.4	1.70	263.5	0.3	3	5	66.45	22.8	2.3	19	1	8						1
29R1 63-65	22	111	11.99	27.9	43.0	1.67	265.23	0.8	8	4	66.61	21.1	2.1	16	1	7						3
29R1 144-146	12	135	10.3	20.26	50.8	1.69	266.04	0.6	6	7	66.69	20.3	2.0	25	1	13						2
29R2 59-61	13	135	9.12	19.81	46.0	1.72	266.69	0.7	7	7	66.75	19.6	2.0	25	1	13						2
29R2 143-145	16	131	9.7	23.49	41.3	1.69	267.53	0.7	7	6	66.83	18.8	1.9	19	1	10						2
29R3 58-60	18	166	9.32	22.08	42.2	1.64	268.18	0.8	8	8	66.89	18.1	1.8	23	1	13						2
29R3 140-142	22	199	13.46	19.18	70.2	1.63	269	1.1	11	10	66.96	17.3	1.7	30	1	17						3
29R4 43-45	5	145	5.56	16.91	32.9	1.65	269.53	0.3	3	9	67.02	16.8	1.7	24	1	14						1
29R4 125-127	11	180	13.62	27.45	49.6	1.66	270.35	0.4	4	7	67.09	15.9	1.6	18	1	11						1
29R5 63-65	4	145	7.36	19.04	38.7	1.67	271.05	0.2	2	8	67.16	15.2	1.5	20	1	13						1
29R5 143-145	8	183	10.47	25.17	41.6	1.57	271.85	0.3	3	8	67.23	14.4	1.4	17	1	12						1
29R6 20-22	8	186	6.61	24.25	27.3	1.53	272.12	0.3	3	8	67.26	14.1	1.4	17	1	12						1
29R6 140-142	9	161	4.27	16.38	26.1	1.56	273.32	0.5	5	10	67.37	12.9	1.3	21	1	16						1
29R7 50-52	4	159	6.3	21.16	29.8	1.68	273.92	0.2	2	8	67.43	12.3	1.2	16	1	13						0
29R CC 3-5	9	151	6.51	21.63	30.1	1.69	274.37	0.4	4	7	67.47	11.9	1.2	15	1	12						1
30R1 60-62	8	198	8.4	23.93	35.1	1.44	274.8	0.3	3	9	67.51	11.4	1.1	15	1	13						1
30R1 143-145	3	146	9.04	19.4	46.6	1.50	275.63	0.2	2	8	67.59	10.6	1.1	13	1	13						0
30R2 55-57	12	142	8.79	19	46.3	1.54	276.25	0.6	6	8	67.65	10.7	1.1	13	1	12						1
30R2 135-137	15	215	6.34	25.1	25.3	1.60	277.05	0.6	6	9	67.72	10.8	1.1	16	1	14						1
30R3 63-65	7	228	13.52	35.61	38.0	1.65	277.83	0.2	2	7	67.8	10.9	1.1	13	1	12		Tie points				0
30R3 143-145	10	199	10.1	23.76	42.5	1.72	278.63	0.4	4	9	67.87	11	1.1	17	1	15		K/Pg	252,58 m	66,04 Ma		1
30R4 41-43	5	191	17.57	31.25	56.2	1.76	279.11	0.2	2	7	67.92	11.1	1.1	13	1	12		C29r*	262,77 m	66,38 Ma		0
31R1 65-67	6	183	12.95	23.35	55.5	1.67	284.55	0.3	3	8	68.43	11.9	1.2	17	1	14		C31n*	293,52 m	69,27 Ma		1
31R1 145-147	5	183	12.88	26.41	48.8	1.58	285.35	0.2	2	7	68.5	12	1.2	14	1	12		C31r*	330,34 m	71,45 Ma		0
31R2 63-65	3	206	13.99	38.44	36.4	1.45	286.03	0.1	1	6	68.57	12.1	1.2	10	1	8						0
31R2 143-145	1	192	2.94	17.21	17.1	1.49	286.83	0.1	1	12	68.64	12.2	1.2	21	1	17						0
31R3 18-20	4	169	9.47	23.6	40.1	1.54	287.08	0.2	2	8	68.66	12.3	1.2	14	1	12						0
31R3 63-65		205	5.05	17.24	29.3	1.63	287.53	0.0	0	12	68.71	12.4	1.2	24	1	20						0
31R3 143-145	8	168	15.68	31.39	50.0	1.68	288.33	0.3	3	6	68.78	12.5	1.3	12	1	10						1
31R4 63-65	9	153	16.78	29.86	56.2	1.66	289.03	0.3	3	5	68.85	12.6	1.3	11	1	9						1
31R4 143-145	8	173	12.08	27.39	44.1	1.64	289.83	0.3	3	7	68.92	12.7	1.3	14	1	11						1
31R5 63-65	4	184	9.12	17.04	53.5	1.62	290.53	0.2	2	11	68.99	12.8	1.3	23	1	18						0
31R5 143-145	6	171	4.38	16.42	26.7	1.61	291.33	0.4	4	11	69.06	12.9	1.3	22	1	17						1
31R6 64-66	5	164	3.78	14.23	26.6	1.59	292.04	0.4	4	12	69.13	13	1.3	25	1	19						1
31R6 143-145	4	194	4.48	24.06	18.6	1.65	292.83	0.2	2	8	69.2	13.1	1.3	18	1	14						0
31R7 58-60	8	153	15.24	29.49	51.7	1.71	293.48	0.3	3	5	69.27	13.2	1.3	12	1	9						1
32R1 24-28	4	137	4.94	26.81	18.4	1.72	293.76	0.1	1	5	69.28	13.3	1.3	12	1	9						0
32R1 105-108	9	147	6.56	23.65	27.7	1.72	294.56	0.4	4	7	69.33	13.4	1.3	16	1	12						1
32R2 25-27	5	143	15.17	27.11	56.0	1.73	295.25	0.2	2	6	69.37	13.5	1.4	14	1	10						0
32R2 105-107	7	140	7.67	28.95	26.5	1.68	296.05	0.2	2	5	69.42	13.6	1.4	13	1	9						1
32R3 22-24	4	177	11.47	36.3	31.6	1.61	296.72	0.1	1	5	69.46	13.7	1.4	11	1	8						0
32R3 105-107	9	156	10.95	23.12	47.4	1.60	297.55	0.4	4	7	69.51	13.8	1.4	16	1	11						1
32R4 23-25	1	131	6.84	15.87	43.1	1.63	298.23	0.1	1	9	69.55	13.9	1.4	21	1	15						0
32R4 105-107	11	132	10.62	22.53	47.1	1.66	299.05	0.5	5	7	69.6	14	1.4	15	1	11						1
32R5 16-18	12	143	12.56	28.4	44.2	1.68	299.66	0.4	4	5	69.63	14.1	1.4	13	1	9						1
32R5 95-97	4	129	5.76	15.08	38.2	1.71	300.45	0.3	3	10	69.68	14.2	1.4	23	1	16						1
32R6 20-22	4	122	11.86	23.11	51.3	1.73	301.2	0.2	2	6	69.72	14.3	1.4	14	1	10						0
32R6 101-103	14	131	9.17	19.03	48.2	1.68	302.01	0.7	7	7	69.77	14.4	1.4	18	1	13						2
33R1 60-62	5	127	9.87	30.15	32.7	1.53	303.7	0.2	2	5	69.87	14.5	1.5	11	1	7						0
33R1 140-142	15	178	6.95	19.33	36.0	1.47	304.5	0.8	8	10	69.92	14.6	1.5	22	1	15						2
33R2 18-20	7	143	11.79	21.81	54.1	1.47	304.78	0.3	3	7	69.94	14.7	1.5	16	1	11						1
33R2 97-100	6	128	7.06	17.61	40.1	1.43	305.58	0.3	3	8	69.98	14.8	1.5	17	1	11						1
33R3 20-22	8	145	5.11	18.5	27.6	1.42	306.3	0.4	4	9	70.03	14.9	1.5	18	1	12						1
33R3 98-100	3	324	3.52	19.97	17.6	1.45	307.1	0.2	2	17	70.07	15	1.5	37	1	24						0
33R4 15-17	5	219	5.15	27.94	18.4	1.52	307.75	0.2	2	8	70.11	15.1	1.5	19	1	12						0
33R4 103-105	4	137	6.02	20.94	28.7	1.60	308.65	0.2	2	7	70.16	15.2	1.5	17	1	11						0
33R5 25-27	4	153	11.31	24.62	45.9	1.56	309.35	0.2	2	7	70.21	15.3	1.5	17	1	11			Tie points			0
33R5 63-65	9	130	8.4	19.84	42.3	1.54	309.73	0.5	5	7	70.23	15.4	1.5	17	1	11			K/Pg	252,58 m	66,04 Ma	1
33R5 102-104	4	109	11.08	19.67	56.3	1.56	310.12	0.2	2	6	70.25	15.5	1.6	15	1	10			C29r*	262,77 m	66,38 Ma	0
33R6 23-25	9	116	10.85	21.02	51.6	1.60	310.83	0.4	4	6	70.29	15.6	1.6	15	1	10			C31n*	293,52 m	69,27 Ma	1
33R6 103-105	7	133	7.65	22.38	34.2	1.64	311.63	0.3	3	7	70.34	15.7	1.6	17	1	11			C31r*	330,34 m	71,45 Ma	1
33R7 68-70	3	123	9.22	20.21	45.6	1.62	312.78	0.1	1	7	70.41	15.8	1.6	17	1	11						0
34R1 62-64	6	166	8.49	21.48	39.5	1.64	313.42	0.3	3	8	70.45	15.9	1.6	21	1	13						1
34R1 144-146	8	137	9.76	28.45	34.3	1.62	314.24	0.3	3	5	70.5	16	1.6	14	1	9						1
34R2 60-62	3	190	1.66	16.29	10.2	1.60	314.8	0.2	2	13	70.53	16.1	1.6	32	1	20						0
34R2 143-145	3	277	1.69	19.15	8.8	1.56	315.73	0.2	2	15	70.58	16.2	1.6	38	1	23						0
34R3 64-66	4	175	8.22	19.55	42.0	1.51	316.43	0.2	2	9	70.63	16.3	1.6	23	1	14						1
34R3 142-144	2	153	1.68	24.59	6.8	1.50	317.21	0.1	1	7	70.67	16.4	1.6	17	1	10						0
34R4 41-43	4	263	6.56	27.15	24.2	1.50	317.71	0.1	1	10	70.7	16.5	1.7	26	1	16						0
34R4 118-119	10	160	6.23	15.19	41.0	1.51	318.47	0.7	7	12	70.75	16.7	1.7	29	1	17						2
34R CC 5-7	5	193	2.38	28.51	8.3	1.55	320.11	0.2	2	7	70.84	16.9	1.7	18	1	10						0

ubular and calcareous uniserial forms (fragmented)

TABLE S2 δ13c AND δ18O VALUES, AND ELEMENTAL COMPOSITION DATA (XRF ANALYSES) OF HOLE 1258A (XRF DATA)

Nr	Ident	Mg	Al	Si	S	K	Ca	Ti	Cr	Mn	Fe	Ni	Cu	Zn	Rb	Sr	Zr	Ba	Co	V	Ga		
		C	C	C	C	C	C	C	C	C	C	C	C	C	C	C	C	C	C	C	C		
1	DEM28R2-110-112	-1,794	276,683	2,709,797	14,001	963,822	70431.64	325,882	6,238	334,380	8,931,762	4,625	4,737	22,166	75,168	2,401,467	177,268	31,255	68,804	23,852	2,953	126.8146	3.483488
2	DEM28R2-148-150	2,025	326,041	3,108,446	18,517	1,011,808	64333.93	414,815	11,546	323,778	12,238,810	7,346	5,553	30,268	98,230	2,543,283	214,522	27,318	96,431	36,358	5,662	190.2388	3.103315
3	DEM28R3-23-25NEW	1,607	311,663	3,006,161	20,060	1,049,470	56018.42	438,705	13,903	292,430	15,043,630	10,678	10,725	34,128	116,250	2,752,737	243,599	21,655	125,836	34,162	7,388	268.5479	3.367323
4	DEM28R3-61-63	-2,175	238,229	2,273,680	13,203	712,889	53697.32	348,813	10,369	261,046	13,155,430	10,262	12,682	30,155	82,368	2,197,176	186,760	18,103	108,210	32,508	6,072	244.9923	2.992453
5	DEM28R3-103-105	-1,246	266,120	2,553,741	26,193	852,311	63520.73	357,732	6,736	284,295	9,986,524	4,913	24,644	26,104	89,166	2,550,691	209,219	21,420	79,071	21,678	4,286	157.2168	3.202732
6	DEM28R3-141-143	-1,183	326,398	2,741,973	15,700	892,670	67776.74	378,519	9,542	300,526	10,022,380	8,071	9,092	59,017	92,874	2,592,713	208,182	20,414	81,609	31,013	5,465	147.8734	2.734913
7	DEM28R4-21-23	2,242	215,763	2,049,576	24,402	717,036	63099.6	286,433	3,446	271,122	6,486,944	4,773	11,941	19,819	65,664	2,156,213	148,346	16,554	52,968	16,634	3,344	102.8048	3.323257
8	DEM28R4-63-65NEW3	1,508	288,322	2,500,702	30,961	854,541	77236.99	298,664	4,929	312,805	6,749,400	2,082	5,895	21,421	73,711	2,684,324	173,032	20,429	51,297	24,232	2,557	87.38559	2.963843
9	DEM28R4-103-105	-4,481	189,633	1,850,831	14,780	673,915	60736.61	264,391	3,592	260,262	6,340,322	3,874	5,747	17,200	60,318	2,062,815	140,675	12,076	53,359	17,506	2,750	104.3904	3.553785
10	DEM28R4-143-145	1,157	266,100	2,468,336	28,617	850,299	78079.47	300,958	5,916	315,929	7,259,001	3,916	7,881	24,235	76,503	2,543,221	179,930	22,341	59,542	24,119	3,357	92.96939	3.195411
11	DEM28R5-13-15	3,222	277,393	2,390,362	24,252	803,180	74943.59	303,595	3,227	314,480	7,307,827	1,409	5,949	18,469	70,990	2,556,492	175,253	25,369	54,248	19,988	2,412	97.51103	2.895459
12	DEM28R5-48-50	0.731	244,282	2,308,027	19,741	782,837	70983.01	294,274	4,675	281,169	7,310,015	3,107	7,547	18,199	66,162	2,379,016	159,187	16,484	62,009	15,906	3,295	102.9826	3.204645
13	DEM28R5-93-95	0.276	285,238	2,577,674	36,679	846,477	73127.06	334,219	6,401	276,711	8,103,102	4,256	7,971	19,358	80,716	2,543,578	185,113	23,399	62,161	20,543	3,743	110.8085	2.967617
14	DEM28R5-133-135	-0.486	285,424	2,571,418	36,319	879,908	71452.07	323,559	7,337	264,322	7,835,520	4,067	9,044	27,540	83,266	2,584,110	194,288	25,300	59,184	24,219	2,552	109.6612	3.08281
15	DEM28R6-30-32	0.144	276,262	2,349,843	26,245	780,159	76965.2	300,181	4,883	253,162	7,062,510	1,979	10,129	20,557	67,513	2,496,033	176,499	23,529	53,876	25,234	2,465	91.76238	2.823982
16	DEM28R6-70-72	3,296	286,407	2,461,579	24,755	817,858	76330.08	296,525	4,497	241,976	7,364,793	2,547	6,213	56,871	74,928	2,759,407	183,481	27,511	57,923	19,158	3,422	96.48612	2.85558
17	DEM28R6-110-112	-0.334	294,993	2,583,991	26,672	873,256	70082.53	356,515	5,330	235,539	8,708,109	4,853	8,461	39,788	93,297	2,879,606	216,440	27,002	79,339	25,344	5,355	124.2551	2.96026
18	DEM29R1-21-24	0.211	213,314	2,162,877	27,131	771,424	64091.94	296,667	6,871	209,603	7,017,536	3,073	5,769	20,840	71,415	2,352,856	159,890	22,137	57,146	10,485	3,269	109.4917	3.616378
19	DEM29R1-63-65	-2,746	237,304	2,328,928	26,187	796,834	73504.01	291,387	4,053	233,623	7,069,907	1,909	6,311	16,532	74,256	2,619,052	181,983	25,609	56,965	23,893	4,564	96.18396	3.357862
20	DEM29R1-103-105	-1,445	256,567	2,450,301	37,085	926,157	69075.16	318,958	6,427	214,612	8,061,781	6,484	9,155	24,382	93,817	2,942,233	209,166	23,617	70,638	19,722	3,076	116.7103	3.609806
21	DEM29R1-144-146	0.561	259,831	2,729,965	42,420	944,705	72414.95	332,912	6,648	213,688	7,189,943	8,011	22,811	16,586	84,955	2,526,419	186,340	17,486	55,763	24,301	3,066	99.2881	3.635844
22	DEM29R2-18-20	-3,273	306,605	2,897,881	39,101	1,055,032	63259.97	392,166	9,880	190,390	9,956,497	11,879	10,430	31,597	113,835	3,035,185	248,791	38,377	95,482	22,214	5,278	157.3902	3.442687
23	DEM29R2-59-61	-0.510	210,396	2,093,693	25,367	796,350	68556.73	275,846	4,327	204,159	6,199,634	1,171	7,144	16,721	64,574	2,343,628	154,276	24,623	50,847	22,063	4,160	90.43071	3.785005
24	DEM29R2-104-106	0.114	257,861	2,531,440	33,689	903,525	74264.77	292,652	4,345	213,341	6,915,946	4,216	6,299	62,984	79,078	2,784,432	183,421	25,382	58,350	21,179	3,277	93.12553	3.503923
25	DEM29R21-43-145	0.941	236,012	2,256,105	27,653	804,214	71550.48	281,483	5,305	209,160	6,782,986	4,149	10,033	16,153	69,490	2,576,156	176,191	27,387	50,679	19,627	3,774	94.80001	3.407513
26	DEM29R3-20-22	-3,122	212,140	2,073,649	22,939	743,179	59299.33	294,782	5,783	172,033	7,085,692	2,523	6,143	14,703	69,423	2,109,860	151,905	19,112	57,924	15,759	2,795	119.4903	3.503248
27	DEM29R3-58-60	-3,775	188,296	1,914,446	21,454	739,963	61582.84	264,038	3,980	177,484	6,636,843	2,874	8,330	33,608	72,371	2,191,045	146,267	24,760	54,960	8,757	4,537	107.771	3.929786
28	DEM29R3-98-100	-3,837	241,582	2,398,556	45,776	825,276	76213.06	275,673	1,988	209,005	6,767,734	4,490	6,128	45,077	74,930	2,670,494	171,202	27,308	49,942	14,649	3,224	88.80019	3.416132
29	DEM29R3-140-142	-2,722	176,775	1,868,938	31,517	722,492	63760.14	255,757	4,388	185,450	6,192,779	1,847	5,445	19,195	68,173	2,301,219	154,297	29,423	50,403	15,422	3,403	97.12618	4.087071
30	DEM29R4-5-7	2,595	234,491	2,405,025	32,957	932,020	60148.97	323,752	8,176	166,013	8,010,737	5,421	9,612	21,685	92,886	2,916,357	208,421	24,401	68,012	17,961	3,559	133.1816	3.974651
31	DEM29R4-43-45	0.033	205,719	2,260,106	39,308	856,117	55507.88	313,334	4,821	161,562	7,382,735	7,218	7,238	96,354	84,714	2,417,917	181,460	22,820	62,956	15,927	3,723	133.0034	4.161584
32	DEM29R4-85-87	-1,060	190,633	2,225,179	33,034	888,643	54478.14	312,839	6,132	155,475	7,449,449	8,386	8,052	25,638	86,834	2,418,141	179,871	21,998	59,626	15,513	3,726	136.742	4.661538
33	DEM29R4-125-127	0.597	282,616	2,707,266	42,856	913,809	74923.44	315,591	6,384	188,189	7,322,542	3,560	5,620	18,793	79,826	2,639,768	182,037	27,330	57,203	21,272	2,724	97.73366	3.233394
34	DEM29R5-21-23	1,603	285,915	2,821,454	60,174	1,039,749	61038.32	413,399	11,232	176,942	10,835,580	11,976	10,227	26,463	120,937	2,845,453	239,335	31,251	93,091	20,146	4,925	177.5209	3.636567
35	DEM29R5-63-65	3,086	280,567	2,775,031	60,539	939,717	72546.19	338,683	5,580	190,900	8,209,813	5,304	7,872	30,989	86,213	2,695,974	201,062	34,910	71,260	20,372	5,298	113.1667	3.34935
36	DEM29R5-103-105	2,869	279,498	2,915,800	60,536	1,032,600	68055.6	373,948	9,540	175,093	9,393,020	7,233	8,971	26,505	105,235	3,054,862	222,770	34,637	77,636	28,848	5,093	138.0198	3.694481
37	DEM29R5-143-145	-2,145	238,340	2,227,503	37,207	873,380	66088.84	307,891	6,723	177,925	7,603,639	5,037	7,702	41,904	89,880	2,671,063	200,465	27,963	66,233	23,557	3,819	115.0518	3.664429
38	DEM29R6-20-22	0.705	273,648	2,676,293	41,221	1,007,189	65321.1	354,015	8,783	165,356	8,846,161	10,398	8,778	30,743	104,953	3,031,190	238,486	34,482	81,199	19,963	3,850	135.4258	3.680601
39	DEM29R6-60-62	0.768	248,520	2,577,072	50,464	975,186	60800.5	366,994	7,300	155,466	8,838,310	7,836	8,678	43,204	102,536	2,705,986	226,519	46,545	80,076	21,229	4,743	145.3657	3.923974
40	DEM29R6-105-107	2,156	233,721	2,476,396	43,018	859,321	64721.52	325,768	9,809	171,682	8,689,137	10,373	8,837	17,007	82,967	2,332,092	181,709	20,687	74,002	13,464	3,166	134.2542	3.676696
41	DEM29R6-140-142	-1,513	267,461	2,731,438	90,886	1,062,131	62717.18	357,425	6,775	137,672	8,523,063	8,574	8,235	31,877	110,930	3,477,761	248,628	36,807	77,098	22,509	5,888	135.8968	3.971162
42	DEM29R7-13-15	-0.557	231,758	2,493,947	33,595	919,576	73141.26	295,109	6,593	152,194	7,006,743	3,467	6,677	21,999	82,868	2,971,256	192,914	33,603	56,672	19,510	3,400	95.79741	3.967829
43	DEM29R7-50-52	0.150	244,649	2,536,412	94,170	972,777	60039.1	365,505	10,219	152,549	10,397,770	13,492	13,759	21,589	116,200	3,193,527	247,903	34,583	98,197	21,170	4,492	173.1833	3.976215
44	DEM29R-CC3-5	0.295	267,693	2,818,116	41,875	1,022,299	69385.56	331,288	7,517	148,039	8,312,880	5,593	10,862	26,259	100,411	3,462,354	236,332	36,595	69,591	23,518	5,438	119.8071	3.818923
45	DEM29R7-93-95NEW2	1,356	183,160	1,891,242	30,546	687,668	57443.91	230,362	6,689	126,665	5,520,065	1,823	7,559	18,479	58,651	2,014,786	125,819	18,784	41,619	15,170	2,273	96.09487	3.754466
46	DEM30R1-20-22	-3,249	228,942	2,363,377	37,112	932,546	58397.56	325,692	9,241	123,650	7,957,694	3,401	7,827	20,306	90,635	2,728,066	201,727	32,173	64,391	15,848	4,294	136.2676	4.073285
47	DEM30R1-60-62	-1,244	257,338	2,508,713	49,924	971,864	68796.27	327,508	7,519	147,064	8,140,501	4,899	11,345	25,354	96,237	3,127,688	217,507	46,707	72,427	19,768	4,348	118.3277	3.776605
48	DEM30R1-108-110	0.142	256,388	2,508,225	44,717	898,701	72174.15	311,462	5,650	158,470	7,499,956	4,674	6,514	21,160	80,104	2,600,430	175,248	30,972	55,026	17,800	3,513	103.9147	3.505238
49	DEM30R1-143-145	-0.807	239,158	2,334,626	41,997	869,355	72416.13	290,581	5,625	169,657	7,206,323	2,411	6,532	20,737	76,038	2,569,532	176,495	31,140	53,322	13,553	2,927	99.51268	3.635066
50	DEM30R2-10-12	1,363	244,697	2,587,640	49,655	1,009,885	59369.61	383,204	9,261	140,546	9,414,812	8,950	26,365	32,853	104,565	2,751,480	218,132	34,111	86,285	17,494	4,419	158.5797	4.127084
51	DEM30R2-55-57new	-1,251	236,161	2,520,298	40,283	956,846	67893.55	323,012	5,989	154,522	7,617,760	2,965	9,050	34,368	83,972	2,794,612	192,356	32,007	58,221	23,311	3,807	112.2015	4.051668
52	DEM30R2-95-97	-0.881	289,119	2,900,143	42,400	1,053,740	63351.71	410,240	9,879	169,933	10,245,010	5,526	7,479	25,162	113,806	2,848,646	250,812	35,411	84,815	23,964	4,465	161.7164	3.644658
53	DEM30R2-135-137	-0.610	268,145	2,694,448	32,146	1,016,503	61623.35	374,766	7,948	152,885	9,630,138	3,932	7,939	23,613	107,745	3,056,338	252,191	40,122	85,604	17,704	5,177	156.2742	3.790871
54	DEM30R3-18-22	-0.938	279,555	2,977,957	32,488	1,105,851	64594.46	386,678	9,973	152,790	9,335,322	5,332	8,060	32,628	113,577	3,181,275	248,105	35,426	78,827	20,322	4,386	144.522	3.955755
55	DEM30R3-63-65	-1,931	241,733	2,333,923	22,922	917,435	59399.14	333,651	9,054	165,981	8,894,063	6,977	10,252	28,917	102,276	2,868,212	225,632	37,367	74,420	22,532	4,767	149.7339	3.795241
56	DEM30R3-102-105	-1,756	267,304	2,765,317	28,940	937,520	74267.32	315,083	7,826	177,785	7,317,258	1,799	7,312	18,582	70,781	2,436,007	178,153	39,443	60,262	21,095	3,196	98.52595	3.507318
57	DEM30R3-143-145	0.389	261,683	2,609,510	21,634	900,242	69477.73	340,070	8,084	184,562	8,089,588	3,474	7,184	17,543	81,634	2,620,330	182,871	29,634	61,890	21,221	3,429	116.4343	3.440201
58	DEM30R4-10-12	-1,028	259,282	2,952,777	46,919	1,109,373	59054.62	408,522	11,080	166,800	10,584,980	4,861	9,941	27,208	119,087	3,194,599	265,038	49,894	99,251	26,279	5,760	179.2405	4.278635
59	DEM30R4-41-43	2,079	236,763	2,366,543	42,876	821,678	72889.38	265,715	4,122	177,675	6,246,484	4,438	8,941	16,303	60,844	2,344,263	144,150	32,201	46,414	14,413	2,442	85.69814	3.470466
60	DEM31R1-23-25	2,460	251,049	2,585,123	44,337	896,941	72947.15	324,505	7,904	182,676	7,890,256	3,625	7,994	30,260	81,128	2,485,653	184,985	37,830	61,013	13,651	2,683	108.164	3.572773
61	DEM31R1-65-67	-0.902	249,229	2,519,128	35,821	965,173	67559.55	347,965	7,374	192,576	8,828,510	4,549	6,980	19,706	94,596	2,565,202	203,032	77,105	68,722	22,769	4,070	130.6775	3.872635
62	DEM31R1-105-107	4,780	275,911	2,754,533	42,382	1,027,780	72958.6	339,281	7,004	179,836	7,714,703	3,483	5,852	36,729	82,403	2,508,618	178,486	132,891	62,907	22,916	2,148	105.7408	3.725042
63	DEM31R1-145-147	-5,112	250,165	2,515,709	27,854	1,020,782	62216.46	350,769	11,065	165,589	8,646,972	5,977	9,661	23,525	97,665	2,697,997	206,645	73,585	71,951	22,560	5,412	138.9821	4.080435
64	DEM31R2-23-25	-1,389	299,247	2,978,862	27,672	1,077,562	67058.57	437,212	11,454	182,916	10,450,570	4,785	9,643	26,744	105,864	2,425,867	208,102	44,178	88,368	23,341	4,199	155.8424	3.600912
65	DEM31R2-63-65	-2,130	214,741	2,053,802	49,184	816,855	50195.49	344,882	12,002	160,925	9,850,899	12,176	10,005	23,046	101,115	2,161,135	190,674	33,136	85,267	18,366	3,934	196.2507	3.803908
66	DEM31R2-103-105	-0.230	319,982	3,119,688	102,835	1,210,526	52467.1	524,909	18,060	169,124	14,101,730	15,961	13,404	41,020	150,630	2,997,773	301,537	40,654	123,410	32,526	6,241	268.7728	3.783107
67	DEM31R2-143-145	-1,546	289,548	2,898,207	157,102	1,217,523	45218.74	552,825	16,641	148,247	15,708,440	21,846	14,860	42,256	183,783	2,991,177	341,172	41,529	158,529	29,194	7,322	347.3878	4.204909
68	DEM31R3-18-20	-0.986	289,286	3,157,464	49,510	1,220,576	66513.13	422,906	9,897	175,412	9,281,308	4,834	11,398	27,311	110,655	2,814,412	244,532	87,128	79,368	27,434	4,339	139.541	4.219271
69	DEM31R3-63-65	-0.849	322,910	3,286,208	82,213	1,375,435	52404.13	538,124	13,512	144,158	12,700,120	14,600	12,809	40,264	165,995	3,152,076	337,224	79,117	114,484	30,064	8,947	242.3496	4.2595
70	DEM31R3-103-105	-1,933	312,961	3,357,388	68,714	1,358,563	52354.11	531,559	12,868	150,560	12,842,990	13,006	13,575	34,217	165,441	3,088,697	304,410	59,443	112,636	34,335	7,745	245.3101	4.340998
71	DEM31R3-143-145	-2,855	212,871	2,229,064	77,416	889,174	61377.27	301,590	5,906	166,616	7,031,237	3,007	7,394	18,874	78,299	2,152,554	166,030	86,214	48,023	11,259	3,698	114.5577	4.177056
72	DEM31R4-23-25	-1,238	207,538	2,283,322	38,393	906,426	59958.51	310,135	6,242	147,093	6,647,827	3,406	6,430	22,062	72,983	2,127,614	158,852	19,447	53,808	15,071	2,848	110.8738	4.367518
73	DEM31R4-63-65	-2,425	193,468	2,145,688	70,404	859,452	61169.65	290,815	6,860	160,702	6,364,845	3,620	5,797	19,061	75,132	2,116,675	155,887	9,916	53,217	12,610	2,798	104.0523	4.442347
74	DEM31R4-103-105	-3,243	305,247	3,187,260	148,573	1,243,544	58386.2	485,052	14,400	159,014	11,108,930	7,819	11,073	34,852	144,164	2,952,092	283,144	17,301	96,468	26,084	5,262	190.2664	4.073894
75	DEM31R4-143-145	2,489	237,851	2,711,330	88,713	1,122,009	52782.53	419,128	11,503	152,884	9,933,972	8,717	11,519	38,711	119,966	2,556,491	233,109	9,603	84,136	23,170	6,387	188.2057	4.717277
76	DEM31R5-22-24	2,399	278,928	2,821,555	34,699	1,040,452	69394.17	357,561	10,175	173,708	7,814,798	2,997	5,587	23,527	84,830	2,325,439	192,907	9,209	62,627	20,677	4,129	112.6146	3.730181
77	DEM31R5-63-65	0.573	244,262	2,679,865	45,305	1,033,621	65809.25	350,284	7,457	162,842	7,588,885	2,751	7,196	45,912	88,522	2,353,540	198,088	14,423	61,915	22,381	4,041	115.3164	4.231608
78	DEM31R5-103-105	0.787	249,620	2,660,451	33,482	1,113,058	54754.3	382,865	11,946	163,329	8,963,730	4,639	8,528	70,449	115,499	2,874,946	240,540	15,900	79,143	18,363	5,052	163.7082	4.45901
79	DEM31R5-143-145	-2,155	306,232	3,249,524	79,786	1,405,062	52543.75	498,722	16,165	141,217	11,609,700	8,707	23,296	61,314	161,945	3,391,319	323,751	18,671	107,238	32,318	6,922	220.953	4.588227
80	DEM31R6-22-24	2,071	250,904	2,842,497	40,313	1,173,531	50328.63	446,726	11,263	159,912	9,667,628	7,781	12,761	47,505	120,252	2,539,596	254,092	93,767	86,367	19,551	5,459	192.09	4.677211
81	DEM31R6-64-66	-0.528	339,337	3,517,997	49,971	1,398,062	51195.65	569,663	16,229	169,929	12,687,520	11,007	35,857	96,230	172,013	3,240,282	310,338	60,738	113,890	37,439	7,572	247.8242	4.119981
82	DEM31R6-103-105	0.774	275,720	2,844,624	74,091	1,114,557	51895.78	461,458	11,718	195,363	10,994,200	12,503	34,588	33,432	121,750	2,294,510	237,646	107,565	102,861	25,374	4,649	211.8515	4.042351
83	DEM31R6-143-145	0.110	215,647	2,489,882	35,148	1,072,070	38852.47	484,071	14,963	165,900	12,276,760	10,415	21,245	30,112	133,123	2,142,155	236,705	13,252	109,218	27,925	7,553	315.984	4.971412
84	DEM31R7-30-32	-0.406	282,397	2,892,695	26,914	1,121,637	63184.68	394,210	11,102	212,700	8,351,255	4,522	23,250	22,679	94,917	2,332,173	201,152	10,068	74,121	24,650	3,946	132.1721	3.971845
85	DEM31R7-58-60	1,506	285,411	3,135,540	76,663	1,180,288	60300.25	454,989	13,004	227,504	10,267,110	6,694	22,684	28,210	113,902	2,379,384	234,897	11,196	82,694	35,886	5,225	170.2665	4.135398
86	DEM31RCC-9-11	0.332	281,016	3,073,106	127,801	1,104,886	51589.81	501,425	14,667	201,885	11,725,180	8,080	28,232	33,768	120,341	2,191,821	239,425	8,327	94,972	31,131	6,271	227.2771	3.931755
87	DEM32R1-24-28	2,512	304,858	3,278,460	6,808	1,286,585	43601.1	610,804	15,319	178,127	16,444,090	13,162	16,294	42,638	186,876	2,783,808	343,947	35,271	136,978	45,558	8,354	377.1485	4.220276
88	DEM32R1-65-67	1,179	240,519	2,603,665	13,696	975,293	57270.36	403,062	11,533	190,656	9,972,346	6,123	14,610	23,388	95,397	2,056,382	178,988	10,091	87,816	23,150	4,096	174.1275	4.054952
89	DEM32R1-105-108	-0.884	215,621	2,349,589	14,382	838,801	46586.45	442,984	13,768	173,061	13,278,020	10,495	8,447	29,351	103,976	1,784,624	203,938	12,054	113,566	27,764	5,646	285.0189	3.890164
90	DEM32R1-144-146	1,428	283,406	3,180,911	46,372	1,105,384	48136.89	610,738	18,587	185,509	18,479,570	17,787	10,966	43,282	168,451	2,246,651	344,842	37,266	153,956	37,965	10,037	383.8962	3.900355
91	DEM32R2-25-27	-0.126	226,788	2,216,112	23,727	825,577	67448.5	328,156	7,656	224,001	8,321,652	3,761	6,847	24,158	79,253	2,024,931	176,889	23,086	64,540	20,865	4,650	123.3779	3.640303
92	DEM32R2-65-67	-0.719	249,461	2,778,169	35,933	993,341	52497.73	495,014	15,503	208,662	12,914,200	11,532	9,140	39,898	116,774	1,762,191	231,674	17,231	109,174	24,911	7,505	245.9954	3.981949
93	DEM32R2-105-107	0.775	272,366	3,075,065	141,013	1,055,905	57326	530,437	12,958	196,560	15,006,740	10,801	11,584	37,812	128,659	2,204,371	270,254	26,061	116,929	32,139	6,807	261.7789	3.876787
94	DEM32R2-145-147	-2,011	287,447	2,662,546	151,937	958,857	67432.91	342,465	9,323	190,267	9,116,199	5,861	7,850	25,877	79,510	2,092,688	205,751	13,933	72,311	25,318	3,896	135.1892	3.33577
95	DEM32R3-22-24	-1,606	252,759	2,638,347	109,414	989,402	46671.02	477,080	14,672	153,511	13,682,450	12,572	9,376	34,044	111,942	1,705,213	219,631	90,464	113,440	23,610	6,173	293.168	3.914409
96	DEM32R3-65-67	0.075	242,495	2,794,942	61,450	1,104,202	50360.17	458,019	13,729	108,637	12,588,100	10,696	13,510	34,160	126,143	2,231,082	222,470	15,909	113,218	24,944	5,325	249.9614	4.553504
97	DEM32R3-105-107	-2,957	287,051	2,859,207	119,959	1,050,728	66139.87	401,625	8,566	175,462	11,202,450	7,659	7,219	72,755	103,779	2,125,740	207,163	21,554	98,639	23,844	4,436	169.3751	3.660423
98	DEM32R3-145-147	-2,723	302,992	3,066,793	67,283	1,109,619	69649.12	404,458	8,646	166,704	10,042,070	4,705	7,224	28,433	102,961	2,263,742	203,332	19,756	79,111	29,511	3,108	144.1809	3.662206
99	DEM32R4-23-25	-0.911	248,488	2,887,396	86,995	1,111,290	57532.64	453,632	11,153	173,291	12,136,820	10,602	9,614	296,658	116,119	1,940,108	223,711	12,669	99,555	21,812	5,458	210.9554	4.472208
100	DEM32R4-65-67	4,293	285,865	3,090,795	124,748	1,190,976	55818.92	490,280	13,941	160,548	14,069,380	11,220	10,798	40,351	135,607	2,298,251	253,036	14,167	121,020	31,906	5,806	252.054	4.166218
101	DEM32R4-105-107	-0.289	255,981	2,634,801	130,991	1,026,674	59200.98	386,456	9,974	173,795	9,806,150	6,299	13,221	26,737	92,588	1,781,545	194,992	82,433	76,405	14,307	5,640	165.6417	4.010743
102	DEM32R4-145-147	-0.675	301,363	2,970,192	296,666	1,099,480	66656.34	399,820	8,628	188,064	11,957,870	5,988	7,871	37,804	94,332	2,107,740	206,638	54,567	101,197	25,558	6,061	179.3958	3.648358
103	DEM32R5-16-18	0.412	289,988	3,116,099	131,962	1,148,493	62148.91	445,752	12,990	173,578	12,483,470	9,228	10,689	36,583	116,748	2,311,918	236,497	28,368	101,700	28,329	6,984	200.8639	3.960485
104	DEM32R5-55-57	-1,752	313,892	3,091,096	53,322	1,197,857	58706.98	459,698	15,658	153,876	12,549,270	9,015	7,423	44,830	130,726	2,336,030	240,852	15,667	101,801	29,324	6,388	213.7611	3.816144
105	DEM32R5-95-97	-1,641	309,633	3,298,252	27,249	1,243,264	60195.41	494,438	12,859	158,770	13,018,290	9,632	10,651	44,043	130,905	2,357,889	252,528	14,741	113,642	28,796	6,383	216.2672	4.015283
106	DEM32R5-135-137	-1,775	242,921	2,534,167	17,542	976,478	55461.25	381,799	10,827	136,262	9,980,607	8,290	9,383	28,340	92,698	1,875,894	174,233	30,772	80,164	20,592	3,618	179.9564	4.019735
107	DEM32R6-20-22	-1,665	217,628	2,444,124	17,240	951,650	59281.66	354,119	7,455	154,697	9,306,693	7,424	9,403	38,135	82,940	1,802,151	162,124	25,011	72,159	17,036	3,911	156.9911	4.372829
108	DEM32R6-65-67	0.777	277,571	2,740,472	92,264	1,031,384	69429.22	379,058	8,987	172,210	9,846,690	5,439	6,835	26,767	96,268	2,252,039	195,292	93,406	78,138	21,532	5,098	141.8234	3.715748
109	DEM32R6-101-103	-3,452	293,084	3,023,769	107,751	1,086,811	64248.42	440,997	11,048	151,922	11,561,020	5,894	5,941	35,384	103,377	2,267,660	216,274	19,826	92,149	25,665	5,537	179.9425	3.708189
110	DEM33R1-20-22	-0.402	280,998	3,038,149	154,253	1,163,090	56668.7	489,342	15,699	117,748	13,431,440	10,468	11,989	39,752	125,011	2,406,718	244,552	49,270	112,250	31,171	7,121	237.0169	4.13914
111	DEM33R1-60-62	-0.200	240,187	2,340,314	84,801	928,473	47712.42	419,427	13,969	150,170	13,440,400	12,143	12,060	36,697	129,771	2,211,050	256,049	15,274	108,653	25,182	5,495	281.696	3.865626
112	DEM33R1-108-110	-1,806	248,695	2,765,005	80,160	1,169,979	51409.09	444,306	14,083	130,850	9,943,136	9,288	12,700	39,321	124,792	2,506,789	248,811	13,703	91,433	27,148	4,849	193.412	4.704473
113	DEM33R1-140-142	-3,514	260,938	2,955,300	59,996	1,171,719	54731.96	475,778	13,662	152,482	12,336,830	10,830	12,072	36,702	147,712	2,787,356	287,989	30,702	112,160	29,599	7,125	225.4045	4.490412
114	DEM33R2-18-20	0.767	237,588	2,518,979	37,918	1,056,976	61942.21	360,554	9,229	160,626	7,986,870	5,166	25,648	28,654	96,700	2,482,580	192,811	16,283	67,198	20,383	3,704	128.9407	4.448777
115	DEM33R2-58-60	0.605	302,664	3,146,402	19,784	1,186,741	66737.33	397,578	10,082	193,864	8,614,200	4,727	10,454	27,764	101,042	2,647,876	209,084	29,911	76,203	24,620	4,727	129.0762	3.920985
116	DEM33R2-97-100	-1,147	270,311	2,908,758	34,984	1,125,652	56390.89	440,635	15,482	187,591	10,375,910	11,530	6,986	32,436	117,474	2,373,510	226,970	38,589	94,985	22,879	5,213	183.9998	4.164285
117	DEM33R2-140-142	0.999	260,028	3,057,995	26,312	1,173,197	61087.43	405,644	8,827	188,579	8,801,971	5,359	33,599	29,094	114,489	2,720,456	218,762	11,163	69,876	29,038	4,762	144.0881	4.51181
118	DEM33R320-22	0.150	243,748	2,708,091	18,316	1,114,287	46453.04	495,851	15,910	179,372	14,569,980	13,407	11,387	43,667	172,609	2,654,210	311,761	18,212	123,071	32,552	7,433	313.6497	4.571471
119	DEM33R3-60-62	-0.241	268,300	2,908,722	51,955	1,057,177	62381.65	418,846	7,158	188,493	10,290,280	5,532	7,389	28,765	111,345	2,327,075	221,208	357,958	79,028	25,277	5,068	164.9568	3.94028
120	DEM33R3-98-100	-1,007	199,832	2,265,573	16,999	887,554	42476.14	447,681	14,615	124,320	12,647,780	10,869	10,748	35,758	129,663	1,863,074	259,234	14,965	112,581	28,236	5,407	297.762	4.441501
121	DEM33R3-140-142	-2,088	165,470	2,067,396	12,262	815,780	38766.52	382,851	12,602	112,123	10,138,970	9,656	8,524	27,910	101,777	1,564,318	181,373	8,258	84,026	29,561	4,491	261.5393	4.930078
122	DEM33R4-15-17NEW2	-1,979	197,699	2,128,255	6,810	868,099	33697.5	464,458	13,551	121,579	14,227,790	12,075	11,935	41,285	150,440	1,802,984	247,528	27,432	116,115	25,149	7,325	422.2209	4.391014
123	DEM33R4-55-57	1,477	199,543	2,405,005	558,223	935,787	28021.28	374,704	-37,300	103,092	13,434,970	12,033	35,685	36,979	129,149	2,393,118	229,087	2,619,157	122,761	164,595	6,341	479.456	4.689651
124	DEM33R4-103-105	-0.507	245,611	3,127,945	18,256	1,229,755	51916.17	457,081	16,169	161,410	12,032,060	10,694	15,132	30,597	164,283	2,770,271	292,093	22,899	97,548	35,099	6,630	231.7594	5.006922
125	DEM33R4-145-147NEW	1,868	310,071	3,290,725	203,639	1,195,772	52960.95	448,298	-5,856	177,384	11,591,350	9,584	14,721	32,208	138,342	2,580,668	238,147	958,953	96,704	49,662	5,893	218.866	3.856446
126	DEM33R5-25-27	-0.950	267,567	3,333,962	26,501	1,240,367	55967.94	469,779	11,775	197,763	10,985,500	7,620	10,682	34,365	150,691	2,438,460	248,241	78,323	83,840	26,572	6,782	196.282	4.635725
127	DEM33R5-63-65	0.338	264,166	3,515,112	45,206	1,169,894	58495.89	421,746	8,693	188,777	9,888,220	6,880	12,023	34,935	128,583	2,462,620	222,174	108,983	93,046	32,091	4,949	169.0413	4.428632
128	DEM33R5-102-104	-0.558	197,276	2,906,818	19,273	921,810	55568.41	320,917	6,809	171,341	7,187,034	3,430	6,515	22,775	90,137	2,013,071	167,208	129,727	61,567	14,478	4,167	129.3367	4.672692
129	DEM33R5-145-147	-0.118	245,669	3,273,838	32,540	1,127,515	60573.85	401,143	10,293	183,361	9,477,768	6,590	9,083	30,170	123,935	2,430,552	209,718	129,805	74,390	25,270	4,233	156.4663	4.58957
130	DEM33R6-23-25	-0.908	242,511	3,380,155	33,344	1,091,077	60191.96	389,064	10,007	172,006	8,860,396	4,296	8,399	37,768	117,208	2,455,300	217,448	119,066	77,664	22,691	5,107	147.2023	4.499083
131	DEM33R6-63-65	3,030	253,539	3,347,414	46,236	1,303,738	50388.68	485,266	14,037	153,141	11,601,450	6,963	13,431	54,845	173,122	2,861,060	301,674	60,899	101,588	32,315	7,402	230.2392	5.14216
132	DEM33R6-103-105	0.761	237,678	2,808,111	60,904	1,079,354	56576.92	408,665	11,128	175,442	10,199,230	8,299	17,314	37,874	133,073	2,487,966	241,953	86,585	97,111	20,528	4,785	180.2719	4.541245
133	DEM33R6-142-144	2,754	233,717	2,754,358	50,147	1,013,781	58240.52	354,347	9,778	164,622	8,406,518	8,291	9,318	35,399	107,950	2,091,930	176,910	86,540	72,817	18,025	4,172	144.3414	4.337643
134	DEM33R7-22-24	-0.656	267,503	3,480,722	65,791	1,055,029	63876.68	369,555	8,373	153,101	8,273,094	4,204	20,278	47,794	104,359	2,476,419	218,766	141,582	71,544	21,218	3,053	129.5167	3.943989
135	DEM33R7-68-70	-0.371	199,716	2,471,862	58,628	912,254	56309.23	305,208	6,758	158,120	7,548,835	5,383	6,447	28,368	92,129	1,983,722	169,366	145,185	58,657	12,946	3,392	134.0603	4.567756
136	DEM34R1-23-25	0.756	280,302	3,265,746	61,836	1,108,047	65361.52	387,645	8,801	168,645	8,878,313	6,077	10,091	26,531	107,380	2,523,508	201,920	169,654	78,741	22,179	6,267	135.8339	3.953047
137	DEM34R1-62-64	-0.008	264,165	2,973,180	46,440	1,100,702	60326.29	407,783	7,944	167,015	10,635,560	7,180	13,642	30,214	129,262	2,414,686	219,968	154,123	86,070	17,423	6,207	176.3006	4.166722
138	DEM34R1-103-105	0.254	227,407	2,796,125	57,299	1,031,850	51845.72	357,367	9,771	117,881	8,194,308	5,926	18,274	48,302	104,034	2,284,802	179,963	164,021	70,855	14,434	4,777	158.0518	4.537459
139	DEM34R1-144-146	-3,377	276,122	2,966,547	50,526	1,080,078	60768.85	380,700	8,585	158,977	9,496,076	4,025	10,262	30,430	115,516	2,583,140	233,550	240,626	81,834	18,552	4,605	156.2655	3.911597
140	DEM34R2-25-27	-0.988	294,696	3,621,346	55,160	1,399,634	46025.53	570,734	16,138	123,134	14,426,260	16,451	20,359	65,326	196,382	3,120,672	364,127	123,946	131,492	25,390	8,036	313.4404	4.749416
141	DEM34R2-60-62	0.501	272,461	3,168,035	82,534	1,280,990	50302.82	474,430	11,593	132,575	12,111,370	10,214	17,941	46,490	168,669	3,297,364	320,637	97,834	112,718	25,761	7,993	240.7692	4.701554
142	DEM34R2-102-104	-2,985	298,902	3,349,066	82,534	1,282,938	48397.17	551,835	17,320	139,603	15,485,440	13,381	12,192	44,665	196,038	3,026,107	342,071	98,718	144,064	31,300	7,792	319.9658	4.292169
143	DEM34R2-143-145	-1,968	238,637	2,698,967	46,465	1,144,080	36844.55	476,164	14,058	97,640	12,413,980	12,968	13,642	42,676	156,113	2,573,371	304,031	60,094	110,689	27,113	8,431	336.9285	4.794227
144	DEM34R3-23-25	-0.569	239,205	3,293,877	135,825	1,053,396	63937.08	338,731	-1,897	153,401	7,957,644	2,969	6,483	24,608	96,058	2,590,847	213,558	911,998	63,033	31,162	3,398	124.4605	4.403737
145	DEM34R3-64-66	-1,369	272,730	3,593,243	112,892	1,171,789	61833.12	376,882	3,731	142,310	8,833,669	4,258	12,230	29,972	109,038	2,855,373	233,484	416,221	75,911	20,785	5,226	142.8631	4.296517
146	DEM34R3-102-104	1,990	225,285	2,931,200	57,651	1,059,459	45963.82	424,492	12,918	117,624	9,980,263	11,488	16,979	38,513	126,979	2,404,490	221,779	57,310	85,575	22,208	4,903	217.133	4.70275
147	DEM34R3-142-144NEW2	-2,491	290,279	3,230,353	161,089	1,282,511	43209.27	578,394	19,807	107,939	14,840,010	25,007	18,237	58,298	195,611	3,517,179	372,443	80,172	142,344	25,883	9,289	343.4451	4.418201
148	DEM34R4-8-10	-0.605	278,839	3,372,622	201,305	1,245,517	48209.96	517,145	15,071	133,296	13,698,630	12,312	18,175	45,299	177,418	3,326,674	311,035	78,718	122,565	29,419	6,011	284.1452	4.466796
149	DEM34R4-41-43	-1,348	247,294	3,014,524	67,803	1,108,356	54805	417,116	10,321	138,136	10,246,840	8,002	11,131	31,549	129,747	3,092,408	285,472	81,582	89,216	17,042	6,761	186.9691	4.481936
150	DEM34R4-78-80	1,031	286,503	3,294,545	100,253	1,192,239	50120.25	530,382	16,530	142,528	14,061,950	17,811	10,805	33,272	172,335	2,967,839	334,156	82,138	127,885	21,001	7,390	280.5642	4.161349
151	DEM34R4-118-119	1,300	204,728	2,838,509	111,857	996,234	54467.8	377,118	6,481	143,256	9,105,702	7,293	79,554	86,217	107,140	2,495,794	211,733	84,981	82,270	14,832	3,986	167.1759	4.866135
152	DEM34RCC-5-7	2,533	310,064	3,538,492	157,440	1,174,008	43380.41	619,115	7,427	146,140	17,105,800	16,349	16,530	59,068	176,589	2,773,181	336,500	632,266	138,703	47,049	8,483	394.3208	3.786341

TABLE S2 δ13c AND δ18O VALUES, AND ELEMENTAL COMPOSITION DATA (XRF ANALYSES) OF HOLE 1258A (XRF NORMALIZED DATA)

Mg NMS	Al NMS	Si NMS	S NMS	K NMS	Ca NMS	Ti NMS	Cr NMS	Mn NMS	Fe NMS	Ni NMS	Cu NMS	Zn NMS	Rb NMS	Sr NMS	Zr NMS	Ba NMS	Co NMS	V NMS	Ga NMS	
-0.01091	1.682629	16.47944	0.085146	5.861417	0.428325	1.981829	0.037936	2.033509	54.3179	0.028127	0.028808	0.134801	0.457129	14.60436	1.078043	0.190075	0.418427	0.145054	0.017958	100
0.009837	1.58387	15.10047	0.089953	4.915247	0.312527	2.015123	0.056089	1.572876	59.45473	0.035686	0.026976	0.147038	0.47719	12.35498	1.042123	0.132708	0.468451	0.176623	0.027505	100
0.006812	1.321121	12.74293	0.085033	4.44864	0.237459	1.859644	0.058934	1.239593	63.76904	0.045263	0.045463	0.144667	0.492777	11.66869	1.032601	0.091794	0.533411	0.144811	0.031317	100
-0.01101	1.206255	11.51261	0.066852	3.60966	0.271892	1.766189	0.052503	1.321787	66.61154	0.051961	0.064214	0.152688	0.417064	11.12524	0.945645	0.091663	0.547913	0.164602	0.030745	100
-0.00715	1.527045	14.65383	0.1503	4.890717	0.364494	2.052732	0.038652	1.631337	57.3045	0.028192	0.141412	0.14979	0.511651	14.63633	1.200577	0.122912	0.453724	0.124392	0.024594	100
-0.00662	1.827255	15.35023	0.087892	4.997382	0.379431	2.119041	0.053418	1.682417	56.1077	0.045183	0.050899	0.330391	0.519931	14.51463	1.165453	0.114283	0.456867	0.173618	0.030594	100
0.017771	1.71019	16.24543	0.193416	5.683401	0.500143	2.270337	0.027314	2.148979	51.41709	0.037832	0.094647	0.15709	0.520469	17.09067	1.175826	0.131211	0.419837	0.131845	0.026505	100
0.010636	2.03358	17.63784	0.218373	6.027212	0.544765	2.106524	0.034765	2.206263	47.60458	0.014685	0.041578	0.151086	0.519895	18.93296	1.220422	0.144089	0.361806	0.170912	0.018035	100
-0.03725	1.576295	15.38474	0.122856	5.601813	0.504864	2.197709	0.029858	2.163387	52.70293	0.032202	0.047771	0.142972	0.501384	17.14683	1.169339	0.10038	0.443538	0.145516	0.022859	100
0.007969	1.832716	17.00022	0.197094	5.856281	0.537758	2.072794	0.040745	2.175904	49.99506	0.026971	0.054279	0.166914	0.526901	17.51597	1.239235	0.15387	0.410085	0.166115	0.023121	100
0.022324	1.921928	16.56171	0.168031	5.564863	0.519249	2.103469	0.022358	2.178886	50.63255	0.009762	0.041218	0.127963	0.491857	17.71275	1.214287	0.17577	0.375859	0.138488	0.017712	100
5.2E-06	1.739044	16.43085	0.140536	5.573017	0.505328	2.094937	0.033281	2.001642	52.04	0.022119	0.053727	0.129559	0.471007	16.93622	1.133252	0.11735	0.441442	0.113235	0.023457	100
1.78E-06	1.841378	16.64039	0.236784	5.464503	0.472078	2.157579	0.041322	1.786331	52.31025	0.027475	0.051457	0.124967	0.521069	16.42028	1.195012	0.151054	0.401286	0.132617	0.024163	100
-3.2E-06	1.866879	16.81893	0.237553	5.755235	0.467348	2.11631	0.047989	1.728857	51.24997	0.026601	0.059154	0.180132	0.54462	16.90195	1.270784	0.16548	0.387106	0.15841	0.016692	100
1.03E-06	1.97217	16.77498	0.187357	5.569372	0.549437	2.142922	0.034859	1.807264	50.4176	0.014128	0.072309	0.146752	0.481959	17.81859	1.259985	0.167968	0.384608	0.18014	0.017597	100
0.022316	1.939182	16.66666	0.167609	5.537488	0.51681	2.007688	0.030448	1.638352	49.86495	0.017245	0.042066	0.385058	0.507317	18.68317	1.242299	0.186269	0.39218	0.129713	0.023169	100
-2E-06	1.784163	15.62837	0.161316	5.281586	0.42387	2.156257	0.032237	1.424576	52.66798	0.029352	0.051173	0.240644	0.564275	17.4163	1.309062	0.163312	0.479854	0.153284	0.032388	100
1.57E-06	1.582877	16.04943	0.201323	5.724282	0.475588	2.201391	0.050615	1.55534	52.07299	0.022803	0.042808	0.154641	0.529929	17.45916	1.186449	0.164266	0.424047	0.077803	0.024257	100
-0.01952	1.686589	16.55237	0.186119	5.663333	0.522415	2.070973	0.028806	1.660427	50.2479	0.013568	0.044854	0.117498	0.527759	18.61437	1.293406	0.182011	0.404867	0.169815	0.032438	100
-0.00918	1.629845	15.56556	0.235583	5.883422	0.438801	2.026184	0.040828	1.363325	51.21255	0.04119	0.058157	0.154887	0.595973	18.69057	1.328729	0.150027	0.442479	0.125284	0.01954	100
3.81E-06	1.762969	18.52297	0.287822	6.409879	0.49134	2.258828	0.045107	1.449886	48.78419	0.054355	0.154774	0.112537	0.576425	17.1419	1.264328	0.118644	0.378355	0.164884	0.020803	100
-0.01767	1.655434	15.64636	0.211116	5.699142	0.341556	2.117399	0.053345	1.027962	53.75753	0.064138	0.056314	0.1706	0.614623	16.3877	1.343283	0.207207	0.51553	0.119939	0.028497	100
-4.1E-06	1.674123	16.65954	0.201845	6.336565	0.545507	2.194909	0.03443	1.624495	49.33055	0.009318	0.056845	0.133049	0.513816	18.64827	1.227576	0.195925	0.40459	0.175556	0.033101	100
7.89E-07	1.783804	17.51173	0.23305	6.25031	0.513741	2.024477	0.030057	1.475828	47.84241	0.029165	0.043575	0.435704	0.547037	19.26185	1.268851	0.175585	0.403648	0.14651	0.022669	100
6.9E-06	1.731803	16.55479	0.202912	5.901142	0.525021	2.065459	0.038927	1.534769	49.77203	0.030444	0.07362	0.118527	0.509902	18.90325	1.29285	0.20096	0.371871	0.144019	0.027693	100
-0.0238	1.61735	15.80944	0.174886	5.665976	0.452096	2.24741	0.044089	1.311575	54.02112	0.019235	0.046834	0.112095	0.529279	16.08551	1.15812	0.145709	0.441611	0.120146	0.021309	100
-0.03008	1.500149	15.25234	0.170923	5.895264	0.490629	2.103583	0.031709	1.41401	52.87554	0.022897	0.066365	0.267754	0.576578	17.45599	1.165305	0.197262	0.437865	0.069767	0.036146	100
-0.02759	1.737324	17.24908	0.329196	5.934927	0.548082	1.982487	0.014297	1.503048	48.66979	0.03229	0.044069	0.324169	0.538855	19.20471	1.23119	0.196384	0.359155	0.105347	0.023185	100
-0.02241	1.455182	15.38479	0.259443	5.947434	0.524863	2.105349	0.036121	1.526594	50.97793	0.015204	0.044822	0.15801	0.561189	18.94325	1.270147	0.242205	0.414909	0.112677	0.028013	100
0.016694	1.50854	15.47214	0.212021	5.995923	0.386954	2.182779	0.052598	1.068004	51.53512	0.034875	0.061836	0.139505	0.597559	18.76167	1.340826	0.156978	0.437539	0.115548	0.022896	100
2.33E-07	1.450816	15.93921	0.277216	6.037694	0.391465	2.209762	0.034	1.139403	52.06612	0.050904	0.051045	0.679529	0.597438	17.05216	1.279731	0.160936	0.443992	0.112324	0.026256	100
-0.0075	1.347936	15.73389	0.233578	6.283454	0.385206	2.212035	0.043358	1.099339	52.67388	0.059296	0.056934	0.181282	0.613989	17.09829	1.271839	0.155544	0.421606	0.10969	0.026346	100
4.01E-06	1.897731	18.17895	0.287773	6.136113	0.503102	2.119154	0.042868	1.263666	49.16995	0.023905	0.037738	0.126193	0.536022	17.72571	1.222356	0.183518	0.384111	0.142839	0.018291	100
0.008388	1.496084	14.76359	0.314868	5.44061	0.31939	2.163159	0.057873	0.92587	56.69846	0.062666	0.053514	0.138471	0.632817	14.88917	1.252349	0.163525	0.48711	0.105416	0.025771	100
0.019245	1.749638	17.30531	0.377526	5.86015	0.452404	2.112054	0.034797	1.190468	51.19705	0.033076	0.04909	0.19325	0.537631	16.81231	1.253839	0.217702	0.444383	0.127041	0.033039	100
0.016043	1.562948	16.3051	0.338516	5.77428	0.380566	2.09111	0.053348	0.979117	52.52559	0.040447	0.050166	0.148215	0.588472	17.08273	1.245726	0.193689	0.434139	0.161317	0.02848	100
-0.01462	1.624214	15.17975	0.253544	5.951817	0.450375	2.298183	0.045815	1.212504	51.81647	0.034326	0.052487	0.285563	0.612505	18.20247	1.366107	0.190559	0.451358	0.160534	0.026025	100
4.15E-06	1.609502	15.74102	0.242844	5.923934	0.384196	2.082193	0.051659	0.972566	52.03003	0.061157	0.051629	0.18082	0.617297	17.8284	1.402691	0.202811	0.477584	0.117415	0.022644	100
4.65E-06	1.503679	15.59266	0.305334	5.900397	0.367876	2.2051	0.044169	0.940652	53.4765	0.047412	0.052507	0.261407	0.620398	16.37266	1.370561	0.281622	0.484503	0.128447	0.028698	100
0.013803	1.49629	15.85397	0.275403	5.501403	0.414349	2.085578	0.062798	1.099114	55.62816	0.066408	0.056575	0.108879	0.531158	14.93013	1.163307	0.132439	0.473763	0.086197	0.020269	100
-0.00876	1.549029	15.81942	0.526376	6.151446	0.363233	2.070065	0.039238	0.797342	49.36224	0.049657	0.047694	0.184619	0.642463	20.14183	1.439956	0.213172	0.446521	0.130363	0.034101	100
-3.8E-06	1.586838	17.07596	0.230024	6.2963	0.500795	2.2026	0.045142	1.042066	47.97489	0.023738	0.045717	0.150626	0.567394	20.34407	1.320874	0.230078	0.388031	0.133584	0.02328	100
8.06E-07	1.315388	13.63736	0.506317	5.230264	0.322808	1.965186	0.054944	0.8202	55.90499	0.072542	0.073977	0.116076	0.624765	17.17042	1.332883	0.18594	0.527969	0.113823	0.024152	100
1.74E-06	1.575031	16.58101	0.246381	6.014923	0.408245	1.949206	0.044228	0.87102	48.91067	0.032908	0.063909	0.154501	0.59079	20.37153	1.390512	0.215315	0.409454	0.133873	0.031996	100
0.012282	1.659034	17.13057	0.276681	6.228787	0.520318	2.086582	0.060588	1.147311	49.99986	0.016512	0.068468	0.16738	0.531251	18.24961	1.139648	0.170142	0.376978	0.137407	0.020588	100
-0.02137	1.505992	15.54642	0.244125	6.134335	0.384142	2.142419	0.060788	0.813376	52.34612	0.022372	0.051486	0.133574	0.596202	17.94536	1.326971	0.211636	0.423567	0.104249	0.028246	100
-0.00772	1.59795	15.57794	0.310005	6.034824	0.427193	2.033673	0.04669	0.913199	50.54873	0.030421	0.070447	0.157437	0.597589	19.42149	1.350618	0.290029	0.449738	0.12275	0.026999	100
9.63E-07	1.738084	17.00355	0.303142	6.092399	0.489277	2.111437	0.038302	1.074287	50.84308	0.031686	0.044159	0.143446	0.543034	17.62862	1.188027	0.209963	0.373028	0.120668	0.023815	100
-5.7E-06	1.686298	16.4614	0.29612	6.129805	0.510605	2.048881	0.039962	1.196248	50.81164	0.017	0.046057	0.146216	0.536142	18.11772	1.244463	0.219568	0.375972	0.095562	0.020638	100
0.007931	1.423892	15.05747	0.288942	5.87652	0.345472	2.229864	0.05389	0.817837	54.78478	0.05208	0.153418	0.191172	0.608464	16.01086	1.26931	0.198492	0.502092	0.101798	0.025714	100
-0.00825	1.558183	16.62884	0.265786	6.313239	0.447959	2.131223	0.039515	1.019531	50.26173	0.019563	0.059712	0.226759	0.554045	18.43876	1.269159	0.211181	0.38414	0.153805	0.025118	100
-4.7E-06	1.55575	15.60567	0.228154	5.670177	0.340896	2.207502	0.053159	0.91441	55.12842	0.029735	0.040245	0.135397	0.61239	15.32857	1.34962	0.190547	0.45639	0.12895	0.024026	100
-3.4E-06	1.503142	15.10428	0.180201	5.698217	0.345442	2.100828	0.044554	0.857028	53.98372	0.022042	0.044504	0.132368	0.603987	17.13293	1.413709	0.224912	0.479871	0.099243	0.029021	100
-5.2E-06	1.546798	16.47725	0.179758	6.118752	0.357406	2.139517	0.055181	0.845398	51.653	0.029502	0.044597	0.180533	0.62843	17.60222	1.372783	0.196015	0.436155	0.112443	0.024268	100
-0.0118	1.477804	14.26814	0.140131	5.608622	0.363129	2.039733	0.05535	1.014704	54.37272	0.042653	0.062674	0.17678	0.625251	17.53445	1.379373	0.228438	0.454957	0.137747	0.029142	100
-0.01192	1.815163	18.77824	0.196521	6.366351	0.504322	2.139612	0.053143	1.207272	49.68879	0.012216	0.049653	0.126183	0.480648	16.54202	1.209771	0.267843	0.409217	0.143248	0.021703	100
2.51E-06	1.686747	16.82029	0.139448	5.802749	0.447837	2.192011	0.052108	1.189643	52.14359	0.022393	0.046306	0.113078	0.526194	16.89003	1.178744	0.191014	0.398928	0.136786	0.022103	100
-0.0053	1.336527	15.22075	0.241855	5.718513	0.30441	2.105818	0.057114	0.859808	54.56266	0.025057	0.051243	0.14025	0.613861	16.46728	1.366198	0.25719	0.511612	0.135461	0.029691	100
0.016102	1.833775	18.32933	0.332083	6.364055	0.564542	2.058014	0.031926	1.376127	48.38023	0.034373	0.06925	0.12627	0.471249	18.15677	1.11647	0.249403	0.359485	0.111631	0.018914	100
0.016219	1.65523	17.04437	0.292325	5.913759	0.480959	2.139544	0.052113	1.204429	52.02245	0.023901	0.052706	0.199512	0.534897	16.38854	1.219653	0.249423	0.402274	0.090004	0.01769	100
-5.5E-06	1.530884	15.4737	0.22003	5.928557	0.414983	2.137369	0.045295	1.182894	54.22896	0.027942	0.042875	0.121044	0.581054	15.75671	1.24712	0.473616	0.422124	0.139858	0.025	100
0.030927	1.785184	17.82223	0.274218	6.649887	0.472053	2.195198	0.045317	1.163565	49.91526	0.022536	0.037863	0.237642	0.533159	16.23112	1.15483	0.859824	0.407017	0.14827	0.013898	100
-0.03144	1.538437	15.47083	0.171293	6.277491	0.382612	2.15712	0.068046	1.018321	53.17618	0.036757	0.059412	0.144671	0.600609	16.59184	1.270802	0.452525	0.442476	0.138737	0.033282	100
-0.00752	1.619981	16.12614	0.149803	5.833408	0.363023	2.366858	0.062007	0.99022	56.57441	0.025904	0.052203	0.144779	0.573097	13.13249	1.126565	0.239159	0.478382	0.126357	0.022731	100
-0.01316	1.326363	12.68546	0.303789	5.045364	0.310036	2.130189	0.074131	0.993965	60.84479	0.075206	0.061797	0.142345	0.624544	13.34841	1.177712	0.204667	0.526658	0.113439	0.024299	100
-9.9E-07	1.370814	13.36485	0.440549	5.185936	0.224771	2.248729	0.07737	0.724533	60.41231	0.068377	0.057423	0.175731	0.645304	12.84257	1.291795	0.174163	0.528693	0.139343	0.026737	100
-0.00622	1.164533	11.6563	0.631848	4.896755	0.181865	2.223407	0.066928	0.596235	63.17777	0.087862	0.059765	0.169949	0.739157	12.03021	1.372159	0.167025	0.637588	0.117415	0.029448	100
-5.5E-06	1.599654	17.45971	0.273774	6.749375	0.367795	2.338528	0.054727	0.969969	51.32251	0.02673	0.063027	0.151021	0.611885	15.56275	1.35218	0.481789	0.438878	0.151701	0.023993	100
-3.8E-06	1.437029	14.62444	0.365868	6.121025	0.233211	2.394785	0.060132	0.641539	56.51867	0.064974	0.057003	0.179185	0.738719	14.02752	1.50073	0.35209	0.509482	0.133792	0.039816	100
-0.00858	1.389732	14.90878	0.305131	6.032822	0.232483	2.360436	0.057142	0.668575	57.03046	0.057754	0.060281	0.151944	0.734656	13.71564	1.35176	0.263962	0.50017	0.152468	0.034392	100
-0.02107	1.571265	16.45339	0.571431	6.56326	0.453044	2.226126	0.043594	1.229843	51.89967	0.022196	0.054577	0.139315	0.577948	15.88865	1.225517	0.636371	0.354472	0.083106	0.027296	100
-0.00946	1.585686	17.44563	0.29334	6.925511	0.458111	2.369574	0.047692	1.123858	50.79246	0.026023	0.049128	0.168564	0.557624	16.25595	1.213702	0.148584	0.411118	0.115149	0.02176	100
-0.01924	1.534767	17.02158	0.55851	6.817968	0.485254	2.307013	0.05442	1.274837	50.49183	0.028717	0.045987	0.151209	0.596016	16.79142	1.23664	0.078663	0.422166	0.100034	0.022196	100
-0.01599	1.50476	15.71207	0.732413	6.130235	0.287823	2.391136	0.070987	0.783883	54.76312	0.038545	0.054586	0.171808	0.710678	14.55278	1.3958	0.085288	0.475553	0.128585	0.02594	100
0.013964	1.334407	15.21128	0.497703	6.294768	0.296124	2.351419	0.064535	0.85772	55.73221	0.048905	0.064625	0.217179	0.673041	14.34259	1.307803	0.053875	0.472025	0.12999	0.035833	100
0.015643	1.818827	18.39873	0.226264	6.784554	0.452504	2.331575	0.066349	1.132711	50.95855	0.019543	0.036432	0.153414	0.553157	15.16367	1.257903	0.06005	0.408377	0.13483	0.026924	100
3.83E-06	1.630903	17.89308	0.302495	6.901343	0.439399	2.338797	0.049789	1.087273	50.66992	0.018368	0.048047	0.306548	0.591049	15.71426	1.322606	0.0963	0.413398	0.149435	0.026981	100
4.61E-06	1.462649	15.58892	0.196188	6.521966	0.320833	2.243398	0.069998	0.957027	52.523	0.027182	0.04997	0.412796	0.676767	16.84575	1.409445	0.093166	0.463739	0.107598	0.029602	100
-0.01003	1.424847	15.1195	0.371231	6.53752	0.244477	2.320471	0.075213	0.657059	54.01801	0.040512	0.108392	0.285284	0.753503	15.77924	1.50636	0.086873	0.498961	0.15037	0.032207	100
0.011614	1.407019	15.94016	0.226067	6.580927	0.282233	2.50515	0.063161	0.896755	54.21413	0.043634	0.071561	0.266399	0.674349	14.24155	1.424897	0.525827	0.484329	0.109638	0.030613	100
-2.3E-06	1.482775	15.37232	0.218354	6.109004	0.223706	2.489213	0.070915	0.742526	55.43968	0.048096	0.156682	0.420489	0.751632	14.15881	1.35606	0.265402	0.497656	0.163594	0.033087	100
4.07E-06	1.451272	14.97288	0.389983	5.866551	0.273157	2.428917	0.061679	1.028307	57.86876	0.06581	0.182056	0.175972	0.64084	12.07732	1.250867	0.566176	0.541416	0.133558	0.02447	100
5.63E-07	1.104466	12.75228	0.180015	5.490756	0.198988	2.479237	0.076635	0.84968	62.87714	0.053342	0.108809	0.154223	0.681808	10.97135	1.212318	0.067872	0.559375	0.143022	0.038684	100
-2.5E-06	1.748851	17.91412	0.166675	6.946165	0.391295	2.441296	0.068753	1.317226	51.71833	0.028004	0.143984	0.140448	0.58781	14.44287	1.24571	0.06235	0.459023	0.152655	0.024437	100
0.008087	1.532565	16.83684	0.411656	6.337768	0.323793	2.443145	0.069827	1.221623	55.13108	0.035945	0.121806	0.151479	0.611617	12.77653	1.261321	0.060119	0.44404	0.192696	0.028057	100
1.67E-06	1.416131	15.48638	0.644031	5.567881	0.259978	2.526844	0.073912	1.017364	59.087	0.040718	0.14227	0.170168	0.606438	11.0453	1.206541	0.041962	0.478595	0.156879	0.031602	100
0.009742	1.182351	12.71507	0.026404	4.989848	0.169101	2.368922	0.059413	0.690842	63.77621	0.051047	0.063194	0.165366	0.724774	10.79663	1.333953	0.136794	0.531251	0.176691	0.0324	100
0.006948	1.417381	15.34342	0.080711	5.74741	0.337495	2.375248	0.067964	1.123537	58.76712	0.036083	0.086097	0.137826	0.562175	12.11828	1.054778	0.059466	0.5175	0.136423	0.024138	100
-4.5E-06	1.096043	11.94342	0.073106	4.263788	0.236808	2.251773	0.069985	0.879703	67.49474	0.053348	0.042938	0.149197	0.52853	9.071589	1.036656	0.061273	0.577278	0.14113	0.0287	100
0.005283	1.048439	11.76753	0.17155	4.089283	0.178079	2.259378	0.068761	0.686276	68.36374	0.065802	0.040568	0.160118	0.623171	8.311312	1.275716	0.137863	0.569548	0.140449	0.037131	100
-8.6E-07	1.54592	15.10632	0.161737	5.627618	0.459769	2.236904	0.052188	1.526922	56.72527	0.025637	0.046673	0.164675	0.540235	13.80312	1.205779	0.157368	0.439943	0.142228	0.031697	100
-3.6E-06	1.242781	13.84046	0.179013	4.948689	0.261537	2.466092	0.077234	1.039526	64.33678	0.057451	0.045534	0.198766	0.581752	8.778995	1.154168	0.085842	0.54389	0.124103	0.037389	100
3.34E-06	1.174306	13.25814	0.607977	4.552534	0.247161	2.286979	0.055868	0.847468	64.70155	0.046569	0.049944	0.163026	0.554713	9.504144	1.1652	0.112362	0.504139	0.138567	0.029348	100
-0.01232	1.761592	16.31716	0.931132	5.876265	0.413256	2.098764	0.057135	1.166033	55.86776	0.035919	0.048108	0.158585	0.48727	12.82484	1.260926	0.085387	0.443151	0.155159	0.023876	100
-0.00776	1.221697	12.75231	0.528847	4.782223	0.225582	2.305941	0.070916	0.741987	66.13341	0.060766	0.045318	0.16455	0.541066	8.242058	1.061575	0.437253	0.548306	0.114118	0.029837	100
3.71E-07	1.199319	13.82308	0.303916	5.461104	0.249069	2.265246	0.0679	0.537291	62.25756	0.0529	0.066817	0.168947	0.623871	11.03437	1.10028	0.078682	0.559948	0.123367	0.026336	100
-0.01569	1.523543	15.17544	0.636691	5.576811	0.351042	2.131652	0.045465	0.931277	59.45777	0.040651	0.038315	0.386152	0.550814	11.28251	1.099532	0.114399	0.523533	0.126554	0.023544	100
-0.01515	1.685407	17.05918	0.374265	6.172309	0.387427	2.249817	0.048094	0.927299	55.85949	0.026172	0.040184	0.15816	0.572725	12.59217	1.131044	0.109894	0.440059	0.164156	0.017288	100
-4.6E-06	1.248501	14.50741	0.437097	5.583557	0.289067	2.279225	0.056037	0.870682	60.98015	0.053269	0.048305	1.490526	0.583427	9.747865	1.124012	0.063654	0.500203	0.109592	0.027423	100
0.019158	1.275681	13.79277	0.556692	5.314768	0.249094	2.18789	0.062212	0.71645	62.78505	0.05007	0.048186	0.180068	0.60515	10.25602	1.129181	0.063221	0.540056	0.142382	0.025909	100
-1.7E-06	1.525677	15.70373	0.780722	6.119099	0.352845	2.303324	0.059446	1.035839	58.44582	0.037543	0.078799	0.159356	0.551835	10.61822	1.162175	0.49131	0.455383	0.085271	0.033615	100
-3.4E-06	1.511615	14.89827	1.488055	5.514911	0.334343	2.005468	0.043277	0.943315	59.9798	0.030035	0.03948	0.189622	0.473162	10.57227	1.036481	0.273704	0.507597	0.128197	0.030402	100
1.99E-06	1.39743	15.01624	0.635915	5.534499	0.299491	2.148045	0.062598	0.836459	60.15688	0.044469	0.051509	0.176291	0.5626	11.14095	1.139661	0.136703	0.490084	0.136515	0.033655	100
-0.00842	1.508104	14.85127	0.256187	5.755143	0.28206	2.208634	0.075229	0.739302	60.29337	0.043313	0.035664	0.215387	0.628077	11.22353	1.157181	0.075273	0.489106	0.140888	0.030691	100
-0.0076	1.434116	15.27639	0.126208	5.758379	0.278805	2.29007	0.059559	0.735369	60.29633	0.044612	0.049332	0.203992	0.606308	10.92095	1.169624	0.068275	0.526351	0.133373	0.029564	100
-0.01066	1.45826	15.21266	0.105305	5.86182	0.332935	2.291948	0.064995	0.817984	59.91381	0.049765	0.056326	0.170126	0.556468	11.26104	1.045925	0.184725	0.481226	0.123614	0.021719	100
-0.01058	1.383389	15.53648	0.109589	6.049321	0.376834	2.251016	0.047389	0.983357	59.15954	0.047192	0.059772	0.242411	0.527222	11.45567	1.030568	0.158987	0.458691	0.108292	0.024861	100
4.47E-06	1.595338	15.75085	0.530287	5.927876	0.399044	2.178634	0.051653	0.989776	56.59382	0.031261	0.039284	0.153843	0.5533	12.94359	1.12244	0.536851	0.449098	0.123755	0.029301	100
-0.01769	1.501847	15.49466	0.552147	5.569133	0.329227	2.259796	0.056613	0.778492	59.242	0.030203	0.030443	0.181318	0.529734	11.62014	1.10825	0.101594	0.472198	0.131515	0.028373	100
-1.8E-06	1.289828	13.94562	0.708047	5.33878	0.260119	2.246163	0.072061	0.540483	61.65258	0.04805	0.055032	0.182468	0.573822	11.04724	1.122535	0.226158	0.515246	0.14308	0.032687	100
-9.8E-07	1.172913	11.42853	0.414111	4.534041	0.232996	2.048201	0.068215	0.73333	65.63392	0.059298	0.058893	0.179204	0.633715	10.79729	1.250372	0.074588	0.530589	0.122972	0.026834	100
-0.01008	1.387447	15.42571	0.447205	6.527207	0.286807	2.478743	0.078568	0.73	55.47185	0.051817	0.070852	0.219368	0.696203	13.98515	1.388094	0.076448	0.510096	0.151456	0.027052	100
-0.01678	1.246112	14.11307	0.286512	5.595556	0.261373	2.272083	0.065243	0.728179	58.91466	0.051719	0.05765	0.175271	0.7054	13.31105	1.375294	0.146618	0.535621	0.14135	0.034026	100
4.99E-06	1.54581	16.38914	0.246704	6.876962	0.403012	2.345859	0.060046	1.045075	51.96466	0.033611	0.166873	0.18643	0.629155	16.15231	1.254479	0.105941	0.437208	0.132617	0.024099	100
3.54E-06	1.772612	18.42753	0.115869	6.950386	0.390861	2.328495	0.059047	1.135403	50.45079	0.027685	0.061226	0.162605	0.591773	15.50782	1.224542	0.17518	0.446298	0.144192	0.027685	100
-0.00625	1.473475	15.85574	0.190699	6.135969	0.307389	2.401917	0.084393	1.022565	56.55945	0.06285	0.038081	0.17681	0.640355	12.93809	1.237221	0.21035	0.517767	0.124714	0.028416	100
5.8E-06	1.510014	17.75814	0.152797	6.812896	0.354742	2.355623	0.051259	1.095101	51.1141	0.03112	0.195113	0.168952	0.664851	15.79801	1.270377	0.064825	0.405778	0.168627	0.027654	100
6.58E-07	1.069994	11.88785	0.080403	4.891446	0.203917	2.176664	0.069841	0.787399	63.95864	0.058853	0.049986	0.191687	0.757711	11.65133	1.368554	0.079946	0.540251	0.142895	0.032629	100
-1.3E-06	1.456414	15.78943	0.282028	5.738679	0.338627	2.273624	0.038856	1.023197	55.85878	0.030029	0.04011	0.156145	0.604415	12.63207	1.200784	1.943105	0.428988	0.137211	0.027511	100
-0.00527	1.045346	11.85149	0.088924	4.642903	0.222198	2.341874	0.076453	0.650333	66.16208	0.056857	0.056224	0.187054	0.678283	9.745967	1.356085	0.078284	0.588925	0.147706	0.028285	100
-0.01325	1.049668	13.11464	0.077785	5.174947	0.245918	2.428637	0.079942	0.711259	64.31713	0.061253	0.054072	0.177049	0.645628	9.92334	1.15055	0.052385	0.533024	0.187522	0.028489	100
-0.00965	0.964281	10.3806	0.033216	4.234169	0.16436	2.265403	0.066095	0.593004	69.39631	0.058896	0.058213	0.201368	0.733774	8.794088	1.207322	0.1338	0.566353	0.122665	0.035728	100
0.006218	0.840095	10.1253	2.350172	3.939753	0.117972	1.57754	-0.15704	0.434027	56.56251	0.05066	0.150237	0.155685	0.54373	10.07526	0.964478	11.0269	0.516836	0.692961	0.026696	100
-2.4E-06	1.181649	15.04872	0.087831	5.916423	0.249772	2.199043	0.07779	0.776553	57.88694	0.051449	0.072801	0.147204	0.790375	13.32793	1.405276	0.110168	0.469309	0.168863	0.031897	100
0.008733	1.449533	15.38362	0.95198	5.590046	0.247584	2.095723	-0.02738	0.829242	54.18774	0.044804	0.068818	0.150567	0.646727	12.06422	1.1133	4.482954	0.452076	0.232162	0.027549	100
-4.8E-06	1.359951	16.94538	0.134695	6.304357	0.284466	2.387725	0.059848	1.005161	55.83551	0.03873	0.054293	0.174665	0.76591	12.39385	1.261723	0.398089	0.42613	0.135056	0.034471	100
1.81E-06	1.41518	18.83103	0.242176	6.267314	0.313372	2.259362	0.04657	1.011309	52.97281	0.036857	0.064409	0.187153	0.68884	13.19266	1.190222	0.58384	0.498463	0.171917	0.026513	100
-3.9E-06	1.37956	20.32751	0.134777	6.446259	0.388592	2.244187	0.047616	1.198195	50.25926	0.023986	0.04556	0.159267	0.630332	14.0775	1.169293	0.907187	0.430541	0.101245	0.02914	100
-6.6E-07	1.3758	18.33421	0.182231	6.31433	0.339227	2.246488	0.057643	1.026862	53.07757	0.036905	0.050867	0.168959	0.694063	13.61162	1.174467	0.726936	0.4166	0.141518	0.023706	100
-5.2E-06	1.401498	19.53429	0.192699	6.305456	0.347856	2.248444	0.057832	0.994042	51.20522	0.024827	0.048539	0.218265	0.677358	14.18945	1.256656	0.688096	0.448829	0.131134	0.029514	100
0.014517	1.21476	16.03818	0.221527	6.246487	0.241423	2.325013	0.067254	0.733731	55.58503	0.033361	0.064351	0.262774	0.829464	13.70795	1.445385	0.29178	0.48673	0.154828	0.035465	100
4.19E-06	1.307894	15.45246	0.335142	5.939466	0.311331	2.2488	0.061235	0.965422	56.12429	0.045668	0.095275	0.208413	0.732274	13.69077	1.331418	0.47646	0.534382	0.112961	0.026331	100
0.017587	1.492482	17.58893	0.320231	6.473857	0.371915	2.262808	0.062441	1.051252	53.68279	0.052945	0.059503	0.226053	0.689353	13.35876	1.129721	0.552632	0.464999	0.115105	0.026642	100
-3.9E-06	1.587907	20.66169	0.390538	6.262689	0.379174	2.193692	0.049702	0.908813	49.10938	0.024955	0.120371	0.283707	0.619479	14.70011	1.298603	0.840436	0.424688	0.125951	0.018123	100
-2.6E-06	1.404148	17.37898	0.412197	6.413807	0.395895	2.145833	0.047514	1.111698	53.07378	0.037846	0.045327	0.199448	0.647734	13.947	1.190766	1.020756	0.412401	0.09102	0.023848	100
4.35E-06	1.613059	18.79345	0.355849	6.376498	0.376137	2.230788	0.050647	0.970504	51.09219	0.034971	0.058071	0.152678	0.617942	14.52208	1.161993	0.976311	0.453132	0.127634	0.036065	100
-4.3E-08	1.40949	15.86382	0.247787	5.872951	0.321879	2.175784	0.042386	0.891132	56.74753	0.03831	0.072789	0.161211	0.689696	12.8839	1.17367	0.822345	0.459239	0.092963	0.033118	100
1.61E-06	1.444841	17.76531	0.364052	6.555907	0.329404	2.270548	0.06208	0.748962	52.06291	0.037651	0.116105	0.306889	0.660985	14.51659	1.143403	1.042115	0.450181	0.091707	0.030351	100
-0.01897	1.551461	16.6683	0.283893	6.068692	0.341445	2.139059	0.048237	0.893253	53.35611	0.022615	0.05766	0.170979	0.649056	14.51403	1.31226	1.352018	0.459805	0.104239	0.025874	100
-4E-06	1.19672	14.70579	0.223997	5.683722	0.186903	2.317673	0.065534	0.50003	58.58307	0.066805	0.082675	0.26528	0.79748	12.67262	1.47867	0.503328	0.533971	0.103105	0.032633	100
2.31E-06	1.256165	14.60603	0.380518	5.905925	0.231918	2.18733	0.053449	0.611229	55.83872	0.047091	0.082716	0.214339	0.777638	15.20229	1.478277	0.451058	0.519679	0.118769	0.036851	100
-0.01186	1.187562	13.30611	0.327914	5.097218	0.192286	2.192486	0.068814	0.554654	61.52492	0.053164	0.04844	0.177458	0.778875	12.02297	1.359076	0.392215	0.572378	0.124357	0.030958	100
-0.00961	1.165561	13.18241	0.226946	5.587966	0.179958	2.325701	0.068663	0.476898	60.63291	0.063339	0.066631	0.20844	0.762494	12.56897	1.484962	0.293514	0.540632	0.132427	0.041179	100
-3.3E-06	1.392489	19.17471	0.790681	6.132156	0.372198	1.971862	-0.01104	0.892996	46.324	0.017284	0.03774	0.143251	0.559184	15.08215	1.24319	5.309033	0.366935	0.181404	0.019781	100
-0.00747	1.487872	19.60285	0.61588	6.392666	0.337329	2.05607	0.020354	0.776369	48.19186	0.023229	0.06672	0.163512	0.594854	15.57742	1.273766	2.270683	0.414131	0.113392	0.02851	100
0.01115	1.262308	16.42398	0.323028	5.936319	0.257543	2.378497	0.072382	0.659066	55.92102	0.064369	0.095136	0.215795	0.711484	13.47274	1.242663	0.321117	0.47949	0.124435	0.027472	100
-0.00997	1.161322	12.92371	0.64447	5.130955	0.172868	2.313987	0.079242	0.431833	59.37058	0.100046	0.072961	0.233233	0.782583	14.07121	1.490036	0.320745	0.569477	0.10355	0.037163	100
-2.6E-06	1.179609	14.26764	0.851607	5.269072	0.203949	2.187746	0.063757	0.563899	57.95109	0.052085	0.076888	0.191634	0.750554	14.07326	1.315812	0.333011	0.518503	0.124455	0.025429	100
-0.00707	1.297671	15.81866	0.355795	5.816079	0.287588	2.188809	0.054159	0.724866	53.77011	0.04199	0.05841	0.165553	0.680845	16.22736	1.498009	0.4281	0.468159	0.089428	0.035478	100
0.004396	1.221724	14.04881	0.427505	5.08402	0.213726	2.261688	0.070488	0.607777	59.96385	0.075951	0.046075	0.141881	0.734882	12.65564	1.424929	0.350258	0.545335	0.089554	0.031513	100
0.007641	1.20333	16.68391	0.657462	5.855566	0.320145	2.216587	0.038093	0.842016	53.5206	0.042866	0.467595	0.506758	0.629737	14.66953	1.244503	0.499493	0.483559	0.087178	0.023429	100
0.009275	1.135386	12.95718	0.576511	4.29896	0.15885	2.267063	0.027196	0.535133	62.63769	0.059866	0.060529	0.216294	0.64663	10.15478	1.232189	2.315219	0.5079	0.172283	0.031063	100

TABLE S2 δ13c AND δ18O VALUES, AND ELEMENTAL COMPOSITION DATA (XRF ANALYSES) OF HOLE 1258A (REDOX CONDITIONS)

Cu/Al	Cu/Al (10*-2)	Depth (mbsf)	Zn/Al	Zn/Al (10*-1)	Depth (mbsf)	V/Al	V/Al (10*-1)	Depth (mbsf)	V/Cr	Age (Ma)
0.017121	1.71	257.5	0.080113	0.8	257.5	0.086207	0.86	257.5	3.823661	66.2
0.017032	1.7	257.88	0.092835	0.93	257.88	0.111514	1.12	257.88	3.148969	66.21
0.034412	3.44	258.13	0.109503	1.1	258.13	0.109612	1.1	258.13	2.457168	66.22
0.053234	5.32	258.51	0.12658	1.26	258.51	0.136457	1.36	258.51	3.135114	66.23
0.092605	9.26	258.93	0.098091	0.98	258.93	0.081459	0.81	258.93	3.21823	66.25
0.027856	2.78	259.31	0.180813	1.81	259.31	0.095016	0.95	259.31	3.250157	66.26
0.055343	5.53	259.61	0.091855	0.92	259.61	0.077094	0.77	259.61	4.827046	66.27
0.020446	2.04	260.01	0.074295	0.74	260.01	0.084045	0.84	260.01	4.91621	66.28
0.030306	3.03	260.41	0.090702	0.9	260.41	0.092315	0.92	260.41	4.873608	66.3
0.029617	2.96	260.81	0.091075	0.91	260.81	0.090639	0.91	260.81	4.07691	66.31
0.021446	2.14	261.03	0.066581	0.66	261.03	0.072057	0.72	261.03	6.193988	66.32
0.030895	3.09	261.38	0.0745	0.74	261.38	0.065113	0.65	261.38	3.402353	66.33
0.027945	2.79	261.83	0.067866	0.68	261.83	0.072021	0.72	261.83	3.209342	66.35
0.031686	3.17	261.23	0.096488	0.96	261.23	0.084853	0.85	261.23	3.30094	66.36
0.036664	3.67	262.7	0.074411	0.74	262.7	0.091341	0.91	262.7	5.167725	66.38
0.021693	2.17	263.1	0.198567	1.98	263.1	0.066891	0.67	263.1	4.260173	66.41
0.028682	2.87	263.5	0.134878	1.35	263.5	0.085914	0.86	263.5	4.754972	66.45
0.027045	2.7	264.82	0.097696	0.98	264.82	0.049153	0.49	264.82	1.537165	66.57
0.026595	2.66	265.23	0.069666	0.7	265.23	0.100685	1.01	265.23	5.895139	66.61
0.035683	3.57	265.63	0.095032	0.95	265.63	0.076869	0.77	265.63	3.068617	66.65
0.087792	8.78	266.04	0.063834	0.64	266.04	0.093526	0.94	266.04	3.655385	66.69
0.034018	3.4	266.28	0.103054	1.03	266.28	0.072452	0.72	266.28	2.248381	66.71
0.033955	3.39	266.69	0.079474	0.79	266.69	0.104864	1.05	266.69	5.098914	66.75
0.024428	2.44	267.14	0.244256	2.44	267.14	0.082133	0.82	267.14	4.874338	66.79
0.042511	4.25	267.53	0.068441	0.68	267.53	0.083161	0.83	267.53	3.699717	66.83
0.028957	2.9	267.8	0.069308	0.69	267.8	0.074286	0.74	267.8	2.725056	66.85
0.044239	4.42	268.18	0.178485	1.78	268.18	0.046507	0.46	268.18	2.200251	66.89
0.025366	2.54	268.58	0.186591	1.86	268.58	0.060638	0.61	268.58	7.368712	66.92
0.030802	3.08	269	0.108584	1.08	269	0.087241	0.87	269	3.514585	66.96
0.040991	4.1	269.15	0.092477	0.93	269.15	0.076596	0.76	269.15	2.196795	66.98
0.035184	3.52	269.53	0.468377	4.68	269.53	0.077421	0.77	269.53	3.303671	67.02
0.042238	4.22	269.95	0.134489	1.34	269.95	0.081376	0.81	269.95	2.529843	67.06
0.019886	1.99	270.35	0.066497	0.66	270.35	0.075268	0.75	270.35	3.33208	67.09
0.035769	3.58	270.63	0.092555	0.92	270.63	0.070462	0.7	270.63	1.793625	67.12
0.028057	2.8	271.05	0.110451	1.1	271.05	0.07261	0.73	271.05	3.650896	67.16
0.032097	3.21	271.45	0.094831	0.95	271.45	0.103214	1.03	271.45	3.023899	67.2
0.032315	3.23	271.85	0.175816	1.76	271.85	0.098838	0.99	271.85	3.503942	67.23
0.032078	3.21	272.12	0.112345	1.12	272.12	0.072951	0.73	272.12	2.272914	67.26
0.034919	3.49	272.52	0.173845	1.74	272.52	0.085422	0.85	272.52	2.908082	67.28
0.03781	3.78	272.97	0.072766	0.73	272.97	0.057607	0.58	272.97	1.372617	67.3
0.03079	3.08	273.32	0.119184	1.19	273.32	0.084158	0.84	273.32	3.322362	67.37
0.02881	2.88	273.55	0.094922	0.95	273.55	0.084183	0.84	273.55	2.959199	67.4
0.05624	5.62	273.92	0.088245	0.88	273.92	0.086532	0.86	273.92	2.071631	67.43
0.040576	4.06	274.37	0.098094	0.98	274.37	0.087854	0.88	274.37	3.128642	67.47
0.04127	4.13	274.39	0.10089	1.01	274.39	0.082824	0.83	274.39	2.267903	67.47
0.034188	3.42	274.4	0.088695	0.89	274.4	0.069223	0.69	274.4	1.714966	67.48
0.044086	4.41	274.8	0.098524	0.98	274.8	0.076817	0.77	274.8	2.629073	67.51
0.025407	2.54	275.28	0.082531	0.82	275.28	0.069426	0.69	275.28	3.150442	67.56
0.027312	2.73	275.63	0.086708	0.87	275.63	0.05667	0.57	275.63	2.409422	67.59
0.107745	1.08	275.8	0.13426	1.34	275.8	0.071492	0.71	275.8	1.888997	67.61
0.038321	3.83	276.25	0.145528	1.46	276.25	0.098708	0.99	276.25	3.892303	67.65
0.025868	2.59	276.65	0.08703	0.87	276.65	0.082886	0.83	276.65	2.425752	67.68
0.029607	2.96	277.05	0.088061	0.88	277.05	0.066024	0.66	277.05	2.227479	67.72
0.028832	2.88	277.4	0.116714	1.17	277.4	0.072694	0.73	277.4	2.037702	67.76
0.04241	4.24	277.83	0.119624	1.2	277.83	0.09321	0.93	277.83	2.488624	67.8
0.027355	2.73	278.23	0.069516	0.7	278.23	0.078918	0.79	278.23	2.695502	67.84
0.027453	2.74	278.63	0.067039	0.67	278.63	0.081094	0.81	278.63	2.625062	67.87
0.03834	3.83	278.8	0.104936	1.05	278.8	0.101353	1.01	278.8	2.371751	67.89
0.037764	3.78	279.11	0.068858	0.69	279.11	0.060875	0.61	279.11	3.496604	67.92
0.031842	3.18	284.13	0.120534	1.2	284.13	0.054376	0.54	284.13	1.7271	68.39
0.028006	2.8	284.55	0.079068	0.79	284.55	0.091358	0.91	284.55	3.087741	68.43
0.02121	2.12	284.95	0.133119	1.33	284.95	0.083056	0.83	284.95	3.271845	68.46
0.038619	3.86	285.35	0.094038	0.94	285.35	0.09018	0.9	285.35	2.038861	68.5
0.032224	3.22	285.63	0.089371	0.89	285.63	0.077999	0.78	285.63	2.037803	68.53
0.046591	4.66	286.03	0.10732	1.07	286.03	0.085526	0.86	286.03	1.530245	68.57
0.04189	4.19	286.43	0.128195	1.28	286.43	0.101649	1.02	286.43	1.800997	68.6
0.051321	5.13	286.83	0.145938	1.46	286.83	0.100826	1.01	286.83	1.754342	68.64
0.0394	3.94	287.08	0.094408	0.94	287.08	0.094833	0.95	287.08	2.771951	68.66
0.039667	3.97	287.53	0.124691	1.25	287.53	0.093103	0.93	287.53	2.224985	68.71
0.043376	4.34	287.93	0.109333	1.09	287.93	0.10971	1.1	287.93	2.668247	68.74
0.034735	3.47	288.33	0.088664	0.89	288.33	0.052891	0.53	288.33	1.906366	68.78
0.030982	3.1	288.63	0.106303	1.06	288.63	0.072618	0.73	288.63	2.41445	68.81
0.029964	3	289.03	0.098523	0.98	289.03	0.065179	0.65	289.03	1.838192	68.85
0.036276	3.63	289.43	0.114176	1.14	289.43	0.085452	0.85	289.43	1.811389	68.88
0.048429	4.84	289.83	0.162753	1.63	289.83	0.097414	0.97	289.83	2.014257	68.92
0.02003	2	290.12	0.084348	0.84	290.12	0.07413	0.74	290.12	2.032138	68.95
0.02946	2.95	290.53	0.187962	1.88	290.53	0.091627	0.92	290.53	3.001341	68.99
0.034164	3.42	290.93	0.282225	2.82	290.93	0.073564	0.74	290.93	1.537167	69.02
0.076073	7.61	291.33	0.200221	2	291.33	0.105534	1.06	291.33	1.999258	69.06
0.05086	5.09	291.62	0.189335	1.89	291.62	0.077922	0.78	291.62	1.735861	69.09
0.105668	10.7	292.04	0.283582	2.84	292.04	0.11033	1.1	292.04	2.30692	69.13
0.125446	12.5	292.43	0.121253	1.21	292.43	0.092028	0.92	292.43	2.165387	69.16
0.098517	9.85	292.83	0.139636	1.4	292.83	0.129494	1.29	292.83	1.86627	69.2
0.082331	8.23	293.2	0.080309	0.8	293.2	0.087288	0.87	293.2	2.220321	69.24
0.079478	7.95	293.48	0.09884	0.99	293.48	0.125734	1.26	293.48	2.759612	69.27
0.100464	10	293.68	0.120164	1.2	293.68	0.11078	1.11	293.68	2.12252	69.28
0.053448	5.34	293.76	0.139862	1.4	293.76	0.14944	1.49	293.76	2.973954	69.28
0.060744	6.07	294.15	0.09724	0.97	294.15	0.09625	0.96	294.15	2.007283	69.3
0.039175	3.92	294.56	0.136123	1.36	294.56	0.128763	1.29	294.56	2.01656	69.33
0.038694	3.87	294.93	0.152721	1.53	294.93	0.13396	1.34	294.93	2.042557	69.35
0.030191	3.02	295.25	0.106522	1.06	295.25	0.092002	0.92	295.25	2.725313	69.37
0.036639	3.67	295.65	0.159937	1.6	295.65	0.099859	0.99	295.65	1.60685	69.4
0.042531	4.25	296.05	0.138828	1.39	296.05	0.117999	1.18	296.05	2.480244	69.42
0.027309	2.73	296.45	0.090024	0.9	296.45	0.088079	0.88	296.45	2.715649	69.44
0.037095	3.71	296.72	0.13469	1.35	296.72	0.093409	0.93	296.72	1.609188	69.46
0.055712	5.57	297.15	0.140869	1.41	297.15	0.102864	1.03	297.15	1.816884	69.48
0.025149	2.51	297.55	0.253457	2.53	297.55	0.083065	0.83	297.55	2.783563	69.51
0.023842	2.38	297.95	0.093841	0.94	297.95	0.097399	0.97	297.95	3.413255	69.53
0.03869	3.87	298.23	1.193852	11.9	298.23	0.087779	0.88	298.23	1.955707	69.55
0.037773	3.78	298.65	0.141154	1.41	298.65	0.111612	1.12	298.65	2.288645	69.58
0.051648	5.16	299.05	0.104449	1.04	299.05	0.055891	0.56	299.05	1.43443	69.6
0.026118	2.61	299.45	0.125443	1.25	299.45	0.084808	0.84	299.45	2.962216	69.62
0.03686	3.69	299.66	0.126153	1.26	299.66	0.09769	0.98	299.66	2.180831	69.63
0.023648	2.36	300.05	0.14282	1.43	300.05	0.093421	0.93	300.05	1.872781	69.65
0.034399	3.44	300.45	0.142243	1.42	300.45	0.093	0.93	300.45	2.239365	69.68
0.038626	3.86	300.85	0.116663	1.17	300.85	0.084768	0.85	300.85	1.901912	69.7
0.043207	4.32	301.2	0.17523	1.75	301.2	0.07828	0.78	301.2	2.285178	69.72
0.024624	2.46	301.65	0.096433	0.96	301.65	0.077573	0.78	301.65	2.395905	69.75
0.020271	2.03	302.01	0.12073	1.21	302.01	0.087569	0.88	302.01	2.323045	69.77
0.042666	4.27	303.3	0.141467	1.41	303.3	0.11093	1.11	303.3	1.98554	69.85
0.050211	5.02	303.7	0.152785	1.53	303.7	0.104843	1.05	303.7	1.802706	69.87
0.051067	5.11	304.18	0.158109	1.58	304.18	0.109162	1.09	304.18	1.927714	69.9
0.046264	4.63	304.5	0.140654	1.41	304.5	0.113433	1.13	304.5	2.16652	69.92
0.107952	1.08	304.78	0.120604	1.21	304.78	0.085791	0.86	304.78	2.208582	69.94
0.03454	3.45	305.18	0.091732	0.92	305.18	0.081344	0.81	305.18	2.441976	69.96
0.025844	2.58	305.58	0.119995	1.2	305.58	0.08464	0.85	305.58	1.477781	69.98
0.129213	12.9	306	0.111888	1.12	306	0.111673	1.12	306	3.289679	70.01
0.046716	4.67	306.3	0.179148	1.79	306.3	0.133548	1.34	306.3	2.046009	70.03
0.02754	2.75	306.7	0.107212	1.07	306.7	0.094212	0.94	306.7	3.531294	70.05
0.053785	5.38	307.1	0.17894	1.79	307.1	0.141299	1.41	307.1	1.931988	70.07
0.051514	5.15	307.5	0.168671	1.69	307.5	0.178649	1.79	307.5	2.345739	70.08
0.06037	6.04	307.75	0.208828	2.09	307.75	0.127209	1.27	307.75	1.855878	70.11
0.178834	17.9	308.15	0.185318	1.85	308.15	0.82486	8.25	308.15	-4.41273	70.13
0.06161	6.16	308.65	0.124575	1.24	308.65	0.142905	1.43	308.65	2.170759	70.16
0.047476	4.75	309.05	0.103873	1.04	309.05	0.160163	1.6	309.05	-8.48053	70.19
0.039923	3.99	309.35	0.128435	1.28	309.35	0.09931	0.99	309.35	2.256645	70.21
0.045513	4.55	309.73	0.132246	1.32	309.73	0.12148	1.21	309.73	3.691591	70.23
0.033025	3.3	310.12	0.115447	1.15	310.12	0.07339	0.73	310.12	2.126303	70.25
0.036973	3.7	310.55	0.122808	1.23	310.55	0.102862	1.03	310.55	2.455067	70.27
0.034633	3.36	310.83	0.155737	1.56	310.83	0.093567	0.94	310.83	2.267513	70.29
0.052974	5.3	311.23	0.216318	2.16	311.23	0.127456	1.27	311.23	2.30213	70.32
0.072846	7.28	311.63	0.15935	1.59	311.63	0.086369	0.86	311.63	1.844716	70.34
0.039869	3.99	312.02	0.151461	1.51	312.02	0.077123	0.77	312.02	1.843424	70.36
0.075805	7.58	312.32	0.178667	1.79	312.32	0.079319	0.79	312.32	2.534098	70.38
0.032281	3.23	312.78	0.142042	1.42	312.78	0.064822	0.65	312.78	1.915656	70.41
0.036	3.6	313.03	0.094651	0.95	313.03	0.079125	0.79	313.03	2.520055	70.42
0.051642	5.16	313.42	0.114375	1.14	313.42	0.065955	0.66	313.42	2.193228	70.45
0.080358	8.04	313.83	0.212403	2.12	313.83	0.063472	0.63	313.83	1.477229	70.48
0.037165	3.72	314.24	0.110205	1.1	314.24	0.067188	0.67	314.24	2.160978	70.5
0.069085	6.91	314.55	0.221673	2.22	314.55	0.086157	0.86	314.55	1.573305	70.52
0.065848	6.58	314.8	0.17063	1.71	314.8	0.094549	0.94	314.8	2.222117	70.53
0.040789	4.08	315.22	0.14943	1.49	315.22	0.104717	1.05	315.22	1.807159	70.55
0.057166	5.72	315.73	0.178832	1.79	315.73	0.113616	1.14	315.73	1.928653	70.58
0.027102	2.71	316.02	0.102874	1.03	316.02	0.130273	1.3	316.02	-16.427	70.6
0.044843	4.48	316.43	0.109896	1.1	316.43	0.076211	0.76	316.43	5.570893	70.63
0.075367	7.54	316.81	0.170952	1.71	316.81	0.098577	0.98	316.81	1.719152	70.65
0.062826	6.28	317.21	0.200834	2.01	317.21	0.089166	0.89	317.21	1.30676	70.67
0.065181	6.52	317.38	0.162456	1.62	317.38	0.105505	1.06	317.38	1.952027	70.67
0.045011	4.5	317.71	0.127577	1.28	317.71	0.068914	0.69	317.71	1.651197	70.7
0.037713	3.77	318.08	0.116131	1.16	318.08	0.073301	0.73	318.08	1.270478	70.72
0.388584	3.88	318.47	0.421129	4.21	318.47	0.072447	0.72	318.47	2.288536	70.75
0.053312	5.33	320.11	0.190503	1.9	320.11	0.15174	1.51	320.11	6.334859	70.84
		Outliers			Outliers			Outliers		

TABLE S2 δ13c AND δ18O VALUES, AND ELEMENTAL COMPOSITION DATA (XRF ANALYSES) OF HOLE 1258A (SOURCE AND WEATHERING)																	
Ident	Depth (mbsf)	Si NMS	K NMS	Al NMS	Fe NMS	Ca NMS	Ti NMS	Si/Ti (10*-5)	Si/Ti	Si/Al	K/Al	log(Fe/Ca)		K/Fe	Fe/K		Age (Ma)
DEM28R2-110-112	257.5	16.47944	5.861417	1.682629	54.3179	0.428325	1.981829	5.06	5.06E-05	9.79	3.48	2.10	0.11	0.108	9.27	0.007886	66.2
DEM28R2-148-150	257.88	15.10047	4.915247	1.58387	59.45473	0.312527	2.015123	3.64	3.64E-05	9.53	3.10	2.28	0.08	0.083	12.10	0.005257	66.21
DEM28R3-23-25NEW	258.13	12.74293	4.44864	1.321121	63.76904	0.237459	1.859644	2.9	2.9E-05	9.65	3.37	2.43	0.07	0.070	14.33	0.003724	66.22
DEM28R3-61-63	258.51	11.51261	3.60966	1.206255	66.61154	0.271892	1.766189	3.3	3.3E-05	9.54	2.99	2.39	0.05	0.054	18.45	0.004082	66.23
DEM28R3-103-105	258.93	14.65383	4.890717	1.527045	57.3045	0.364494	2.052732	4.1	4.1E-05	9.60	3.20	2.20	0.09	0.085	11.72	0.006361	66.25
DEM28R3-141-143	259.31	15.35023	4.997382	1.827255	56.1077	0.379431	2.119041	4.06	4.06E-05	8.40	2.73	2.17	0.09	0.089	11.23	0.006763	66.26
DEM28R4-21-23	259.61	16.24543	5.683401	1.71019	51.41709	0.500143	2.270337	5.67	5.67E-05	9.50	3.32	2.01	0.11	0.111	9.05	0.009727	66.27
DEM28R4-63-65NEW3	260.01	17.63784	6.027212	2.03358	47.60458	0.544765	2.106524	5.91	5.91E-05	8.67	2.96	1.94	0.13	0.127	7.90	0.011444	66.28
DEM28R4-103-105	260.41	15.38474	5.601813	1.576295	52.70293	0.504864	2.197709	5.82	5.82E-05	9.76	3.55	2.02	0.11	0.106	9.41	0.009579	66.3
DEM28R4-143-145	260.81	17.00022	5.856281	1.832716	49.99506	0.537758	2.072794	5.65	5.65E-05	9.28	3.20	1.97	0.12	0.117	8.54	0.010756	66.31
DEM28R5-13-15	261.03	16.56171	5.564863	1.921928	50.63255	0.519249	2.103469	5.46	5.46E-05	8.62	2.90	1.99	0.11	0.110	9.10	0.010255	66.32
DEM28R5-48-50	261.38	16.43085	5.573017	1.739044	52.04	0.505328	2.094937	5.58	5.58E-05	9.45	3.20	2.01	0.11	0.107	9.34	0.00971	66.33
DEM28R5-93-95	261.83	16.64039	5.464503	1.841378	52.31025	0.472078	2.157579	4.98	4.98E-05	9.04	2.97	2.04	0.10	0.104	9.57	0.009025	66.35
DEM28R5-133-135	262.23	16.81893	5.755235	1.866879	51.24997	0.467348	2.11631	5.2	5.2E-05	9.01	3.08	2.04	0.11	0.112	8.90	0.009119	66.36
DEM28R6-30-32	262.7	16.77498	5.569372	1.97217	50.4176	0.549437	2.142922	5.59	5.59E-05	8.51	2.82	1.96	0.11	0.110	9.05	0.010898	66.38
DEM28R6-70-72	263.1	16.66666	5.537488	1.939182	49.86495	0.51681	2.007688	5.62	5.62E-05	8.59	2.86	1.98	0.11	0.111	9.00	0.010364	66.41
DEM28R6-110-112	263.5	15.62837	5.281586	1.784163	52.66798	0.42387	2.156257	4.38	4.38E-05	8.76	2.96	2.09	0.10	0.100	9.97	0.008048	66.45
DEM29R1-21-24	264.82	16.04943	5.724282	1.582877	52.07299	0.475588	2.201391	5.41	5.41E-05	10.14	3.62	2.04	0.11	0.110	9.10	0.009133	66.57
DEM29R1-63-65	265.23	16.55237	5.663333	1.686589	50.2479	0.522415	2.070973	5.68	5.68E-05	9.81	3.36	1.98	0.11	0.113	8.87	0.010397	66.61
DEM29R1-103-105	265.63	15.56556	5.883422	1.629854	51.21255	0.438801	2.026184	4.88	4.88E-05	9.55	3.61	2.07	0.11	0.115	8.70	0.008568	66.65
DEM29R1-144-146	266.04	18.52297	6.409879	1.762969	48.78419	0.49134	2.258828	5.56	5.56E-05	10.51	3.64	2.00	0.13	0.131	7.61	0.010072	66.69
DEM29R2-18-20	266.28	15.64636	5.699142	1.655434	53.75753	0.341556	2.117399	3.99	3.99E-05	9.45	3.44	2.20	0.11	0.106	9.43	0.006354	66.71
DEM29R2-59-61	266.69	16.65954	6.336565	1.674123	49.33055	0.545507	2.194909	6.04	6.04E-05	9.95	3.79	1.96	0.13	0.128	7.79	0.011058	66.75
DEM29R2-104-106	267.14	17.51173	6.25031	1.783804	47.84241	0.513741	2.024477	5.98	5.98E-05	9.82	3.50	1.97	0.13	0.131	7.65	0.010738	66.79
DEM29R21-43-145	267.53	16.55479	5.901142	1.731803	49.77203	0.525021	2.065459	5.88	5.88E-05	9.56	3.41	1.98	0.12	0.119	8.43	0.010549	66.83
DEM29R3-20-22	267.8	15.80944	5.665976	1.61735	54.02112	0.452096	2.24741	5.36	5.36E-05	9.77	3.50	2.08	0.10	0.105	9.53	0.008369	66.85
DEM29R3-58-60	268.18	15.26348	5.895264	1.500149	52.87554	0.490629	2.103583	5.78	5.78E-05	10.17	3.93	2.03	0.11	0.111	8.97	0.009279	66.89
DEM29R3-98-100	268.58	17.24908	5.934927	1.737324	48.66979	0.548082	1.982487	6.26	6.26E-05	9.93	3.42	1.95	0.12	0.122	8.20	0.011261	66.92
DEM29R3-140-142	269	15.38479	5.947434	1.455182	50.97793	0.524863	2.105349	6.02	6.02E-05	10.57	4.09	1.99	0.12	0.117	8.57	0.010296	66.96
DEM29R4-5-7	269.15	15.47214	5.995923	1.50854	51.53512	0.386954	2.082779	4.78	4.78E-05	10.26	3.97	2.12	0.12	0.116	8.60	0.007509	66.98
DEM29R4-43-45	269.53	15.93921	6.037694	1.450816	52.06612	0.391465	2.209762	5.09	5.09E-05	10.99	4.16	2.12	0.12	0.116	8.62	0.007519	67.02
DEM29R4-85-87	269.95	15.73389	6.283454	1.347936	52.67388	0.385206	2.212035	5.03	5.03E-05	11.67	4.66	2.14	0.12	0.119	8.38	0.007313	67.06
DEM29R4-125-127	270.35	18.17895	6.136113	1.897731	49.16995	0.503102	2.119154	5.76	5.76E-05	9.58	3.23	1.99	0.12	0.125	8.01	0.010232	67.09
DEM29R5-21-23	270.63	14.76359	5.44061	1.496084	56.69846	0.31939	2.163159	3.57	3.57E-05	9.87	3.64	2.25	0.10	0.096	10.42	0.005633	67.12
DEM29R5-63-65	271.05	17.30531	5.86015	1.749638	51.19705	0.452404	2.112054	5.11	5.11E-05	9.89	3.35	2.05	0.11	0.114	8.74	0.008837	67.16
DEM29R5-103-105	271.45	16.3051	5.77428	1.562948	52.52559	0.380566	2.09111	4.36	4.36E-05	10.43	3.69	2.14	0.11	0.110	9.10	0.007245	67.2
DEM29R5-143-145	271.85	15.17975	5.951817	1.624214	51.81647	0.450375	2.098183	4.93	4.93E-05	9.35	3.66	2.06	0.11	0.115	8.71	0.008692	67.23
DEM29R6-20-22	272.12	15.74102	5.923934	1.609502	52.03003	0.384196	2.082193	4.45	4.45E-05	9.78	3.68	2.13	0.11	0.114	8.78	0.007384	67.26
DEM29R6-60-62	272.52	15.59266	5.900397	1.503679	53.4765	0.367876	2.22051	4.25	4.25E-05	10.37	3.92	2.16	0.11	0.110	9.06	0.006879	67.28
DEM29R6-105-107	272.97	15.85397	5.501403	1.49629	55.62816	0.414349	2.085578	4.87	4.87E-05	10.60	3.68	2.13	0.10	0.099	10.11	0.007449	67.3
DEM29R6-140-142	273.32	15.81942	6.151446	1.549029	49.36224	0.363233	2.070065	4.43	4.43E-05	10.21	3.97	2.13	0.12	0.125	8.02	0.007359	67.37
DEM29R7-13-15	273.55	17.07894	6.2963	1.586838	47.97489	0.500795	2.0206	5.79	5.79E-05	10.76	3.97	1.98	0.13	0.131	7.62	0.010439	67.4
DEM29R7-50-52	273.92	13.63736	5.230264	1.315388	55.90499	0.322808	1.965186	3.73	3.73E-05	10.37	3.98	2.24	0.09	0.094	10.69	0.005774	67.43
DEM29R-CC3-5	274.37	16.58101	6.014923	1.575031	48.91067	0.408245	1.949206	5.01	5.01E-05	10.53	3.82	2.08	0.12	0.123	8.13	0.008347	67.47
DEM29R7-93-95NEW2	274.39	17.13057	6.228787	1.659034	49.99986	0.520318	2.086582	7.44	7.44E-05	10.33	3.75	1.98	0.12	0.125	8.03	0.010406	67.47
DEM30R1-20-22	274.4	15.54642	6.134335	1.505992	52.34612	0.384142	2.142419	4.77	4.77E-05	10.32	4.07	2.13	0.12	0.117	8.53	0.007339	67.48
DEM30R1-60-62	274.8	15.57794	6.034824	1.59795	50.54873	0.427193	2.033673	4.76	4.76E-05	9.75	3.78	2.07	0.12	0.119	8.38	0.008451	67.51
DEM30R1-108-110	275.28	17.00355	6.092399	1.739068	50.84308	0.489277	2.111437	5.46	5.46E-05	9.78	3.51	2.02	0.12	0.120	8.35	0.009623	67.56
DEM30R1-143-145	275.63	16.4614	6.129805	1.686298	50.81164	0.510605	2.048881	5.66	5.66E-05	9.76	3.64	2.00	0.12	0.121	8.29	0.010049	67.59
DEM30R2-10-12	275.8	15.05747	5.87652	1.423892	54.78478	0.345472	2.229864	3.93	3.93E-05	10.57	4.13	2.20	0.11	0.107	9.32	0.006306	67.61
DEM30R2-55-57new	276.25	16.62884	6.313239	1.558183	50.26173	0.447959	2.131223	5.15	5.15E-05	10.67	4.05	2.05	0.13	0.126	7.96	0.008913	67.65
DEM30R2-95-97	276.65	15.60567	5.670177	1.55575	55.12842	0.340896	2.207502	3.8	3.8E-05	10.03	3.64	2.21	0.10	0.103	9.72	0.006184	67.68
DEM30R2-135-137	277.05	15.10428	5.698217	1.503246	53.98372	0.345442	2.100828	4.03	4.03E-05	10.05	3.79	2.19	0.11	0.106	9.47	0.006399	67.72
DEM30R3-18-22	277.4	16.47725	6.118752	1.546798	51.653	0.357406	2.139517	4.26	4.26E-05	10.65	3.96	2.16	0.12	0.118	8.44	0.006919	67.76
DEM30R3-63-65	277.83	14.26814	5.608622	1.477804	54.37272	0.363129	2.039733	4.28	4.28E-05	9.65	3.80	2.18	0.10	0.103	9.69	0.006679	67.8
DEM30R3-102-105	278.23	18.77824	6.366351	1.815163	49.68879	0.504322	2.139612	5.96	5.96E-05	10.35	3.51	1.99	0.13	0.128	7.80	0.01015	67.84
DEM30R3-143-145	278.63	16.82029	5.802749	1.686747	52.14359	0.447837	2.192011	4.95	4.95E-05	9.97	3.44	2.07	0.11	0.111	8.99	0.008589	67.87
DEM30R4-10-12	278.8	15.22075	5.718513	1.336527	54.56266	0.30441	2.105818	3.73	3.73E-05	11.39	4.28	2.25	0.10	0.105	9.54	0.005579	67.89
DEM30R4-41-43	279.11	18.32933	6.364055	1.833775	48.38023	0.564542	2.058014	6.9	6.9E-05	10.00	3.47	1.93	0.13	0.132	7.60	0.011669	67.92
DEM31R1-21-25	284.13	17.04437	5.913759	1.65523	52.02245	0.480959	2.139544	5.25	5.25E-05	10.30	3.57	2.03	0.11	0.114	8.80	0.009245	68.39
DEM31R1-65-67	284.55	15.4737	5.928557	1.530884	54.22896	0.414983	2.137369	4.45	4.45E-05	10.11	3.87	2.12	0.11	0.109	9.15	0.007652	68.43
DEM31R1-105-107	284.95	17.82223	6.649887	1.785184	49.91526	0.472053	2.195198	5.25	5.25E-05	9.98	3.73	2.02	0.13	0.133	7.51	0.009457	68.46
DEM31R1-145-147	285.35	15.47083	6.277491	1.538437	53.17618	0.382612	2.15712	4.41	4.41E-05	10.06	4.08	2.14	0.12	0.118	8.47	0.007195	68.5
DEM31R2-23-25	285.63	16.12614	5.833408	1.619981	56.57441	0.363023	2.366858	3.69	3.69E-05	9.95	3.60	2.19	0.10	0.103	9.70	0.006417	68.53
DEM31R2-63-65	286.03	12.68546	5.045364	1.326363	60.84479	0.310036	2.130189	3.68	3.68E-05	9.56	3.80	2.29	0.08	0.083	12.06	0.005096	68.57
DEM31R2-103-105	286.43	13.36485	5.185936	1.370814	60.41231	0.224771	2.248729	2.55	2.55E-05	9.75	3.78	2.43	0.09	0.086	11.65	0.003721	68.6
DEM31R2-143-145	286.83	11.6563	4.896755	1.164533	63.17777	0.181865	2.223407	2.11	2.11E-05	10.01	4.20	2.54	0.08	0.078	12.90	0.002879	68.64
DEM31R3-18-20	287.08	17.45971	6.749375	1.599654	51.32251	0.367795	2.338528	4.13	4.13E-05	10.91	4.22	2.14	0.13	0.132	7.60	0.007166	68.66
DEM31R3-63-65	287.53	14.62444	6.121025	1.437029	56.51867	0.233211	2.394785	2.72	2.72E-05	10.18	4.26	2.38	0.11	0.108	9.23	0.004126	68.71
DEM31R3-103-105	287.93	14.90878	6.032822	1.389732	57.03046	0.232483	2.360436	2.8	2.8E-05	10.73	4.34	2.39	0.11	0.106	9.45	0.004076	68.74
DEM31R3-143-145	288.33	16.45339	6.56326	1.571265	51.89967	0.453044	2.226126	5.46	5.46E-05	10.47	4.18	2.06	0.13	0.126	7.91	0.008729	68.78
DEM31R4-23-25	288.73	17.44563	6.925511	1.585686	50.79246	0.458111	2.369574	5.63	5.63E-05	11.00	4.37	2.04	0.14	0.136	7.33	0.009019	68.81
DEM31R4-63-65	289.03	17.02158	6.817968	1.534767	50.49183	0.485254	2.307013	5.85	5.85E-05	11.09	4.44	2.02	0.14	0.135	7.41	0.009611	68.85
DEM31R4-103-105	289.43	15.71207	6.130235	1.50476	54.76312	0.287823	2.391136	3.24	3.24E-05	10.44	4.07	2.28	0.11	0.112	8.93	0.005256	68.88
DEM31R4-143-145	289.83	15.21128	6.294768	1.334407	55.73221	0.296124	2.351419	3.63	3.63E-05	11.40	4.72	2.27	0.11	0.113	8.85	0.005313	68.92
DEM31R5-22-24	290.12	18.39873	6.784554	1.818827	50.95855	0.452504	2.331575	5.15	5.15E-05	10.12	3.73	2.05	0.13	0.133	7.51	0.00888	68.95
DEM31R5-63-65	290.53	17.89308	6.901343	1.630903	50.66992	0.439399	2.338797	5.11	5.11E-05	10.97	4.23	2.06	0.14	0.136	7.34	0.008672	68.99
DEM31R5-103-105	290.93	15.58892	6.521966	1.462649	52.523	0.320833	2.243398	4.07	4.07E-05	10.66	4.46	2.21	0.12	0.124	8.05	0.006108	69.02
DEM31R5-143-145	291.33	15.1195	6.53752	1.424847	54.01801	0.244477	2.320471	3.03	3.03E-05	10.61	4.59	2.34	0.12	0.121	8.26	0.004526	69.06
DEM31R6-22-24	291.62	15.94016	6.580927	1.407019	54.21413	0.282233	2.50515	3.57	3.57E-05	11.33	4.68	2.28	0.12	0.121	8.24	0.005206	69.09
DEM31R6-64-66	292.04	15.37232	6.109004	1.482775	55.43968	0.223706	2.489213	2.7	2.7E-05	10.37	4.12	2.39	0.11	0.110	9.08	0.004035	69.13
DEM31R6-103-105	292.43	14.97288	5.866551	1.451272	57.86876	0.273157	2.428917	3.24	3.24E-05	10.32	4.04	2.33	0.10	0.101	9.86	0.00472	69.16
DEM31R6-143-145	292.83	12.75228	5.490756	1.104466	62.87714	0.198988	2.479237	2.63	2.63E-05	11.55	4.97	2.50	0.09	0.087	11.45	0.003165	69.2
DEM31R7-30-32	293.2	17.91412	6.946165	1.748851	51.71833	0.391295	2.441296	4.54	4.54E-05	10.24	3.97	2.12	0.13	0.134	7.45	0.007566	69.24
DEM31R7-58-60	293.48	16.83684	6.337768	1.532565	55.13108	0.323793	2.443145	3.7	3.7E-05	10.99	4.14	2.23	0.11	0.115	8.70	0.005873	69.27
DEM31RCC-9-11	293.68	15.48638	5.567881	1.416131	59.087	0.259978	2.526844	3.09	3.09E-05	10.94	3.93	2.36	0.09	0.094	10.61	0.0044	69.28
DEM32R1-21-28	293.76	12.71507	4.989848	1.182351	63.77621	0.169101	2.368922	2.08	2.08E-05	10.75	4.22	2.58	0.08	0.078	12.78	0.002651	69.28
DEM32R1-65-67	294.15	15.34342	5.74741	1.417381	58.76712	0.337495	2.375248	3.81	3.81E-05	10.83	4.05	2.24	0.10	0.098	10.22	0.005743	69.3
DEM32R1-105-108	294.56	11.94342	4.263788	1.096043	67.49474	0.236808	2.251773	2.7	2.7E-05	10.90	3.89	2.45	0.06	0.063	15.83	0.003509	69.33
DEM32R1-144-146	294.93	11.76753	4.089283	1.048439	68.36374	0.178079	2.259378	1.93	1.93E-05	11.22	3.90	2.58	0.06	0.060	16.72	0.002605	69.35
DEM32R2-25-27	295.25	15.10632	5.627618	1.54592	56.72527	0.459769	2.236904	4.6	4.6E-05	9.77	3.64	2.09	0.10	0.099	10.08	0.008105	69.37
DEM32R2-65-67	295.65	13.84046	4.948689	1.242781	64.33678	0.261537	2.466092	2.8	2.8E-05	11.14	3.98	2.39	0.08	0.077	13.00	0.004065	69.4
DEM32R2-105-107	296.05	13.25814	4.552534	1.174306	64.70155	0.247161	2.286979	2.5	2.5E-05	11.29	3.88	2.42	0.07	0.070	14.21	0.00382	69.42
DEM32R2-145-147	296.45	16.31716	5.876265	1.761592	55.86776	0.413256	2.098764	4.76	4.76E-05	9.26	3.34	2.13	0.11	0.105	9.51	0.007397	69.44
DEM32R3-22-24	296.72	12.75231	4.782223	1.221697	66.13341	0.225582	2.305941	2.67	2.67E-05	10.44	3.91	2.47	0.07	0.072	13.83	0.003411	69.46
DEM32R3-65-67	297.15	13.82308	5.461104	1.199319	62.25756	0.249069	2.265246	3.02	3.02E-05	11.53	4.55	2.40	0.09	0.088	11.40	0.004001	69.48
DEM32R3-105-107	297.55	15.17544	5.576811	1.523543	59.45777	0.351042	2.131652	3.78	3.78E-05	9.96	3.66	2.23	0.09	0.094	10.66	0.005904	69.51
DEM32R3-145-147	297.95	17.05918	6.172309	1.685407	55.85949	0.387427	2.249817	4.22	4.22E-05	10.12	3.66	2.16	0.11	0.110	9.05	0.006936	69.53
DEM32R4-23-25	298.23	14.50741	5.583557	1.248501	60.98015	0.289067	2.279225	3.2	3.2E-05	11.62	4.47	2.32	0.09	0.092	10.92	0.00474	69.55
DEM32R4-65-67	298.65	13.79277	5.314768	1.275681	62.78505	0.249094	2.18789	2.81	2.81E-05	10.81	4.17	2.40	0.08	0.085	11.81	0.003967	69.58
DEM32R4-105-107	299.05	15.70373	6.119099	1.525677	58.44582	0.352845	2.303324	4.06	4.06E-05	10.29	4.01	2.22	0.10	0.105	9.55	0.006037	69.6
DEM32R4-145-147	299.45	14.89827	5.514911	1.511615	59.9798	0.334343	2.005468	3.73	3.73E-05	9.86	3.65	2.25	0.09	0.092	10.88	0.005574	69.62
DEM32R5-16-18	299.66	15.01624	5.534499	1.39743	60.15688	0.299491	2.148045	3.37	3.37E-05	10.75	3.96	2.30	0.09	0.092	10.87	0.004978	69.63
DEM32R5-55-57	300.05	14.85127	5.755143	1.508104	60.29337	0.28206	2.208634	3.23	3.23E-05	9.85	3.82	2.33	0.10	0.095	10.48	0.004678	69.65
DEM32R5-95-97	300.45	15.27639	5.758379	1.434116	60.29633	0.278805	2.29007	3.09	3.09E-05	10.65	4.02	2.33	0.10	0.096	10.47	0.004624	69.68
DEM32R5-135-137	300.85	15.21266	5.86182	1.45826	59.91381	0.332935	2.291948	3.98	3.98E-05	10.43	4.02	2.26	0.10	0.098	10.22	0.005557	69.7
DEM32R6-20-22	301.2	15.53648	6.049321	1.383389	59.15954	0.376834	2.251016	4.39	4.39E-05	11.23	4.37	2.20	0.10	0.102	9.78	0.00637	69.72
DEM32R6-65-67	301.65	15.75085	5.927876	1.595338	56.59382	0.399044	2.178634	4.16	4.16E-05	9.87	3.72	2.15	0.10	0.105	9.55	0.007051	69.75
DEM32R6-101-103	302.01	15.49466	5.569133	1.501847	59.242	0.329227	2.259796	3.51	3.51E-05	10.32	3.71	2.26	0.09	0.094	10.64	0.005557	69.77
DEM33R1-20-22	303.3	13.94562	5.33878	1.289828	61.65258	0.260119	2.246163	2.85	2.85E-05	10.81	4.14	2.37	0.09	0.087	11.55	0.004219	69.85
DEM33R1-60-62	303.7	11.42853	4.534041	1.172913	65.63392	0.232996	2.048201	2.72	2.72E-05	9.74	3.87	2.45	0.07	0.069	14.48	0.00355	69.87
DEM33R1-108-110	304.18	15.42571	6.527207	1.387447	55.47185	0.286807	2.478743	3.47	3.47E-05	11.12	4.70	2.29	0.12	0.118	8.50	0.00517	69.9
DEM33R1-140-142	304.5	14.11307	5.595556	1.246112	58.91466	0.261373	2.272083	2.97	2.97E-05	11.33	4.49	2.35	0.09	0.095	10.53	0.004436	69.92
DEM33R2-18-20	304.78	16.38914	6.876962	1.54581	51.96466	0.403012	2.345859	4.55	4.55E-05	10.60	4.45	2.11	0.13	0.132	7.56	0.007756	69.94
DEM33R2-58-60	305.18	18.42753	6.950386	1.772612	50.45079	0.390861	2.328495	4.63	4.63E-05	10.40	3.92	2.11	0.14	0.138	7.26	0.007747	69.96
DEM33R2-97-100	305.58	15.85574	6.135969	1.473475	56.55166	0.307389	2.401917	3.6	3.6E-05	10.76	4.16	2.26	0.11	0.108	9.22	0.005435	69.98
DEM33R2-140-142	306	17.75814	6.812896	1.510014	51.1141	0.354742	2.355623	4.38	4.38E-05	11.76	4.51	2.16	0.13	0.133	7.50	0.00694	70.01
DEM33R320-22	306.3	11.88785	4.891446	1.069994	63.95864	0.203917	2.176664	2.4	2.4E-05	11.11	4.57	2.50	0.08	0.076	13.08	0.003188	70.03
DEM33R3-60-62	306.7	15.78943	5.738679	1.456414	55.85878	0.338627	2.273624	3.77	3.77E-05	10.84	3.94	2.22	0.10	0.103	9.73	0.006062	70.05
DEM33R3-98-100	307.1	11.85149	4.642903	1.045346	66.16208	0.222198	2.341874	2.65	2.65E-05	11.34	4.44	2.47	0.07	0.070	14.25	0.003358	70.07
DEM33R3-140-142	307.5	13.11464	5.174947	1.049668	64.31713	0.245918	2.428637	3.43	3.43E-05	12.49	4.93	2.42	0.08	0.080	12.43	0.003824	70.08
DEM33R4-15-17NEW2	307.75	10.3806	4.234169	0.964281	69.39631	0.16436	2.265403	2.23	2.23E-05	10.77	4.39	2.63	0.06	0.061	16.39	0.002368	70.11
DEM33R4-55-57	308.15	10.1253	3.939753	0.840095	56.56251	0.117972	1.57754	2.7	2.7E-05	12.05	4.69	2.68	0.07	0.070	14.36	0.002086	70.13
DEM33R4-103-105	308.65	15.04872	5.916423	1.181649	57.88694	0.249772	2.199043	3.29	3.29E-05	12.74	5.01	2.37	0.10	0.102	9.78	0.004315	70.16
DEM33R4-145-147NEW	309.05	15.38362	5.590046	1.449533	54.18774	0.247584	2.095723	3.43	3.43E-05	10.61	3.86	2.34	0.10	0.103	9.69	0.004569	70.19
DEM33R5-25-27	309.35	16.94538	6.304357	1.359951	55.83551	0.284466	2.387725	3.61	3.61E-05	12.46	4.64	2.29	0.11	0.113	8.86	0.005095	70.21
DEM33R5-63-65	309.73	18.83103	6.267314	1.41518	52.97281	0.313372	2.259362	4.47	4.47E-05	13.31	4.43	2.23	0.12	0.118	8.45	0.005916	70.23
DEM33R5-102-104	310.12	20.32751	6.446259	1.37956	50.25926	0.388592	2.244187	6.33	6.33E-05	14.73	4.67	2.11	0.13	0.128	7.80	0.007732	70.25
DEM33R5-145-147	310.55	18.33421	6.31433	1.3758	53.07757	0.339227	2.246488	4.57	4.57E-05	13.33	4.59	2.19	0.12	0.119	8.41	0.006391	70.27
DEM33R6-23-25	310.83	19.53429	6.305456	1.401498	51.20522	0.347856	2.248444	5.02	5.02E-05	13.94	4.50	2.17	0.12	0.123	8.12	0.006793	70.29
DEM33R6-63-65	311.23	16.03818	6.246487	1.21476	55.58503	0.241423	2.325013	3.31	3.31E-05	13.20	5.14	2.36	0.11	0.112	8.90	0.004343	70.32
DEM33R6-103-105	311.63	15.45246	5.939466	1.307894	56.12429	0.311331	2.2488	3.78	3.78E-05	11.81	4.54	2.26	0.11	0.106	9.45	0.005547	70.34
DEM33R6-142-144	312.02	17.58893	6.473857	1.492482	53.68279	0.371915	2.262808	4.96	4.96E-05	11.79	4.34	2.16	0.12	0.121	8.29	0.006928	70.36
DEM33R7-22-24	312.32	20.66169	6.262689	1.587907	49.10938	0.379174	2.193692	5.59	5.59E-05	13.01	3.94	2.11	0.13	0.128	7.84	0.007721	70.38
DEM33R7-68-70	312.78	17.37898	6.413807	1.404148	53.07378	0.395895	2.145833	5.69	5.69E-05	12.38	4.57	2.13	0.12	0.121	8.27	0.007459	70.41
DEM34R1-23-25	313.03	18.79345	6.376498	1.613059	51.09219	0.376137	2.230788	4.85	4.85E-05	11.65	3.95	2.13	0.12	0.125	8.01	0.007362	70.42
DEM34R1-62-64	313.42	15.86382	5.872951	1.40949	56.74753	0.321879	2.175784	3.89	3.89E-05	11.26	4.17	2.25	0.10	0.103	9.66	0.005672	70.45
DEM34R1-103-105	313.83	17.76531	6.555907	1.444841	52.06291	0.329404	2.270548	4.97	4.97E-05	12.30	4.54	2.20	0.13	0.126	7.94	0.006327	70.48
DEM34R1-144-146	314.24	16.6683	6.068692	1.551461	53.35611	0.341445	2.139059	4.38	4.38E-05	10.74	3.91	2.19	0.11	0.114	8.79	0.006399	70.5
DEM34R2-25-27	314.55	14.70579	5.683722	1.19672	58.58307	0.186903	2.317673	2.58	2.58E-05	12.29	4.75	2.50	0.10	0.097	10.31	0.00319	70.52
DEM34R2-60-62	314.8	14.60603	5.905925	1.256165	55.83872	0.231918	2.18733	3.08	3.08E-05	11.63	4.70	2.38	0.11	0.106	9.45	0.004153	70.53
DEM34R2-102-104	315.22	13.30611	5.097218	1.187562	61.52492	0.192286	2.192486	2.41	2.41E-05	11.20	4.29	2.51	0.08	0.083	12.07	0.003125	70.55
DEM34R2-143-145	315.73	13.18824	5.587966	1.165561	60.63291	0.179958	2.325701	2.77	2.77E-05	11.31	4.79	2.53	0.09	0.092	10.85	0.002968	70.58
DEM34R3-23-25	316.02	19.17471	6.132156	1.392489	46.324	0.372198	1.971862	5.66	5.66E-05	13.77	4.40	2.10	0.13	0.132	7.55	0.008035	70.6
DEM34R3-64-66	316.43	19.60285	6.392666	1.487872	48.19186	0.337329	2.05607	5.2	5.2E-05	13.18	4.30	2.15	0.13	0.133	7.54	0.007	70.63
DEM34R3-102-104	316.81	16.42398	5.936319	1.262308	55.92102	0.257543	2.378497	3.87	3.87E-05	13.01	4.70	2.34	0.11	0.106	9.42	0.004605	70.65
DEM34R3-142-144NEW2	317.21	12.92371	5.130955	1.161322	59.37058	0.172868	2.313987	2.23	2.23E-05	11.13	4.42	2.54	0.09	0.086	11.57	0.002912	70.67
DEM34R4-8-10	317.38	14.26764	5.269072	1.179609	57.95109	0.203949	2.187746	2.76	2.76E-05	12.10	4.47	2.45	0.09	0.091	11.00	0.003519	70.67
DEM34R4-41-43	317.71	15.81866	5.816079	1.297671	53.77011	0.287588	2.188809	3.79	3.79E-05	12.19	4.48	2.27	0.11	0.108	9.25	0.005348	70.7
DEM34R4-78-80	318.08	14.04881	5.08402	1.221724	59.90385	0.213726	2.261688	2.65	2.65E-05	11.50	4.16	2.45	0.08	0.085	11.79	0.003564	70.72
DEM34R4-118-119	318.47	16.68391	5.855566	1.20333	53.5206	0.320145	2.216587	4.42	4.42E-05	13.86	4.87	2.22	0.11	0.109	9.14	0.005982	70.75
DEM34RCC-5-7	320.11	12.95718	4.29896	1.135386	62.63769	0.15885	2.267063	2.09	2.09E-05	11.41	3.79	2.60	0.07	0.069	14.57	0.002536	70.84

TABLE S2 δ13c AND δ18O VALUES, AND ELEMENTAL COMPOSITION DATA (XRF ANALYSES) OF HOLE 1258A (PALEOPRODUCTIVITY AND CCD)

Ident	Depth (mbsf)	Ba NMS	Ca NMS	Al NMS	Ba/Ca	Ba/Al	Ident	Depth (mbsf)	Dry weight (g)	Final weight (g)	>63 fraction (%)	Ba NMS	Ti NMS		Age (Ma)
DEM28R2-110-112	257.5	0.190075	0.428325	1.682629	0.443764	0.112963	DEM28R2-110-112	257.5	20.42	10.35	50.7	0.190075	1.981829	0.095909	66.2
DEM28R2-148-150	257.88	0.132708	0.312527	1.58387	0.424628	0.083787	DEM28R2-148-150	257.88	16.77	6.43	38.3	0.132708	2.015123	0.065856	66.21
DEM28R3-23-25NEW	258.13	0.091794	0.237459	1.321121	0.386569	0.069482	DEM28R3-23-25NEW	258.13	24.08	6.24	25.9	0.091794	1.859644	0.049361	66.22
DEM28R3-61-63	258.51	0.091663	0.271892	1.206255	0.33713	0.07599	DEM28R3-61-63	258.51	16.73	3.85	23.0	0.091663	1.766189	0.051899	66.23
DEM28R3-103-105	258.93	0.122912	0.364494	1.527045	0.337213	0.08049	DEM28R3-103-105	258.93	22.21	8.29	37.3	0.122912	2.052732	0.059877	66.25
DEM28R3-141-143	259.31	0.114283	0.379431	1.827255	0.301195	0.062543	DEM28R3-141-143	259.31	27.69	9.37	33.8	0.114283	2.119041	0.053931	66.26
DEM28R4-21-23	259.61	0.131211	0.500143	1.71019	0.262347	0.076723	DEM28R4-21-23	259.61	29.54	10.33	35.0	0.131211	2.270337	0.057794	66.27
DEM28R4-63-65NEW3	260.01	0.144089	0.544765	2.03358	0.264498	0.070855	DEM28R4-63-65NEW3	260.01	31.38	13.56	43.2	0.144089	2.106524	0.068401	66.28
DEM28R4-103-105	260.41	0.10038	0.504864	1.576295	0.198826	0.063681	DEM28R4-103-105	260.41	30.04	10.89	36.3	0.10038	2.197709	0.045675	66.3
DEM28R4-143-145	260.81	0.15387	0.537758	1.832716	0.286132	0.083957	DEM28R4-143-145	260.81	28.7	11.41	39.8	0.15387	2.072794	0.074233	66.31
DEM28R5-13-15	261.03	0.17577	0.519249	1.921928	0.338508	0.091455	DEM28R5-13-15	261.03	31.92	11.57	36.2	0.17577	2.103469	0.083562	66.32
DEM28R5-48-50	261.38	0.11735	0.505328	1.739044	0.232225	0.067479	DEM28R5-48-50	261.38	35.13	12.24	34.8	0.11735	2.094937	0.056016	66.33
DEM28R5-93-95	261.83	0.151054	0.472078	1.841378	0.319977	0.082033	DEM28R5-93-95	261.83	34.3	8.9	25.9	0.151054	2.157579	0.070011	66.35
DEM28R5-133-135	262.23	0.16548	0.467348	1.866879	0.354084	0.08864	DEM28R5-133-135	262.23	33.48	13.92	41.6	0.16548	2.11631	0.078193	66.36
DEM28R6-30-32	262.7	0.167968	0.549437	1.97217	0.30571	0.085169	DEM28R6-30-32	262.7	30.73	11.17	36.3	0.167968	2.142922	0.078383	66.38
DEM28R6-70-72	263.1	0.186269	0.51681	1.939182	0.360421	0.096056	DEM28R6-70-72	263.1	27.98	10.39	37.1	0.186269	2.007688	0.092778	66.41
DEM28R6-110-112	263.5	0.163312	0.42387	1.784163	0.385289	0.091534	DEM28R6-110-112	263.5	28.81	7.03	24.4	0.163312	2.156257	0.075739	66.45
DEM29R1-21-24	264.82	0.164266	0.475588	1.582877	0.345394	0.103777	DEM29R1-21-24	264.82	29.64	11.79	39.8	0.164266	2.201391	0.074619	66.57
DEM29R1-63-65	265.23	0.182011	0.522415	1.686589	0.348403	0.107916	DEM29R1-63-65	265.23	27.9	11.99	43.0	0.182011	2.070973	0.087887	66.61
DEM29R1-103-105	265.63	0.150027	0.438801	1.629845	0.341903	0.09205	DEM29R1-103-105	265.63	33.17	11.94	36.0	0.150027	2.026184	0.074044	66.65
DEM29R1-144-146	266.04	0.118644	0.49134	1.762969	0.241469	0.067298	DEM29R1-144-146	266.04	20.26	10.3	50.8	0.118644	2.258828	0.052524	66.69
DEM29R2-18-20	266.28	0.207207	0.341556	1.655434	0.606655	0.125168	DEM29R2-18-20	266.28	16.39	3.5	21.4	0.207207	2.117399	0.097859	66.71
DEM29R2-59-61	266.69	0.195925	0.545507	1.674123	0.359162	0.117032	DEM29R2-59-61	266.69	19.81	9.12	46.0	0.195925	2.194909	0.089264	66.75
DEM29R2-104-106	267.14	0.175585	0.513741	1.783804	0.341777	0.098433	DEM29R2-104-106	267.14	19.42	8.88	45.7	0.175585	2.024477	0.086731	66.79
DEM29R21-43-145	267.53	0.20096	0.525021	1.731803	0.382765	0.116041	DEM29R2-143-145	267.53	23.49	9.7	41.3	0.20096	2.065459	0.097295	66.83
DEM29R3-20-22	267.8	0.145709	0.452096	1.61735	0.322297	0.090091	DEM29R3-20-22	267.8	19.35	4	20.7	0.145709	2.24741	0.064834	66.85
DEM29R3-58-60	268.18	0.197262	0.490629	1.500149	0.40206	0.131495	DEM29R3-58-60	268.18	22.08	9.32	42.2	0.197262	2.103583	0.093774	66.89
DEM29R3-98-100	268.58	0.196384	0.548082	1.737324	0.358311	0.113038	DEM29R3-98-100	268.58	33.04	13.22	40.0	0.196384	1.982487	0.099059	66.92
DEM29R3-140-142	269	0.242205	0.524863	1.455182	0.461464	0.166443	DEM29R3-140-142	269	19.18	13.46	70.2	0.242205	2.105349	0.115043	66.96
DEM29R4-5-7	269.15	0.156978	0.386954	1.50854	0.405676	0.104059	DEM29R4-5-7	269.15	22.32	5.89	26.4	0.156978	2.082779	0.075369	66.98
DEM29R4-43-45	269.53	0.160936	0.391465	1.450816	0.411113	0.110928	DEM29R4-43-45	269.53	16.91	5.56	32.9	0.160936	2.209762	0.07283	67.02
DEM29R4-85-87	269.95	0.155544	0.385206	1.347936	0.403795	0.115395	DEM29R4-85-87	269.95	19.7	6.23	31.6	0.155544	2.212035	0.070317	67.06
DEM29R4-125-127	270.35	0.183518	0.503102	1.897731	0.364772	0.096704	DEM29R4-125-127	270.35	27.45	13.62	49.6	0.183518	2.119154	0.086599	67.09
DEM29R5-21-23	270.63	0.163525	0.31939	1.496084	0.51199	0.109302	DEM29R5-21-23	270.63	31.35	9.81	31.3	0.163525	2.163159	0.075595	67.12
DEM29R5-63-65	271.05	0.217702	0.452409	1.749638	0.481211	0.124427	DEM29R5-63-65	271.05	19.04	7.36	38.7	0.217702	2.112054	0.103076	67.16
DEM29R5-103-105	271.45	0.193689	0.380566	1.562948	0.508952	0.123926	DEM29R5-103-105	271.45	25.84	7.11	27.5	0.193689	2.09111	0.092625	67.2
DEM29R5-143-145	271.85	0.190559	0.450375	1.624214	0.423112	0.117324	DEM29R5-143-145	271.85	25.17	10.47	41.6	0.190559	2.098183	0.090821	67.23
DEM29R6-20-22	272.12	0.202811	0.384196	1.609502	0.527885	0.126009	DEM29R6-20-22	272.12	24.25	6.61	27.3	0.202811	2.082193	0.097403	67.26
DEM29R6-60-62	272.52	0.281622	0.367876	1.503679	0.765536	0.187289	DEM29R6-60-62	272.52	22.26	7.67	34.5	0.281622	2.22051	0.126828	67.28
DEM29R6-105-107	272.97	0.132439	0.414349	1.49629	0.319631	0.088512	DEM29R6-105-107	272.97	20.27	6.89	34.0	0.132439	2.085578	0.063502	67.3
DEM29R6-140-142	273.32	0.213172	0.363233	1.549029	0.586873	0.137616	DEM29R6-140-142	273.32	16.38	4.27	26.1	0.213172	2.070065	0.102978	67.37
DEM29R7-13-15	273.55	0.230078	0.500795	1.586838	0.459426	0.144992	DEM29R7-13-15	273.55	31.1	11.8	37.9	0.230078	2.0206	0.113866	67.4
DEM29R7-50-52	273.92	0.18594	0.322808	1.315388	0.576008	0.141358	DEM29R7-50-52	273.92	21.16	6.3	29.8	0.18594	1.965186	0.094617	67.43
DEM29R-CC3-5	274.37	0.215315	0.408245	1.575031	0.527415	0.136705	DEM29R-CC3-5	274.37	21.63	6.51	30.1	0.215315	1.949206	0.110463	67.47
DEM29R7-93-95NEW2	274.39	0.170142	0.520318	1.659034	0.326997	0.102555	DEM29R7-93-95NEW2	274.39	35.89	15.25	42.5	0.170142	2.086582	0.081541	67.47
DEM30R1-20-22	274.4	0.211636	0.384142	1.505992	0.550931	0.140529	DEM30R1-20-22	274.4	12.76	3.5	27.4	0.211636	2.142419	0.098784	67.48
DEM30R1-60-62	274.8	0.290029	0.427193	1.59795	0.678918	0.181501	DEM30R1-60-62	274.8	23.93	8.4	35.1	0.290029	2.033673	0.142613	67.51
DEM30R1-108-110	275.28	0.209963	0.489277	1.738084	0.429129	0.120801	DEM30R1-108-110	275.28	26.3	11.11	42.2	0.209963	2.111437	0.099441	67.56
DEM30R1-143-145	275.63	0.219568	0.510605	1.686298	0.430015	0.130207	DEM30R1-143-145	275.63	19.4	9.04	46.6	0.219568	2.048881	0.107165	67.59
DEM30R2-10-12	275.8	0.198492	0.345472	1.423892	0.574553	0.139401	DEM30R2-10-12	275.8	26.41	6.81	25.8	0.198492	2.229864	0.089015	67.61
DEM30R2-55-57new	276.25	0.211181	0.447959	1.558183	0.471429	0.13553	DEM30R2-55-57new	276.25	19	8.79	46.3	0.211181	2.131223	0.099089	67.65
DEM30R2-95-97	276.65	0.190547	0.340896	1.55575	0.558959	0.122479	DEM30R2-95-97	276.65	28.96	7.53	26.0	0.190547	2.207502	0.086318	67.68
DEM30R2-135-137	277.05	0.224912	0.345442	1.503142	0.651084	0.149628	DEM30R2-135-137	277.05	25.1	6.34	25.3	0.224912	2.100828	0.107059	67.72
DEM30R3-18-22	277.4	0.196015	0.357406	1.546798	0.548437	0.126723	DEM30R3-18-22	277.4	18.13	6.56	36.2	0.196015	2.139517	0.091616	67.76
DEM30R3-63-65	277.83	0.228438	0.363129	1.477804	0.629083	0.15458	DEM30R3-63-65	277.83	35.61	13.52	38.0	0.228438	2.039733	0.111994	67.8
DEM30R3-102-105	278.23	0.267843	0.504322	1.815163	0.531095	0.147559	DEM30R3-102-105	278.23	24.82	12.87	51.9	0.267843	2.139612	0.125183	67.84
DEM30R3-143-145	278.63	0.191014	0.447837	1.686747	0.426525	0.113244	DEM30R3-143-145	278.63	23.76	10.1	42.5	0.191014	2.192011	0.087141	67.87
DEM30R4-10-12	278.8	0.25719	0.30441	1.336527	0.844879	0.192431	DEM30R4-10-12	278.8	31.77	6.53	20.6	0.25719	2.105818	0.122133	67.89
DEM30R4-41-43	279.11	0.249403	0.564542	1.833775	0.441779	0.136005	DEM30R4-41-43	279.11	31.25	17.57	56.2	0.249403	2.058014	0.121186	67.92
DEM31R1-23-25	284.13	0.249423	0.480959	1.65523	0.518595	0.150688	DEM31R1-23-25	284.13	34.52	8.46	24.5	0.249423	2.139544	0.116578	68.39
DEM31R1-65-67	284.55	0.473616	0.414983	1.530884	1.141289	0.309374	DEM31R1-65-67	284.55	23.35	12.95	55.5	0.473616	2.137369	0.221588	68.43
DEM31R1-105-107	284.95	0.859824	0.472053	1.785184	1.821458	0.481644	DEM31R1-105-107	284.95	35.18	18.13	51.5	0.859824	2.195198	0.391684	68.46
DEM31R1-145-147	285.35	0.452525	0.382612	1.538437	1.182726	0.294146	DEM31R1-145-147	285.35	26.41	12.88	48.8	0.452525	2.15712	0.209782	68.5
DEM31R2-23-25	285.63	0.239159	0.363023	1.619981	0.658797	0.147631	DEM31R2-23-25	285.63	26.7	11.12	41.6	0.239159	2.366858	0.101045	68.53
DEM31R2-63-65	286.03	0.204667	0.310036	1.326363	0.660139	0.154307	DEM31R2-63-65	286.03	38.44	13.99	36.4	0.204667	2.130189	0.096079	68.57
DEM31R2-103-105	286.43	0.174163	0.224771	1.370814	0.774847	0.127051	DEM31R2-103-105	286.43	32.92	6.04	18.3	0.174163	2.248729	0.07745	68.6
DEM31R2-143-145	286.83	0.167025	0.181865	1.164533	0.918402	0.143427	DEM31R2-143-145	286.83	17.21	2.94	17.1	0.167025	2.223407	0.075121	68.64
DEM31R3-18-20	287.08	0.481789	0.367795	1.599654	1.309937	0.301183	DEM31R3-18-20	287.08	23.6	9.47	40.1	0.481789	2.338528	0.206022	68.66
DEM31R3-63-65	287.53	0.35209	0.233211	1.437029	1.509747	0.245013	DEM31R3-63-65	287.53	17.24	5.05	29.3	0.35209	2.394785	0.147024	68.71
DEM31R3-103-105	287.93	0.263962	0.232483	1.389732	1.135403	0.189937	DEM31R3-103-105	287.93	14.52	3.7	25.5	0.263962	2.360436	0.111828	68.74
DEM31R3-143-145	288.33	0.636371	0.453044	1.571265	1.404657	0.405006	DEM31R3-143-145	288.33	31.39	15.68	50.0	0.636371	2.226126	0.285865	68.78
DEM31R4-23-25	288.63	0.148584	0.458111	1.585686	0.324341	0.093703	DEM31R4-23-25	288.63	34.28	18.28	53.3	0.148584	2.369574	0.062705	68.81
DEM31R4-63-65	289.03	0.078663	0.485254	1.534767	0.162107	0.051254	DEM31R4-63-65	289.03	29.86	16.78	56.2	0.078663	2.307013	0.034097	68.85
DEM31R4-103-105	289.43	0.085288	0.287823	1.50476	0.29632	0.056679	DEM31R4-103-105	289.43	20.71	6.12	29.6	0.085288	2.391136	0.035668	68.88
DEM31R4-143-145	289.83	0.053875	0.296124	1.334407	0.181935	0.040374	DEM31R4-143-145	289.83	27.39	12.08	44.1	0.053875	2.351419	0.022912	68.92
DEM31R5-22-24	290.12	0.06005	0.452504	1.818827	0.132706	0.033016	DEM31R5-22-24	290.12	18.18	9.45	52.0	0.06005	2.331575	0.025755	68.95
DEM31R5-63-65	290.53	0.0963	0.439399	1.630903	0.219164	0.059047	DEM31R5-63-65	290.53	17.04	9.12	53.5	0.0963	2.338797	0.041175	68.99
DEM31R5-103-105	290.93	0.093166	0.320833	1.462649	0.290388	0.063697	DEM31R5-103-105	290.93	24.89	13.5	54.2	0.093166	2.243398	0.041529	69.02
DEM31R5-143-145	291.33	0.086873	0.244477	1.424847	0.355342	0.06097	DEM31R5-143-145	291.33	16.42	4.38	26.7	0.086873	2.320471	0.037438	69.06
DEM31R6-22-24	291.62	0.525827	0.282233	1.407019	1.863095	0.373717	DEM31R6-22-24	291.62	28.35	9.89	34.9	0.525827	2.50515	0.209898	69.09
DEM31R6-64-66	292.04	0.265402	0.223706	1.482775	1.18639	0.17899	DEM31R6-64-66	292.04	14.23	3.78	26.6	0.265402	2.489213	0.106621	69.13
DEM31R6-103-105	292.43	0.566176	0.273157	1.451272	2.072712	0.390124	DEM31R6-103-105	292.43	25.14	9.51	37.8	0.566176	2.428917	0.233098	69.16
DEM31R6-143-145	292.83	0.067872	0.198988	1.104466	0.341085	0.061452	DEM31R6-143-145	292.83	24.06	4.48	18.6	0.067872	2.479237	0.027376	69.2
DEM31R7-30-32	293.2	0.06235	0.391295	1.748851	0.159342	0.035652	DEM31R7-30-32	293.2	24.56	12.58	51.2	0.06235	2.441296	0.02554	69.24
DEM31R7-58-60	293.48	0.060119	0.323793	1.532565	0.185671	0.039228	DEM31R7-58-60	293.48	29.49	15.24	51.7	0.060119	2.443145	0.024607	69.27
DEM31RCC-9-11	293.68	0.041962	0.259978	1.416131	0.161408	0.029632	DEM31RCC-9-11	293.68	24.73	9.05	36.6	0.041962	2.526844	0.016607	69.28
DEM32R1-24-28	293.76	0.136794	0.169101	1.182351	0.808947	0.115696	DEM32R1-24-28	293.76	26.81	4.94	18.4	0.136794	2.368922	0.057745	69.28
DEM32R1-65-67	294.15	0.059466	0.337495	1.417381	0.176199	0.041955	DEM32R1-65-67	294.15	16.85	6.59	39.1	0.059466	2.375248	0.025036	69.3
DEM32R1-105-108	294.56	0.061273	0.236808	1.096043	0.258745	0.055904	DEM32R1-105-108	294.56	26.35	6.56	24.9	0.061273	2.251773	0.027211	69.33
DEM32R1-144-146	294.93	0.137863	0.178079	1.048439	0.774167	0.131493	DEM32R1-144-146	294.93	22.18	4.05	18.3	0.137863	2.259378	0.061018	69.35
DEM32R2-25-27	295.25	0.157368	0.459769	1.54592	0.342276	0.101796	DEM32R2-25-27	295.25	27.11	15.17	56.0	0.157368	2.236904	0.070351	69.37
DEM32R2-65-67	295.65	0.085842	0.261537	1.242781	0.328224	0.069073	DEM32R2-65-67	295.65	34.12	12.1	35.5	0.085842	2.466092	0.034809	69.4
DEM32R2-105-107	296.05	0.112362	0.247161	1.174306	0.45461	0.095684	DEM32R2-105-107	296.05	28.95	7.67	26.5	0.112362	2.286979	0.049131	69.42
DEM32R2-145-147	296.45	0.085387	0.413256	1.761592	0.20662	0.048472	DEM32R2-145-147	296.45	16.18	8.48	52.4	0.085387	2.098764	0.040684	69.44
DEM32R3-22-24	296.72	0.437253	0.225582	1.221697	1.938333	0.357906	DEM32R3-22-24	296.72	36.3	11.47	31.6	0.437253	2.305941	0.18962	69.46
DEM32R3-65-67	297.15	0.078682	0.249069	1.199319	0.315904	0.065605	DEM32R3-65-67	297.15	20.21	4.93	24.4	0.078682	2.265246	0.034734	69.48
DEM32R3-105-107	297.55	0.114399	0.351042	1.523543	0.325885	0.075088	DEM32R3-105-107	297.55	23.12	10.95	47.4	0.114399	2.131652	0.053667	69.51
DEM32R3-145-147	297.95	0.109894	0.387427	1.685407	0.28365	0.065203	DEM32R3-145-147	297.95	20.32	8.73	43.0	0.109894	2.249817	0.048846	69.53
DEM32R4-23-25	298.23	0.063654	0.289067	1.248501	0.220205	0.050984	DEM32R4-23-25	298.23	15.87	6.84	43.1	0.063654	2.279225	0.027928	69.55
DEM32R4-65-67	298.65	0.063221	0.249094	1.275681	0.253803	0.049558	DEM32R4-65-67	298.65	25.7	8.88	34.6	0.063221	2.18789	0.028896	69.58
DEM32R4-105-107	299.05	0.49131	0.352845	1.525677	1.392426	0.322028	DEM32R4-105-107	299.05	22.53	10.62	47.1	0.49131	2.303324	0.213305	69.6
DEM32R4-145-147	299.45	0.273704	0.334343	1.511615	0.818632	0.181067	DEM32R4-145-147	299.45	19.26	9.96	51.7	0.273704	2.005468	0.136479	69.62
DEM32R5-16-18	299.66	0.136703	0.299491	1.39743	0.456452	0.097825	DEM32R5-16-18	299.66	28.4	12.56	44.2	0.136703	2.148045	0.063641	69.63
DEM32R5-55-57	300.05	0.075273	0.28206	1.508104	0.266868	0.049912	DEM32R5-55-57	300.05	24.41	9.89	40.5	0.075273	2.208634	0.034081	69.65
DEM32R5-95-97	300.45	0.068275	0.278805	1.434116	0.244886	0.047608	DEM32R5-95-97	300.45	15.08	5.76	38.2	0.068275	2.29007	0.029814	69.68
DEM32R5-135-137	300.85	0.184725	0.332935	1.45826	0.554838	0.126675	DEM32R5-135-137	300.85	22.44	9.37	41.8	0.184725	2.291948	0.080597	69.7
DEM32R6-20-22	301.2	0.158987	0.376834	1.383389	0.421901	0.114925	DEM32R6-20-22	301.2	23.11	11.86	51.3	0.158987	2.251016	0.070629	69.72
DEM32R6-65-67	301.65	0.536851	0.399044	1.595338	1.345341	0.336512	DEM32R6-65-67	301.65	23.22	12.4	53.4	0.536851	2.178634	0.246416	69.75
DEM32R6-101-103	302.01	0.101594	0.329227	1.501847	0.308583	0.067646	DEM32R6-101-103	302.01	19.03	9.17	48.2	0.101594	2.259796	0.044957	69.77
DEM33R1-20-22	303.3	0.226158	0.260119	1.289828	0.869439	0.175339	DEM33R1-20-22	303.3	17.53	8.88	50.7	0.226158	2.246163	0.100686	69.85
DEM33R1-60-62	303.7	0.074588	0.232996	1.172913	0.320126	0.063592	DEM33R1-60-62	303.7	30.15	9.87	32.7	0.074588	2.048201	0.036416	69.87
DEM33R1-108-110	304.18	0.076448	0.286807	1.387447	0.266548	0.0551	DEM33R1-108-110	304.18	31.58	10.13	32.1	0.076448	2.478743	0.030841	69.9
DEM33R1-140-142	304.5	0.146618	0.261373	1.246112	0.560952	0.11766	DEM33R1-140-142	304.5	19.33	6.95	36.0	0.146618	2.272083	0.06453	69.92
DEM33R2-18-20	304.78	0.105941	0.403012	1.54581	0.262874	0.068535	DEM33R2-18-20	304.78	21.81	11.79	54.1	0.105941	2.345859	0.045161	69.94
DEM33R2-58-60	305.18	0.17518	0.390861	1.772612	0.44819	0.098826	DEM33R2-58-60	305.18	19.27	10.32	53.6	0.17518	2.328495	0.075233	69.96
DEM33R2-97-100	305.58	0.21035	0.307389	1.473475	0.684313	0.142758	DEM33R2-97-100	305.58	17.61	7.06	40.1	0.21035	2.401917	0.087576	69.98
DEM33R2-140-142	306	0.064825	0.354742	1.510014	0.182738	0.04293	DEM33R2-140-142	306	26.67	10.86	40.7	0.064825	2.355623	0.027519	70.01
DEM33R320-22	306.3	0.079946	0.203917	1.069994	0.392052	0.074717	DEM33R320-22	306.3	18.5	5.11	27.6	0.079946	2.176664	0.036729	70.03
DEM33R3-60-62	306.7	1.943105	0.338627	1.456414	5.738194	1.334171	DEM33R3-60-62	306.7	33.85	13.81	40.8	1.943105	2.273624	0.854629	70.05
DEM33R3-98-100	307.1	0.078284	0.222198	1.045346	0.352315	0.074888	DEM33R3-98-100	307.1	19.97	3.52	17.6	0.078284	2.341874	0.033428	70.07
DEM33R3-140-142	307.5	0.052385	0.245918	1.049668	0.213019	0.049906	DEM33R3-140-142	307.5	28.38	6.09	21.5	0.052385	2.428637	0.02157	70.08
DEM33R4-15-17NEW2	307.75	0.1338	0.16436	0.964281	0.814066	0.138756	DEM33R4-15-17NEW2	307.75	27.94	5.15	18.4	0.1338	2.265403	0.059062	70.11
DEM33R4-55-57	308.15	11.0269	0.117972	0.840095	93.47028	13.12578	DEM33R4-55-57	308.15	35.06	12.58	35.9	11.0269	1.57754	6.989936	70.13
DEM33R4-103-105	308.65	0.110168	0.249772	1.181649	0.441076	0.093233	DEM33R4-103-105	308.65	20.94	6.02	28.7	0.110168	2.199043	0.050098	70.16
DEM33R4-145-147NEW	309.05	4.482954	0.247584	1.449533	18.10679	3.092688	DEM33R4-145-147NEW	309.05	22.04	8.25	37.4	4.482954	2.095723	2.139097	70.19
DEM33R5-25-27	309.35	0.398089	0.284466	1.359951	1.399426	0.292723	DEM33R5-25-27	309.35	24.62	11.31	45.9	0.398089	2.387725	0.166723	70.21
DEM33R5-63-65	309.73	0.58384	0.313372	1.41518	1.863088	0.412555	DEM33R5-63-65	309.73	19.84	8.4	42.3	0.58384	2.259362	0.258409	70.23
DEM33R5-102-104	310.12	0.907187	0.388592	1.37956	2.334546	0.657591	DEM33R5-102-104	310.12	19.67	11.08	56.3	0.907187	2.244187	0.404238	70.25
DEM33R5-145-147	310.55	0.726936	0.339227	1.3758	2.142921	0.528374	DEM33R5-145-147	310.55	22.65	8.65	38.2	0.726936	2.246488	0.323588	70.27
DEM33R6-23-25	310.83	0.688096	0.347856	1.401498	1.978105	0.490972	DEM33R6-23-25	310.83	21.02	10.85	51.6	0.688096	2.248444	0.306032	70.29
DEM33R6-63-65	311.23	0.29178	0.241423	1.21476	1.208585	0.240196	DEM33R6-63-65	311.23	18.07	3.6	19.9	0.29178	2.325013	0.125496	70.32
DEM33R6-103-105	311.63	0.47646	0.311331	1.307894	1.530394	0.364295	DEM33R6-103-105	311.63	22.38	7.65	34.2	0.47646	2.2488	0.211873	70.34
DEM33R6-142-144	312.02	0.552632	0.371915	1.492482	1.485907	0.370277	DEM33R6-142-144	312.02	25.62	9.29	36.3	0.552632	2.262808	0.244224	70.36
DEM33R7-22-24	312.32	0.840436	0.379174	1.587907	2.21649	0.529273	DEM33R7-22-24	312.32	19.25	9.29	48.3	0.840436	2.193692	0.383115	70.38
DEM33R7-68-70	312.78	1.020756	0.395895	1.404148	2.578352	0.726957	DEM33R7-68-70	312.78	20.21	9.22	45.6	1.020756	2.145833	0.475692	70.41
DEM34R1-23-25	313.03	0.976311	0.376137	1.613059	2.595625	0.605254	DEM34R1-23-25	313.03	28.96	12.73	44.0	0.976311	2.230788	0.437653	70.42
DEM34R1-62-64	313.42	0.822345	0.321879	1.40949	2.554823	0.583435	DEM34R1-62-64	313.42	21.48	8.49	39.5	0.822345	2.175784	0.377953	70.45
DEM34R1-103-105	313.83	1.042115	0.329404	1.444841	3.163636	0.721266	DEM34R1-103-105	313.83	21.9	6.25	28.5	1.042115	2.270548	0.458971	70.48
DEM34R1-144-146	314.24	1.352018	0.341445	1.551461	3.959693	0.871448	DEM34R1-144-146	314.24	28.45	9.76	34.3	1.352018	2.139059	0.632062	70.5
DEM34R2-25-27	314.55	0.503328	0.186903	1.19672	2.692984	0.420589	DEM34R2-25-27	314.55	23.19	2.45	10.6	0.503328	2.317673	0.217169	70.52
DEM34R2-60-62	314.8	0.451058	0.231918	1.256165	1.944901	0.359075	DEM34R2-60-62	314.8	16.29	1.66	10.2	0.451058	2.18733	0.206214	70.53
DEM34R2-102-104	315.22	0.392215	0.192286	1.187562	2.039747	0.330269	DEM34R2-102-104	315.22	18.35	1.58	8.6	0.392215	2.192486	0.17889	70.55
DEM34R2-143-145	315.73	0.293514	0.179958	1.165561	1.631015	0.251822	DEM34R2-143-145	315.73	19.15	1.69	8.8	0.293514	2.325701	0.126204	70.58
DEM34R3-23-25	316.02	5.309033	0.372198	1.392489	14.26399	3.812621	DEM34R3-23-25	316.02	24.26	11.51	47.4	5.309033	1.971862	2.692396	70.6
DEM34R3-64-66	316.43	2.270683	0.337329	1.487872	6.73136	1.526128	DEM34R3-64-66	316.43	19.55	8.22	42.0	2.270683	2.05607	1.10438	70.63
DEM34R3-102-104	316.81	0.321117	0.257543	1.262308	1.24685	0.254389	DEM34R3-102-104	316.81	14.85	3.65	24.6	0.321117	2.378497	0.135008	70.65
DEM34R3-142-144NEW2	317.21	0.320745	0.172868	1.161322	1.855435	0.276189	DEM34R3-142-144NEW2	317.21	24.59	1.68	6.8	0.320745	2.313987	0.138611	70.67
DEM34R4-8-10	317.38	0.333011	0.203949	1.179609	1.632816	0.282306	DEM34R4-8-10	317.38	15.05	1.44	9.6	0.333011	2.187746	0.152216	70.67
DEM34R4-41-43	317.71	0.4281	0.287588	1.297671	1.488587	0.329899	DEM34R4-41-43	317.71	27.45	6.56	23.9	0.4281	2.188809	0.195586	70.7
DEM34R4-78-80	318.08	0.350258	0.213726	1.221724	1.638819	0.286692	DEM34R4-78-80	318.08	27.36	2.05	7.5	0.350258	2.261688	0.154866	70.72
DEM34R4-118-119	318.47	0.499493	0.320145	1.20333	1.560206	0.415092	DEM34R4-118-119	318.47	15.19	6.23	41.0	0.499493	2.216587	0.225343	70.75
DEM34RCC-5-7	320.11	2.315219	0.15885	1.135386	14.57492	2.039147	DEM34RCC-5-7	320.11	28.51	2.38	8.3	2.315219	2.267063	1.021242	70.84

TABLE S2 δ13c AND δ18O VALUES, AND ELEMENTAL COMPOSITION DATA (XRF ANALYSES) OF HOLE 1258A (ISOTOPES ITT OCEANEON)

Consecutive	Sample	Depth (mbsf)	δ 18O/16O	Depth (mbsf)	$^{13}C_{VPDB}$	Age (Ma)
1	28R-2, 69–70	257.09	-2.03	257.09	1.61	66.19
2	DEM28R2-110-112	257.5	-2.18	257.5	1.61	66.2
3	28R-3, 70–71	258.6	-1.94	258.6	1.77	66.24
4	DEM28R3-103-105	258.93	-2.15	258.93	1.57	66.25
5	DEM28R4-103-105	260.41	-2.16	260.41	1.66	66.3
6	28R-5, 70–71	261.6	-2.02	261.6	1.68	66.34
7	DEM28R5-93-95	261.83	-2.3	261.83	1.49	66.35
8	28R-6, 70–71	263.1	-2.11	263.1	1.56	66.43
9	DEM28R6-110-112	263.5	-1.94	263.5	1.64	66.45
10	DEM29R1-144-146	266.04	-2.27	266.04	1.68	66.69
11	29R-2, 70–71	266.8	-1.89	266.8	1.49	66.76
12	DEM29R2-143-145	267.53	-2.1	267.53	1.61	66.83
13	DEM29R3-140-142	269	-2.07	269	1.71	66.96
14	DEM29R4-125-127	270.35	-2.48	270.35	1.59	67.09
15	29R-5, 70–71	271.12	-2.38	271.12	1.66	67.16
16	DEM29R5-143-145	271.85	-2.14	271.85	1.54	67.23
17	29R-6, 70–71	272.62	-2.15	272.62	1.46	67.3
18	DEM29R6-140-142	273.32	-2.21	273.32	1.79	67.37
19	29R-7, 70–71	274.12	-2.06	274.12	1.62	67.45
20	DEM30R1-20-22	274.4	-2.55	274.4	1.61	67.48
21	DEM30R2-55-57	276.25	-2.04	276.25	1.51	67.65
22	30R-2, 70–71	276.4	-2.02	276.4	1.6	67.66
23	DEM30R3-63-65	277.83	-2.19	277.83	1.57	67.8
24	30R-3, 70–71	277.9	-2.12	277.9	1.72	67.81
25	DEM30R4-41-43	279.11	-2.59	279.11	1.66	67.92
26	31R1 23-25	284.13	-2.71	284.13	1.69	68.39
27	31R1 65-67	284.55	-2.63	284.55	1.49	68.43
28	31R1 105-107	284.95	-2.6	284.95	1.46	68.46
29	DEM31R1-145-147	285.35	-2.55	285.35	1.56	68.5
30	31R2 23-25	285.63	-2.78	285.63	1.31	68.53
31	31R2 63-65	286.03	-2.45	286.03	1.29	68.57
32	31R-2, 70–71	286.1	-2.67	286.1	1.29	68.58
33	31R2 103-105	286.43	-2.32	286.43	1.57	68.6
34	DEM31R2-143-145	286.83	-2.22	286.83	1.65	68.64
35	31R3 18-20	287.08	-2.77	287.08	1.38	68.66
36	31R3 63-65	287.53	-2.31	287.53	1.75	68.71
37	31R-3, 70–71	287.6	-2.32	287.6	1.61	68.72
38	31R3 103-105	287.93	-2.35	287.93	1.69	68.74
39	DEM31R3-143-145	288.33	-2.63	288.33	1.24	68.78
40	31R4 23-25	288.63	-2.89	288.63	1.34	68.81
41	31R4 63-65	289.03	-2.75	289.03	1.35	68.85
42	31R4 103-105	289.43	-2.62	289.43	1.5	68.88
43	DEM31R4-143-145	289.83	-2.35	289.83	1.65	68.92
44	31R5 22-24	290.12	-2.83	290.12	1.27	68.95
45	31R5 63-65	290.53	-2.74	290.53	1.32	68.99
46	31R-5, 70–71	290.6	-2.22	290.6	1.52	69
47	31R5 103-105	290.93	-2.62	290.93	1.47	69.02
48	DEM31R5-143-145	291.33	-2.3	291.33	1.87	69.06
49	31R6 22-24	291.62	-2.27	291.62	1.61	69.09
50	31R6 64-66	292.04	-2.21	292.04	1.69	69.13
51	31R-6, 70–71	292.1	-2.45	292.1	1.78	69.14
52	31R6 103-105	292.43	-2.46	292.43	1.34	69.16
53	DEM31R6-143-145	292.83	-2.3	292.83	1.39	69.2
54	31R7 30-32	293.2	-2.84	293.2	1.15	69.24
55	31R7 58-60	293.48	-2.75	293.48	1.15	69.27
56	31R-7, 70–71	293.6	-2.9	293.6	1.11	69.28
57	31RCC 9-11	293.68	-2.67	293.68	1.17	69.28
58	DEM32R1-24-28	293.76	-2.28	293.76	1.77	69.28
59	32R1 65-67	294.15	-2.6	294.15	1.27	69.3
60	32R1 105-108	294.56	-2.3	294.56	1.39	69.33
61	32R1 144-146	294.93	-2.35	294.93	1.15	69.35
62	DEM32R2-25-27	295.25	-2.67	295.25	1.1	69.37
63	32R2 65-67	295.65	-2.66	295.65	1	69.4
64	32R-2, 70–70.5	295.7	-2.46	295.7	1.04	69.4
65	32R2 105-107	296.05	-2.64	296.05	1.11	69.42
66	32R2 145-147	296.45	-2.52	296.45	1.01	69.44
67	DEM32R3-22-24	296.72	-2.5	296.72	1.03	69.46
68	32R3 65-67	297.15	-2.52	297.15	1.47	69.48
69	32R-3, 70–70.5	297.2	-2.35	297.2	1.5	69.48
70	32R3 105-107	297.55	-2.32	297.55	1.05	69.51
71	32R3 145-147	297.95	-2.58	297.95	1.11	69.53
72	DEM32R4-23-25	298.23	-2.5	298.23	1.27	69.55
73	32R4 65-67	298.65	-2.62	298.65	1.18	69.58
74	32R4 105-107	299.05	-2.22	299.05	1.1	69.6
75	32R4 145-147	299.45	-2.19	299.45	1.2	69.62
76	DEM32R5-16-18	299.66	-2.23	299.66	1.53	69.63
77	32R5 55-57	300.05	-2.34	300.05	1.33	69.65
78	32R-5, 69–69.5	300.19	-2.27	300.19	1.82	69.66
79	32R5 95-97	300.45	-2.14	300.45	1.43	69.68
80	32R5 135-137	300.85	-2.48	300.85	1.42	69.7
81	DEM32R6-20-22	301.2	-2.27	301.2	1.27	69.72
82	32R6 65-67	301.65	-2.26	301.65	1.25	69.75
83	32R-6, 69–69.5	301.69	-2.32	301.69	1.13	69.75
84	32R6 101-103	302.01	-2.32	302.01	1.18	69.77
85	33R1 20-22	303.3	-2.52	303.3	1.32	69.85
86	DEM33R1-60-62	303.7	-2.7	303.7	0.89	69.87
87	33R1 108-110	304.18	-2.5	304.18	1.49	69.9
88	33R1 140-142	304.5	-2.41	304.5	1.31	69.92
89	33R2 18-20	304.78	-2.43	304.78	1.45	69.94
90	33R2 58-60	305.18	-2.65	305.18	1.07	69.96
91	33R-2, 70–71	305.3	-2.8	305.3	1.15	69.97
92	DEM33R2-97-100	305.58	-2.71	305.58	1.27	69.98
93	33R2 140-142	306	-2.8	306	1.19	70.01
94	33R3 20-22	306.3	-2.47	306.3	1.25	70.03
95	33R3 60-62	306.7	-2.68	306.7	1.05	70.05
96	33R-3, 70–71	306.8	-2.37	306.8	1.67	70.06
97	33R3 98-100	307.1	-2.57	307.1	1.19	70.07
98	33R3 140-142	307.5	-2.41	307.5	1.22	70.08
99	33R4 15-17	307.75	-2.35	307.75	1.07	70.11
100	33R4 55-57	308.15	-2.33	308.15	0.79	70.13
101	DEM33R4-103-105	308.65	-2.25	308.65	1.4	70.16
102	33R4 145-147	309.05	-2.24	309.05	1.26	70.19
103	33R5 25-27	309.35	-2.32	309.35	1.14	70.21
104	33R5 63-65	309.73	-2.48	309.73	1.14	70.23
105	33R-5, 70–71	309.8	-2.23	309.8	1.1	70.23
106	DEM33R5-102-104	310.12	-2.27	310.12	1.12	70.25
107	33R5 145-147	310.55	-2.5	310.55	0.95	70.27
108	33R6 23-25	310.83	-2.33	310.83	1.02	70.29
109	33R6 63-65	311.23	-2.03	311.23	1.4	70.32
110	33R-6, 70–71	311.3	-2.27	311.3	0.96	70.32
111	DEM33R6-103-105	311.63	-2.05	311.63	1.07	70.34
112	33R6 142-144	312.02	-2.05	312.02	1.04	70.36
113	33R7 22-24	312.32	-2.37	312.32	0.96	70.38
114	33R7 68-70	312.78	-2.17	312.78	0.95	70.41
115	33R-7, 70–71	312.8	-2.48	312.8	0.96	70.41
116	34R1 23-25	313.03	-2.23	313.03	1	70.42
117	DEM34R1-62-64	313.42	-2.34	313.42	1.02	70.45
118	34R1 103-105	313.83	-2.16	313.83	1.09	70.48
119	34R1 144-146	314.24	-2.09	314.24	0.92	70.5
120	34R2 25-27	314.55	-2.05	314.55	1.21	70.52
121	DEM34R2-60-62	314.8	-2.04	314.8	1.33	70.53
122	34R-2, 70–71	315	-2.08	315	1.21	70.54
123	34R2 102-104	315.22	-1.42	315.22	1.81	70.55
124	34R2 143-145	315.73	-1.88	315.73	1.27	70.58
125	34R3 23-25	316.02	-2.15	316.02	1	70.6
126	DEM34R3-64-66	316.43	-2.39	316.43	0.99	70.63
127	34R-3, 70–71	316.5	-2.42	316.5	1.02	70.63
128	34R3 102-104	316.81	-2.04	316.81	1.16	70.65
129	34R3 142-144	317.21	-1.65	317.21	1.62	70.67
130	34R4 8-10	317.38	-1.91	317.38	1.44	70.67
131	DEM34R4-41-43	317.71	-1.63	317.71	1.11	70.7
132	34R-3, 70–71	318	-2.21	318	1.02	70.72
133	34R4 78-80	318.08	-1.94	318.08	1.24	70.72
134	34R4 118-119	318.47	-2.25	318.47	1.09	70.75
135	DEM34RCC-5-7	320.11	-1.86	320.11	1.16	70.84
136	35R-2, 67–70	324.57	-2.33	324.57	1.07	71.17
137	35R-3, 70–71	326.1	-2.14	326.1	0.93	71.26
138	35R-4, 69–71	327.59	-2.04	327.59	1.08	71.34
139	35R-5, 71–72	329.11	-2.24	329.11	0.5	71.42
140	35R-6, 70–71	330.6	-1.81	330.6	1.9	71.5

Previous data (MacLeod 2006)

itt Oceaneon

CHAPTER 4

Table S1 Bulk sediment $\delta^{13}C$ and elemental composition data (XRF analyses) of Hole 1001B.

Table S2 Foraminiferal data (total counts) of Hole 1001B.

Figure S1 Petrographic thin sections from Hole 1001B (Nicaraguan Rise). Photos in 5x. Gt: Globotruncanids, Ht: Heterohelicids, Fr: fish remains.

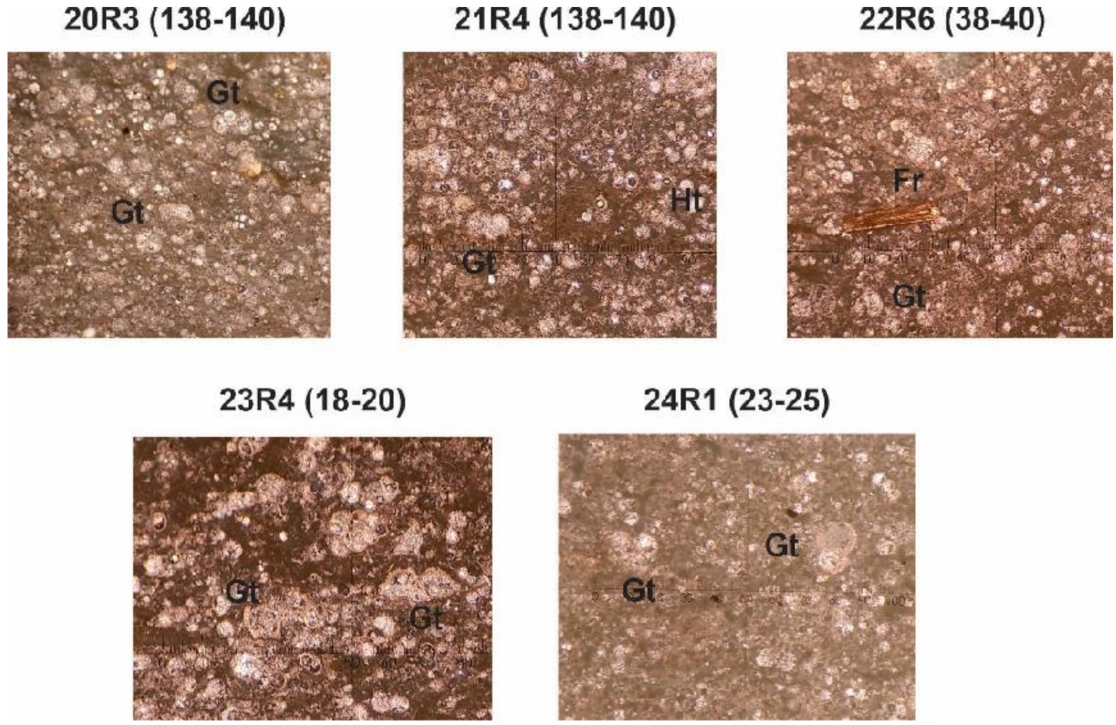

Figure S2 Age model of Hole 1001B. Chronostratigraphic datums based on Sigurdsson et al (1997) and Louvel and Galbrun (2000). Planktonic foraminifera (PF) and calcareous nannofossil (CN) biozones based on Sigurdsson et al (1997).

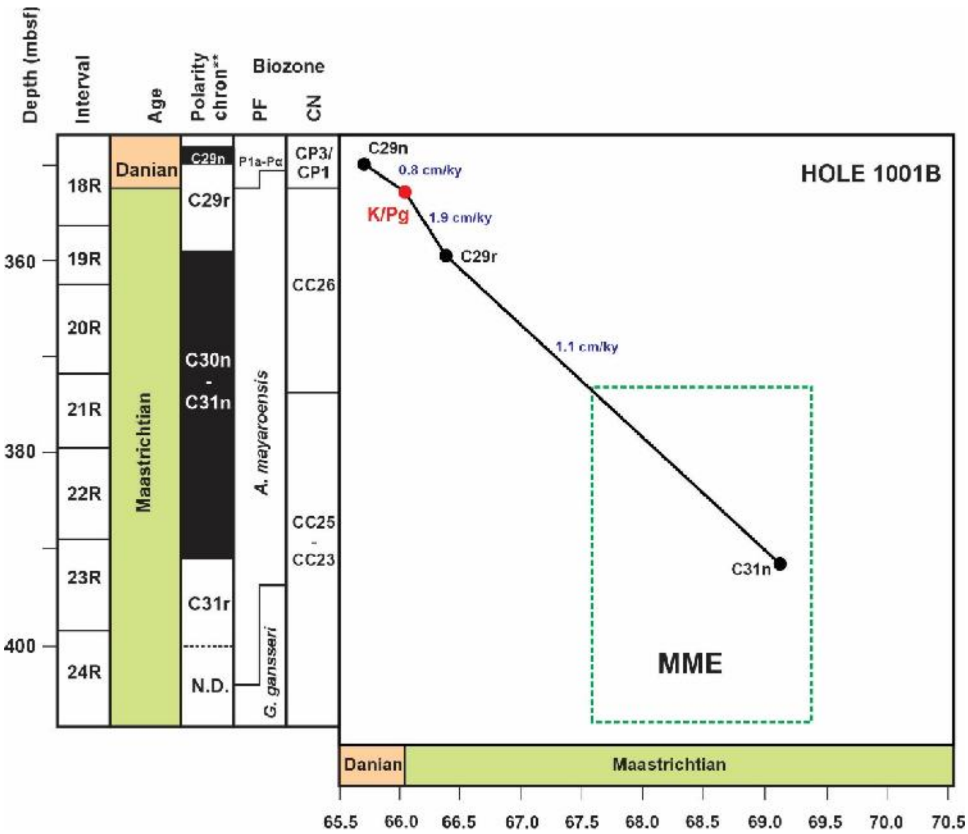

TABLE S1 BULK SEDIMENT δ13C AND ELEMENTAL COMPOSITION DATA (XRF ANALYSES) OF HOLE 1001B (ISOTOPES)

Consecutive	Sample	Depth (mcsd)		Depth (mbsf)	Age (My)	Sample	δ 13C/12C (‰)	Std Dev	δ 18O/16O (‰)	Std Dev
	16R1 70-75	332.15		341.83	64.11	17R1 68-73	0.957	0.023	-3,814	0.040
	16R2 71-76	333.66		343.19	64.37	17R2 69-74	0.825	0.034	-3,745	0.041
	16R3 70-76	335.16		344.66	64.64	17R3 69-74	0.940	0.015	-4,866	0.025
	16R4 70-75	336.65		345.91	64.76	17R4 69-74	1,167	0.018	-3,918	0.035
	16R5 70-75	338.15		348.77	65.36	18R1 72-77	0.939	0.019	-3,973	0.031
	16R6 70-76	339.76		349.96	65.69	18R2 77-82	0.691	0.010	-3,900	0.023
	16R7 20-24	340.64		351.13	65.83	18R3 72-77	0.715	0.018	-3,690	0.035
	17R1 68-73	341.83		352.27	65.97	18R4 70-75	1,000	0.023	-4,056	0.043
	17R2 69-74	343.19		353.22	66.06	18R5 55-60	1,830	0.017	-4,116	0.045
	17R3 69-74	344.66		353.79	66.08	18R6 55-59	2,057	0.026	-3,430	0.028
	17R4 69-74	345.91		357.12	66.26	19R1 77-82	1,987	0.025	-3,976	0.028
	18R1 72-77	348.77		358.4	66.32	19R2 69-74	2,070	0.016	-4,030	0.017
	18R2 77-82	349.96		359.68	66.4	19R3 70-76	2,056	0.017	-4,577	0.041
	18R3 72-77	351.13		362.2	66.61	20R1 29-32	2,021	0.025	-2,935	0.055
Paleogene	18R4 70-75	352.27		363.87	66.76	20R2 5-7	2,098	0.021	-3,700	0.032
	18R5 55-60	353.22		365.4	66.89	20R3 8-10	2,117	0.021	-4,246	0.029
	18R6 55-59	353.79		366.95	67.03	20R4 13-15	2,159	0.019	-3,851	0.039
	19R1 77-82	357.12		368.45	67.16	20R5 13-15	2,170	0.014	-4,314	0.041
	19R2 69-74	358.4		369.91	67.28	20R6 9-11	2,162	0.009	-4,159	0.026
	19R3 70-76	359.68		372.33	67.49	21R1 31-33	2,155	0.022	-4,370	0.038
	20R1 29-32	362.2		373.67	67.61	21R2 30-32	2,298	0.008	-4,400	0.038
	20R1 55-57	362.87		374.82	67.71	21R3 10-12	2,328	0.012	-4,771	0.026
	20R1 69-74	363.03		376.25	67.84	21R4 3-5	2,370	0.028	-4,277	0.028
	20R1 85-87	363.17		377.73	67.96	21R5 0-2	2,274	0.023	-4,348	0.028
	20R1 145-147	363.77		379.27	68.1	21R6 5-7	2,218	0.011	-3,794	0.036
	20R2 5-7	363.87		379.97	68.16	22 R1 35-37	1,834	0.026	-4,090	0.043
	20R2 45-47	364.24		381.31	68.27	22R2 19-21	1,593	0.019	-2,529	0.048
	20R2 68-70	364.47		383	68.42	22R3 38-40	2,086	0.011	-4,461	0.013
	20R2 77-82	364.59		384.43	68.54	22R4 33-35	2,040	0.037	-3,330	0.028
	20R2 88-90	364.7		385.75	68.66	22R5 13-15	2,088	0.030	-4,239	0.035
	20R2 128-130	365.1		387.44	68.8	22R6 38-40	2,144	0.039	-4,543	0.019
	20R3 8-10	365.4		388.5	68.9	22R7 13-17	2,244	0.011	-4,367	0.018
	20R3 48-50	365.8		389.54	68.99	23R1 32-34	2,288	0.027	-3,773	0.032
	20R3 73-75	366.05		390.92	69.11	23R2 20-22	2,305	0.015	-3,661	0.044
	20R3 78-83	366.13		392.45	69.24	23R3 23-25	2,113	0.022	-4,104	0.039
	20R3 113-115	366.45		393.9	69.36	23R4 18-20	2,093	0.029	-4,104	0.020
	20R3 138-140	366.7		395.32	69.49	23R5 10-12	2,168	0.017	-4,617	0.028
	20R4 13-15	366.95		396.87	69.62	23R6 15-17	2,055	0.020	-3,437	0.046
	20R4 53-55	367.35		398.5	69.76	23R7 13-15	2,041	0.030	-4,219	0.025
	20R4 75-80	367.6		399.05	69.81	24R1 23-25	1,992	0.019	-4,024	0.033
	20R4 93-95	367.75		400.53	69.94	24R2 23-25	1,998	0.014	-3,153	0.028
	20R4 140-142	368.12		402.03	70.07	24R3 23-25	2,196	0.015	-3,612	0.036
	20R5 13-15	368.45		403.53	70.2	24R4 23-25	2,160	0.015	-3,894	0.032
	20R5 70-72	369.02								
	20R5 69-73	369.03								
	20R5 120-122	369.52								
	20R5 148-150	369.8								
	20R6 9-11	369.91								
	20R6 50-52	370.32								
	20R6 73-78	370.58								
	20R6 90-92	370.72								
	21R1 31-33	372.33								
	21R1 70-74	372.74								
	21R1 108-110	373.1								
	21R1 133-135	373.35								
	21R2 30-32	373.67								
	21R2 69-73	374.08								
	21R2 110-112	374.49								
	21R3 10-12	374.82								
	21R3 50-52	375.24								
	21R3 71-74	375.44								
	21R3 110-112	375.88								
	21R3 148-150	376.2								
	21R4 3-5	376.25								
	21R4 42-44	376.64								
	21R4 76-78	376.98								
	21R4 98-100	377.2								
	21R4 138-140	377.62								
	21R5 0-2	377.73								
	21R5 60-62	378.32								
	21R5 71-76	378.46								
	21R5 120-122	378.92								
	21R5 140-142	379.12								
	21R6 5-7	379.27								
	21R6 40-42	379.6								
	21R6 71-75	379.75								
	21R6 85-87	379.9								
	22R1 35-37	379.97								
	22R1 78-80	380.2								
	21RCC 13-15	380.3								
	22R1 118-120	380.8								
	22R1 138-140	381.1								
	22R2 0-2	381.12								
	22R2 19-21	381.31								
	22R2 65-67	381.87								
	22R2 105-107	382.2								
	22R2 145-147	382.57								
	22R3 3-5	382.65								
	22R3 38-40	383								
	22R3 78-80	383.4								
	22R3 117-119	383.79								
	22R4 33-35	384.43								
	22R4 75-77	384.87								
	22R4 115-117	385.27								
	22R4 148-150	385.6								
	22R5 13-15	385.75								
	22R5 55-57	386.17								
	22R5 70-75	386.35								
	22R5 113-115	386.75								
	22R6 0-2	387.06								
	22R6 38-40	387.44								
	22R6 80-82	387.86								
	22R6 118-120	388.24								
	22R7 13-17	388.5								
	22RCC 15-17	388.8								
	23R1 32-34	389.54								
	23R1 70-74	389.94								
	23R1 110-112	390.32								
	23R1 148-150	390.7								
	23R2 20-22	390.92								
	23R2 60-62	391.32								
	23R2 99-101	391.71								
	23R2 140-142	392.13								
	23R3 23-25	392.45								
	23R3 64-66	392.86								
	23R3 115-117	393.37								
	23R3 148-150	393.7								
	23R4 18-20	393.9								
	23R4 45-47	394.17								
	23R4 86-88	394.58								
	23R4 125-127	394.97								
	23R5 10-12	395.32								
	23R5 53-55	395.75								
	23R5 93-95	396.15								
	23R5 135-137	396.57								
	23R6 15-17	396.87								
	23R6 55-57	397.27								
	23R6 95-97	397.67								
	23R6 125-127	397.97								
	23R7 13-15	398.5								
	24R1 23-25	399.05								
	24R1 63-65	399.45								
	24R1 103-105	399.85								
	24R1 143-145	400.25								
	24R2 23-25	400.53								
	24R2 63-65	400.93								
	24R2 103-105	401.33								
	24R2 143-145	401.73								
	24R3 3-5	401.83								
	24R3 23-25	402.03								
	24R3 43-45	402.23								
	24R3 63-65	402.43								
	24R3 83-85	402.63								
	24R3 105-107	402.85								
	24R3 123-125	403.03								
	24R3 143-145	403.23								
	24R4 23-25	403.53								
	24R4 60-62	403.9								
	Extra									
	First round									

TABLE S1 BULK SEDIMENT δ13C AND ELEMENTAL COMPOSITION DATA (XRF ANALYSES) OF HOLE 1001B (XRF NORMALIZED DATA)

Nr	Ident	Depth (mbsf)	Mg	Al	Si	S	K	Ca	Ti	Cr	Mn	Fe	Ni	Cu	Zn	Rb	Sr	Zr	Ba	Co	V	Ga	Raw sum
1	NIC20R1-29-32	362.2	3328	138180	2578442	144825	730242	71616.45	236671	-0.812	202945	7218571	9242	27274	32622	44905	2485450	171535	341591	66277	25350	1653	14530719
2	NIC20R1-55-57	362.87	0.568	121285	3150550	208289	623569	68867.01	211101	-1011	237453	5695001	10345	22386	33405	38572	2229349	139496	316131	53023	30483	3604	13191899
3	NIC20R1-85-87	363.17	1429	114744	1950589	141805	465384	75177.3	153098	-0.821	207663	4272482	5021	16054	18564	22571	1788627	107251	188616	33203	15842	1229	9579348
4	NIC20R1-145-147	363.77	1706	126556	2139308	111716	466180	84240.02	143560	-0.284	228543	4096310	4205	14606	17913	25624	1898074	105239	201589	25710	21571	1986	9714636
5	NIC20R2-5-7	363.87	3932	103174	1575023	96587	345234	68062.36	114032	-0.159	188568	3222499	2892	9768	15164	14519	1402479	75260	119665	20303	12539	0.818	7389701
6	NIC20R2-45-47	364.24	1763	145740	2518927	175490	776707	70038.09	251498	0.035	217788	8055511	9037	28554	31221	45998	2531161	166945	366904	69626	31779	2717	15494704
7	NIC20R2-68-70	364.47	-1246	121114	2405503	145696	628773	70877.39	211303	0.02	230114	6326437	7335	22718	24603	35784	1934071	131765	256998	45215	17923	2331	12617314
8	NIC20R2-88-90	364.7	0.632	119770	2147869	154346	515681	81836.67	140719	-1700	234325	4515669	3581	19366	20210	30065	1877003	110961	228653	37333	20188	0.673	10255877
9	NIC20R2-128-130	365.1	2058	116568	2883870	203316	750337	64530.39	254191	-1417	180770	8027608	10306	40796	39132	53990	3329840	204962	484822	75563	33021	2982	16757245
10	NIC20R3-8-10	365.4	6358	124181	2617528	121983	544875	76762.73	174294	-1290	217479	5276672	6679	20095	24775	34843	2114113	123660	297828	42357	23122	0.925	11846406
11	NIC20R3-48-50	365.8	4771	119803	2608843	156038	546890	77831.37	178640	-0.423	233297	5319395	9058	22957	26132	27425	2146824	133914	272133	43128	16305	0.776	11943385
12	NIC20R3-73-75	366.05	6317	142488	2565266	129372	591862	78534.16	169577	-1398	267955	5286774	6991	16645	19769	34159	1722010	114176	250167	41316	23446	1743	11467169
13	NIC20R3-113-115	366.45	2443	119073	2091337	156725	596662	61330.95	205976	-2048	202707	5814066	8172	30906	27661	36011	2006197	133313	299214	47883	26410	2145	11866184
14	NIC20R3-138-140	366.7	-1528	106398	1927951	133136	490708	72407.13	139341	-1552	196546	4159999	3806	16442	21805	24112	2015755	110645	222341	32332	13218	1165	9685027
15	NIC20R4-13-15	366.95	-0.137	125250	2261392	204393	581786	73989.17	172114	-1885	222681	5347344	5092	19291	22612	30838	1866730	122447	257953	42834	19806	1706	11376373
16	NIC20R4-53-55	367.35	2743	119226	3058078	140744	634667	71403.81	192784	-1074	211126	5910939	6616	21316	28322	42988	2235046	159591	309315	53455	26107	2209	13225602
17	NIC20R4-93-95	367.75	2110	94662	2152536	166116	567035	58750.14	176156	-0.012	171686	5193476	5869	21393	23363	33716	1774072	120387	221515	40528	17455	2329	10843154
18	NIC20R4-140-142	368.12	0.076	99349	2000616	110624	346852	91311.93	92322	-2370	227782	2769813	2014	10109	14774	17105	1685705	85637	185048	17149	13791	-0.12	7767632
19	NIC20R5-13-15	368.45	-1784	90294	1592016	109127	379292	67166.88	106951	-0.343	178429	3342625	4388	13477	16110	18194	1319541	79343	143379	17394	9740	0.785	7485683
20	NIC20R570-72NEW2	369.02	5398	67679	4240702	190883	454770	48844.87	167710	-1066	136630	5294232	15050	23734	30146	31862	2007457	122747	240368	55537	19453	2070	13154207
21	NIC20R5-120-122	369.52	-3313	84081	1936548	105355	472660	66409.58	134053	0.621	169746	3954548	4655	14102	18249	23757	1655330	106132	196296	32549	10874	2227	8984259
22	NIC20R5-148-150	369.8	1763	93452	2100384	179364	459767	75991.7	130868	-3090	184670	3670571	2808	14997	16328	28129	1883605	112127	226637	29524	16490	1203	9225489
23	NIC20R6-9-11	369.91	-0.314	119290	1686205	166569	480490	81893.6	129993	-1911	197014	3429799	3406	14116	17193	22014	1783817	106539	221808	27083	13693	0.026	8502011
24	NIC20R6-50-52	370.32	1641	83845	2140586	86983	346304	87383.47	91892	0.804	204455	2596703	3025	11099	12432	13599	1731072	85682	151456	16446	15795	1100	7681499
25	NIC20R6-90-92	370.72	0.303	96149	1934984	92012	406725	86345.37	104970	-0.052	229700	2806995	0.808	10588	35909	19165	1540819	81300	140342	18019	10137	1066	7615226
26	NIC21R1-31-33	372.33	1579	110195	2147186	186101	453311	83038.29	119092	-0.312	201527	3429681	2065	10388	14983	23650	1512995	86537	177805	24800	6780	1105	8592818
27	NIC21R1-70-74	372.74	0.85	78461	1809436	116119	388602	65598.16	114793	-0.014	170381	3313745	3590	9759	15032	18919	1387957	84469	113829	20814	7205	0.957	7736911
28	NIC21R1-108-110	373.1	4004	139134	2713903	143375	706725	70139.65	217687	-0.89	181500	6494750	7623	34367	34618	48572	2315287	173137	333535	47703	17943	1659	13685211
29	NIC21R1-133-135	373.35	4973	102302	4274226	153867	636495	44195.35	208197	-0.574	142136	5729710	9625	23784	30249	48798	1598307	139949	228575	49777	20135	2865	13448165
30	NIC21R2-30-32	373.67	-6620	105013	1793939	101857	414823	94810.13	102058	-1405	204286	2812349	2350	16357	14084	18323	1510694	75788	167993	16012	13794	0.735	7456775
31	NIC21R2-69-73	374.08	-2320	92232	1421993	80412	328204	74072.02	81230	-0.703	172525	2168764	1924	12057	14976	14238	1153741	61958	92665	12979	3727	0.751	5785377
32	NIC21R2-110-112	374.49	2126	157391	2633213	188123	810944	75159.58	202831	-0.504	184314	6017304	7229	33846	25487	57629	2093880	170975	332663	47041	23301	2518	13065974
33	NIC21R3-10-12	374.82	0.365	97703	1825168	84893	286709	91812.91	74317	-0.559	185618	2003714	1327	10159	21974	13619	1316798	66140	124883	9432	5428	-0.241	6214843
34	NIC21R3-50-52	375.24	0.207	111823	1877212	118994	444852	81357.41	117449	-0.161	179713	3496316	3847	17562	17800	21320	1573735	85678	171552	24884	9061	1116	8354221
35	NIC21R3-71-74	375.44	-5967	76520	1258334	76876	319255	60325.7	82646	-0.483	133533	2624381	2257	8198	10362	19859	1228562	70082	109442	17767	9524	0.268	6101956
36	NIC21R3-110-112	375.88	-1220	114449	1827778	117309	435109	91598.35	107113	-1382	190372	3225955	5071	14153	15563	20804	1821932	99614	210993	21570	13024	0.922	8329806
37	NIC21R3-148-150	376.2	0.392	84715	1447190	83179	286680	84799.85	69193	-0.003	182687	1916876	2173	11297	9520	13097	1495906	70986	122334	11574	3831	0.106	5896038
38	NIC21R4-3-5	376.25	-2610	96267	1483244	97726	311651	94795.71	74672	-1050	198495	1862767	0.308	13704	18165	15087	1674666	74765	147787	9769	8196	0.621	6178098
39	NIC21R4-42-44	376.64	2484	150473	2688185	155044	795046	68000.57	226679	-2317	179621	7154166	8590	37442	33231	51874	2150427	179940	336950	65233	24629	2628	14307826
40	NIC21R4-76-78	376.98	0.241	91263	1736069	107995	327241	94620.37	83226	-0.905	189306	2369471	1519	15510	12368	15996	1751312	85414	172651	18847	10983	0.091	7083791
41	NIC21R4-98-100	377.2	-1806	142501	2148112	132417	610247	76283.98	169285	-0.66	175791	4800287	5509	19341	19808	31255	1595549	112474	210624	41413	14341	1168	10304599
42	NIC21R4-138-140	377.62	-0.008	85637	2181591	124656	301007	89369.32	72398	-1719	184770	2259384	2097	11381	15274	14912	1656797	82098	167179	15193	8591	0.773	7270616
43	NIC21R5-0-2	377.73	-2098	100442	1973622	119851	304835	82069.32	79188	-1454	180870	2366389	1816	12641	15457	15269	1565674	79196	155088	13790	7067	1015	7070727
44	NIC21R5-60-62	378.32	0.482	85013	1965376	104025	372440	80361.37	98015	-2286	169157	3139988	3318	35007	18892	20237	2050206	98143	188079	23233	12284	0.728	8461490
45	NIC21R5-120-122	378.92	5478	124131	2475039	154581	722958	69268.13	317830	-0.595	183435	7075244	10761	56241	34012	46152	2264717	193537	304069	63337	24782	1579	14127151
46	NIC21R5-140-142	379.12	-1539	83579	1962340	170709	308494	92169.8	83006	-1193	221291	2189171	2040	29673	14828	16640	1504417	79146	138681	16625	12299	0.588	6926677
47	NIC21R6-5-7	379.27	3058	75603	1968459	76878	311492	80036.02	92058	-1084	200998	2626488	3222	20484	13360	17084	1402821	75372	114238	21766	7044	1021	7110398
48	NIC21R6-40-42	379.6	2743	151044	2319093	147828	735254	73028.54	209417	-1143	206122	6591653	9372	22522	36040	47233	1683835	145661	253901	57253	25815	3223	12719895
49	NIC21R6-85-87	379.9	-1495	73522	1958562	64780	280336	74270.85	82216	0.098	182389	2150295	0.255	7499	9252	15175	1136689	63839	76615	13492	1820	1055	6190312
50	NIC22R135-37	379.97	-0.333	123641	2061931	162293	494182	78268.33	141196	-0.059	196623	4175036	2756	11786	19010	30053	1615919	96703	194199	30189	14578	0.713	9448364
51	NIC22RCC-13-15	380.2	-3045	75890	1400877	89374	276756	65941.6	76448	0.892	167669	2387196	2413	7775	10226	12911	1057327	48880	87435	19666	10867	0.462	5794608
52	NIC22R1-78-80	380.3	-0.231	122429	2332736	163904	559725	82202.77	155666	-1654	199325	5070283	6578	21042	26632	39691	1997417	140094	303866	38559	21665	1900	11281578
53	NIC22R-1118-120	380.8	-1324	94344	1822371	73240	250800	86552.15	73031	0.253	169440	1875979	0.539	7770	10054	9447	1319965	60737	116017	10901	6511	1535	5987371
54	NIC22R1-138-140	381.1	1335	174342	3381964	231355	1023872	55068.77	335035	-1646	180972	10370.36	16442	28217	42573	84826	2165883	260199	337894	88666	25546	4151	8437565
55	NIC22R2-0-2	381.12	-1851	59794	1344109	71294	165494	67349.8	48135	0.029	130286	1353339	0.583	5626	7149	8692	946869	42320	48453	8931	3790	0.203	4309781
56	NIC22R2-19-21	381.31	7633	80066	4907717	110703	626909	42735.14	201696	-1147	138656	5800280	6121	15612	20552	47523	1534150	115990	163473	55573	13331	2590	13890163
57	NIC22R2-65-67	381.87	-1426	65539	1428892	86061	291868	62192.73	80496	-0.594	131845	2328242	0.944	6573	10983	15563	1126516	70380	88060	17555	8257	-0.003	5818386
58	NIC22R2-105-107	382.2	0.422	108221	3010772	103574	514334	79780.82	139732	-0.902	186487	4275385	3133	9029	16538	32112	1407293	85822	149854	26133	12843	0.829	10161081
59	NIC22R2-145-147	382.57	5152	103749	4675228	139548	702536	38899.59	236684	-0.046	140826	6362026	11962	16493	38253	54922	1208128	126654	151117	61679	16880	2137	14092694
60	NIC22R3-3-5	382.65	-1480	69439	1787189	95806	195194	78692.45	65479	-0.615	172151	1955740	0.837	7281	11142	10228	1313371	57345	90728	11572	4344	0.776	5924222
61	NIC22R3-38-40	383	0.692	86771	1898453	78937	268166	89286.82	70855	-0.39	195733	2064223	0.975	6595	8364	10942	1308321	64946	101955	12102	6132	0.128	6271783
62	NIC22R3-78-80	383.4	1797	95091	2079072	102388	343232	89808.12	86101	-0.41	197040	2471227	0.603	7210	9797	15812	1403820	76725	141636	17364	12716	0.507	7150837
63	NIC22R3-117-119	383.79	6999	98664	4496289	121691	701567	39387.89	225413	-0.024	138634	6914051	8919	15687	53508	59682	1337595	136301	162867	62448	14795	2580	14597078
64	NIC22R4-33-35	384.43	-2058	94798	2138363	97981	447452	80817.12	131720	-1094	193261	3742901	1127	12449	24084	27376	1770706	107132	205851	25659	17977	-0.317	9116552
65	NIC22R4-75-77	384.87	2497	110303	1867583	61659	270578	86744.45	64492	-0.273	176968	1948327	-0.808	3886	7849	11053	1156182	59906	84384	4964	1493	-0.048	5918867
66	NIC22R4-115-117	385.27	0.448	116431	2188410	105625	426731	87695.96	99785	-0.095	186496	3306928	3191	9248	15419	19743	1654365	91003	187550	23684	15939	1416	8539660
67	NIC22R4-148-150	385.6	-0.445	114295	1993797	103279	383179	83997.59	87646	-0.669	171060	2576888	0.394	9139	16736	15738	1349511	72092	119717	8645	3784	0.59	7117549
68	NIC22R5-13-15	385.75	-1042	86226	2215816	72356	311753	88115.43	76200	-0.749	177622	2354679	1150	7864	13959	14319	1437708	70820	127915	9967	9372	0.548	7074879
69	NIC22R5-55-57	386.17	3031	110393	2447868	125437	640108	69914.16	194554	-2194	177786	5916185	7117	17720	21342	37032	1699926	129580	207395	45889	17487	1284	11867854
70	NIC22R5-71-75	386.35	1677	102985	2461535	131354	392295	87248.99	99766	-1798	179486	3004955	2403	8555	17439	19439	1478096	81841	139783	13618	11508	0.915	8238387
71	NIC22R5-113-115	386.75	-1551	88790	2203229	110535	508612	64285.21	151680	-1161	158972	5004064	6139	13656	19443	33313	1760476	115762	197543	42220	14605	1544	10491856
72	NIC22R6-0-2	387.06	5277	126227	2438239	273815	634152	75943.37	156386	-1197	178609	5185765	6766	14306	20422	42053	1713927	115784	179192	39047	18013	1521	11224247
73	NIC22R6-38-40	387.44	-0.129	79475	1690281	64089	253646	87384.41	67420	0.06	167650	1897206	0.677	5703	55869	14897	1254178	64313	85102	9112	7540	-0.022	5803866
74	NIC22R6-80-82	387.86	1274	122756	2637057	194880	697761	73725.52	185910	-1547	194747	6208013	6310	18541	27648	48928	2220659	145409	313095	47313	20570	1128	13164178
75	NIC22R6-118-120	388.24	-4688	83279	1684656	116529	362736	73728.05	90942	0.062	181113	2919972	2594	8846	13749	19584	1421513	76352	138027	20741	11995	0.866	7221669
76	NIC22R7-13-17	388.5	-4292	109533	1718720	122713	359807	92931.13	84756	-0.891	197423	2717942	1252	8371	14182	17441	1670096	81571	171406	17591	13480	0.904	7394923
77	NIC22RCC-15-17	388.8	0.022	114789	2082517	138834	506175	81944.27	126780	-1513	183940	3853090	3827	11538	15590	27372	1620471	102388	209034	26381	13533	0.28	9116691
78	NIC23R1-32-34	389.54	-3212	99994	1472152	165666	377775	83266.06	95890	-1454	169793	2878689	3949	10112	15924	17413	1623977	81424	173211	17738	5222	0.132	7287529
79	NIC23R1-70-74	389.94	-0.242	103003	1999455	189626	463493	88893.31	103318	-0.274	175758	3653032	1431	9234	14756	24403	1877064	103333	178846	22394	14999	1514	9024552
80	NIC23R1-110-112	390.32	-4546	96768	1718309	105901	351650	91779.29	85172	-2184	186289	2712823	0.761	7111	11663	17584	1734480	85004	162047	18669	14620	1890	7395030
81	NIC23R1-148-150	390.7	-0.343	79670	1493260	152836	370697	63458.35	106716	-0.564	136337	3668412	3181	9052	18626	17446	1238409	76474	129779	30035	14257	0.912	7608645
82	NIC23R2-20-22	390.92	-0.187	111593	1685773	110140	464957	79866.25	117462	-1063	168718	3598509	1632	10403	14638	24105	1550561	86353	174162	22141	8782	1138	8229870
83	NIC23R2-60-62	391.32	-1971	72932	1189586	75210	189334	74152.24	46635	0.841	142766	1368122	0.992	5141	7599	6163	1060848	47852	86439	6171	7924	0.212	4384905
84	NIC23R2-99-101	391.71	-2178	98071	1839727	119120	337934	89269.88	89235	-0.989	169433	2937217	0.856	10524	15588	19065	2042627	96362	193514	17950	15047	0.645	8088506
85	NIC23R-2-140-142	392.13	-4910	102053	1593739	96237	276670	91692.25	61965	-2252	174164	2111250	1175	5460	10932	9917	1458776	63541	122885	9962	3023	0.337	6186280
86	NIC23R3-23-25	392.45	1123	108954	2090795	88594	391992	91748.29	86810	-2521	176886	3018341	1119	8734	13827	19194	1551457	76109	150806	16199	12713	0.714	7902881
87	NIC23R3-64-66	392.86	1485	149668	3063715	179841	854368	60674.65	305889	-2174	152336	8420346	8284	33265	42247	59770	2207110	176335	323297	76640	27228	3125	16143450
88	NIC23R3-115-117	393.37	-2613	68290	1271863	78333	183549	80941.45	48245	0.107	147866	1469207	-0.038	13690	22044	11477	1256036	52970	92850	6069	8192	-0.925	4809009
89	NIC23R3-148-150	393.7	2691	114287	1718528	142835	403833	81967.99	97373	-1098	161125	2764723	1758	28786	31528	21831	1402349	78954	114068	25175	7870	0.592	7198585
90	NIC23R4-18-20	393.9	-3541	100779	1689055	94543	281329	93622.02	72120	-0.584	168410	2128255	-0.763	31183	14648	15503	1623871	76936	144346	15692	13963	0.422	6560713
91	NIC23R4-45-47	394.17	8632	12545	5887934	224771	471333	40415.12	150067	-0.651	110592	4604216	4298	81803	18392	32770	1192166	98584	140883	38388	12990	3351	13134129
92	NIC23R4-86-88	394.58	8031	26086	7128097	133782	488266	37449.73	184593	0.409	85577	4617518	3384	22336	21630	43847	1060785	122255	167968	41634	12821	3389	14209449
93	NIC23R4-125-127	394.97	1189	122901	2125784	79088	509454	82063.38	116782	0.977	155678	3453113	2605	10493	30377	28067	1303225	88853	105182	22629	6164	1209	8244857
94	NIC23R5-10-12	395.32	1001	153276	1909730	93745	592219	85130.64	141341	-1431	161933	4115909	2680	13590	23035	34078	1516079	101910	158524	35261	7342	2316	9147669
95	NIC23R5-53-55	395.75	-1206	95306	1383414	100986	266081	92655.31	73569	-0.037	162736	1966189	-0.672	11374	16243	9346	1465203	67600	114949	9313	3247	-0.184	5837004
96	NIC23R5-93-95	396.15	-2239	87689	1582673	126048	369805	76366.38	96738	-1882	150428	2705882	2105	16352	16136	21773	1467973	75846	144354	23040	6271	0.328	6965359
97	NIC23R5-135-137	396.57	7113	108960	1899685	186054	603718	67646.52	187223	-1300	119775	5105472	14740	64891	33959	41449	2583285	163230	315125	55229	21542	2278	11580075
98	NIC23R6-15-17	396.87	-0.642	118351	1686545	128120	370699	93064.13	79622	-1600	169803	2484421	-0.168	12531	10862	23021	1790670	87592	207055	17923	12189	-0.081	7290867
99	NIC23R6-55-57	397.27	7287	85667	1723183	213009	319179	87261.59	77055	-0.52	164507	2039156	2388	10590	9395	15089	1580556	83454	145560	16291	9155	0.197	6588782
100	NIC23R6-95-97	397.67	-1153	85210	1869510	137575	310564	73976.4	94622	-0.4	142982	2390757	0.384	13929	12455	18670	1712742	78929	156932	19067	10731	0.378	7127499
101	NIC23R6-125-127	397.97	0.589	101983	1476823	120400	439060	53396.21	159922	-1441	99131	4363800	6336	43592	24514	31852	1941643	132938	188272	43947	18101	1310	9245580
102	NIC23R7-13-15	398.5	0.062	79787	1452206	107868	214931	83898.14	72867	-1525	154029	1730781	-0.11	12062	9081	11447	1243757	58577	117400	8609	3206	1717	5360698
103	NIC24R1-23-25	399.05	0.885	93146	1824470	104304	271915	85260.05	81143	-0.822	172934	2403003	0.68	12064	17969	13981	1504433	78442	154357	18654	7764	0.922	6843841
104	NIC24R1-63-65	399.45	2401	133018	2105069	143918	612559	83728.61	135408	-1420	175573	4508937	1470	20586	33969	38984	1777504	121457	244772	32852	19590	2206	10192582
105	NIC24R1-103-105	399.85	-3271	77816	1445186	100446	227426	71054.71	65104	-0.662	138732	1840904	1936	17085	158157	14235	1237159	64868	107247	13865	9212	-0.068	5587161
106	NIC24R1-143-145	400.25	1352	144496	2732394	163421	609268	76267.13	205578	-1304	173855	6929470	4852	33595	37922	45960	2130345	145133	301395	59336	25346	1187	13819868
107	NIC24R2-23-25	400.53	1634	134090	2040108	155912	595149	78064.95	153201	-1455	165937	4236801	5301	41629	25193	32523	1806730	118918	204478	42055	16828	0.875	9853098
108	NIC24R2-63-65	400.93	-0.051	183501	1821801	145980	981475	70197.78	239013	-0.28	146271	6903500	7880	20059	32053	57708	1614604	130176	209476	56147	16888	1931	12638660
109	NIC24R2-103-105	401.33	-5338	91083	1570109	97782	281185	86667.42	72156	-0.974	156008	2160893	-0.082	8925	9312	18093	1421574	73972	127436	10810	11589	-0.325	6192255
110	NIC24R2-143-145	401.73	1086	80372	1512125	92404	285743	77389.74	72352	-0.207	133846	2205897	0.062	8530	12433	14630	1448753	68326	128793	12284	6417	0.187	6161381
111	NIC24R3-3-5	401.83	0.416	91975	1633006	114756	292778	87771.77	88310	1164	153664	2505750	1968	9967	14788	13997	1494130	69943	126720	9893	9340	-0.117	6719921
112	NIC24R3-23-25	402.03	-3797	113833	1497617	149251	406301	91749.07	86072	-1864	164523	2917478	0.514	9853	23271	25060	1950844	90216	228249	17171	18242	1212	7785282
113	NIC24R3-43-45	402.23	1817	81018	1272057	92561	238764	84186.63	62126	0.317	156541	1845772	-1023	7246	11463	13214	1575228	69939	143907	9616	7217	0.291	5671650
114	NIC24R3-63-65	402.43	-2099	101558	1478079	102410	304481	95258.69	80826	-1307	156805	2191469	-1810	7387	8518	17383	1870473	86626	160380	10930	11570	0.809	6678938
115	NIC24R3-83-85	402.63	-4975	114042	1350189	112281	505901	78686.87	104311	-0.75	142748	3126554	0.692	9873	11517	27641	1401630	83101	146966	16458	14230	0.75	7241155
116	NIC24R3-105-107	402.85	3881	108877	1625613	95498	331056	95495.77	91768	-0.88	163809	2483104	-1278	7917	9416	17585	1681454	78858	175313	16515	20335	1419	7006635
117	NIC24R3-123-125	403.03	-3703	81134	1390535	138067	280439	73127.97	70754	0.06	125885	2132754	0.654	9794	8536	15090	1429428	65984	135154	14103	9684	0.662	5976767
118	NIC24R3-143-145	403.23	-1293	109206	1624295	112480	419373	95212.77	85809	-0.615	155416	2565602	0.11	11974	10063	21695	1583129	81829	138074	16576	14123	1554	7045117
119	NIC24R4-23-25	403.53	0.101	144830	1715186	155639	694327	78497.88	156530	0.834	143425	4414665	1266	21595	17829	45481	1710555	115482	152898	34305	12546	2331	9617389
120	NIC24R4-60-62	403.9	-3669	128255	1339804	130952	531484	89703.95	122954	-0.799	133186	3546744	2611	26062	17192	31174	2222656	108534	194353	27233	20392	1149	8670769

Nr	Mg NMS	Al NMS	Si NMS	S NMS	K NMS	Ca NMS	Ti NMS	Cr NMS	Mn NMS	Fe NMS	Ni NMS	Cu NMS	Zn NMS	Rb NMS	Sr NMS	Zr NMS	Ba NMS	Co NMS	V NMS	Ga NMS	
1	0.022903	0.950951	17.74477	0.996682	5.025505	0.492862	1.628763	-5.6E-06	1.396662	49.678	0.063603	0.187699	0.224504	0.309035	17.1048	1.180499	2.35082	0.456116	0.174458	0.011376	100
2	4.31E-06	0.91939	23.88246	1.578916	4.726909	0.52204	1.600232	-0.00766	1.799991	43.17044	0.078419	0.169695	0.253224	0.292392	16.89938	1.057437	2.396403	0.401936	0.231074	0.02732	100
3	0.014918	1.197827	20.36244	1.48032	4.858201	0.784785	1.598209	-8.6E-06	2.16782	44.60097	0.052415	0.16759	0.193792	0.235621	18.6717	1.119606	1.968986	0.34661	0.165377	0.01283	100
4	0.017561	1.302735	22.02149	1.149976	4.798739	0.867145	1.47777	-2.9E-06	2.352564	42.16638	0.043285	0.15035	0.184392	0.263767	19.53829	1.083304	2.075106	0.264652	0.222046	0.020443	100
5	0.053209	1.396186	21.31376	1.307049	4.671826	0.921043	1.543121	-2.2E-06	2.551768	43.60798	0.039136	0.132184	0.205205	0.196476	18.97883	1.018444	1.619348	0.274747	0.169682	1.11E-05	100
6	0.011378	0.940579	16.2567	1.132581	5.012726	0.452013	1.623122	2.26E-07	1.405564	51.9888	0.058323	0.184282	0.201495	0.296863	16.33565	1.077433	2.367932	0.431928	0.205096	0.017535	100
7	-0.00988	0.959903	19.0651	1.154731	4.983414	0.561747	1.674707	1.59E-07	1.823795	50.14092	0.058134	0.180054	0.194994	0.28361	15.32871	1.044319	2.036868	0.358357	0.142051	0.018475	100
8	6.16E-06	1.167818	20.94281	1.504952	5.028151	0.797949	1.372082	-0.01658	2.284788	44.03006	0.034917	0.188829	0.197058	0.293149	18.30173	1.081926	2.229483	0.364016	0.196843	6.56E-06	100
9	0.012281	0.695627	17.20969	1.213302	4.477687	0.385089	1.516902	-0.00846	1.078757	47.9053	0.061502	0.243453	0.233523	0.322189	19.87105	1.223125	2.893208	0.450927	0.197055	0.017795	100
10	0.05367	1.048259	22.09555	1.029705	4.599496	0.647983	1.471282	-0.01013	1.835823	44.54239	0.05638	0.16963	0.209135	0.294123	17.84603	1.043861	2.514079	0.357551	0.195182	7.81E-06	100
11	0.039947	1.003091	21.84341	1.306481	4.57902	0.651669	1.495723	-3.5E-06	1.953357	44.53842	0.075841	0.192215	0.218799	0.229625	17.975	1.12124	2.278525	0.361104	0.136519	6.5E-06	100
12	0.055088	1.242573	22.37053	1.128195	5.161361	0.684861	1.478804	-0.01219	2.336714	46.10357	0.060965	0.145154	0.172397	0.297885	15.01687	0.995677	2.181593	0.360298	0.204462	0.0152	100
13	0.020588	1.003465	17.62434	1.32077	5.028255	0.516855	1.735823	-0.01726	1.708275	48.99693	0.068868	0.260454	0.233108	0.303476	16.90684	1.12347	2.521569	0.403525	0.222565	0.018077	100
14	-0.01578	1.098582	19.90651	1.374658	5.066666	0.747619	1.438726	-0.01602	2.02938	42.95289	0.039298	0.169767	0.225141	0.248962	20.81311	1.142424	2.295719	0.333835	0.136479	0.012029	100
15	-1.2E-06	1.100966	19.87797	1.796645	5.113985	0.650376	1.512907	-0.01657	1.957399	47.00394	0.044759	0.169571	0.198763	0.271071	16.40883	1.076327	2.267445	0.376517	0.174098	0.014996	100
16	0.02074	0.901479	23.12241	1.064178	4.798776	0.539891	1.457658	-0.00812	1.596343	44.69331	0.050024	0.161172	0.214145	0.325036	16.89939	1.206682	2.338759	0.404178	0.197397	0.016702	100
17	0.019459	0.873012	19.85157	1.53199	5.229429	0.541818	1.624583	-1.1E-07	1.583358	47.89636	0.054126	0.197295	0.215463	0.310943	16.36122	1.110258	2.042902	0.373766	0.160977	0.021479	100
18	9.78E-07	1.279013	25.7558	1.424166	4.465351	1.175544	1.188548	-0.03051	2.932451	35.6584	0.025928	0.130143	0.1902	0.220209	21.70166	1.102485	2.382296	0.220775	0.177544	-1.5E-06	100
19	-0.02383	1.206223	21.26748	1.457809	5.066899	0.897271	1.428741	-4.6E-06	2.383603	44.65357	0.058619	0.180037	0.215211	0.243051	17.62753	1.05993	1.915376	0.232364	0.130115	1.05E-05	100
20	0.041036	0.514505	32.23837	1.451118	3.457221	0.371325	1.274953	-0.0081	1.038679	40.24744	0.114412	0.180429	0.229174	0.242219	15.26095	0.933139	1.827339	0.4222	0.147884	0.015736	100
21	-0.03688	0.93587	21.5549	1.172662	5.260979	0.739177	1.492087	6.91E-06	1.889371	44.01641	0.051813	0.156963	0.203122	0.264429	18.42478	1.181311	2.184888	0.362289	0.121034	0.024788	100
22	0.01911	1.012976	22.76718	1.944222	4.98366	0.823715	1.418548	-0.03349	2.001737	39.78728	0.030437	0.16256	0.176988	0.304905	20.4174	1.215404	2.455556	0.320026	0.178744	0.01304	100
23	-3.7E-06	1.40308	19.83301	1.959172	5.651486	0.963226	1.564253	-0.02248	2.317263	40.34103	0.040061	0.166031	0.202223	0.258927	20.98112	1.253103	2.608889	0.318548	0.161056	3.06E-07	100
24	0.021363	1.091519	27.86677	1.13237	4.508287	1.137584	1.196277	1.05E-05	2.661655	33.80464	0.03938	0.14449	0.161843	0.177036	22.5356	1.115433	1.971698	0.214099	0.205624	0.01432	100
25	3.98E-06	1.262589	25.40941	1.208263	5.340944	1.133852	1.378423	-6.8E-07	3.016325	36.8603	1.06E-05	0.139037	0.471542	0.251667	20.2334	1.067598	1.842913	0.236618	0.133115	0.013998	100
26	0.018376	1.282408	24.98815	2.165774	5.275464	0.966369	1.385948	-3.6E-06	2.345296	39.91334	0.024032	0.120892	0.174367	0.27523	17.60767	1.007085	2.069228	0.288613	0.078903	0.01286	100
27	1.1E-05	1.014113	23.38706	1.500844	5.022702	0.84786	1.483706	-1.8E-07	2.202184	42.83034	0.046401	0.126136	0.194289	0.244529	17.93942	1.09177	1.703897	0.269022	0.093125	1.24E-05	100
28	0.029258	1.016674	19.83092	1.047664	5.160863	0.512522	1.590673	-6.5E-06	1.326249	47.45817	0.055702	0.251125	0.252959	0.354923	16.91817	1.265139	2.437193	0.348573	0.131112	0.012123	100
29	0.036979	0.760713	31.78297	1.144149	4.732951	0.328635	1.548144	-4.3E-06	1.056917	42.60589	0.071572	0.176857	0.22493	0.36286	11.88495	1.040655	1.699674	0.37014	0.149723	0.021304	100
30	-0.08878	1.40829	24.05784	1.365966	5.563035	1.271463	1.368661	-0.01884	2.739603	37.71535	0.031514	0.219356	0.188875	0.245723	20.25962	1.016363	2.252891	0.214731	0.184986	9.86E-06	100
31	-0.0401	1.594226	24.57909	1.389918	5.672992	1.280332	1.404057	-1.2E-05	2.982087	37.48699	0.033256	0.208405	0.25886	0.246103	19.94236	1.070941	1.601711	0.224341	0.064421	1.3E-05	100
32	0.016271	1.204587	20.15321	1.439793	6.206533	0.575231	1.55236	-3.9E-06	1.410641	46.05324	0.055327	0.259039	0.195064	0.441062	16.02544	1.308552	2.546025	0.360027	0.178333	0.019271	100
33	5.87E-06	1.572091	29.36788	1.365972	4.613294	1.477317	1.195798	-9E-06	2.986688	32.24078	0.021352	0.163463	0.353573	0.207181	21.12185	1.064226	2.009431	0.151766	0.087339	-3.9E-06	100
34	2.48E-06	1.338521	22.47022	1.424358	5.324877	0.973848	1.405864	-1.9E-06	2.151164	41.85089	0.046049	0.210217	0.213066	0.2552	18.8376	1.024967	2.053477	0.297861	0.10846	0.013359	100
35	-0.09779	1.254024	20.62181	1.259858	5.23201	0.988629	1.354418	-7.9E-06	2.188364	43.00884	0.036988	0.13435	0.169814	0.325453	20.1339	1.148517	1.793556	0.291169	0.156081	4.39E-06	100
36	-0.01465	1.37397	21.94262	1.408304	5.223519	1.099646	1.2859	-0.01659	2.285431	38.72785	0.060878	0.169908	0.186835	0.249754	21.87244	1.195874	2.532988	0.25895	0.156354	1.11E-05	100
37	6.65E-06	1.436812	24.54513	1.410761	4.862248	1.438251	1.173551	-5.1E-08	3.09847	32.51125	0.036855	0.191603	0.161464	0.222132	25.37138	1.203961	2.074851	0.196301	0.064976	1.8E-06	100
38	-0.04225	1.558198	24.0081	1.581814	5.044449	1.534383	1.208657	-0.017	3.212882	30.15114	4.99E-06	0.221816	0.294023	0.244201	27.1065	1.210162	2.392112	0.158123	0.132662	1.01E-05	100
39	0.017361	1.051683	18.78821	1.083631	5.556721	0.475268	1.584301	-0.01619	1.255404	50.00177	0.060037	0.261689	0.232258	0.359062	15.02973	1.257633	2.355005	0.455925	0.172137	0.018368	100
40	3.4E-06	1.288336	24.50763	1.524537	4.619575	1.335731	1.174879	-1.3E-05	2.672383	33.4492	0.021443	0.218952	0.174596	0.225811	24.72281	1.205767	2.437268	0.266058	0.155044	1.28E-06	100
41	-0.01753	1.382887	20.84615	1.285028	5.922084	0.740291	1.64281	-6.4E-06	1.705947	46.58393	0.053462	0.187693	0.192225	0.303311	15.48385	1.091493	2.04398	0.401889	0.139171	0.011335	100
42	-1.1E-07	1.177851	30.00559	1.714518	4.140048	1.229185	0.995762	-0.02364	2.541325	31.07555	0.028842	0.156534	0.210078	0.2051	22.78757	1.129175	2.299379	0.208964	0.118161	1.06E-05	100
43	-0.02967	1.420533	27.91257	1.695031	4.311226	1.160691	1.119941	-0.02056	2.558011	33.46741	0.025683	0.178779	0.218606	0.215947	22.14304	1.120055	2.193381	0.195029	0.099947	0.014355	100
44	5.7E-06	1.004705	23.22731	1.229393	4.401589	0.949731	1.158366	-0.02702	1.99914	37.10916	0.039213	0.413721	0.22327	0.239166	24.22985	1.159879	2.222765	0.274573	0.145175	8.6E-06	100
45	0.038776	0.87867	17.51973	1.094212	5.117508	0.490319	2.249781	-4.2E-06	1.298457	50.0826	0.076172	0.398106	0.240756	0.326689	16.03095	1.369965	2.152373	0.448335	0.175421	0.011177	100
46	-0.02223	1.207322	28.34655	2.465939	4.456282	1.331418	1.199045	-0.01723	3.19661	31.62318	0.029468	0.428635	0.214193	0.240369	21.73606	1.143286	2.003286	0.240153	0.177662	8.49E-06	100
47	0.043007	1.063274	27.68423	1.081205	4.380796	1.125619	1.294695	-0.01525	2.826818	36.93869	0.045314	0.288085	0.187894	0.240268	19.72915	1.060025	1.606633	0.306115	0.099066	0.014359	100
48	0.021565	1.187463	18.23201	1.162179	5.780347	0.574129	1.646374	-0.00899	1.620469	51.8216	0.07368	0.177061	0.283336	0.371332	13.23781	1.145143	1.996094	0.450106	0.20295	0.025338	100
49	-0.02415	1.187695	31.63915	1.046474	4.528625	1.199792	1.32814	1.58E-06	2.946362	34.73645	4.12E-06	0.121141	0.149459	0.245141	18.36239	1.031273	1.23766	0.217953	0.029401	0.017043	100
50	-3.5E-06	1.308597	21.82315	1.717684	5.230345	0.82838	1.494396	-6.2E-07	2.081027	44.18793	0.029169	0.124742	0.201199	0.318076	17.10263	1.023489	2.055372	0.319516	0.154291	7.55E-06	100
51	-0.05255	1.309666	24.17553	1.542365	4.776095	1.137982	1.319295	1.54E-05	2.893535	41.19685	0.041642	0.134176	0.176474	0.222807	18.24674	0.843543	1.508903	0.339384	0.187536	7.97E-06	100
52	-2E-06	1.085212	20.67739	1.452846	4.961407	0.728646	1.379825	-0.01466	1.766819	44.94303	0.058307	0.186516	0.236066	0.351821	17.70512	1.241794	2.69349	0.341787	0.192039	0.016842	100
53	-0.02211	1.575717	30.43691	1.223241	4.188817	1.445579	1.219751	4.23E-06	2.829957	31.33227	9E-06	0.129773	0.16792	0.157782	22.04582	1.014419	1.937695	0.182067	0.108746	0.025637	100
54	0.015822	2.06626	40.08223	2.741964	12.13469	0.652662	3.970755	-0.01951	2.144837	0.122907	0.194866	0.334421	0.504565	1.005337	25.55693	3.083816	4.004639	1.050848	0.302765	0.049197	100
55	-0.04295	1.387402	31.18741	1.654237	3.839963	1.56272	1.116878	6.73E-07	3.023031	31.40158	1.35E-05	0.13054	0.165879	0.201681	21.97024	0.981953	1.124257	0.207226	0.08794	4.71E-06	100
56	0.054953	0.576422	35.33232	0.796988	4.513331	0.307665	1.452078	-0.00826	0.998232	41.75818	0.044067	0.112396	0.147961	0.342134	11.04492	0.835051	1.176898	0.400089	0.095975	0.018646	100
57	-0.02451	1.126412	24.55822	1.479122	5.016305	1.0689	1.383476	-1E-05	2.266006	40.01525	1.62E-05	0.112969	0.188764	0.26748	19.36131	1.209614	1.527039	0.301716	0.141912	-5.2E-08	100
58	4.15E-06	1.065054	29.63043	1.019321	5.061788	0.785161	1.375169	-8.9E-06	1.835297	42.07608	0.030833	0.088859	0.162759	0.316029	13.84983	0.844615	1.474784	0.257187	0.126394	8.16E-06	100
59	0.036558	0.73619	33.17484	0.990215	4.983831	0.276027	1.67948	-3.3E-07	0.999284	45.14414	0.084881	0.117032	0.271439	0.38972	8.572726	0.898721	1.072307	0.437667	0.119778	0.015164	100
60	-0.02498	1.17212	30.16749	1.617191	3.294846	1.328317	1.105276	-1E-05	2.905883	33.0126	1.41E-05	0.122902	0.188075	0.172647	22.16951	0.967975	1.531475	0.195334	0.073326	1.31E-05	100
61	1.1E-05	1.383514	30.26975	1.258605	4.275754	1.423627	1.129742	-6.2E-06	3.120851	32.91286	1.55E-05	0.105154	0.133359	0.174464	20.86043	1.035527	1.625614	0.192959	0.097771	2.04E-06	100
62	0.02513	1.329788	29.07453	1.431832	4.799886	1.255911	1.204069	-5.7E-06	2.755482	34.55857	8.43E-06	0.100827	0.137005	0.221121	19.63155	1.072944	1.980701	0.242825	0.177825	7.09E-06	100
63	0.047948	0.675916	30.80267	0.833667	4.806215	0.269834	1.544234	-1.6E-07	0.949738	47.36599	0.061101	0.107467	0.366567	0.408863	9.163444	0.933755	1.115751	0.427812	0.101356	0.017675	100
64	-0.02257	1.039845	23.45583	1.074759	4.908128	0.886488	1.444845	-0.012	2.119891	41.0561	0.012362	0.136554	0.264179	0.300289	19.42297	1.175137	2.257992	0.281455	0.197191	-3.5E-06	100
65	0.042187	1.863583	31.55305	1.041736	4.571449	1.465558	1.0896	-4.6E-06	2.989896	32.91723	-1.4E-05	0.065654	0.13261	0.186742	19.53384	1.012119	1.425678	0.083867	0.025224	-8.1E-07	100
66	5.25E-06	1.363415	25.62643	1.236876	4.997049	1.026926	1.168489	-1.1E-06	2.183881	38.72435	0.037367	0.108295	0.180558	0.231192	19.37273	1.065653	2.196223	0.277341	0.186647	0.016581	100
67	-6.3E-06	1.60582	28.01241	1.451047	5.38358	1.180148	1.234217	-9.4E-06	2.403355	36.20471	5.54E-06	0.128401	0.235137	0.221115	18.96033	1.012879	1.682054	0.231639	0.053164	8.29E-06	100
68	-0.01473	1.218763	31.31949	1.022717	4.406478	1.245455	1.07705	-1.1E-05	2.510601	33.28225	0.016254	0.111154	0.197304	0.202392	20.32138	1.001007	1.808017	0.140879	0.132469	7.75E-06	100
69	0.02554	0.930185	20.62604	1.056948	5.393629	0.589105	1.639336	-0.01849	1.498047	49.8505	0.059969	0.149311	0.17983	0.312035	14.32379	1.091857	1.747536	0.386666	0.147348	0.010819	100
70	0.020356	1.250063	29.87885	1.594414	4.761794	1.059054	1.210989	-0.02182	2.178665	36.47504	0.029168	0.103843	0.21168	0.235956	17.94157	0.993417	1.696728	0.165299	0.139688	1.11E-05	100
71	-0.01478	0.846275	20.99942	1.053531	4.847684	0.612715	1.445695	-0.01107	1.515194	47.69474	0.058512	0.130158	0.185315	0.317513	16.77945	1.100349	1.882822	0.402407	0.139203	0.014716	100
72	0.047014	1.124592	21.72296	2.439495	5.64984	0.676601	1.393287	-0.01066	1.591278	46.20145	0.06028	0.127456	0.181945	0.374662	15.26986	1.031552	1.596472	0.347881	0.160482	0.013551	100
73	-2.2E-06	1.369346	29.12336	1.104247	4.370294	1.505624	1.16164	1.03E-06	2.888592	32.68866	1.17E-05	0.098262	0.962617	0.256674	21.60935	1.108106	1.466298	0.156999	0.129913	-3.8E-07	100
74	0.009678	0.9325	20.03207	1.480381	5.300453	0.560047	1.412242	-0.01175	1.479371	47.15838	0.047933	0.140844	0.210025	0.371675	16.86895	1.104581	2.378386	0.359407	0.156257	0.008569	100
75	-0.06492	1.153182	23.32779	1.613602	5.022883	1.020928	1.259293	8.59E-07	2.507911	40.43348	0.03592	0.122492	0.190385	0.271184	19.684	1.057263	1.911289	0.287205	0.166097	1.2E-05	100
76	-0.05804	1.481192	23.24189	1.659422	4.865595	1.256688	1.146138	-1.2E-05	2.66971	36.75416	0.016931	0.113199	0.19178	0.235851	22.58436	1.103068	2.317888	0.237879	0.182287	1.22E-05	100
77	2.41E-07	1.259108	22.84291	1.522855	5.552179	0.898838	1.390636	-0.0166	2.017618	42.26413	0.041978	0.126559	0.171005	0.300241	17.77477	1.123083	2.292872	0.28937	0.148442	3.07E-06	100
78	-0.04408	1.372125	20.20098	2.273281	5.183856	1.142583	1.315809	-0.01995	2.329912	39.50158	0.054188	0.138758	0.21851	0.238942	22.28433	1.117306	2.376814	0.243402	0.071657	1.81E-06	100
79	-2.7E-06	1.141364	22.15573	2.101223	5.135912	0.985016	1.144855	-3E-06	1.947554	40.47882	0.015857	0.102321	0.16351	0.270407	20.79953	1.145021	1.981772	0.248145	0.166202	0.016776	100
80	-0.06147	1.308555	23.236	1.432056	4.755221	1.241094	1.151747	-0.02953	2.519111	36.68441	1.03E-05	0.096159	0.157714	0.237781	23.45467	1.149475	2.191296	0.252453	0.1977	0.025558	100
81	-4.5E-06	1.047098	19.62583	2.008715	4.87205	0.83403	1.402562	-7.4E-06	1.79187	48.21373	0.041808	0.11897	0.2448	0.229292	16.27634	1.005094	1.705678	0.394748	0.187379	1.2E-05	100
82	-2.3E-06	1.355951	20.48359	1.338296	5.649627	0.970444	1.427264	-0.01292	2.050069	43.72498	0.01983	0.126405	0.177864	0.292896	18.84065	1.049263	2.116218	0.269032	0.106709	0.013828	100
83	-0.04495	1.663251	27.12912	1.715202	4.317858	1.69108	1.063535	1.92E-05	3.255851	31.20072	2.26E-05	0.117243	0.173299	0.14055	24.19318	1.091289	1.971285	0.140733	0.180711	4.83E-06	100
84	-0.02693	1.212474	22.74495	1.472707	4.177953	1.103663	1.103232	-1.2E-05	2.094738	36.31347	1.06E-05	0.130111	0.192718	0.235705	25.25345	1.191345	2.392457	0.22192	0.186029	7.97E-06	100
85	-0.07937	1.649667	25.76248	1.555652	4.472316	1.482187	1.001652	-0.0364	2.815327	34.12794	0.018994	0.08826	0.176714	0.160306	23.58083	1.027128	1.986412	0.161034	0.048866	5.45E-06	100
86	0.01421	1.378662	26.45611	1.121034	4.960115	1.160947	1.09846	-0.0319	2.238247	38.19292	0.014159	0.110517	0.174962	0.242873	19.63154	0.963054	1.908241	0.204976	0.160865	9.03E-06	100
87	0.009199	0.927113	18.97807	1.114018	5.292351	0.375847	1.894818	-0.01347	0.94364	52.15952	0.051315	0.206059	0.261697	0.370243	13.67186	1.092301	2.002651	0.474744	0.168663	0.019358	100
88	-0.05434	1.420043	26.44751	1.62888	3.816774	1.683121	1.003221	2.22E-06	3.074771	30.55114	-7.9E-07	0.284674	0.45839	0.238656	26.1184	1.101474	1.930751	0.126201	0.170347	-1.9E-05	100
89	0.037382	1.587632	23.87314	1.98421	5.609894	1.138668	1.352669	-0.01525	2.238287	38.40648	0.024421	0.399884	0.437975	0.303268	19.4809	1.096799	1.584589	0.349722	0.109327	8.22E-06	100
90	-0.05397	1.536098	25.74499	1.441048	4.288086	1.42701	1.099271	-8.9E-06	2.566947	32.43939	-1.2E-05	0.475299	0.223268	0.236301	24.75144	1.172677	2.200157	0.239181	0.212827	6.43E-06	100
91	0.065722	0.095515	44.82927	1.711351	3.588612	0.307711	1.142573	-5E-06	0.84202	35.05536	0.032724	0.622828	0.140032	0.249503	9.076856	0.750594	1.072648	0.292277	0.098903	0.025514	100
92	0.056519	0.183582	50.16449	0.9415	3.436206	0.263555	1.299086	2.88E-06	0.602254	32.49611	0.023815	0.157191	0.152223	0.308576	7.465349	0.860378	1.182087	0.293002	0.090229	0.02385	100
93	0.014421	1.490638	25.78315	0.95924	6.179052	0.995328	1.416422	1.18E-05	1.888183	41.88202	0.031595	0.127267	0.368436	0.340418	15.80652	1.077678	1.275729	0.274462	0.074762	0.014664	100
94	0.010943	1.675574	20.87669	1.024797	6.473988	0.930627	1.545104	-0.01564	1.770211	44.99408	0.029297	0.148562	0.251813	0.372532	16.57339	1.114054	1.732944	0.385464	0.080261	0.025318	100
95	-0.02066	1.63279	23.70075	1.7301	4.55852	1.587378	1.26039	-6.3E-07	2.788005	33.6849	-1.2E-05	0.19486	0.278276	0.160116	25.10197	1.158128	1.969315	0.159551	0.055628	-3.2E-06	100
96	-0.03214	1.25893	22.72206	1.809641	5.309203	1.096374	1.388844	-0.02702	2.159659	38.8477	0.030221	0.234762	0.231661	0.31259	21.07534	1.088903	2.072456	0.33078	0.090031	4.71E-06	100
97	0.061424	0.940927	16.40477	1.606674	5.213421	0.584163	1.616769	-0.01123	1.03432	44.08842	0.127288	0.560368	0.293254	0.357934	22.30802	1.409576	2.721269	0.476931	0.186026	0.019672	100
98	-8.8E-06	1.623277	23.1323	1.757267	5.084429	1.276448	1.092079	-0.02195	2.328982	34.0758	-2.3E-06	0.171873	0.148981	0.315751	24.56045	1.201393	2.839923	0.245828	0.167182	-1.1E-06	100
99	0.110597	1.300195	26.15328	3.232904	4.844279	1.324396	1.169488	-7.9E-06	2.496774	30.94891	0.036243	0.160728	0.142591	0.22901	23.98859	1.266607	2.209209	0.247254	0.138948	2.99E-06	100
100	-0.01618	1.195511	26.22954	1.9302	4.357265	1.037901	1.327562	-5.6E-06	2.006061	33.54272	5.39E-06	0.195426	0.174746	0.261943	24.03006	1.107387	2.201782	0.267513	0.150558	5.3E-06	100
101	6.37E-06	1.103046	15.97329	1.302244	4.748864	0.577532	1.729713	-0.01559	1.072199	47.19877	0.06853	0.47149	0.265143	0.344511	21.00077	1.437855	2.036346	0.47533	0.19578	0.014169	100
102	1.16E-06	1.48837	27.08987	2.012201	4.009385	1.56506	1.359282	-0.02845	2.873301	32.28649	-2.1E-06	0.225008	0.1694	0.213536	23.2014	1.092712	2.190013	0.160595	0.059806	0.032029	100
103	1.29E-05	1.361019	26.65857	1.524057	3.973135	1.245792	1.185635	-1.2E-05	2.526856	35.11191	9.94E-06	0.176275	0.262557	0.204286	21.98229	1.146169	2.255415	0.272566	0.113445	1.35E-05	100
104	0.023556	1.305047	20.65295	1.411988	6.009851	0.821466	1.328496	-0.01393	1.722557	44.23744	0.014422	0.20197	0.333272	0.382474	17.43919	1.191622	2.401472	0.322313	0.192199	0.021643	100
105	-0.05854	1.392765	25.8662	1.7978	4.070511	1.27175	1.165243	-1.2E-05	2.48305	32.94883	0.034651	0.30579	2.830722	0.254781	22.14289	1.161019	1.919526	0.248158	0.164878	-1.2E-06	100
106	0.009783	1.045567	19.77149	1.182508	4.408638	0.551866	1.487554	-0.00944	1.258008	50.14136	0.035109	0.243092	0.274402	0.332565	15.41509	1.050176	2.180882	0.429353	0.183403	0.008589	100
107	0.016584	1.360892	20.70524	1.582365	6.040222	0.792288	1.554851	-0.01477	1.68411	42.99968	0.0538	0.422497	0.255686	0.330079	18.33667	1.20691	2.075266	0.42682	0.170789	8.88E-06	100
108	-4E-07	1.451902	14.41451	1.155027	7.765657	0.555421	1.891126	-2.2E-06	1.15733	54.62209	0.062348	0.158711	0.253611	0.456599	12.77512	1.029983	1.657422	0.444248	0.133622	0.015279	100
109	-0.0862	1.470918	25.35601	1.579102	4.540914	1.39961	1.165262	-1.6E-05	2.519405	34.89671	-1.3E-06	0.144132	0.150381	0.292188	22.95729	1.194589	2.05799	0.174573	0.187153	-5.2E-06	100
110	0.017626	1.304448	24.54198	1.499729	4.637646	1.256045	1.174282	-3.4E-06	2.172338	35.80199	1.01E-06	0.138443	0.201789	0.237447	23.51345	1.10894	2.090327	0.199371	0.104149	3.04E-06	100
111	6.19E-06	1.368692	24.30097	1.707699	4.356867	1.306143	1.314152	0.017322	2.286694	37.28838	0.029286	0.14832	0.220062	0.208291	22.23434	1.040831	1.885736	0.147219	0.13899	-1.7E-06	100
112	-0.04877	1.462156	19.23652	1.917092	5.218835	1.178494	1.105573	-0.02394	2.113257	37.47428	6.6E-06	0.126559	0.29891	0.321889	25.0581	1.158802	2.931801	0.220557	0.234314	0.015568	100
113	0.032037	1.428473	22.42834	1.631994	4.20978	1.484341	1.095378	5.59E-06	2.760061	32.54383	-0.01804	0.127758	0.20211	0.232983	27.77372	1.233133	2.537304	0.169545	0.127247	5.13E-06	100
114	-0.03143	1.520571	22.13045	1.533327	4.558823	1.426255	1.210162	-0.01957	2.347753	32.81164	-0.0271	0.110601	0.127535	0.260266	28.00554	1.297003	2.40128	0.163649	0.173231	1.21E-05	100
115	-0.0687	1.574915	18.64605	1.550595	6.986469	1.086662	1.44053	-1E-05	1.971343	43.17756	9.56E-06	0.136346	0.159049	0.381721	19.35644	1.147621	2.029593	0.227284	0.196516	1.04E-05	100
116	0.05539	1.553913	23.20105	1.362965	4.724893	1.362933	1.30973	-1.3E-05	2.337913	35.43932	-0.01824	0.112993	0.134387	0.250976	23.99803	1.125476	2.5021	0.235705	0.290225	0.020252	100
117	-0.06196	1.35749	23.26567	2.310061	4.692152	1.223537	1.183817	1E-06	2.106239	35.68407	1.09E-05	0.163868	0.14282	0.252478	23.91641	1.104008	2.261323	0.235964	0.162027	1.11E-05	100
118	-0.01835	1.550095	23.05561	1.596567	5.952676	1.351472	1.217993	-8.7E-06	2.20601	36.41674	1.56E-06	0.169962	0.142837	0.307944	22.47129	1.161499	1.959854	0.235284	0.200465	0.022058	100
119	1.05E-06	1.505918	17.83422	1.618308	7.219496	0.816208	1.627573	8.67E-06	1.491309	45.90295	0.013164	0.224541	0.185383	0.472904	17.78606	1.200763	1.589808	0.356698	0.130451	0.024237	100
120	-0.04231	1.479165	15.45196	1.51027	6.129606	1.034556	1.418029	-9.2E-06	1.536034	40.90461	0.030113	0.300573	0.198275	0.35953	25.6339	1.251723	2.241474	0.314078	0.235181	0.013251	100

TABLE S1 BULK SEDIMENT δ13C AND ELEMENTAL COMPOSITION DATA (XRF ANALYSES) OF HOLE 1001B (REDOX CONDITIONS)

Ident	Depth (mbsf)	V NMS	Cr NMS	Ni NMS	Cu NMS	Zn NMS	Al NMS	V/Cr	Ni/Al	Ni/Al (10*-2)	Cu/Al	Cu/Al (10*-1)	Zn/Al	Zn/Al (10*-1)	V/Al	V/Al (10*-1)
NIC20R1-29-32	362.2	0.174458	-5.6E-06	0.063603	0.187699	0.224504	0.950951	-31219.2	0.066884	6.69	0.19738	1.97	0.236083	2.36	0.183456	1.83
NIC20R1-55-57	362.87	0.231074	-0.00766	0.078419	0.169695	0.253224	0.91939	-30.1513	0.085295	8.53	0.184574	1.84	0.275426	2.75	0.251334	2.51
NIC20R1-85-87	363.17	0.165377	-8.6E-06	0.052415	0.16759	0.193792	1.197827	-19296	0.043758	4.38	0.139911	1.39	0.161786	1.62	0.138064	1.38
NIC20R1-145-147	363.77	0.222046	-2.9E-06	0.043285	0.15035	0.184392	1.302735	-75954.2	0.033226	3.32	0.115411	1.15	0.141542	1.42	0.170446	1.7
NIC20R2-5-7	363.87	0.169682	-2.2E-06	0.039136	0.132184	0.205205	1.396186	-78861.6	0.02803	2.8	0.094675	0.95	0.146975	1.47	0.121533	1.21
NIC20R2-45-47	364.24	0.205096	2.26E-07	0.058323	0.184282	0.201495	0.940579	907971.4	0.062008	6.2	0.195924	1.96	0.214224	2.14	0.218053	2.18
NIC20R2-68-70	364.47	0.142051	1.59E-07	0.058134	0.180054	0.194994	0.959903	896150	0.060563	6.06	0.187575	1.88	0.203139	2.03	0.147985	1.48
NIC20R2-88-90	364.7	0.196843	-0.01658	0.034917	0.188828	0.197058	1.167818	-11.8753	0.029899	2.99	0.161693	1.62	0.16874	1.69	0.168556	1.68
NIC20R2-128-130	365.1	0.197055	-0.00846	0.061502	0.243453	0.233523	0.695627	-23.3035	0.088412	8.84	0.349976	3.49	0.335701	3.36	0.283277	2.83
NIC20R3-8-10	365.38	0.195182	-0.01013	0.05638	0.16963	0.209135	1.048259	-19.2683	0.053784	5.38	0.16182	1.62	0.199507	1.99	0.186196	1.86
NIC20R3-48-50	365.8	0.136519	-3.5E-06	0.075841	0.192215	0.218799	1.003091	-38546.1	0.075607	7.56	0.191623	1.92	0.218125	2.18	0.136098	1.36
NIC20R3-73-75	366.05	0.204462	-0.01219	0.060965	0.145154	0.172397	1.242573	-16.7711	0.049064	4.9	0.116817	1.17	0.138742	1.39	0.164547	1.64
NIC20R3-113-115	366.45	0.222565	-0.01726	0.068868	0.260454	0.233108	1.003465	-12.8955	0.06863	6.86	0.259555	2.59	0.232303	2.32	0.221797	2.21
NIC20R3-138-140	366.7	0.136479	-0.01602	0.039298	0.169767	0.225141	1.098582	-8.51675	0.035771	3.58	0.154533	1.54	0.204938	2.05	0.124232	1.24
NIC20R4-13-15	366.95	0.174098	-0.01657	0.044759	0.169571	0.198763	1.100966	-10.5072	0.040655	4.06	0.15402	1.54	0.180535	1.8	0.158132	1.58
NIC20R4-53-55	367.35	0.197397	-0.00812	0.050024	0.161172	0.214145	0.901479	-24.3082	0.055491	5.55	0.178787	1.79	0.237549	2.38	0.218971	2.19
NIC20R4-93-95	367.75	0.160977	-1.1E-07	0.054126	0.197295	0.215463	0.873012	-1454583	0.062	6.2	0.225994	2.26	0.246804	2.47	0.184393	1.84
NIC20R4-140-142	368.12	0.177544	-0.03051	0.025928	0.130143	0.1902	1.279013	-5.81899	0.020272	2.03	0.101752	1.02	0.148708	1.49	0.138814	1.39
NIC20R5-13-15	368.45	0.130115	-4.6E-06	0.058619	0.180037	0.215211	1.206223	-28396.5	0.048597	4.86	0.149257	1.49	0.178417	1.78	0.10787	1.08
NIC20R570-72NEW2	369.02	0.147884	-0.0081	0.114412	0.180429	0.229174	0.514505	-18.2486	0.222373	22.2	0.350685	3.51	0.445426	4.45	0.28743	2.87
NIC20R5-120-122	369.52	0.120926	6.91E-06	0.051813	0.156963	0.203122	0.93587	17510.47	0.055363	5.54	0.167719	1.68	0.217041	2.17	0.129328	1.29
NIC20R5-148-150	369.8	0.178744	-0.03349	0.030437	0.16256	0.176988	1.012976	-5.33657	0.030048	3	0.160478	1.6	0.174721	1.74	0.176454	1.76
NIC20R6-9-11	369.91	0.161056	-0.02248	0.040061	0.166031	0.202223	1.40308	-7.16536	0.028552	2.86	0.118333	1.18	0.144128	1.44	0.114787	1.15
NIC20R6-50-52	370.32	0.205624	1.05E-05	0.03938	0.14449	0.161843	1.091519	19645.52	0.036078	3.61	0.132375	1.32	0.148274	1.48	0.188383	1.88
NIC20R6-90-92	370.72	0.133115	-6.8E-07	1.06E-05	0.139037	0.471542	1.262589	-194942	8.4E-06	0.08	0.110121	1.1	0.373472	3.73	0.10543	1.05
NIC21R1-31-33	372.33	0.078903	-3.6E-06	0.024032	0.120892	0.174367	1.282408	-21730.8	0.01874	1.87	0.094269	0.94	0.135968	1.36	0.061527	0.61
NIC21R1-70-74	372.74	0.093125	-1.8E-07	0.046401	0.126136	0.194289	1.014113	-514643	0.045755	4.58	0.12438	1.24	0.191586	1.92	0.091829	0.92
NIC21R1-108-110	373.1	0.131112	-6.5E-06	0.055702	0.251125	0.252959	1.016674	-20160.7	0.054789	5.48	0.247006	2.47	0.24881	2.49	0.128962	1.29
NIC21R1-133-135	373.35	0.149723	-4.3E-06	0.071571	0.176857	0.22493	0.760713	-35078.4	0.094084	9.41	0.232488	2.32	0.295683	2.96	0.196819	1.97
NIC21R2-30-32	373.67	0.184986	-0.01884	0.031515	0.219358	0.188875	1.40829	-9.81779	0.022378	2.24	0.155762	1.56	0.134117	1.34	0.131355	1.31
NIC21R2-69-73	374.08	0.064421	-1.2E-05	0.033256	0.208405	0.25886	1.594226	-5301.56	0.02086	2.09	0.130725	1.31	0.162373	1.62	0.040409	0.4
NIC21R2-110-112	374.49	0.178333	-3.9E-06	0.055327	0.259039	0.195064	1.204587	-46232.1	0.04593	4.59	0.215044	2.15	0.161934	1.62	0.148045	1.48
NIC21R3-10-12	374.82	0.087339	-9E-06	0.021352	0.163463	0.353573	1.572091	-9710.2	0.013582	1.36	0.103978	1.04	0.224906	2.25	0.055556	0.56
NIC21R3-50-52	375.24	0.10846	-1.9E-06	0.046049	0.210217	0.213066	1.338521	-56279.5	0.034403	3.44	0.157052	1.57	0.15918	1.59	0.08103	0.81
NIC21R3-71-74	375.44	0.156081	-7.9E-06	0.036988	0.13435	0.169814	1.254024	-19718.4	0.029496	2.95	0.107135	1.07	0.135416	1.35	0.124464	1.24
NIC21R3-110-112	375.88	0.156354	-0.01659	0.060878	0.169908	0.186835	1.37397	-9.42402	0.044308	4.43	0.123662	1.24	0.135982	1.36	0.113797	1.13
NIC21R3-148-150	376.2	0.064976	-5.1E-08	0.036855	0.191603	0.161464	1.436812	-1277000	0.025651	2.56	0.133353	1.33	0.112377	1.12	0.045222	0.45
NIC21R4-3-5	376.25	0.132662	-0.017	4.99E-06	0.221816	0.294023	1.558198	-7.80571	3.2E-06	0.03	0.142354	1.42	0.188694	1.89	0.085138	0.85
NIC21R4-42-44	376.64	0.172137	-0.01619	0.060037	0.261689	0.232258	1.051683	-10.6297	0.057087	5.71	0.248829	2.49	0.220844	2.21	0.163677	1.64
NIC21R4-76-78	376.98	0.155044	-1.3E-05	0.021443	0.218951	0.174596	1.288336	-12135.9	0.016644	1.66	0.169948	1.69	0.13552	1.36	0.120344	1.2
NIC21R4-98-100	377.2	0.139171	-6.4E-06	0.053462	0.187693	0.192225	1.382887	-21728.8	0.038659	3.87	0.135725	1.36	0.139003	1.39	0.100638	1
NIC21R4-138-140	377.62	0.118161	-0.02364	0.028842	0.156534	0.210078	1.177851	-4.99767	0.024487	2.45	0.132898	1.33	0.178357	1.78	0.100319	1
NIC21R5-0-2	377.73	0.099947	-0.02056	0.025683	0.178779	0.218606	1.420533	-4.86039	0.01808	1.81	0.125854	1.26	0.15389	1.54	0.070359	0.7
NIC21R5-60-62	378.32	0.145175	-0.02702	0.039213	0.413721	0.22327	1.004705	-5.37358	0.039029	3.9	0.411784	4.12	0.222225	2.22	0.144496	1.44
NIC21R5-120-122	378.92	0.175421	-4.2E-06	0.076172	0.398106	0.240756	0.87867	-41650.4	0.086691	8.67	0.453078	4.53	0.274001	2.74	0.199644	1.99
NIC21R5-140-142	379.12	0.177662	-0.01723	0.029468	0.428635	0.214195	1.207322	-10.3093	0.024408	2.44	0.355029	3.55	0.177413	1.77	0.147154	1.47
NIC21R6-5-7	379.27	0.099066	-0.01525	0.045314	0.288085	0.187894	1.063274	-6.49815	0.042617	4.26	0.270942	2.71	0.176713	1.77	0.093171	0.93
NIC21R6-40-42	379.6	0.20295	-0.00899	0.07368	0.177061	0.283336	1.187463	-22.5853	0.062048	6.2	0.149109	1.49	0.238606	2.39	0.17091	1.71
NIC21R6-85-87	379.9	0.029401	1.58E-06	4.12E-06	0.121141	0.149459	1.187695	18571.43	3.47E-06	0.03	0.101997	1.02	0.12584	1.26	0.024754	0.25
NIC22R135-37	379.97	0.154291	-6.2E-07	0.029169	0.124741	0.201199	1.308597	-247085	0.02229	2.23	0.095324	0.95	0.153752	1.54	0.117906	1.18
NIC21RCC-13-15	380.2	0.187536	1.54E-05	0.041642	0.134176	0.176474	1.309666	12182.74	0.031796	3.18	0.102451	1.02	0.134748	1.35	0.143194	1.43
NIC22R1-78-80	380.3	0.192039	-0.01466	0.058307	0.186516	0.236066	1.085212	-13.0985	0.053729	5.37	0.171871	1.72	0.21753	2.18	0.17696	1.77
NIC22R-1118-120	380.8	0.108746	4.23E-06	9E-06	0.129773	0.16792	1.575717	25735.18	5.71E-06	0.05	0.082358	0.82	0.106567	1.07	0.069013	0.69
NIC22R1-138-140	381.1	0.302765	-0.01951	0.194867	0.334421	0.504565	2.06626	-15.52	0.094309	9.43	0.161849	1.62	0.244192	2.44	0.146528	1.46
NIC22R2-0-2	381.12	0.08794	6.73E-07	1.35E-05	0.13054	0.165879	1.387402	130689.7	9.75E-06	0.09	0.09409	0.94	0.11956	1.19	0.063384	0.63
NIC22R2-19-21	381.31	0.095974	-0.00826	0.044067	0.112396	0.147961	0.576422	-11.6225	0.076449	7.64	0.194989	1.95	0.256688	2.57	0.1665	1.66
NIC22R2-65-67	381.87	0.139012	-1E-05	1.62E-05	0.112969	0.188764	1.126412	-13900.7	1.44E-05	0.14	0.100291	1	0.16758	1.68	0.125986	1.26
NIC22R2-105-107	382.2	0.126394	-8.9E-06	0.030833	0.088859	0.162758	1.065054	-14238.4	0.02895	2.89	0.083431	0.83	0.152817	1.52	0.118674	1.19
NIC22R2-145-147	382.57	0.119778	-3.3E-07	0.084881	0.117032	0.271439	0.73619	-366957	0.115297	1.15	0.15897	1.59	0.368707	3.68	0.1627	1.63
NIC22R3-3-5	382.65	0.073326	-1E-05	1.41E-05	0.122902	0.188075	1.17212	-7063.41	1.21E-05	0.21	0.104855	1.05	0.160457	1.6	0.062559	0.62
NIC22R3-38-40	383	0.097771	-6.2E-06	1.55E-05	0.105154	0.133359	1.383514	-15723.1	1.12E-05	0.12	0.076005	0.76	0.096392	0.96	0.070669	0.71
NIC22R3-78-80	383.4	0.177825	-5.7E-06	8.43E-06	0.100827	0.137005	1.329788	-31014.6	6.34E-06	0.06	0.075822	0.76	0.103028	1.03	0.133725	1.34
NIC22R3-117-119	383.79	0.101356	-1.6E-07	0.061101	0.107467	0.366567	0.675916	-616458	0.090398	9.04	0.158994	1.59	0.542325	5.42	0.149953	1.49
NIC22R4-33-35	384.43	0.197191	-0.012	0.012362	0.136554	0.264179	1.039845	-16.4324	0.011888	1.19	0.131321	1.31	0.254056	2.54	0.189635	1.89
NIC22R4-75-77	384.87	0.025224	-4.6E-06	-1.4E-05	0.065654	0.13261	1.863583	-5468.86	-7.3E-06	-0.07	0.03523	0.35	0.071159	0.71	0.013535	0.14
NIC22R4-115-117	385.27	0.186647	-1.1E-06	0.037367	0.108295	0.180558	1.363415	-167779	0.027407	2.74	0.079429	0.79	0.13243	1.32	0.136897	1.37
NIC22R4-148-150	385.6	0.053164	-9.4E-06	5.54E-06	0.128401	0.235137	1.60582	-5656.2	3.45E-06	0.03	0.07996	0.79	0.146428	1.46	0.033107	0.33
NIC22R5-13-15	385.75	0.132469	-1.1E-05	0.016255	0.111154	0.197304	1.218763	-12512.7	0.013337	1.33	0.091202	0.91	0.161889	1.62	0.108691	1.09
NIC22R5-55-57	386.17	0.147348	-0.01849	0.059969	0.149311	0.17983	0.930185	-7.97037	0.06447	6.45	0.160517	1.6	0.193327	1.93	0.158407	1.58
NIC22R5-71-75	386.35	0.139688	-0.02182	0.029168	0.103843	0.21168	1.250063	-6.40044	0.023333	2.33	0.08307	0.83	0.169335	1.69	0.111744	1.11
NIC22R5-113-115	386.75	0.139203	-0.01107	0.058512	0.130158	0.185315	0.846275	-12.5797	0.069141	6.91	0.153801	1.54	0.218977	2.19	0.164489	1.64
NIC22R6-0-2	387.06	0.160572	-0.01066	0.06028	0.127456	0.181945	1.124592	-15.0568	0.053602	5.36	0.113335	1.13	0.161788	1.62	0.142782	1.43
NIC22R6-38-40	387.44	0.129913	1.03E-06	1.17E-05	0.098262	0.962617	1.369346	125666.7	8.52E-06	0.08	0.071758	0.72	0.702976	7.03	0.094873	0.95
NIC22R6-80-82	387.86	0.156257	-0.01175	0.047933	0.140844	0.210025	0.9325	-13.2967	0.051403	5.14	0.151039	1.51	0.225227	2.25	0.167568	1.68
NIC22R6-118-120	388.24	0.166097	8.59E-07	0.03592	0.122492	0.190385	1.153182	193467.7	0.031148	3.11	0.106221	1.06	0.165096	1.65	0.144034	1.44
NIC22R7-13-17	388.5	0.182287	-1.2E-05	0.016931	0.113199	0.19178	1.481192	-15129.1	0.01143	1.14	0.076424	0.76	0.129477	1.29	0.123068	1.23
NIC22RCC-15-17	388.8	0.148442	-0.0166	0.041978	0.126559	0.171005	1.259108	-8.94448	0.033339	3.33	0.100515	1	0.135814	1.36	0.117895	1.18
NIC23R1-32-34	389.54	0.071657	-0.01995	0.054188	0.138758	0.21851	1.372125	-3.59147	0.039492	3.95	0.101126	1.01	0.15925	1.59	0.052223	0.52
NIC23R1-70-74	389.94	0.166202	-3E-06	0.015857	0.102321	0.16351	1.141364	-54740.9	0.013893	1.39	0.089648	0.89	0.143258	1.43	0.145617	1.46
NIC23R1-110-112	390.32	0.1977	-0.02953	1.03E-05	0.096159	0.157714	1.308555	-6.69414	7.86E-06	0.07	0.073485	0.73	0.120525	1.2	0.151083	1.51
NIC23R1-148-150	390.7	0.187379	-7.4E-06	0.041808	0.11897	0.2448	1.047098	-25278.4	0.039927	3.99	0.113619	1.14	0.233789	2.34	0.178951	1.79
NIC23R2-20-22	390.92	0.106709	-0.01292	0.01983	0.126405	0.177864	1.355951	-8.26152	0.014625	1.46	0.093223	0.93	0.131173	1.31	0.078697	0.79
NIC23R2-60-62	391.32	0.180711	1.92E-05	2.26E-05	0.117243	0.173299	1.663251	9422.117	1.36E-05	0.14	0.07049	0.7	0.104193	1.04	0.108649	1.09
NIC23R2-99-101	391.71	0.186029	-1.2E-05	1.06E-05	0.130111	0.192718	1.212474	-15214.4	8.73E-06	0.08	0.10731	1.07	0.158946	1.59	0.15343	1.53
NIC23R-2-140-142	392.13	0.048866	-0.0364	0.018994	0.08826	0.176714	1.649667	-1.34236	0.011514	1.15	0.053502	0.54	0.107121	1.07	0.029622	0.29
NIC23R3-23-25	392.45	0.160865	-0.0319	0.014159	0.110517	0.174962	1.378662	-5.04284	0.01027	1.03	0.080162	0.8	0.126907	1.27	0.116682	1.17
NIC23R3-64-66	392.86	0.168663	-0.01347	0.051315	0.206059	0.261697	0.927113	-12.5244	0.055349	5.53	0.222259	2.22	0.282271	2.82	0.181923	1.82
NIC23R3-115-117	393.37	0.170347	2.22E-06	-7.9E-07	0.284674	0.45839	1.420043	76560.75	-5.6E-07	-0.005	0.200469	2	0.3228	3.23	0.119959	1.19
NIC23R3-148-150	393.7	0.109327	-0.01525	0.024421	0.399884	0.437975	1.587632	-7.16758	0.015382	1.54	0.251875	2.52	0.275867	2.76	0.068862	0.69
NIC23R4-18-20	393.9	0.212827	-8.9E-06	-1.2E-05	0.475299	0.223268	1.536098	-23909.2	-7.6E-06	-0.07	0.30942	3.09	0.145348	1.45	0.138551	1.39
NIC23R4-45-47	394.17	0.098903	-5E-06	0.032724	0.622828	0.140032	0.095515	-19953.9	0.342607	3.43	6.520765	65.2	1.466082	14.7	1.035472	10.4
NIC23R4-86-88	394.58	0.090229	2.88E-06	0.023815	0.157191	0.152223	0.183582	31347.19	0.129725	1.29	0.856245	8.56	0.82918	8.29	0.49149	4.91
NIC23R4-125-127	394.97	0.074762	1.18E-05	0.031595	0.127267	0.368436	1.490638	6309.11	0.021196	2.12	0.085378	0.85	0.247166	2.47	0.050154	0.5
NIC23R5-10-12	395.32	0.080261	-0.01564	0.029297	0.148562	0.251813	1.675574	-5.13068	0.017485	1.75	0.088664	0.89	0.150284	1.5	0.047901	0.48
NIC23R5-53-55	395.75	0.055628	-6.3E-07	-1.2E-05	0.19486	0.278276	1.63279	-87756.8	-7.1E-06	-0.07	0.119342	1.19	0.17043	1.7	0.034069	0.34
NIC23R5-93-95	396.15	0.090031	-0.02702	0.030221	0.234762	0.231661	1.25893	-3.33209	0.024005	2.4	0.186477	1.86	0.184014	1.84	0.071514	0.71
NIC23R5-135-137	396.57	0.186026	-0.01123	0.127288	0.560368	0.293254	0.940927	-16.5708	0.135279	1.35	0.595549	5.96	0.311665	3.12	0.197706	1.98
NIC23R6-15-17	396.87	0.167182	-0.02195	-2.3E-06	0.171873	0.148981	1.623277	-7.61813	-1.4E-06	-0.01	0.10588	1.06	0.091778	0.92	0.10299	1.03
NIC23R6-55-57	397.27	0.138948	-7.9E-06	0.036243	0.160728	0.142591	1.300195	-17605.8	0.027875	2.79	0.123618	1.24	0.109669	1.09	0.106867	1.07
NIC23R6-95-97	397.67	0.150558	-5.6E-06	5.39E-06	0.195426	0.174746	1.195511	-26827.5	4.51E-06	0.04	0.163467	1.63	0.146168	1.46	0.125936	1.26
NIC23R6-125-127	397.97	0.19578	-0.01559	0.06853	0.47149	0.265143	1.103046	-12.5614	0.062128	6.21	0.427444	4.27	0.240373	2.4	0.17749	1.77
NIC23R7-13-15	398.5	0.059806	-0.02845	-2.1E-06	0.225008	0.1694	1.48837	-2.1023	-1.4E-06	-0.01	0.151178	1.51	0.113816	1.14	0.040182	0.4
NIC24R1-23-25	399.05	0.113445	-1.2E-05	9.94E-06	0.176275	0.262557	1.361019	-9445.26	7.3E-06	0.07	0.129517	1.29	0.192912	1.93	0.083353	0.83
NIC24R1-63-65	399.45	0.192199	-0.01393	0.014422	0.20197	0.333272	1.305047	-13.7958	0.011051	1.1	0.154761	1.55	0.255371	2.55	0.147273	1.47
NIC24R1-103-105	399.85	0.164878	-1.2E-05	0.034651	0.30579	2.830722	1.392765	-13915.4	0.024879	2.49	0.219556	2.19	2.032448	20.3	0.118382	1.18
NIC24R1-143-145	400.25	0.183403	-0.00944	0.035109	0.243092	0.274402	1.045567	-19.4371	0.033579	3.36	0.232498	2.32	0.262443	2.62	0.17541	1.75
NIC24R2-23-25	400.53	0.170789	-0.01477	0.0538	0.422497	0.255686	1.360892	-11.5656	0.039533	3.95	0.310456	3.1	0.187881	1.88	0.125498	1.25
NIC24R2-63-65	400.93	0.133622	-2.2E-06	0.062348	0.158711	0.253611	1.451902	-60314.3	0.042943	4.29	0.109313	1.09	0.174675	1.75	0.092032	0.92
NIC24R2-103-105	401.33	0.187153	-1.6E-05	-1.3E-06	0.144132	0.150381	1.470918	-11898.4	-9E-07	-0.009	0.097988	0.98	0.102236	1.02	0.127236	1.27
NIC24R2-143-145	401.73	0.104149	-3.4E-06	1.01E-06	0.138443	0.201569	1.304448	-31000	7.71E-07	-0.007	0.106131	1.06	0.154693	1.55	0.079841	0.79
NIC24R3-3-5	401.83	0.13899	0.017322	0.029286	0.14832	0.220062	1.368692	8.024055	0.021397	2.14	0.108366	1.08	0.160783	1.61	0.101549	1.01
NIC24R3-23-25	402.03	0.234314	-0.02394	6.6E-06	0.126559	0.29891	1.462156	-9.78648	4.52E-06	0.04	0.086557	0.86	0.204431	2.04	0.160252	1.6
NIC24R3-43-45	402.23	0.127247	5.59E-06	-0.01804	0.127758	0.20211	1.428473	22766.56	-0.01263	-1.26	0.089437	0.89	0.141487	1.41	0.089079	0.89
NIC24R3-63-65	402.43	0.173231	-0.01957	-0.0271	0.110601	0.127535	1.520571	-8.85233	-0.01782	-1.78	0.072737	0.73	0.083873	0.84	0.113925	1.14
NIC24R3-83-85	402.63	0.196516	-1E-05	9.56E-06	0.136346	0.159049	1.574915	-18973.3	6.07E-06	0.006	0.086573	0.86	0.100989	1.01	0.124779	1.25
NIC24R3-105-107	402.85	0.290225	-1.3E-05	-0.01824	0.112993	0.134387	1.553913	-23108	-0.01174	-1.17	0.072715	0.73	0.086483	0.86	0.18677	1.87
NIC24R3-123-125	403.03	0.162027	1E-06	1.09E-05	0.163868	0.14282	1.35749	161400	8.06E-06	0.08	0.120714	1.21	0.105209	1.05	0.119358	1.19
NIC24R3-143-145	403.23	0.200465	-8.7E-06	1.56E-06	0.169962	0.142837	1.550095	-22964.2	1.01E-06	0.01	0.109646	1.09	0.092147	0.92	0.129324	1.29
NIC24R4-23-25	403.53	0.130451	8.67E-06	0.013164	0.224541	0.185383	1.505918	15043.17	0.008741	8.74	0.149106	1.49	0.123103	1.23	0.086626	0.87
NIC24R4-60-62	403.9	0.235181	-9.2E-06	0.030113	0.300573	0.198275	1.479165	-25521.9	0.020358	2.04	0.203205	2.03	0.134045	1.34	0.158996	1.59

Outliers

TABLE S1 BULK SEDIMENT δ13C AND ELEMENTAL COMPOSITION DATA (XRF ANALYSES) OF HOLE 1001B (SOURCE AND WEATHERING)

Ident	Depth (mbsf)	Si NMS	K NMS	Al NMS	Fe NMS	Ca NMS	Ti NMS	Si/Ti	Si/Al	K/Al	log(Fe/Ca)	K/Fe	Fe/K
NIC20R1-29-32	362.2	17.74477	5.025505	0.950951	49.678	0.492862	1.628763	10.89463	18.66002	5.284716	2.0034384	0.101162	9.885176
NIC20R1-55-57	362.87	23.88246	4.726909	0.91939	43.17044	0.52204	1.600232	14.92437	25.97642	5.141353	1.9174826	0.109494	9.132912
NIC20R1-85-87	363.17	20.36244	4.858201	1.197822	44.60097	0.784785	1.598209	12.74079	16.99937	4.055846	1.7545935	0.108926	9.180552
NIC20R1-145-147	363.77	22.02149	4.798739	1.302735	42.16638	0.867145	1.47777	14.90184	16.90404	3.683587	1.6868744	0.113805	8.786971
NIC20R2-5-7	363.87	21.31376	4.671826	1.396186	43.60798	0.921043	1.543121	13.81211	15.2657	3.346134	1.6752858	0.107132	9.334246
NIC20R2-45-47	364.24	16.2567	5.012726	0.940579	51.9888	0.452013	1.623122	10.01569	17.2837	5.329402	2.0607588	0.096419	10.37136
NIC20R2-68-70	364.47	19.0651	4.983414	0.959903	50.14092	0.561747	1.674707	11.38414	19.86148	5.19158	1.9506515	0.099388	10.06156
NIC20R2-88-90	364.7	20.94281	5.028151	1.167818	44.03006	0.797949	1.372082	15.26353	17.93328	4.305594	1.7417742	0.114198	8.75671
NIC20R2-128-130	365.1	17.20969	4.477687	0.695627	47.9053	0.385089	1.516902	11.34529	24.73981	6.436904	2.0948219	0.09347	10.69867
NIC20R3-8-10	365.4	22.09555	4.599496	1.048259	44.54239	0.647983	1.471282	15.01789	21.07833	4.387749	1.8372097	0.103261	9.684188
NIC20R3-48-50	365.8	21.84341	4.57902	1.003091	44.53842	0.651669	1.495723	14.60391	21.77611	4.564911	1.8347076	0.102811	9.726627
NIC20R3-73-75	366.05	22.37053	5.161361	1.242573	46.10357	0.684861	1.478804	15.12744	18.00338	4.153767	1.8281321	0.111951	8.932444
NIC20R3-113-115	366.45	17.62434	5.028255	1.003465	48.99693	0.516855	1.735823	10.1533	17.56349	5.010892	1.9768003	0.102624	9.744321
NIC20R3-138-140	366.7	19.90651	5.066666	1.098582	42.95289	0.747619	1.438726	13.83621	18.12018	4.612004	1.7593119	0.117959	8.477545
NIC20R4-13-15	366.95	19.87797	5.113985	1.100966	47.00394	0.650376	1.512907	13.13892	18.05503	4.644998	1.85897	0.108799	9.191256
NIC20R4-53-55	367.35	23.12241	4.798776	0.901479	44.69316	0.539891	1.457658	15.86272	25.64942	5.323226	1.9179351	0.107372	9.313449
NIC20R4-93-95	367.75	19.85157	5.229429	0.873012	47.89636	0.541818	1.624583	12.21949	22.73918	5.990102	1.9464492	0.109182	9.159004
NIC20R4-140-142	368.12	25.7558	4.465351	1.279013	35.6584	1.175544	1.188548	21.66998	20.13725	3.491248	1.4819229	0.125226	7.985576
NIC20R5-13-15	368.45	21.26748	5.066899	1.206223	44.65357	0.897271	1.428741	14.88547	17.63147	4.200633	1.6969325	0.113471	8.812801
NIC20R570-72NEW2	369.02	32.23837	3.457221	0.514505	40.24744	0.371325	1.274953	25.28592	62.65905	6.719514	2.034984	0.085899	11.64156
NIC20R5-120-122	369.52	21.5549	5.260979	0.93587	44.01641	0.739177	1.492087	14.44614	23.03193	5.621484	1.7748661	0.119523	8.366581
NIC20R5-148-150	369.8	22.76718	4.98366	1.012976	39.78728	0.823715	1.418548	16.04964	22.47554	4.91982	1.6839675	0.125258	7.983546
NIC20R6-9-11	369.91	19.83301	5.651486	1.40308	40.34103	0.963226	1.564253	12.6789	14.13534	4.027915	1.6220187	0.140093	7.138128
NIC20R6-50-52	370.32	27.86677	4.508287	1.091519	33.80464	1.137584	1.196277	23.29458	25.53028	4.130288	1.472993	0.133363	7.498334
NIC20R6-90-92	370.72	25.40941	5.340944	1.262589	36.8603	1.133852	1.378423	18.43369	20.12485	4.230153	1.5120026	0.144897	6.901457
NIC21R1-31-33	372.33	24.98815	5.275464	1.282408	39.91334	0.966369	1.385948	18.02964	19.48533	4.113717	1.6159753	0.132173	7.565846
NIC21R1-70-74	372.74	23.38706	5.022702	1.014113	42.83034	0.84786	1.483706	15.7626	23.0616	4.952805	1.7034274	0.11727	8.527349
NIC21R1-108-110	373.1	19.83092	5.160863	1.016674	47.45817	0.512522	1.590673	12.467	19.50568	5.076221	1.9665988	0.108746	9.195781
NIC21R1-133-135	373.35	31.78297	4.732951	0.760713	42.60589	0.328635	1.548144	20.52972	41.78047	6.221726	2.1127561	0.111087	9.001972
NIC21R2-30-32	373.67	24.05784	5.563035	1.40829	37.71535	1.271463	1.368661	17.57764	17.08302	3.950206	1.4722145	0.147501	6.779636
NIC21R2-69-73	374.08	24.57909	5.672992	1.594226	37.48699	1.280332	1.404057	17.50576	15.41757	3.558461	1.4665581	0.151332	6.607976
NIC21R2-110-112	374.49	20.15321	6.206533	1.204587	46.05324	0.575231	1.55236	12.9823	16.73039	5.152417	1.9034176	0.134769	7.420123
NIC21R3-10-12	374.82	29.36788	4.613294	1.572091	32.24078	1.477317	1.195798	24.55923	18.68078	2.934495	1.338932	0.143089	6.988668
NIC21R3-50-52	375.24	22.47022	5.324877	1.338521	41.85089	0.973848	1.405864	15.98321	16.78735	3.97818	1.6332136	0.127234	7.859504
NIC21R3-71-74	375.44	20.62181	5.23201	1.254024	43.00884	0.988629	1.354418	15.22559	16.44451	4.172177	1.6385245	0.12165	8.220329
NIC21R3-110-112	375.88	21.94262	5.223519	1.37397	38.72785	1.099646	1.2859	17.06402	15.97024	3.801772	1.5467707	0.134878	7.414131
NIC21R3-148-150	376.2	24.54513	4.862248	1.436812	32.51125	1.438251	1.173551	20.91527	17.08304	3.384052	1.3541989	0.149556	6.686466
NIC21R4-3-5	376.25	24.0081	5.044449	1.558198	30.15114	1.534383	1.208657	19.86346	15.40761	3.237361	1.2933699	0.167305	5.977093
NIC21R4-42-44	376.64	18.78821	5.556721	1.051683	50.00177	0.475268	1.584301	11.85899	17.8649	5.283646	2.0220465	0.11113	8.99843
NIC21R4-76-78	376.98	24.50763	4.619575	1.288336	33.4492	1.335731	1.174879	20.8597	19.0227	3.585692	1.3986668	0.138107	7.240752
NIC21R4-98-100	377.2	20.84615	5.922084	1.382887	46.58393	0.740291	1.64281	12.68932	15.07436	4.282405	1.7988339	0.127127	7.866138
NIC21R4-138-140	377.62	30.00559	4.140048	1.177851	31.07555	1.229185	0.995762	30.1333	25.47486	3.514918	1.4028016	0.133225	7.506085
NIC21R5-0-2	377.73	27.91257	4.311226	1.420533	33.46741	1.160691	1.119941	24.92325	19.64937	3.034936	1.4599053	0.128819	7.762852
NIC21R5-60-62	378.32	23.22731	4.401589	1.004705	37.10916	0.949731	1.158366	20.05179	23.11853	4.380977	1.5918807	0.118612	8.430856
NIC21R5-120-122	378.92	17.51973	5.117508	0.87867	50.08026	0.490319	2.249781	7.787305	19.93893	5.824154	2.009208	0.102181	9.786521
NIC21R5-140-142	379.12	28.34655	4.456282	1.207322	31.62318	1.331418	1.199045	23.64094	23.47886	3.691047	1.375691	0.140918	7.096316
NIC21R6-5-7	379.27	27.68423	4.380796	1.063274	36.93869	1.125618	1.294695	21.38281	26.03678	4.120101	1.5160899	0.118596	8.43196
NIC21R6-40-42	379.6	18.23201	5.780347	1.187463	51.8216	0.574129	1.646374	11.07404	15.35376	4.867813	1.9555017	0.111543	8.965137
NIC21R6-85-87	379.9	31.63915	4.528625	1.187695	34.74645	1.199792	1.32814	23.82215	26.63913	3.812954	1.4616797	0.130371	7.67042
NIC22R135-37	379.97	21.82315	5.230345	1.308597	44.18793	0.82838	1.494396	14.60332	16.67676	3.99691	1.7270742	0.118366	8.448377
NIC21RCC-13-15	380.2	24.17553	4.776095	1.309666	41.19685	1.137982	1.319295	18.32457	18.45931	3.646805	1.5587286	0.115934	8.625634
NIC22R1-78-80	380.3	20.67739	4.961407	1.085212	44.94303	0.728646	1.379825	14.98552	19.05379	4.571833	1.7901457	0.110393	9.058525
NIC22R-1118-120	380.8	30.43691	4.188817	1.575717	31.33227	1.445579	1.219751	24.95339	19.31624	2.658357	1.3359501	0.13369	7.47998
NIC22R1-138-140	381.1	40.08223	12.13469	2.06626	0.122907	0.652662	3.970755	10.09436	19.39845	5.872779	-0.725112	98.73061	0.010129
NIC22R2-0-2	381.12	31.18741	3.839963	1.387402	31.40158	1.56272	1.116878	27.92374	22.47899	2.767736	1.3030703	0.122286	8.177571
NIC22R2-19-21	381.31	35.33232	4.513331	0.576422	41.75818	0.307665	1.452078	24.33225	61.29589	7.829903	2.1326638	0.108083	9.252188
NIC22R2-65-67	381.87	24.55822	5.016305	1.126412	40.01525	1.0689	1.383476	17.75109	21.80216	4.453348	1.5732885	0.12536	7.977038
NIC22R2-105-107	382.2	29.63043	5.062788	1.065054	42.07608	0.785161	1.375169	21.54676	27.82059	4.753551	1.7290767	0.120325	8.310852
NIC22R2-145-147	382.57	33.17484	4.983831	0.73619	45.14414	0.276027	1.67948	19.75304	45.06287	6.769762	2.2136504	0.110398	9.058122
NIC22R3-3-5	382.65	30.16749	3.294846	1.17212	33.0126	1.328317	1.105276	27.29408	25.73754	2.811014	1.3953781	0.099806	10.01947
NIC22R3-38-40	383	30.26975	4.275754	1.383514	32.91286	1.423627	1.129742	26.79349	21.87889	3.090503	1.3639693	0.129911	7.697557
NIC22R3-78-80	383.4	29.07453	4.799886	1.329788	34.55857	1.255911	1.204069	24.1469	21.86402	3.609511	1.439597	0.138891	7.199874
NIC22R3-117-119	383.79	30.80267	4.806215	0.675916	47.36599	0.269834	1.544234	19.94689	45.57173	7.110669	2.2443699	0.10147	9.855154
NIC22R4-33-35	384.43	23.45583	4.908128	1.039845	41.0561	0.886488	1.444845	16.23416	22.55705	4.720057	1.665705	0.119547	8.364922
NIC22R4-75-77	384.87	31.55305	4.571449	1.863583	32.91723	1.465558	1.0896	28.95837	16.93139	2.453043	1.3514202	0.138877	7.200611
NIC22R4-115-117	385.27	25.62643	4.997049	1.363415	38.72435	1.026926	1.168489	21.93125	18.79577	3.665098	1.5764452	0.129042	7.749444
NIC22R4-148-150	385.6	28.01241	5.38358	1.60582	36.20471	1.180148	1.234217	22.6965	17.44431	3.352544	1.4868287	0.148698	6.725024
NIC22R5-13-15	385.75	31.31949	4.406478	1.218763	33.28225	1.245469	1.07705	29.07895	25.69777	3.615534	1.4268797	0.132397	7.553028
NIC22R5-55-57	386.17	20.62604	5.393629	0.930185	49.8505	0.589105	1.639336	12.58195	22.17412	5.798447	1.9274766	0.108196	9.242479
NIC22R5-71-75	386.35	29.87885	4.761794	1.250063	36.47504	1.059054	1.210989	24.67309	23.90188	3.809244	1.5370776	0.130549	7.659937
NIC22R5-113-115	386.75	20.99942	4.847684	0.846275	47.69474	0.612715	1.445693	14.52551	24.81393	5.728258	1.8912118	0.10164	9.838667
NIC22R6-0-2	387.06	21.72296	5.64984	1.124592	46.20145	0.676601	1.393287	15.59116	19.3163	5.023901	1.834323	0.122287	8.17748
NIC22R6-38-40	387.44	29.12336	4.370294	1.369346	32.68866	1.505624	1.16164	25.07091	21.26808	3.191519	1.3366805	0.133694	7.479739
NIC22R6-80-82	387.86	20.03207	5.300453	0.9325	47.15838	0.560047	1.412242	14.18459	21.4821	5.684129	1.9253348	0.112397	8.897048
NIC22R6-118-120	388.24	23.32779	5.022883	1.153182	40.43348	1.020928	1.259293	18.52451	20.22906	4.355672	1.5977459	0.124226	8.049854
NIC22R7-13-17	388.5	23.24189	4.865595	1.481192	36.75416	1.256688	1.146138	20.27845	15.69134	3.284919	1.466079	0.132382	7.553889
NIC22RCC-15-17	388.8	22.84291	5.552179	1.259108	42.26413	0.898838	1.390636	16.42623	18.14213	4.409612	1.6722906	0.131369	7.61217
NIC23R1-32-34	389.54	20.20098	5.183856	1.372125	39.50158	1.142583	1.315809	15.35251	14.7224	3.777977	1.5387267	0.131232	7.620115
NIC23R1-70-74	389.94	22.15573	5.135912	1.141364	40.47882	0.985016	1.144855	19.35244	19.41162	4.499801	1.6137844	0.126879	7.881526
NIC23R1-110-112	390.32	23.236	4.755221	1.308555	36.68441	1.241094	1.151747	20.17458	17.757	3.633949	1.4706768	0.129625	7.714554
NIC23R1-148-150	390.7	19.62583	4.87205	1.047098	48.21373	0.83403	1.402562	13.99284	18.74307	4.652906	1.7619893	0.101051	9.895985
NIC23R2-20-22	390.92	20.48359	5.649627	1.355951	43.72498	0.970444	1.427264	14.35165	15.10644	4.166543	1.6537593	0.129208	7.739445
NIC23R2-60-62	391.32	27.12912	4.317858	1.663251	31.20072	1.69108	1.063535	25.50844	16.31089	2.596035	1.2660006	0.13839	7.225971
NIC23R2-99-101	391.71	22.74495	4.177953	1.212474	36.31347	1.103663	1.103232	20.61665	18.75913	3.44581	1.5172311	0.115052	8.691688
NIC23R-2-140-142	392.13	25.76248	4.472316	1.649667	34.12794	1.482187	1.001652	25.71999	15.61678	2.711042	1.362207	0.131046	7.630932
NIC23R3-23-25	392.45	26.45611	4.960115	1.378662	38.19292	1.160947	1.09846	24.08473	19.1897	3.597775	1.5171703	0.12987	7.700007
NIC23R3-64-66	392.86	18.97807	5.292351	0.927113	52.15952	0.375847	1.894818	10.01577	20.47007	5.708421	2.1423227	0.101465	9.855643
NIC23R3-115-117	393.37	26.44751	3.816774	1.420043	30.55114	1.683121	1.003221	26.36259	18.62444	2.687787	1.258912	0.124931	8.00444
NIC23R3-148-150	393.7	23.87314	5.609894	1.587632	38.40648	1.138668	1.352669	17.64892	15.03695	3.533499	1.5280073	0.146066	6.846204
NIC23R4-18-20	393.9	25.74499	4.288086	1.536098	32.43939	1.42701	1.099271	23.42006	16.75999	2.791544	1.3566457	0.132188	7.565004
NIC23R4-45-47	394.17	44.82927	3.588612	0.095515	35.05536	0.307711	1.142573	39.23537	469.3451	37.57138	2.0566118	0.10237	9.768499
NIC23R4-86-88	394.58	50.16449	3.436206	0.183582	32.49611	0.263555	1.299086	38.61521	273.2537	18.71755	2.0909599	0.105742	9.456972
NIC23R4-125-127	394.97	25.78315	6.179052	1.490638	41.88202	0.995328	1.416422	18.20301	17.29672	4.145239	1.6240614	0.147535	6.778066
NIC23R5-10-12	395.32	20.87669	6.473988	1.675574	44.99408	0.930627	1.545104	13.51151	12.45942	3.863743	1.6843799	0.143885	6.949978
NIC23R5-53-55	395.75	23.70075	4.55852	1.63279	33.6849	1.587378	1.26039	18.80431	14.5155	2.79186	1.3267549	0.135328	7.389438
NIC23R5-93-95	396.15	22.72206	5.309203	1.25893	38.8477	1.096374	1.388844	16.36041	18.04871	4.217234	1.5494066	0.136667	7.317051
NIC23R5-135-137	396.57	16.40477	5.213421	0.940927	44.06884	0.584163	1.616769	10.14664	17.4347	5.540731	1.8777904	0.118249	8.456717
NIC23R6-15-17	396.87	23.1323	5.084429	1.623277	34.0758	1.276448	1.092079	21.1819	14.25037	3.1322	1.4264429	0.149209	6.70199
NIC23R6-55-57	397.27	26.15328	4.844279	1.300195	30.94891	1.324396	1.169488	22.36303	20.1149	3.72581	1.3686273	0.156525	6.388754
NIC23R6-95-97	397.67	26.22954	4.357265	1.195511	33.54272	1.037901	1.327562	19.75767	21.94003	3.64469	1.5094422	0.129902	7.698114
NIC23R6-125-127	397.97	15.97329	4.748864	1.103046	47.19877	0.577532	1.729713	9.234646	14.48107	4.305227	1.9123544	0.100614	9.938961
NIC23R7-13-15	398.5	27.08987	4.009385	1.48837	32.28649	1.56506	1.359282	19.92954	18.20104	2.69381	1.3144898	0.124182	8.052729
NIC24R1-23-25	399.05	26.65857	3.973135	1.361019	35.11191	1.245792	1.185635	22.48463	19.58721	2.919234	1.4500087	0.113156	8.837332
NIC24R1-63-65	399.45	20.65295	6.009851	1.305047	44.23744	0.821466	1.328496	15.54612	15.82544	4.605084	1.7312003	0.135854	7.360821
NIC24R1-103-105	399.85	25.8662	4.070511	1.392765	32.94883	1.27175	1.165243	22.19811	18.57184	2.922612	1.4134383	0.12354	8.094519
NIC24R1-143-145	400.25	19.77149	4.408638	1.045567	50.14136	0.551866	1.487554	13.29128	18.90982	4.216504	1.9583626	0.087924	11.37344
NIC24R2-23-25	400.53	20.70524	6.040222	1.360892	42.99968	0.792288	1.554851	13.31654	15.21447	4.438429	1.734582	0.140471	7.118891
NIC24R2-63-65	400.93	14.41451	7.765657	1.451902	54.62209	0.555421	1.891126	7.622184	9.928017	5.348608	1.992746	0.142171	7.033801
NIC24R2-103-105	401.33	25.35601	4.540914	1.470918	34.89671	1.39961	1.165262	21.75992	17.23822	3.087129	1.3967774	0.130124	7.684951
NIC24R2-143-145	401.73	24.54198	4.637646	1.304448	35.80199	1.256045	1.174282	20.89956	18.81408	3.555256	1.4549018	0.129536	7.719864
NIC24R3-3-5	401.83	24.30097	4.356867	1.368692	37.28838	1.306143	1.314152	18.49174	17.75489	3.183235	1.4555829	0.116842	8.558532
NIC24R3-23-25	402.03	19.23652	5.218835	1.462156	37.47428	1.178494	1.105573	17.39958	13.15626	3.569273	1.5024059	0.139264	7.180583
NIC24R3-43-45	402.23	22.42834	4.20978	1.428473	32.54383	1.484341	1.095378	20.47544	15.70092	2.947049	1.3409349	0.129357	7.730529
NIC24R3-63-65	402.43	22.13045	4.558823	1.520571	32.81164	1.426255	1.210162	18.28717	14.55404	2.9981	1.3618307	0.138939	7.197392
NIC24R3-83-85	402.63	18.64605	6.986469	1.574915	43.17756	1.086662	1.44053	12.94388	11.8394	4.436094	1.5991637	0.161808	6.18017
NIC24R3-105-107	402.85	23.20105	4.724893	1.553913	35.43932	1.362933	1.30973	17.71438	14.93073	3.040642	1.4150108	0.133323	7.500556
NIC24R3-123-125	403.03	23.26567	4.692152	1.35749	35.68407	1.223537	1.183817	19.65309	17.13875	3.456492	1.4648572	0.131491	7.605055
NIC24R3-143-145	403.23	23.05561	5.952676	1.550095	36.41674	1.351472	1.217993	18.92919	14.87368	3.840201	1.4304941	0.16346	6.117709
NIC24R4-23-25	403.53	17.83422	7.219496	1.505918	45.90295	0.816208	1.627573	10.95755	11.84275	4.794083	1.7500398	0.157277	6.358193
NIC24R4-60-62	403.9	15.45196	6.129606	1.479165	40.90461	1.034556	1.418029	10.89679	10.44641	4.143963	1.5970183	0.149851	6.673285

TABLE S1 BULK SEDIMENT δ13C AND ELEMENTAL COMPOSITION DATA (XRF ANALYSES) OF HOLE 1001B (PALEOPRODUCTIVITY)

Ident	Depth (mbsf)	Ba NMS	Ca NMS	Al NMS	Ba/Ca	Ba/Al
NIC20R1-29-32	362.2	2.35082	0.492862	0.950951	4.769728	2.472073
NIC20R1-55-57	362.87	2.396403	0.52204	0.91939	4.590456	2.606514
NIC20R1-85-87	363.17	1.968986	0.784785	1.197827	2.508949	1.643798
NIC20R1-145-147	363.77	2.075106	0.867145	1.302735	2.393031	1.592884
NIC20R2-5-7	363.87	1.619348	0.921043	1.396186	1.758167	1.159837
NIC20R2-45-47	364.24	2.367932	0.452013	0.940579	5.238635	2.517524
NIC20R2-68-70	364.47	2.036868	0.561747	0.959903	3.625952	2.121951
NIC20R2-88-90	364.7	2.229483	0.797949	1.167818	2.794016	1.909101
NIC20R2-128-130	365.1	2.893208	0.385089	0.695627	7.51308	4.159135
NIC20R3-8-10	365.4	2.514079	0.647983	1.048259	3.879852	2.398338
NIC20R3-48-50	365.8	2.278525	0.651669	1.003091	3.496444	2.271504
NIC20R3-73-75	366.05	2.181593	0.684861	1.242573	3.185455	1.755706
NIC20R3-113-115	366.45	2.521569	0.516855	1.003465	4.878679	2.512862
NIC20R3-138-140	366.7	2.295719	0.747619	1.098582	3.070706	2.08971
NIC20R4-13-15	366.95	2.267445	0.650376	1.100966	3.486362	2.059505
NIC20R4-53-55	367.35	2.338759	0.539891	0.901479	4.331912	2.594359
NIC20R4-93-95	367.75	2.042902	0.541818	0.873012	3.770459	2.340063
NIC20R4-140-142	368.12	2.382296	1.175544	1.279013	2.026548	1.862606
NIC20R5-13-15	368.45	1.915376	0.897271	1.206223	2.134668	1.587913
NIC20R570-72NEW2	369.02	1.827309	0.371325	0.514505	4.921049	3.551589
NIC20R5-120-122	369.52	2.184888	0.739177	0.93587	2.955839	2.334606
NIC20R5-148-150	369.8	2.455556	0.823715	1.012976	2.981076	2.4241
NIC20R6-9-11	369.91	2.608889	0.963226	1.40308	2.70849	1.859401
NIC20R6-50-52	370.32	1.971698	1.137584	1.091519	1.733234	1.806381
NIC20R6-90-92	370.72	1.842913	1.133852	1.262589	1.625356	1.45963
NIC21R1-31-33	372.33	2.069228	0.966369	1.282408	2.141241	1.613549
NIC21R1-70-74	372.74	1.703897	0.84786	1.014113	2.009645	1.680185
NIC21R1-108-110	373.1	2.437193	0.512522	1.016674	4.755299	2.397221
NIC21R1-133-135	373.35	1.699674	0.328635	0.760713	5.171924	2.234316
NIC21R2-30-32	373.67	2.252891	1.271463	1.40829	1.771889	1.599735
NIC21R2-69-73	374.08	1.601711	1.280332	1.594226	1.251012	1.004695
NIC21R2-110-112	374.49	2.546025	0.575231	1.204587	4.426089	2.113609
NIC21R3-10-12	374.82	2.009431	1.477317	1.572091	1.36019	1.27819
NIC21R3-50-52	375.24	2.053477	0.973848	1.338521	2.108622	1.534139
NIC21R3-71-74	375.44	1.793556	0.988629	1.254024	1.814185	1.43024
NIC21R3-110-112	375.88	2.532988	1.099646	1.37397	2.303459	1.843555
NIC21R3-148-150	376.2	2.074851	1.438251	1.436812	1.44262	1.444065
NIC21R4-3-5	376.25	2.392112	1.534383	1.558198	1.559005	1.535178
NIC21R4-42-44	376.64	2.355005	0.475268	1.051683	4.955106	2.239272
NIC21R4-76-78	376.98	2.437268	1.335731	1.288336	1.824671	1.891796
NIC21R4-98-100	377.2	2.04398	0.740291	1.382887	2.761052	1.478053
NIC21R4-138-140	377.62	2.299379	1.229185	1.177851	1.870653	1.952182
NIC21R5-0-2	377.73	2.193381	1.160691	1.420533	1.88972	1.544055
NIC21R5-60-62	378.32	2.222765	0.949731	1.004705	2.340416	2.212356
NIC21R5-120-122	378.92	2.152373	0.490319	0.87867	4.389739	2.449581
NIC21R5-140-142	379.12	2.003286	1.331418	1.207322	1.504625	1.65928
NIC21R6-5-7	379.27	1.606633	1.125619	1.063274	1.427332	1.511025
NIC21R6-40-42	379.6	1.996094	0.574129	1.187463	3.476737	1.680974
NIC21R6-85-87	379.9	1.23766	1.199792	1.187695	1.031562	1.042069
NIC22R135-37	379.97	2.055372	0.82838	1.308597	2.481195	1.570668
NIC21RCC-13-15	380.2	1.508903	1.137982	1.309666	1.325946	1.152128
NIC22R1-78-80	380.3	2.68919	0.728646	1.085212	3.690666	2.478032
NIC22R-1118-120	380.8	1.937695	1.445579	1.575717	1.340429	1.229723
NIC22R1-138-140	381.1	4.004639	0.652662	2.06626	6.135855	1.93811
NIC22R2-0-2	381.12	1.124257	1.56272	1.387402	0.719423	0.810332
NIC22R2-19-21	381.31	1.176898	0.307665	0.576422	3.825259	2.041728
NIC22R2-65-67	381.87	1.527039	1.0689	1.126412	1.428607	1.355666
NIC22R2-105-107	382.2	1.474784	0.785161	1.065054	1.878321	1.384704
NIC22R2-145-147	382.57	1.072307	0.276027	0.73619	3.884797	1.456563
NIC22R3-3-5	382.65	1.531475	1.328317	1.17212	1.152944	1.306586
NIC22R3-38-40	383	1.625614	1.423627	1.383514	1.141882	1.174989
NIC22R3-78-80	383.4	1.980691	1.255911	1.329788	1.577096	1.489478
NIC22R3-117-119	383.79	1.115751	0.269834	0.675916	4.134951	1.650724
NIC22R4-33-35	384.43	2.257992	0.886488	1.039845	2.547121	2.17147
NIC22R4-75-77	384.87	1.425678	1.465558	1.863583	0.972788	0.76502
NIC22R4-115-117	385.27	2.196223	1.026926	1.363415	2.138639	1.610825
NIC22R4-148-150	385.6	1.682054	1.180148	1.60582	1.425291	1.047474
NIC22R5-13-15	385.75	1.808017	1.245469	1.218763	1.451675	1.483485
NIC22R5-55-57	386.17	1.747536	0.589105	0.930185	2.966423	1.878697
NIC22R5-71-75	386.35	1.696728	1.059054	1.250063	1.602116	1.357314
NIC22R5-113-115	386.75	1.882822	0.612715	0.846275	3.072915	2.224834
NIC22R6-0-2	387.06	1.596472	0.676601	1.124592	2.359548	1.419601
NIC22R6-38-40	387.44	1.466298	1.505624	1.369346	0.973881	1.070802
NIC22R6-80-82	387.86	2.378386	0.560047	0.9325	4.246766	2.550547
NIC22R6-118-120	388.24	1.911289	1.020928	1.153182	1.87211	1.657405
NIC22R7-13-17	388.5	2.317888	1.256688	1.481192	1.844441	1.56488
NIC22RCC-15-17	388.8	2.292872	0.898838	1.259108	2.550929	1.821028
NIC23R1-32-34	389.54	2.376814	1.142583	1.372125	2.080211	1.732214
NIC23R1-70-74	389.94	1.981772	0.985016	1.141364	2.011917	1.736318
NIC23R1-110-112	390.32	2.191296	1.241094	1.308555	1.765616	1.674593
NIC23R1-148-150	390.7	1.705678	0.83403	1.047098	2.045105	1.628957
NIC23R2-20-22	390.92	2.116218	0.970444	1.355951	2.180671	1.560689
NIC23R2-60-62	391.32	1.971285	1.69108	1.663251	1.165696	1.1852
NIC23R2-99-101	391.71	2.392457	1.103663	1.212474	2.167741	1.973203
NIC23R-2-140-142	392.13	1.986412	1.482187	1.649667	1.34019	1.204129
NIC23R3-23-25	392.45	1.908241	1.160947	1.378662	1.643693	1.384125
NIC23R3-64-66	392.86	2.002651	0.375847	0.927113	5.32837	2.160094
NIC23R3-115-117	393.37	1.930751	1.683121	1.420043	1.147125	1.359643
NIC23R3-148-150	393.7	1.584589	1.138668	1.587632	1.391616	0.998084
NIC23R4-18-20	393.9	2.200157	1.42701	1.536098	1.541795	1.432302
NIC23R4-45-47	394.17	1.072648	0.307711	0.095515	3.485898	11.23021
NIC23R4-86-88	394.58	1.182087	0.263555	0.183582	4.485159	6.439009
NIC23R4-125-127	394.97	1.275729	0.995328	1.490638	1.281717	0.855827
NIC23R5-10-12	395.32	1.732944	0.930627	1.675574	1.862126	1.034239
NIC23R5-53-55	395.75	1.969315	1.587378	1.63279	1.240609	1.206105
NIC23R5-93-95	396.15	2.072456	1.096374	1.25893	1.890282	1.646204
NIC23R5-135-137	396.57	2.721269	0.584163	0.940927	4.658407	2.892116
NIC23R6-15-17	396.87	2.839923	1.276448	1.623277	2.224864	1.749499
NIC23R6-55-57	397.27	2.209209	1.324396	1.300195	1.668088	1.699137
NIC23R6-95-97	397.67	2.201782	1.037901	1.195511	2.121379	1.841709
NIC23R6-125-127	397.97	2.036346	0.577532	1.103046	3.525943	1.846112
NIC23R7-13-15	398.5	2.190013	1.56506	1.48837	1.399316	1.471418
NIC24R1-23-25	399.05	2.255415	1.245792	1.361019	1.810426	1.657151
NIC24R1-63-65	399.45	2.401472	0.821466	1.305047	2.923397	1.840142
NIC24R1-103-105	399.85	1.919526	1.27175	1.392765	1.509358	1.378213
NIC24R1-143-145	400.25	2.180882	0.551866	1.045567	3.951834	2.085836
NIC24R2-23-25	400.53	2.075266	0.792288	1.360892	2.619332	1.524931
NIC24R2-63-65	400.93	1.657422	0.555421	1.451902	2.984083	1.141552
NIC24R2-103-105	401.33	2.05799	1.39961	1.470918	1.470403	1.399119
NIC24R2-143-145	401.73	2.090327	1.256045	1.304448	1.664213	1.602461
NIC24R3-3-5	401.83	1.885736	1.306143	1.368692	1.443744	1.377766
NIC24R3-23-25	402.03	2.931801	1.178494	1.462156	2.487753	2.005122
NIC24R3-43-45	402.23	2.537304	1.484341	1.428473	1.709381	1.776235
NIC24R3-63-65	402.43	2.40128	1.426255	1.520571	1.683626	1.579196
NIC24R3-83-85	402.63	2.029593	1.086662	1.574915	1.867732	1.288701
NIC24R3-105-107	402.85	2.5021	1.362933	1.553913	1.83582	1.610193
NIC24R3-123-125	403.03	2.261323	1.223537	1.35749	1.848185	1.665812
NIC24R3-143-145	403.23	1.959854	1.351472	1.550095	1.450163	1.264344
NIC24R4-23-25	403.53	1.589808	0.816208	1.505918	1.947798	1.055707
NIC24R4-60-62	403.9	2.241474	1.034556	1.479165	2.166605	1.515364

TABLE S1 BULK SEDIMENT δ13C AND ELEMENTAL COMPOSITION DATA (XRF ANALYSES) OF HOLE 1001B (ISOTOPES)

Consecutive	Sample	Depth (mcd)	Depth (mbsf)	Age (My)	Sample	δ 13C/12C (‰)	Std Dev	δ 18O/16O (‰)	Std Dev
	16R1 70-75	332.15	341.83	64.11	17R1 68-73	0.957	0.023	-3,814	0.040
	16R2 71-76	333.66	343.19	64.37	17R2 69-74	0.825	0.034	-3,745	0.041
	16R3 70-76	335.16	344.66	64.64	17R3 69-74	0.940	0.015	-4,866	0.025
	16R4 70-75	336.65	345.91	64.76	17R4 69-74	1,167	0.018	-3,918	0.035
	16R5 70-75	338.15	348.77	65.36	18R1 72-77	0.939	0.019	-3,973	0.031
	16R6 70-76	339.76	349.96	65.69	18R2 77-82	0.691	0.010	-3,900	0.023
	16R7 20-24	340.64	351.13	65.83	18R3 72-77	0.715	0.018	-3,690	0.035
	17R1 68-73	341.83	352.27	65.97	18R4 70-75	1,000	0.023	-4,056	0.043
	17R2 69-74	343.19	353.22	66.06	18R5 55-60	1,830	0.017	-4,116	0.045
	17R3 69-74	344.66	353.79	66.08	18R6 55-59	2,057	0.026	-3,430	0.028
	17R4 69-74	345.91	357.12	66.26	19R1 77-82	1,987	0.025	-3,976	0.028
	18R1 72-77	348.77	358.4	66.32	19R2 69-74	2,070	0.016	-4,030	0.017
	18R2 77-82	349.96	359.68	66.4	19R3 70-76	2,056	0.017	-4,577	0.041
	18R3 72-77	351.13	362.2	66.61	20R1 29-32	2,021	0.025	-2,935	0.055
Paleogene	18R4 70-75	352.27	363.87	66.76	20R2 5-7	2,098	0.021	-3,700	0.032
	18R5 55-60	353.22	365.4	66.89	20R3 8-10	2,117	0.021	-4,246	0.029
	18R6 55-59	353.79	366.95	67.03	20R4 13-15	2,159	0.019	-3,851	0.039
	19R1 77-82	357.12	368.45	67.16	20R5 13-15	2,170	0.014	-4,314	0.041
	19R2 69-74	358.4	369.91	67.28	20R6 9-11	2,162	0.009	-4,159	0.026
	19R3 70-76	359.68	372.33	67.49	21R1 31-33	2,155	0.022	-4,370	0.038
	20R1 29-32	362.2	373.67	67.61	21R2 30-32	2,298	0.008	-4,400	0.038
	20R1 55-57	362.87	374.82	67.71	21R3 10-12	2,328	0.012	-4,771	0.026
	20R1 69-74	363.03	376.25	67.84	21R4 3-5	2,370	0.028	-4,277	0.028
	20R1 85-87	363.17	377.73	67.96	21R5 0-2	2,274	0.023	-4,348	0.028
	20R1 145-147	363.77	379.27	68.1	21R6 5-7	2,218	0.011	-3,794	0.036
	20R2 5-7	363.87	379.97	68.16	22 R1 35-37	1,834	0.026	-4,090	0.043
	20R2 45-47	364.24	381.31	68.27	22R2 19-21	1,593	0.019	-2,529	0.048
	20R2 68-70	364.47	383	68.42	22R3 38-40	2,086	0.011	-4,461	0.013
	20R2 77-82	364.59	384.43	68.54	22R4 33-35	2,040	0.037	-3,330	0.023
	20R2 88-90	364.7	385.75	68.66	22R5 13-15	2,088	0.030	-4,239	0.035
	20R2 128-130	365.1	387.44	68.8	22R6 38-40	2,144	0.039	-4,543	0.019
	20R3 8-10	365.4	388.5	68.9	22R7 13-17	2,244	0.011	-4,367	0.018
	20R3 48-50	365.8	389.54	68.99	23R1 32-34	2,288	0.027	-3,773	0.032
	20R3 73-75	366.05	390.92	69.11	23R2 20-22	2,305	0.015	-3,661	0.044
	20R3 78-83	366.13	392.45	69.24	23R3 23-25	2,113	0.022	-4,104	0.039
	20R3 113-115	366.45	393.9	69.36	23R4 18-20	2,093	0.029	-4,104	0.020
	20R3 138-140	366.7	395.32	69.49	23R5 10-12	2,168	0.017	-4,617	0.028
	20R4 13-15	366.95	396.87	69.62	23R6 15-17	2,055	0.020	-3,437	0.046
	20R4 53-55	367.35	398.5	69.76	23R7 13-15	2,041	0.030	-4,219	0.025
	20R4 75-80	367.6	399.05	69.81	24R1 23-25	1,992	0.019	-4,024	0.033
	20R4 93-95	367.75	400.53	69.94	24R2 23-25	1,998	0.014	-3,153	0.028
	20R4 140-142	368.12	402.03	70.07	24R3 23-25	2,196	0.015	-3,612	0.036
	20R5 13-15	368.45	403.53	70.2	24R4 23-25	2,160	0.015	-3,894	0.032
	20R5 70-72	369.02							
	20R5 69-73	369.03							
	20R5 120-122	369.52							
	20R5 148-150	369.8							
	20R6 9-11	369.91							
	20R6 50-52	370.32							
	20R6 73-78	370.58							
	20R6 90-92	370.72							
	21R1 31-33	372.33							
	21R1 70-74	372.74							
	21R1 108-110	373.1							
	21R1 133-135	373.35							
	21R2 30-32	373.67							
	21R2 69-73	374.08							
	21R2 110-112	374.49							
	21R3 10-12	374.82							
	21R3 50-52	375.24							
	21R3 71-74	375.44							
	21R3 110-112	375.88							
	21R3 148-150	376.2							
	21R4 3-5	376.25							
	21R4 42-44	376.64							
	21R4 76-78	376.98							
	21R4 98-100	377.2							
	21R4 138-140	377.62							
	21R5 0-2	377.73							
	21R5 60-62	378.32							
	21R5 71-76	378.46							
	21R5 120-122	378.92							
	21R5 140-142	379.12							
	21R6 5-7	379.27							
	21R6 40-42	379.6							
	21R6 71-75	379.75							
	21R6 85-87	379.9							
	22R1 35-37	379.97							
	22R1 78-80	380.2							
	21RCC 13-15	380.3							
	22R1 118-120	380.8							
	22R1 138-140	381.1							
	22R2 0-2	381.12							
	22R2 19-21	381.31							
	22R2 65-67	381.87							
	22R2 105-107	382.2							
	22R2 145-147	382.57							
	22R3 3-5	382.65							
	22R3 38-40	383							
	22R3 78-80	383.4							
	22R3 117-119	383.79							
	22R4 33-35	384.43							
	22R4 75-77	384.87							
	22R4 115-117	385.27							
	22R4 148-150	385.6							
	22R5 13-15	385.75							
	22R5 55-57	386.17							
	22R5 70-75	386.35							
	22R5 113-115	386.75							
	22R6 0-2	387.06							
	22R6 38-40	387.44							
	22R6 80-82	387.86							
	22R6 118-120	388.24							
	22R7 13-17	388.5							
	22RCC 15-17	388.8							
	23R1 32-34	389.54							
	23R1 70-74	389.94							
	23R1 110-112	390.32							
	23R1 148-150	390.7							
	23R2 20-22	390.92							
	23R2 60-62	391.32							
	23R2 99-101	391.71							
	23R2 140-142	392.13							
	23R3 23-25	392.45							
	23R3 64-66	392.86							
	23R3 115-117	393.37							
	23R3 148-150	393.7							
	23R4 18-20	393.9							
	23R4 45-47	394.17							
	23R4 86-88	394.58							
	23R4 125-127	394.97							
	23R5 10-12	395.32							
	23R5 53-55	395.75							
	23R5 93-95	396.15							
	23R5 135-137	396.57							
	23R6 15-17	396.87							
	23R6 55-57	397.27							
	23R6 95-97	397.67							
	23R6 125-127	397.97							
	23R7 13-15	398.5							
	24R1 23-25	399.05							
	24R1 63-65	399.45							
	24R1 103-105	399.85							
	24R1 143-145	400.25							
	24R2 23-25	400.53							
	24R2 63-65	400.93							
	24R2 103-105	401.33							
	24R2 143-145	401.73							
	24R3 3-5	401.83							
	24R3 23-25	402.03							
	24R3 43-45	402.23							
	24R3 63-65	402.43							
	24R3 83-85	402.63							
	24R3 105-107	402.85							
	24R3 123-125	403.03							
	24R3 143-145	403.23							
	24R4 23-25	403.53							
	24R4 60-62	403.9							
	Extra								
	First round								

TABLE S2 FORAMINIFERAL DATA (TOTAL COUNTS) OF HOLE 1001B

Sample	Depth (mbsf)	*Ammobaculites* sp.	*Clavulinoides trilatera*	*Marssonella oxycona*	*Rhabdammina* sp.	Textulariina indet.	*Anomalinoides* sp.	*Cibicidoides* sp.	*Coryphostoma incrassatum*	*Gyrodinoides girardana*	*Gyroidinoides nitida*	*Lenticulina* sp.	*Marginulina* sp.	*Nodosaria* sp.	*Nutallides truempyi*	*Pleurostomella* sp.	*Praebulimina* sp.	*Pyramidulina* sp.	*Reusssolina* sp.	Rotaliina indet	TOTAL
21R1 70-75	372.75							3	3		1	1			1				2	2	13
21R2 69-74	374.09											1	1				2			4	8
21R3 71-76	375.46					2	1			1		1			4					6	15
21R4 71-76	376.96							2								1	1			7	11
21R5 71-76	378.46																1	1			2
21R6 71-75	379.76																				0
22R5 70-75	386.35																			1	1
23R1 (70-75)	389.95																				0
23R5 (70-75)	396.95																				0
24R1 68-73	399.53	1		6	1	2		1		3				2							16
24R2 70-75	401.03					1															1
24R3 70-75	402.43		1	1								1								3	6
24R4 62-68	403.96											1				1					2

No recovery

Samples from Aumond et al. (2009)

CHAPTER 5

Table S1 $\delta^{13}C$ and Hg concentrations of Core Diablito-1E.

Table S2 Hg concentrations of Holes 1258A and 1001B.

Figure S1 Cross-plots of Hg concentrations (ppb) and Hg/S ratio (ppb/wt%) against normalized mean scale (NMS) Al, Fe, K intensities, and the V/Cr ratio at Core Diablito-1E. Note the low correlation coefficients for all plots. Upper section of the core: 574.7-637.4 m. Lower section: 640.7-700.3 m.

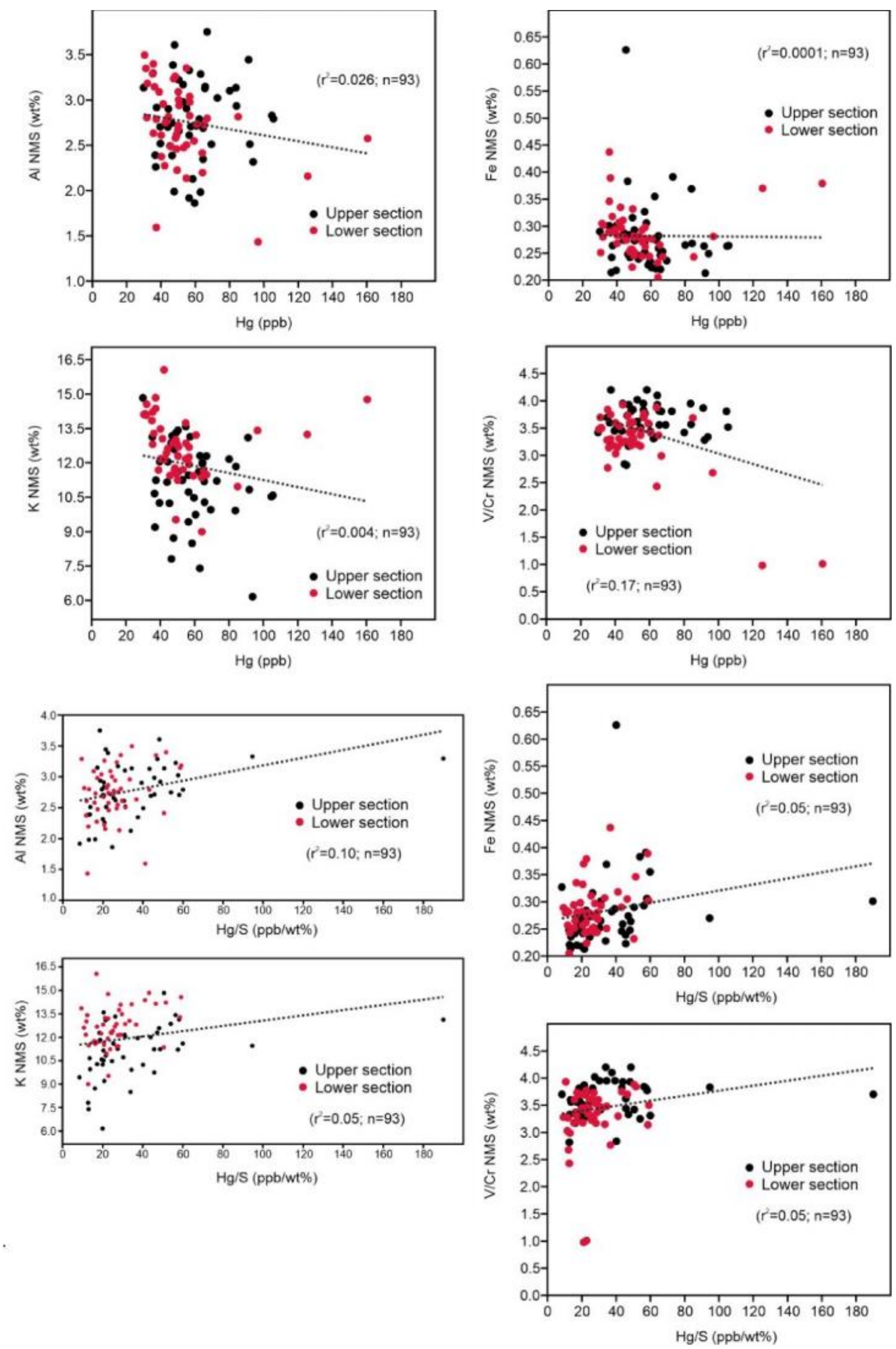

Figure S2 Mercury chemostratigraphy of selected Maastrichtian locations. Blue caption: marine settings, green caption: continental settings. Our data: Holes 1001B (Nicaraguan Rise) and 1258A (Demerara Rise). Previous studies: Bidart, France (Font et al., 2016, 2021); ODP Site 174AX, Bass River (Percival et al., 2018); Seymour Island, Antarctica (Percival et al., 2018); Nirvana, USA (Fendley et al., 2019); Elles, Tunisia (Keller et al., 2020), Songliao basin, China (Gu et al., 2022).

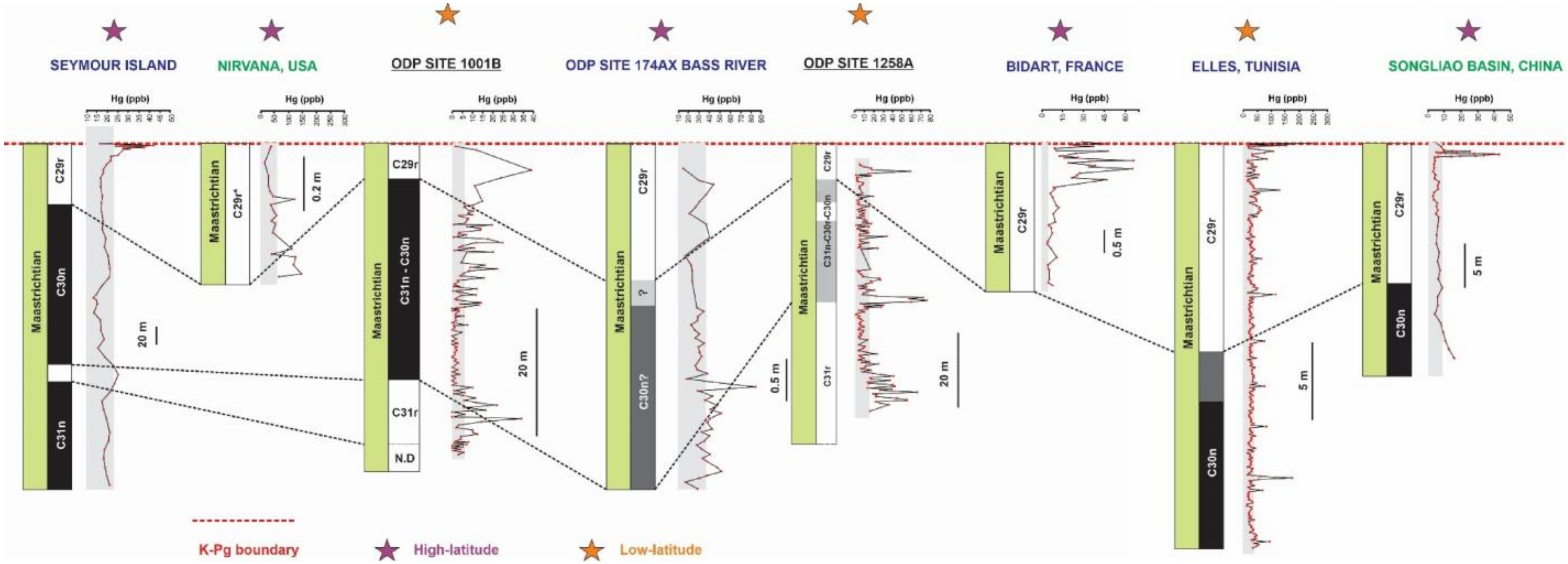

TABLE S1 δ13C AND HG CONCENTRATIONS OF CORE DIABLITO-1E (HG DATA)

Consecutive	Label	Depth (ft)	Depth (m)	Hg (ppb)	Hg/S (NMS)	Age (My)	COT (%)	Hg/COT			
1	DI1885.5	1885.5	574.7	52.7666	45.682	66.71	0.603	87.5			
2	DI1891.5	1891.5	576.5	50.3111	56.362	66.73	0.454	110.8			
3	DI1895.3	1895.3	577.7	66.8391	18.393	66.74	0.568	117.7			
4	DI1898	1898	578.5	65.6969	17.140	66.75	0.691	95.1			
5	DI1902.8	1902.8	580.0	83.7530	34.391	66.76	1.064	78.7			
6	DI1908.3	1908.3	581.6	56.4299	30.279	66.78	1.485	38.0			
7	DI1912.2	1912.2	582.8	56.4565	94.669	66.79	0.638	88.5			
8	DI1919.4	1919.4	585.0	59.5730	24.600	66.81	0.556	107.1			
9	DI1921	1921	585.5	84.0767	18.671	66.82	1.304	64.5			
10	DI1925.2	1925.2	586.8	104.7028	20.363	66.83	1.729	60.6			
11	DI1929.1	1929.1	588.0	72.8884	57.538	66.84	0.663	109.9			
12	DI1932.3	1932.3	589.0	52.8752	27.461	66.85	0.483	109.5			
13	DI1935.6	1935.6	590.0	47.9652	48.216	66.86	0.568	84.4			
14	DI1938.3	1938.3	590.8	64.4972	43.934	66.87	0.817	78.9			
15	DI1943	1943	592.2	58.4613	33.913	66.88	0.935	62.5			
16	DI1946.2	1946.2	593.2	65.5287	43.329	66.89	0.818	80.1			
17	DI1948.4	1948.4	593.9	60.5052	45.760	66.9	0.903	67.0			
18	DI1957.8	1957.8	596.7	49.2314	26.250	66.92	0.535	92.0			
19	DI1960.2	1960.2	597.5	64.4569	37.516	66.93	0.845	76.3			
20	DI1965.6	1965.6	599.1	93.8000	19.904	66.94	1.021	91.9			
21	DI1968.2	1968.2	599.9	91.1145	21.353	66.95	0.801	113.8			
22	DI1971.4	1971.4	600.9	62.2959	59.965	66.96	0.804	77.5			
23	DI1977.2	1977.2	602.7	57.3917	58.136	66.97	0.562	102.1			
24	DI1981.3	1981.3	603.9	46.3608	54.031	66.98	0.507	91.4			
25	DI1989	1989	606.2	37.4882	48.686	67	0.407	92.1			
26	DI1991	1991	606.9	35.4519	190.010	67.01	0.429	82.6			
27	DI1993	1993	607.5	54.8760	20.405	67.02	0.385	142.5			
28	DI1995	1995	608.1	46.9868	22.492	67.03	0.368	127.7			
29	DI2010.2	2010.2	612.7	29.9269	50.647	67.06	0.296	101.1			
30	DI2016	2016	614.5	105.6044	19.419	67.08	0.431	245.0			
31	DI2022.2	2022.2	616.4	43.9792	20.285	67.1	0.351	125.3			
32	DI2033	2033	619.7	69.3608	13.695	67.13	0.464	149.5			
33	DI2037.9	2037.9	621.2	36.9778	20.737	67.14	0.352	105.1			
34	DI2046.5	2046.5	623.8	46.5090	12.722	67.17	0.645	72.1			
35	DI2050.3	2050.3	624.9	62.9721	12.952	67.18	0.462	136.3			
36	DI2055.8	2055.8	626.6	47.7065	16.086	67.19	0.342	139.5			
37	DI2057.4	2057.4	627.1	50.4217	25.303	67.2	0.356	141.6			
38	DI2062.9	2062.9	628.8	80.1148	30.969	67.21	0.473	169.4			
39	DI2065.8	2065.8	629.7	56.3694	8.425	67.22	0.336	167.8			
40	DI2068.3	2068.3	630.4	39.7213	31.185	67.23	0.450	88.3			
41	DI2070.1	2070.1	631.0	44.3549	39.325	67.24	0.489	90.7			
42	DI2075.3	2075.3	632.6	45.3755	40.164	67.25	0.458	99.1			
43	DI2078.4	2078.4	633.5	63.0645	47.211	67.26	0.469	134.5			
44	DI2082.1	2082.1	634.6	91.8476	21.515	67.27	0.433	212.1			
45	DI2088.5	2088.5	636.6	39.5943	19.931	67.29	0.544	72.8			
46	DI2091.3	2091.3	637.4	36.7035	13.481	67.29	0.591	62.1			
47	DI2102	2102	640.7	31.7922	28.941	67.32	0.422	75.3			
48	DI2105.5	2105.5	641.8	40.1539	29.568	67.34	0.517	77.7			
49	DI2113	2113	644.0	30.5001	34.489	67.36	0.367	83.1			
50	DI2115	2115	644.7	37.3151	41.165	67.37	0.334	111.7			
51	DI2117.8	2117.8	645.5	35.6110	36.700	67.37	0.371	96.0			
52	DI2120.5	2120.5	646.3	36.2765	58.564	67.38	0.356	101.9			
53	DI2127	2127	648.3	85.0592	21.813	67.39	0.572	148.7			
54	DI2129.3	2129.3	649.0	49.0700	22.860	67.4	0.647	75.8			
55	DI2133.2	2133.2	650.2	50.0977	23.694	67.41	0.506	99.0			
56	DI2135.2	2135.2	650.8	54.8344	28.911	67.42	0.510	107.5			
57	DI2152	2152	655.9	64.0227	50.530	67.46	0.690	92.8			
58	DI2162.4	2162.4	659.1	59.2330	27.343	67.49	0.569	104.1			
59	DI2165.6	2165.6	660.1	48.3206	20.680	67.5	0.476	101.5			
60	DI2167.5	2167.5	660.7	39.0026	15.365	67.51	0.392	99.5			
61	DI2174.7	2174.7	662.8	64.1648	12.730	67.53	0.625	102.7			
62	DI2178.6	2178.6	664.0	96.6433	12.288	67.54	0.494	195.6			
63	DI2181	2181	664.8	66.8824	13.037	67.55	0.426	157.0			
64	DI2185.2	2185.2	666.0	42.6797	27.623	67.56	0.357	119.6			
65	DI2190.8	2190.8	667.8	44.3884	10.686	67.57	0.352	126.1			
66	DI2193.4	2193.4	668.5	56.7413	17.124	67.58	0.346	164.0			
67	DI2196.5	2196.5	669.5	50.1996	23.982	67.59	0.373	134.6			
68	DI2201	2201	670.9	50.3507	24.482	67.6	0.420	119.9			
69	DI2206.4	2206.4	672.5	43.6212	25.471	67.62	0.352	123.9			
70	DI2210	2210	673.6	49.3861	20.603	67.63	0.366	134.9			
71	DI2211.9	2211.9	674.2	160.5258	22.706	67.64	0.37	433.9			
72	DI2220.7	2220.7	676.9	45.6955	26.864	67.66	0.405	112.8			
73	DI2225	2225	678.2	56.7357	22.548	67.66	0.401	141.5			
74	DI2227.2	2227.2	678.9	53.2064	17.293	67.68	0.349	152.5			
75	DI2233.7	2233.7	680.8	56.6690	19.164	67.69	0.318	178.2			
76	DI2235	2235	681.2	60.7525	22.697	67.7	0.267	227.5			
77	DI2237.3	2237.3	681.9	48.5207	15.765	67.71	0.258	188.1			
78	DI2242.3	2242.3	683.5	65.2820	16.261	67.72	0.284	229.9			
79	DI2245.5	2245.5	684.4	49.0370	11.865	67.73	0.267	183.7			Age
80	DI2247.2	2247.2	684.9	49.8251	20.199	67.74	0.284	175.4		K/Pg	66.04
81	DI2253.5	2253.5	686.8	47.4376	26.906	67.75	0.253	187.5		Top S. bramletti (FO P. hariaensis)	67.30
82	DI2255.2	2255.2	687.4	54.8	28.204	67.76	0.253	216.5			
83	DI2258.4	2258.4	688.4	50.5826	26.068	67.77	0.286	176.9			
84	DI2263.7	2263.7	690.0	54.9388	31.233	67.78	0.283	194.1			
85	DI2265.2	2265.2	690.4	41.3232	33.398	67.78	0.276	149.7			
86	DI2268.5	2268.5	691.4	40.2581	11.575	67.79	0.254	158.5			
87	DI2271.4	2271.4	692.3	125.5481	21.107	67.8	0.446	281.5			
88	DI2275.4	2275.4	693.5	32.0793	59.127	67.81	0.341	94.1			
89	DI2278.5	2278.5	694.5	37.3170	43.222	67.82	0.495	75.4			
90	DI2283.2	2283.2	695.9	31.2729	46.581	67.83	0.418	74.8			
91	DI2284.2	2284.2	696.2	35.5983	51.572	67.84	0.373	95.4			
92	DI2286.5	2286.5	696.9	35.1832	9.394	67.85	0.342	102.9			
93	DI2297.5	2297.5	700.3	42.2097	16.870	67.88	0.302	139.8			
				56.2851	31.105			124.4			
First group											
Second group											
Third group											

TABLE S1 δ13C AND HG CONCENTRATIONS OF CORE DIABLITO-1E (ISOTOPES)						
Consecutive	(ft)	Depth (m)	delta 13C/12C	Age (My)	Depth (m)	Age (My)
1	**1971.4**	**585**	**-5.35**	66.81	585.0	66.81
2	**2033**	**619.7**	**-5.03**	67.13	619.7	67.13
3	**2037.9**	**621.2**	**-4.91**	67.14	621.2	67.14
4	2044.1	623	-6.20	67.16	624.9	67.18
5	2046.5	623.8	-6.65	67.17	626.6	67.19
6	**2050.3**	**624.9**	**-6.33**	67.18	627.1	67.2
7	**2055.8**	**626.6**	**-5.44**	67.19	628.8	67.21
8	**2057.4**	**627.1**	**-5.01**	67.2	630.4	67.23
9	**2062.9**	**628.8**	**-5.59**	67.21	631.0	67.24
10	**2068.3**	**630.4**	**-4.82**	67.23	633.5	67.26
11	**2070.1**	**631**	**-4.14**	67.24	634.6	67.27
12	**2078.4**	**633.5**	**-3.71**	67.26	636.6	67.29
13	2080.1	634	-3.45	67.27	637.4	67.29
14	**2082.1**	**634.6**	**-4.26**	67.27	641.8	67.34
15	**2088.5**	**636.6**	**-3.41**	67.29	644.0	67.36
16	**2091.3**	**637.4**	**-3.77**	67.29	644.7	67.37
17	2097.1	639.2	-4.24	67.31	646.3	67.38
18	2099.3	639.9	-3.26	67.32	648.3	67.39
19	**2105.5**	**641.8**	**-4.00**	67.34	649.0	67.4
20	**2113**	**644**	**-4.74**	67.36	650.2	67.41
21	**2115**	**644.7**	**-3.23**	67.37	650.8	67.42
22	2117.8	645.5	-4.39	67.37	655.9	67.46
23	**2120.5**	**646.3**	**-3.13**	67.38	659.1	67.49
24	**2127**	**648.3**	**-2.45**	67.39	660.1	67.5
25	**2129.3**	**649**	**-3.51**	67.4	660.7	67.51
26	**2133.2**	**650.2**	**-3.42**	67.41	662.8	67.53
27	**2135.2**	**650.8**	**-3.38**	67.42	664.8	67.55
28	**2152**	**655.9**	**-4.07**	67.46	670.9	67.6
29	**2162.4**	**659.1**	**-3.68**	67.49	672.5	67.62
30	**2165.6**	**660.1**	**-4.65**	67.5	673.6	67.63
31	**2167.5**	**660.7**	**-2.78**	67.51	676.9	67.66
32	**2174.7**	**662.8**	**-2.36**	67.53	678.2	67.66
33	**2181**	**664.8**	**-4.17**	67.55	678.9	67.68
34	**2201**	**670.9**	**-4.12**	67.6	680.8	67.69
35	**2206.4**	**672.5**	**-4.14**	67.62	681.2	67.7
36	**2210**	**673.6**	**-4.99**	67.63	681.9	67.71
37	2216.4	675.6	-5.57	67.65	683.5	67.72
38	**2220.7**	**676.9**	**-4.98**	67.66	684.4	67.73
39	**2225**	**678.2**	**-5.39**	67.66	684.9	67.74
40	**2227.2**	**678.9**	**-4.54**	67.68	686.8	67.75
41	**2233.7**	**680.8**	**-5.84**	67.69	687.4	67.76
42	**2235**	**681.2**	**-5.50**	67.7	688.4	67.77
43	**2237.3**	**681.9**	**-5.49**	67.71	690.0	67.78
44	**2242.3**	**683.5**	**-4.28**	67.72	690.4	67.78
45	**2245.5**	**684.4**	**-4.56**	67.73	691.4	67.79
46	**2247.2**	**684.9**	**-4.25**	67.74	693.5	67.81
47	**2253.3**	**686.8**	**-3.31**	67.75	695.9	67.83
48	**2255.2**	**687.4**	**-3.88**	67.76	696.2	67.84
49	2257.5	688.1	-6.19	67.77		
50	**2258.4**	**688.4**	**-4.27**	67.77		
51	2262.3	689.5	-5.78	67.78		
52	**2263.7**	**690**	**-3.94**	67.78		
53	**2265.2**	**690.4**	**-4.12**	67.78		
54	2267.2	691	-4.14	67.79		
55	**2268.5**	**691.4**	**-4.35**	67.79		
56	2271.4	692.3	-4.64	67.8		
57	**2275.4**	**693.5**	**-5.53**	67.81		
58	**2283.2**	**695.9**	**-4.64**	67.83		
59	**2284.2**	**696.2**	**-4.31**	67.84		
60	2299.5	700.9	-3.55	67.99		

TABLE S1 δ13C AND HG CONCENTRATIONS OF CORE DIABLITO-1E (TOC)

	Diablito-1E		
Consecutive	Sample	COT	Depth (m)
1	1888.5	0.603	574.7
2	1891.5	0.454	576.5
3	1895.3	0.568	577.7
4	1898	0.691	578.5
5	1902.8	1.064	580.0
6	1908.3	1.485	581.6
7	1912.2	0.638	582.8
8	1919.4	0.556	585.0
9	1921	1.304	585.5
10	1925.2	1.729	586.8
11	1929.1	0.663	588.0
12	1932-3	0.483	589.0
13	1935.6	0.568	590.0
14	1938.3	0.817	590.8
15	1943	0.935	592.2
16	1946.2	0.818	593.2
17	1948.4	0.903	593.9
18	1957.8	0.535	596.7
19	1960.2	0.845	597.5
20	1965.6	1.021	599.1
21	1968.3	0.801	599.9
22	1971.4	0.804	600.9
23	1977.2	0.562	602.7
24	1981.3	0.507	603.9
25	1989	0.407	606.2
26	1991	0.429	606.9
27	1993	0.385	607.5
28	1995	0.368	608.1
29	2010.2	0.296	612.7
30	2016	0.431	614.5
31	2022.2	0.351	616.4
32	2033	0.464	619.7
33	2037.9	0.352	621.2
34	2046.5	0.645	623.8
35	2050.3	0.462	624.9
36	2055.8	0.342	626.6
37	2057.4	0.356	627.1
38	2062.9	0.473	628.8
39	2065.8	0.336	629.7
40	2068.3	0.45	630.4
41	2070.1	0.489	631.0
42	2075.3	0.458	632.6
43	2078.4	0.469	633.5
44	2082.1	0.433	634.6
45	2088.5	0.544	636.6
46	2091.3	0.591	637.4
47	2102	0.422	640.7
48	2105.5	0.517	641.8
49	2113	0.367	644.0
50	2115	0.334	644.7
51	2117.8	0.371	645.5
52	2120.5	0.356	646.3
53	2127	0.572	648.3
54	2129.3	0.647	649.0
55	2133.2	0.506	650.2
56	2135.2	0.51	650.8
57	2152	0.69	655.9
58	2162.4	0.569	659.1
59	2165.6	0.476	660.1
60	2167.5	0.392	660.7
61	2174.7	0.625	662.8
62	2178.6	0.494	664.0
63	2181	0.426	664.8
64	2185.2	0.357	666.0
65	2190.8	0.352	667.8
66	2193.4	0.346	668.5
67	2196.5	0.373	669.5
68	2201	0.42	670.9
69	2206.4	0.352	672.5
70	2210	0.366	673.6
71	2211.9	0.37	674.2
72	2220.7	0.405	676.9
73	2225	0.401	678.2
74	2227.2	0.349	678.9
75	2233.7	0.318	680.8
76	2235	0.267	681.2
77	2237.3?	0.258	681.9
78	2242.3?	0.284	683.5
79	2245.5	0.267	684.4
80	2247.2?	0.284	684.9
81	2253.5?	0.253	686.8
82	2255.2?	0.253	687.4
83	2258.4	0.286	688.4
84	2263.7?	0.283	690.0
85	2265.2?	0.276	690.4
86	2268.5?	0.254	691.4
87	2271.4	0.446	692.3
88	2275.4?	0.341	693.5
89	2278.5	0.495	694.5
90	2283.2?	0.418	695.9
91	2284.2?	0.373	696.2
92	2286.5?	0.342	696.9
93	2297.5?	0.302	700.3

TABLA S2 HG CONCENTRATIONS OF HOLE 1258A AND 1001B (DEMERARA)

Consecutive	Sample	Depth (mbsf)	Age (Ma)	Mercury (µg/kg)	TOC (%wt)*	*Scientific report	TOC tt	Mercury (µg/kg)	Hg/TOC (average)
1	28R2 110-112	257.5	66.2	5.1756	0.06		0.10	5.1756	51.8
2	28R2 148-150	257.88	66.21	6.2217	0.06		0.10	6.2217	62.2
3	28R3 23-25	258.13	66.22	9.4234	0.06		0.10	9.4234	94.2
4	28R3 61-63	258.51	66.23	17.2703	0.06		0.10	17.2703	172.7
5	28R3 103-105	258.93	66.25	17.8103	0.06		0.1	17.8103	178.1
6	28R3 141-143	259.31	66.26	58.8718	0.06		0.12	58.8718	490.6
7	28R4 21-23	259.61	66.27	14.2868	0.06		0.1	14.2868	142.9
8	28R4 63-65	260.01	66.28	3.8278	0.06		0.1	3.8278	38.3
9	28R4 103-105	260.41	66.3	16.5906	0.05		0.1	16.5906	165.9
10	28R4 143-145	260.81	66.31	2.3472	0.05		0.1	2.3472	23.5
11	28R5 13-15	261.03	66.32	2.0243	0.05		0.1	2.0243	20.2
12	28R5 48-50	261.38	66.33	2.5418	0.05		0.1	2.5418	25.4
13	28R5 93-95	261.83	66.35	2.4878	0.05		0.1	2.4878	24.9
14	28R5 133-135	262.23	66.36	8.8305	0.05		0.1	8.8305	88.3
15	28R6 28-30	262.7	66.38	8.2659	0.05		0.1	8.2659	82.7
16	28R6 70-72	263.1	66.41	5.1132	0.04		0.1	5.1132	51.1
17	28R6 110-112	263.5	66.45	4.7464	0.04		0.1	4.7464	47.5
18	29R1 21-24	264.82	66.57	7.9614	0.04		0.1	7.9614	79.6
19	29R1 63-65	265.23	66.61	2.3181	0.04		0.1	2.3181	23.2
20	29R1 103-105	265.63	66.65	17.6117	0.04		0.1	17.6117	176.1
21	29R1 144-146	266.04	66.69	5.6451	0.03		0.1	5.6451	56.5
22	29R2 18-20	266.28	66.71	7.2897	0.03		0.1	7.2897	72.9
23	29R2 59-61	266.69	66.75	2.8309	0.03		0.1	2.8309	28.3
24	29R2 104-106	267.14	66.79	4.3537	0.03		0.1	4.3537	43.5
25	29R2 143-145	267.53	66.83	3.0787	0.03		0.1	3.0787	30.8
26	29R3 20-22	267.8	66.85	4.5432	0.04		0.1	4.5432	45.4
27	29R3 58-60	268.18	66.89	14.0939	0.04		0.1	14.0939	140.9
28	29R3 98-100	268.58	66.92	7.526	0.04		0.1	7.526	75.3
29	29R3 140-142	269	66.96	3.5723	0.04		0.1	3.5723	35.7
30	29R4 5-7	269.15	66.98	9.9452	0.04		0.1	9.9452	99.5
31	29R4 43-45	269.53	67.02	4.4054	0.05		0.1	4.4054	44.1
32	29R4 85-87	269.95	67.06	9.9422	0.05		0.1	9.9422	99.4
33	29R4 125-127	270.35	67.09	5.6464	0.05		0.1	5.6464	56.5
34	29R5 21-23	270.63	67.12	9.462	0.05		0.1	9.462	94.6
35	29R5 63-65	271.05	67.16	3.1401	0.06		0.1	3.1401	31.4
36	29R5 103-105	271.45	67.2	9.9269	0.06		0.1	9.9269	99.3
37	29R5 143-145	271.85	67.23	12.7195	0.06		0.1	12.7195	127.2
38	29R6 20-22	272.12	67.26	9.0151	0.06		0.1	9.0151	90.2
39	29R6 60-62	272.52	67.28	16.3791	0.06		0.1	16.3791	163.8
40	29R6 105-107	272.97	67.3	2.6735	0.07		0.1	2.6735	26.7
41	29R6 140-142	273.32	67.37	13.0265	0.07		0.1	13.0265	130.3
42	29R7 13-15	273.55	67.4	3.7506	0.07		0.1	3.7506	37.5
43	29R7 50-52	273.92	67.43	2.798	0.07		0.1	2.798	28.0
44	29R CC 3-5	274.37	67.47	11.8297	0.08		0.1	11.8297	118.3
45	29R7 93-95	274.39	67.47	13.1466	0.08		0.1	13.1466	131.5
46	30R1 20-22	274.4	67.48	7.2103	0.08		0.1	7.2103	72.1
47	30R1 60-62	274.8	67.51	13.8135	0.08		0.1	13.8135	138.1
48	30R1 108-110	275.28	67.56	5.2191	0.08		0.1	5.2191	52.2
49	30R1 143-145	275.63	67.59	5.5799	0.08		0.1	5.5799	55.8
50	30R2 10-12	275.8	67.61	33.7083	0.08		0.1	33.7083	337.1
51	30R2 55-57	276.25	67.65	13.1532	0.09		0.1	13.1532	131.5
52	30R2 95-97	276.65	67.68	4.9843	0.09		0.1	4.9843	49.8
53	30R2 135-137	277.05	67.72	6.4821	0.09		0.1	6.4821	64.8
54	30R3 18-22	277.4	67.76	14.0145	0.09		0.1	14.0145	140.1
55	30R3 63-65	277.83	67.8	5.2121	0.10		0.1	5.2121	52.1
56	30R3 102-105	278.23	67.84	5.9754	0.10		0.1	5.9754	59.8
57	30R3 143-145	278.63	67.87	3.7912	0.10		0.1	3.7912	37.9
58	30R4 10-12	278.8	67.89	24.1898	0.10		0.1	24.1898	241.9
59	30R4 41-43	279.11	67.92	6.7119	0.10		0.1	6.7119	67.1
60	31R1 23-25	284.13	68.39	16.2616	0.09		0.1	16.2616	162.6
61	31R1 65-67	284.55	68.43	3.1764	0.09		0.1	3.1764	31.8
62	31R1 105-107	284.95	68.46	4.381	0.09		0.1	4.381	43.8
63	31R1 145-147	285.35	68.5	6.147	0.09		0.1	6.147	61.5
64	31R2 23-25	285.63	68.53	7.8194	0.09		0.1	7.8194	78.2
65	31R2 63-65	286.03	68.57	8.3991	0.09		0.1	8.3991	84.0
66	31R2 103-105	286.43	68.6	26.0313	0.09		0.1	26.0313	260.3
67	31R2 143-145	286.83	68.64	26.9656	0.09		0.1	26.9656	269.7
68	31R3 18-20	287.08	68.66	16.4206	0.09		0.1	16.4206	164.2
69	31R3 63-65	287.53	68.71	18.1784	0.09		0.1	18.1784	181.8
70	31R3 103-105	287.93	68.74	11.577	0.09		0.1	11.577	115.8
71	31R3 143-145	288.33	68.78	4.8003	0.09		0.1	4.8003	48.0
72	31R4 23-25	288.63	68.81	11.6707	0.09		0.1	11.6707	116.7
73	31R4 63-65	289.03	68.85	5.8204	0.09		0.1	5.8204	58.2
74	31R4 103-105	289.43	68.88	19.753	0.09		0.1	19.753	197.5
75	31R4 143-145	289.83	68.92	13.2567	0.09		0.1	13.2567	132.6
76	31R5 22-24	290.12	68.95	9.1904	0.09		0.1	9.1904	91.9
77	31R5 63-65	290.53	68.99	8.1501	0.09		0.1	8.1501	81.5
78	31R5 103-105	290.93	69.02	22.2791	0.09		0.1	22.2791	222.8
79	31R5 143-145	291.33	69.06	72.3049	0.09		0.1	72.3049	723.0
80	31R6 22-24	291.62	69.09	57.6155	0.09		0.1	57.6155	576.2
81	31R6 64-66	292.04	69.13	76.0114	0.09		0.1	76.0114	760.1
82	31R6 103-105	292.43	69.16	59.5835	0.09		0.1	59.5835	595.8
83	31R6 143-145	292.83	69.2	6.1883	0.08		0.1	6.1883	61.9
84	31R7 30-32	293.2	69.24	30.3176	0.08		0.1	30.3176	303.2
85	31R7 58-60	293.48	69.27	9.9666	0.08		0.1	9.9666	99.7
86	31RCC 9-11	293.68	69.28	27.9504	0.08		0.1	27.9504	279.5
87	32R1 24-28	293.76	69.28	11.3906	0.08		0.1	11.3906	113.9
88	32R1 65-67	294.15	69.3	13.4933	0.08		0.1	13.4933	134.9
89	32R1 105-108	294.56	69.33	4.6794	0.08		0.1	4.6794	46.8
90	32R1 144-146	294.93	69.35	9.7194	0.08		0.1	9.7194	97.2
91	32R2 25-27	295.25	69.37	3.6622	0.08		0.1	3.6622	36.6
92	32R2 65-67	295.65	69.4	0.9297	0.08		0.1	0.9297	9.3
93	32R2 105-107	296.05	69.42	5.0737	0.08		0.1	5.0737	50.7
94	32R2 145-147	296.45	69.44	3.3807	0.08		0.1	3.3807	33.8
95	32R3 22-24	296.72	69.46	5.9961	0.08		0.1	5.9961	60.0
96	32R3 65-67	297.15	69.48	8.3499	0.08		0.1	8.3499	83.5
97	32R3 105-107	297.55	69.51	5.9237	0.08		0.1	5.9237	59.2
98	32R3 145-147	297.95	69.53	4.7	0.08		0.1	4.7	47.0
99	32R4 23-25	298.23	69.55	5.9007	0.08		0.1	5.9007	59.0
100	32R4 65-67	298.65	69.58	9.926	0.08		0.1	9.926	99.3
101	32R4 105-107	299.05	69.6	4.9336	0.08		0.1	4.9336	49.3
102	32R4 145-147	299.45	69.62	3.9409	0.08		0.1	3.9409	39.4
103	32R5 16-18	299.66	69.63	9.1325	0.08		0.1	9.1325	91.3
104	32R5 55-57	300.05	69.65	8.1495	0.08		0.1	8.1495	81.5
105	32R5 95-97	300.45	69.68	5.1993	0.08		0.1	5.1993	52.0
106	32R5 135-137	300.85	69.7	6.9978	0.08		0.1	6.9978	70.0
107	32R6 20-22	301.2	69.72	4.0854	0.08		0.1	4.0854	40.9
108	32R6 65-67	301.65	69.75	5.3472	0.08		0.1	5.3472	53.5
109	32R6 101-103	302.01	69.77	13.3538	0.08		0.1	13.3538	133.5
110	33R1 20-22	303.3	69.85	4.0994	0.08		0.1	4.0994	41.0
111	33R1 60-62	303.7	69.87	10.668	0.08		0.1	10.668	106.7
112	33R1 110-112	304.18	69.9	8.5404	0.08		0.1	8.5404	85.4
113	33R1 140-142	304.5	69.92	4.6339	0.08		0.1	4.6339	46.3
114	33R2 18-20	304.78	69.94	3.597	0.08		0.1	3.597	36.0
115	33R2 58-60	305.18	69.96	12.3631	0.08		0.1	12.3631	123.6
116	33R2 98-100	305.58	69.98	22.1607	0.09		0.1	22.1607	221.6
117	33R2 140-142	306	70.01	4.7686	0.09		0.1	4.7686	47.7
118	33R3 20-22	306.3	70.03	6.4369	0.09		0.1	6.4369	64.4
119	33R3 60-62	306.7	70.05	9.677	0.09		0.1	9.677	96.8
120	33R3 98-100	307.1	70.07	4.1075	0.09		0.1	4.1075	41.1
121	33R3 140-142	307.5	70.08	14.1707	0.09		0.1	14.1707	141.7
122	33R4 15-17	307.75	70.11	8.7208	0.09		0.1	8.7208	87.2
123	33R4 55-57	308.15	70.13	23.5179	0.09		0.1	23.5179	235.2
124	33R4 103-105	308.65	70.16	11.7673	0.09		0.1	11.7673	117.7
125	33R4 145-147	309.05	70.19	10.4262	0.09		0.1	10.4262	104.3
126	33R5 25-27	309.35	70.21	6.5246	0.09		0.1	6.5246	65.2
127	33R5 63-65	309.73	70.23	16.2143	0.09		0.1	16.2143	162.1
128	33R5 102-104	310.12	70.25	8.2353	0.09		0.1	8.2353	82.4
129	33R5 145-147	310.55	70.27	18.8434	0.09		0.1	18.8434	188.4
130	33R6 23-25	310.83	70.29	27.3452	0.09		0.1	27.3452	273.5
131	33R6 63-65	311.23	70.32	38.9438	0.09		0.155	38.9438	251.3
132	33R6 103-105	311.63	70.34	16.0874	0.09		0.10	16.0874	160.9
133	33R6 142-144	312.02	70.36	17.3933	0.09		0.10	17.3933	173.9
134	33R7 22-24	312.32	70.38	37.1772	0.09		0.10	37.1772	371.8
135	33R7 68-70	312.78	70.41	13.3559	0.09		0.10	13.3559	133.6
136	34R1 23-25	313.03	70.42	14.6914	0.09		0.10	14.6914	146.9
137	34R1 62-64	313.42	70.45	39.9287	0.09		0.10	39.9287	399.3
138	34R1 103-105	313.83	70.48	42.4085	0.09		0.10	42.4085	424.1
139	34R1 144-146	314.24	70.5	13.1219	0.09		0.10	13.1219	131.2
140	34R2 25-27	314.55	70.52	38.7651	0.09		0.10	38.7651	387.7
141	34R2 60-62	314.8	70.53	26.63	0.09		0.10	26.63	266.3
142	34R2 102-104	315.22	70.55	66.3086	0.09		0.10	66.3086	663.1
143	34R2 143-145	315.73	70.58	20.1468	0.10		0.10	20.1468	201.5
144	34R3 23-25	316.02	70.6	23.168	0.10		0.10	23.168	231.7
145	34R3 64-66	316.43	70.63	22.2212	0.11		0.10	22.2212	222.2
146	34R3 102-104	316.81	70.65	44.0819	0.12		0.10	44.0819	440.8
147	34R3 142-144	317.21	70.67	55.0406	0.12		0.10	55.0406	550.4
148	34R4 8-10	317.38	70.67	55.3435	0.13		0.10	55.3435	553.4
149	34R4 42-43	317.71	70.7	22.5152	0.13		0.10	22.5152	225.2
150	34R4 78-80	318.08	70.72	27.0376	0.14		0.10	27.0376	270.4
151	34R4 118-119	318.47	70.75	36.0707	0.15		0.10	36.0707	360.7
152	34R CC 5-7	320.11	70.84	15.9877	0.17		0.10	15.9877	159.9
				14.55419342			0.10	14.55419342	144.0

TABLA S2 HG CONCENTRATIONS OF HOLE 1258A AND 1001B (NICARAGUA)

Consecutive	Sample	Depth (mbsf)	Weight (g)	Mercury (µg/kg)	TOC*			Mercury (µg/kg)	Hg/TOC		S NMS	Depth (mbsf)	Age (My)
	16R1 70-75	332.15		2.6181	0.09		*Scientific results 1001A	2.6181	29.09	0.09		332.15	62.28
	16R2 71-76	333.66		1.4787	0.09			1.4787	16.43	0.09		333.66	62.56
	16R3 70-76	335.16		0.8886	0.09			0.8886	9.87	0.09		335.16	62.85
	16R4 70-75	336.65		6.4878	0.09			6.4878	72.09	0.09		336.65	63.13
	16R5 70-75	338.15		2.5151	0.09			2.5151	27.95	0.09		338.15	63.42
	16R6 70-76	339.76		2.7077	0.09			2.7077	30.09	0.09		339.76	63.72
	16R7 20-24	340.64		4.1894	0.09			4.1894	46.55	0.09		340.64	63.89
	17R1 68-73	341.83		2.8899	0.09			2.8899	32.11	0.09		341.83	64.11
	17R2 69-74	343.19		3.8965	0.09			3.8965	43.29	0.09		343.19	64.37
	17R3 69-74	344.66		2.7409	0.09			2.7409	30.45	0.09		344.66	64.64
	17R4 69-74	345.91		1.0715	0.09			1.0715	11.91	0.09		345.91	64.76
	18R1 72-77	348.77		6.3108	0.09		SET EXTRA	6.3108	70.12	0.09		348.77	65.36
	18R2 77-82	349.96		4.0033	0.09			4.0033	44.48	0.09		349.96	65.69
	18R3 72-77	351.13		1.3045	0.09			1.3045	14.49	0.09		351.13	65.83
Paleogene	18R4 70-75	352.27		4.7374	0.09			4.7374	52.64	0.09		352.27	65.97
	18R5 55-60	353.22		1.5273	0.09			1.5273	16.97	0.09		353.22	66.06
	18R6 55-59	353.79		11.7196	0.09			11.7196	130.22	0.09		353.79	66.08
	19R1 77-82	357.12		38.8293	0.09			38.8293	431.44	0.09		357.12	66.26
	19R2 69-74	358.4		23.823	0.09			23.823	264.70	0.09		358.4	66.32
	19R3 70-76	359.68		11.0699	0.09			11.0699	123.00	0.09		359.68	66.4
	20R1 29-32	362.2		14.674	0.09	K		14.674	163.04	0.09	0.996682	362.2	66.61
	20R1 55-57	362.87		10.2335	0.09	K		10.2335	113.71	0.09	1.578916	362.87	66.67
	20R1 69-74	363.03		6.1915	0.09			6.1915	68.79	0.09		363.03	66.69
	20R1 85-87	363.17		5.7995	0.09	K		5.7995	64.44	0.09	1.48032	363.17	66.7
	20R1 145-147	363.77		8.1635	0.09			8.1635	90.71	0.09	1.149976	363.77	66.75
	20R2 5-7	363.87		10.2556	0.09			10.2556	113.95	0.09	1.307049	363.87	66.76
	20R2 45-47	364.24		7.7595	0.09			7.7595	86.22	0.09	1.132581	364.24	66.79
	20R2 68-70	364.47		9.7817	0.09			9.7817	108.69	0.09	1.154731	364.47	66.81
	20R2 77-82	364.59		3.3616	0.09			3.3616	37.35	0.09		364.59	66.82
	20R2 88-90	364.7		4.2379	0.09	K		4.2379	47.09	0.09	1.504952	364.7	66.83
	20R2 128-130	365.1		7.8796	0.09	K		7.8796	87.55	0.09	1.213302	365.1	66.87
	20R3 8-10	365.4		7.0279	0.09	K		7.0279	78.09	0.09	1.029705	365.4	66.89
	20R3 48-50	365.8		6.3239	0.09	K		6.3239	70.27	0.09	1.306481	365.8	66.93
	20R3 73-75	366.05		0.7487	0.09	K		0.7487	8.32	0.09	1.128195	366.05	66.95
	20R3 78-83	366.13		19.4782	0.09			19.4782	216.42	0.09		366.13	66.96
	20R3 113-115	366.45		8.2324	0.09	K		8.2324	91.47	0.09	1.32077	366.45	66.98
	20R3 138-140	366.7		13.9312	0.09	K		13.9312	154.79	0.09	1.374658	366.7	67
	20R4 13-15	366.95		13.692	0.09	K		13.692	152.13	0.09	1.796645	366.95	67.03
	20R4 53-55	367.35		3.4679	0.09	K		3.4679	38.53	0.09	1.064178	367.35	67.06
	20R4 75-80	367.6		2.9849	0.09			2.9849	33.17	0.09		367.6	67.08
	20R4 93-95	367.75		6.3672	0.09	Pg		6.3672	70.75	0.09	1.53199	367.75	67.1
	20R4 140-142	368.12		1.2084	0.09	Pg		1.2084	13.43	0.09	1.424166	368.12	67.13
	20R5 13-15	368.45		17.5397	0.09	Pg		17.5397	194.89	0.09	1.457809	368.45	67.16
	20R5 70-72	369.02		24.079	0.09	Pg		24.079	267.54	0.09	1.451118	369.02	67.21
	20R5 69-73	369.03		11.7349	0.09			11.7349	130.39	0.09		369.03	67.21
	20R5 120-122	369.52		5.0669	0.09	K		5.0669	56.30	0.09	1.172662	369.52	67.25
	20R5 148-150	369.8		3.4491	0.09	K		3.4491	38.32	0.09	1.944222	369.8	67.27
	20R6 9-11	369.91		10.7513	0.09	Pg		10.7513	119.46	0.09	1.959172	369.91	67.28
	20R6 50-52	370.32		1.0171	0.09	Pg		1.0171	11.30	0.09	1.13237	370.32	67.32
	20R6 73-78	370.58		20.0221	0.09			20.0221	222.47	0.09		370.58	67.34
	20R6 90-92	370.72		6.8754	0.09	Pg		6.8754	76.39	0.09	1.208263	370.72	67.35
	21R1 31-33	372.33		4.4407	0.09	Pg		4.4407	49.34	0.09	2.165774	372.33	67.49
	21R1 70-74	372.74		15.4674	0.09	Pg		15.4674	171.86	0.09	1.500844	372.74	67.53
	21R1 108-110	373.1		9.6338	0.09	Pg		9.6338	107.04	0.09	1.047664	373.1	67.56
	21R1 133-135	373.35		22.1188	0.09	Pg		22.1188	245.76	0.09	1.144149	373.35	67.58
	21R2 30-32	373.67		8.2959	0.09	Pg		8.2959	92.18	0.09	1.365966	373.67	67.61
	21R2 69-73	374.08		5.4721	0.09	Pg		5.4721	60.80	0.09	1.389918	374.08	67.64
	21R2 110-112	374.49		3.8247	0.09	Pg		3.8247	42.50	0.09	1.439793	374.49	67.68
	21R3 10-12	374.82		15.52	0.09	Pg		15.52	172.44	0.09	1.365972	374.82	67.71
	21R3 50-52	375.24		2.5976	0.09	Pg		2.5976	28.86	0.09	1.424358	375.24	67.75
	21R3 71-74	375.44		2.8182	0.09			2.8182	31.31	0.09	1.259858	375.44	67.76
	21R3 110-112	375.88		1.0709	0.09	26 additional		1.0709	11.90	0.09	1.408304	375.88	67.8
	21R3 148-150	376.2		3.2723	0.09			3.2723	36.36	0.09	1.410761	376.2	67.83
	21R4 3-5	376.25		0.8796	0.09			0.8796	9.77	0.09	1.581814	376.25	67.84
	21R4 42-44	376.64		11.0036	0.09			11.0036	122.26	0.09	1.083631	376.64	67.87
	21R4 76-78	376.98		0.813	0.09			0.813	9.03	0.09	1.524537	376.98	67.9
	21R4 98-100	377.2		3.5788	0.09			3.5788	39.76	0.09	1.285028	377.2	67.92
	21R4 138-140	377.62		11.5775	0.09			11.5775	128.64	0.09	1.714518	377.62	67.95
	21R5 0-2	377.73		4.1711	0.09			4.1711	46.35	0.09	1.695031	377.73	67.96
	21R5 60-62	378.32		1.2701	0.09			1.2701	14.11	0.09	1.229393	378.32	68.01
	21R5 71-76	378.46		2.3363	0.09			2.3363	25.96	0.09		378.46	68.02
	21R5 120-122	378.92		14.1429	0.09			14.1429	157.14	0.09	1.094212	378.92	68.06
	21R5 140-142	379.12		3.7856	0.09			3.7856	42.06	0.09	2.465939	379.12	68.08
	21R6 5-7	379.27		13.0942	0.09			13.0942	145.49	0.09	1.081205	379.27	68.1
	21R6 40-42	379.6		6.1732	0.09			6.1732	68.59	0.09	1.162179	379.6	68.12
	21R6 71-75	379.75		2.1416	0.09			2.1416	23.80	0.09		379.75	68.14
	21R6 85-87	379.9		0.0003	0.09			0.0003	0.00	0.09	1.046474	379.9	68.15
	22R1 35-37	379.97		2.6135	0.09			2.6135	29.04	0.09	1.717684	379.97	68.16
	22R1 78-80	380.2		0.3541	0.09			0.3541	3.93	0.09	1.542365	380.2	68.18
	21RCC 13-15	380.3		3.0951	0.09			3.0951	34.39	0.09	1.452846	380.3	68.19
	22R1 118-120	380.8		1.5308	0.09			1.5308	17.01	0.09	1.223241	380.8	68.23
	22R1 138-140	381.1		1.7147	0.09			1.7147	19.05	0.09	2.741964	381.1	68.25
	22R2 0-2	381.12		4.4743	0.09			4.4743	49.71	0.09	1.654237	381.12	68.26
	22R2 19-21	381.31		1.5067	0.09			1.5067	16.74	0.09	0.796988	381.31	68.27
	22R2 65-67	381.87		1.7279	0.09			1.7279	19.20	0.09	1.479122	381.87	68.32
	22R2 105-107	382.2		0.0003	0.09			0.0003	0.00	0.09	1.019321	382.2	68.35
	22R2 145-147	382.57		6.4956	0.09			6.4956	72.17	0.09	0.990215	382.57	68.38
	22R3 3-5	382.65		0.7708	0.09			0.7708	8.56	0.09	1.617191	382.65	68.39
	22R3 38-40	383		1.0334	0.09			1.0334	11.48	0.09	1.258605	383	68.42
	22R3 78-80	383.4		0.0003	0.09			0.0003	0.00	0.09	1.431832	383.4	68.45
	22R3 117-119	383.79		4.6171	0.09			4.6171	51.30	0.09	0.833667	383.79	68.49
	22R4 33-35	384.43		0.0003	0.09			0.0003	0.00	0.09	1.074759	384.43	68.54
	22R4 75-77	384.87		1.8432	0.09			1.8432	20.48	0.09	1.041736	384.87	68.58
	22R4 115-117	385.27		0.0002	0.09			0.0002	0.00	0.09	1.236876	385.27	68.62
	22R4 148-150	385.6		2.3904	0.09			2.3904	26.56	0.09	1.451047	385.6	68.64
	22R5 13-15	385.75		0.0003	0.09			0.0003	0.00	0.09	1.022717	385.75	68.66
	22R5 55-57	386.17		2.2539	0.09			2.2539	25.04	0.09	1.056948	386.17	68.69
	22R5 70-75	386.35		1.3679	0.09			1.3679	15.20	0.09	1.594414	386.35	68.71
	22R5 113-115	386.75		2.1059	0.09			2.1059	23.40	0.09	1.053531	386.75	68.74
	22R6 0-2	387.06		1.1589	0.09			1.1589	12.88	0.09	2.439495	387.06	68.77
	22R6 38-40	387.44		1.2638	0.09			1.2638	14.04	0.09	1.104247	387.44	68.8
	22R6 80-82	387.86		0.0003	0.09			0.0003	0.00	0.09	1.480381	387.86	68.84
	22R6 118-120	388.24		1.6731	0.09			1.6731	18.59	0.09	1.613602	388.24	68.87
	22R7 13-17	388.5		1.0752	0.09			1.0752	11.95	0.09	1.659422	388.5	68.9
	22RCC 15-17	388.8		2.8575	0.09			2.8575	31.75	0.09	1.522855	388.8	68.92
	23R1 32-34	389.54		0.0003	0.09			0.0003	0.00	0.09	2.273281	389.54	68.99
	23R1 70-74	389.94		2.5576	0.09			2.5576	28.42	0.09	2.101223	389.94	69.02
	23R1 110-112	390.32		0.0003	0.09			0.0003	0.00	0.09	1.432056	390.32	69.05
	23R1 148-150	390.7		3.6405	0.09			3.6405	40.45	0.09	2.008715	390.7	69.09
	23R2 20-22	390.92		0.0003	0.09			0.0003	0.00	0.09	1.338296	390.92	69.11
	23R2 60-62	391.32		1.3975	0.09			1.3975	15.53	0.09	1.715202	391.32	69.14
	23R2 99-101	391.71		0.0003	0.09			0.0003	0.00	0.09	1.472707	391.71	69.18
	23R2 140-142	392.13		1.7843	0.09			1.7843	19.83	0.09	1.555652	392.13	69.21
	23R3 23-25	392.45		0.0003	0.09			0.0003	0.00	0.09	1.121034	392.45	69.24
	23R3 64-66	392.86		9.585	0.09			9.585	106.50	0.09	1.114018	392.86	69.28
	23R3 115-117	393.37		1.2122	0.09			1.2122	13.47	0.09	1.62888	393.37	69.32
	23R3 148-150	393.7		5.4536	0.09			5.4536	60.60	0.09	1.98421	393.7	69.35
	23R4 18-20	393.9		1.364	0.09			1.364	15.16	0.09	1.441048	393.9	69.36
	23R4 45-47	394.17		5.1351	0.09			5.1351	57.06	0.09	1.711351	394.17	69.39
	23R4 86-88	394.58		10.9315	0.09			10.9315	121.46	0.09	0.9415	394.58	69.42
	23R4 125-127	394.97		6.1229	0.09			6.1229	68.03	0.09	0.95924	394.97	69.46
	23R5 10-12	395.32		11.6073	0.09			11.6073	128.97	0.09	1.024797	395.32	69.49
	23R5 53-55	395.75		21.0609	0.09			21.0609	234.01	0.09	1.7301	395.75	69.53
	23R5 93-95	396.15		6.8131	0.09			6.8131	75.70	0.09	1.809641	396.15	69.56
	23R5 135-137	396.57		16.352	0.09			16.352	181.69	0.09	1.606674	396.57	69.6
	23R6 15-17	396.87		0.0003	0.09			0.0003	0.00	0.09	1.757267	396.87	69.62
	23R6 55-57	397.27		5.7021	0.09			5.7021	63.36	0.09	3.232904	397.27	69.66
	23R6 95-97	397.67		0.0003	0.09			0.0003	0.00	0.09	1.9302	397.67	69.69
	23R6 125-127	397.97		34.0157	0.09			34.0157	377.95	0.09	1.302244	397.97	69.72
	23R7 13-15	398.5		14.2436	0.09			14.2436	158.26	0.09	2.012201	398.5	69.76
	24R1 23-25	399.05		3.1289	0.09			3.1289	34.77	0.09	1.524057	399.05	69.81
	24R1 63-65	399.45		2.0599	0.09			2.0599	22.89	0.09	1.411988	399.45	69.85
	24R1 103-105	399.85		9.9245	0.09			9.9245	110.27	0.09	1.7978	399.85	69.88
	24R1 143-145	400.25		10.1655	0.09			10.1655	112.95	0.09	1.182508	400.25	69.92
	24R2 23-25	400.53		12.3616	0.09			12.3616	137.35	0.09	1.582365	400.53	69.94
	24R2 63-65	400.93		4.0541	0.09			4.0541	45.05	0.09	1.155027	400.93	69.98
	24R2 103-105	401.33		4.1365	0.09			4.1365	45.96	0.09	1.579102	401.33	70.01
	24R2 143-145	401.73		1.5429	0.09			1.5429	17.14	0.09	1.499729	401.73	70.04
	24R3 3-5	401.83		7.9755	0.09			7.9755	88.62	0.09	1.707699	401.83	70.05
	24R3 23-25	402.03		0.8382	0.09			0.8382	9.31	0.09	1.917092	402.03	70.07
	24R3 43-45	402.23		6.0306	0.09			6.0306	67.01	0.09	1.631994	402.23	70.09
	24R3 63-65	402.43		0.4324	0.09			0.4324	4.80	0.09	1.533327	402.43	70.1
	24R3 83-85	402.63		4.4821	0.09			4.4821	49.80	0.09	1.550595	402.63	70.12
	24R3 105-107	402.85		0.0003	0.09			0.0003	0.00	0.09	1.362965	402.85	70.14
	24R3 123-125	403.03		3.4635	0.09			3.4635	38.48	0.09	2.310061	403.03	70.16
	24R3 143-145	403.23		0.6849	0.09			0.6849	7.61	0.09	1.596567	403.23	70.18
	24R4 23-25	403.53		5.5162	0.09			5.5162	61.29	0.09	1.618308	403.53	70.2
	24R4 60-62	403.9		2.8929	0.09			2.8929	32.14	0.09	1.51027	403.9	70.23
				5.83272027				5.83272027	64.81				

	Depth (mbsf)	Age (My)
C27r**	338.8	63,54 My
C28n**	344.6	64,64 My
C28r**	347	64,86 My
C29n**	350	65,7 My
K/Pg*	352.9	66,04 My
C29r**	359.5	66,38 My
C31n**	392.8	69,27 My

*Scientific results

**Louvel and Galbrun (2000)

Ash layers		Depth (mbsf)	Age (My)
16R2 12-15	333.02	333.05	62.34
16R2 41-42	333.31	333.32	62.5
16R4 19-21	336.09	336.11	63.03
16R4 37-45	336.27	336.35	63.08
16R4 148-150	337.38	337.4	63.27
16R5 14-16	337.54	337.56	63.3
16R5 30-37	337.7	337.77	63.33
17R2 38-41	342.83	342.86	64.31
17R2 45-47	342.9	342.92	64.32
18R3 100-103	351.36	351.39	65.09

Sample	Depth (mbsf)	Age (My)	Mercury (µg/kg)	S NMS	Hg/S NMS
20R1 29-32	362.2	66.61	14.674	0.996682	14.722856
20R1 55-57	362.87	66.67	10.2335	1.578916	6.4813453
20R1 85-87	363.17	66.7	5.7995	1.48032	3.9177343
20R1 145-147	363.77	66.75	8.1635	1.149976	7.0988425
20R2 5-7	363.87	66.76	10.2556	1.307049	7.8463787
20R2 45-47	364.24	66.79	7.7595	1.132581	6.8511685
20R2 68-70	364.47	66.81	9.7817	1.154731	8.4709796
20R2 88-90	364.7	66.83	4.2379	1.504952	2.8159707
20R2 128-130	365.1	66.87	7.8796	1.213302	6.4943433
20R3 8-10	365.4	66.89	7.0279	1.029705	6.8251604
20R3 48-50	365.8	66.93	6.3239	1.306481	4.8404088
20R3 73-75	366.05	66.95	0.7487	1.128195	0.6636266
20R3 113-115	366.45	66.98	8.2324	1.32077	6.2330306
20R3 138-140	366.7	67	13.9312	1.374658	10.134303
20R4 13-15	366.95	67.03	13.692	1.796645	7.6208725
20R4 53-55	367.35	67.06	3.4679	1.064178	3.2587581
20R4 93-95	367.75	67.1	6.3672	1.53199	4.1561638
20R4 140-142	368.12	67.13	1.2084	1.424166	0.8484964
20R5 13-15	368.45	67.16	17.5397	1.457809	12.031545
20R5 70-72	369.02	67.21	24.079	1.451118	16.593418
20R5 120-122	369.52	67.25	5.0669	1.172662	4.3208526
20R5 148-150	369.8	67.27	3.4491	1.944222	1.7740256
20R6 9-11	369.91	67.28	10.7513	1.959172	5.4876762
20R6 50-52	370.32	67.32	1.0171	1.13237	0.8982046
20R6 90-92	370.72	67.35	6.8754	1.208263	5.6903152
21R1 31-33	372.33	67.49	4.4407	2.165774	2.0503988
21R1 70-74	372.74	67.53	15.4674	1.500844	10.305798
21R1 108-110	373.1	67.56	9.6338	1.047664	9.1955071
21R1 133-135	373.35	67.58	22.1188	1.144149	19.332103
21R2 30-32	373.67	67.61	8.2959	1.365966	6.073285
21R2 69-73	374.08	67.64	5.4721	1.389918	3.9369947
21R2 110-112	374.49	67.68	3.8247	1.439793	2.6564232
21R3 10-12	374.82	67.71	15.52	1.365972	11.361876
21R3 50-52	375.24	67.75	2.5976	1.424358	1.8236991
21R3 71-74	375.44	67.76	2.8182	1.259858	2.2369184
21R3 110-112	375.88	67.8	1.0709	1.408304	0.7604182
21R3 148-150	376.2	67.83	3.2723	1.410761	2.3195285
21R4 3-5	376.25	67.84	0.8796	1.581814	0.5560705
21R4 42-44	376.64	67.87	11.0036	1.083631	10.154381
21R4 76-78	376.98	67.9	0.813	1.524537	0.5332767
21R4 98-100	377.2	67.92	3.5788	1.285028	2.7849974
21R4 138-140	377.62	67.95	11.5775	1.714518	6.7526278
21R5 0-2	377.73	67.96	4.1711	1.695031	2.4607814
21R5 60-62	378.32	68.01	1.2701	1.229393	1.0331111
21R5 120-122	378.92	68.06	14.1429	1.094212	12.92519
21R5 140-142	379.12	68.08	3.7856	2.465939	1.5351556
21R6 5-7	379.27	68.1	13.0942	1.081205	12.110743
21R6 40-42	379.6	68.12	6.1732	1.162179	5.3117443
21R6 85-87	379.9	68.15	0.0003	1.046474	0.0002867
22R1 35-37	379.97	68.16	2.6135	1.717684	1.5215258
22R1 78-80	380.2	68.18	0.3541	1.542365	0.2295825
21RCC 13-15	380.3	68.19	3.0951	1.452846	2.1303696
22R1 118-120	380.8	68.23	1.5308	1.223241	1.2514292
22R1 138-140	381.1	68.25	1.7147	2.741964	0.6253547
22R2 0-2	381.12	68.26	4.4743	1.654237	2.7047509
22R2 19-21	381.31	68.27	1.5067	0.796988	1.8904916
22R2 65-67	381.87	68.32	1.7279	1.479122	1.1681934
22R2 105-107	382.2	68.35	0.0003	1.019321	0.0002943
22R2 145-147	382.57	68.38	6.4956	0.990215	6.5597859
22R3 3-5	382.65	68.39	0.7708	1.617191	0.4766289
22R3 38-40	383	68.42	1.0334	1.258605	0.8210675
22R3 78-80	383.4	68.45	0.0003	1.431832	0.0002095
22R3 117-119	383.79	68.49	4.6171	0.833667	5.5383034
22R4 33-35	384.43	68.54	0.0003	1.074759	0.0002791
22R4 75-77	384.87	68.58	1.8432	1.041736	1.7693534
22R4 115-117	385.27	68.62	0.0002	1.236876	0.0001617
22R4 148-150	385.6	68.64	2.3904	1.451047	1.647362
22R5 13-15	385.75	68.66	0.0003	1.022717	0.0002933
22R5 55-57	386.17	68.69	2.2539	1.056948	2.1324614
22R5 70-75	386.35	68.71	1.3679	1.594414	0.8579327
22R5 113-115	386.75	68.74	2.1059	1.053531	1.9988963
22R6 0-2	387.06	68.77	1.1589	2.439495	0.4750573
22R6 38-40	387.44	68.8	1.2638	1.104247	1.1444906
22R6 80-82	387.86	68.84	0.0003	1.480381	0.0002027
22R6 118-120	388.24	68.87	1.6731	1.613602	1.0368727
22R7 13-17	388.5	68.9	1.0752	1.659422	0.6479364
22RCC 15-17	388.8	68.92	2.8575	1.522855	1.8764095
23R1 32-34	389.54	68.99	0.0003	2.273281	0.000132
23R1 70-74	389.94	69.02	2.5576	2.101223	1.2171956
23R1 110-112	390.32	69.05	0.0003	1.432056	0.0002095
23R1 148-150	390.7	69.09	3.6405	2.008715	1.8123527
23R2 20-22	390.92	69.11	0.0003	1.338296	0.0002242
23R2 60-62	391.32	69.14	1.3975	1.715202	0.8147727
23R2 99-101	391.71	69.18	0.0003	1.472707	0.0002037
23R2 140-142	392.13	69.21	1.7843	1.555652	1.1469787
23R3 23-25	392.45	69.24	0.0003	1.121034	0.0002676
23R3 64-66	392.86	69.28	9.585	1.114018	8.6039871
23R3 115-117	393.37	69.32	1.2122	1.62888	0.7441921
23R3 148-150	393.7	69.35	5.4536	1.98421	2.7485001
23R4 18-20	393.9	69.36	1.364	1.441048	0.9465336
23R4 45-47	394.17	69.39	5.1351	1.711351	3.0006125
23R4 86-88	394.58	69.42	10.9315	0.9415	11.610724
23R4 125-127	394.97	69.46	6.1229	0.95924	6.3830717
23R5 10-12	395.32	69.49	11.6073	1.024797	11.326442
23R5 53-55	395.75	69.53	21.0609	1.7301	12.173229
23R5 93-95	396.15	69.56	6.8131	1.809641	3.76489
23R5 135-137	396.57	69.6	16.352	1.606674	10.177549
23R6 15-17	396.87	69.62	0.0003	1.757267	0.0001707
23R6 55-57	397.27	69.66	5.7021	3.232904	1.7637703
23R6 95-97	397.67	69.69	0.0003	1.9302	0.0001554
23R6 125-127	397.97	69.72	34.0157	1.302244	26.120836
23R7 13-15	398.5	69.76	14.2436	2.012201	7.0786183
24R1 23-25	399.05	69.81	3.1289	1.524057	2.0530079
24R1 63-65	399.45	69.85	2.0599	1.411988	1.4588654
24R1 103-105	399.85	69.88	9.9245	1.7978	5.5203571
24R1 143-145	400.25	69.92	10.1655	1.182508	8.5965616
24R2 23-25	400.53	69.94	12.3616	1.582365	7.8121026
24R2 63-65	400.93	69.98	4.0541	1.155027	3.5099598
24R2 103-105	401.33	70.01	4.1365	1.579102	2.6195274
24R2 143-145	401.73	70.04	1.5429	1.499729	1.028786
24R3 3-5	401.83	70.05	7.9755	1.707699	4.6703205
24R3 23-25	402.03	70.07	0.8382	1.917092	0.4372247
24R3 43-45	402.23	70.09	6.0306	1.631994	3.6952338
24R3 63-65	402.43	70.1	0.4324	1.533327	0.2820011
24R3 83-85	402.63	70.12	4.4821	1.550595	2.8905673
24R3 105-107	402.85	70.14	0.0003	1.362965	0.0002201
24R3 123-125	403.03	70.16	3.4635	2.310061	1.4993107
24R3 143-145	403.23	70.18	0.6849	1.596567	0.428983
24R4 23-25	403.53	70.2	5.5162	1.618308	3.4086212
24R4 60-62	403.9	70.23	2.8929	1.51027	1.9154857
					4.0504687